UNITED STATES DEPARTMENT OF THE INTERIOR
GEOLOGICAL SURVEY

PROCEEDINGS OF
CONFERENCE XXXIX

Directions in Paleoseismology

22-25 April 1987
Albuquerque, New Mexico

Sponsored by

U.S. GEOLOGICAL SURVEY
NATIONAL EARTHQUAKE-HAZARDS REDUCTION PROGRAM

Editors
Anthony J. Crone and Eleanor M. Omdahl
U.S. Geological Survey
Denver, Colorado 80225

Convenor
Anthony J. Crone

Organizing Committee

Randall W. Jibson	U.S. Geological Survey,	Reston, Virginia
Alan R. Nelson	U.S. Geological Survey,	Denver, Colorado
Thomas K. Rockwell	San Diego State Univ.,	San Diego, California
David P. Schwartz	U.S. Geological Survey,	Menlo Park, California

OPEN-FILE REPORT 87-673

Denver, Colorado

1987

CONTENTS

CONTENTS--Continued

CONTENTS--Continued

*Editor's Note: Pages 100, 190, 360, and 416 are blank pages and are not included in copies of this report distributed by Open File Services Section.

LIST OF PARTICIPANTS

Allen, Clarence R.
Seismological Laboratory 252-21
California Institute of Technology
Pasadena, CA 91125
(818) 356-6904

Anderson, R. Ernest
U.S. Geological Survey
MS 966, Box 25046 DFC
Denver, CO 80225
(303) 236-1584

Andrews, D. Joe
U.S. Geological Survey
MS 977
345 Middlefield Road
Menlo Park, CA 94025
(415) 329-2752

Atwater, Brian F.
U.S. Geological Survey
c/o University of Washington
Department of Geological Sciences
AJ-20
Seattle, WA 98195
(206) 543-1912

Birkeland, Peter W.
University of Colorado
Department of Geological Sciences
Campus Box 250
Boulder, CO 80309-0250
(303) 492-6985

Bruhn, Ronald L.
University of Utah
Department of Geology & Geophysics
Salt Lake City, UT 84112-1183
(801) 581-6619

Bull, William B.
University of Arizona
Department of Geosciences
Tucson, AZ 85721
(602) 621-2219

Carver, Gary A.
Humboldt State University
Department of Geology
Arcata, CA 95521
(707) 826-3950

Clark, Malcolm M.
U.S. Geological Survey
MS 977
345 Middlefield Road
Menlo Park, CA 94025
(415) 329-2591

Colman, Steven M.
U.S. Geological Survey
Quissett Campus
Woods Hole, MA 02543
(617) 548-8700

Crone, Anthony J.
U.S. Geological Survey
MS 966, Box 25046 DFC
Denver, CO 80225
(303) 236-1595

Damon, Paul E.
Laboratory of Isotope Geochemistry
Department of Geosciences
University of Arizona
Tucson, Arizona 85721
(602) 621-4659

Edwards, R. Lawrence
California Institute of Technology
Division of Geological &
Planetary Sciences, 170-25
Pasadena, CA 91125
(818) 356-6894

Ellsworth, William L.
U.S. Geological Survey
MS 977
345 Middlefield Road
Menlo Park, CA 94025
(415) 329-4784

Forman, Steve
Institute of Arctic and Alpine Research
Campus Box 450
University of Colorado
Boulder, CO 80302
(303) 492-1196

Hall, N. Timothy
Earth Sciences Associates
701 Welch Road
Palo Alto, CA 94304
(415) 321-4071

Hanks, Thomas C.
U.S. Geological Survey
MS 977
345 Middlefield Road
Menlo Park, CA 94025
(415) 329-5634

Harden, Jennifer W.
U.S. Geological Survey
MS 975
345 Middlefield Road
Menlo Park, CA 94025
(415) 329-4949

Harrington, Charles D.
ESS-1, MS D462
Los Alamos National Laboratory
Los Alamos, New Mexico 87545
(505) 667-0078

Hemphill-Haley, Mark A.
Woodward-Clyde Consultants
100 Pringle Ave, Suite 300
Walnut Creek, CA 94596-3564
(415) 945-3483

Hull, Alan G.
Department of Geological Sciences
University of California, Santa Barbara
Santa Barbara, CA 93106
(805) 961-3471

Jacoby, Gordon
Tree-Ring Laboratory
Lamont-Doherty Geological Observatory
Palisades, NY 10964
(914) 359-2900 x 616

Jibson, Randy,
U.S. Geological Survey
MS 922, National Center
Reston, VA 22092
(703) 648-6787

Johnston, Arch C., Director
Tennessee Earthquake Information Center
Memphis State University
Memphis, TN 38152
(901) 454-2007

Keefer, David K.
U.S. Geological Survey
MS 998
345 Middlefield Road
Menlo Park, CA 94025
(415) 329-4893

King, Kenneth W.
U.S. Geological Survey
MS 966, Box 25046 DFC
Denver, CO 80225
(303) 236-1591

Knuepfer, Peter
Department of Geological Sciences
State University of New York, Binghamton
Binghamton, NY 13901
(607) 777-2389

Lettis, William
Geomatrix Consultants
1 Market Plaza
Spear Street Tower, Suite 717
San Francisco, CA 94105
(415) 957-9557

Maccini, John A.
Division of Earth Sciences
National Science Foundation
1800 G Street, N.W.
Washington, D.C. 20550
(202) 357-7866

Machette, Michael N.
U.S. Geological Survey
MS 966, Box 25046 DFC
Denver, CO 80225
(303) 236-1243

Mayer, Larry
Department of Geology
Miami University
Oxford, OH 45056
(513) 529-3241

McCalpin, James P.
Utah State University
Department of Geology UMC
Logan, UT 84322-0705
(801) 750-1220

McMullen, Richard D.
Office of Research
U.S. Nuclear Regulatory
Commission, NL 007
Washington, D. C. 20555
(301) 492-7000

Menges, Christopher
Department of Geology
Northrop Hall
University of New Mexico
Albuquerque, New Mexico 87131
(505) 277-5261

Muhs, Daniel R.
U.S. Geological Survey
MS 963, Box 25046 DFC
Denver, CO 80225
(303) 236-4772

Naeser, Charles W.
U.S. Geological Survey
MS 424, Box 25046 DFC
Denver, CO 80225
(303) 236-4720

Nash, David
University of Cincinnati
Department of Geology
Cincinnati, OH 45221-0013
(513) 475-2834

Nelson, Alan R.
U.S. Geological Survey
MS 966, Box 25046 DFC
Denver, CO 80225
(303) 236-1596

Nishenko, Stuart
U.S. Geological Survey
MS 967, Box 25046 DFC
Denver CO 80225
(303) 236-1506

Obermeier, Stephen F.
U.S. Geological Survey
MS 922, National Center
Reston, VA 22092
(703) 648-6791

Ostenaa, Dean
U.S. Bureau of Reclamation, D-1632
P.O. Box 25007
Denver, CO 80225
(303) 236-4195

Pavich, Milan
U.S. Geological Survey
MS 928, National Center
Reston, VA 22092
(703) 648-6952

Perkins, David M.
U.S. Geological Survey
Ms 966, Box 25046 DFC
Denver, CO 80225
(303) 236-1616

Pierce, Kenneth L.
U.S. Geological Survey
MS 913, Box 25046 DFC
Denver, CO 80225
(303) 236-1244

Plafker, George
U.S. Geological Survey
MS 904
345 Middlefield Road
Menlo Park, CA 94025
(415) 329-5689

Reilinger, Robert
Earth Resources Laboratory, E-34
Department of Earth, Atmospheric, &
Planetary Science
Massachusetts Institute of Technology
Cambridge, MA 02139
(617) 253-7860

Rockwell, Thomas K.
Department of Geological Sciences
San Diego State University
San Diego, CA 92182
(619) 265-4441

Rogers, Albert M.
U.S. Geological Survey
MS 966, Box 25046 DFC
Denver, CO 80225
(303) 236-1585

Russ, David P.
U.S. Geological Survey
MS 905, National Center
Reston, VA 22092
(202) 959-6708

Rymer, Michael J.
U.S. Geological Survey
MS 977
345 Middlefield Road
Menlo Park, CA 94025
(415) 329-5649

Sarna-Wojcicki, Andrei M.
U.S. Geological Survey
MS 975
345 Middlefield Road
Menlo Park, CA 94025
(415) 329-4930

Schumm, Stanley A.
Colorado State University
Department of Earth Resources
Fort Collins, CO 80523
(303) 491-5294

Schwarcz, Henry
McMaster University
Department of Geology
Hamilton, Ontario
Canada L8S-4M1
(416) 525-9140 x4186

Schwartz, David P.
U.S. Geological Survey
MS 977
345 Middlefield Road
Menlo Park, CA 94025
(415) 329-5651

Seeber, Leonardo
Lamont-Doherty Geological Observatory
Palisades, NY 10964
(914) 359-2900 x 385

Shlemon, Roy J.
Shlemon and Associates
P.O. Box 3066
Newport Beach, CA 92663-0620
(714) 675-2696

Sibson, Richard H.
University of California, Santa Barbara
Department of Geological Sciences
Santa Barbara, CA 93106
(805) 961-4530

Sieh, Kerry E.
California Institute of Technology
Division of Geological &
Planetary Science
Pasadena, CA 91125
(818) 356-6115

Slemmons, D. Burton
University of Nevada
Mackay School of Mines
Department of Geological Sciences
Reno, NV 89506
(702) 784-6067

Stein, Ross S.
U.S. Geological Survey
MS 977
345 Middlefield Road
Menlo Park, CA 94025
(415) 329-4840

Swan, Bert
Geomatrix Consultants
1 Market Plaza
Spear Street Tower, Suite 717
San Francisco, CA 94105
(415) 957-9557

Tapponier, Paul
Institute du Physique du Globe
4 Place Jussieu
75252 Paris Cedux 05
(33) (1) 43.54.87.72

Tsukuda, Eikichi
Geological Survey of Japan
Higashi 1-1-3, Yatabe, Tsukuba
Ibaraki 305, JAPAN
(0208) 54-3693

Verosub, Kenneth L.
Department of Geology
University of California, Davis
Davis, California 95616
(916) 752-6911

Wallace, Robert E.
U.S. Geological Survey
MS 977
345 Middlefield Road
Menlo Park, CA 94025
(415) 329-5159

Wells, Stephen
Deparment of Geology, Northrop Hall
University of New Mexico
Albuquerque, New Mexico 87131
(505) 277-2348

Wesnowsky, Steven G.
Memphis State University
Department of Geological Sciences
Memphis, TN 38152
(901) 454-2007

Wheeler, Russell L.
U.S. Geological Survey
MS 966, Box 25046 DFC
Denver, CO 80225
(303) 236-1592

Yeats, Robert S.
Oregon State University
Department of Geology
Corvallis, OR 97331
(503) 754-2484

Youd, Les
Brigham Young University
Department of Civil Engineering
Provo, UT 84602
(801) 378-6327

Zoback, Mary Lou
U.S. Geological Survey
MS 977
345 Middlefield Road
Menlo Park, CA 94025
(415) 329-4760

Workshop Staff:

Haller, Kathleen
U.S. Geological Survey
MS 966, Box 25046 DFC
Denver, CO 80225

Omdahl, Eleanor
U.S. Geological Survey
MS 966, Box 25046 DFC
Denver, CO 80225

Tibbetts, Reva
U.S. Geological Survey
MS 966, Box 25046 DFC
Denver, CO 80225

INTRODUCTION TO DIRECTIONS IN PALEOSEISMOLOGY

by

Anthony J. Crone
U.S. Geological Survey
Denver, Colorado 80225

Earthquakes are one of the most terrorizing, destructive, and deadly natural phenomena known to mankind. Historical records contain numerous accounts of earthquakes that caused extensive damage, thousands of deaths, and serious economic hardship throughout the world. Despite the constant threat of destruction and death for thousands of years, we possess only a rudimentary knowledge of the causes of earthquakes; only now are we starting to develop a basic understanding of some of the physical processes that produce such destructive events. In the United States, serious, destructive shocks in Alaska in 1964 and in southern California in 1971 drew national attention to the peril of earthquakes. These events provided some impetus for Federal approval of the Earthquake Hazards Reduction Act of 1977 which included funding for the National Earthquake Hazards Reduction Program (NEHRP) (Hanks, 1985). Three major goals of the national program are to (1) identify those parts of the country where earthquakes pose a significant hazard, (2) mitigate those hazards through better design of structures and modifications in land-use policy, and (3) increase our understanding of the earthquake-generation process through a comprehensive program of basic and applied scientific research.

Earthquake hazards are assessed by using the past behavior of seismogenic faults to predict their future behavior. These assessments require information on the location, the timing and recurrence, and the size or magnitude of paleoseismic events (ancient earthquakes). Regional and worldwide seismic networks, which have been installed during the past few decades, now supply accurate information on the location, time, and magnitude of major earthquakes. For events that predate our instrumental records, we must extract earthquake information from the historic record if possible. For events that predate the local historic record, our only source of information on past earthquakes is the geologic record.

Plate tectonics provides us with a unified perspective of global dynamics and orogenesis. This perspective, combined with a modern overview of worldwide seismicity from instrumental and historic data, allows us to identify those areas most susceptible to large-magnitude, damaging earthquakes. In those areas prone to large earthquakes, now we need to carefully map all potentially seismogenic faults, especially where these faults are near heavily populated areas. However, even in carefully mapped areas, some seismogenic faults may escape detection because (1) they may not break the ground surface, (2) they may lie under water, or (3) their expression may be completely obliterated by urbanization. Two examples of recent earthquakes associated with unmapped or concealed faults in carefully mapped areas are the Coalinga earthquake in May 1983 (Stein and King, 1984) and the Whittier Narrows earthquake in southern California in October 1987.

In some parts of the world, historic accounts provide a relatively complete record of large earthquakes during the past few thousand years. However, even in these areas, the historic record is of minimal value for determining the recurrence time between large events. In tectonically active

regions, the recurrence of major earthquakes on a specific part of a fault is commonly measured in hundreds to thousands of years; in less active regions, recurrence is measured in tens or even hundreds of thousands of years. Under the best circumstances in very active areas, such as China, the historic record is incomplete and subject to varying amounts of interpretation. Where earthquake recurrence is measured in tens of thousands of years, the historic record is essentially useless. Given the limitations of the historic record and the typical recurrence time of large earthquakes, the geologic record is our only source of information to characterize the long-term temporal behavior of seismogenic faults.

Estimating the magnitude of pre-instrumental earthquakes is also subject to the incompleteness and vagaries in the historic record. Magnitude estimates of pre-instrumental events are commonly derived from empirical comparisons of the relation between magnitude (commonly, m_b) and the distribution of Modified Mercalli intensities (for example, see Nuttli and others, 1979). In addition to the limitations of historic record, these estimates are influenced by terrestrial effects such as variations in attenuation and focusing of seismic energy that can produce anomalously high or low intensities. Again, only the geologic record can provide us with some basic information on the magnitude of selected historic and all prehistoric earthquakes.

Thus, our knowledge of the long-term behavior of seismogenic faults has been restricted by the constraints of the historic record, which is useful in some places but of minimal value elsewhere. In the past, we have had few clues to the regularity or variability in the timing between successive events on a single fault or fault zone. We have had little information on how individual segments of lengthy faults interact during major earthquakes. We did not know if measurements of contemporary slip rates were representative of long-term geological rates. Thus, our general lack of knowledge concerning the temporal and spatial behavior of seismogenic faults has hampered our ability to accurately assess and mitigate earthquake hazards.

During the past decade, the new subdiscipline of paleoseismology (Wallace, 1981) has attempted to deal with some of these problems; it offers great promise in contributing to more realistic earthquake-hazard assessments. Simply defined, paleoseismology is the study of the age, frequency, and size of prehistoric earthquakes. Paleoseismology relies on stratigraphic evidence to decipher the record of prehistoric earthquakes, and utilizes techniques from a diverse variety of geoscience disciplines including geomorphology and Quaternary geology, Quaternary dating methods, structural geology, seismology, geodesy, and geophysics. Paleoseismology provides the means to expand the limited view of earthquakes offered by the historic record and can help us understand the long-term behavior of seismogenic faults (Allen, 1986). Through studies of individual prehistoric surface-faulting events, we hope to characterize the coseismic behavior of seismogenic faults, to identify variations in the spatial and temporal distribution of earthquakes, and to detect patterns of long-term, regional deformation (Schwartz, 1987).

Despite this optimistic potential, the scientific conclusions of paleoseismologic studies still contain significant uncertainties and ambiguities. These uncertainties are not trivial because, in many cases, important societal decisions having substantial economic impacts are based on those conclusions. Paleoseismologic investigations can and do have major implications that affect hundreds of thousands of people and involve the expenditure of millions of dollars.

In April 1987, the U.S. Geological Survey sponsored this workshop on "Directions in Paleoseismology", which was the first forum dedicated solely to paleoseismology. The workshop was especially timely because of increasing public awareness of earthquake hazards and because the scientific community now recognizes that paleoseismology has made and will continue to make substantial contributions to minimizing earthquake hazards. Seventy two geoscientists, practitioners, and scientific managers from academic institutions, the business community, and government organizations convened to review the past accomplishments, current status, and future objectives of paleoseismology. At the workshop, participants exchanged ideas and information, discussed the current limitations and future developments of paleoseismologic techniques, and expressed concern on how some paleoseismologic data is being used and abused.

This volume summarizes the proceedings of the workshop and, thereby, presents a realistic picture of the current status of paleoseismology. The format of the workshop was designed to encourage and stimulate dialog, and consisted of a series of brief reviews of pertinent scientific topics followed by discussion sessions involving all of the participants. Discussion in these sessions was moderated by a chairman and stimulated by a panel of individuals familiar with the appropriate topics. This volume is organized in the same format as the meetings. I prepared the summaries of the discussion sessions from transcripts of the individual sessions; in the summaries, I attempted to capture the overall content of the discussions, and identify the major thoughts and concerns expressed by the participants. These summaries are meant solely to provide readers with a sense of the content of the discussion sessions. Readers should also realize that some comments in the discussions were offered purely in the spirit of stimulating discussion; some of these controversial comments were not challenged as unrealistic or impractical. Furthermore, the topics included in the summaries do not represent a consensus of the attendees, nor do they necessarily represent my personal opinions or policies of the U.S. Geological Survey.

Quaternary geology has a critical role in paleoseismology because most of the evidence of major prehistoric earthquakes is preserved in Quaternary deposits or interpreted from geomorphic features. Quaternary dating techniques are especially important to paleoseismology because of the need to determine the timing and recurrence of prehistoric events. Thus, the first technical session of the workshop reviewed the status of Quaternary dating techniques, including recent developments in novel methods that may expand our ability to date a greater variety of deposits. Subsequent technical sessions and presentations dealt with the problems of recognizing and characterizing individual paleoseismic events in the geologic record, the difficulties in estimating Quaternary slip rates and the amounts of coseismic deformation, the variations in long-term and short-term behavior of seismogenic faults, and the application of paleoseismic data to various aspects of seismic-hazard analysis. The final panel discussion examined the needs and possible future directions of paleoseismologic studies from the viewpoint of both practitioners and scientific managers.

The nascent discipline of paleoseismology has already made substantial contributions to evaluating seismic hazards. In the future, paleoseismology has the potential to answer fundamental questions about the behavior of faults that can be answered in no other way. These opportunities make paleoseismology an exciting and dynamic field of scientific research whose potential is only now being recognized.

RECOMMENDATIONS AND RESEARCH PRIORITIES

The discussions at this workshop covered a wide range of topics related to the past, present, and future activities in paleoseismology. During the discussions, several significant research topics and objectives seemed to draw the enthusiastic support of most participants. I have summarized some of these topics below; this list is not comprehensive and is based largely on my sense of what the group felt was important objectives for paleoseismology. I should emphasize that not all participants endorsed all of these recommendations.

1. Test and stimulate development of new dating techniques. The crux of virtually all paleoseismic studies is reliable, consistent age control. Without age control, paleoseismic data has limited value. Several new, potentially valuable techniques and further refinements in standard techniques could have widespread application in paleoseismology. Developing and refining dating techniques requires not only improvements in laboratory procedures, but also careful, systematic field testing. The field testing should be done first in areas where geologic relations are unambiguous and well documented. Subsequent testing should apply the techniques to more complex areas. An important part of any testing program should be to apply several independent dating methods to the same stratigraphic section. The resulting age determinations will permit calibration of the different techniques, and will help identify specific physical and chemicla factors that affect individual techniques.

2. Systematic investigation of historic events. A program to carefully and systematically study deformation associated with historic surface-faulting earthquakes offers numerous benefits to paleoseismology and to earthquake hazard assessments. The recognition and characterization of prehistoric earthquakes often depends on accurately interpreting small-scale geologic features and subtle stratigraphic relations. In the past decade, we have learned a great deal about near-surface deformation, tectonic geomorphology, and scarp-modification processes that allow us to decipher significant, subtle details in the geologic record. By systematically studying the geologic features formed by historic surface-faulting events, we will understand better the features and stratigraphic relations we observe in the geologic record. Our improved understanding will contribute to better interpretations. These studies should include historic events worldwide because the short historic record in the United States severely limits the number of events available for study.

   Studying of historic earthquakes has other benefits. Estimating the timing and recurrence of moderate-magnitude (M 6-6.5) earthquakes are a serious problem in earthquake hazard assessments. Geologists must study the surface effects of historic, moderate-magnitude earthquakes to recognize similar-size events in the geologic record. In addition, studies of historic events may help geologists identify features that may be diagnostic of moderate-magnitude earthquakes.

The concept of fault segmentation has profound implications for understanding the process of rupture propagation and for evaluating seismic hazards. An important objective of future studies in paleoseismology will be to define segments of various fault zones and to characterize geologic structures that bound individual segments. Studies of historic earthquakes will provide invaluable insight into how different segment boundaries respond to propagating ruptures and how effectively different boundaries halt coseismic ruptures.

Estimates of the magnitude of paleoseismic events are commonly based on a comparison of the amount of surface displacement and (or) length of surface faulting of prehistoric events with similar parameters for historic events. However, the quality these measurements for historic events is extremely variable. Detailed studies of selected historic earthquakes could substantially improve our data on the displacement and length of ruptures, and thus contribute to better estimates of magnitude for prehistoric events.

The morphology of fault scarps is a convenient and efficient way to estimate the age of many surface-faulting events. Improving these age estimates will depend on a better understanding of scarp degradation processes and the rates of degradation in various climates and various materials. Studies of historic and prehistoric fault scarps of known age could clarify the role of different degradation processes and contribute to better numeric age estimates for fault scarps based on scarp morphology.

3. Characterize long-term versus short-term behavior of faults. Paleoseismic studies have uncovered tantalizing bits of information about differences in the long-term and short-term behavior of faults. The behavior of some faults seems to be regular and predictable, whereas the behavior of others seems to be dominated by temporal clustering of earthquakes and long periods of quiescence. Studies to characterize the regularity or randomness in fault behavior will improve probabilistic models of seismic hazards.

4. Increase general awareness of the value of paleoseismology as a scientific discipline. Paleoseismology has made major contributions to the national earthquake program, many of which were initially unexpected. Future studies should provide insight into fundamental aspects of earthquake research that no other discipline offers. In these times of strong competition for limited resources, geoscientists need to educate their peers, the public, and legislative bodies about the unique contributions that paleoseismology can make in future earthquake hazard programs. At the same time, we should vigorously pursue research opportunities using new and developing technologies.

ACKNOWLEDGMENTS

The success of this conference depended on the cooperation and support of many people. The organizing committee of Randy Jibson (USGS, Reston, Va.), Alan Nelson (USGS, Denver, Colo.), Tom Rockwell (San Diego State Univ., San Diego, Calif.), and David Schwartz (USGS, Menlo Park, Calif.) was vital to planning the excellent technical program. They also moderated the discussion sessions at the meetings. I thank John Filson (Chief, Office of Earthquakes, Volcanoes, and Engineering), Elaine Padovani (Deputy Office Chief) and Albert Rogers (Chief, Branch of Geologic Risk Assessment) for their interest and support. Eleanor Omdahl was indispensable in supervising and coordinating numerous aspects of the workshop, and in assisting in the editing responsibilities. Kathleen Haller provided invaluable logistical assistance at the workshop and during the preparation of this volume.

REFERENCES CITED

Allen, C.R., 1986, Seismological and paleoseismological techniques of research in active tectonics, in Active tectonics: Washington, D.C., National Academy Press, p. 148-154.

Hanks, T.C., 1985, The National Earthquake Hazards Reduction Program--Scientific status: U.S. Geological Survey Bulletin 1659, 40 p.

Nuttli, O.W., Bollinger, G.A., and Griffiths, D.W., 1979, On the relation between modified Mercalli intensity and body-wave magnitude: Bulletin of the Seismological Society of America, v. 69, no. 3, p. 893-909.

Schwartz, D.P., 1987, Earthquakes of the Holocene: Reviews of Geophysics, v. 25, no. 6, p. 1197-1202.

Stein, R.S., and King, G.C.P., 1984, Seismic potential revealed by surface folding--1983 Coalinga, California earthquake: Science, v. 224, p. 869-872.

Wallace, R.E., 1981, Active faults, paleoseismology, and earthquake hazards in the western United States, in Simpson, D.W., and Richards, P.G., eds., Earthquake prediction--An international review: Washington, D.C., American Geophysical Union, Maurice Ewing Series 4, p. 209-216.

A PERSPECTIVE OF PALEOSEISMOLOGY

by

Robert E. Wallace

U.S. Geological Survey
Menlo Park, California 94025

HISTORY

This is the first conference devoted to "paleoeismology." We are always intrigued by "firsts"; in sports, exploration, or discoveries in science; we list such things in books of records. "Firsts" are punctuation marks in the flow of history, and for a first in "paleoseismology" I select, not surprisingly, a paper by Grove Karl Gilbert. In 1883 he wrote in the Salt Lake Tribune (later published in American Journal of Science, 1884), these very modern concepts:

> "Mountains rise little by little" and a "little cliff, in geologic parlance a 'fault scarp' is formed." Alternate "cohesion and sliding" characterize this motion... There is one place where scarps are conspicuously absent, strain is slowly increasing, and someday it (strain) will overcome friction, lift the mountains a few feet, and re-enact on a more fearful scale the catastrophe of Owens Valley."

Here are paleoseismology, earthquake prediction, and the evaluation of earthquake hazards encompassed in a few words. This is what our new subdiscipline is all about. Gilbert's paper also happened to be the first paper devoted to earthquakes that was authored by a member of the fledgling U.S. Geological Survey and, to the best of my knowledge, it is the first paper on earthquake prediction using the scientific method.

Paleoseismology can be defined as "the identification and study of prehistoric earthquakes" (Wallace, 1981a). Records of historical earthquakes, especially in North America, do not even span one full cycle of recurrence of magnitude 8 earthquakes at any given site. For intracontinental areas in countries where the useful seismic history is thousands of years long, great earthquakes on a given segment of a fault seem to recur at even longer intervals. Large earthquakes in subduction zones, of course, occur more frequently.

The study of active faults, the generators of earthquakes, is the major focus of paleoseismology. I have suggested that active faults be defined as "those that may have displacement within a future period of concern to humans" (Wallace, 1981b). Thus, a predictive frame of thinking is proper and useful in the study of active faults.

The techniques of paleoseismology are primarily geologic, including analysis of: microstratigraphic relations along faults, fault-scarp and fault-trace geomorphology, regional tectonic relations, seismically induced sedimentary structures, and river and marine terraces related to uplift and faulting. Dating techniques for Quaternary geology serve to determine the timing and rates of occurrence of prehistoric earthquakes.

The first use of the term "paleoseismology" in the title of a paper, or at least a term very closely related, appears to have been by the Russian, Kuchay (1971). His term was "paleosysmodislokatsiy." In English I believe Engelder (1974) used the term first in the title, "Microscopic wear grooves on slickensides: Indicators of Paleoseismology."

Between Gilbert's time and the 1970's, however, many paleoseismologic studies and discoveries were made, even though they were not termed paleoseismology. The following is a sketch of the history of the past 100 years of paleoseismology, highlighted only by selected events to portray the flow of ideas and development of techniques. Each of you undoubtedly might choose different events to note.

Before the turn of the century the work of Dutton (1889) on the Charleston, S. C., earthquake of 1886 contained much information pertinent to paleoseismology. Work on the 1906 San Francisco, Calif., earthquake saw a major milestone, with research reports by Gilbert, Branner, Lawson, and others (Lawson, 1908). The weight of geologic opinion only then turned strongly to the concepts that faults generate earthquakes, and that faults break again and again in the same place, even though Gilbert had noted these relations more than two decades earlier.

In the decades from 1910 to 1940, few large earthquakes occurred in the Western United States, but studies of two in Nevada, Pleasant Valley, 1915 (Jones, 1915), and Cedar Mountain, 1932 (Gianella and Callaghan, 1934) laid the groundwork for later paleoseismologic analyses of fault scarps.

The year 1940 was marked by the Imperial Valley earthquake, and data gathered by J.P. Buwalda, Charles Richter (1958) and others became a base line about surface faulting to which the faulting of 1979 could be compared. In 1950, J.T. Pardee used many modern techniques of paleoseismology in

analyzing Cenozoic faults in western Montana (Pardee, 1950). He wrote of "recent scarps" having angles of repose of 30^{o}-35^{o}, noted that young scarps lay at the base of higher dissected fault scarps constituting range fronts, and described "segmentation" of range-front faults. He also counted growth rings on stumps of trees that grew on the fault scarps and estimated when previous faulting might have occurred. Perhaps many of these techniques and concepts were not entirely original, but Pardee combined them to create a distinctly modern paleoseismologic analysis, well ahead of common practice.

The 1950's saw significant studies of fault scarps, including those at Fairview Peak and Dixie Valley, Nevada, in 1954 (Slemmons, 1957), and at Hebgen Lake, Montana, in 1959 (Myers and Hamilton, 1964; Witkind, 1964). A study of the Hebgen scarps made 18 years later documented some of the styles and rates of scarp degradation (Wallace, 1980). In studying the 1954 earthquake Slemmons and colleagues (1959) described, for the first time, evidence that a fault having had surface displacement in 1903 had similar surface displacement in 1954. As likely as this behavior seemed to most geologists, no clear documentation was available before. Now, 30 years later, the record is so replete with examples, it is difficult to appreciate our lack of information in 1954.

In Richter's Elementary Seismology (1958) many paleoseismologic observations are made. He noted in New Zealand, for example, that "Everywhere in the principal active areas of both islands, are scarplets of the right height and extent to have originated in single seismic events, without indication of accumulation or repetition, as if the locus of fracture were constantly shifting" (Richter, 1958, p. 460-461).

The great Alaskan earthquake of 1964 was a benchmark for all subsequent earthquake studies in the United States. A succession of reports prepared at national level proposed actions to mitigate against the hazards of great earthquakes, and these efforts culminated in 1977 in the enactment of the National Earthquake Hazard Reduction Act.

One of the most significant paleoseismic studies following the 1964 event was conducted by George Plafker (Plafker and Rubin, 1978) who compared the newly created marine terraces on Middleton and Montague Islands with similar prehistoric marine terraces. Clearly several prehistoric uplifts of the same tectonic blocks had occurred at intervals of from 500 to 1,400 years. In 1968, Plafker used this technique in Chile to analyze the region of the great 1960 earthquake. There, rather than uplift, he found that the accessible part of the coastline had been subjected to subsidence, consistent with a dislocation model of subduction zone faulting.

In the late 1960s, Slemmons (1967) compiled a map of the young fault scarps in the Great Basin province and on this map reported the distribution of scarps of different ages. He based his analysis on fault-scarp degradation. In 1968, a symposium on the San Andreas fault was organized by W.R. Dickinson and Arthur Grantz and included paleoseismologically significant reports on stream offsets by Wallace (1968) and on long-term characteristics of different segments of the San Andreas fault by Allen (1968). An important synthesis on rates of slip on the San Andreas fault based on geological offsets was prepared by the conveners Grantz and Dickinson (1968, p. 117-119).

Excavations specifically for paleoseismological studies were first made in the late 1960s. Although such excavations are useful only if fortuitous arrangements of sedimentary structures, faults, and datable materials are found, extremely important data about prehistoric earthquakes have been recovered using this approach. In 1968, Jay Smith of Converse, Davis and Associates (1968) may have been the first to gather paleoseismic data by trenching in San Bernardino, Calif. At about the same time Malde (1971) was conducting similar studies in Idaho. In addition, Clark, Grantz and others (1972), in the aftermath of the 1968 Borrego Mountain, Calif., earthquake, were obtaining clear evidence in trenches excavated across the Coyote Mountain fault that displacements had recurred again and again. Similar studies were made by Bonilla (1973) following the 1971 San Fernando earthquake. In 1978, a site of great significance was found by Kerry Sieh at Pallett Creek, Calif., on the San Andreas fault (Sieh, 1978). By meticulous and detailed analysis, he identified a series of prehistoric offsets along the San Andreas fault which had occurred at intervals averaging between 140 and 150 years; presumably each displacement was accompanied by a great earthquake. These findings have had a profound influence on analyses of earthquake hazards and on programs of hazard reduction in southern California.

The first in a continuing series of excavation for paleoseismological studies was made in Japan in 1976. Special shapes of excavations have since been developed to best display stratigraphic and structural relations, and remarkably complete written, photographic, and sample records have been collected. In the Peoples Republic of China paleoseismology captured the attention of geologists at the State Seismological Bureau in the late 1970s, and the first trenches excavated for this purpose were opened in late 1978 and early 1979.

Other new techniques for studying prehistoric earthquakes were developed, including measurement of profiles of fault scarps. Interpretation of the changes that had occurred in a scarp's profile since its inception provided evidence of the age of the scarp and, in places, evidence of repeated events (Wallace, 1977). Further mathematical refinements of

scarp-profile analyses followed in a series of papers by Nash (1980), Colman and Watson (1983), Hanks and others (1984), and Andrews and Hanks (1985). A diffusion model was the principal basis for these later analyses.

As interest in paleoseismology grew, Quaternary dating techniques became more clearly recognized as crucial to dating prehistoric seismic events. Support by the Earthquake-Hazard-Reduction Program of the U.S. Geological Survey became an important stimulus for a variety of studies in dating techniques, including further attention to rates of soil development and dating of soils (Harden, 1982). Dendrochronologic studies along the Fairweather fault in Alaska were reported by Page (1970), and Lamarche and Wallace (1972) evaluated the effects on trees by movements on the San Andreas fault. A study by Janet Hoare (1982) first used lichenometric methods to date fault scarps in Nevada.

WHAT NEXT?

Since about the time of enactment of the National Earthquake Hazard Reduction Act of 1977, paleoseismology has received rapidly expanding attention and credit for significant advancements relating to earthquake prediction and seismic-hazard assessment.

Among the important paleoseismologic concepts that have emerged over the past ten or fifteen years are: (1) the importance of slip rates on faults, (2) the usefulness of average recurrence interval of faulting events and related earthquakes, and (3) the significance of segmentation of faults and related characteristic earthquakes. These three themes are interrelated and can form a framework for developing questions and significant future research.

To provide a first-order approximation, long-term average slip rates translate into average recurrence intervals for earthquakes of a given size. This is a powerful concept and builds both on the elastic-rebound theory and on long-established methods of field analyses of faults, such as the offset of geologic units or geomorphic features of known age. But slip may be either aseismic by tectonic creep, or by stick-slip mechanisms that generate earthquakes. As yet, we have no specific way to distinguish between these two styles of slip in the geologic record.

Both the loading and the release of elastic strain may be at nonuniform rates. The accumulation of strain may accelerate or decelerate at constant or variable rates or in spasmodic fashions (Pierce, 1986). Grouping and migration of slip or other variations in either short or long term may occur (Wallace, 1987). Documenting these variations in fault behavior not only should help assess earthquake hazards, but should help reveal how the crust of the earth behaves physically.

Fault segmentation leads to the idea of the "characteristic earthquake" (Schwartz and Coppersmith, 1984). But although faults clearly are segmented, a variety of styles of segmentation are known, including longitudinal, branching, en echelon, parallel, and conjugate segmentation. Each style of segmentation presents different possibilities in interpreting characteristic behavior from patterns of faulting. Can we learn to predict which single seismic events may involve more than one major segment, as has happened? What are the characteristics of transitions between segments? Transitions at depth between brittle and ductile behavior of materials are extremely significant to the problems at hand, but are little-known or understood.

The rates of processes, ranging from rates of strain accumulation and release, to rates of geomorphic and sedimentary processes, are critical to the science of paleoseismology. It is gratifying to see the emphasis at this conference on dating techniques. Several of us who are participating here also were involved in preparing the "Active Tectonics" volume for The National Research Council/National Academy of Sciences (1986). In the recommendations presented in that volume, the highest research priority was assigned to the furtherance of methods for dating Quaternary materials. In that same volume, Pierce (1986) presented a review of more than two dozen dating techniques, including radioactive carbon, cosmogenic isotopes, soil development, geomorphic forms, and thermoluminescence.

Progress in paleoseismology has been exciting and gratifying; new advances seem to be just ahead. I fear, however, that at times we have exploited some of our new ideas too enthusiastically. In our enthusiasm, our interpretations can be, and some may have been, carried too far, too soon. I believe that some statements that I, and possibly others, have made in public have been too far-reaching, too positive, and have lacked appropriate caveats of uncertainty. As a result, I believe, some people have misconceptions as to the imminence and destructive power of earthquakes. How should we report significant findings on a timely basis--often before ideas have matured--to provide useful decisions now and to educate users of our information in the uncertainties we recognize? How can we help the public react to earthquake hazards with well-measured responses, with tendencies neither toward panic nor complacency?

We need a constant flow of new ideas, and indeed, they abound. We should encourage the evolution of these ideas, but should constantly be on guard for inadequacies. Gilbert (1886, p. 287) said:

> "The great investigator is primarily and preeminently the man who is rich in hypotheses. In the plentitude of his wealth he can spare the weaklings without

regret; and having many from which to select, his mind maintains a judicial attitude. The man who can produce but one, cherishes and champions that one as his own, and is blind to its faults."

We have just now reached what might be called a critical mass of earth scientists involved in paleoseismology--just look around at those who attended the paleoseismology workshop. Progress in the science is accelerating. To maintain this pace will require great effort on behalf of each of us, not only to conduct research but to apply the findings, to publicize the accomplishments, and to seek new support for critically needed studies. This is not an easy assignment in these times of eroding budgets for earth science. We must put forward a sequence of initiatives, and have up-to-date versions always available, should opportunity knock.

Although we may not always gain the level of support for our research that we might wish, whatever we do must be done with intellectual integrity, with willingness to discard or modify ideas that prove incomplete or inadequate, and to move on to test the myriad other concepts that await attention. We must emulate G.K. Gilbert's style as expressed by Davis (1926): "He *** presented a conclusion *** as a ball might be placed on the outstretched hand--not gripped as if to prevent its fall, not grasped as if to hurl it at an objector, but poised on the open palm, free to roll off if any breath of disturbing evidence should displace it; yet there it would rest in satisfied stability."

REFERENCES CITED

Allen, C.R., 1968, The tectonic environments of seismically active and inactive areas along the San Andreas fault system, in Dickinson, W.R., and Grantz, Arthur, eds., Conference on geologic problems of San Andreas fault system: Stanford, Calif., Stanford University Publications in Geological Sciences, v. 11, p. 70-80.

Andrews, D.J., and Hanks, T.C., 1985, Scarp degraded by linear diffusion--Inverse solution for age: Journal of Geophysical Research, v. 90, no. B12, p. 10, 193-10,208.

Bonilla, M.G., 1973, Trench exposure across surface fault rupture associated with San Fernando earthquake, in San Fernando, California, earthquake of February 9, 1971, Geological and Geophysical Studies: U.S. Department of Commerce, National Oceanic and Atmospheric Administration, v. 3, p. 173-182.

Clark, M.M., Grantz, Arthur, and Rubin, Meyer, 1972, Holocene activity of the Coyote Creek fault as recorded in sediments of Lake Cahuilla, in The Borrego Mountain earthquake of April 9, 1968: U.S. Geological Survey Professional Paper 787, p. 112-130.

Colman, S.M., and Watson, K., 1983, Ages estimated from a diffusion equation model for scarp degradation: Science, v. 221, p. 263-265.

Converse, Davis and Associates, 1968, Geologic report on the probability of faulting at the Paramedical Building site, San Bernardino Valley Joint Union College District: unpublished report, 11 p.

Davis, W.M., 1926, Biographical Memoir--Grove Karl Gilbert, 1843-1918: National Academy of Sciences Biographical Memoir, 5th Memoir, v. 21, 303 p.

Dutton, C.E., 1889, The Charleston, South Carolina earthquake 1886: U.S. Geological Survey, 9th Annual Report 1887-88, p. 203-528.

Engelder, J. T., 1974, Microscopic wear grooves on slickensides--Indicators of Paleoseismology: Journal of Geophysical Research, v. 79, no. 29, p. 4387-4392.

Gianella, V.P., and Callaghan, Eugene, 1934, The Cedar Mountain, Nevada, earthquake of December 20, 1932: Bulletin of the Seismological Society of America, v. 24, no. 4, p. 345-384. Gilbert, G.K., 1884, A theory of the earthquakes of the Great Basin, with a practical application: American Journal of Science, 3rd series, v. 27, p. 49-53.

------1886, The inculcation of scientific method by example: American Journal of Science, 3rd series, v. 31, p. 284-299.

Grantz, Arthur, and Dickinson, W.R., 1968, Indicated cumulative offsets along the San Andreas fault in the California Coast Ranges, in Dickinson, W.R., and Grantz, Arthur, eds., Conference on geologic problems of the San Andreas fault system: Stanford., Calif., Stanford University Publications in the Geological Sciences,

v. 11, p. 117-119.
Hanks, T.C., Bucknam, R.C., Lajoie, K.R., and Wallace, R.E., 1984, Modification of wave-cut and faulting controlled landforms: Journal of Geophysical Research, v. 89, no. B7, p. 5771-5790.
Harden, J.W., 1982, A quantitative index of soil development from field descriptions--Examples from a chronosequence in central California: Geoderma, v. 28, p. 1-28.
Hoare, J.K., An evaluation of lichenometric methods in dating prehistoric earthquakes in the Tobin Range, Nevada: San Francisco, Calif., San Francisco State University M.S. Thesis, 33 p.
Jones, J.C., 1915, The Pleasant Valley, Nevada, earthquake of October 2, 1915: Bulletin of the Seismological Society of America, v. 5, p. 190-205.
Kuchay, V.K., 1971, Ispol' zovanie paleosysmodislokatsiy pri izuchenii seysmicheskogo rezhima (na primere chatkal' skogo) Pleystoseystovoy oblasti zemletryseniya 1946 g [Use of paleoseismic dislocations in the study of seismic regimes with an example from the Pleistocene region (northeast Fergana) affected by the Chatkal earthquake of 1946]: Geological Geofiz (Akad Nauk SSSR, Sib Otd), no. 4, p. 124-129.
LaMarche, V.C., and Wallace, R.E., 1972, Evaluation of effects on trees of past movements on the San Andreas fault, northern California: Geological Society of American Bulletin, v. 83, p. 2665-2676.
Lawson, A.C., 1908, The California earthquake of April 18, 1906--Report of the State Earthquake Investigation Commission: Carnegie Institute Washington Publication no. 87, 2 volumes with atlas.
Malde, H.E., 1971, Geologic investigations of faulting near the National Reactor Testing Station, Idaho: U.S. Geological Survey Open-File Report, 267 p.
Myers, W.B., and Hamilton, Warren, 1964, Deformation accompanying the Hebgen Lake earthquake of August 17, 1959: U.S. Geological Survey Professional Paper 435, p. 55-98.
Nash, D.B., 1980, Morphologic dating of degraded normal fault scarps: Journal of Geology, v. 88, p. 353-360.
National Research Council, 1986, Active Tectonics: Washington, D.C., National Academy Press, 266 p.
Page, Robert, 1970, Dating episodes of faulting from tree rings--Effects of the 1958 rupture of the Fairweather fault on tree growth: Geological Society of American Bulletin, v. 81, p. 3085-3094.
Pardee, J.T., 1950, Late Cenozoic block faulting in western Montana: Geological Society of America Bulletin, v. 61, p. 359-406.
Pierce, K.L., 1986, Dating Methods, in Active Tectonics: Washington, D.C., National Academy Press, p. 195-214.
Plafker, George, and Rubin, Meyer, 1978, Uplift history of earthquake recurrence as deduced from marine terraces on Middleton Island, Alaska, in Isacks, B.L., and Plafker, George, Co-organizers, Proceedings of Conference VI,

Methodology for identifying seismic gaps and soon-to-break gaps: U.S. Geological Survey Open-File Report 78-943, p. 687-722.
Richter, C.F., 1958, Elementary seismology: San Francisco, Calif., W.H. Freeman and Co., 768 p.
Schwartz, D.P., and Coppersmith, K.J., 1984, Fault behavior and characteristic earthquakes--examples from the Wasatch and San Andreas fault zones: Journal of Geophysical Research, v. 89, no. B7, p. 5681-5698.
Sieh, K.E., 1978, Prehistoric large earthquakes produced by slip on the San Andreas fault at Pallet Creek, California: Journal of Geophysical Research, v. 83, no. B8, p. 3907-3939.
Slemmons, D.B., 1957, Geological effects of the Dixie Valley-Fairview Peak, Nevada, earthquakes of December 16, 1954: Bulletin of the Seismological Socity of America, v. 47, no. 4, p. 353-375.
------1967, Pliocene and Quaternary crustal movements of the Basin and Range province, USA: Osaka City University Journal of Geosciences, v. 10, p. 91-103.
Slemmons, D.B., Steinbrugge, K.V., Tocher, Don, Oakeshott, G.B., and Gianella, V.P., 1959, Wonder, Nevada, earthquake of 1903: Bulletin of the Seismological Society of America, v. 49, no. 3, p. 251-265.
Wallace, R.E., 1968, Notes on stream channels offset by the San Andreas fault, southern Coast Ranges, California, in Dickenson, W.R., and Grantz, Arthur, eds., Proceedings of conference on geological problems of San Andreas fault system: Stanford, Calif., Stanford University Publications, v. 11, p. 6-21.
------1977, Profiles and ages of young fault scarps north-central Nevada: Geological Society of America Bulletin, v. 88, p. 1267-1281.
------1980, Degradation of the Hebgen Lake fault scarps of 1959: Geology, v. 8, p. 225-229.
------1981a, Paleoseismology [abs.]: Geological Society of America Abstracts with Programs, v. 13, no. 7, p. 575.
------1981b, Active faults, paleoseismology, and earthquake hazards in the Western United States, in Simpson, D.W., and Richards, P.G., eds., Earthquake prediction--an international review--Washington, D.C.: American Geophysical Union, Maurice Ewing Series 4, p. 209-216.
------1987, Grouping and migration of surface faulting and variations in slip rates on faults in the Great Basin Province: Bulletin of the Seismological Society of America, v. 77, no. 3, p. 868-876.
Witkind, I.J., 1964, Reactivated faults north of Hebgen Lake: U.S. Geological Survey Professional Paper 435, p. 37-50.

QUATERNARY DATING TECHNIQUES

POTENTIAL AND LIMITS FOR DATING PREHISTORIC EARTHQUAKES USING TREE-RING ANALYSIS

by

Gordon C. Jacoby
Tree-Ring Laboratory
Lamont-Doherty Geological Observatory
Palisades, New York 10964

Dendrochronology is the determination of absolute year-dates of the formation of annual growth-rings of trees. Analysis of the dated rings can yield information about environmental changes during the lives of the trees. The science is made possible by the strong tendency of trees in temperate to subpolar regions to grow concentric, identifiable radial-growth increments around the circumference of their trunks each year. It must be emphasized that this strong tendency does not always prevail. There are false rings and rings that are locally missing. Only rigorous dating procedures will determine the absolute year of growth. Mere counting of rings will have a "strong tendency" to lead to errors in dating, analysis, and interpretation. Different disturbances could be erroneously attributed to the same year or different years assigned to what was a single traumatic event.

Initially used in archaeological dating and studies of past climate variations, dendrochronology has increasing numbers of applications in hydrology, forestry, pollution studies, and earth sciences. Tree-ring analysis has yielded new information about volcanic (Yamaguchi, 1983) and seismic (Jacoby and Ulan, 1981) events. Virtually all sampling can be done by coring, which is nondestructive of trees.

Dating of severely traumatized trees such as those disturbed by earthquakes is often difficult. Growth can be very suppressed, causing extremely narrow rings for many years or even no radial growth in the lower trunk in some cases. The portion of the sample prior to the trauma must be dated and the last year of normal growth determined. Counting in from the bark would be totally misleading as an age determination in these cases. Only after the date(s) of a ring or rings is fixed in time should the analysis proceed and comparisons be made between trees.

The strong point of tree-ring analysis is that absolute year-dates and sometimes even seasons of disturbance events can be obtained. Most other dating methods have uncertainties attached. The limitations of tree-ring analysis are the time range and geographic distribution of trees. In the

Western United States the general time range is about 400 to 600 yrs B. P., in unusual cases perhaps 1,000 to 1,200 yrs B. P. There are older trees but their geographic range is severely limited. Geographic range of all tree growth is restricted by moisture and temperature.

Tree rings can record evidence of seismic events two ways:

1. There can be direct damage to the branch, trunk or root systems.
2. Coseismic environmental change can cause tree growth changes.

In the direct evidence category, there is also a probabilistic limitation. Higher magnitude events (MM VI - VIII) may kill or destroy trees. By definition of magnitude VIII and above, trees are destroyed. The sample pool is limited to the traumatized survivors. In years or centuries following an event, there is additional attrition of the sample pool due to other natural causes of tree death, decay or removal by human activities. The sample pool diminishes through time for both categories.

A simultaneous potential and problem in tree-ring analysis is the response of tree growth to a variety of factors. Therefore an essential element in this application of the science is a "control" set of tree-ring data that determines growth patterns of undisturbed trees of the same or very similar species in a similar growth environment. Since climatic variation is a ubiquitous cause of tree-ring variations, the control data set must be from the same climatic region. Knowledge of normal, undisturbed growth variations is crucial for correct interpretation of evidence for seismic disturbance or coseismic environmental change (Jacoby and Ulan, 1981). Fire, severe storms, disease, drought, or other phemonena can impact tree growth. Therefore tree-ring sampling must be sufficient to determine a seismic cause for growth change and rule out other alternative causes.

An illustrative example of tree-ring analysis applied to paleoseismology is a study of trees in the vicinity of Wrightwood, Calif., a town transected by the San Anrdreas fault. Both fault-zone trees and trees distant from the fault were sampled. Figure 1 displays a time series based on annual ring widths from a distrubed tree and a composite, "control" time series from trees growing in the same general area. The former is interpreted to be disturbed by two earthquakes and the latter time series is representative of normal tree growth in the area. A very real problem in southern California is the occurrence of suppressed growth due to moisture stress or drought. This stress unfortunately coincides with two major earthquake events. It is therefore essential to define the effects of drought stress and differentiate between it and the effects of earthquake disturbance. The plots of figure 1

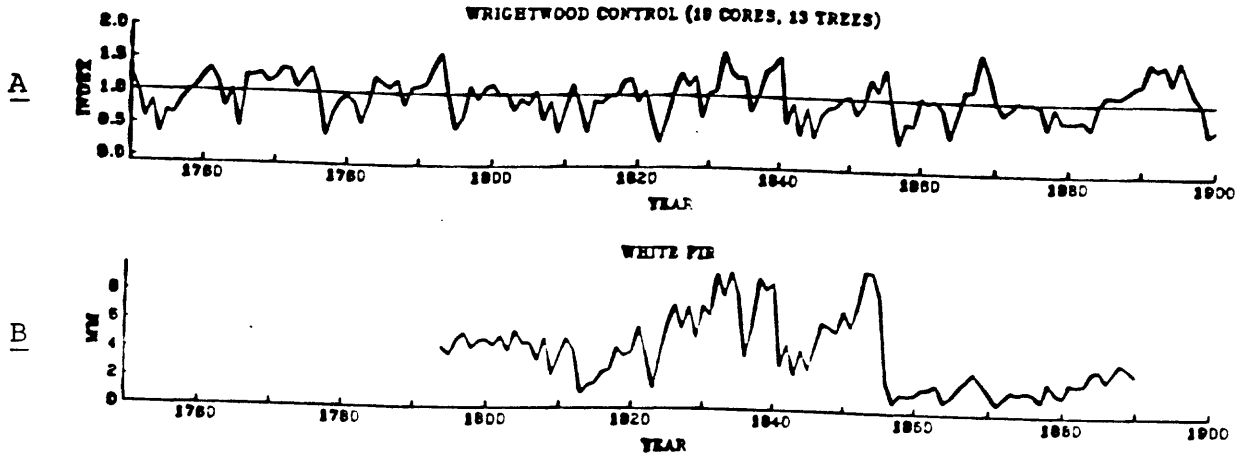

FIGURE 1--A, Ring-width indices for undisturbed trees near Wrightwood, Calif. The main cause of variation is moisture stress due to variations in precipitation. B, Ring widths from a white fir that is moderately sensitive to drought. Many of the narrower rings match, but the extended sequences of narrow rings beginning in 1813 and 1857 indicate more than merely moisture stress. The tree was very young and small during the earthquake in 1812 and not as damaged as in the 1857 earthquake.

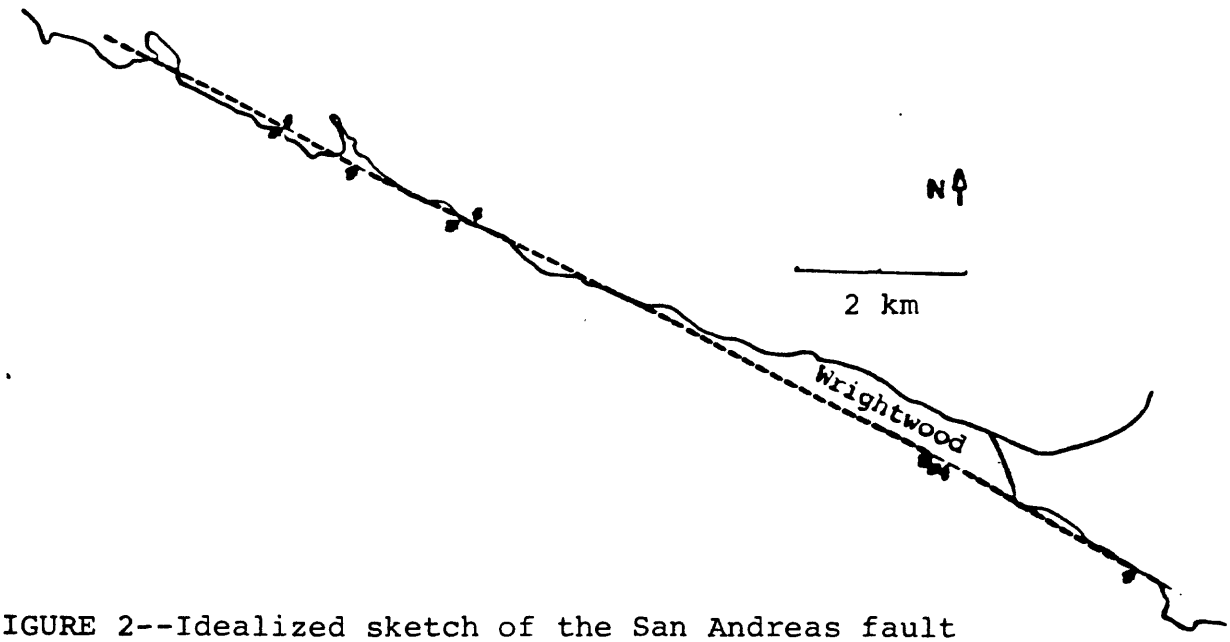

FIGURE 2--Idealized sketch of the San Andreas fault (dashed line) and the Angeles Crest Highway near Wrightwood (solid line). Arrowheads indicate disturbed trees. All trees are within about 10 m of the fault. All the control trees are farther away. None of the trees farther away show the 1813 decrease in ring widths.

show unusual growth changes in a fault-line tree beginning in 1813 and 1857. The 1857 earthquake is an historically known event but the event affecting growth in 1813 was hitherto unknown as a San Andreas earthquake (Jacoby and others, 1987). The different effects can and must be defined on individual-tree and tree-location basis. Figure 2 is a location map for earthquake trees in the Wrightwood, Calif., area. Note that the traumatized trees are restricted to the fault zone. Because of the wide variety of stresses that can affect tree growth, the concept of needing a control set of tree-ring data applies to all regions of possible study. The trees in this study thus far exhibit evidence of direct effect.

Direct response can also be produced in trees away from an actual fault. Major earthquakes can cause tsunami, seiches, landslides, liquefaction and other ground disturbance. Examples of secondary but still direct effects are trees scarred by the ice-rafting seich of Kenai Lake, Alaska, in March of 1964 and beach-ridge trees shaken and tilted by the same earthquake at Cape Suckling, Alaska, many kilometers from the activated fault.

Indirectly, tree-ring dating of coseismic environmental change can also be helpful; however, great caution must be exercised in making the inference of seismic cause for both the environmental and the tree-growth changes. Destruction of a competitor tree can produce an environmental change and tree response (Page, 1970). Coseismic geomorphic change can also lead to environmental change and tree response (Jacoby and Ulan, 1981). Dating of the annual rings must still be absolute, but, due to biological lag in tree response, the dating of the environmental change may not be absolute. An increase or decrease in radial growth can lag a growth-site change as the whole crown, trunk and root systems adjust to the change. The interpretation of such tree-ring data is more complex and is greatly aided by supplemental information.

A relatively new technique for tree-ring analysis can enhance the use of trees in paleoseismology. X-ray densitometry as applied to tree-ring studies is the measurement of wood density variations within and between rings (Telewski and Jacoby, 1987). Density variations are more sensitive to environmental change and can therefore yield dating and other information in trees where ring-width data are too uniform to be of much value. For example, in the Pacific Northwest many coastal Douglas firs have very uniform ring widths but have substantial density variations and achieve ages of over 1,000 yrs (Parker and Jozsa, 1974). As interest in earthquake hazards increases in this region, these trees have potential for producing important paleoseismic information.

There is much potential for application of tree-ring analysis to

paleoseismology. Unknown events can be dated and increased information can be gained about speculatively known events. Analysis of subfossil trees buried or killed by coseismic earth disturbances may even produce information about events in more distant past than the lifetime of living trees. However, with the exception of carbon-14 dating of tree fragments, absolute dating is required along with comprehensive sampling in order to isolate seismic effects from other tree-ring variations.

ACKNOWLEDGEMENTS

Data collection and analysis was supported by NSF Grant EAR 85-19039 and USGS Contract 14-08-0001-G1329. Manuscript was reviewed and improved by P. R. Sheppard. Lamont-Doherty Geological Observatory publication number 4190.

REFERENCES CITED

Jacoby, G. C. and Ulan, L.D., 1983, Tree-ring evidence for uplift at Icy Cape, Alaska, related to 1899 earthquakes: Journal of Geophysical Research, v. 88, no. B11, p. 9305-9313.

Jacoby, G. C., Sheppard, P.R., and Sieh, K.E., 1987, Was the 8 December 1812 California earthquake produced by the San Andreas fault?--Evidence from trees near Wrightwood: Seismological Research Letters, Abstracts, 82nd Annual Meeting, Seismological Society of America, v. 58, no. 1, p.14.

Parker, M. L. and Jozsa, L.A., 1974, Width and Density Chronologies of 1289 Annual Rings of a British Columbia Douglas Fir Tree: Unpub. report to Faculty of Forestry, Univ. of British Columbia, Vancouver, B. C., XX p.

Page, R., 1970, Dating episodes of faulting from tree rings--Effects of the 1958 rupture of the Fairweather fault on tree growth, Bulletin Geological Society of America, 81:3085-3094.

Telewski, F. and Jacoby, G.C., 1987, Current status of x-ray densitometry, in Jacoby. G.C. and Hornbeck, J.W., compilers, Proceedings of the International Symposium on Ecological Aspects of Tree-Ring Analysis: Tarrytown, N.Y., 726 p.

Yamaguchi, D. K.,1983, New tree-ring dates for recent eruptions of Mount St. Helens: Quaternary Research, v. 20, p. 246-250.

RADIOCARBON DATING TECHNIQUES: TAMS VERSUS QUANTULUS

by

Paul E. Damon
N.S.F.-Arizona Accelerator Facility for Radioisotope Analysis
and Laboratory of Isotope Geochemistry,
Department of Geosciences, University of Arizona
Tucson, AZ 85721

ABSTRACT

The tandem accelerator mass spectrometer, which counts ^{14}C atoms directly rather than beta particles from radioactive decay, has revolutionized ^{14}C dating. Its inherent superiority results from a high ratio of modern count rate, S_o, to background, B, expressed either as figure of merit, S_o^2/B, or factor of merit, $S_o/B^{1/2}$. In practice, much of this inherent advantage is used in reduction of sample size by three orders of magnitude and counting time by a factor of 30. At present, the oldest age measurable is limited primarily by chemical contamination.

The stability of conventional, state-of-the-art beta-counting techniques permits longer counting times resulting in higher precision and a greater maximum measurable age. The conventional methods are also less expensive. State-of-the-art scintillation counting vs. gas-proportional counting has the inherent advantage of smaller sample volume yielding very low background counting rates.

Reduction of the chemical background would allow fuller advantage to be taken of the inherent potential of the TAMS method in dating old samples. The beta-counting methods would still be competitive for large samples and at lower cost. However, it should be kept in mind that the TAMS method is still on the steep side of the sigma curve of instrument development and technique, whereas the beta counting methods have reached the plateau.

INTRODUCTION

The rate of ^{14}C disintegration from 1 g of modern wood is 13.6 per minute (13.6 dpm/gC). Modern wood is defined as A.D. 1850 wood with $\delta^{13}C = -25‰$, age corrected to A.D. 1950. The reference age of A.D. 1850 is chosen to avoid anthropogenic dilution of ^{14}C by fossil fuel combustion and enrichment by nuclear technology. In traditional dating by ^{14}C, the beta particles emitted during disintegration are counted by the electronic pulses produced in a gas-proportional counter or by scintillations of light converted to electronic pulses in a scintillation counter. Here, at the University of Arizona, we use the state-of-the-art scintillation counter manufactured by LKB-Wallac Corporation in Finland, the Quantulus. With this instrument, at 75 percent efficiency, we obtain about 10 cpm/gC.

Tandem accelerator mass spectrometry (TAMS) permits the separation and direct detection of ^{14}C atoms. This makes available the 5.9×10^{10} atoms of ^{14}C present in a gram of carbon without waiting for the atoms to decay. It is necessary to detect only 10 per minute of this large population of ^{14}C atoms to equal the count rate of the Quantulus. In practice, much higher count

rates are obtainable with much smaller samples than are used in the beta-counting methods. Thus, the TAMS method has revolutionized ^{14}C dating, in particular with respect to sample size.

THE QUANTULUS

Scintillation counting of ^{14}C has been brought to its present state-of-the-art by adding passive and active shielding to lower background radiation plus energy discrimination and pulse-shape filtering (Kojola and others, 1984). The passive shielding includes 630 kg of asymmetric lead shielding plus a layer of cadmium which is very effective in absorbing low energy or thermal neutrons. The lead shielding is thickest above the sample as shown in figure 1 because the most intense cosmic-ray flux enters from above the counter. In addition to the lead-cadmium shielding, the University of Arizona Quantulus is housed in an underground laboratory 10 m below ground level. The active shielding is an asymmetric, liquid scintillation guard containing a mineral-oil based scintillator. The guard has a copper wall to shield against cadmium x-ray fluorescence. Also, the Finnish engineers cleverly included a high level of electronic noise suppression. The counter is also a spectrometer including two, two-stage, multichannel analyzers and software that excludes pulses with energy above the ^{14}C beta cutoff energy.

The Quantulus is very versatile; for example, samples can be programmed to be counted in any order and for any time or number of counts. The electronic circuitry can be readily programmed for ^{14}C to optimize for the specific counting function. Figure 1 shows the electronic arrangement for ^{14}C dating used at the University of Arizona. Coincidence between the two photomultipliers viewing the sample is required and discriminators eliminate low-level noise pulses. If a pulse meets the coincidence criteria and is in anticoincidence with the guard ring, it is passed to the first half of multichannel analyzer 1 (MC1) and the information stored in the computer memory where it can be retrieved by display on the cathode-ray screen or as hard copy. Rejected pulses are passed to the second half of MC1. The guard is monitored in a similar way. Coincident guard pulses are passed to the first half of MC2 and anticoincident pulses to the second half. This is useful for diagnostic purposes in case of unusual events or system failure.

THE TAMS

A block diagram of the Arizona tandem accelerator mass spectrometer is shown in figure 2. The graphitized samples to be dated are contained in a 10-position carousel. The 1-mm-diameter graphite targets are sputtered sequentially by a cesium beam focused on the target surface. The sputtering process produces carbon anions with a single negative charge, C^{-1}. Initial acceleration as an anion is the key to the success of the TAMS method of ^{14}C dating. Fortunately, the abundant isobar of ^{14}C, ^{14}N does not form a measurably metastable anion allowing very effective discrimination of the two isobars. The ion optics, including an Einzel (gridded) lens, focuses the beam which is initially accelerated at 25 KV. The injection (analyzing) magnet splits the beam into components with the same ratio of mass to charge, M/q. A "bouncer" sequentially selects M/q ratios of 12, 13, 14 to pass into the accelerator where the anions are accelerated initially by an additional 2 MV. The anions enter an argon gas stripper where electrons are removed and interfering molecules, such as ^{12}CH, $^{12}CH_2$ and ^{13}C, are disassociated. The resulting

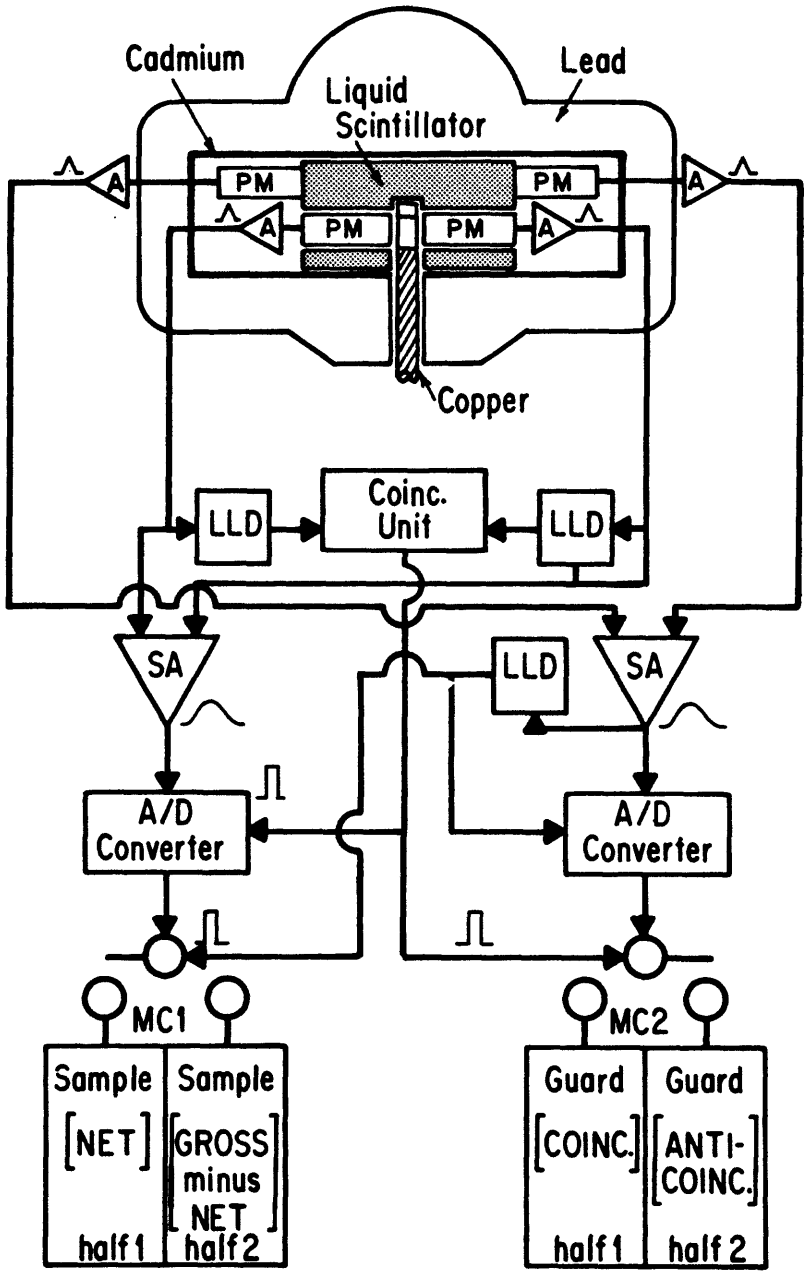

FIGURE 1.--Schematic diagram of the Quantulus ^{14}C dating apparatus at the University of Arizona. PM = photomultiplier, A = amplifier, SA = sum amplifier, LLD = lower level discriminator, A/D = analog to digital. The passive shielding consists of lead and cadmium. Active shielding is by liquid scintillator. the sample vial is between two matched photomultiplier tubes and rests on a copper lift. The multichannel analyzers monitor the net count, gross passively shielded background and the guard ring.

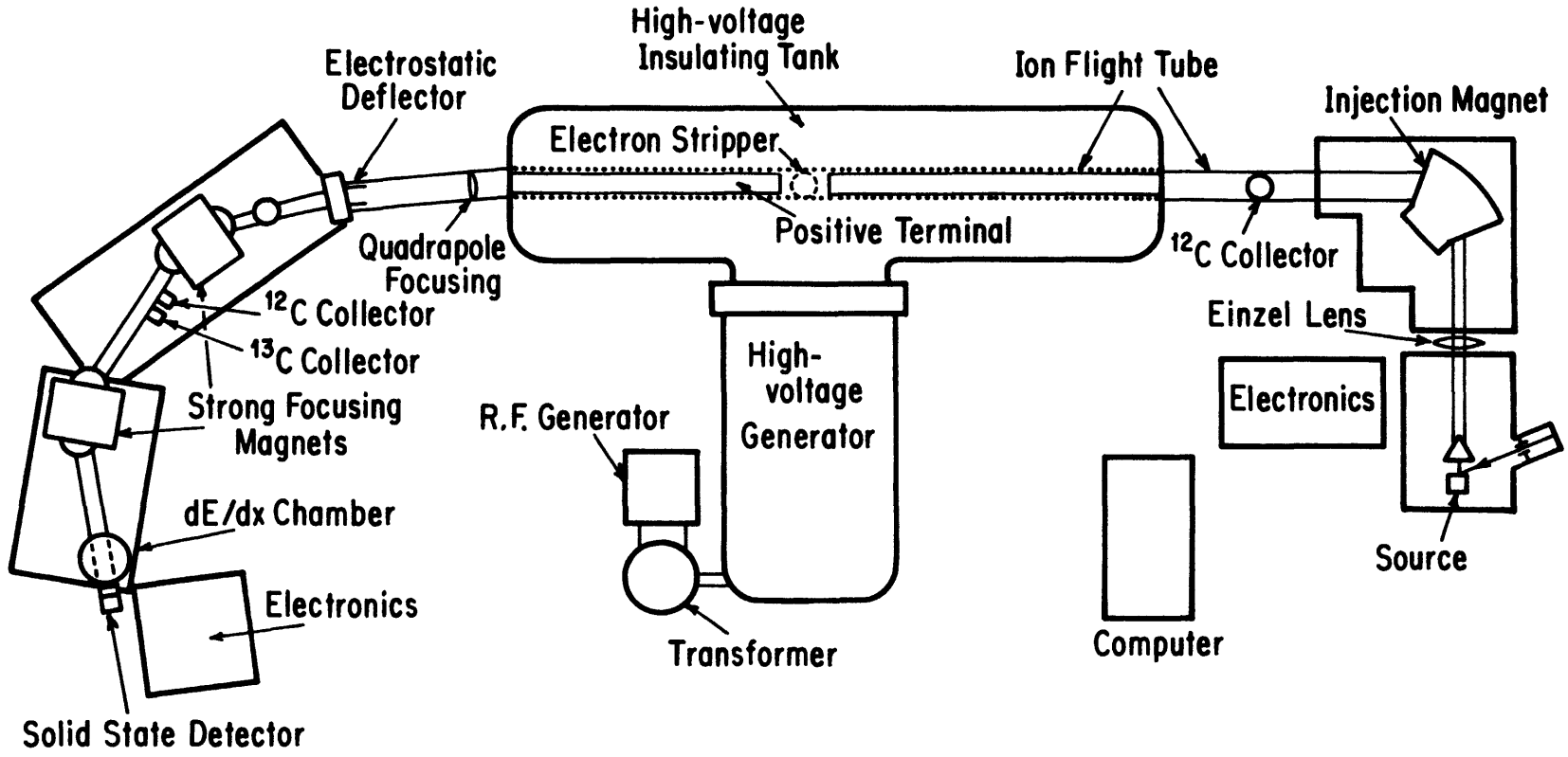

FIGURE 2.--Schematic diagram of the N.S.F.-Arizona tandem accelerator mass spectrometer (TAMS) for radioisotope analysis. The graphitized samples are included in the 10-position source carousel (R.F. = radio frequency).

atoms have various charges with C^{3+} being selected for analysis. The positive ions are now further accelerated by 2 MV to a total energy of 8.025 MeV upon exiting into an electrostatic quadrapole focusing unit, and the voltage on the electrostatic deflector is set to select ions of charge +3 with 8.025 MeV energy (E/q selection). After passing through the first high-energy magnet, $^{12}C^{3+}$ and $^{13}C^{3+}$ are sequentially detected on Faraday cups. The ^{14}C beam passes through another high-energy magnet and enters a dE/dx ionization chamber containing about 7 torr of isobutane. The energy loss in the gas by ^{14}N is greater than the loss by ^{14}C, allowing for good operation without overlap of their residual energies. The residual energy after passing through the ionization chamber is measured by a silicon surface-barrier detector. Residual $^{14}N^{3+}$, $^{13}C^{3+}$ and $^{12}C^{3+}$ ions are well resolved in order of increasing energy: $^{14}N^{3+}$, $^{14}C^{3+}$, $^{13}C^{3+}$ and $^{12}C^{3+}$. For further details on operation of the Arizona TAMS see Linick and others (1986).

Experiments with natural, geologically old graphite demonstrate that most of the ^{14}C background is of chemical origin contained in the graphite target and not introduced by the TAMS itself. Removal of this chemically introduced component would extend the oldest age measurable under routine conditions by an additional 11,000 yrs.

COMPARISON OF TAMS AND QUANTULUS

Table 1 shows a comparison of the Quantulus and TAMS for routine sample sizes and counting times. State-of-the-art proportional counting with the same sample size (2.6 g) and counting time (2,000 min) as the Quantulus is

TABLE 1.--Comparison of TAMS with conventional ^{14}C dating methods

	TAMS	Quantulus	Gas (CO_2)
Sample weight	1 mg	2.6 g	2.6 g
Modern count rate (S_o, cpm)	900	26.5	30.0
Standard counting time (s.c.t.)	60 m	2000 m	2000 m
Background (B, cpm)	3.78	0.176	0.745
Background (% modern)	0.42	0.666	2.48
Background, 1σ (%, s.c.t.).	28.6	5.25	2.58
Figure of merit (S_o^2/B).	2.14×10^5	3.99×10^3	1.21×10^3
Factor of merit ($S_o/B^{1/2}$)	462	63	35
Precision (s.c.t., modern sample) . . .	±52 y	±35 y	±35 y
Oldest age (s.c.t.)	46,000 y	55,000 y	50,700 y
Oldest age (4 x s.c.t.)	46,000 y	61,000 y	56,900 y
Samples per day (no break down)	7	0.7	0.7
Cost per analysis (s.c.t.).	[1]$500	[1]$250	[1]$250

[1]includes $\delta^{13}C$ for fractionation correction.

also shown for comparison. The porportional-counter data were interpolated from figure 9 of Stuiver and others (1979). Larger samples can be used in the two conventional methods to improve performance as measured by the figure of merit, S_o^2/B, and factor of merit, $S_o/B^{1/2}$ (Oeschger and Wahlen, 1975). The figure of merit is a measure of the precision obtainable in a given counting time, whereas the factor of merit is a measure of the oldest age obtainable (2σ criteria). For example, increasing the sample size for proportional counting from 2.6 gC to 6.4 gC increases the factor of merit from 19 to 67 and the oldest measurable age, in 8,000 min, from 56,900 to 61,600 yrs. The precision is improved by a factor of 2, to ±18 yrs.

It can be seen from table 1 that the TAMS has both a higher figure of merit and factor of merit and, so, it is intrinsically the superior method because of the very high count rates obtainable by direct counting of ^{14}C atoms rather than beta particles emitted during ^{14}C decay. The TAMS is suitable for dating milligram size samples which is a great advantage considering that such small samples were previously undatable. The short counting time allows for greater throughput. Unfortunately, the small sample size and reduced counting time also reduces the precision obtainable under routine counting parameters to lower than that of the beta-counting methods. Because of the chemical blank in the graphite, the background is much less precisely known which also puts severe limits on the oldest age obtainable. Also, since the precision is largely determined by the chemical blank and not by the counts accumulated, increasing the counting time does not improve the oldest obtainable age.

The excellent stability of the beta-counting methods permits the accumulation of data for the modern count rate which is a significant factor in the better precision of the conventional methods. The precisions given in table 1 assume that sixteen 2,000-min standard counts have been obtained under stable counting conditions. Precision of 2‰ is obtainable for the conventional methods by increasing the counting time by a factor of 4. By doubling the counting time for the TAMS sample and devoting a carousel to the measurement of one sample (four standards, four sample targets and two backgrounds), 2‰ precision is also obtainable. However, considering that the sample throughput is reduced by almost a factor of fourteen to obtain a factor of two improvement in precision, the cost is prohibitive for all but special cases.

As noted earlier, elimination of the chemical blank would improve the oldest measurable age under standard counting conditions to 57,000 yrs. The nature of the remaining machine blank has yet to be determined. For example, we do not yet know whether it will be subject to Poisson counting statistics. The 57,000-yr estimate assumes that its randomness is similar to the chemical blank. If it is subject to Poisson counting statistics, the TAMS will approach closer to the full potential of its high factor of merit. The only remaining advantages of the conventional methods would be long-term counting stability and lower cost.

Lastly, the smaller size of the sample volume of the Quantulus compared to gas counting yields a lower background under similar passive and active shielding conditions. Thus the Quantulus has an intrinsic advantage over state-of-the-art CO_2 gas counting, particularly for dating old samples.

SUMMARY AND CONCLUSIONS

At the present state of development, the TAMS has the advantage of much smaller sample size, shorter counting time, and greater throughput. The current advantage of the beta-counting methods is higher precision and the ability to measure older sample ages at a lower cost per sample. An intrinsic advantage of the Quantulus over CO_2 or CH_4 gas-proportional counting is lower background under similar shielding conditions permitting the measurement of older ages.

Much of the advantage of the Quantulus over the TAMS for dating older samples would be lost upon removal of the chemical blank from the milligram-size TAMS samples. Reduction of the chemical blank should be an obtainable objective.

At the present time, it is preferable on both a cost and performance basis to date large samples by conventional methods. However, it should be kept in mind that the conventional methods have essentially plateaued out on the sigma curve of development whereas the TAMS is probably still on the steep part of the sigma curve. Nevertheless, considering the high demand for ^{14}C dating, the excellent performance and intrinsically lower cost of operation, it would be a mistake to phase out the conventional methods at the present time. In particular, the Quantulus probably has a useful life of a decade or more before becoming obsolete for ^{14}C dating.

ACKNOWLEDGMENTS

I am grateful to Timothy Jull, Austin Long and Robert Kalin for reviewing this paper. I benefited from helpful discussions with them and with Douglas Donahue, Timothy Linick and Dave Steinke. The word processing was done by Jo Ann Overs and the final illustrations were done by James Abbot. This work was supported by N.S.F. Grants EAR-8512761 to Damon and Donahue and ATM-8607161 to Damon and Linick and the State of Arizona.

REFERENCES

Kojola, H., Polach, H., Nurmi, J., Oikari, T., and Soini, E., 1984, High-resolution low-level liquid scintillation β-spectrometer: Applied Radiation and Isotopes, v. 35, p. 949-952.

Linick, T.W., Jull, A.J.T., Toolin, L.J., and Donahue, D.J., 1986, Operation of the NSF-Arizona Accelerator Facility for Radioisotope Analysis and results from selected collaborative research projects, in Stuiver, M., and Kra, R., eds., International Radiocarbon Conference, 12th, Proceedings: Radiocarbon, v. 28, no. 2A, p. 522-533.

Oeschger, H. and Wahlen, M., 1975, Low-level counting techniques: Annual Review of Nuclear Science, v. 25, p. 423-463.

Stuiver, M., Robinson, S.W., and Yang, I.C., 1979, ^{14}C dating to 60,000 years B.P. with proportional counters, in Berger, R., and Suess, H.E., eds., Radiocarbon dating; International Radiocarbon Conference, 9th, Proceedings: Los Angeles, Calif., University of California Press, p. 202-215.

HIGH-PRECISION THORIUM-230 DATING OF CORALS USING THERMAL IONIZATION MASS SPECTROMETRY: APPLICATIONS TO PALEOSEISMOLOGY

by

R. Lawrence Edwards[1], F. W. Taylor[2], J. H. Chen[1] and G. J. Wasserburg[1]

[1] The Lunatic Asylum of the Charles Arms Laboratory, Division of Geological and Planetary Sciences, California Institute of Technology, Pasadena, California 91125

[2] Institute for Geophysics, University of Texas at Austin, Austin, Texas 78759

ABSTRACT

The recent development of mass spectrometric methods for determining ^{230}Th abundances reduces the analytical error in ^{230}Th ages of corals. Errors of ±3 yrs (2σ) for a 17 yr old coral, ±5 yrs at 180 yrs, ±44 yrs at 8,294 yrs, and ±1.1 ky at 123.1 ky (1 ky = 1,000 yrs) were obtained using these techniques. Within the error of the measurements, ^{230}Th ages agree with ages determined by counting of annual growth bands. These measurements indicate that the maximum amount of ^{230}Th incorporated into a coral skeleton during growth is equivalent to the amount of ^{230}Th generated by radioactive decay in <6 yrs. Using these techniques, we have dated two emerged corals from north Malekula Island and two from northwest Santo Island, Vanuatu. By analogy to partially emerged corals that were killed by coseismic uplift on Santo in 1973 (M_s = 7.5) and on Malekula in 1965 (M_s = 7.5), it appears that each pair of emerged corals was killed by an earlier coseismic uplift event. Pairs of emerged coral heads from each of the localities yield similar ^{230}Th ages. This demonstrates that each pair of corals died at the same time and is consistent with the idea that they were killed by the same event (presumed to be coseismic emergence). The ^{230}Th growth dates of the emerged corals (A.D. 1864±4 (2σ) and A.D. 1865±4 for Santo; A.D. 1729±3 and A.D. 1718±5 for Malekula) in conjunction with the dates of historical earthquakes yield recurrence intervals of 108 yrs for northwest Santo Island and 236 yrs for north Malekula Island. If a slip-predictable model is used, average uplift rates over the past few centuries are similar to uplift rates averaged over the past 6,126 yrs. It may be possible to extend this approach back in time and to other localities because coral features that represent paleoseismic events are preserved in the geologic record and we have the ability to recognize these features in the field. However, the difficulties in recognizing and sampling corals that represent paleoseismic uplifts become increasingly greater with increasing age.

INTRODUCTION

We have recently developed high-precision mass spectrometric techniques to measure ^{230}Th and ^{234}U abundances in small amounts of coral (Edwards and others, 1987a, b). Use of these techniques reduces the analytical error in a ^{230}Th age, decreases the sample size required for an analysis, and increases the time range over which useful ages can be determined. The purpose of this note is to review the systematics and assumptions used in ^{230}Th dating, to

summarize the recent technical improvements in ^{230}Th measurements, and to examine situations where use of these techniques will have immediate impact in paleoseismologic studies.

SYSTEMATICS

^{230}Th dating of corals is based on the decay of ^{238}U through a series of intermediate daughters:

$$^{238}U \xrightarrow[6.446\times10^{9}\ yr]{} {}^{234}U \xrightarrow[352.7\times10^{3}\ yr]{} {}^{230}Th \xrightarrow[108.8\times10^{3}\ yr]{} {}^{206}Pb,$$

where the numbers below the arrows are mean lives and only the pertinent intermediate daughters are shown. The differential equations for radioactive production and decay can be solved for time as a function of the measured $^{234}U/^{238}U$ and $^{230}Th/^{238}U$ ratios if: (1) the initial $^{230}Th/^{238}U$ ratio, when the coral grew, is assumed to be zero, and (2) corals are assumed to be closed systems with respect to U and Th. The solutions are:

$$[^{230}Th/^{238}U]_{act} - 1 = [(\delta^{234}U(0)/1000)(\lambda_{230}/(\lambda_{230}-\lambda_{234})][1-e^{(\lambda_{234}-\lambda_{230})T}) - e^{-\lambda_{230}T} \quad (1)$$

and

$$\delta^{234}U(T) = \delta^{234}U(0)e^{\lambda_{234}T}. \quad (2)$$

Equation 1 (modified from Kaufman and Broecker, 1965) is used to calculate the ^{230}Th age. T is the age; the λ's are decay constants; $[^{230}Th/^{238}U]_{act}$ is the measured $^{230}Th/^{238}U$ atomic ratio times $\lambda_{230}/\lambda_{238}$; and $\delta^{234}U$ is the fractional enrichment of the $^{234}U/^{238}U$ ratio (at any given time) relative to the $^{234}U/^{238}U$ ratio at secular equilibrium in parts per thousand:

$$\delta^{234}U = [(^{234}U/^{238}U)(\lambda_{234}/\lambda_{238})-1](1000). \quad (3)$$

The value of $\delta^{234}U$ changes with time. The relationship between the present value $[\delta^{234}U(0)]$ and the initial value when the coral grew $[\delta^{234}U(T)]$ is given by equation 2. Equation 2 provides an independent test of the closed system assumption used in solving the radioactive decay equations. The initial uranium isotopic composition can be calculated using the age, T (from eq. 1) and the measured uranium isotopic composition. If the isotopic composition of uranium in seawater does not change with time, then differences between the calculated $\delta^{234}U(T)$ of the fossil coral and the present $\delta^{234}U$ value of seawater (Chen and others, 1986) would indicate open system behavior.

MEASUREMENT OF ^{230}Th AND ^{234}U BY THERMAL IONIZATION MASS SPECTROMETRY

^{230}Th ages of corals were first measured by Barnes and others (1956) using α-spectrometry to determine the $^{230}Th/^{238}U$ ratios. Thurber and others (1965) and Broecker and Thurber (1965) measured $^{234}U/^{238}U$ ratios as well as $^{230}Th/^{238}U$ ratios (again by α-spectrometry) and calculated ^{230}Th ages taking into account the fact that the $^{234}U/^{238}U$ ratio in seawater differs from the value at secular equilibrium (Thurber, 1962). Improvements in detector systems increased the resolution of α-spectra (see Rosholt, 1984) and obviated some of the problems associated with α-counting measurements, but major

improvements in the precision of ^{230}Th, ^{234}U and ^{238}U measurements (by α-spectrometry) have not been made since the pioneering work of Broecker and coworkers. This is because the precision of a measurement is limited by the number of atoms (or α-particles) that can be detected during a measurement. By α-spectrometry, only decaying particles can be detected. ^{230}Th has a mean life of ~ 10^5 yrs, so for a laboratory counting time of one week, only one out of 10^7 ^{230}Th atoms in a sample can be detected. In mass spectrometric measurements, ions are detected, and the precision of a measurement is limited by the fraction of ^{230}Th atoms that one can ionize. We have obtained ionization efficiencies of one out of 10^3 (Edwards and others, 1987a) for Th. For the same size sample, 10^4 times more atoms of ^{230}Th can be detected by mass spectrometric determination than by α-counting methods. Based solely on counting statistics, a ^{230}Th measurement by mass spectrometry should be about 10^2 times more precise than a ^{230}Th measurement (on the same size sample) by α-counting. Both methods of measurement have other sources of error (Harmon and others, 1979; Rosholt, 1984; Edwards and others, 1987a). Table 1 compares the methods and shows that, for a 120,000 yr old (120 ky) sample, the error in age is about an order of magnitude smaller and the sample size around fifty times smaller for mass spectrometric measurements.

TABLE 1.-- Comparison between mass spectrometric and α-counting methods for measuring ^{230}Th and ^{234}U in a ~ 120 ky old coral

Method	Coral sample size	Number of ions or alpha particles measured/run		2σ uncertainty[1]		
		^{230}Th	^{234}U	$^{230}Th/^{238}U$	$^{234}U/^{238}U$	Age(ky)
Mass spectrometry	200 mg	5×10^6	2×10^6	±2°/oo	±5°/oo	±1
α-counting	10 g	3×10^3	5×10^3	±40°/oo	±30°/oo	±10

[1] The α-counting uncertainties are taken from Harmon and others (1979) and are based on counting statistics. °/oo indicates parts per thousand.

Table 2 shows samples that were dated by ^{14}C, counting of coral growth bands, ^{230}Th (α-counting) and ^{230}Th (mass spectrometric). The errors in the mass spectrometric ages, based on analytical errors, range from ±3 yrs (2σ) for a coral that is 17 yrs old to ±1.1 ky for samples that are around 120 ky old. Assuming typical analytical errors, we calculate that, for a 500 ky old sample, the error in age due to analytical uncertainty would be ±50 ky (2σ). Samples CWS-A, CWS-A-1d and TAN-E-1g were collected when the surface of the coral head was still alive, and their ages were determined from the counting of annual growth bands. For all three samples, the ^{230}Th ages and growth band ages agree within the error of the measurements (fig. 1). The ^{230}Th ages were calculated assuming that the initial amount of ^{230}Th incorporated into the coral skeleton was zero. The agreement between the ^{230}Th ages and the growth band ages indicates that this assumption is valid, within errors. For CWS-A,

the ^{230}Th age is three yrs older than the mean growth band age and the 2σ error is ±3 yrs, so the maximum amount of initial ^{230}Th incorporated into the skeleton is equivalent to the amount of ^{230}Th produced by radioactive decay in 6 yrs.

TABLE 2.— Coral ages determined by different methods or techniques[1]

Sample[2]	^{14}C[3] (conventional) (yrs)	^{14}C[4] (corrected) (yrs)	Growth Bands (yrs)	^{238}U-^{234}U-^{230}Th[5] (α-counting) (ky)	^{238}U-^{234}U-^{230}Th[6] (mass spectrometric)
CWS-A	---	---	13-15	---	17±3 yrs
CWS-A-1d	---	---	49-51	---	54±5 yrs
TAN-E-1g	270±120	30-70, 180-270, or 300-500	176-182	---	180±5 yrs
CWS-F-1	980±120	780-1010	---	---	845±8 yrs
CH-8	8990±120	~10,000	---	---	8294±44 yrs
AFS-12 A	---	---	---	129±9	122.1±1.1 ky
B					122.7±1.3 ky
C					124.5±1.3 ky
E-T-2 A	---	---	---	141±16	129.9±1.1 ky
B					129.2±1.1 ky

[1] Ages refer to the ages in 1986. Reported errors are 2σ. For ^{14}C and α-counting, the errors are based on counting statistics. Errors in mass spectrometric ages are based on the standard deviation of the mean of 60-300 isotope ratios measured in the course of a mass spectrometric run.

[2] For AFS-12, A and B are different fractions of the same powder; C is a different fragment of coral. For E-T-2, A and B are different fragments of coral.

[3] ^{14}C ages are as reported by Taylor and others (1985) in radiocarbon years; the mean life of 8033 yrs was used; no corrections have been made for natural fractionation of carbon isotopes, the difference between $^{14}C/C$ in surface water and the atmosphere, or differences in initial $^{14}C/C$.

[4] ^{14}C ages have been corrected by us to dendroyears using the curves of Stuiver (1982) for TAN-E-1g and CWS-F-1 and for CH-8, assuming a $^{14}C/C$ initial ratio from Klein and others (1982) for tree rings ~ 8,000 yrs old. No corrections have been made for natural fractionation of carbon isotopes or the difference between $^{14}C/C$ in the surface water and the atmosphere.

[5] Ages from T.-L. Ku (written commun., 1986) except for E-T-2 which is from Bloom and others (1978).

[6] From Edwards and others (1987b) and R. L. Edwards (unpub. data).

For TAN-E-1g and CWS-F-1, the ^{230}Th age and ^{14}C age agree within the analytical errors (table 2). For TAN, however, the ^{14}C age has three ranges that span several centuries. This is because of changes in the initial $^{14}C/C$ ratio in the atmosphere with time. For CH-8, the ^{14}C and ^{230}Th ages do not agree. The reasons for this are unclear and the discrepancy emphasizes the importance of more detailed studies comparing ^{14}C and ^{230}Th ages.

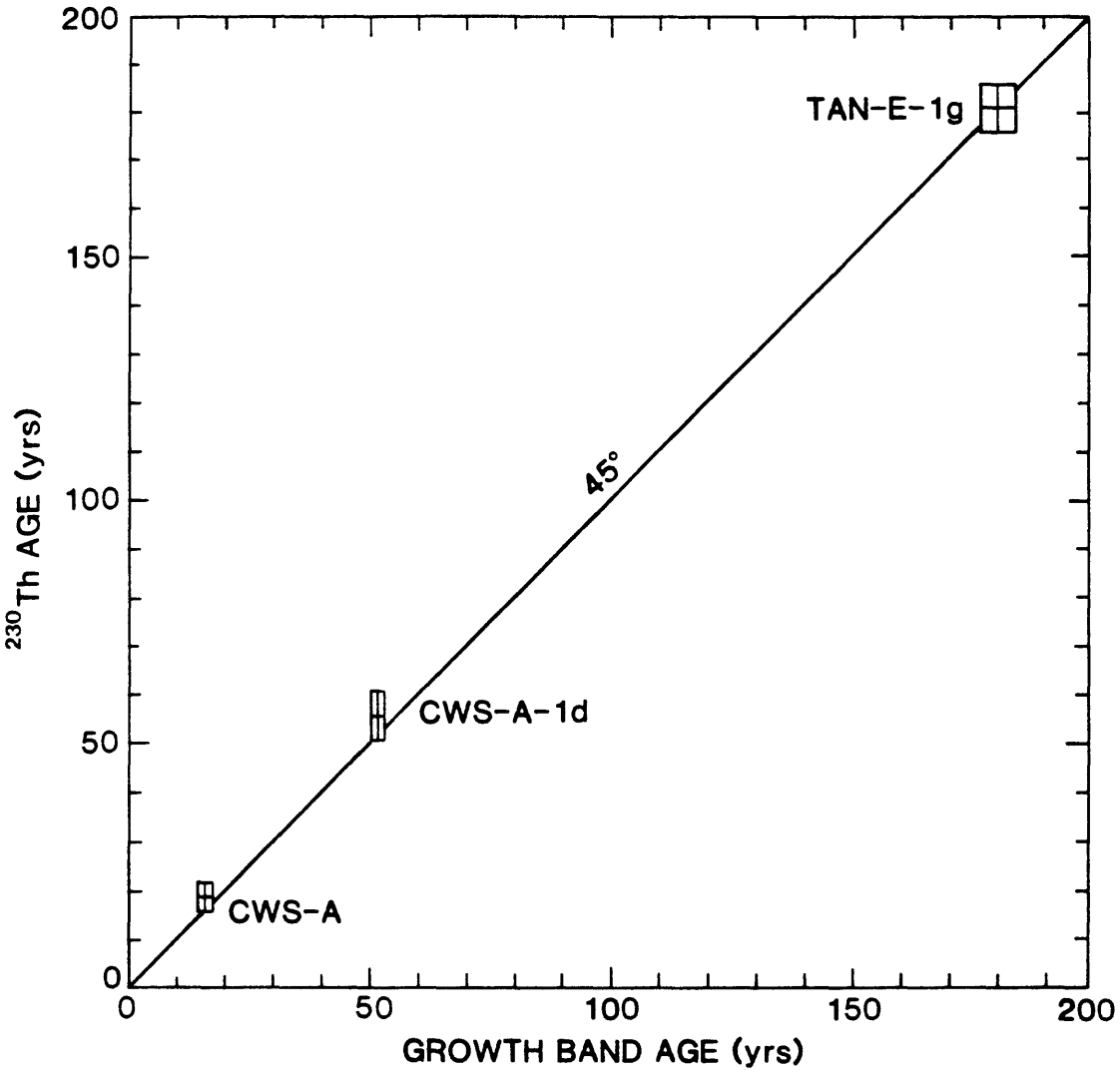

FIGURE 1.--^{230}Th age versus age determined by counting of annual growth bands. The error in the ^{230}Th age is 2σ and is based on analytical errors. The error in the growth band age is the range of ages in the sample which was analyzed. Boxes indicate the error limits of the age determinations.

Samples AFS-12 and E-T-2 are beyond the range of ^{14}C dating. The mass spectrometric ages agree with the α-counting ages but the errors for the mass spectrometric determinations are about an order of magnitude smaller. Replicate analyses of different fragments of AFS-12 and E-T-2 agree within analytical error. This indicates not only analytical reproducibility but also shows that different fragments of the same hand specimen could not have been altered to different degrees.

In summary, errors in ^{230}Th ages of corals due to analytical uncertainty are significantly lower when analysis is done by mass spectrometry instead of α-spectrometry. The error in mass spectrometric ^{230}Th ages are also lower than the errors in ^{14}C ages (due to analytical uncertainty). Mass spectrometric ^{230}Th ages have 2σ errors of ±3 yrs for a 17 yr old coral, ±5 yrs at 180 yrs, ±44 yrs at 8,294 yrs, ±1.1 ky at 123.1 ky, and an estimated error of ±50 ky at 500 ky. The sample size for the corals younger than 10 ky is ~ 3 g and for the 123.1 ky old sample, ~ 250 mg. For corals that grew during the past two centuries, ^{230}Th ages agree with ages determined from counting of growth bands. These measurements place an upper limit on the amount of initial ^{230}Th incorporated during coral growth (equivalent to the amount generated by radioactive decay in <6 yrs). This shows that the assumption that initial ^{230}Th is zero is valid. Future studies will address the validity of the assumption that corals can be chosen which have been closed with respect to U and Th exchange. The strongest evidence that diagenetic alteration is not a problem is the agreement between analyses of different fragments of the same sample (AFS-12 and E-T-2). This shows that different parts of the same hand specimen could not have been altered to different degrees.

APPLICATIONS IN PALEOSEISMOLOGY

Corals grow close to the sea surface. Therefore, the elevations and ages of fossil corals record changes in sea level with time. Apparent changes in sea level are caused by tectonic uplift (or subsidence), isostatic readjustments, and glacio-eustatic fluctuations in sea level. To the extent that eustatic and isostatic fluctuations in sea level (and apparent sea level) can be subtracted off, corals provide a record of tectonic movement. This approach has been used in a number of localities to determine uplift and subsidence rates averaged over ~ 10^5 yrs (see, for example, Moore and Fornari, 1984; Mesolella and others, 1969; Bloom, 1980).

There are two ways in which mass spectrometric ^{230}Th measurements will extend this approach. The first takes advantage of the ability to measure small samples. Reef-forming corals generally grow in the tropics. However, solitary corals grow in marine environments worldwide. Fossil solitary corals are only found in small masses in marine terraces. Therefore, dating by α-counting methods has only been possible in a few localities. Dating by mass spectrometric methods should extend this approach.

The second way takes advantage of the ability to date young corals (last several thousand years) very precisely. It may be possible to date corals which were killed by coseismic uplift and thereby date earthquakes. The ability to do this depends not only on the ability to date corals precisely, but also on the ability to identify fossil corals that were killed by coseismic uplift. The rest of this note will describe our results on samples from a specific locality where F. W. Taylor (unpub. data) found fossil corals presumed to have been killed by coseismic uplift.

Taylor and others (1987) examined partially emerged coral heads from Vanuatu. The tops of these coral heads were above sea level and were dead. The portions of the heads below sea level were still alive. The time of emergence and death of the upper part of a coral head could be determined by counting annual growth bands starting with the living portion of the coral. Using this approach, Taylor and others (1987) showed that the times of coral emergence correlated with the times of major earthquakes on northwest Santo Island (1973, M_S = 7.5) and north Malekula Island (1965, M_S = 7.5). The amount of emergence was 0.6 m on northwest Santo in 1973 and 0.8 m at the north Malekula locality in 1965.

At both localities, there are also completely emerged coral heads whose heights are 1.8 m above the highest living corals at northwest Santo and 1.3 m above the highest living corals on north Malekula. By analogy to the corals killed by coseismic uplift in 1965 and 1973, we considered the completely emerged corals also to have been killed by coseismic uplifts at earlier times. If this is true, then the ages of emerged coral heads at a given locality should be the same. We have dated the tops of two coral heads from each of the localities by ^{230}Th methods (table 3). At the northwest Santo locality, the growth dates of the two heads agree within analytical error (A.D. 1864±4, 1866±4), and at north Malekula, the dates of the two heads are similar to each other (A.D. 1729±3, 1718±4). The slight difference in growth date for the north Malekula locality is outside of analytical error and may be due to erosion of the outer (younger) part of the MAG coral head.

TABLE 3.-- ^{230}Th ages of emerged corals

Sample	Island	Height[1] (m)	Date of growth (from ^{230}Th)[2] (yrs A.D.)
CWS-C	N.W. Santo	1.8	1866 ± 4
CWS-D-1[3]	N.W. Santo	1.8	1864 ± 4
CWS-D-2[3]	N.W. Santo	1.8	1868 ± 9
MAF	N. Malekula	1.3	1729 ± 3
MAG	N. Malekula	1.3	1718 ± 5

[1] Above the highest living corals at the same locality (F. W. Taylor, unpub. data).

[2] Determined by subtracting the ^{230}Th age from the date of analysis; dates are rounded to January 1 of the indicated year; reported errors are 2σ of the mean (R. L. Edwards, unpub. data).

[3] CWS-D-1 and CWS-D-2 are replicate analyses of the same coral.

The general agreement between growth dates of corals at a given locality is consistent with the idea that the heads were killed by coseismic uplift. The difference in growth dates between the north Malekula and northwest Santo corals indicates that they were killed by different events. The seismic recurrence interval at northwest Santo is (1973-1865) 108 yrs; the amount of uplift at this locality for the 1973 event was 0.6 m and for the 1865 event, 1.2 m. The uplift rate calculated by dividing 0.6 m by 108 yrs (slip-predictable model; see Shimazaki and Nakata, 1980) is 5.6 mm/y. The average uplift rate for the latter part of the Holocene can be estimated by dividing

the height of coral collected near the top of the Holocene terrace by its age. For northwest Santo, the average uplift rate over the past 6,126 yrs is 4.2 mm/y (see Taylor and others, 1987). Similarly, the seismic recurrence interval at north Malekula is (1965-1729) 236 yrs; the amount of uplift at this locality in 1965 was 0.8 m and in 1729, 0.5 m. The average uplift rate between 1729 and 1965 was 3.0 mm/y (slip-predictable), and the average rate over the last 6,126 yrs was 2.7 mm/y (Taylor and others, 1987). The similarity between short-term and long-term uplift rates at each locality suggests that, if a slip-predictable model is appropriate, uplift rates have been relatively constant throughout the Holocene and the total Holocene uplift can be accounted for by events similar to the 1965 and 1973 events.

In summary, the error in ^{230}Th ages (based on analytical errors) for corals ranges from ±3 yrs for a 17 yr old coral to ±1.1 ky for a 123.1 ky old coral. The correlation between growth band age and ^{230}Th age for living corals shows that initial ^{230}Th is less than the amount of ^{230}Th produced by radioactive decay in 6 yrs. Because of the precision with which the ages of corals can be measured, studies of paleoseismicity may be designed to use dating of corals for time control. The major problems are associated with the preservation of corals in the geologic record which represent paleoseismic events, the identification of such features in the field, and the determination of the depth at which the corals grew. In this note, we have described one instance where we believe identification of such a feature was possible.

ACKNOWLEDGMENTS

Discussions with D. A. Papanastassiou on various aspects of this project have been extremely helpful. We thank the Government of Vanuatu for assistance with fieldwork which was funded by NSF Grant EAR 79-19912 to F. W. Taylor. The age determinations were done in the Lunatic Asylum, supported by NASA Grant NAG 9-43. California Institute of Technology, Division of Geological and Planetary Sciences Contribution No. 4514 (593); University of Texas, Institute for Geophysics Technical Report No. 48.

REFERENCES CITED

Barnes, J.W., Lang, E.J., and Potratz, H.A., 1956, Ratio of ionium to uranium in coral limestones: Science, v. 124, p. 175-176.

Bloom, A.L., 1980, Late Quaternary sea level change on South Pacific coasts--A study of tectonic diversity, in Mörner, M.-A. ed., Earth Rheology, Isostasy and Eustasy: New York, N.Y., John Wiley & Sons, p. 505-516.

Bloom, A.L., Jouannic, C., and Taylor, F.W., 1978, Preliminary radiometric ages from the uplifted Quaternary coral reefs of Efate, appendix to Ash, R.P., Carney, J.N., and MacFarlane, A., Geology of Efate and offshore islands: New Hebrides Geological Survey Report, p. 47-49.

Broecker, W.S., and Thurber, D., 1965, Uranium series dating of corals and oolites from Bahaman and Florida Key limestones: Science, v. 149, p. 58-60.

Chen, J.H., Edwards, R.L., and Wasserburg, G.J., 1986, ^{238}U, ^{234}U, and ^{232}Th in seawater: Earth Planetary Science Letters, v. 80, p. 241-251.

Edwards, R.L., Chen, J.H., and Wasserburg, G.J., 1987a, ^{238}U-^{234}U-^{230}Th-^{232}Th systematics and the precise measurement of time over the past 500,000 years: Earth Planetary Science Letters, v. 81, p. 175-192.

Edwards, R.L., Chen, J.H., Ku, T.-L., and Wasserburg, G.J., 1987b, Precise timing of the last interglacial period: Science, v. 236, p. 1547-1553.

Harmon, R.S., Ku, T.-L., Matthews, R.K., and Smart, P.L., 1979, Limits of U-series analyses--Phase I, results of the Uranium-Series Intercomparison Project: Geology, v. 7, p. 405-409.

Kaufman, A., and Broecker, W.S., 1965, Comparison of ^{230}Th and ^{14}C ages for carbonate materials from lakes Lahontan and Bonneville: Journal Geophysical Research, v. 70, p. 4039-4054.

Klein, J., Lerman, J.C., Damon, P.E., and Ralph, E.K., 1982, Calibration of radiocarbon dates--Tables based on the consensus data of the Workshop on Calibrating the Radiocarbon Time Scale: Radiocarbon, v. 24, p. 103-122.

Mesolella, K.J., Matthews, R.K., Broecker, W.S., and Thurber, D.L., 1969, The astronomical theory of climate change--Barbados data, Journal Geology, v. 77, p. 250-274.

Moore, J.G., and Fornari, D.J., 1984, Drowned reefs as indicators of the rate of subsidence of the island of Hawaii: Journal Geology, v. 92, p. 752-759.

Rosholt, J.N., 1984, Isotope dilution analyses of U and Th in geologic samples using ^{236}U and ^{229}Th: Nuclear Instruments Methods, v. 223, p. 572-576.

Shimazaki, K., and Nakata, T., 1980, Time-predictable recurrence model for large earthquakes: Geophysical Research Letters, v. 7, p. 279-282.

Stuiver, M., 1982, A high precision calibration of the A.D. radiocarbon time scale: Radiocarbon, v. 24, p. 1-26.

Taylor, F.W., Jouannic, C., and Bloom, A.L., 1985, Quaternary uplift of the Torres Islands, northern New Hebrides frontal arc--Comparison with Santo and Malekula Islands, central New Hebrides frontal arc: Journal Geology, v. 93, p. 419-438.

Taylor, F.W., Frohlich, C., Lecolle, J., and Strecker, M., 1987, Analysis of partially emerged corals and reef terraces in the Central Vanuatu Arc--Comparison of contemporary coseismic and non-seismic with Quaternary vertical movements: Journal Geophysical Research, v. 92, p. 4905-4933.

Thurber, D., 1962, Anomalous $^{234}U/^{238}U$ in nature: Journal Geophysical Research, v. 67, p. 4518-4520.

Thurber, D.L., Broecker, W.S., Blanchard, R.L., and Potratz, H.A., 1965, Uranium-series ages of Pacific atoll coral: Science, v. 149, p. 55-58.

APPLICATION OF MASS SPECTROMETRIC MEASUREMENT OF ^{10}Be, ^{26}Al, ^{3}He TO SURFICIAL GEOLOGY

by

Milan J. Pavich
U.S. Geological Survey
Reston, Virginia 22092

Cosmogenic isotopes and isotopes produced in minerals by cosmic rays can potentially be used to date geomorphic surfaces. Many fault studies depend on detailed stratigraphy of regolith units such as soils, fluvial sediments, organic lacustrine deposits, etc. to determine the age of last movement or the frequency of recurrent movement. One critical part of surficial stratigraphy is age control. Dating by ^{14}C is applicable to dating in cases where organic material is preserved, but in many cases, organic material is absent or is too old to be usefully dated. The development of accelerator mass spectrometer measurement of many low abundance isotopes may provide methods of dating surficial materials that have heretofore not been directly datable.

Accelerator mass spectrometry facilitates the determination of extremely small ratios (for example, $\leq 10^{-13}$) of several geologically useful isotopes produced by cosmic rays in the atmosphere or at the earth's surface. Radioactive isotopes such as ^{10}Be (1.5-Ma half-life), ^{26}Al (0.7-Ma half-life), and ^{36}Cl (0.3-Ma half-life) and stable ^{3}He occur in very low quantities relative to their more abundant, stable isotopes. These isotopes occur in measurable quantities in a variety of surficial materials such as soils, saprolite, quartz grains, and, in the case of ^{10}Be and ^{36}Cl, in solutions. The concentration in atoms/per or the inventory through a vertical column in atoms per square centimeter are useful measurements in common geologic materials that span a wide range of mappable regolith units. Inventories of these isotopes can be used to estimate minimum exposure ages of geologic surfaces.

^{10}Be produced in the atmosphere and delivered by precipitation has been investigated in soils, saprolite, fluvial sediments, estuarine sediments, and loess. Atmospherically produced ^{10}Be is delivered to the earth's surface principally in by precipitation, and, at a pH range of about 5 to 8, is rapidly adsorbed by the soil fine fraction (clays and iron oxyhydroxides). ^{10}Be in soils reaches concentrations in excess of 10^{9} atoms/gm (Pavich and others, 1984, 1985, 1986). ^{10}Be concentrations in near-neutral pH solutions are very low ($< 10^{3}$ atom/gm) (Valette-Silver and others, 1985) requiring time periods $> 10^{5}$ years for movement over tens of meters. The inventory of ^{10}Be (atom/cm^2) in a profile sampled to sufficient depth can be used to estimate the minimum residence time of the regolith. The simplest case of age estimation is that of isovolumetric weathered rock (that is, saprolite) developed from metamorphic or igneous rocks sufficiently old to have no inherited inventory of ^{10}Be (Pavich and others, 1985). Soils and a wide variety of clastic sediments can also be analyzed but one must be aware of the ^{10}Be inherited prior to transport (Pavich and others, 1986). Migration of ^{10}Be on fine, suspended sediment during erosion and fluvial transport occurs without evidence of remobilization to solution at common stream pH's. ^{10}Be

attached to sediment can be used to study the acceleration of fluvial erosion relative to a long-term steady-state rate (Brown and others, 1986, in press), and to demonstrate the acceleration and deceleration of Quaternary-sediment deposition rates in "closed" sedimentary basins (Valette-Silver and others, 1986).

^{10}Be and ^{26}Al produced in situ by cosmic rays striking atomic nuclei within mineral grains exposed at geomorphic surfaces can also be measured as demonstrated by quartz-grain analyses by Nishiizumi and others (1986). The in situ production can occur on any exposed rock surface, but production rates vary with altitude due to the atmospheric attenuation of cosmic rays and with depth below the geomorphic surface due to lithospheric attenuation. Since ^{10}Be- and ^{26}Al production and decay rates are different, the ratio of their abundances should change over time following exposure of a substrate to cosmic rays. Their ratio thus provides a potential clock. Bedrock exposed by erosion and bedrock or boulders exposed by geologically recent faulting are potentially useful settings for analysis of in situ production. Stable ^{3}He is also applicable to those cases.

Stable ^{3}He is also produced by cosmic rays in subaerially exposed minerals (Craig and Porreda, 1986; Kurz, 1987). $^{3}He/^{4}He$ ratios are measured by gas mass spectrometry. ^{3}He production rates are higher than ^{10}Be and ^{26}Al production rates making the method applicable to rocks exposed for shorter times.

The $^{10}Be/^{26}Al$ in situ clock should be useful over the 10^4- to 10^5-yr age-range. Atmospherically produced ^{10}Be in soils should be useful over the 10^4 to $>10^6$ yr age-range. ^{3}He would be useful over the 10^2- to $>10^6$-yr age-range. The combination of various techniques on different parts of the same landscape (that is, bare rock surfaces versus regolith cover) should be extremely useful in estimating residence times of regolith and, conversely, rates of erosion.

The accuracy and applicability of these methods is still being investigated. Analytical uncertainty is less a problem than is uncertainty about ages of test materials and variables such as altitude, rainfall delivery of cosmogenic isotopes, and the effects of variable erosion rates. There are few accurately dated standards for the appropriate age ranges such as the archeological samples used to test ^{14}C dating. Appropriate materials dated by any other methods, such as fluvial terraces or lava flows, are rare. The accuracy of any single technique must be assessed relative to other techniques than can be used over the 10^4 to 10^6 yr time scales.

Analytical precision does not appear to be a problem. With properly sampled and processed materials, precision is better than ± 5 percent. In the case of ^{10}Be in soils, this uncertainty is small relative to the order of magnitude differences in concentrations among soil horizons. Precision is more critical with the in situ techniques (^{10}Be, ^{26}Al, ^{3}He) where production rates are small and contamination or leakage is difficult to eliminate.

The main development that will affect accuracy and usefulness is the measurement of more samples by a variety of techniques in a variety of geologic settings. Present information about these isotopes suggests that

their distributions are determined by relatively simple and understandable physical and geochemical processes. For example, ^{10}Be concentration has been observed to follow log-linear distribution with depth in both saprolite in Virginia to depths of 50 ft and sediments in Texas to depths approaching 200 ft.

The usefulness of these techniques to paleoseismologists depends on a sufficient understanding of the field situation. As with ^{14}C dating of organic material, sampling and sample history can only be critically evaluated in the context of the field problem. Perhaps the most relevant application to paleoseismic studies would be to investigate the inventories of ^{10}Be on fluvial or marine terraces offset by faulting. ^{10}Be inventories can be used, cautiously, to estimate soil "ages" and erosion histories (Pavich and others, 1986). In a small area where the delivery flux of ^{10}Be can be assumed to be constant over the area, terrace-soil inventories could be extremely useful in determining relative ages of terraces across a fault or along a fault-trough bounded river. Rock surfaces exposed by faulting might be dated by measurement of in situ isotope production.

REFERENCES CITED

Brown, Louis, Pavich, M.J., Hickman, R.E., Klein, Jeffrey, and Middleton, Roy, in press, Erosion of the Eastern United States observed with ^{10}Be: Earth Surface Processes.

Brown, Louis, Fouad, Tera, Valette-Silver, J.N., Pavich, M.J., Klein, Jeffrey, and Middleton, Roy, 1986, Application of ^{10}Be to the study of erosion and sediment transport: Fourth Federal Interagency Sedimentation Conference Proceedings, Las Vegas, Nevada, 10 p.

Craig, H. and Porreda, R.J., 1986, Cosmogenic ^{3}He in terrestrial rocks--The summit lavas of Maine: Proceedings of National Academy Science, v. 83, p. 1970-1974.

Kurz, M.D., 1987, In situ production of terrestrial cosmogenic believe and some applications to geochronology: Geochimica et Cosmochimica Acta, v. 50, p. 2855-2862.

Nishiizumi, K., Lal, D., Klein, Jeffrey, Middleton, R., and Arnold, J.R., 1986, Production of ^{10}Be and ^{26}Al by cosmic rays in terrestrial quartz in situ: Nature, v. 319, p. 134-136.

Pavich, M.J., Brown, Louis, Klein, Jeffrey, and Middleton, Roy, 1984, Beryllium-10 accumulation in a soil chronosequence: Earth and Planetary Science Letters, v. 68, p. 198-204.

Pavich, M.J., Brown, Louis, Valette-Silver, J.N., Klien, Jeffrey, and Middleton, Roy, 1985, ^{10}Be analysis of a Quaternary weathering profield in the Virginia Piedmont: Geology, v. 13, no. 1, p. 39-41.

Pavich, M.J., Brown, Louis, Harden, J.W., Klein, Jeffrey, and Middleton, Roy, 1986, ^{10}Be distribution in soils from Merced River terraces, California: Geochimica et Cosmochimica Acta, v. 50, p. 1727-1735.

Valette-Silver, J.N., Fouad, Tera, Pavich, M.J., Brown, Louis, Klein, Jeffrey, and Middleton, Roy, 1985, ^{10}Be content of natural waters [abs.]: EOS, (Transaction, American Geophysical Union), v. 66, no. 18, p. 423.

Valette-Silver, J.N., Brown, Louis, Pavich, M.J., Klein, Jeffrey, and Middleton, Roy, 1986, Detection of erosion agents using ^{10}Be profiles--Examples of the impact of agriculture on soil erosion in the Chesapeake Bay area (USA): Earth and Planetary Science Letters, v. 80, p. 82-90.

THE APPLICATION OF THERMOLUMINESCENCE (TL) DATING TO NORMAL FAULTED TERRAIN

by

Steven L. Forman

Center for Geochronological Research
INSTAAR, C.B. 450, University of Colorado,
Boulder, CO 80309

ABSTRACT

The thermoluminescence technique directly dates mineral grains, reflecting the time since the last light exposure of the sediment. During transportation and deposition of the sediment, sunlight exposure removes previously acquired TL. Buried mineral grains acquire a TL signal by ionizing radiation from the decay of radioisotopes. A TL-age estimate is the proportion of TL signal induced from radioactive decay (paleodose) to the radioactivity of the sediment (dose rate). Application of the technique is not completely routine. For meaningful age estimates, investigations are required to determine the sensitivity of mineral grains to acquire TL, the extent of anomalous fading or sensitivity changes, and the extent of possible diagenetic changes in dose rate.

Initial research on modern and Holocene sediments from the Wasatch fault zone indicates that buried A horizons, fine-grained distal colluvial-sediment, and sag-pond silts are adequately light-bleached to be dated by TL. TL-age estimates for these deposits are consistent with radiocarbon ages. Judicious application of the TL technique will provide needed chronologic control in many tectonic settings.

INTRODUCTION

Since the pioneering experiments of Wintle and Huntley (1980) on the thermoluminescence dating of deep sea sediments, the TL method has been successfully applied to many terrestrial deposits (for example, Wintle and others, 1984; Berger, 1985; Forman et al, in press). Recently the TL technique has been extended to date faulted and fault-derived sediment from the Wasatch fault zone, Utah (McCalpin, 1986; Forman et al, 1987). Initial results indicate that the TL technique has the potential for providing needed chronologic control in deciphering the timing of tectonic events.

Thermoluminescence dating is not dependent on the fortuity of finding datable organic material but directly dates mineral grains, reflecting the time since the last exposure of the sediment to sunlight. For the technique to be useful, the sediment must have been exposed to light for a sufficient time during transportation, or shortly after deposition, to drain

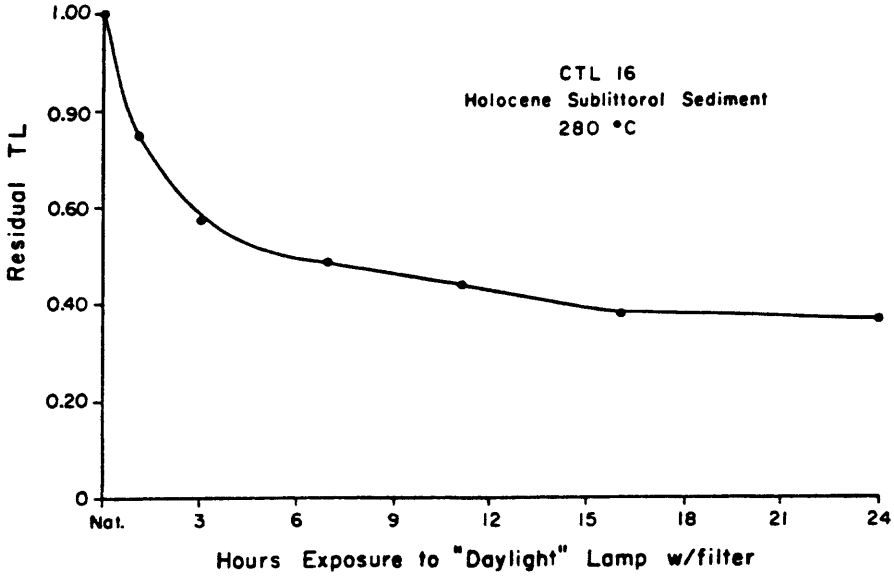

FIGURE 1.--Reduction in thermoluminescence signal of about 10,000 year-old sublittoral sediment after exposure to laboratory light that simulates natural-light conditions (from Forman, in press)

(bleach) previously inherited TL (fig. 1). After deposition and burial, the TL signal accumulates in mineral grains by exposure to the decay products of U, Th, K, and their daughters. This ionizing radiation, mainly alpha, beta, and gamma particles, results in the displacement of electrons from elements into crystallographic defect "traps". Heating or light exposure of the mineral grains results in the migration of some of the electrons to "luminescence centers" from where light is emitted (fig. 2). Thus the number of electrons in traps is a measure of the past ionizing radiation (paleodose) and hence, of the time elasped since the last sunlight exposure. A TL age-estimate is determined by two separate experiments: (1) determination of the paleodose (in Grays, a unit of radiation) which is the quantity of effective radiation that produced the thermoluminescence level of the ancient sediment; and (2) measurement of the dose rate which is the environmental radioactivity of the sediment over a period of time. In the simplest form, a TL age-estimate is calculated as:

$$\text{TL age estimate} = \frac{\text{Paleodose}}{\text{Dose rate}} \qquad (1)$$

DETERMINING THE PALEODOSE

Determining an accurate paleodose for colluvial wedge sediment such as that accumulated after fault displacement, is predicated on the assumption that the TL signal of mineral grains is reduced by natural light during deposition. In order to test this assumption the TL properties of modern and late Holocene materials from the Wasatch fault zone, Utah are presently being studied. Laboratory experiments on buried soils within colluvial-wedge sequences indicate that A-horizon material is well bleached by light (fig. 3). TL age-estimates by the regeneration (Wintle and Prószynska, 1983) and total bleach (Singhvi and others, 1982) techniques have produced consistent results that are in general agreement with associated radiocarbon dates (Forman and Machette, unpubl. data). Fine-grained distal-slope sediment is also adequately light bleached and may produce reliable TL age-estimates. Sag-pond or graben-lake sediments which are derived from adjacent slopes are well light-bleached and thus are a newly targeted sediment-type for dating. Loess, and some lacustrine, near-shore marine and fluvial sediments that have been tectonically displaced may be dated by TL.

Paleodose determinations can be complicated by anomalous fading, which is the short-term instability of the laboratory induced TL signal (Wintle, 1973). However, recently, procedures have been applied to circumvent the effects of anomalous fading in most materials (Lamothe, 1984, Berger, 1984, 1985; Templer, 1985; Forman et al in press). Presently, some questions remain regarding whether laboratory-light exposure and artificial irradiations are effective simulations of natural conditions (Rendell and others, 1983; Wintle, 1985). Laboratory procedures may inadvertently change the natural sensitivity of mineral grain's acquisition of TL. Laboratory-induced sensitivity changes may be a significant problem with dating some sediment older then about 50 ka.

New techniques are being developed and applied to date partially light-bleached sediments, such as proximal colluvial-wedge deposits and deltaic sediments. Laboratory light-bleaching procedures have been devised that simulate the attenuation of spectra and light intensity to which water-lain sediments are exposed during deposition (for example, Berger and others, 1984). These procedures define the residual TL level from which the time-dependent geological TL signal accumulated. Future research will concentrate on determining paleodose on separate mineral fractions, or in reference to the feldspar component (for example, Mejdahl, 1985). Feldspar minerals are more easily light bleached and may yield a more accurate paleodose. Most recently, the advent of a tuneable laser has made it possible to extract the most light-sensitive luminescence signal from mineral grains (Huntley and others, 1985). This technique shows promise in dating well light-bleached sediments as well as those that are rapidly deposited and poorly light-bleached.

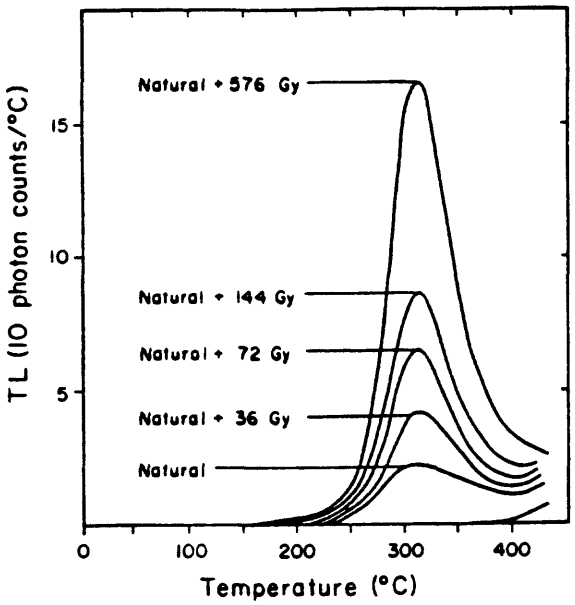

FIGURE 2.--Progressive heating of sediment from 30 °C to 450 °C results in luminescence. The natural curve is the TL emitted by a 10,000 yr-old sediment. Beta dose in grays (Gy) added to the natural TL (that is, natural + 36 Gy) simulates the function in which TL accumulates over geological time.

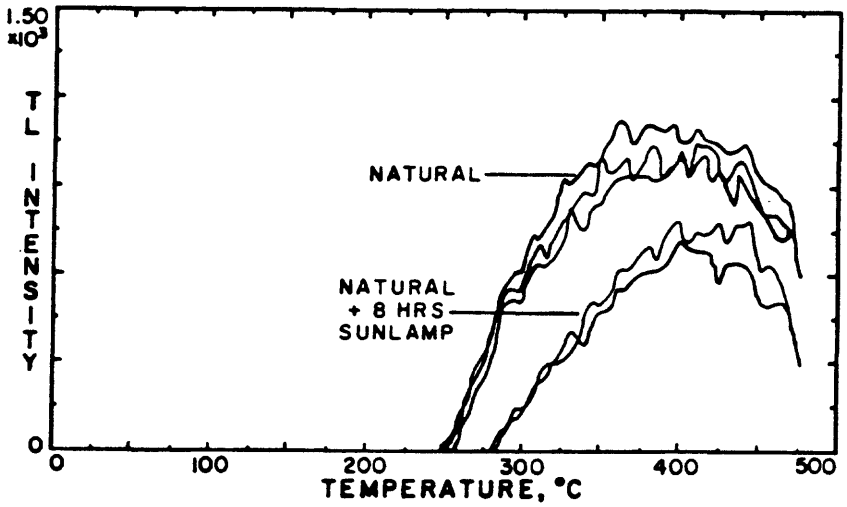

FIGURE 3.--Natural thermoluminescence-glow curves for an about 1,000 yr- old buried A horizon. The natural + 8 hrs sunlamp curves represent the original light-bleached level for this buried A horizon. The difference between these two curve sets is the TL that accumulated over the past 1 ka. Multiple curves in each set represent duplicate analyses.

DOSE-RATE CALCULATION

The dose rate, which is the other half of the TL age equation is calculated from the types and amounts of radioactive elements in the sample and their rates of production of gamma, beta, and alpha particles. The gamma component can be measured directly by field dosimeters in the sediment, by using a gamma spectrometer, or by elemental analysis of the sediment. The alpha and beta contributions usually are determined by measuring the alpha activity of the U and Th decay chains and the K content of the sample. Alpha particles are only 5-20 percent as effective as beta and gamma particles in producing TL because of localized saturation in the alpha track (Zimmerman, 1972). The calculated dose rate is corrected for absorption of alpha, beta, and gamma radiation by water in the sediment. This correction factor can be the greatest potential source of error in the dose-rate estimate because of the uncertainty in determining past moisture conditions.

Additional concerns are possible changes in dose rate due to disequilibrium of the uranium decay-chain or addition of detrital thorium. Post-depositional weathering, accumulations of secondary minerals in soils, and ground-water movement can also change the amounts and types of radioactive elements in the sample. Na-I-and Ge-gamma spectrometry, that detects numerous daughters in the uranium and thorium decay series, is a method to ascertain and compensate for postdepositional changes in radioactivity (Bunker and Bush, 1966).

CONCLUSIONS

The greatest variable in TL dating is the natural spatial and temporal variation in mineralogy, light-bleaching conditions and dose rate. Each sample exhibits unique TL and dosimetric characteristics, thus the technique cannot be simply and routinely applied.

The TL technique can date sediment as young as a few 1,000 yrs to probably 100 ka and possibly as old as 500 ka. TL age estimates presently have a precision of 10-15 percent (2 sigma) and hopefully with additional research errors can be contained at <10 percent.

We will continue to study the TL properties of modern sedimentary environments as a key to judicious applications of the technique to ancient sediments. Future research will focus on obtaining a better understanding of the physical mechanisms of light bleaching in the geologic environment by coupling sedimentologic analysis with TL studies. The temporal limitations of the TL technique are not well known. TL studies of independently dated sediments with clear stratigraphic relations may provide important information on the applicability of the TL technique to the dating of late and middle Pleistocene deposits.

Although the TL technique has limitations (as do most

dating techniques), the greatest asset of thermoluminescence is that it directly dates a wide variety and ages of sediment. Thus the method can provide detailed chronologic information about past tectonic events that cannot be dated by other methods.

ACKNOWLEDGMENTS

This TL research is supported by USGS external grant from the National Earthquake Hazards Reduction Program to J.P. McCalpin and S.L. Forman and University of Colorado Enrichment Award to the Center for Geochronological Research. The author gratefully acknowledges the interest and assistance of M.N. Machette, A.R. Nelson and A.J. Crone as well as valuable discussions on dose rate with C. Bush. Laboratory analyses were completed with the assistance of M.E. Jackson and P. Maat. This paper benefited from the reviews of S. Lehman and R. Walter.

REFERENCES CITED

Berger, G.W., 1984, Thermoluminescence dating studies of glacial silts from Ontario: Canadian Journal of Earth Sciences, v. 21, p. 1393-1399.

_____ 1985, Thermoluminescence dating studies of rapidly deposited silts from south-central British Columbia: Canadian Journal of Earth Sciences, v. 22, p. 704-710.

_____ Huntley, D.J. and Stipp, J.J., 1984, Thermoluminescence studies on a 14C-dated marine core: Canadian Journal of Earth Sciences, v. 21, p. 1145-1150.

Bunker, C.M. and Bush, C.A., 1966, Uranium, thorium, and radium analyses by gamma-ray spectrometry (0.184-0.352 million electron volts): U.S. Geolological Survey Professional, Paper 550-B, p. B-176-181.

Forman, S.L., Jackson, M.J. and McCalpin, J., 1987, Thermoluminescence (TL) studies on colluvial and alluvial sediments from Utah and Colorado-- Preliminary results: Geological Society of America Abstracts with Programs, v. 19, no. 5, p. 506.

_____ Wintle, A.G. Thorleifson, H.L. and Wyatt, P.H., in press, Thermoluminescence properties and preliminary dates for marine sediment from the Hudson Bay Lowland, Canada: Canadian Journal of Earth Sciences.

_____ in press, The solar resetting of thermoluminescence of sediments in a glacier-dominated fjord environment in Spitsbergen-- Geochronologic implications: Arctic and Alpine Research.

Huntley, D.J., Godfrey-Smith, D.I., and Thewalt, M.L.W., 1985, Optical dating of sediments: Nature, v. 313, p. 105-107.

Lamothe, M., 1984, Apparent thermoluminescence ages of St. Pierre sediments at Pierreville, Quebec, and the problem of anomalous fading: Canadian Journal of Earth Sciences, v. 21,p. 1406-1409.

McCalpin, J., 1986, Thermoluminescence (TL) dating in seismic hazard evaluations--An example from Bonneville Basin, Utah: Proceedings of the 22nd Symposium on Engineering Geology and Soils Engineering, Boise, Idaho, p. 156-176.

Mejdahl, V., 1985, Thermoluminescence dating of partially bleached sediment: Nuclear Tracks and radiation measurements, v. 10, no. 4-6, p. 711-715.

Rendell, H.M., Gamble, I.J. A., and Townsend, P.D., 1983, Thermoluminescence dating of loess from the Potwar Plateau, northern Pakistan: PACT (Journal of the European study group on physical, chemical and mathematical techniques applied to archaeology), v. 9, p. 555-562.

Singhvi, A.K., Sharma, Y.P. and Agrawal, D.P., 1982, Thermoluminescence dating of dune sands in Rajasthan, India: Nature, v. 295, p. 313-315.

Templer, R.H., 1985, The removal of anomalous fading in zircons: Nuclear Tracks, v. 10, no. 4-6, p. 531-537.

Wintle, A.G., 1973, Anomalous fading of thermoluminescence in mineral samples: Nature, v. 245, p. 143-144.

_____ 1985, Sensitization of TL signal by exposure to light: Ancient TL, v. 3, no. 3, p. 16-21.

_____, and Huntley, D.J., 1980, Thermoluminescence dating of ocean sediments: Canadian Journal of Earth Sciences, v. 17, p. 348-360.

_____, and Prószynska, H., 1983, TL-dating of loess in Germany and Poland: PACT (Journal of the European study group on physical, chemical and mathematical techniques applied to archaeology), v. 9, p. 547-554.

_____, Shackleton, N.J. and Lautridou, J.P., 1984, Thermoluminescence dating of periods of loess deposition and soil formation in Normandy: Nature, v. 310, p. 491-493.

Zimmmerman, D.W., 1972, Relative thermoluminescence effects of alpha- and beta-radiation: Radiation Effects, v. 14, p. 81-92.

ELECTRON SPIN RESONANCE (ESR) DATING OF FAULT GOUGE

by

Henry P. Schwarcz, W.M. Buhay, and R. Grün*
Department of Geology
McMaster University, Hamilton, ON, L8S 4M1, Canada

*present address: Subdepartment of Quaternary Research, Cambridge University, Free School Lane, Cambridge CB2 3RS, UK

ABSTRACT

Electrons and holes produced by ambient radiation can be trapped in quartz to produce paramagnetic centers. These centers can be released when the quartz is subject to shear strain. By counting the number of centers, N_c, that have subsequently regenerated, the time since shearing can then be measured; this method can thus be used to date the time of last movement in a sample of fault gouge. For a specific center, Nc is proportional to the height of a particular peak in the electron spin resonance (ESR) spectrum of the quartz; N_c is also proportional to the accumulated radiation dose in the sample (AD) which is the product of the dose rate (DR) and the age. DR is found from the concentration of U, Th, and K in the rock. AD is found by the additive dose method using Co-60 γ-rays. The AD of quartz from a single sample of gouge decreases with grain size down to a minimum (plateau) value for particles with a diameter of $<80\mu m$. Of the various ESR signals detectable in quartz, the oxygen-hole center (OH) appears to be the most useful for fault-dating: it is not bleached by light during sample preparation, it is the peak most effectively zeroed by pressure, trapped electrons are stable to fading, and the trap itself is stable to high-temperature annealing.

INTRODUCTION

Quartz and other minerals contain charge defects which are capable of trapping electrons and positively charged "holes". When subjected to shear stress, the electrons and holes can recombine. Associated with each type of trapped electron or hole (paramagnetic center) is a characteristic electron spin resonance (ESR) signal. The shear-induced recombination process results in the zeroing of the ESR signal associated with the particular electron or hole trap. Subsequently, paramagnetic centers produced by ambient radiation in the rock, will repopulate these traps at a steady rate, and the time elapsed since the zeroing event can be determined by measuring the extent to which the traps have been refilled. These processes are shown schematically in figure 1.

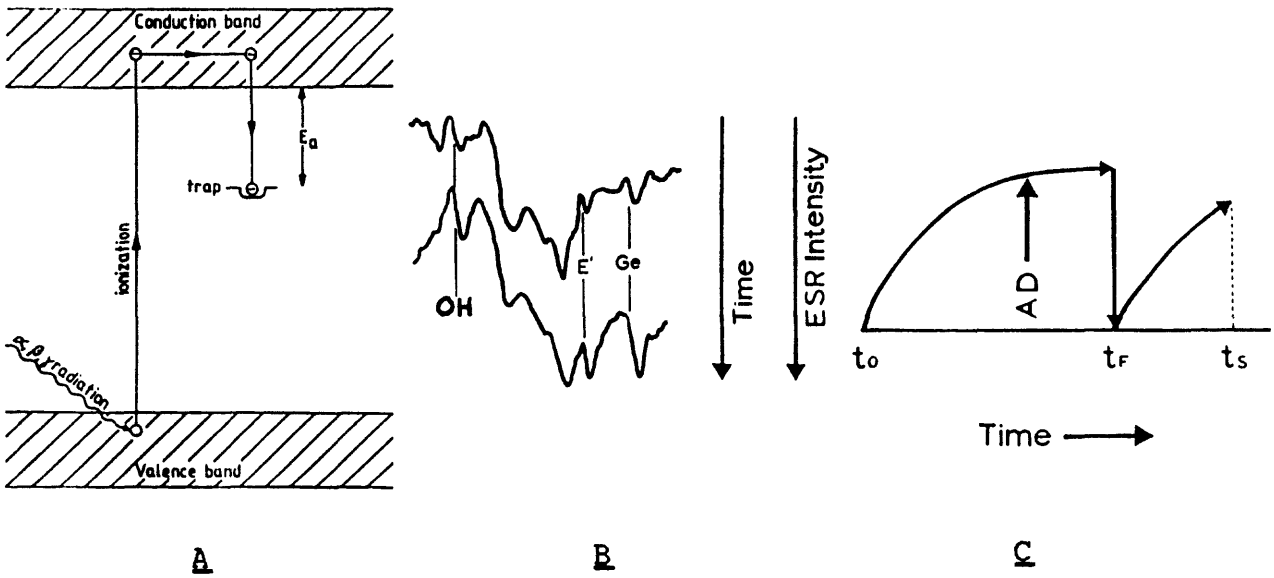

FIGURE 1. A, Schematic energy-level diagram showing electron traps, partly filled by electrons produced by ambient radiation; B, ESR signal produced by trapped electrons showing increase in signal height as a result of increase in number of trapped electrons; C, history of an ESR signal in quartz from rock that has been faulted. Prior to faulting most of the traps are filled (saturated) due to the radiation dose received over geological time. At time t_F the sample is zeroed by shearing along a fault. Subsequently, the trap refills with electrons and the signal increases in proportion to the time since shearing t_S

Ikeya, and others (1982) showed that this phenomenon could be used to date the time of last movement on a fault. Subsequently, he and his colleagues in Japan have used the method to date fault movements in that country. In this paper we discuss some of their results and also report on experiments to test various aspects of the method using materials from active faults in California.

Besides ESR spectroscopy, two other methods can be used to count the number of trapped electrons in minerals: thermoluminscence (Aitken, 1985). and optically-stimulated luminescence (Huntley and others, 1985). Neither of the latter methods has as yet been applied to fault gouge.

EXPERIMENTAL METHODS

ESR Spectra

In this paper we only discuss ESR signals in quartz, although ESR-active electron traps are found in essentially all minerals. Many ESR signals have been observed in quartz (see Marfunin, 1979), but only a few have been tested for their applicability to fault dating. Note that several electron traps (and corresponding ESR signals) can be seen in a single mineral such as quartz, and each can be used independently to obtain an apparent age of last resetting (zeroing). To be useful for dating, such a signal must have three important properties: (1) it must be stable over a geological time scale; (2) it must be sensitive to radiation (that is, it must increase when the sample is exposed to additional doses of γ radiation) and be sufficiently sensitive to be measurable accurately; and (3) it must be easily reset by shearing.

The signals which are believed to best satisfy these criteria are the charge-defect centers called Ge, Ti, and Al (where a germanium, titanium or aluminum atoms have substituted for a Si); the oxygen hole center (OH); and the E' center (SiO_3^-) (figure 2).

The signals for each center have a characteristic peak shape and g-value. The latter is the parameter which determines at what point in the ESR spectrum (at what magnetic field value) the peak will appear.

The measurement of ESR signals is done in an ESR spectrometer; for details for these procedures, see Hennig and Grün (1983) or Marfunin (1979). The Al and Ti signals can only be detected when the sample is cooled to about 100K. The other signals can be detected at room temperature.

The lifetimes of the trapped centers have been measured by thermal annealing studies (Shimokawa and Imai, 1987; Smolyanskiy and Masaytis, 1979) and appear to be on the order of several million years or more at temperatures of a few tens of degrees .

Measurement of AD, Dose and Age

The age of a sample is given by the relation:

Age = AD (accumulated dose)/ DR (dose rate)

To determine the AD, we give the sample additional doses of artificial γ radiation, and observe the rate of increase of the ESR peak-height above the level of the natural signal. Back-extrapolation to zero added dose gives the dose to which the natural signal would correspond (figure 3).

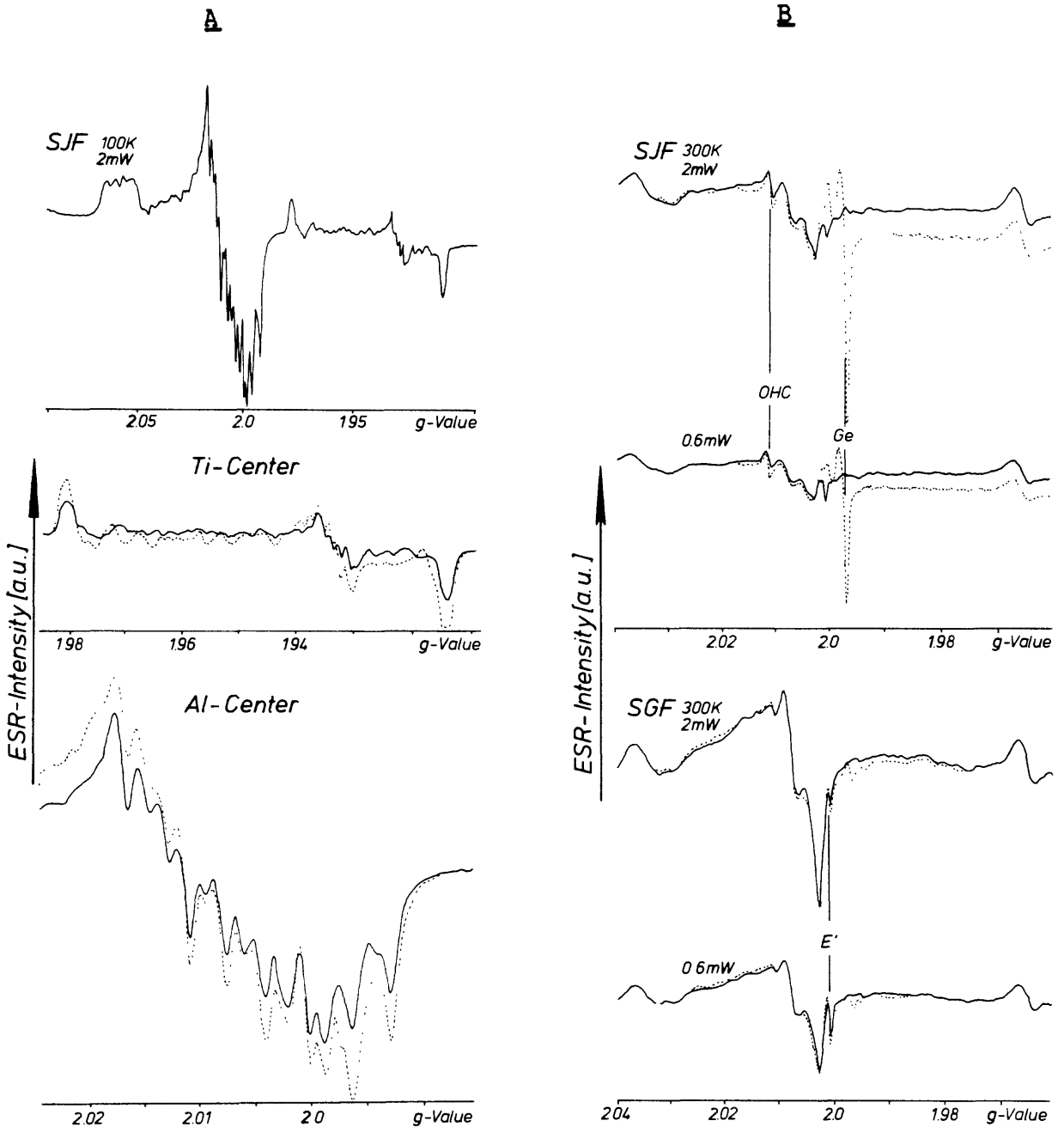

FIGURE 2. Spectra of the principal centers used in ESR dating of quartz. A: spectra at 100K. Top: total spectrum of San Jacinto fault gouge (Anza, CA); middle: detail of Ti center; dashed line shows effect of 100 Gy added dose of ^{60}Co γ-rays; bottom: detail of Al peak, showing hyperfine splitting of peak. B: spectra at 300K; top: OH and Ge centers in San Jacinto fault gouge; bottom: E' center in San Gabriel fault gouge, showing effect of varying microwave power.

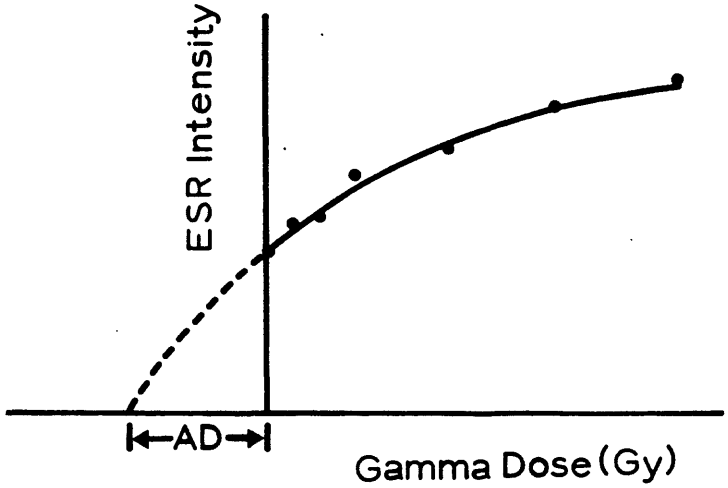

FIGURE 3. Increase in ESR peak height as a function of added dose; Intercept gives AD.

The dose rate is generally calculated from the concentration of uranium, thorium and potassium in the rock surrounding the sample. The γ-ray dose is assumed to penetrate at least 30 cm through the rock; β-particles can penetrate about 2 mm from the immediately surrounding matrix of the quartz grain, while α particles only penetrate a few microns. The quartz is presumed to contribute no internal dose due to its low content of U, Th, and K. Corrections may be made for radon leakage and water content. The concentrations of U, Th, and K are converted to dose rates using published tables (Nambi and Aitken, 1986).

It is important actually to measure the age (or at least, AD) of each sample being studied. In some of the studies reported by other authors, only data on ESR intensity were cited. These will vary greatly from sample to sample, or even as a function of grain size for a single sample (due to differences in packing density in the microwave cavity of the ESR spectrometer). It is only the age, as given by the ratio of AD to dose rate, that gives a meaningful estimate of the time since zeroing of the signal.

Zeroing of ESR Signals in Quartz

Miki and Ikeya (1982) showed that the ESR signal in quartz could be zeroed by crushing or grinding. Ariyama (1986) showed that pressures of at least 20 bars and displacements of 50 cm or more are needed for zeroing of the E' and Ge centers.

We have used a simple compressional apparatus to test the relative sensitivity of the various ESR signals to zeroing under hydrostatic stress. Quartz was separated from samples of gouge from the San Jacinto fault zone, collected by T. Rockwell near Anza, Calif. A sized fraction of quartz particles, between 88 and 210 μm in diameter, was annealed at 550 $^{\circ}$C, after which it displayed no ESR signals. It was then artificially irradiated

with 500 Gy of γ rays from a ^{60}Co source, and then subjected to hydrostatic pressure. The resultant quartz particles were separated by sieving and the ESR signal was studied as a function of compressive stress and grain size (figure 4).

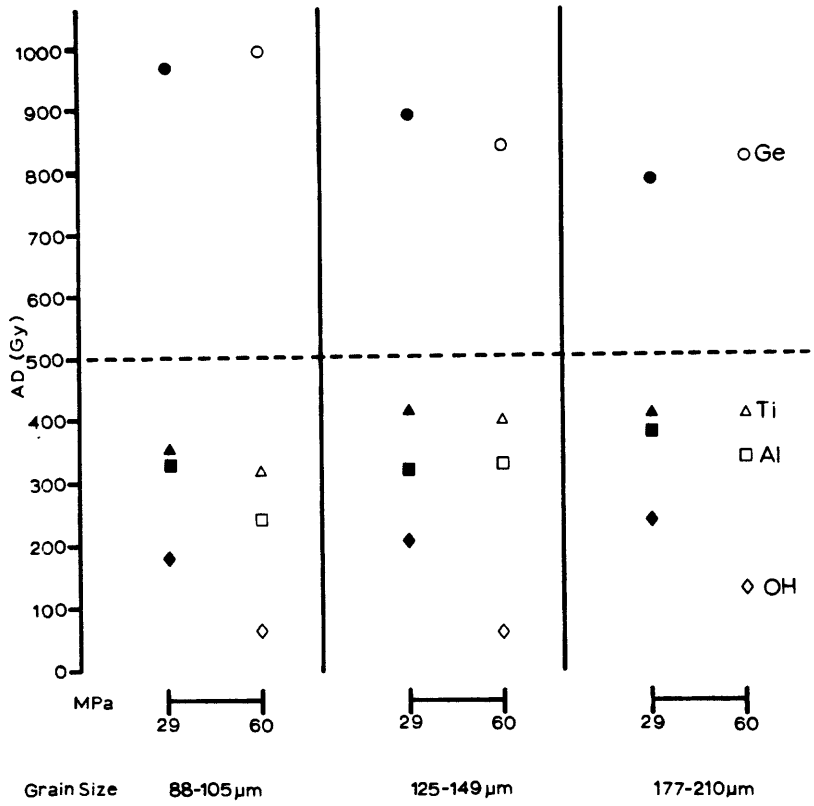

FIGURE 4. Effect of static compressive stress on acquired doses (AD's) of quartz.

It was found that the Ti, Al, and OH signals all decreased markedly as a result of compression, while the Ge signal actually increased (figure 3), contrary to the results of Ariyama (1986), who found that the Ge signal was zeroed by shearing. The largest decrease which we recorded was in the OH signal which would therefore presumably be the most sensitive to resetting in a geological environment. Fukuchi and others (1986) crushed and sieved quartz from a gouge zone and found that, with decreasing size of the particles, the Al and Ge signals decreased in intensity slightly more than the OH signal. They did not, however, measure AD's for the crushed samples.

The Ge signal bleaches very rapidly in sunlight whereas the others (including OH) do not, indicating that quartz samples could be safely processed in the laboratory under normal lighting conditions.

We should note, however, that the actual mechanism of zeroing during shearing is not yet known. Zeroing of ESR signals by heating can be accounted for by a theoretical model in which thermal energy supplies the activation energy needed for electrons to leave the electron traps, and thence to recombine with holes. We presume that, during shearing, a similar delocalization of trapped electrons occurs, possibly as dislocations sweep through the crystal. It can be shown that temperature rise due to frictional heating alone cannot account for the detrapping.

PREVIOUS STUDIES OF FAULT DATING

ESR dating of faults in Japan has been carried out by Fukuchi and others (1986), Ikeya and others (1982), and other authors in the collection edited by Ikeya and Miki (1985). Fukuchi and others (1986) studied samples from several breaks of the Fossa Magna, where independent dating of movement was available from volcanic and fluvial stratigraphy. The ESR ages of quartz from the same fault zone, obtained from the OH, Ge, Al, and E' centers, agreed well at some localities, while at others there was marked disagreement with the ages falling in the sequence OH>Ge>Al>E'. The ages generally fell in the range from 2.0 to 0.25 [my], and were consistent with other dating estimates. The lack of agreement between the dates from the various centers in quartz gives no indication of whether these samples were completely zeroed or not at the time of faulting.

Other studies of fault zones in Japan, mainly using the E' and Ge centers, have also obtained ages ranging from a few hundred thousand to a few million years. Kosaka and Sawada (1986) showed that where several successive stages of movement along the same fault zone could be distinguished structurally, they also show successively younger ESR ages, from 0.58 to 0.22 [my].

EXPERIMENTAL STUDIES

Summarizing these Japanese studies, there is encouraging evidence that resetting of ESR signals has occurred during faulting and that some age estimates are consistent with other geological estimates of the date of faulting. Some of the following questions need to be answered:

1. To what extent is each center reset during shearing?
2. What is the variation in apparent ESR age with particle size? What particles should be measured to obtain the timing of last movement?
3. Does exposure to light or grinding alter the ESR signals?

We have studied some of these parameters in quartz samples from currently active fault zones in California. Samples were kindly provided by the following researchers: D. Schwartz (U.S. Geological Survey), R. Biegel (University of Southern California), and T. Rockwell (California State University at San Diego).

Sample Preparation

All of the samples in this study were extremely friable, and did not need to be crushed. Each sample was treated with fluoboric acid to extract a pure quartz fraction and then passed through a magnetic separator to extract quartz. The quartz was then sieved, and separated into fractions ranging in size from 80 to 450μm. The samples were stored in glass vials at ambient light levels which were later shown to be capable of partially bleaching the Ge signal.

AD Measurement

Aliquots of quartz were weighed into vials and irradiated with γ-rays from a ^{60}Co source. The samples were analysed on a Bruker ER100D spectrometer with a TE4101 cavity. The microwave power was 2 mW, modulation amplitude 1.0 Gpp, sweep width 100G, sweep time 500 s. The Al and Ti spectra could be determined only at 105K. The g-values for the respective peaks are (figure 2):

OH	2.010
E'	1.999
Ge	1.9963
Al	2.017 to 1.985 (hyperfine splitting)
Ti	1.98 to 1.915 (hyperfine splitting)

In almost all cases we observed nonlinear increases in ESR intensity with added dose, indicating that the electron traps were being saturated. We therefore used a logarithmic fit to determine the AD.

AD and Age Dependence on Grain Size

Theoretical model

If a volume of rock has been crushed by shearing along a fault, then we expect that not all the particles produced by this crushing would have undergone the same degree of resetting of their ESR signals. For a given electron trap, in particular, we expect that larger grains would be only partially zeroed because shear strain would have been concentrated along their margins, leaving the interiors relatively unstrained. In general, the smaller the grain, the larger the proportion of it that would have been sufficiently strained to totally zero the ESR signal.

Grains smaller than some critical radius r_c would be totally reset. Immediately after shearing, we would then expect the apparent age distribution in the particles to look like that shown in curve A of figure 5.

After the passage of time, electrons will repopulate the traps and the apparent age of the totally reset (smallest) particles will equal the time elapsed since movement while larger particles will give a a greater apparent age. Thus, in a graph of age versus grain size, we would expect to find a plateau of constant age for grains below some critical size. The age given by this plateau is the true time of last movement. Only samples which exhibit such a plateau (for at least one ESR center) can be shown to have been totally zeroed at the time of last movement. If the sample contains a mixture of totally and partially reset particles, it will not give a satisfactory plateau, but the minimum age (for the smallest particles) will approach that of the last movement.

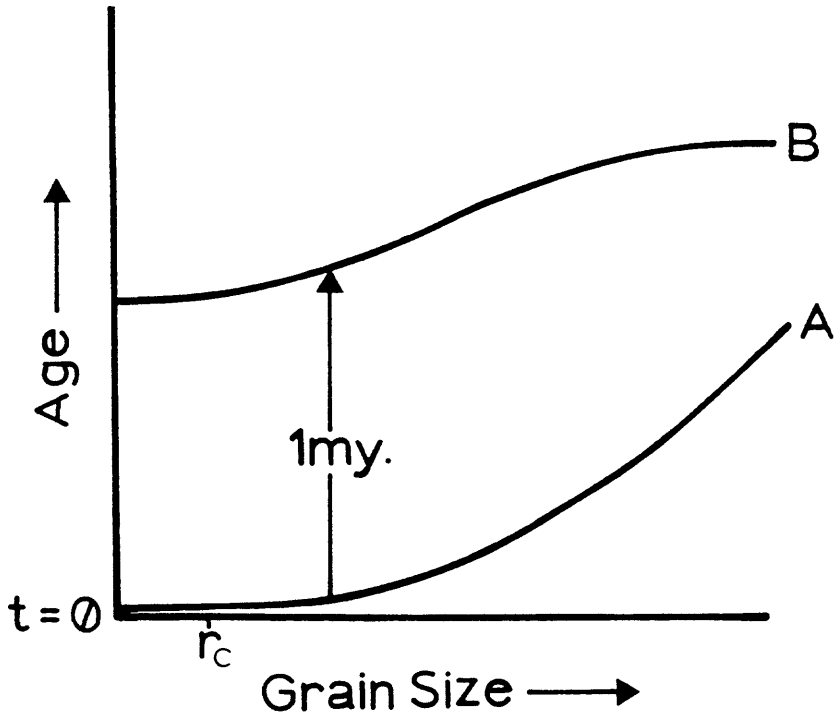

FIGURE 5. Hypothetical distribution of ESR ages in quartz grains as a function of particle size: A. immediately after movement on the fault; B. 1 my later. The maximum age shown is that corresponding to saturation of all electron traps.

AD Variation with size

Figure 6 shows the variation of AD with grain size in various samples.

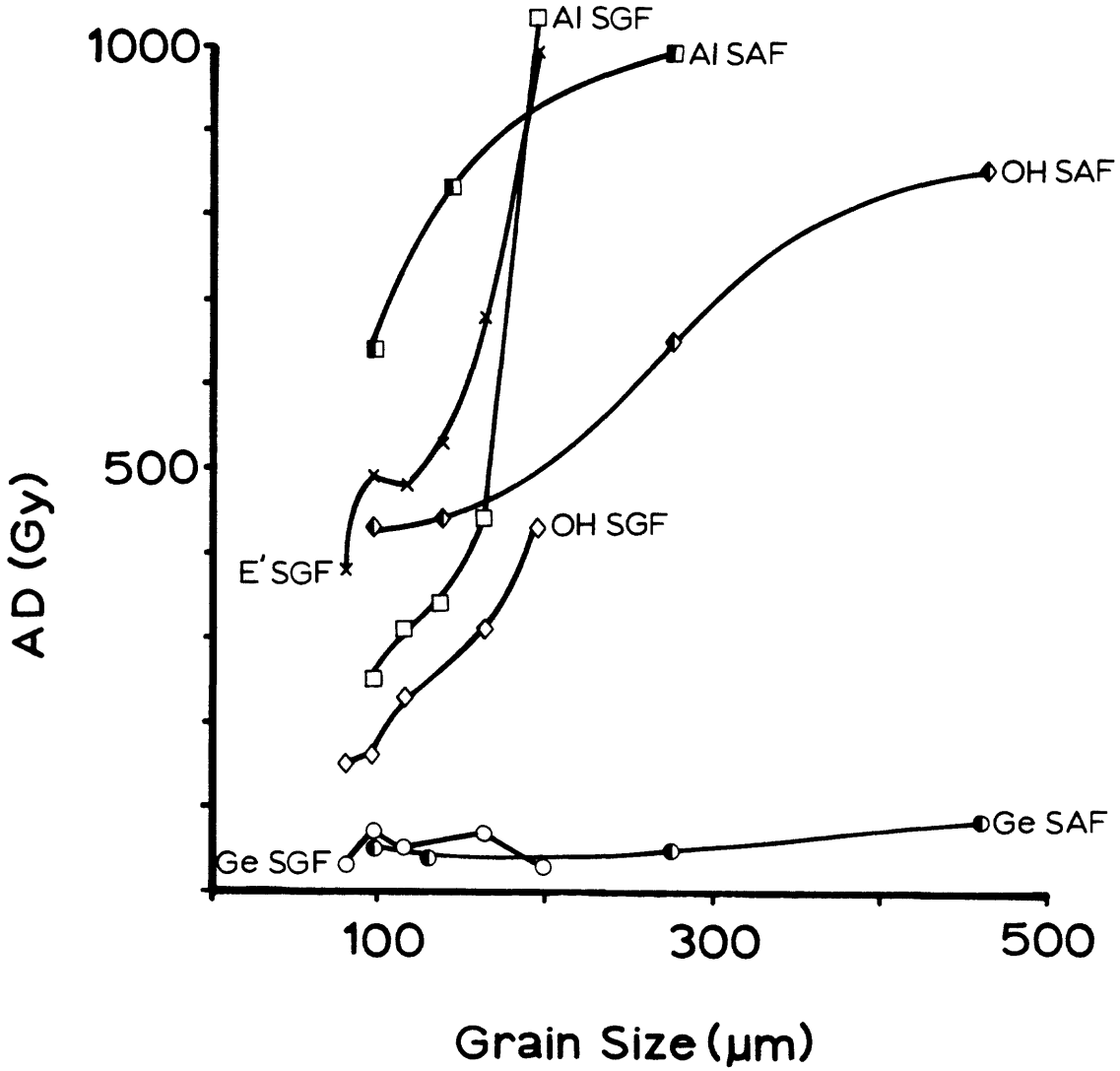

FIGURE 6. Variation of AD with grain size in quartz from samples of fault gouge from southern California. The samples are from: San Andreas fault (SAF) near Palmdale, and the San Gabriel fault (SGF) near Big Tujunga Canyon. Al, OH, E, and Ge refer to various kinds of defect centers described in the text.

As expected, there is a pronounced decrease in AD with decreasing grain size. For the OH center, the AD apparently approaches a plateau for particles smaller than 150μm. Our previous experiments had suggested that the OH centre is the most readily reset by hydrostatic pressure (and presumably also by shear stress). The AD given by the plateau for this center should therefore give the best estimate of the age. The AD's given by the E' and Al signals continue to decrease to the lowest grain size. The Ti center was measurable in only one sample, that from the San Jacinto fault at Anza; it showed, surprisingly, an increase in AD with decreasing grain size, and did not converge on the value for the Al and OH centers.

The Ge center, which was previously found to be easily bleached, gives uniformly low AD's for all grain sizes, suggesting either that it has faded (due to electron de-trapping at ambient temperature) or that it has been bleached during preparation of the sample.

These data suggest that, if we can successfully measure the dose rates for the samples as well, then it should be possible to estimate the time of last resetting of the ESR signal by shearing.

Age variation with grain size

We have so far studied the variation of age with grain size in only one sample from this suite, gouge from the San Jacinto fault near Anza, Calif. The age was calculated using a program (ESR-DATA) that takes into account attenuation of β- and α-particles in the quartz grains (as a function of their size) as well as α-efficiency, energies of α and β particles in the U, Th, and K decays, and γ-doses from the surrounding rock. Attenuation by water in pores, loss of radon, and disequilibrium between daughters of ^{238}U were neglected, as were cosmic rays. The data are shown in figure 7.

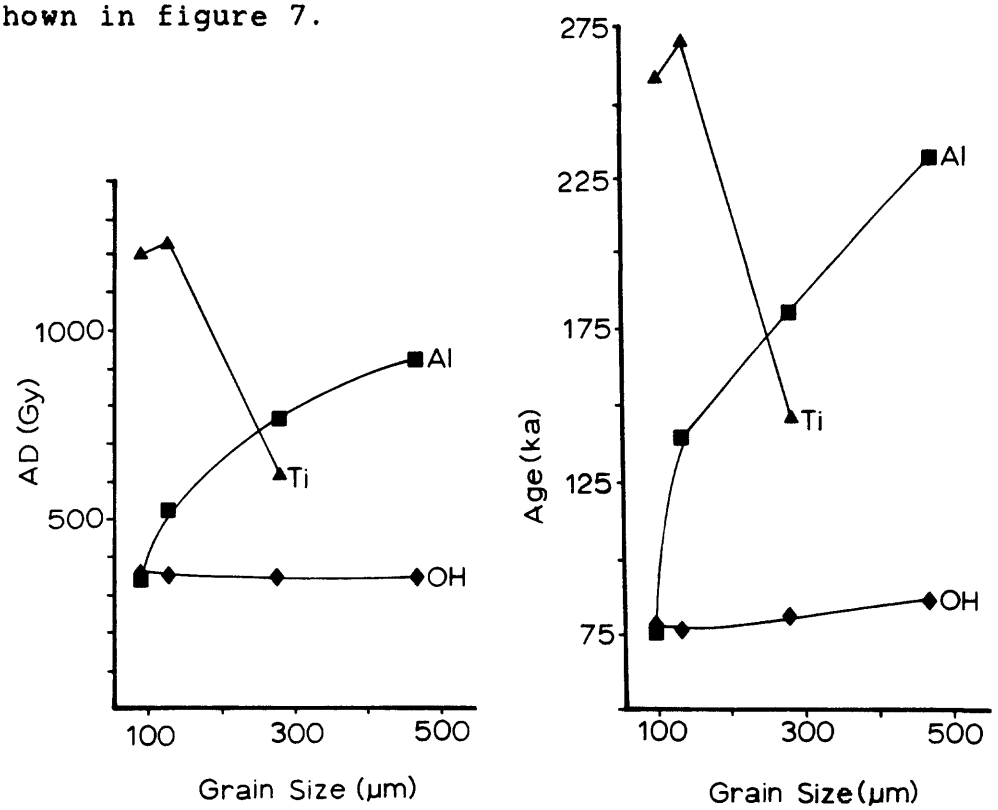

FIGURE 7. Variation of AD and age in various size fractions from fault gouge of the San Jacinto fault, near Anza, California. Al, Ti, and OH are various kinds of defect centers described in the text.

As in the previous examples, the Al signal decreases in AD with decreasing grain size, reaching a lower limit which is equal to the plateau for the OH center. Note that the AD values in this case are not proportional to the age, although the trends in both quantities are parallel.

Although this section of the San Jacinto fault has been active in recent times (T. Rockwell, oral commun., 1987), the ages that we calculate for the various fractions of this sample converge to an age of about 75,000 yrs. Whereas this is consistent with the known continuous activity of this fault through the Pleistocene, the ESR signal apparently does not record the time of last movement on this fault. A possible reason for this will be presented below.

From the increase in the height of the OH-center peak as a function of dose together with the known dose rates observed in typical gouge material, we estimate that we could detect regrowth of the signal a few hundred years after the time of zeroing. For such small signals, we would naturally suppose that some residual signal might have existed in the sample (incomplete zeroing) and that the age estimate was an upper limit to the true age of last movement.

DISCUSSION

We should therefore consider what sort of information might, in principle, be obtainable from the ESR dating of fault gouge. Any currently active fault of moderately large displacement (such as the San Jacinto fault) must consist of a large number of discrete slip surfaces or subzones. Stress and displacement within individual subzones is inhomogeneous, thus creating strands of material within the fault gouge that have been zeroed to different extents at different times. If we select, at random, a sample of fault gouge from somewhere among this set of intertwining strands, it will record in its ESR signal an apparent resetting event at some time $T > 0$. If one of the slip zones was in fact active in the very recent past ($T \simeq 0$) and if there are n such subzones across the width of the fault zone where the sample was taken, then there is a probability of approximately 1/n of obtaining an age of zero for the "time of last movement" assuming that each of the various subzones occupies an equal fraction of the total thickness of the fault zone. There will be, however, some tendency for younger faulting events to obliterate the record of older ones, and the probability of observing a strand-volume with a date T will be a decreasing function of T.

Given these constraints, ESR studies of randomly selected gouge samples will mainly provide information about the frequency of movement on the fault, although there will be a bias towards younger events, as noted above. In addition, such multiple analyses of material from individual subzones should make it possible to converge on the time of last movement. A statistical

treatment of the data may allow us to acquire a probability of there being an even younger event than those analysed, based on the total distribution function f(T), the frequency of events of age T.

Ariyama (1986) showed that resetting will only occur if the overburden is greater than about 20 bars. If movement occurred within the last few hundred years on a particular slip plane, it is possible that the material which was completely zeroed may still be buried at depths of 70 m or more. Using surface samples, the minimum age of movement that we can detect will depend on uplift and erosion rates in the vicinity of the fault. The surprising old age for the San Jacinto fault at Anza may in fact be a result of a relatively low uplift rate at this site. We should also collect samples for ESR dating by core-drilling to some moderate depth (>100 m) in a fault zone, and test the apparent age of samples of core as a function of depth to see if there is some minimum depth below which zeroing is complete.

If the fault being studied consists of a single slip-zone, then there is a greater likelihood of obtaining a true estimate of the time of last movement as long as the sample was collected at sufficient depth.

CONCLUSIONS

We have shown that there is a strong dependence of AD on particlesize, down to a critical size below which the signal is uniform (plateau). The establishment of this plateau assures us that the signal was fully zeroed at the time of last movement. Only samples which exhibit such a plateau of age versus grain size for the smallest particles can be assured to have been fully zeroed, and are thus potentially datable. Furthermore, we should expect to see a plateau in the ages given by more than one paramagnetic center, although plateaus may not necessarily converge on the same age.

It appears that, of the various ESR signals that can be measured in quartz, the oxygen-hole center (OH) is most completely zeroed during faulting, and is thus the most reliable signal for use in dating. Other advantages of the use of this signal are that it is detectable at room temperature, and that it is very commonly observed in samples of quartz. The Al center is also very sensitive, and AD's based on it decrease markedly with grain size, but may not reach a plateau for grains larger than 80 μm. The Ge signal appears to be bleached by visible light, and its use would require preparation of samples in a filtered-light environment, which would greatly complicate the sample preparation procedures.

ACKNOWLEDGEMENTS

We greatly appreciate the assistance in sample collection of R. Biegel, T. Rockwell, and D. Schwartz. Discussions with these individuals as well as with R. Wallace (U.S. Geological Survey) have greatly aided us in this study. We also acknowledge discussions with M. Ikeya, K. Shimokawa, and N. Imai. This research was supported by a grant to HPS from the Natural Science and Engineering Research Council of Canada.

REFERENCES CITED

Aitken, M.J.,1985, Thermoluminescence dating: London, Academic Press, 359 p.

Ariyama, T.,1985, Conditions of resetting the ESR clock during faulting, in: Ikeya, M. and Miki, T., eds, ESR Dating and Dosimetry, Tokyo, p.249-256.

Fukuchi, T., Imai, N., and Shimokawa, K.,1986, ESR dating of fault movement using various defect centres in quartz; the case in the western South Fossa Magna, Japan. Earth and Planetary Science Letters, v.78, p.121-128.

Hennig, G.J. and Grün, R.,1983, ESR dating in quaternary geology. Quaternary Science Reviews, v.2, p.157-238.

Huntley, D.J., Godfrey-Smith, D.I. and Thewalt, M.L.W.,1985, Optical dating of sediments. Nature, v.313, p.105-107.

Ikeya, M. & Miki, N.,1985, eds. ESR dating and Dosimetry. Tokyo, 347 p.

Ikeya, M., Miki, T. Tanaka, K.,1982, Dating of fault by electron spin resonance on intrafault materials. Science, v.215, p.1392-1393.

Kosaka, K. and Sawada, S.,1985, Fault gouge analysis and ESR dating of the Tsurukawa fault, west of Tokyo: significance of minute sampling. in Ikeya, M. & Miki, T. eds. ESR Dating and Dosimetry: Tokyo, p.257-266.

Marfunin, A.S.,1979, Spectroscopy, luminescence and radiation centers in minerals: Berlin, Springer Verlag, 352p.

Miki, T. and Ikeya, M.,1982, Physical basis of fault dating with ESR. Naturwissenschaften, v.69, p.90-91.

Nambi, K.S.V. and Aitken, M.J.,1986, Annual dose conversion factors for TL and ESR dating. Archaeometry, v.28, p.202-205.

Shimokawa, K. and Imai, N.,1987, Simultaneous determination of alteration and eruption ages of volcanic rocks by electron spin resonance. Geochimica et Cosmochimica Acta, v.51 no.1, p.115-119.

Smolyanskiy, P.L. and Masaytis, V.L.,1979, Reconstruction of paleotemperature anomalies of old rocks from radiation-induced defects in quartz: Dokladi Akademii, Nauk, SSSR, v.248, p.1428-1431.

DATING QUATERNARY DEPOSITS USING WEATHERING RINDS AND RELATED PHENOMENA

by

Steven M. Colman
U.S. Geological Survey
Woods Hole, MA 02543

ABSTRACT

Weathering characteristics of Quaternary deposits and surfaces have long been known to change systematically with time. These characteristics have great potential as age indicators because of their widespread occurrence and their general applicability. Recent studies have shown that some dating methods based on weathering measurements, especially weathering rinds and obsidian-hydration rinds, can be used to derive direct numerical ages under favorable conditions and with calíbration by other methods.

INTRODUCTION

Dating Quaternary deposits or events in applications such as paleoseismologic studies is commonly a difficult task. Most isotopic and other numerical dating methods require specific materials, ages, and settings in order to provide accurate age estimates. In contrast, weathered materials are nearly ubiquitous on exposed deposits and surfaces. The development of many weathering phenomena is clearly related to time, and studies that have used weathering observations to differentiate surficial deposits according to age date back at least to Blackwelder (1931). However, the direct use of weathering measurements in estimating ages has been severely limited because of several problems, particularly uncertain initial conditions, questions of representativeness and reproducibility of the measurements, and the confounding effects of environmental variables, especially lithology and climate. Recent work on the use of weathering rinds has attempted to minimize these problems while taking advantage of the wide applicability of methods based on weathering measurements.

WEATHERING RINDS

Weathering rinds have proved useful in estimating ages in a wide variety of subhumid to humid environments. Weathering rinds were first used primarily for relative dating and mapping (see review in Colman and Pierce, 1981), but recent work has extended their use to more quantitative geochronology (Cernohouz and Solc, 1966; Colman and Pierce, 1981, 1985; Chinn, 1981; Whitehouse and others, 1986). Large numbers of measurements can be made in the field, allowing relatively sophisticated sampling designs and statistical tests of reliability and sources of variation. Because the cores of clasts on which rinds are measured are unweathered, the initial conditions for the rinds

are commonly well defined and the effects of different lithologies can be compared. Most clasts in alluvial and glacial deposits are abraded in transport, so they are deposited with fresh, unweathered surfaces. Consequently, the thickness of the rind is a function of the age of the deposit or surface from which it was sampled. Finally, at least within local areas, sampling designs can minimize the effects of all environmental variables other than age.

Weathering-rind data may be examined for time or age information on several different levels (Colman, 1986). Increasingly quantitative age data typically require increasing assumptions and thus carry increasing uncertainty. The lowest level of time information is relative age, which requires virtually no assumptions. The validity of early qualitative and empirical use of weathering rinds in this way have been confirmed by recent statistical tests (Colman and Pierce, 1981; Whitehouse and others, 1986).

The next level of age information derived from weathering-rind thicknesses is the magnitude of the age difference between two deposits. Deposits in a given area are subject to approximately the same set of environmental variables, so the need to account for these variables is essentially eliminated in the comparison. The primary unknown at this level is the exact function that relates rind thickness to age. However, in many cases, reasonable limits can be placed on this function. Where weathering-rind thickness measurements have been calibrated with independent age estimates, they are a logarithmic or a fractional-exponential function of age (fig. 1), in which the rates of rind formation clearly decrease with time (Colman, 1981). As a result, for example, two deposits whose rind thicknesses differ by a factor of 2 must differ in age by more than a factor of 2. Thus, because limits on the general form of the relation between rind thickness and time are known, useful quantitative age information can be derived using assumptions whose validity is virtually certain.

Because of the effects of variables such as climate and lithology, the use of weathering rinds to directly estimate numerical ages requires calibration by independent age estimates (fig. 1). In most cases, at least one independent age, derived from other dating methods or by correlation to deposits of known age, is required for each local area. Because most areas have little or no independent numerical age control, the number of assumptions required for this calibration process is considerable. However, subject to the validity of such assumptions, calibrated rates of weathering-rind development can be used as a true numerical dating method.

OBSIDIAN HYDRATION

Hydration rinds, which are special kinds of weathering rinds formed by the diffusion of water into volcanic glass, have been successfully used to provide accurate ages in many climatic and geologic settings. Although they are restricted to silicic volcanic glass, they represent a much simpler chemical system and depend on fewer variables than do weathering rinds. The thickness of the hydrated layer is proportional to the square root of time and a rate coefficient that depends on temperature and the composition of the glass (fig. 2). The diffusion coefficient is largely independent of moisture conditions and, in many cases, can be determined experimentally in the laboratory for obsidian of a given composition.

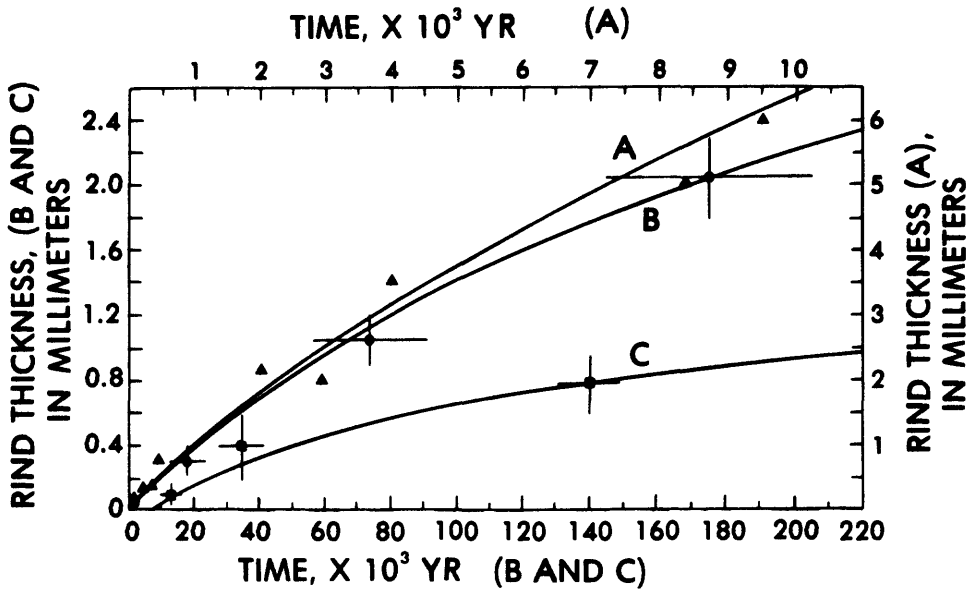

Figure 1. Calibration of the relation between weathering-rind thickness and time. Triangles (curve A), graywacke clasts in New Zealand (Chinn, 1981); circles (curve B), basaltic clasts in Bohemia (Cernohouz and Solc, 1966); squares (curve C), basaltic clasts near West Yellowstone, Montana (Colman and Pierce, 1981).

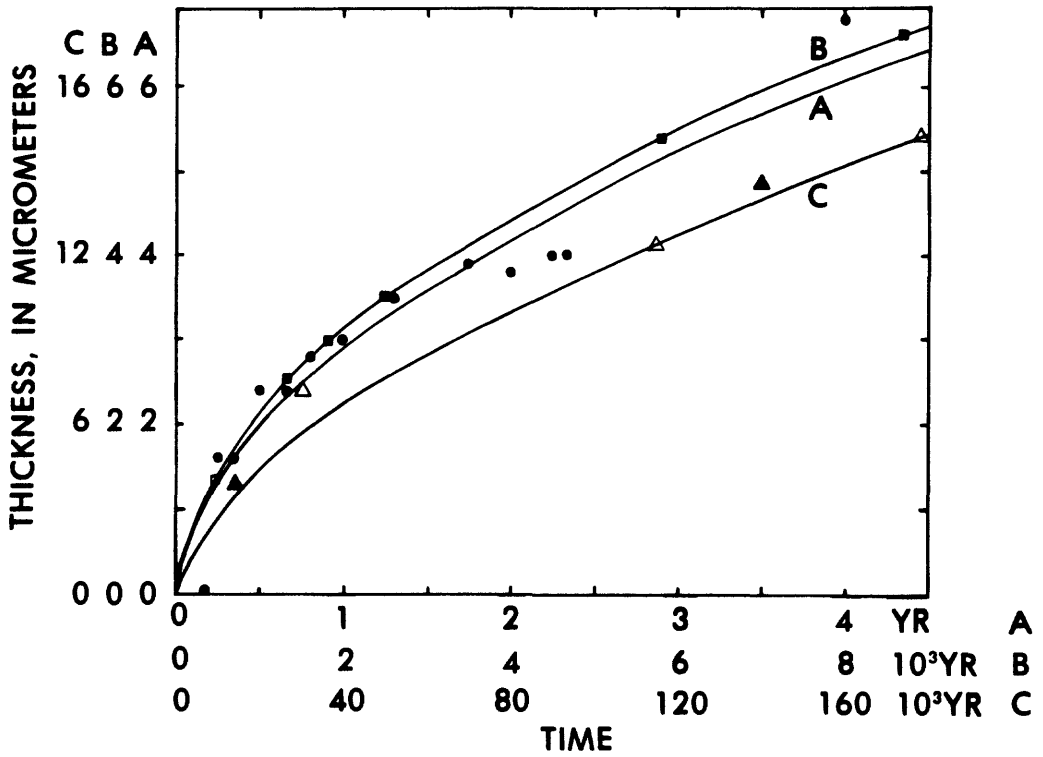

Figure 2. Thickness of obsidian hydration as a function of time. Circles (curve A), laboratory hydration of obsidian at 100°C (Friedman and others, 1966); Squares (curve B), hydration of obsidian from rhyolite flows near Mono Craters, California (Friedman, 1968), open squares are dated flows used for calibration; triangles (curve C), hydration of obsidian near West Yellowstone, Montana (Pierce and others, 1976), open triangles are dated flows used for calibration and solid triangles are obsidian-bearing glacial deposits.

The method has been used to estimate the ages of materials as diverse as archaeological artifacts, glacial deposits, and lava flows (see Taylor, 1976, and Friedman and Long, 1976, for examples). Of particular interest to paleoseismologic studies is the dating of the Pinedale and Bull Lake Glaciations near West Yellowstone, Montana, by this method (fig. 2), because many deposits in tectonically active areas can be correlated to these dated deposits (Pierce and others, 1976).

OTHER WEATHERING MEASUREMENTS

Many other kinds of weathering data, both traditional surface-weathering measurements (Burke and Birkeland, 1979; Brookes, 1982) and newer kinds of analyses, have the potential for use as numerical age indicators in ways similar to those used for weathering and hydration rinds. One recent promising development uses P-wave speeds in weathered boulders (Crook and Gillespie, 1986). Weathering of heavy minerals, especially etching of hornblende (Locke, 1979, 1986; Hall and Martin, 1986) also shows potential. Processes related to obsidian hydration, such as hydration of tephra and filling of vesicles in tephra shards, show time dependency (Steen-McIntyre, 1975). New developments in the use of progressive changes in rock-varnish chemistry to estimate ages are covered elsewhere in this volume. The most serious limitations to the development of new methods based on weathering measurements seems to involve uncertainties about the initial conditions and the preservation of the full history of weathering.

CONCLUSIONS

The use of weathering measurements for estimating the ages of Quaternary deposits has both advantages and disadvantages. Chief among their advantages is their widespread applicability in diverse environments. Under favorable conditions, weathering measurements have been used to directly estimate numerical ages with relatively low uncertainties. On the other hand, age estimates derived from weathering measurements are commonly hampered by uncertainty about initial conditions and by the scarcity of independent calibration. However, as Quaternary stratigraphies become better dated by existing and new dating methods, the positive feedback between new age information and the need for testing and calibration of all dating methods is likely to increase the usefulness of dating methods based on weathering phenomena.

REFERENCES CITED

Blackwelder, E. 1931, Pleistocene glaciation of the Sierra Nevada and Basin Ranges: Geological Society of America Bulletin, v. 42, p. 865-922.

Brookes, I.A., 1982, Dating methods of Pleistocene deposits and their problems--VIII, Weathering: Geoscience Canada, v. 9, p. 188-199.

Burke, R.M., and Birkeland, P.W., 1979, Reevaluation of multiparameter relative dating techniques and their application to the glacial sequence along the eastern escarpment of the Sierra Nevada, California: Quaternary Research, v. 11, p. 21-51.

Cernohouz, J., and Solc, I., 1966, Use of sandstone wanes and weathered basaltic crust in absolute chronology: Nature, v. 212, p. 806-807.

Chinn, T.J.H., 1981, Use of weathering rind thickness for Holocene absolute age-dating in New Zealand: Arctic and Alpine Research, v. 13, p. 33-45.
Colman, S.M., 1981, Rock weathering rates as functions of time: Quaternary Research, v. 15, p. 250-264.
_____1986, Levels of time information in weathering measurements, with examples from weathering rinds on volcanic clasts in the western United States, in Colman, S.M., and Dethier, D.P., eds., Rates of chemical weathering of rocks and minerals: New York, Academic Press, p. 379-394.
Colman, S.M., and Pierce, K.L., 1981, Weathering rinds on andesitic and basaltic stones as a Quaternary age indicator, western United States: U.S. Geological Survey Professional Paper 1210, 56 p.
_____1985, Correlation of Quaternary glacial sequences in the western United States based on weathering rinds and related studies, in Mahaney, W. C., ed., Correlation of Quaternary sequences: Norwich, UK, GeoBooks Ltd., p. 437-454.
Crook, Richard, Jr., and Gillespie, A.R., 1986, Weathering rates in granitic boulders measured by P-wave speeds, in Colman, S.M., and Dethier, D.P., eds., Rates of chemical weathering of rocks and minerals: New York, Academic Press, p. 395-417.
Friedman, I., 1968, Hydration rind dates rhyolite flows: Science, v. 159, p. 878-879.
Friedman, Irving, and Long, W., 1976, Hydration rates of obsidian: Science, v. 191, p. 347-352.
Friedman, I., Smith, R.L., and Long, W.D., 1966, Hydration of natural glass and the formation of perlite: Geological Society of America Bulletin, v. 77, p. 323-328.
Hall, R.D., and Martin, R.E., 1986, The etching of hornblende grains in the matrix of alpine tills and periglacial deposits, in Colman, S.M., and Dethier, D.P., eds., Rates of chemical weathering of rocks and minerals: New York, Academic Press, p. 101-127.
Locke, W.W., 1979, Etching of hornblende grains in arctic soils--An indicator of relative age and paleoclimate: Quaternary Research, v. 11, p. 197-212.
Locke, W.W., 1986, Rates of hornblende etching in soils on glacial deposits, Baffin Island, Canada, in Colman, S.M., and Dethier, D.P., eds., Rates of chemical weathering of rocks and minerals: New York, Academic Press, p. 129-146.
Pierce, K.L., Obradovich, J.D., and Friedman, I., 1976, Obsidian hydration dating and correlation of Bull Lake and Pinedale Glaciations near West Yellowstone, Montana: Geological Society of America Bulletin, v. 87, p. 703-710.
Steen-McIntyre, V., 1975, Hydration and superhydration of tephra glass--A potential tool for estimating the age of Holocene and Pleistocene ash beds in Quaternary studies, in Suggate, R.P., and Cresswell, M.M., eds., Quaternary Studies: Royal Society of New Zealand Bulletin 13, p. 271-278.
Taylor, R.E., ed., 1976, Advances in obsidian glass studies: Park Ridge, N.J., Noyes Press, 360 p.
Whitehouse, I.E., McSaveney, M.J., Knuepfer, P.L.K., and Chinn, T.J.H., 1986, Growth of weathering rinds on Torlesse Sandstone, Southern Alps, New Zealand, in Colman, S.M., and Dethier, D.P., eds., Rates of chemical weathering of rocks and minerals: New York, Academic Press, p. 419-437.

APPLICATION OF ROCK-VARNISH DATING OF QUATERNARY SURFICIAL DEPOSITS IN DETERMINING TIMES OF FAULT MOVEMENT

by

Charles D. Harrington
Earth and Space Sciences Division
Los Alamos National Laboratory
Los Alamos, New Mexico 87545

ABSTRACT

Rock varnish, a coating commonly found on rock surfaces in arid and semiarid regions, has a significant potential in paleoseismic studies, as a wide variety of Quaternary surfaces and surficial deposits can be dated with the rock varnish technique. If the formation of geomorphic surfaces or surficial deposits can be related to times of faulting or if faulting has broken or deformed such features, then rock-varnish dating can be used to constrain maximum and minimum times of motion on the related fault.

INTRODUCTION

Rock varnish, a ubiquitous, manganese and iron-rich coating on boulders in arid and semiarid regions, has long been of interest as a potential age indicator. Recent work (Dorn, 1983; Harrington and Whitney, in press) has demonstrated that rock varnish is an effective medium for dating geomorphic surfaces and surficial deposits over an age range of several thousand to more than a million years. The ratio of several minor elements within the varnish [(K+Ca)/Ti] has been shown to be age-dependent and to decrease with time. Rock-varnish cation ratios (VCRs) for geomorphic surfaces which have been isotopically dated are used to construct calibrated VCR curves (area specific plots of VCR versus log of time). These varnish curves can then be used to date varnish of unknown age throughout the region of calibration. Varnish ages from surface clasts represent the surface-exposure time of the clasts. This in turn represents the time that the surface was incised and stabilized (ceased being a surface of active transport). Thus, using calibrated cation-ratio curves, the time of initial varnish formation on surface clasts (a minimum age estimate for surface formation) can be determined for a variety of geomorphic surfaces within the region.

METHOD

Rock varnish is analyzed using a scanning-electron microscope (SEM) equipped with an energy dispersive x-ray analyzer. Whereas others detach the varnish before analysis (Dorn, 1983, Dorn and others, 1986), with the SEM elemental ratios are calculated for undisturbed varnish on parts of varnished clasts (Harrington and Whitney, in press). Eight to 10 clasts are analyzed for each surface to be dated and a VCR is calculated for the surface by averaging the VCRs determined for all analyzed surface clasts. Geomorphic surfaces dated by a variety of isotopic techniques can be used to calibrate VCR curves. K-Ar, U-series, and U-trend dated surfaces (Harrington and Whitney, in press) and ^{14}C dated surfaces (Dorn and others, 1986) have been used for VCR curve calibration.

Cation-ratio curves have been constructed for the Coso Range and Mojave region in southern California (Dorn, 1983; Dorn and others, 1986) for the Española Basin, New Mexico, and part of the Nevada Test Site (NTS) (Harrington

and Whitney, in press). The Española Basin curve (fig. 1) was calibrated for the time interval of 20-500 ka, using a combination of four uranium-series dated erosion surfaces and four surface ages based on carbonate accumulation in soils (Dethier and others, in press). The curve for the NTS (Harrington and Whitney, in press) was calibrated using three uranium-trend dated alluvial surfaces and two K-Ar dated lava flows, ranging in age from 40 ka to 1.1 Ma. Each of the curves possess a unique y intercept and slope, suggesting that cation-ratio curves are specific to the region of calibration.

Regional differences in dust composition and depositional rates, as well as rainfall type and amount, may be possible causes for differences in VCR curves between regions. The aerial extent over which a VCR curve can be used for dating is not yet known, but probably varies depending on the degree of variability of climatic factors across the region.

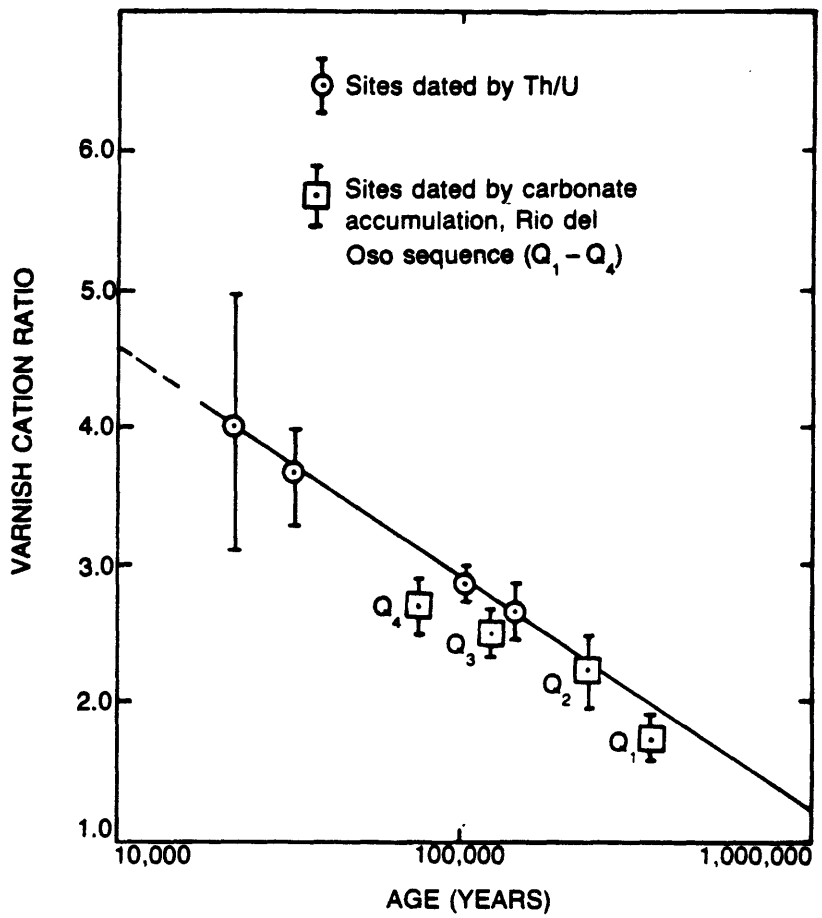

FIGURE 1.--Rock-varnish dating curve for the Española Basin, N. Mex. (from Dethier and others, in press). Line is least-squares fit through the uranium-series-dated points (Harrington and Whitney, in press). Ages of surfaces Q_1, Q_2, Q_3, and Q_4 were estimated using the maximum amount of soil-carbonate accumulation (Dethier and Demsey, 1984) and an estimated $CaCO_3$ accumulation rate of 0.22 $gcm^{-2}ka^{-1}$ (see Dethier and others, in press, for details).

A critical assumption in curve calibration is that dated varnish is the same age as the dated deposit used for calibration. In addition, it must be assumed that the deposit has been continually exposed throughout the time of varnish formation. Dorn and others (1986) have noted that varnish formation begins soon (< 200 yrs) after a deposit has been exposed. Thus, for deposits for which continuous exposure can be demonstrated, the assumption of equality in varnish and deposit age is likely valid. As deposit age increases, demonstrating continuous exposure becomes more difficult and, for very old deposits, continuous exposure often cannot be demonstrated with a high degree of certainty. In the case of K- Ar-dated lava flows, an additional assumption must be that the time between flow deposition and varnish initiation on stable flow surfaces is short when compared to flow age.

Accuracy in determining the age of a geomorphic surface is most severely limited at present by our ability to recognize and select the most mature varnish from the surface to be dated. This becomes increasingly difficult and critical as younger surfaces are sampled. Research to better understand the manner and rate of varnish formation will improve sample selection, resulting in reduced standard deviations for VCR calibration points, VCR curves that are better constrained, and more accurate age estimates.

A cation-ratio curve can be extended into Holocene time by (1) using varnish cation ratios from surfaces or deposits of Holocene age dated by ^{14}C or other isotopic techniques, or (2) extrapolation from the calibrated interval. The standard deviation of VCR's for an individual surface is greater the younger the surface. Thus, calibration curve position is most poorly constrained in the youngest part of the curve. Extrapolating the curve into the Holocene, from calibration points on deposits older than Holocene, increases the uncertainty of curve position.

We have dated the varnish formed on pediment surfaces, alluvial fans, fluvial terraces, colluvial hillslope deposits, stable eolian deposits, and geomorphic surfaces which have been faulted (Dethier and Harrington, 1986; Harrington, 1986a; Harrington, 1986b; Harrington and Dethier, 1987; Dethier and others, in press; Harrington and Whitney, in press). Ideal geomorphic surfaces for rock-varnish dating are on deposits that contain large clasts that project well above the soil surface.

APPLICATION OF ROCK VARNISH DATING IN PALEOSEISMOLOGY

Rock-varnish dating of landforms has a high potential value in paleoseismic investigations. The significance of rock varnish dating to paleoseismic studies lies in the large variety of geomorphic surfaces and deposits potentially datable by this technique. Many such deposits, especially those composed of coarse clastic material, may not be easily datable by conventional isotopic techniques. The age of these deposits, however, may be crucial in constraining times of movement on faults which deform the deposits or to which their formation is related. If formation of geomorphic surfaces or surficial deposits can be related to times of faulting, then rock-varnish dating can yield maximum and/or minimum times for movement of the related fault segments. Dating of surfaces which have been disrupted by faulting yields a maximum age constraint for most recent fault motion. Similarly, varnish dating of surficial deposits (such as colluvial wedge material) which have been shed off or bury the scarp, provides estimates of the minimum time since last fault motion occurred.

We have used rock-varnish dating within the Española Basin to determine the time of formation of landforms that are related to faulting in order to constrain the time of most recent fault motion. Four Quaternary erosion surfaces, formed along the western side of the basin, have been broken or deformed along three groups of related faults which are part of the Pajarito fault system. Estimates of surface ages and correlation of surfaces along the western side of the basin were based on rock-varnish cation ratios from varnished surface clasts (Dethier and others, in press). The four erosion surfaces range in age from about 500 ka to 80 ka, and lie 200-15 m above present base level, the Rio Grande (fig. 2). The maximum time since movement has occurred on a fault can be constrained by the rock-varnish age of the youngest erosion surface displaced by the fault.

Each of the surfaces step down to the east along a series of north-trending scarps which truncate the surfaces along a trend perpendicular to surface slope. Near Hernandez, N. Mex. these north-trending scarps are 8-20 m high and coincide with a series of north-trending fault traces (Harrington and Dethier, 1987). Rock-varnish dating has been used to establish the time of formation of one of these north-trending scarps (fig. 3). The surface that extends back from the top of the scarp yields a rock-varnish age of 103 ka. Varnished clasts on sediment that was deposited on the surface at the foot of the scarp yields an age estimate of 72 ka, while clasts taken from the top of the scarp itself give an age estimate of 31 ka. We thus conclude that the scarp formed between 103 and 72 ka and has undergone regrading until about 31 ka.

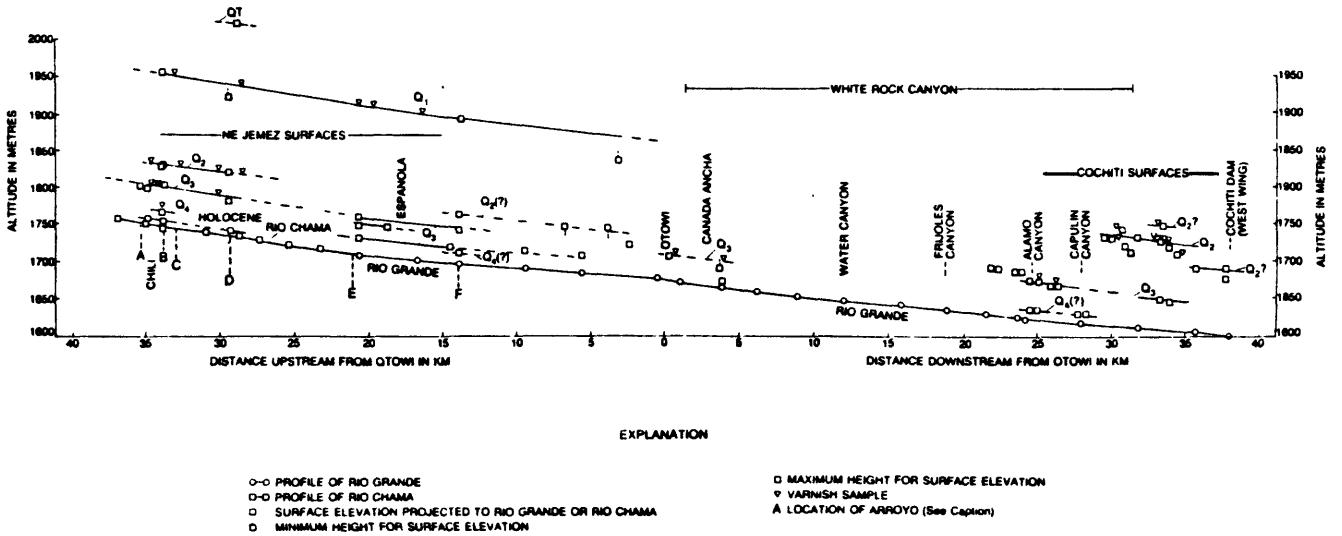

FIGURE 2.--Profiles of geomorphic surfaces projected to the Rio Chama and Rio Grande systems, western Española Basin (from Dethier and others, in press). Letters designate the location of: Arroyo del Placio (A); Rio del Oso (B); Rio Ojo Caliente (C); Arroyo de la Presa (D); Arroyo de la Plaza Larga (E); and Santa Clara Creek (F).

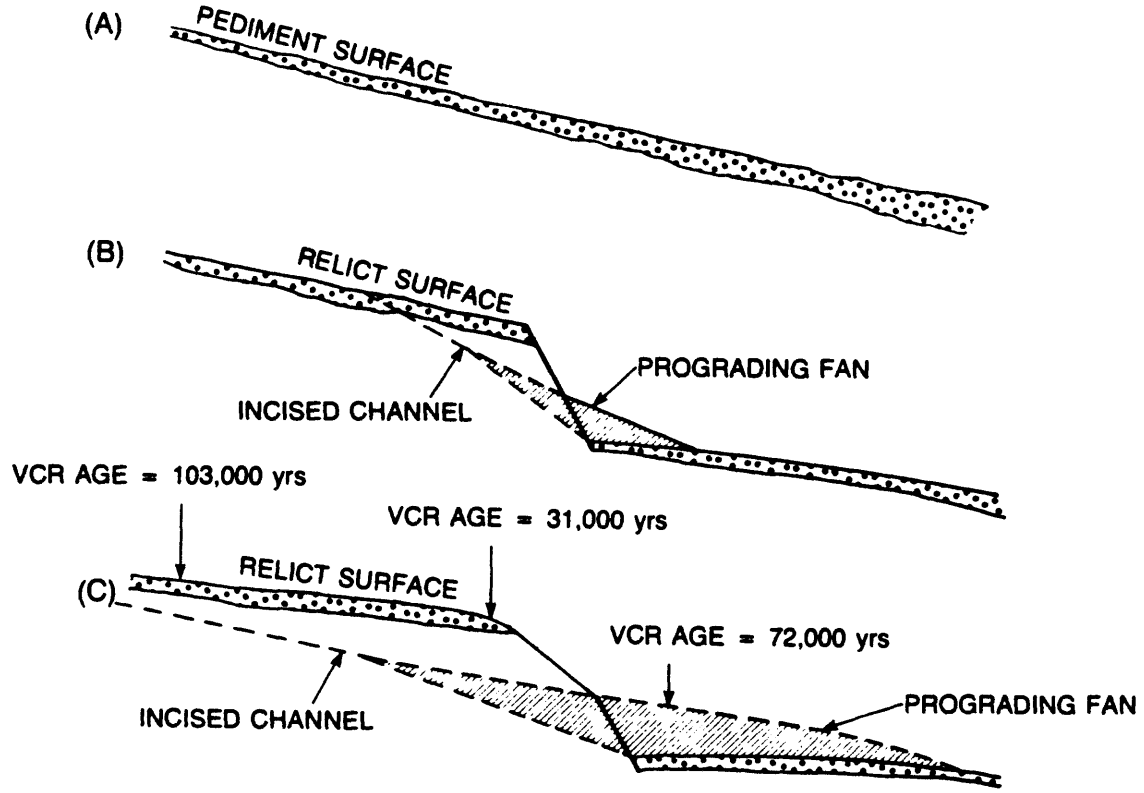

FIGURE 3.--Sketch of relationships along scarp, west of Hernandez, N. Mex. (A) original geomorphic surface, (B) following scarp formation, and (C) rock varnish (VCR) ages derived for surfaces and deposits related to the scarp.

Rock-varnish dating of other geomorphic features has also been used in the Española Basin to constrain the time of last movement on faults. West of Hernandez, N. Mex. a north-northwest-trending fault showing recurrent movement offsets an erosion surface that has a rock-varnish age of 240 ka, a minimum of 6 m. This fault appears to cut the sediment-fill of a paleochannel. Varnished clasts from the surface of the paleochannel fill yield an age estimate of 40 ka. Thus, if the fault cuts the paleochannel, then the 6 m of offset has occurred during a significantly shorter time period than the 240 ka derived by using the age of the erosion surface to constrain the timing of last fault movement.

CONCLUSIONS

The ages of surficial deposits and geomorphic surfaces broken by or related to faulting are often critical to constraining the timing of fault motion. Frequently, imprecise relations between datable materials and pertinent geomorphic features significantly limits the applicability of isotopic techniques (Dohrenwend and others, 1986). Rock-varnish dating can provide age estimates for many geomorphic surfaces or features, especially features formed on coarse clastic materials.

Thus, rock-varnish dating has a significant potential in paleoseismic investigations in arid and semiarid regions because of the large variety of

surficial deposits and geomorphic surfaces which can be dated by the technique. Rock-varnish dating offers the potential for (1) determining the age of many geomorphic surfaces and surficial deposits which may not be readily datable by isotopic techniques; and (2) evaluating whether an isotopic date is an accurate portrayal of deposit age or instead, represents a later event which has reset the isotopic clock for that deposit.

REFERENCES CITED

Dethier, D.P., and Demsey, K.A., 1984, Erosional history and soil development on Quaternary surfaces, northwest Española basin, New Mexico: New Mexico Geological Society, 35th Annual Field Conference Guidebook, p. 227-233.

Dethier, D.P., and Harrington, C.D., 1986, Late Quaternary erosion history of the western Española Basin, New Mexico: [abs.] Geological Society of America Abstracts with Programs, v.18, p. 351.

Dethier, D.P., Harrington, C.D., and Aldrich, M.J., in press, Late Cenozoic rates of erosion in the western Española Basin, New Mexico--Evidence from geologic dating of erosion surfaces: Geological Society of America Bulletin.

Dorn, R.I., 1983, Cation-ratio dating--A new rock varnish age-determination technique: Quaternary Research, v. 20, p. 49-73.

Dorn, R.I., Bamforth, D.B., Cahill, T.A., Dohrenwend, J.C., Turrin, B.D., Donahue, D.J., Jull, A.J.T., Long, A., Macko, M.E., Weil, E.B., Whitley, D.S., and Zabel, T.H., 1986, Cation-ratio and accelerator radiocarbon dating of rock varnish on Mojave artifacts and landforms: Science, v. 231, p. 830-833.

Dohrenwend, J.C., Wells, S.G., and McFadden, L.D., 1986, Penrose conference report-Geomorphic and stratigraphic indicators of Neogene-Quaternary climatic change in arid and semiarid environments: Geology, v. 14, p.263-264.

Harrington, C.D., 1986a, The use of rock varnish as a Quaternary dating method within the central Rio Grande rift, New Mexico, and the Nevada Test Site: [abs.] Geological Society of America Abstracts with Programs, v. 18, p. 360.

_____ 1986b, Rock varnish dating--A new tool in the assessment of fault hazard potential: EOS [Transactions, American Geophysical Union], v. 67, p. 1211.

Harrington, C.D., and Dethier, D.P., 1987, Geomorphic and stratigraphic evidence for Quaternary displacement along the northern Pajarito fault system near Hernandez, New Mexico: [abs.] Geological Society of America Abstracts with Programs, v. 19, p. 281.

Harrington, C.D., and Whitney, J.W., in press, A scanning-electron microscope method for rock-varnish dating: Geology.

APPLICATIONS OF AMINOSTRATIGRAPHY, STRONTIUM-ISOTOPE STRATIGRAPHY, AND URANIUM-TREND DATING TO PALEOSEISMOLOGY AND NEOTECTONICS

by

Daniel R. Muhs
U.S. Geological Survey
Box 25046, MS 963, DFC
Denver, CO 80225

INTRODUCTION

Many of the world's coastlines are located in tectonically active regions. As a result, Quaternary marine deposits are commonly now found at elevations much higher than present sea level, indicating geologically recent tectonic uplift. The rate of uplift is a function of tectonic style; thus, if Quaternary coastal deposits can be accurately dated, it is possible to obtain uplift rates and infer tectonic style. In addition, many marine terraces are deformed over subjacent local structures. For example, shore-parallel profiles of many terraces document Quaternary warping over anticlines and synclines. Finally, terrace deposits are often displaced by faults. For paleoseismic and neotectonic studies, accurate ages of terraces are needed.

Often Quaternary coastal deposits contain fossils of marine organisms. Some organisms, such as corals and certain echinoids, incorporate small amounts of uranium (but little or no thorium) into their skeletal tissue during growth and the skeleton becomes a geochemically closed system after death. The same is true for certain inorganic marine carbonates, such as ooids (Muhs and others, 1987a). Such materials can be dated by the U-series methods $^{230}Th/^{234}U$, $^{234}U/^{238}U$, and $^{231}Pa/^{235}U$, but these techniques are normally limited to materials younger than about 350 ka. In addition, corals and ooids are rare in latitudes outside of the tropics. In higher latitudes, the most common marine fossils are mollusks and echinoids, but unfortunately, mollusks and most echinoids do not yield reliable U-series ages (Kaufman and others, 1971; Muhs and Kennedy, 1985). Thus, two techniques have emerged in recent years that allow use of fossil mollusks for relative age determination and correlation: amino acid geochronology and strontium isotope stratigraphy.

AMINOSTRATIGRAPHY

Amino acid geochronology is based on the observation that the protein of living organisms contains only amino acids of the L structural configuration. Upon death of an organism, amino acids of the L-configuration convert to amino acids of the D-configuration by a process called racemization. Racemization is a reversible reaction that results in increased D/L ratios in a fossil through time until a D/L equilibrium ratio (1.00 to 1.30, depending on the amino acid) is reached. Thus, in a simplified view, a higher D/L ratio in a fossil indicates a relatively greater age. Amino acid ratios do not increase linearly with time to an equilibrium D/L ratio, or in other words, do not follow simple, first-order reversible kinetics. Analyses of reasonably well-dated deep-sea cores indicate that the D/L ratios in foraminifera rapidly change in a linear fashion at first, followed by a much slower rate of change, with an uncertain area in between. Fossil mollusks are thought to follow a

similar pathway, though sufficient data to prove this relationship are lacking.

Several variables are known to affect amino acid racemization rates and observed ratios in fossils. The most important of these include temperature (both the mean annual temperature and the amplitude of the annual temperature cycle), genus of the organism, type of amino acid, and diagenetic processes (Wehmiller, 1982). Temperature history is probably the most critical variable because higher temperatures greatly increase racemization rates. Inasmuch as most areas have experienced climatic changes, it is often difficult to model temperature history accurately.

The simplest application of amino acid ratios in geochronological studies is relative age determination and lateral correlation (fig. 1) or what has been termed "aminostratigraphy" (Miller and Hare, 1980). The main assumption in this approach is that the localities studied have had similar temperature histories. Stratigraphic units that have mollusks clustering around a certain value can be identified as "aminozones" (Nelson, 1982). The method becomes more powerful if at least one of the mollusk-bearing units has coral dated by uranium-series methods. A refinement to this approach is possible on north-south trending coastlines that have had regional temperature gradients that have always been in the same direction (Kennedy and others, 1982; Wehmiller and Belknap, 1982). On such coastlines, one should expect to find systematically lower D/L ratios in deposits of the same age as one moves into higher (hence cooler) latitudes. In this approach, amino acid ratios are plotted as a function of latitude; proximal points with similar, but slightly different D/L ratios are connected into lines that define regional amino acid isochrons. Again, if one or more localities has numerical age control by ^{14}C or U-series dating, the overall chronology is better defined.

Numerical age estimates using amino acid ratios have been attempted by some workers. The usual approach uses one or more independently dated deposits as calibration points, and assumes either linear kinetics for racemization rates or, for mollusks, the kinetic pathways observed in foraminifera (Wehmiller and Belknap, 1978). Sometimes geologically reasonable ages are obtained by this approach, but serious inconsistencies have also resulted (Muhs, 1985). Probably there are still too few calibration points to define accurately a racemization pathway for mollusks.

Amino acid geochronology has proved very useful in developing relative chronologies for marine deposits on many coastlines. There are, however, a number of limitations to the technique. Because racemization rates are a function of genus, long-distance correlation is sometimes impossible because of the geographic limits of the range of a genus. Long distance correlation is also impeded by differing climatic histories among study areas. Finally, in warm regions, racemic equilibrium limits the useful time range of amino acid geochronology.

STRONTIUM-ISOTOPE STRATIGRAPHY

Potentially, many of the shortcomings of amino acid geochronology can be overcome in developing coastal stratigraphic frameworks by using a relatively new technique called strontium-isotope stratigraphy. Strontium is an alkaline earth metal that has geochemical properties similar to calcium; as a result, it occurs as a minor or trace element in marine organisms composed of $CaCO_3$. Strontium has four naturally-occuring isotopes (^{88}Sr, ^{87}Sr, ^{86}Sr, and ^{84}Sr), all of which are stable, but ^{87}Sr forms by decay of ^{87}Rb. Seawater has a mixture of all four isotopes, but at any given point in geologic time, the ratio of oceanic $^{87}Sr/^{86}Sr$ is a function of the ratio in waters delivered

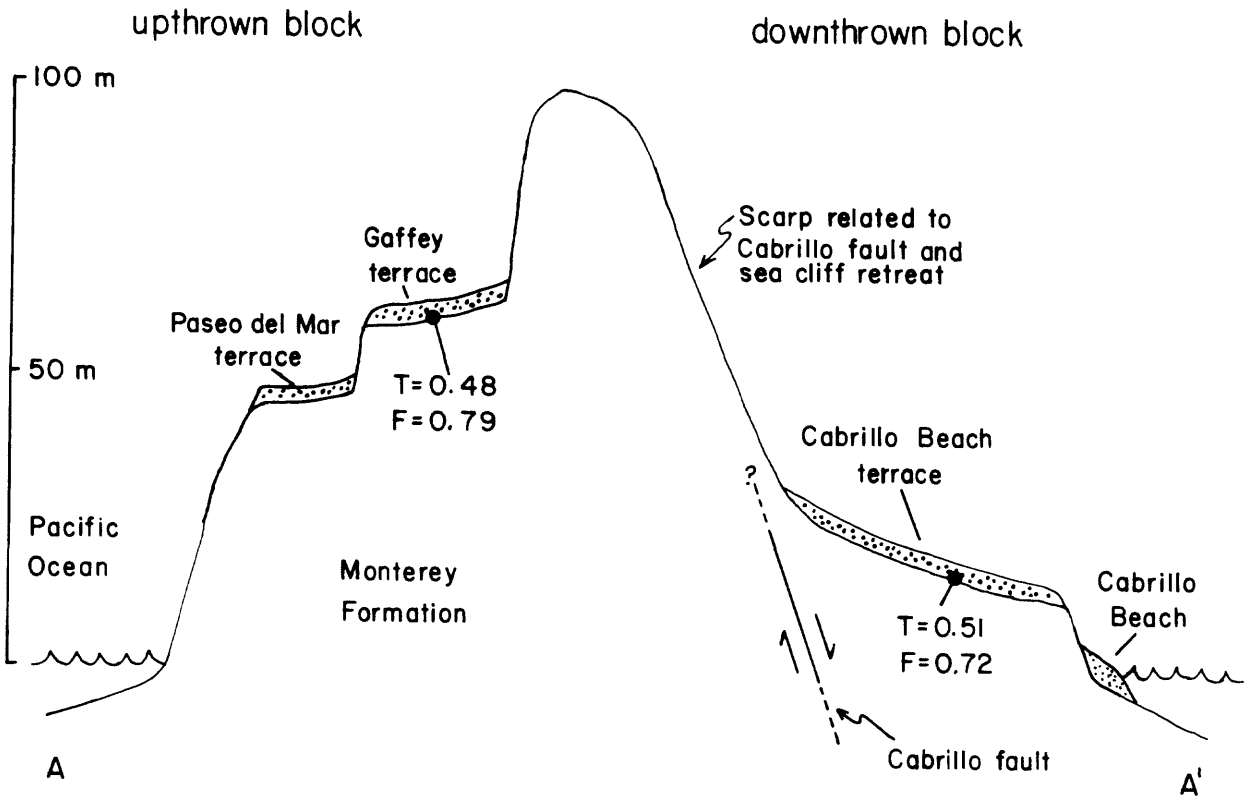

FIGURE 1.--Schematic geologic cross section of bedrock and marine terraces at Point Fermin, near San Pedro, Calif., showing correlation of the Gaffey terrace with the Cabrillo Beach terrace across the Cabrillo fault. Correlation of these two terraces is inferred despite elevation differences because of similar mollusk amino-acid ratios in the free (F) and total (T) extractions (unpublished data of D.R. Muhs).

to the world ocean from the continental crust (via chemical weathering and river systems) and the upper mantle (via mid-ocean ridges, submarine weathering of basalts, and chemical weathering of continental basalts) (Elderfield, 1986). The observation that there has been a relatively rapid, monotonic increase in the $^{87}Sr/^{86}Sr$ ratio in seawater since the early Oligocene (DePaolo and Ingram, 1985) is of most interest to Quaternary geologists. This increase has continued into the Quaternary and has now been roughly calibrated using paleomagnetically-dated deep-sea cores (Capo and DePaolo, 1986).

The basis of strontium-isotope stratigraphy is the fact that marine organisms incorporate Sr into their skeletal structures in isotopic equilibrium with seawater (DePaolo and Ingram, 1985). Thus, a numerical age estimate of a mollusk is possible by measuring the $^{87}Sr/^{86}Sr$ ratio and comparing it with one of the calibration curves. Because variations in this ratio during the Quaternary have been very small, high precision mass spectrometry is required. Error estimates for derived ages are a function not only of instrument precision, but also the slope of the $^{87}Sr/^{86}Sr$ seawater evolution curve. Thus, where the curve is steep as a function of time, age errors will be smaller. Strontium isotope stratigraphy has the advantages of being species-independent and temperature history-independent and can be applied over the entire Quaternary. Because of efficient mixing of the world ocean, one can correlate terraces literally around the world. The main disadvantage is that narrow resolution of ages is at present not possible. For example, one cannot distinguish fossils from the last interglacial (~120 ka) from the present.

Preliminary results from California marine-terrace mollusks suggest that strontium-isotope stratigraphy can be extremely useful in determining long-term Quater-nary uplift rates (Muhs and others, 1987b). On San Nicolas Island, the 2nd, 4th, 5th, and 10th terraces can be clearly distinguished from one another on the basis of $^{87}Sr/^{86}Sr$ ratios, and indicate an uplift rate of ~0.20 m/ka over the last million years. In contrast, $^{87}Sr/^{86}Sr$ ratios in mollusks from the Palos Verdes Hills terraces indicate a higher uplift rate of ~0.34-0.39 m/ka.

URANIUM-TREND DATING

Many marine and continental deposits of Quaternary age cannot be dated by conventional methods either because of a lack of suitable materials or because the deposits are beyond the age range of the methods. Alluvium, colluvium, and glacial till of middle or early Quaternary age commonly fall into this category. Yet, such deposits may be displaced by faults and thus are of interest in paleoseismic or neotectonic studies if ages can be obtained. This need has stimulated the development of a new technique called uranium-trend dating.

Over the past few years, investigators at the U.S. Geological Survey have been studying the migration of uranium and its daughter products through Quaternary soils and sediments (Rosholt, 1985; Rosholt and others, 1985a). Sediments and soils are penetrated continuously or episodically by ground waters or soil waters that contain at least small amounts of dissolved uranium, some of which may include locally leached uranium. As this uranium decays, it leaves a trail of long-lived daughter products (^{234}U and ^{230}Th) adsorbed on solids in the matrix such as silt, clay, and organic matter. Uranium-trend dating is a calibrated method whereby the time-dependent nature of this decay-product trail can be used to determine the age of the host sediment or soil. U-trend dating is calibrated by examination of the distribution of uranium and its daughters in independently dated (by ^{14}C or K/Ar

methods) deposits. This calibrated empirical model is used because there are too many geochemical variables involved to allow the development of a rigorous mathematical model for uranium migration.

Uranium-trend dating has been applied to a wide variety of Quaternary deposits, including alluvium, loess, glacial till, emergent marine sediments, colluvium, and zeolitized volcanic ash. The main requirements are that (1) the sediment has had at least some water movement through it, (2) the sediment contains at least some materials capable of adsorbing daughter products of uranium, and (3) sufficient textural or chemical variation exists in the sediment column such that different amounts of daughter-product adsorption will occur as uranium migrates downward. Some Quaternary sediments do not meet these requirements; examples include well-sorted dune sands (little material capable of adsorbing daughter products and little textural variation with depth), and deposits that are deeply buried or in hyperarid environments (little or no history of water movement in the sediment). We have also found that clay-rich soils in humid tropical environments are not suitable for U-trend dating because such soils experience so much daughter-product adsorption that they cannot be accommodated by the present U-trend model.

For U-trend dating, sediment samples are taken as a function of depth and/or soil horizon; usually 5 to 8 samples are sufficient. The sediment or soil samples are decomposed using HF and HNO_3, and the activities of ^{238}U, ^{234}U, ^{230}Th, and ^{232}Th are measured by alpha spectrometry. The results are plotted as isotopic activity ratios that express the excess or deficiency of ^{230}Th over ^{238}U on one axis and the excess or deficiency of ^{234}U over ^{238}U on the other axis. The slope of a best-fit line drawn through the array of points is a function of the age of the deposit. A poorly fitting line indicates that the sediment or soil does not meet the assumptions of the U-trend model, which may be caused by multiple ages of the sediment, the deposit acting as a closed system, or geologically recent additions of uranium-rich water (Muhs and others, 1988).

The most reliable ages of deposits for U-trend dating appear to be in the range of 60 ka to 600 ka, although theoretically the method can be used for deposits as young as 10 ka and as old as 800 ka (Rosholt, 1985). Errors on age estimates (1σ) in the 60-600 ka range are at best ±10 percent, but deposits less than 20 ka have errors of about ±100 percent, and deposits greater than 600 ka have errors greater than ±20 percent.

U-trend dating has been tested in a number of areas where there is either good geologic control or independent age estimates from other dating methods. Good results have been obtained for alluvium in the Nevada Test Site region (Rosholt and others, 1985b), southern New Mexico (J. N. Rosholt and others, unpub. data); the Grand Canyon (Rosholt and others, 1986; Machette and others, 1986), Fisher Valley, Utah (Colman and others, 1986), and the San Joaquin Valley, California; (J. N. Rosholt and others, unpub. data). Glacial deposits in the Rocky Mountains have also yielded U-trend ages that agree with independent geologic or pedologic data (Rosholt and others, 1985a). U-trend ages of marine deposits on both the east and west coasts of the United States agree with independent age estimates based on conventional U-series ages on coral or amino acid analyses of shell (Rosholt and Szabo, 1982; Muhs and Rosholt, 1984). U-trend ages of marine terraces on the Palos Verdes Hills and San Nicolas Island, Calif., suggest relatively constant long-term rates of uplift (fig. 2); these rates are in agreement with those derived from strontium-isotope ages. Many types of Quaternary deposits have yet to be tested for U-trend dating, including loess, continental glacial till, lacustrine deposits, and eolian sand with imbedded eolian silt and clay. Of

most interest to paleoseismologists are the positive results obtained on alluvium because such deposits are often faulted, and marine-terrace deposits, because they can be used to calculate coastal uplift rates.

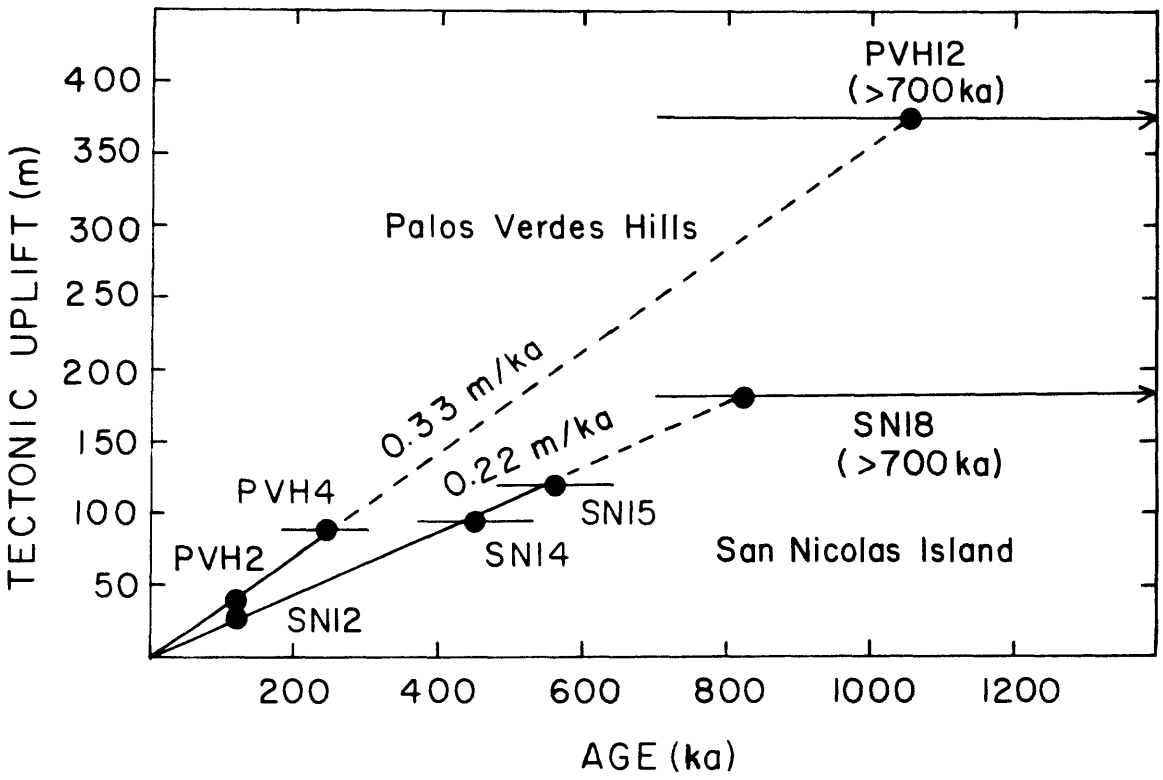

FIGURE 2.--Marine-terace elevations (corrected with sea-level curves to yield tectonic uplift) plotted as functions of uranium-series, amino-acid, or uranium-trend age estimates for San Nicolas Island and the Palos Verdes Hills, Calif.. (from Muhs and others, 1988).

REFERENCES CITED

Capo, R. C., and DePaolo, D. J., 1986, Pleistocene seawater Sr-isotope variation and applications to chronostratigraphy and paleoceanography: Terra Cognita, v. 6, p. 115.

Colman, S. M., Choquette, A. F., Rosholt, J. N., Miller, G. H., and Huntley, D. J., 1986, Dating the upper Cenozoic sediments in Fisher Valley, southeastern Utah: Geological Society of America Bulletin, v. 97, p. 1422-1431.

DePaolo, D. J., and Ingram, B. L., 1985, High-resolution strontium isotope stratigraphy: Science, v. 227, p. 938-941.

Elderfield, H., 1986, Strontium isotope stratigraphy: Palaeogeography, Palaeoclimatology, Palaeoecology, v. 57, p. 71-90.

Kaufman, A., Broecker, W. S., Ku, T. L., and Thurber, D. L., 1971, The status of U-series methods of mollusk dating: Geochimica et Cosmochemica Acta, v. 35, p. 1155-1183.

Kennedy, G. L., Lajoie, K. R., and Wehmiller, J. F., 1982, Aminostratigraphy and faunal correlations of late Quaternary marine terraces, Pacific coast, USA: Nature, v. 299, p. 545-547).

Miller, G. H. and Hare, P. E., 1980, Amino acid geochronology--Integrity of the carbonate matrix and potential of molluscan fossils, in Hare, P. E., Hoering, T. C., and King, K., Jr., eds., Biogeochemistry of Amino Acids: New York, John Wiley and Sons, p. 415-443.

Machette, M. N., Rosholt, J. N., and Bush, C. A., 1986, Uranium-trend ages of Quaternary deposits along the Colorado River, Grand Canyon National Park, Arizona: Geological Society of America Abstracts with Programs, v. 18, no. 5, p. 393.

Muhs, D. R., 1985, Amino acid age estimates of marine terraces and sea levels on San Nicolas Island, California: Geology, v. 13, p. 58-61.

Muhs, D. R., and Rosholt, J. N., 1984, Ages of marine terraces on the Palos Verdes Hills, California, by amino acid and uranium-trend dating: Geological Society of America Abstracts with Programs, v. 16, no. 6, p. 603.

Muhs, D. R. and Kennedy, G. L., 1985, An evaluation of uranium-series dating of fossil echinoids from southern California Pleistocene marine terraces: Marine Geology, v. 69, p. 187-193.

Muhs, D. R., Bush, C. A., and Rowland, T. R., 1987a, Uranium-series age determinations of Quaternary eolianites and implications for sea-level history, New Providence Island, Bahamas: Geological Society of America Abstracts with Programs, v. 19, no. 7, p. 780.

Muhs, D. R., Ludwig, K. R., and Simmons, K. R., 1987, Strontium isotope stratigraphy of California marine terraces and tectonic significance: EOS, Transactions, American Geophysical Union, v. 68, p. 459.

Muhs, D. R., Rosholt, J. N., and Bush, C. A., 1988, Uranium-trend dating of southern California marine terrace deposits, in Brigham-Grette, J. K. and Rutter, N. W., eds., Applied Aspects of Quaternary Geochronology: Quaternary Science Reviews, in press.

Nelson, A. R., 1982, Aminostratigraphy of Quaternary marine and glaciomarine sediments, Qivitu Peninsula, Baffin Island: Canadian Journal of Earth Sciences, v. 19, p. 945-961.

Rosholt, J. N., 1985, Uranium-trend systematics for dating Quaternary sediments: U.S. Geological Survey Open-File Report 85-298, 48 p.

Rosholt, J. N., and Szabo, B. J., 1982, Comparison of uranium-series dating of coral and uranium-trend dating of coral-bearing terraces on the U.S.

Atlantic coastal plain: Geological Society of America Abstracts with Programs, v. 14, no. 7, p. 603.

Rosholt, J. N., Bush, C. A., Shroba, R. R., Pierce, K. L., and Richmond, G. L., 1985a, Uranium-trend dating and calibrations for Quaternary sediments: U.S. Geological Survey Open-File Report 85-299, 48 p.

Rosholt, J. N., Bush, C. A., Carr, W. J., Hoover, D. L., Swadley, WC, and Dooley, J. R., Jr., 1985b, Uranium-trend dating of Quaternary deposits in the Nevada Test Site area, Nevada and California: U.S. Geological Survey Open-File Report 85-540, 72 p.

Rosholt, J. N., Downs, W. R., and O'Malley, P. A., 1986, Uranium-trend ages of surficial deposits in the central Grand Canyon National Park, Arizona: Geological Society of America Abstracts with Programs, v. 18, no. 5, p. 408.

Wehmiller, J. F., 1982, A review of amino acid racemization studies in Quaternary mollusks--Stratigraphic and chronologic applications in coastal and interglacial sites, Pacific and Atlantic coasts, United States, United Kingdom, Baffin Island, and tropical islands: Quaternary Science Reviews, v. 1, p. 83-120.

Wehmiller, J. F., and Belknap, D. F., 1978, Alternative models for the interpretation of amino acid enantiomeric ratios in Pleistocene mollusks: Examples from California, Washington, and Florida: Quaternary Research, v. 9, p. 330-348.

_____ 1982, Amino acid age estimates, Quaternary Atlantic Coastal Plain--Comparison with U-series dates, biostratigraphy, and paleomagnetic control: Quaternary Reserach, v. 8, p. 311-336.

THE APPLICATION OF FISSION-TRACK DATING TO PALEOSEISMOLOGY

by

Charles W. Naeser

USGS, Denver, Co.

Fission-track dating of minerals in a rock can provide information on the thermal and tectonic history of that rock. A fission track is a cylindrical zone of intense damage formed when a fission fragment passes through a solid. When an atom of ^{238}U fissions, the nucleus breaks up into two lighter nuclei, one averaging about 90 atomic mass units (a. m. u.) and the other about 135 a. m. u., with the liberation of about 170 MeV of energy. The two highly charged nuclei recoil in opposite directions and disrupt the electron balance of the atoms along their path in the mineral lattice or glass. This disruption causes the positively charged ions in the lattice to repulse each other and force themselves into the crystal lattice, forming the track or damage zone (Fleischer and others, 1975). The new track is tens of angstroms in diameter and about 10-20 μm in length.

A track in its natural state can only be observed with a transmission electron microscope; however, a suitable chemical etchant can enlarge the damage zone such that it can be observed with an optical microscope at intermediate magnifications (x200-500). Common etchants used to develop tracks include nitric acid (apatite), hydrofluoric acid (mica and glass), concentrated basic solutions (sphene), and alkali fluxes (zircon) (Fleischer and others, 1975; Gleadow and others, 1976). Because ^{238}U fissions spontaneously at a constant rate, fission tracks can therefore be used to date geological materials. Early development of the method has been reviewed by Fleischer and others (1975) and Naeser (1979). The age of a mineral or glass can be calculated from the concentration of uranium and the number of spontaneous fission tracks that it contains. The relative abundance of ^{238}U and ^{235}U is constant in nature, and thus the easiest and most accurate way to determine the amount of uranium present in the area counted is to create a new set of fission tracks by irradiating the sample in a nuclear reactor to induce fission of ^{235}U with a known dose of thermal neutrons. The reader is referred to Naeser and Naeser (1984) for a more detailed discussion of the theory and procedures of the method.

Heating can cause partial to complete fading of the spontaneous tracks. Fission tracks are stable in most nonopaque minerals (opaque minerals do not retain tracks) at temperatures of 50 °C or less. If a mineral is heated above a critical temperature and held there for a period of time, the fission tracks will begin to disappear (anneal). If the mineral is held at that temperature for a sufficiently long time the tracks will completely disappear. The process of annealing is a time-temperature function (Fleischer and others, 1965); a

short time at a high temperature will have the same effect on the fission tracks as a long time at a low temperature. As long as a mineral remains above its annealing temperature it will not retain fission tracks. When this mineral is cooled to temperatures below which annealing can take place the mineral will again begin to accumulate tracks. Therefore, if an apatite or zircon were buried to a depth in the crust where the temperature is sufficient to cause total track annealing, it would have a "0" apparent date. Figure 1 shows the apparent ages of apatite as a function of temperature (depth) in the crust at the time of maximum heating (burial). There is a temperature zone where tracks are only paritally annealed. This is called the partial annealing zone (PAZ). The apparent dates determined on minerals that have resided within the PAZ will never yield a geologically meaningful date. The measured "date" is intermediate between the primary age and the uplift/cooling age. If the rocks containing the apatite age profile in figure 1 were uplifted and cooled, a new fission-track age profile (fig. 2) will develop. The inflection points on the new curve are very diagnostic. The ages from the old total annealing zone yield information about the timing and rate of cooling during uplift and erosion. The date at the inflection point (a, on fig. 2) is the time that the latest cycle of uplift and erosion started.

The annealing temperature of fission tracks in apatite are well known from many laboratory studies and from apatites recovered and dated from deep drill holes where the present temperature is known and the geologic history can be reasonably well established (Naeser, 1979, 1981). Apatite will loose all of its tracks at 105 °C in $\approx 10^8$ yr or at 150 °C in $\approx 10^5$ yr. Thus a fission-track age on apatite records the time when the crystal cooled below 125 °C ± 20 °C for most geologic events.

The annealing temperatures of fission tracks in zircon under geological conditions are not very well known. Limited data suggest that temperatures between ≈160 °C (Naeser, unpublished data) and ≈ 230°C (Hurford, 1986) will completely anneal fission tracks in zircon over periods of time in excess of several million years. The lower value of ≈160 °C was determined from rocks that had undergone very slow cooling in a metamorphic complex in Alaska, while the higher value of ≈230 °C is based upon data from the Alps of Switzerland where the cooling rates are much higher. A zircon fission-track date therefore represents the cooling of the rock below ≈ 200 ° C.

There are three possible applications of fission-track dating to paleoseismology. First, by dating the same mineral species on either side of a fault it is possible to determine the relative movement on that fault (Zimmermann, 1980). Second, if a volcanic ash is displaced by a fault a fission-track age on zircon separated from the ash will place a maximum age on the fault (Naeser and others, 1980). Third, fission-track dating of apatite and zircon from a mountain range can be used to establish an overall cooling rate for the mountain range. This cooling rate is usually related to uplift and erosion.

Zimmermann (1980), in a study of apatite fission-track ages in the Eastern United States, showed that apatite separated from basement rocks on either side of the Fall Line had different apparent fission-track ages. The apatite from the west side of the fall line was always younger than apatite from the east side. This indicates that the Fall Line is a possible fault and that the west side of this feature is up relative to the east.

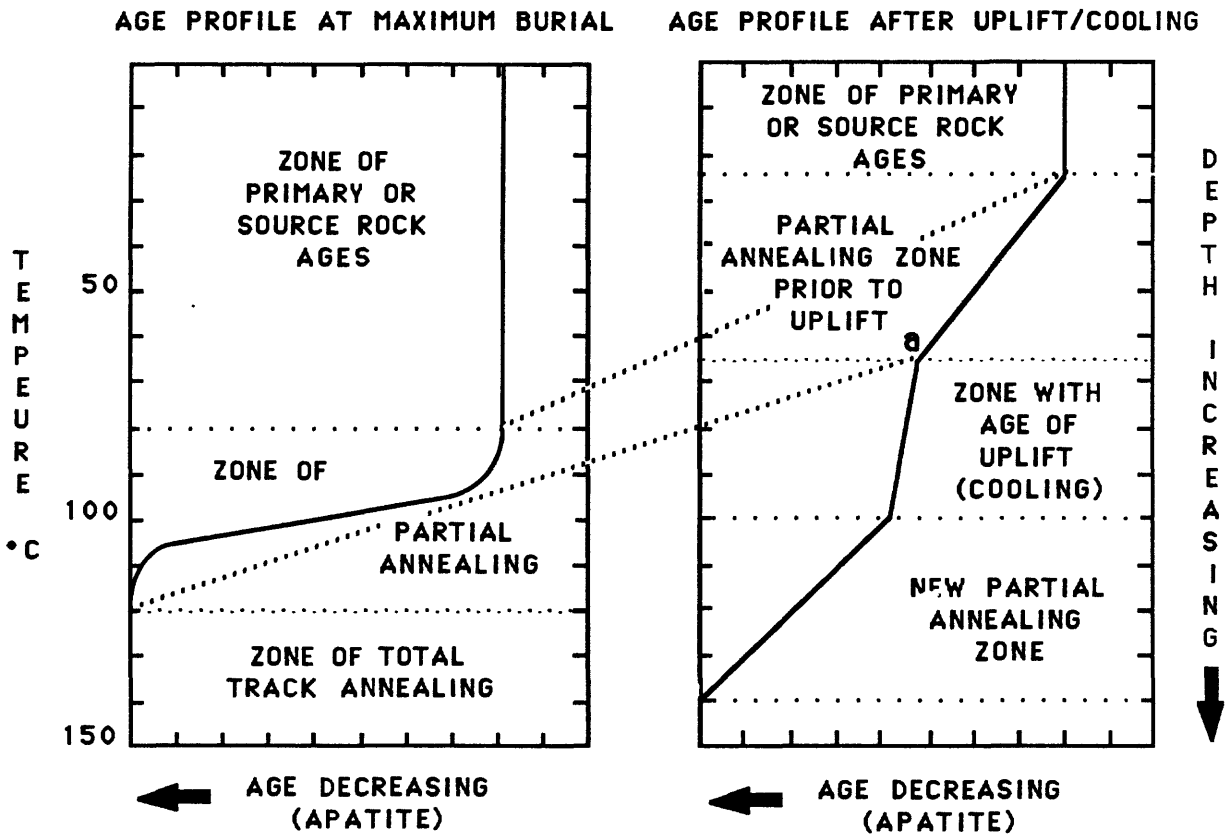

Figure 1. The change of the apatite fission-track age with increasing depth (temperature) at the time of maximum burial (heating).

Figure 2. The age profile of apatite as a function of depth after a period of cooling, usually related to uplift and erosion.

By dating zircons separated from the Mangaroa Ash at several localities near Wellington, New Zealand, Naeser and others (1980) were able to establish that there has been ≈ 266 m of uplift on the northwest side of the Wellington Fault in the last 380,000 yr.

Many studies have used fission-track dates to determine the uplift/cooling history of a mountain range. Examples of this include Naeser and others (1983) and Zeitler and others (1982). Naeser and others (1983) dated apatite from the Farmington Canyon Complex in the Wasatch Mountains of Utah, and found that apatite from these Precambrian rocks yielded fission-track dates as low as ≈ 5 Ma from rocks collected at the base of the range front near the Wasatch fault. The apparent dates of the apatite became older with increased elevation of the samples. Thus, 5 m. y. ago the apatite now at the surface was at a temperature of about 125 °C (a depth of about 3.5 km). Thus, there has been about 3.5 km of uplift on the Wasatch Mountains in the last 5 Ma. A change in the slope of the age versus elevation profile at ≈ 10 Ma which indicatates the initiation of the most recent period of uplift and erosion. Zeitler and others (1982) showed that the area around Nanga Parbat

in northeastern Pakistan is currently being uplifted at a rate of 5 to 10 km per million years. This is based upon fission-track dates of ≈ 1.5 Ma on zircon and ≈ 0.4 Ma on apatite from Precambrian rocks collected along the Indus River where it cuts across the Nanga Parbat massif.

Fission-track dating can be useful as an indicator of the presence of a fault and the relative movement on that fault as well as providing information on long-term tectonic processes.

REFERENCES

Fleischer, R. L., Price, P. B., and Walker, R. M., 1965, Effects of temperature, pressure, and ionization on the formation and stability of fission tracks in minerals and glasses: Journal of Geophysical Research, v. 70, no. 6, p. 1497-1502.

Fleischer, R. L., Price, P. B., and Walker, R. M., 1975, Nuclear tracks in solids--Principles and applications: Berkeley, California, University of California Press, 605 p.

Gleadow, A. J. W., Hurford, A. J., and Quaife, R. D., 1976, Fission track dating of zircon--Improved etching techniques: Earth and Planetary Science Letters, v. 33, p. 273-276.

Hurford, A. J., 1986, Cooling and uplift patterns in the Lepontine Alps, South Central Switzerland and an age of vertical movement on the Insubric fault line: Contributions to Mineralogy and Petrology, v. 92, p. 413-427.

Naeser, C. W., 1979, Fission-track dating and geologic annealing of fission tracks, in Jäger, E., and Hunziker, J. C., eds., Lectures in isotope geology: New York, Springer-Verlag, p. 154-169.

Naeser, C. W., 1981, The fading of fission tracks in the geologic environment--data from deep drill holes: Nuclear Tracks, v. 5, p. 248-250.

Naeser, C. W., Bryant, Bruce, Crittenden, Jr., M. D., and Sorensen, M. L., 1983, Fission-track ages of apatite in the Wasatch Mountains, Utah--An uplift study: Geological Society of America Memoir 157., p. 29-37.

Naeser, C. W., Nishimura, S., and Te Punga, M. T., 1980, Fission-track age of the Mangaroa Ash and tectonic implications at Wellington, New Zealand: New Zealand Journal of Geology and Geophysics, v. 23, p. 615-621.

Naeser, N. D., and Naeser, C. W., 1984, Fission-track dating, in Mahaney, W. C., ed., Quaternary dating dethods: Amsterdam, Elsevier, p. 87-100.

Zeitler, P. K., Johnson, N. M., Naeser, C. W., and Tahirkheli, R. A. K., 1982, Fission track evidence for Quaternary uplift of the Nanga Parbat region, Pakistan: Nature, v. 298, p. 255-257.

Zimmermann, R. A., 1980, Patterns of post-Triassic uplift and inferred Fall Zone faulting in the eastern United States: Geological Society of America Abstracts with Programs, v. 12, no. 7, p. 554.

THE APPLICATION OF PALEOMAGNETISM TO THE DATING OF QUATERNARY MATERIALS

by

Kenneth L. Verosub

Department of Geology
University of California
Davis, California 95616

ABSTRACT

There are two applications of paleomagnetism to the dating of Quaternary materials for paleoseismological studies; namely, magnetostratigraphy and secular-variation dating. Magnetostratigraphy is based on the pattern of normal- and reversed- polarity intervals and can provide a broad chronologic framework for a paleoseismological study. Secular-variation dating is based on the pattern of changes in inclination and declination which occur during a given polarity interval. Under favorable circumstances, secular variation dating can be used to date materials with a resolution of 100-200 yrs.

INTRODUCTION

One of the primary applications of paleomagnetism to geologic studies has been in the area of dating. Long before the discovery of the existence of reversals of the Earth's magnetic field, paleomagnetists proposed that the paleomagnetic record of geomagnetic secular variation could be used for the dating of various materials (Johnson and others, 1948). However, the acquisition of reproducible records of secular variation proved to be quite difficult, and correlation to the pattern of normal- and reversed-polarity intervals, rather than to the pattern of geomagnetic secular variation, came to be the predominant method of paleomagnetic dating. In recent years, however, paleomagnetists have succeeded in obtaining records of geomagnetic secular variation which can be used for high-resolution dating. This paper deals with the applications of both of these approaches to paleoseismological studies. A general discussion of paleomagnetic techniques and procedures can be found in Verosub (1986).

DATING METHODS

Magnetostratigraphy

Magnetostratigraphy is based on the pattern of reversals of the Earth's magnetic field. In the Northern Hemisphere, the present or normal field configuration corresponds to a northward declination and a downward inclination, whereas the opposite or reversed configuration has southward

declinations and upward inclinations. Thus the determination of the polarity of a given sample is relatively simple and usually unambiguous. Indeed, it is possible to do magnetostratigraphic studies with crudely oriented hand samples although fully oriented samples are preferred.

The detailed pattern of the reversals, known as the Magnetic Polarity Time Scale, is now well-established (Harland and others, 1982). The last interval of reversed polarity ended about 730,000 yrs ago so the simplest paleomagnetic method of Quaternary dating involves determination of the polarity of one or more samples from an outcrop of unknown age. If the samples show a reversed polarity, the site must be older than 730,000 yrs old. If the samples show only normal polarity, nothing definite can be said about the age because one does not know to which normal-polarity interval the samples should be assigned. However, if a stratigraphically higher site is of reversed polarity, the normal site must be older than 900,000 yrs which corresponds to the beginning of the last reversed-polarity interval. These possibilities are summarized in figure 1. Although this type of dating does not have high precision, it does represent an important research tool. One common definition of an active fault is that it is one which has shown repeated movement in the last 500,000 yrs. If it can be shown that material of reversed polarity has not been displaced by a fault, the fault is, by definition, inactive. In several cases, glacial deposits which were believed to be younger than 100,000 yrs old have been shown to be of reversed polarity, leading to a substantial revision of the Quaternary stratigraphy of the areas involved (Easterbrook and others, 1981; Stoker and others, 1983; Vincent and others, 1984). None of these glacial deposits was offset by faults, but if it had been, the paleomagnetic result would have had a major impact on the paleoseismological conclusions.

An alternate use of magnetostratigraphy is to determine the actual age of materials rather than their minimum age. To do this, it is necessary to have a continuous sequence of material which spans several polarity intervals. The minimum amount of time involved must be several hundred thousand to a million years, and the sampling horizons must be spaced close enough that there will be several horizons in each of the polarity intervals. Obviously, if little is known about the time span, the initial sampling may not be optimal, and one must plan to return for a second or even a third sampling in order to obtain the necessary resolution.

Analysis of the polarity of the samples leads to the development of a magnetic polarity zonation for the sequence being studied. The problem then is to correlate that zonation to the Magnetic Polarity Time Scale (fig. 2). If the youngest material is known to be younger than 730,000 yrs and if the rate of accumulation of material has been continuous on the scale of tens of thousands of years, one can simply count back the requisite number of polarity intervals.

If the youngest material is not necessarily younger than 730,000 yrs, one can assume that the accumulation rate has been uniform, and one can look for a segment of the Magnetic Polarity Time Scale which shows the same pattern of polarity intervals as the magnetic polarity zonation. The problem with this approach is that the accumulation rate is often not uniform, and the assumption that it is can produce an erroneous correlation. The preferred approach is to use independent data to determine the age of one horizon within

MAGNETOSTRATIGRAPHIC DATING

POLARITY	AGE DETERMINATION
Normal	none
Reversed	>730,000 yrs
Normal under reversed	>900,000 yrs

FIGURE 1.--Summary of the use of magnetostratigraphy to provide a broad chronologic framework for paleoseismological studies.

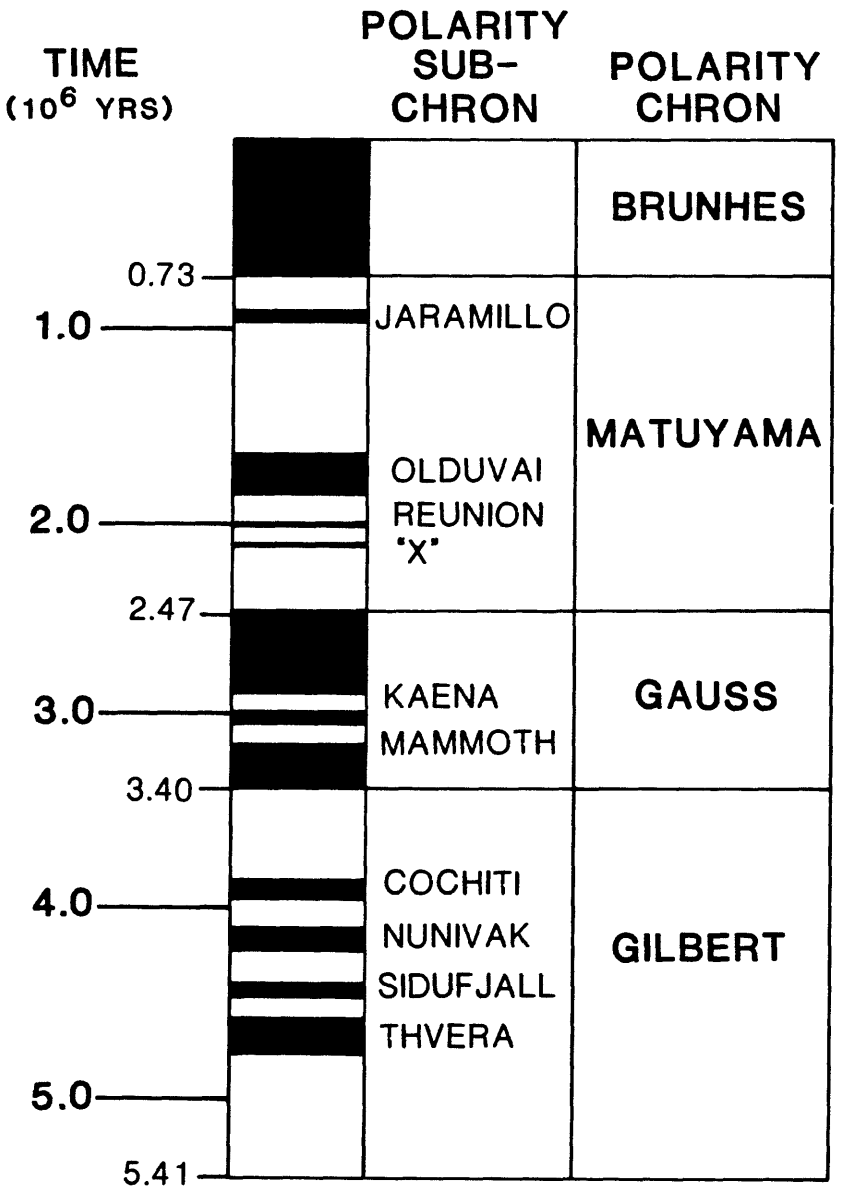

FIGURE 2.--Magnetic Polarity Time Scale for the last 5.4 m.y. The black intervals are normal polarity; the white intervals are reversed polarity.

the sequence. Such information might be obtained from biostratigraphy, tephrochronology, or radiometric dating. In any case, the single date allows one to identify a particular polarity interval, and then the boundaries of overlying and underlying polarity intervals can be used to provide additional high-precision ages. In this way, the two approaches are supplementary. The single age datum provides no information about the duration of a sequence, whereas the magnetic polarity zonation provides detailed information about the duration of a sequence, once a single fixed point is determined.

Secular Variation

In contrast to magnetostratigraphy which deals with time intervals on the order of hundreds of thousands to millions of years, secular variation dating deals with time intervals on the order of a few hundred to a few thousand years. At mid-latitudes in the Northern Hemisphere, the secular variation of the Earth's magnetic field produces changes in the magnetic inclination and declination which are on the order of 20° and 40°, respectively. The time scale over which these changes occur is several hundred years, and the changes are coherent over distances of several hundred to a few thousand kilometers. The simplest application of secular variation to the dating of Quaternary materials is to compare the characteristic paleomagnetic directions associated with two isolated features at a single site or at nearby sites. Such features might be lava flows, thin tephra layers, sandblows, or hearths at archaeological sites. The characteristic direction for each feature is usually the mean direction of 4-10 fully-oriented samples. If the two directions are substantially different, the two sites are probably separated in time by at least several hundred years. However, if the directions are similar, one cannot necessarily conclude that the two features are contemporaneous. The reason why the features may still be of different ages is that a given direction can occur repeatedly over a period of several thousand years. Furthermore, in making these comparisons, it is important to realize that different materials acquire their remanent magnetization through different physical mechanisms and that some of these mechanisms are less accurate than others in recording the ambient geomagnetic field direction (Verosub, 1977). Thus, the comparison between directions is most reliable when the same types of features are involved.

The actual dating of Quaternary materials using secular variation requires the existence of a master curve of secular variation for the region of interest. The master curves are derived from continuous paleomagnetic records which can be obtained by coring small lakes in stable geologic environments. The so-called "second generation" paleomagnetic studies which yield reproducible secular-variation records from these lakes are usually characterized by careful attention to coring procedures, good stratigraphic control, a firm chronologic framework, replicate paleomagnetic sampling, and auxiliary rock magnetic studies (Creer and Tucholka, 1983). Master curves for the Holocene have now been developed for Western and east-central North America (Verosub and others, 1986; Lund and Banerjee, 1985; Creer and Tucholka, 1982a), Europe (Turner and Thompson, 1981; Creer and Tucholka, 1982b), Australia (Barton and McElhinny, 1981; Constable and McElhinny, 1985), and southern South America (Creer and others, 1983). A typical master curve, that from Fish Lake in Harney County, Oreg., is shown in figure 3 (Verosub and others, 1986).

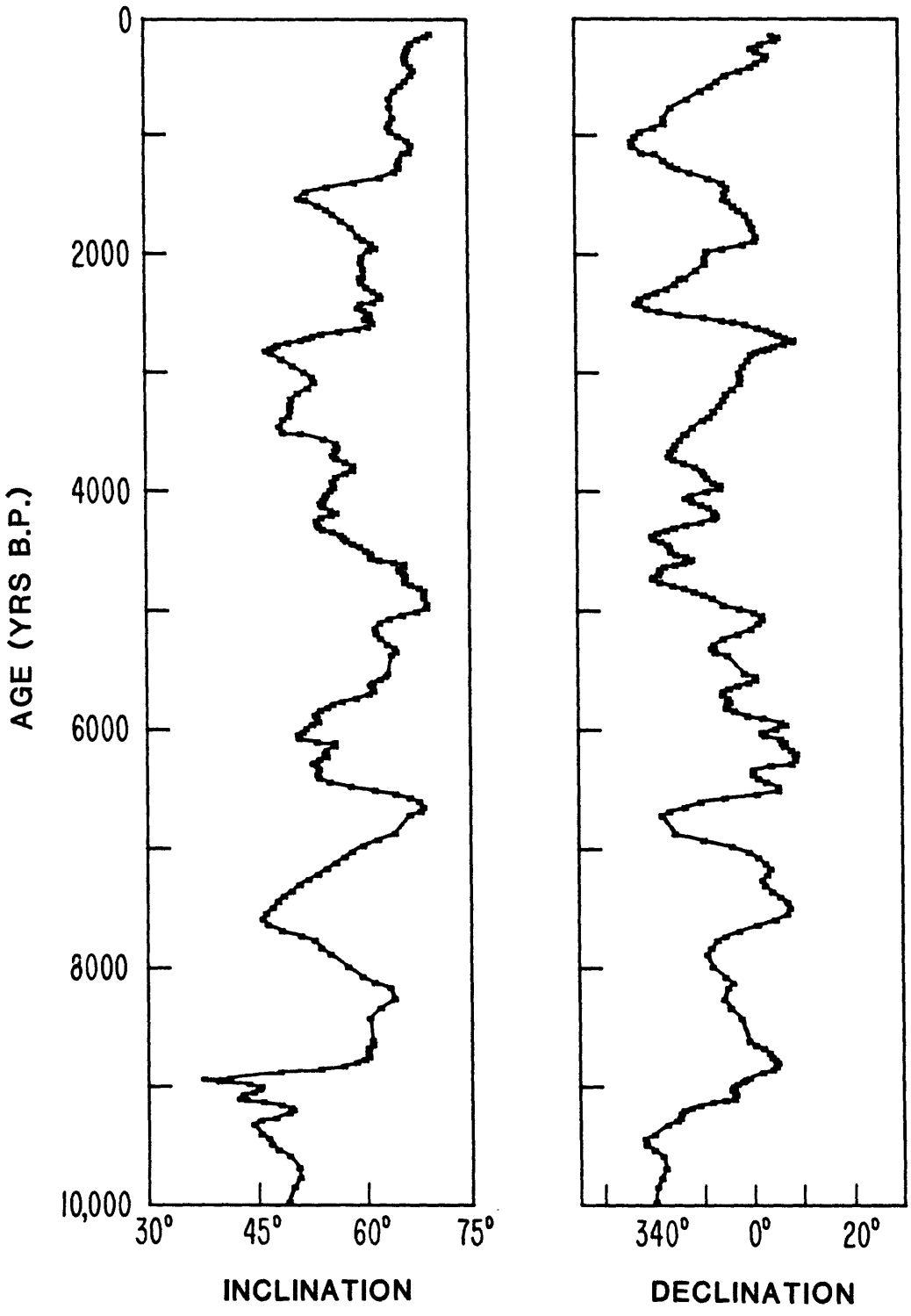

FIGURE 3.--Ten thousand years of secular variation as seen at Fish Lake, Harney County, Oreg. This record is proposed as a master curve for Holocene secular variation in western North America.

The dating of materials using a master curve involves the correlation of the paleomagnetic record of the undated site with the master curve. It is often convenient to represent the master curve as a plot of the declination versus the inclination, with time as an implicit parameter. Typically what is plotted on the inclination axis is the difference between a given inclination and the mean inclination at the site. Such a graph is called a Bauer plot (Bauer, 1896). Figure 4 shows the Bauer plots for 2,500-yr intervals corresponding to the master curve in figure 3.

The resolution which can be obtained by using a master curve for dating depends on the nature of the paleomagnetic record of the undated material and on the nonpaleomagnetic age constraints which might be associated with the material. The Bauer plots in figure 4 show that even in an interval of a few thousand years, a given paleomagnetic direction may occur more than once. Therefore, if the undated material yields only an isolated paleomagnetic direction and if other information can only constrain the age to an interval of a few thousand years, it is unlikely that paleomagnetic dating will be able to improve on the age determination. On the other hand if the age can be restricted to an interval of several hundred years and if the morphology of the master curve is favorable, the uncertainty in the age of the material may be reduced to 100 or 200 yrs. This is particularly true if the isolated direction falls near a point where the Bauer plot has a sharp bend or where the paleomagnetic directions are changing very rapidly. Resolution greater than 100 yrs is unlikely because of the inherent errors in the paleomagnetic recording process.

If the undated material represents a span of time and a sequence of paleomagnetic directions can be obtained, different limitation apply to the dating. In this case the correlation will depend on the recognition that a specific feature in the master curve corresponds to the paleomagnetic record from the undated material. The sequence of directions from the undated site must represent a time span of at least several hundred years. However, if all that is known is that the sequence is Holocene in age, it is again unlikely that an unambiguous correlation will be possible. If the age of the sequence can be estimated to within a few thousand years and if the paleomagnetic record of the undated material contains some distinct feature which is found in the corresponding part of the master curve, dating with a resolution of one or two hundred years is possible. The improvements in resolution which are possible with secular variation dating are summarized in figure 5.

Geomagnetic Excursions

It has also been suggested that the large-scale, short-term directional changes known as geomagnetic excursions can be used at the present time for dating purposes. These excursions have proven difficult to find and to verify (Negrini and others, 1984), and the paleomagnetic literature contains many proposed geomagnetic excursions which have not been confirmed by studies at other sites (Verosub, 1982). Until the existence, age, extent, and nature of geomagnetic excursions are fully understood, it is not appropriate to attempt to use them as time-stratigraphic horizons.

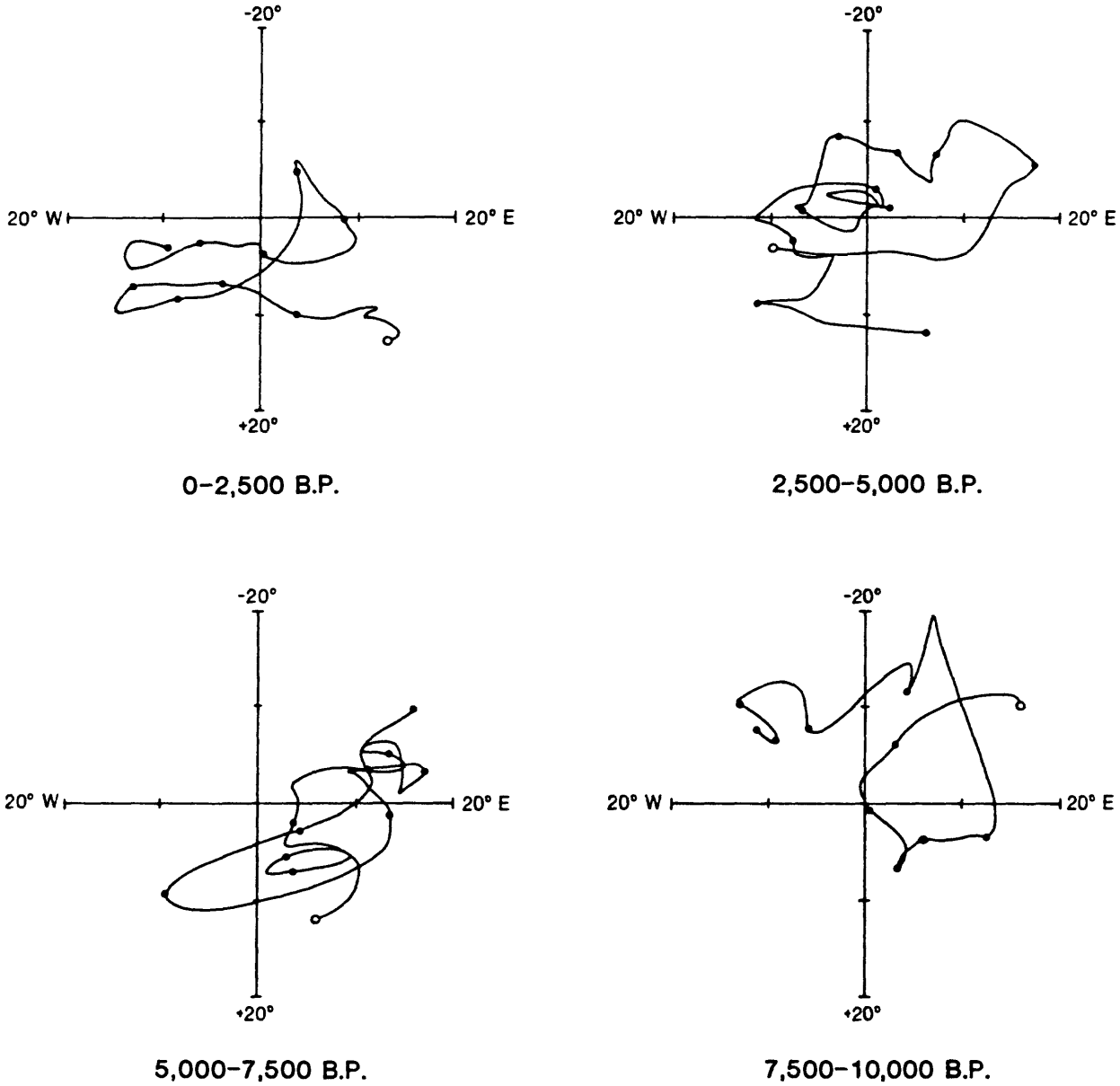

FIGURE 4.--Bauer plots corresponding to 2,500 segments of figure 3. Declination is plotted on the horizontal axis. The difference between the measured inclination and the mean inclination is plotted on the vertical axis. A positive value on the inclination axis indicates that the measured direction was steeper than the mean inclination. The closed circles mark 250-yr intervals. The open circles mark the youngest point of each record.

SECULAR VARIATION DATING

NATURE OF MATERIAL	EXISTING AGE RESOLUTION	POSSIBILITY OF IMPROVEMENT
Sequence	"Holocene"	Unlikely
	within about 2,500 yrs	Likely
Isolated	within about 2,500 yrs	Unlikely
	within about 500 yrs	Likely

FIGURE 5.--Summary of the likelihood that secular-variation dating can improve the chronologic constraints on isolated paleomagnetic directions and sequences of directions.

CONCLUSIONS

An important component in any paleoseismological study is the determination of the age of the materials involved. Paleomagnetic studies can contribute to paleoseismology in two ways. First, magnetostratigraphy can be used to provide a broad chronologic framework for the material being studied. In particular, it can be used to determine that a given deposit is older than 730,000 yrs. For long continuous sequences, it can provide age determinations with a resolution of about a hundred thousand years. On a different time scale, the records of Holocene geomagnetic secular variation that are becoming available make it possible to consider high-resolution dating of isolated paleomagnetic directions as well as sequences of directions spanning several hundred years. Successful use of geomagnetic secular variation depends on a number of factors, including the nature of the materials involved, the morphology of the master curve of secular variation in the time interval of interest, and other existence of other constraints on the age of the material. However, the nature of the paleomagnetic recording process places a limitation of 100 yrs on any secular variation date. At this time, geomagnetic excursions are not understood well enough to be used for the dating purposes.

ACKNOWLEDGMENTS

This work was supported in part by NSF grant EAR-86-18356

REFERENCES CITED

Barton, C.E. and McElhinny, M.W., 1981, A 10,000 yr geomagnetic secular variation record from three Australian maars: Geophysical Journal of the Royal Astronomical Society, v. 67, p. 465-485.

Bauer, L.A., 1896, On the secular variation of a free magnetic needle, II: Physical Review, v. 3, p. 34-48.

Constable, C.G. and McElhinny, M.W., 1985, Holocene geomagnetic secular variation records from north-eastern Australian lake sediments: Geophysical Journal of the Royal Astronomical Society, v. 81, p. 103-120.

Creer, K.M. and Tucholka, P., 1982a, Construction of type curves of geomagnetic secular variation for dating lake sediments from east central North America: Canadian Journal of Earth Sciences, v. 19, p. 1106-1115.

_____, 1982b, Secular variation as recorded in lake sediments--A discussion of North American and European results: Philosophical Transactions, Royal Society, London, v. A 306, p. 87-102.

_____, 1983, On the current state of lake sediment palaeomagnetic research: Geophysical Journal of the Royal Astronomical Society, v. 74, p. 223-238.

Creer, K.M., Valencio, D.A., Sinito, A.M., Tucholka, P. and Vilas, J.F.A., 1983, Geomagnetic secular variations 0-14000 yr BP as recorded by lake sediments from Argentina: Geophysical Journal of the Royal Astronomical Society, v. 74, p. 223-238.

Easterbrook, D.J., Briggs, N.D., Westgate J.A. and Gorton, M.P., 1981, Age of the Salmon Springs Glaciation in Washington: Geology, v. 9, p. 87-93.

Harland, W.B., Cox, A.V., Llewellyn, P.G., Smith, A.G. and Walters, R., 1982, A Geologic Time Scale: Cambridge, Cambridge Univ. Press, 131 p.

UNITED STATES DEPARTMENT OF THE INTERIOR
GEOLOGICAL SURVEY

PROCEEDINGS OF
CONFERENCE XXXIX

Directions in Paleoseismology

22-25 April 1987
Albuquerque, New Mexico

Sponsored by

U.S. GEOLOGICAL SURVEY
NATIONAL EARTHQUAKE-HAZARDS REDUCTION PROGRAM

Editors
Anthony J. Crone and Eleanor M. Omdahl
U.S. Geological Survey
Denver, Colorado 80225

Convenor
Anthony J. Crone

Organizing Committee

Randall W. Jibson	U.S. Geological Survey,	Reston, Virginia
Alan R. Nelson	U.S. Geological Survey,	Denver, Colorado
Thomas K. Rockwell	San Diego State Univ.,	San Diego, California
David P. Schwartz	U.S. Geological Survey,	Menlo Park, California

OPEN-FILE REPORT 87-673

Denver, Colorado

1987

Johnson, E.A., Murphy, T. and Torreson, O.W., 1948, Pre-history of the earth's magnetic field: Terrestrial Magnetism and Atmospheric Electricity, v. 53, p. 349-372.

Lund, S.P. and Banerjee, S.K., 1985, Late Quaternary paleomagnetic field secular variation from two Minnesota lakes: Journal of Geophysical Research, v. 90, p. 803-825.

Negrini, R., Davis, J.O. and Verosub, K.L., 1984, Mono Lake geomagnetic excursion found at Summer Lake, Oregon: Geology, v. 12, p. 643-646.

Stoker, M.S., Skinner, A.C., Fyfe J.A. and Long, D., 1983, Palaeomagnetic evidence for early Pleistocene in the central and northern North Sea: Nature, v. 304, p. 332-334.

Turner, G.M. and Thompson, R., 1981, Lake sediment record of the geomagnetic secular variation in Britain during Holocene times: Geophysical Journal of the Royal Astronomical Society, v. 65, p. 703-725.

Verosub, K.L., 1977, Depositional and postdepositional processes in the magnetization of sediments: Reviews of Geophysics and Space Physics, v. 15, p. 129-143.

_____, 1982, Geomagnetic excursions--A critical assessment of the evidence as recorded in sediments of the Brunhes Epoch: Philosophical Transactions, Royal Society, London, v. A306, p. 161-168.

_____, 1986, Principles and applications of paleomagnetism in the dating of young sediments, in Hurford, A.J., Jager, E., and Ten Cate, J.A.M. -- eds., Dating Young Sediments: CCOP Technical Secretariat, Bangkok, p. 247-267.

Verosub, K.L., Mehringer, P.J. Jr. and Waterstraat, P., 1986, Holocene secular variation in Western North America--The paleomagnetic record from Fish Lake, Harney Co., Oregon: Journal of Geophysical Research, v. 91, p. 3609-3623.

Vincent, J.S., Morris, W.A. and Occhietti, S., 1984, Glacial and nonglacial sediments of Matuyama paleomagnetic age on Banks Island, Canadian Arctic Archipelago: Geology, v. 12, p. 139-142.

page 101 follows

RECOGNITION OF PALEOSEISMIC EVENTS IN THE GEOLOGIC RECORD

GEOLOGIC CRITERIA FOR RECOGNITION OF INDIVIDUAL PALEOSEISMIC EVENTS IN EXTENSIONAL ENVIRONMENTS

by

James McCalpin
Department of Geology
Utah State University
Logan, UT 84322-0705

ABSTRACT

Geologic criteria for recognizing individual paleoseismic events in extensional tectonic environments fall into one of three categories: (1) relations between fault scarps and geomorphic surfaces, (2) multiple-event fault-scarp morphology, and (3) fault-scarp stratigraphy. Where fault scarps displace multiple geomorphic surfaces, increasing scarp heights on older surfaces indicate recurrent fault movement. Multiple-event scarps may preserve multiple profile convexities on the upthrown block, representing degraded scarp crests of several paleoseismic events. More detailed data on number of events, displacement, and recurrence come from fault-scarp stratigraphy in natural exposures and trenches. Individual colluvial wedges preserved at the scarp base record individual paleoseismic events. Colluvial wedges of multiple events are best differentiated when displacements are large (>1.5 m), material exposed in the free face is coarse, and the time between events is long enough for significant soil formation on the wedge surface. Future research should investigate wedge sedimentology, pursue direct sediment-dating techniques, and document surface-rupture patterns of earthquakes just above the magnitude threshold for surface faulting (M_L 5.5-6.5).

INTRODUCTION

This paper summarizes existing knowledge of and techniques for recognizing individual paleoseismic events in extensional tectonic environments. Bonilla (1982), Sieh (1981), and Wallace (1981, 1984), compiled data on styles and patterns of normal faulting, citing both historic and prehistoric earthquakes. Many other recent papers describing Quaternary faulting at specific localities have been analyzed for this summary.

Evidence for individual surface-rupturing events in the geologic record consists of: (1) relations between fault scarps and geomorphic surfaces, (2) multiple-event fault-scarp morphology, and (3) fault-scarp stratigraphy. Each topic will be addressed in the following sections.

RELATIONSHIPS BETWEEN FAULT SCARPS AND GEOMORPHIC SURFACES

The interaction between normal fault scarps and geomorphic surfaces (such as fluvial terraces) yields a first approximation of the number of paleoseismic events recorded. Figure 1 contrasts the relations between two fluvial terraces and a single- versus multiple-event scarp. Recurrent faulting subsequent to the formation of each terrace is recorded in the increased scarp height on older terraces. If the smallest scarp

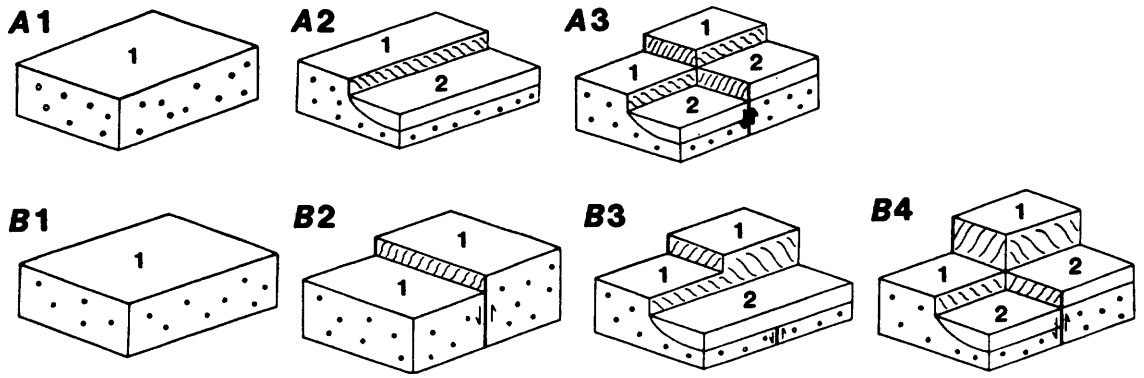

FIGURE 1.--Schematic block diagrams of fault scarp/ terrace relations. A. earlier alluvium (1) is deposited, younger terrace (2) is incised into it, then a single faulting event occurs. B. Earlier alluvium is deposited (1), then faulted (2). After faulting a younger terrace is incised into both the upthrown and downthrown blocks (3), then is re-faulted along the same trace (4). The multiple-event scarp on terrace 1 is twice as high as the single-event scarp on terrace 2 if displacements are equal.

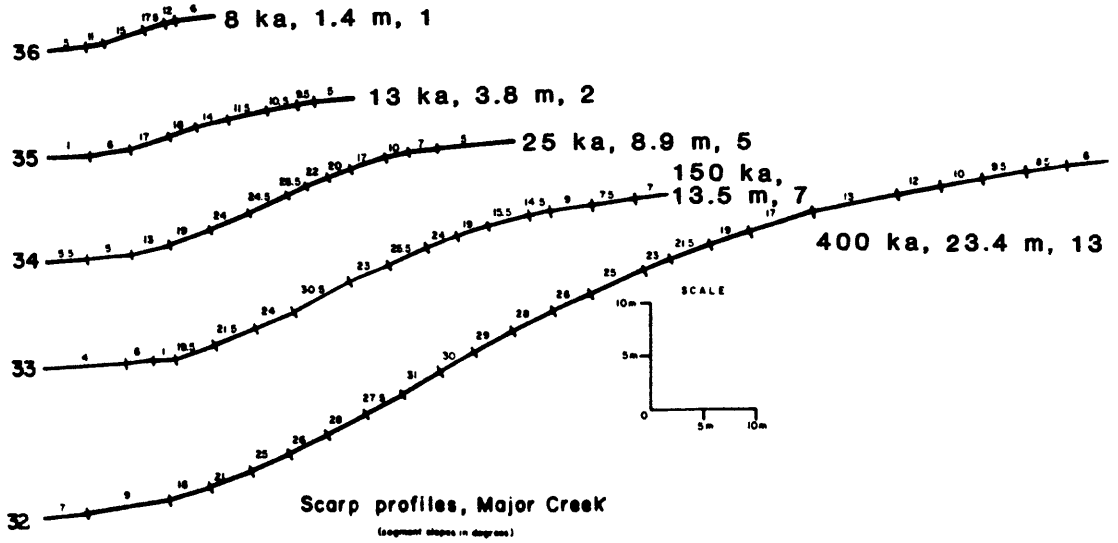

FIGURE 2.--Profiles of scarps on Quaternary units of five different ages at Major Creek, San Luis Valley, Colorado. Scarps on younger units (larger profile numbers, at left) are smaller. The age of the faulted surface (in kilo-annum, Ka), cumulative net vertical tectonic displacement in meters (m), and inferred number of faulting events are shown to the right of each scarp profile. Number of events is derived by dividing the inferred displacement per event (1.4-2.4 m) into the cumulative displacement for each scarp.

represents a single event, then the number of events displacing older surfaces can be roughly estimated if one assumes that past displacements have been equal to the most recent displacement.

Scarps traversing embayed valley mouths along mountain fronts often displace multiple terrace sets. McCalpin (1987c) describes terraces and fans of five ages in the Rio Grande rift displaced by recurrent Quaternary faulting. At Major Creek, scarps range from 2.0 to 24.2 m high. The smallest scarp represents a single event (displacement=1.4 m), and the second smallest represents two events, with a total of 3.8 m of displacement (1.4+2.4 m). The number of individual displacements represented in higher scarps can be estimated by dividing their cumulative net-vertical tectonic displacement by 1.4 or 2.4 m (fig. 2).

Geomorphic relations usually cannot bracket the number, displacement, and age of individual paleoseismic events with much accuracy. Dividing single-event scarp displacements into larger scarp displacements assumes that displacements through time have been constant, but the example cited above shows short-term variations of 170 percent at one site. In addition, using faulted geomorphic surfaces that may be crudely dated can yield only average recurrence intervals. For example, if it appears that six paleoseismic events have occurred between the stabilization of a 140 ka and a 400 ka terrace, one can derive an average recurrence of 42 ka (six events in 260 ka). In actuality, events could have been temporally clustered within that interval.

FAULT-SCARP MORPHOLOGY

Although early studies described fault scarps produced by historic normal-fault earthquakes (Jones, 1915 in Pleasant Valley, Nev.; Slemmons, 1957 in Dixie Valley, Nev.), it was not until 1977 that their paleoseismic value was addressed (Wallace, 1977). The degradation of scarps was qualitatively described by Wallace (1977), and later an empirical relation between scarp-height, slope-angle, and age was proposed by Bucknam and Anderson (1979). Since then, various equations modeling scarp decline have been proposed (Nash, 1980), and numerous workers have attempted to refine this diffusion-equation model (Nash, 1986; Mayer, 1984; Hanks and others, 1984; Pierce and Colman, 1986; Andrews and Hanks, 1986).

Renewed faulting on a preexisting scarp creates a new free face and scarp degradation begins all over again (Wallace, 1977). The new scarp crest retreats headward, but remains distinct from the original scarp crest (fig. 3). Wallace (1977) suggested that multiple slope convexities on the upper part of the scarp each represent a paleoseismic event.

Several problems exist in relating details of scarp morphology to individual paleoseismic events. Multiple slope convexities on scarps could result from multiple small scarplets (longitudinal step-faults) occurring in a single event, rather than from multiple events on the same fault trace.Given the variability in initial scarp geometry along strike in historic earthquakes (for example, Crone and Machette, 1984), profiles should be measured at many locations to determine if multiple crests are relatively rare (suggesting step-faulting) or common (suggesting multiple faulting). Finally, the absence of multiple crests on a scarp does not prove it is a single-event scarp. Most large (>10-m-high) fault scarps profiled on the Sangre de Cristo fault (McCalpin, 1983) and on the Wasatch fault (Peterson, 1981) produced by multiple events (based on geomorphic relations or trenching studies), do not

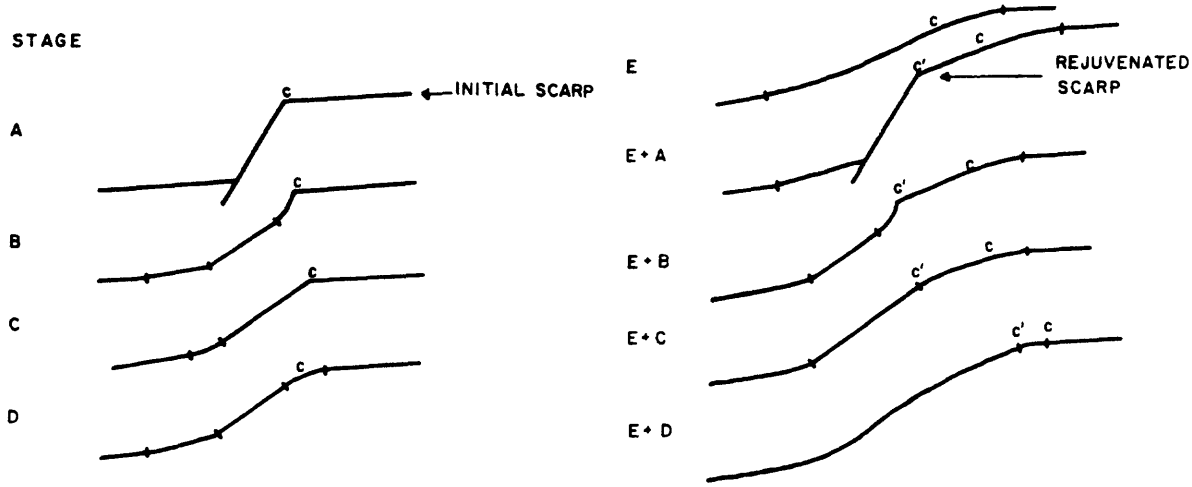

FIGURE 3.--Conceptual diagrams of the degradation of a rejuvenated fault scarp, (adapted from Wallace, 1977, fig. 2). Degradation of the original scarp occurs in stages A through E. The crest of the scarp is shown by C. At E+A, the scarp is re-faulted, and a new crest forms (c'). With time, c' retreats headward and approaches the original crest (c), but has not overtaken it by stage E+D.

have multiple crests. Recurrent faulting has evidently regraded the entire scarp face, obliterating traces of former events.

FAULT-SCARP STRATIGRAPHY

Degradation of a normal-fault scarp creates a wedge-shaped deposit of colluvium at the scarp base. Swan and others (1980) recognized that repeated surface faulting on the same trace creates stacked colluvial wedges, each of which represents an individual paleoseismic event (fig. 4). Wedges can be more easily differentiated if: (1) well-developed soils occur between wedges, and (2) sedimentary facies within the wedge are distinct. Nelson (this volume) defines two colluvial-wedge facies which he terms proximal and distal. The proximal wedge is a poorly sorted talus and debris deposit shed from the scarp free face by gravity fall and debris-flow processes. This facies accumulates rapidly; at Borah Peak, Idaho, much of the free face of the October 1983 scarp was half buried by colluvium by October 1986. After the free face is completely buried, debris and slopewash processes degrade the scarp at a slower rate (Wallace, 1977, figs. 3 and 7). During this stage of wedge deposition, distal colluvium is deposited over and downslope of the proximal wedge. Distal colluvium is finer grained, better sorted, and better stratified than is proximal colluvium. In the Western United States, distal colluvium often contains a higher percentage of silt than is present in the faulted parent material. McCalpin (1983, p. 45) ascribed the silt to eolian influx which is washed over the scarp and concentrated at the scarp base. Numerous trench logs (summarized by Nelson, this volume) show a sharp contact between the clast-rich proximal and finer grained, stratified distal colluviums.

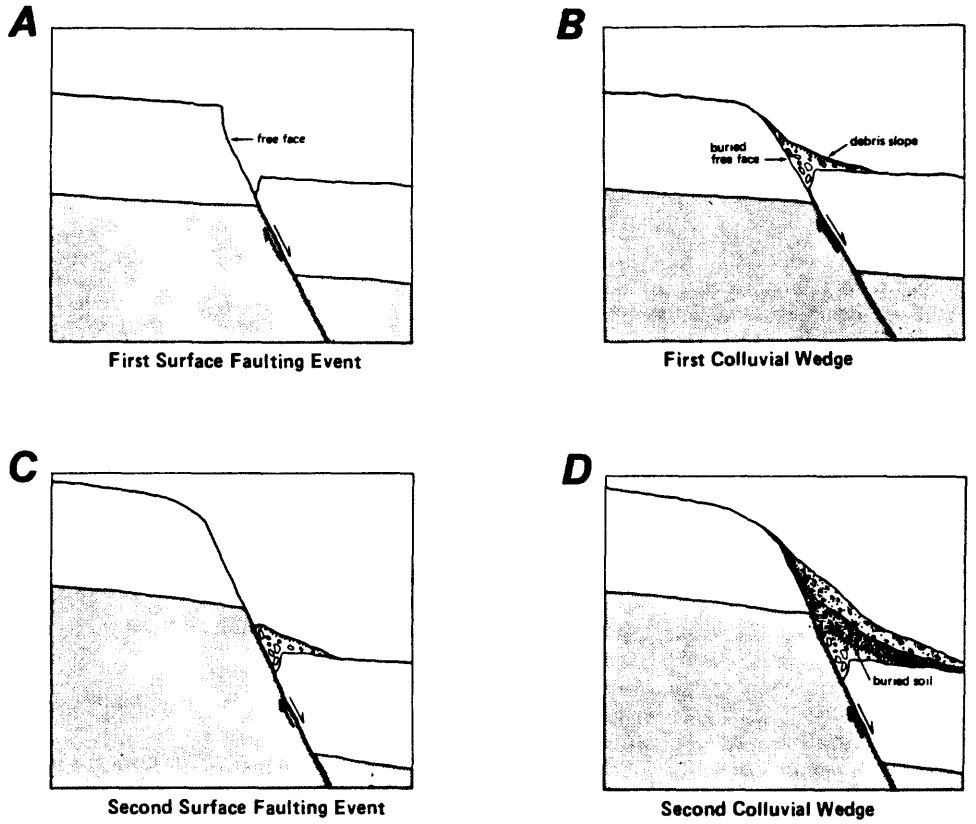

FIGURE 4.--Conceptual diagrams of the formation of two colluvial wedges from recurrent surface faulting on a single fault trace. Note that the younger colluvial wedge is less wedge shaped than is the older colluvium because it was deposited on a preexisting debris slope. From Schwartz and others, 1983.

Determining the Number of Events

If each paleoseismic event creates a free face which degrades to form a colluvial wedge, then simply counting the number of individual wedges at a site should yield the number of faulting events. The key to correct interpretation is differentiating one wedge from another, and (or) differentiating scarp-derived colluvium from other nontectonic deposits (for example, debris flows, eolian deposits) which are commonly deposited below scarps. Figure 5 shows a trench log displaying two colluvial wedges. Note the sharp upslope contact, wedge shape, facies differentiation, and soil development on unit 5. It is easier to make generalizations about wedge geometry than about wedge lithology, because of the wide range of faulted parent materials. In general, good differentiation of wedges is facilitated if parent materials are gravelly, free faces are large, and a long time (several kilo-annum) separates faulting events. If parent materials do not contain abundant clasts, there may be no grain-size contrast between proximal and distal colluvium. This can occur in sandy alluvium, lake beds, and loess. If displacements are small, all wedge features will be small, and subject to possible reworking by scarp-slope processes. Downhill creep may distort or destroy original fabric or sedimentary structures within roughly

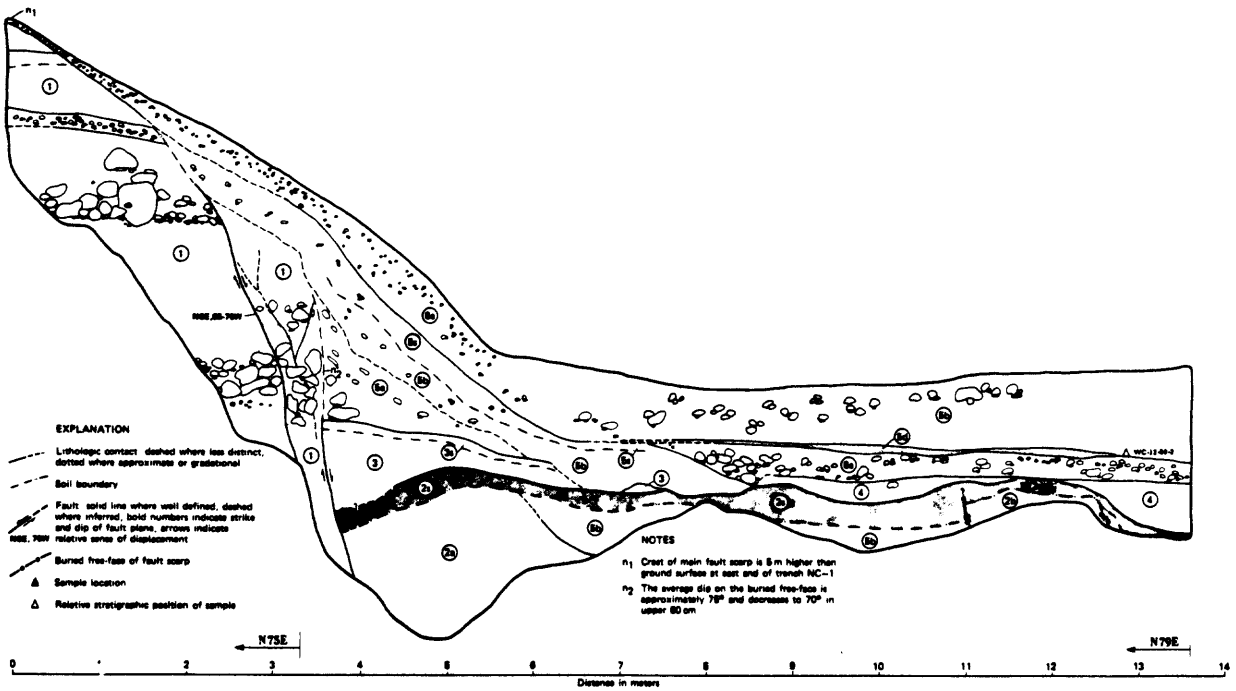

FIGURE 5.--Log of a trench exhibiting at least two colluvial wedges (units 5 and 6). The younger wedge (unit 5) is composed primarily of proximal facies (5a), with the stone-free downslope part of 5b representing the incipient distal wedge. Unit 6, in contrast, does not display comparable facies because: (1) it was deposited on a preexisting slope, and (2) it has not had as much time to develop as has unit 5. Unit 3 is a mudflow deposited against the scarp after initial faulting, but later faulted against unit 1. Units 2a and 2b may be the proximal part of an even earlier wedge (from Crone, 1983).

0.5 m of the ground surface. If events occur within a short time of each other, soils separating the wedges will be poorly developed.

Faulting of scarp-derived colluvium is de facto evidence of more than one paleoseismic event. In any two-event scarp, the lower (older) wedge should be in fault contact with upthrown-block materials, while the upper (younger) wedge must be in depositional contact with the buried free face of the second event. In gravelly colluvium, evidence for faulting is a strong pebble orientation parallel to the fault. Where faults dip steeply (average dip of 78° for 40 trenches; McCalpin, 1987a) this near-vertical fabric is often distinguishable from the nearly angle-of-repose (30°-40°) fabric of the undisturbed proximal wedge. However, intact pieces of upthrown-block gravel may topple into tension fissures at the scarp base, creating vertical pebble fabrics which are not the result of shearing.

Recurrent faulting may sometimes be observed in complex graben zones where minor faults extend upwards to different stratigraphic levels through mixed colluvial, fluvial, and eolian sediments. An example from the Wasatch fault (fig. 6) shows a 22 cm displacement abruptly truncated by a soil, while adjacent faults cut upward nearly to the surface indicating younger movement. Abrupt truncations of substantial displacements (as cited above)

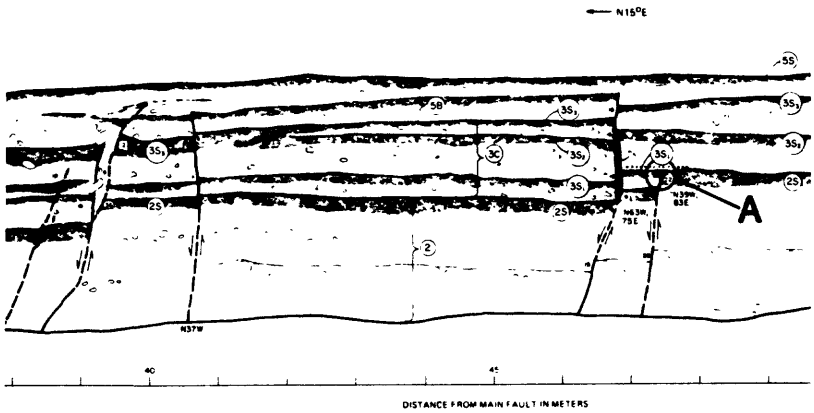

FIGURE 6.--Trench log showing an abrupt truncation of a fault trace (A, at 47 m on log) in contrast to adjacent faults which cut up higher in the colluvial section. The 22 cm displacement offsets soil 2s and 3_{s1}, but does not offset $3s_2$, as do most other faults. However, some displacements do die out gradually upwards; for example, the fault at the far left at 39 m has a displacement that decreases upward from 36 cm to 12 cm to 0 cm. From Swan and others, 1980.

must be differentiated from displacements that slowly decrease toward the surface; these cracks may terminate at any level. Bonilla (1987) states that many fault strands commonly die out upward, but more rarely on normal faults than on strike-slip or reverse faults.

In summary, the simplest case of recurrent surface faulting produces simple scarps along the same fault trace (as in fig. 4). Each successive free face ravels to create a colluvial deposit marked by a basal concentration of clasts and perhaps intact blocks of soil horizons. The colluvium fines upward, and if sufficient time is available, an organic horizon caps each colluvial wedge. Because the scarp is larger after each successive event, colluvium from later events is deposited on a higher and steeper preexisting slope. As a result, each successive wedge is thinner and spreads farther downslope than underlying wedges (fig. 4). In units deposited on steeper slopes, facies are less differentiated, and only the basal stone line may be recognizable. The juxtaposition of stony debris atop finer, organic-rich colluvium is still the key criteria for recognizing separate faulting events.

Conditions Complicating Colluvial-Wedge Geometry

Numerous conditions may occur to complicate this simple geometry, either tectonic or depositional. Figure 7 presents a three-event scarp sequence which displays several complicating conditions described below.

1. Open tension fissures at the scarp base may trap proximal colluvium, depriving the wedge of all or part of this facies. This fissure fill is sometimes hard to distinguish from <u>in-situ</u> sheared alluvium or colluvium.

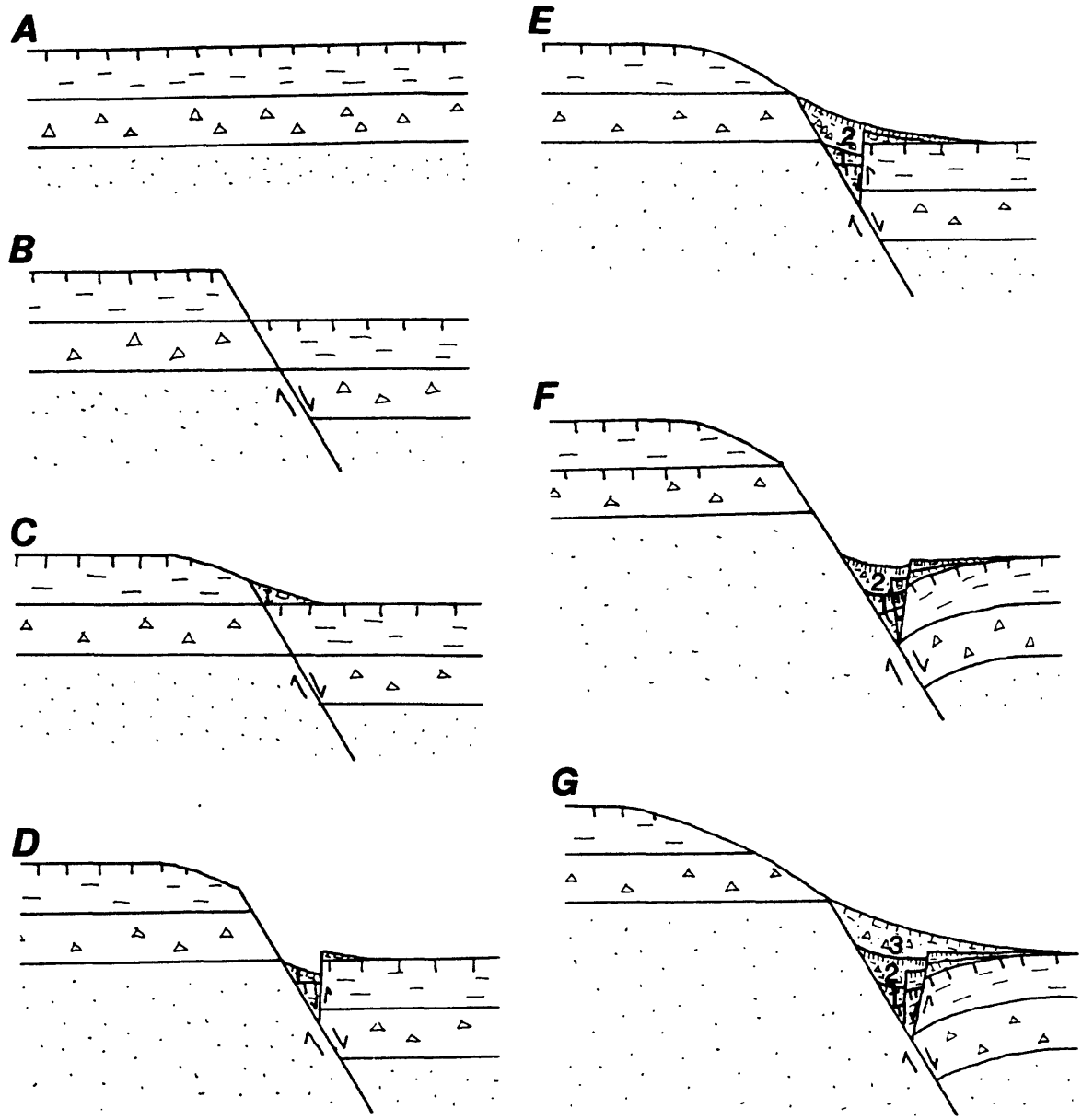

FIGURE 7.--Idealized evolution of a three-event normal fault scarp successively exposing three stratigraphic units in the free face. A-initial conditions (vertical lines indicate soil); B-first faulting event; C-colluvial wedge is derived from upper unit, weak soil develops; D-second faulting event, graben forms, middle unit exposed in free face; E second wedge forms, primarily derived from middle unit, buries antithetic fault, weak soil develops; F-third faulting event, new antithetic fault develops, older colluvium and downthrown block are rotated into the main fault; G-third wedge is derived from all three units, buries both antithetic faults, and weak soil develops. Due to complex tectonic and depositional controls, all three wedges have different lithologies and shapes. The key criteria for recognizing individual wedges is coarse material overlying organic horizons and truncating antithetic faults.

2. If displacement is small, the low free face may be developed in preexisting slope colluvium subject to downhill creep. During scarp degradation, distinctive wedge facies may not develop, and the wedge may be represented only by a downhill thickening of the colluvial mantle (Ostenaa, 1984).
3. If multiple step-fault scarps occur on a preexisting slope, the wedge derived from the uphill scarp may extend downslope to overlie the downhill scarp and wedge. Thus, the stratigraphic superposition of the upslope over the downslope wedge may be interpreted as representing two separate events. If step-faults are close together, there should be little grain-size difference and no soil between the two wedges. However, if faults are widely separated, it may take the upper wedge a considerable time to prograde over the downslope scarp and wedge, so facies contrasts are possible, although soils will not likely be present.
4. Earlier colluvial wedges will probably be faulted and rotated by later faulting events. Therefore the initial shape of each wedge could be altered by block faulting, which may juxtapose intact blocks of later colluvium of one facies against blocks of earlier colluvium of another facies. Soils developed atop earlier wedges are often rotated into the fault, leading to greater anti-slope dips for successively older soils (for example, unit 2s in fig. 5).
5. If scarps are large (>8-10 m high), the colluvial wedge may be so thick that the bottom of the trench barely deep enough to expose the prefaulting ground surface. Poorly stratified material near the trench floor, often with a weakly developed soil, may be interpreted as: (1) the upper part of an early colluvial wedge, or (2) the youngest prefaulting deposit, with stratification obscured by soil-forming processes. The uncertain origin of the lowest deposit in the trench often causes ambiguity in interpreting the number of paleoseismic events, leading to statements such as ". . . at least two and possibly three ruptures have occurred in Holocene time . . .".

Depositional complications may include:

1. Material exposed in the free face may contain few clasts, so no clear sedimentologic contrast occurs between proximal and distal colluvium. If local sedimentary systems also lack clasts, then graben-fill debris flows and loess may also resemble the scarp-derived colluvium.
2. Repeated faulting may expose different stratigraphic units in the free face, leading to colluvial wedges with different lithologies.
3. Time between surface-faulting events may be insufficient for development of recognizable soils. Combined with a lack of clasts, this condition can lead to thick, but undifferentiated wedges of colluvium.

Determining the Timing of Events

In general, faulting events are bracketed between the age of the youngest faulted deposit and that of the oldest unfaulted deposit. Faulted Quaternary deposits of nontectonic origin may be alluvial, glacial, lacustrine, eolian, or colluvial. Techniques for dating Quaternary deposits are summarized by Mahaney (1984) and Pierce (1986). In cases of recurrent faulting, dates from the colluvial-wedge sequence typically provide the key data. The soil developed on the prefaulting geomorphic surface will be buried by the first

colluvial wedge, and may be datable by ^{14}C. If faulting events are separated by sufficient time, the scarp may stabilize and an organic horizon may form on the wedge surface. Even weakly developed soils may have sufficient carbon in the A horizon for dating; M.N. Machette and A.R. Nelson, (oral commun., 1986) report organic matter contents of 0.2-5 percent from soils developed in Holocene wedges on the Wasatch Front. Finding discrete woody material or charcoal in wedges is more difficult.

Soils may be better developed on the distal part of the wedge, where colluvial scarp-derived sediments are often complexly interfingered with alluvial or eolian deposits. These latter deposits do occasionally contain detrital charcoal. Finally, direct dating of the fine grained fraction of distal and proximal wedges by thermoluminescence (TL) (Wintle and Huntley, 1982) is now being tested. Forman and others (1987) report that distal wedge sediments, buried soils, and sag pond silts along the Wasatch fault show stable TL signals and are amenable to direct dating.

One method proposed for relating multiple absolute dates from exposures to the timing of individual paleoseismic events is the "fault window" method (West, in press) (fig. 8). Within a single fault segment, events should be bracketed between the overlap range of all fault windows. If a single line cannot be drawn through all fault windows, then two separate events are suggested.

SUGGESTIONS FOR FUTURE RESEARCH

The preceeding analysis of methods for recognizing individual paleoseismic events suggests several new research directions:

1. Determine the uniformity of individual displacements over time at particular sites (characteristic earthquakes). This would involve trenching multiple sites along the same scarp where scarp height changes dramatically across geomorphic surfaces of different ages.
2. Analyze similarities and differences between the geometries of roughly 100 trench logs already existing. Preliminary work by Nelson (this volume) on 60 trenches, and McCalpin (1987a) on 40 trenches have produced new insights into wedge facies and rupture style, respectively.
3. Improve dating techniques. New techniques aimed at direct dating of sediment, such as thermoluminescence (McCalpin, 1986, 1987b; Forman and others, 1987) should be pursued.
4. Study wedge sedimentation processes on historical and late Holocene scarps. The interpretation of wedge geometry, textures, fabric, and dating potential need to depend on a better understanding of wedge sedimentology.
5. Determine the lower limit of paleomagnitude resolution of geologic methods. Study of small historical fault scarps from earthquakes in the M_L 5.5-6.5 range are needed to define the size, style, and longevity of geologic features produced by moderate-magnitude, but potentially damaging, earthquakes.

CONCLUSIONS

Present methods for recognizing individual paleoseismic events in extensional environments rely on geomorphic relations, fault-scarp morphology, and colluvial-wedge stratigraphy. Features produced by historical earthquakes, particularly colluvial wedges, have been used as analogues for

similar features attributed to paleoseismic events, but without detailed sedimentologic studies. Future research should concentrate on wedge sedimentology, direct sediment-dating techniques, and defining the lower limit of resolution of geologic methods for identifying individual surface-faulting events.

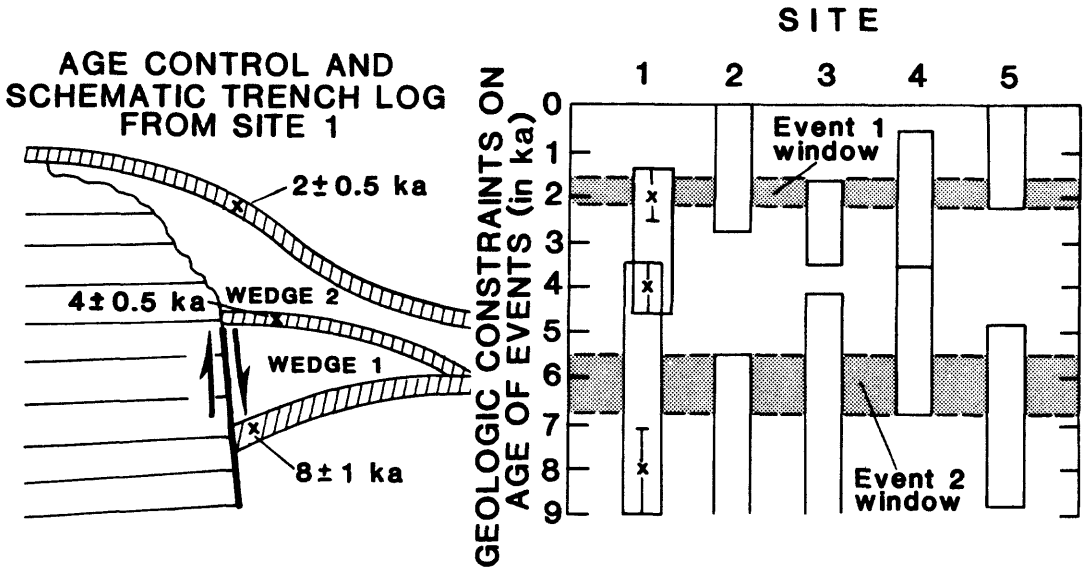

FIGURE 8.--Diagram showing the "fault window" method (adopted from West, in press) of relating limiting dates on colluvium to faulting. At left, sketch shows two colluvial wedges with A horizons, both burying the A horizon of the prefaulting surface. A horizons are indicated by vertical lines. At site 1, event 1 occurred between 1.5 ka and 4.5 ka (includes 1 standard deviation from mean), while event 2 occurred between 3.5 ka and 9 ka. If the same events are also dated at sites 2 through 5, their ages must fall within the fault windows.

ACKNOWLEDGMENTS

This summary was improved by discussions with M.N. Machette, A.R. Nelson, A.J. Crone (U.S. Geological Survey, Denver), D.A. Ostenaa (U.S. Bureau of Reclamation) and M.W. West (Colorado School of Mines). The manuscript benefited by reviews by D.P. Schwartz and A.R. Nelson.

REFERENCES CITED

Andrews, D.J. and Hanks, T.C., 1985, Scarp degraded by linear diffusion--Inverse solution for age: Journal of Geophysical Research, v. 90, p. 10,193-10,208.

_____ 1982, Evaluation of potential surface faulting and other tectonic deformation: U.S. Geological Survey, Open-File Report 82-732, 91 p.

_____ 1987, Surface faulting studies, in Jacobson, M.L. and Rodriguez, T.R. (compilers), National Earthquake Hazards Reduction Program, Summaries of Technical Reports, Volume XXIII: U.S. Geological Survey Open-File Report 87-63, p. 130.

Bucknam, R.C. and Anderson, R.E., 1979, Estimation of fault-scarp ages from a scarp-height-slope-angle relationship: Geology, v. 7, p. 11-14.

Crone, A.J., ed., 1983, Paleoseismicity along the Wasatch Front and adjacent areas, central Utah, in Gurgel, K.D., ed., Geologic excursions in neotectonics and engineering geology in Utah, Guidebook-part 1V: Utah Geological and Mineral Survey Special Studies 62, p. 1-45.

Crone, A.J. and Machette, M.N., 1984, Surface faulting accompanying the Borah Peak earthquake, central Idaho: Geology, v. 12, p. 664-669.

Forman, S.L., Jackson, M.J., and McCalpin, James, 1987, Thermoluminescence (TL) dating studies on colluvial and alluvial sediments from Utah and Colorado--Preliminary results [abs.]: Geological Society of America Abstracts with Programs, v. 19, no. 5, p. 175.

Hanks, T.C., Bucknam, R.C., LaJoie, K.R., and Wallace, R.E., 1984, Modification of wave-cut and faulting-controlled landforms: Journal of Geophysical Research, v. 89, no. B7, p. 5771-5790.

Jones, J.C., 1915, The Pleasant Valley, Nevada, earthquake of October 2, 1915: Bulletin of the Seismological Society of America, v. 5, p. 190-205.

Mahaney, W.C., ed., 1984, Quaternary dating methods: Elsevier, Amsterdam, 431 p.

Mayer, Larry, 1984, Dating Quaternary fault scarps in alluvium using morphologic parameters: Quaternary Research, v. 22, no. 3, p. 300-313.

McCalpin, James, 1983, Quaternary geology and neotectonics of the west flank of the northern Sangre de Cristo Mountains, south-central Colorado: Colorado School of Mines Quarterly, v. 77, no. 3, 97 p.

_____ 1986, Thermoluminescence (TL) dating in seismic hazard evaluations--An example from the Bonneville Basin, Utah: in Wood, S.H., ed., Proceedings of the 22nd Symposium on Engineering Geology and Soils Engineering, Boise, Idaho, p. 156-176.

_____ 1987a, Recommended setback distances from active normal faults, in McCalpin, James (ed.), Proceedings of the 23rd Symposium on Engineering Geology and Soils Engineering, Logan, UT, p. 35-56.

_____ 1987b, Late Quaternary tectonics and earthquake hazard in Cache Valley, Utah: Final Technical Report, U.S. Geological Survey, Contract No. 14-08-0001-G1091, 187 p.

_____ 1987c, Recurrent Quaternary normal faulting at Major Creek, Colorado--An example of youthful tectonism on the eastern boundary of the Rio Grande rift zone: Geological Society of America, Centennial Field Guide, v. 2, Rocky Mountain Section, p. 353-356.

Nash, D.B., 1980, Morphologic dating of degraded normal fault scarps: Journal of Geology, v. 88, p. 353-360.

_____ 1986, Morphologic dating of fault scarps: Final Technical Report, U.S. Geological Survey, Contract No. 14-08-0001-21960, 83 p.

Ostenaa, D.A., 1984, Relationships affecting estimates of surface fault displacements based on scarp-derived colluvial deposits: Geological Society of America Abstracts with Programs, v. 16, no. 5, p. 327.
Peterson, J.F., 1981, Topographic profile analysis of piedmont scarps, northern Wasatch Front: M.S. Thesis, Salt Lake City, University of Utah, 125 p.
Pierce, K.L., 1986, Dating methods, in Active Tectonics: Washington, D.C., National Academy Press, p. 195-214.
Pierce, K.L. and Colman, S.M., 1986, Effect of height and orientation (microclimate) on geomorphic degradation rates and processes, late glacial terrace scarps in central Idaho: Geological Society of America Bulletin, v. 97, no. 7, p. 869-885.
Schwartz, D.P. Hanson, K.L. and Swan, F.H. III, 1983, Paleoseismic investigations along the Wasatch Fault Zone--An update, in Gurgel, K.D., Geologic excursions in neotectonics and engineering geology in Utah, Guidebook - part lV: Utah Geological and Mineral Survey Special Studies No. 62, p. 45-48.
Sieh, K.E., 1981, A review of geological evidence for recurrence times for large earthquakes, in Simpson, D.W. and Richards, P.G., eds., Earthquake prediction--An international review: Washington, D.C., American Geophysical Union, Maurice Ewing Series, v. 4, p. 181-207.
Slemmons, D.B., 1957, Geological effects of the Dixie Valley-Fairview Peak, Nevada, earthquakes of December 16, 1954: Bulletin of the Seismological Society of America, v. 47, no. 4, p. 353-375.
Swan, F.H. III, Schwartz, D.P. and Cluff, L.S., 1980, Recurrence of moderate-to-large magnitude earthquakes produced by surface faulting on the Wasatch Fault Zone, Utah: Bulletin of the Seismological Society of America, v. 70, no. 5, p. 1431-1462.
Wallace, R.E., 1977, Profiles and ages of young fault scarps, north-central Nevada: Geological Society of America Bulletin, v. 88, p. 1267-1281.
_____ 1981, Active faults, paleoseismology, and earthquake hazards in the Western United States, in Simpson, D.W. and Richards, P.G., eds., Earthquake prediction--An international review: Washington, D.C., American Geophysical Union, Maurice Ewing Series, v. 4, p. 209-216.
_____ 1984, Patterns and timing of late Quaternary faulting in the Great Basin province and relation to some regional tectonic features: Journal of Geophysical Research, v. 89, no. B7, p. 5763-5769.
West, M.W., in press, Neotectonics of the Bear River fault zone, Uinta County, Wyoming and Summit County, Utah: Ph.D. Dissertation, Golden, Colorado, Colorado School of Mines.
Wintle, A.G., and Huntley, D.J., 1982, Thermoluminescence dating of sediments: Quaternary Science Reviews, Pergamon Press, v. 1, no. 1, p. 31-53.

Geologic Criteria for Recognition of Individual Paleoseismic Events in Compressional Tectonic Environments

by

Gary A. Carver

Department of Geology
Humboldt State University
Arcata, CA 95521

ABSTRACT

Geologic evidence of individual paleoseismic events in compressional tectonic environments generally is recognized as a sudden change in micro sedimentary sequences and small-scale landforms resulting from coseismic processes. Surface faulting, folding, uplift, subsidence, shaking-triggered ground failure, and tsunamis have generated deposits and geomorphic features during large historic earthquakes. Structural, stratigraphic, and geomorphic relations interpreted to have resulted from these coseismic processes have been found in the near-surface deposits of some active compressional tectonic environments. Indicators of paleoseismicity often require special micro environments to form, and must be evaluated in terms of their local and regional tectonic, sedimentary, and geomorphic setting. Paleoseismic features associated with thrust faults are related to the mechanics and structure of the fault at the surface.

INTRODUCTION

Paleoseismology is the science and art of reconstructing the nature, timing, and location of prehistoric earthquakes from the geologic record. Paleoseismology is a relatively new, rapidly evolving specialization in neotectonics which combines the concepts of seismology with the methods and principles of geology. Its chief goal is to develop detailed pre-instrumental seismic histories of specific faults or seismogenic regions as part of the assessment of their seismic potential.

Observations of the geologic effect of large historic earthquakes provide most of the basis for defining the criteria useful in paleoseismic analysis. Relationships of geologic factors such as coseismic uplift and subsidence, surface-rupture length and displacement, and fault geometry to seismologic factors such as magnitude, source mechanism, strong ground motion, and isoseismal area for large historic earthquakes provide a framework for assessing paleoseismic events from the geologic record. Detailed field investigations of faults and associated tectonic structures active in the Holocene and late Pleistocene, and more complete and detailed seismicity data from expanded seismograph networks has allowed better characterization and location of

paleoseismic sources. Although most paleoseismic investigations have focused on extensional and strike-slip environments, significant information has been generated concerning the geologic record of individual seismic events in tectonic environments dominated by compression.

COMPRESSIONAL TECTONIC ENVIRONMENTS

Convergent plate margins constitute the primary compressional tectonic environment. Deformation from plate convergence and subduction involves large regions and a broad spectrum of structures dominated by thrust faults and folds (Davis and others, 1983; Moore and Silver, 1987). Great subduction-zone earthquakes have been accompanied by tectonic subsidence of large portions of the forearc region and uplift, folding, and faulting of the accretionary prism (Plafker,1965; Plafker and Savage, 1970). Such earthquakes may generate tsunamies capable of leaving enduring stratigraphic and geomorphic evidence (Plafker and Kachadoorian, 1966; Abe, 1979; Nishenko, 1985).

Fold and thrust belts are commonly accessory to strike-slip tectonics along transform margins, such as in the Transverse Ranges of California and the northern and central South Island of New Zealand (Yeats, 1983, 1987). Intraplate compressional structures are associated with a wide range of local and regional tectonic settings, and in many cases are part of complex deformation patterns dominated by strike-slip or extensional tectonics. For example, localized compression frequently occurs at restraining bends and curving ends of large strike-slip faults. Important in the paleoseismic interpretation of field relations is the compatibility of the feature with the local and regional tectonic setting.

Coseismic deformation in compressional tectonic environments includes both horizontal (distance) and vertical (elevation) changes of the earth's surface. Even for large individual seismic events, the magnitude of these changes is small over most of the affected area, generally ranging from a few centimeters to a few meters (Gordon, 1971; Stein, 1983; Atwater, 1987). The horizontal component, principally shortening perpendicular to the trend of major compressional structures, is difficult to detect in the geologic record. Evidence of vertical movements of the earths surface, especially where associated with sensitive geomorphic and sedimentary environments such as shorelines and floodplains, is easier to identify and measure. Localized folding or displacement of initially horizontal strata across thrust and reverse faults provides the most obvious evidence of deformation from compression.

In many instances, geologic evidence of individual earthquakes results from coseismically triggered changes in the regime of geomorphic and sedimentary systems. Coseismic uplift, subsidence, fault displacement, and folding modify base levels and gradients of geomorphic and sedimentary systems. Most geologic evidence of individual paleoseismic events in compressional tectonic environments are recognized by stratigraphic, sedimentary, or geomorphic evidence of a single, sudden, vertical movement or growth of adjacent compressional tectonic structures.

Historic earthquakes in compressional environments have resulted in complex patterns of deformation, commonly including large areas of subsidence and uplift. Localized growth of folds and surface faulting has accompanied many large compressional earthquakes. Where surface processes are affected by coseismic deformation, or other seismic processes such as shaking or tsunamis, the resulting process response may record the seismic event in the stratigraphic or geomorphic record. Because the surface process response to an individual compressional tectonic event is driven by vertical land-level changes of a few meters or less, the recognition of geologic features representing an individual paleoseismic event usually requires the application of micro geomorphic and micro stratigraphic techniques (Allen, 1987).

Coseismic deformation in compressional tectonic environments is not always accommodated on structures that directly record crustal shortening. Tear faults and other strike-slip faults linking segments of thrusts, normal faults, and grabens along the axis of folds and the leading edge of thrusts, and secondary flexure-slip faults in fold limbs may be activated during large compressional earthquakes (Yielding and others, 1981; Philip and Meghraoui, 1983; Yeats, 1987). Thus, paleoseismic indicators of individual events in compressional environments may be expressed as coseismic growth of related extensional or strike-slip structures.

PALEOSEISMIC INDICATORS OF INDIVIDUAL EVENTS

The spectrum of geologic relations indicative of individual paleoseismic events reflects the variety of coseismic processes accompanying large earthquakes. Most are the result of shaking-induced ground failure, tsunamies, changes in elevation of the land surface, and surface folding and faulting. Table 1 lists some of the field relations and geologic features which have been proposed to identify individual paleo-earthquakes. Those geologic relations resulting from single slip events on faults which intersect the ground surface generally can be physically traced to the causative fault in the field . Geologic evidence of past earthquakes resulting from shaking, seismic sea waves, warping, folding, subsidence, or uplift cannot often be directly matched to the seismogenic structure. The ability to identify the source structure for paleoseismic events greatly increases the usefulness of the data for seismic potential assessment and allows more rigorous evaluation of the validity of the evidence.

PALEOSEISMIC INDICATORS FROM SHAKING

Many large historic earthquakes have caused shaking-induced failure of surficial geologic materials. Some landslide deposits, and contorted lacustrine and marine sediments have been interpreted as evidence of past earthquakes (Sims, 1975; Allen, 1987). Since the cause of slope failure and liquefaction may be non-seismic, it is often difficult to demonstrate a seismic orgin for these kind of deposits. Coeval ages for ground failure at different locations are suggestive of earthquake generated landslides and liquefaction. The geographic distribution of such deposits is important in assessing

TABLE 1. -- Extent and coseismic relations for different types of geologic features resulting from individual paleoseismic events in compressional tectonic environments

Geologic feature	Coseismic relation	Extent	Reference
Coeval turbidites from varied sources.	Shaking triggered submarine landslides.	Beyond area of seismic shaking.	Adams, 1984.
Tsunami deposits in coastal marshes.	Tsunami.	Do.	Atwater, 1987.
Coeval landslide deposits.	Shaking triggered landslides.	Within area of seismic shaking.	Plafker, 1972.
Coeval liquefaction deposits.	Shaking triggered liquefaction.	Do.	Allen, 1987.
Coastal sedimentation indicating sudden subsidence.	Subsidence.	Within area of regional co-seismic deformation.	Atwater, 1987.
Raised terraces and coastal shoreline datums.	Uplift.	Do.	Plafker, 1965; Lajoie, 1987.
Deformed stream profiles and and fluvial terrace profiles.	Folding-faulting.	Within area of localized co-seismic deformation near or above the causative fault.	King & Stein, 1983.
Drainage ponding-lacustrine sedimentation	Do.	Do.	King & Vita-Finzi, 1981.
Deformed holocene coastal shoreline and intertidal datums.	Do.	Do.	Plafker, 1965; Lajoie, 1987.
Stratigraphic bracketed faults in depositional settings.	Fault displacement at the ground surface.	Localized along the surface trace of the causative fault or related fault.	Allen, 1987; fig. 1, this paper.
Morphostratigraphic bracketed fault slip in erosional setting.	Do.	Do.	Yeats, 1987.
Buried collapsed fault tips, faultline landslides.	Do.	Do.	Woodward-Clyde Consultants, 1980.
Buried or stacked scarp colluviums.	Fault displacement or fault propagation folding.	Do.	fig. 3, this paper.
Sedimentary onlapping on fold limbs-differentially folded sediments	Fault-bend folding.	Do.	fig. 1, this paper.
Stratigraphic bracketed differential fault-line folding.	Fault-line folding of fault contact strata.	Do.	fig. 1, this paper.

their paleoseismic significance, especially if coeval occurrences define isoseismal areas consistent with the location of major active seismogenic structures. The lack of alternative mechanisms for generating failure of surface materials at some sites also may be suggestive of a seismic origin. Additionally, the lack of evidence of liquefaction or slope failure at susceptible sites suggest the absence of large paleoseismic events in the region.

Landslides formed along the leading edge of the upper plate of thrust and reverse faults constitutes a special class of slope failure with coseismic implications. Such landslides are triggered by simultaneous strong shaking and fault displacement of the toe of the slope. Landslides of this type were formed almost continuously along the length of the Patton Bay fault during the 1964 Alaskan earthquake (Plafker,1965).

Coseismic submarine landslides along continental margins are known to generate extensive turbidite deposits at considerable distances from their sources. Adams (1984) has suggested that turbidites deposited in several submarine channels which head on the continental slope along the Cascadia subduction zone are evidence of large subduction earthquakes. Similarities in the ages of the turbidite sequences and the number of individual turbidite layers, as well as their geographic distribution relative to the subduction zone provide a basis for interpretating of a coseismic origin. Particularly significant are the apparently synchronous flows from tributary channels into the main channel indicated by similar numbers of individual turbidite layers in both. This suggests large submarine landslides were triggered by widespread seismic shaking at widely separated locations.

PALEOSEISMIC INDICATORS OF COSEISMIC UPLIFT, SUBSIDENCE, AND FOLDING

Regional and local coseismic subsidence and uplift can disrupt sensitive erosion and sedimentation processes, and result in lasting geomorphic and stratigraphic evidence of large earthquakes. Paleoseismic information in compressional environments has been developed from the study of deformed fluvial terraces (King and Vita-Finzi, 1981; King and Stein, 1983; Yeats,1987) and raised shore platforms (Matsuda and others, 1978; Plafker and Ruben, 1978; LaJoie, 1987). As with landslides and liquefaction, difficulty often arises in demonstrating seismic, rather than non-tectonic, origins for the changes in elevation of the ground surface and the associated erosional or depositional features.

Coseismic subsidence of large forearc regions during great subduction earthquakes and resulting sudden changes in intertidal sedimentation along adjacent coastlines has occurred historically in Alaska (Bartsch-Winkler and Schmoll, 1987). Sedimentary sequences of alternating mud and peat in intertidal marshes along the Oregon and Washington coasts have been interpreted to represent individual paleoseismic events on the Cascadia subduction zone (Atwater, 1987). Sediment sequences reflecting "jerky" subsidence consist of intertidal mud interstratified with layers of peat which are now below sea level. The peats were developed on stable

salt-marsh surfaces at the upper limit of the intertidal zone. Sharp upper contacts between the peat and overlaying mud are interpreted as evidence of the sudden (coseismic) submergence. Sand layers on the top of some of the peats in the salt-marsh sediments in the Pacific Northwest have been cited as possible tsunami deposits (Atwater, 1987) resulting from large local waves generated at the time of subsidence.

Localized uplift and subsidence, usually accompanying local or regional folding above buried thrusts, can produce geomorphic and stratigraphic evidence of individual seismic events. Incision and terrace cutting by streams responding to coseismic arching of their long profiles (King and Vita-Finzi, 1981; King and Stein, 1983) have been documented during coseismic growth of anticlines in California and Algeria. At these locations fluvial terraces similar to those formed historically have been interpreted as resulting from previous earthquakes. In Algera, folding and faulting across the course of the Cheliff River caused ponding and deposition of lacustrine sediments adjacent to the fault. Buried sequences of similar lake sediments record previous lacustrine sedimentation cycles interpreted to have resulted from prior coseismic ponding of the river (King and Vita-Finzi, 1981).

Criteria for evaluating the paleoseismic significance of geologic features resulting from shaking, tsunamis, and coseismic uplift or subsidence include the geographic distribution of the relations. Important is the location of the paleoseismic evidence relative to the active tectonic structures and long-term patterns of deformation in the region. Also important for evaluating geologic evidence of past strong shaking, tsunamis, and coseismic land elevation changes is the multiple occurrence of coeval paleoseismic relations. Evidence supporting a sudden origin for the geologic features interpreted as resulting from a single paleoseismic event is important in demonstrating a seismic relationship. Stratigraphic, geomorphic, and structural indicators of quiescence, or gradual and uniform geological process between the paleoseismic events is consistent with coseismic and interseismic cycles. Such interseismic indicators include conformable stratigraphic sequences from constant and uniform sedimentation, and geomorphic surfaces exhibiting weathering profiles and soil development. In some instances the degree of soil developement can be used to estimate the length of interseismic intervals (Burke and Carver, 1987).

PALEOSEISMIC INDICATORS OF INDIVIDUAL FAULTING AND FAULT-LINE FOLDING EVENTS

Surface faulting produces a variety of coseismic geologic features which are preserved in the near-surface geology along active thrust faults. Vertical separation and overthrusting of the ground surface, near-surface sediments, soils, and the formation and growth of small-scale tectonic structures result directly from fault displacement. These features, which include stratigraphically bracketed fault-line folds, fault splays and fractures, offset strata, and fault-related buried soils, may be useful as paleoseismic indicators (fig. 1). Coseismically initiated changes in local meso or micro

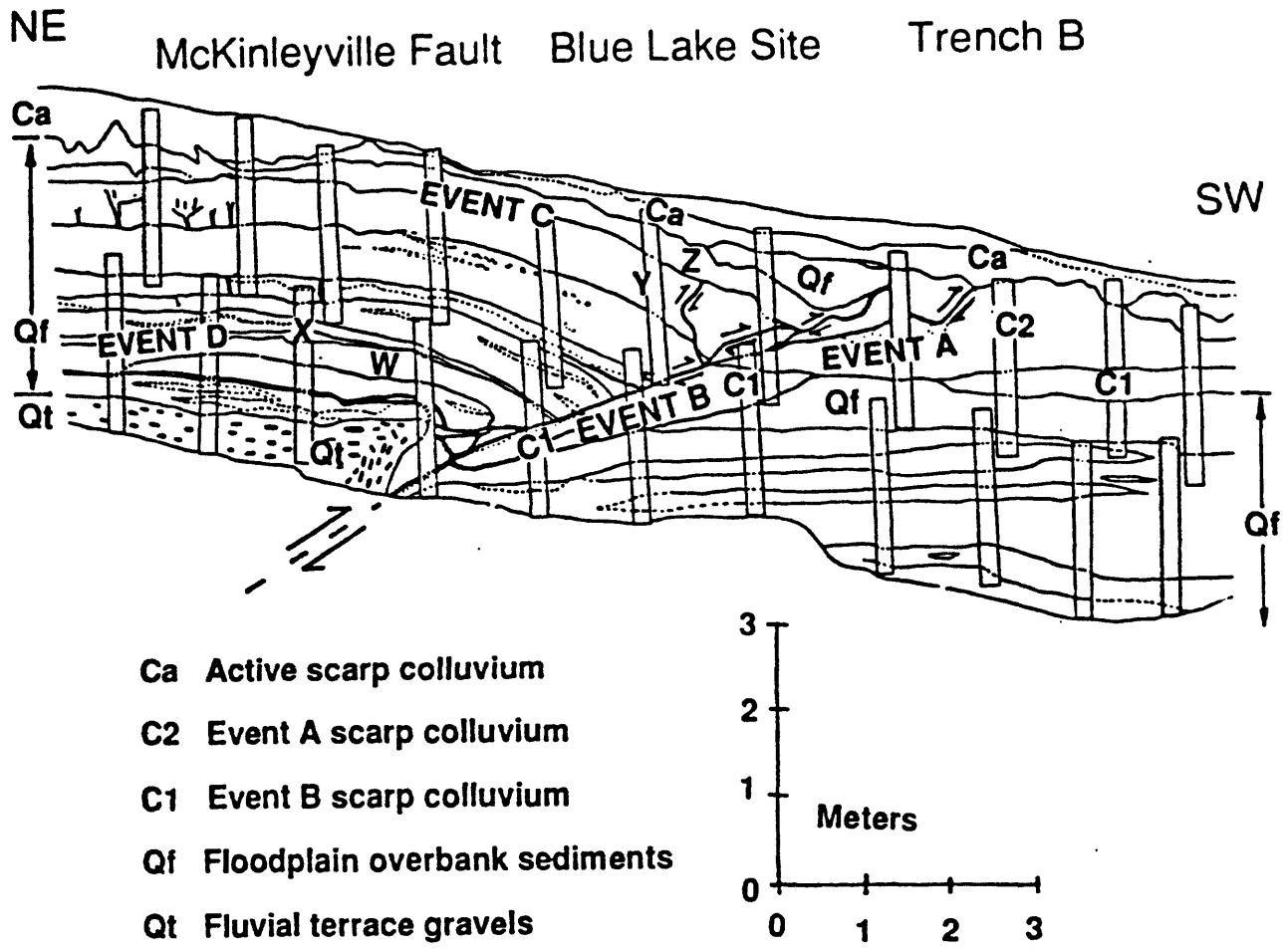

FIGURE 1 -- Portion of a trench log across the McKinleyville fault near Blue Lake, Humboldt County, Calif. The McKinleyville fault at this locality is a low-angle thrust displacing a sequence of well-bedded floodplain and fluvial terrace deposits and scarp-derived colluviums. Four paleoseismic events are present in the exposure. Event A, the most recent, and the previous event B, are indicated by overthrust scarp-derived colluvial wedges (C1 and C2). Both represent fault-slip episodes following the development of a scarp and cessation of floodplain sedimentation. Prior events C and D occurred during the vertical accretion of the floodplain. Event C is represented by fault splays displacing pre-event strata (bed Y) and covered by post-event strata (bed Z). Paleoseismic event D, the first event recorded in the terrace sequence, is expressed as a micro-unconformity near the base of the floodplain sequence with post-event strata (beds X) depositionally onlapping the more deformed pre-event strata (beds W) and by sharply increased fault-line folding of pre-event strata in the upper plate.

geomorphic and sedimentary processes along faults are important in producing lasting paleoseismic evidence, particularly by preserving datable material and depositing strata which bracket tectonic structures.

Geologic relations which record individual slip events on thrust faults are strongly influenced by the character of surface deformation and the local response of erosion and deposition processes to displacement along the fault. In general, geomorphic evidence of paleoseismic events on thrusts is the consequence of deformation-initiated erosion and is concentrated on the upper plate of the thrust. Geomorphic indicators of individual paleo-slip events on thrusts faults include fault-line landslides and debris slopes along the Patton Bay fault in Alaska (Plafker, 1967), and folded, faulted, and incised fluvial terraces along the Cheliff River near El Asnam, Algeria (King and Vita-Finzi, 1981). Interseismic intervals are commonly represented by diminishing erosion, weathering, and soil development.

Depositional settings such as floodplains, bays, estuaries, and lake margins commonly preserve stratigraphic and structural evidence of coseismic displacement on thrust faults. Depositional evidence of individual paleoseismic slip events occurs most often on the footwall of thrusts and is frequently buried beneath the thrust tip. Except for great subduction earthquakes, vertical separations on thrusts at the surface during historic earthquakes range from a few centimeters to a few meters (Krinitzsky, 1974; Slemmons, 1977). Vertical components of faulting on Montague Island, Alaska, in 1964 were as large as 15 m (Plafker, 1976). Generally, techniques for detecting and measuring micro-stratigraphic and micro-geomorphic features resulting from individual events include trenching and detailed surveying.

The surface expression of thrust faults is remarkable in the range of fault geometry and variety of scarp morphology generated from place to place along a thrust. Gordon (1971) described eight general scarp types that formed during the 1968 Meckering, Australia, earthquake. The variation in surface expression reflects differences in deformation process and fault structure resulting from variations in surficial materials and structural complexities deeper on the fault. Both brittle (fracture) and ductile (pervasive distributed shear) deformation processes are important components of near-surface thrusting. Near-surface structure and mechanics of thrust faults displacing fluvial and marine terraces in coastal northern California strongly influences the form of the fault scarp (Carver and Burke, 1987; O'Dea and others,1987). Thrust displacement may be accommodated on a single fault plane, or may involve distributed slip on many synthetic and antithetic meso-scale faults across a wide zone (fig. 2). Folding generally accommodates some of the total displacement and often is dominant. Thrust-related folds commonly occur in the form of broad, open, fault-bend anticlines with multiple hinges, planar limbs, and flat crests, or as tight, overturned fault-propagation folds (Suppe, 1983).

Fault scarp morphology is strongly influenced by the mechanics of surface deformation. Scarps developed in unconsolidated surficial material by slip on single fault surfaces are generally composed of rubble from the collapsed tip of the upper plate, and are narrow and steep. Scarps resulting from fault propagation folding at the

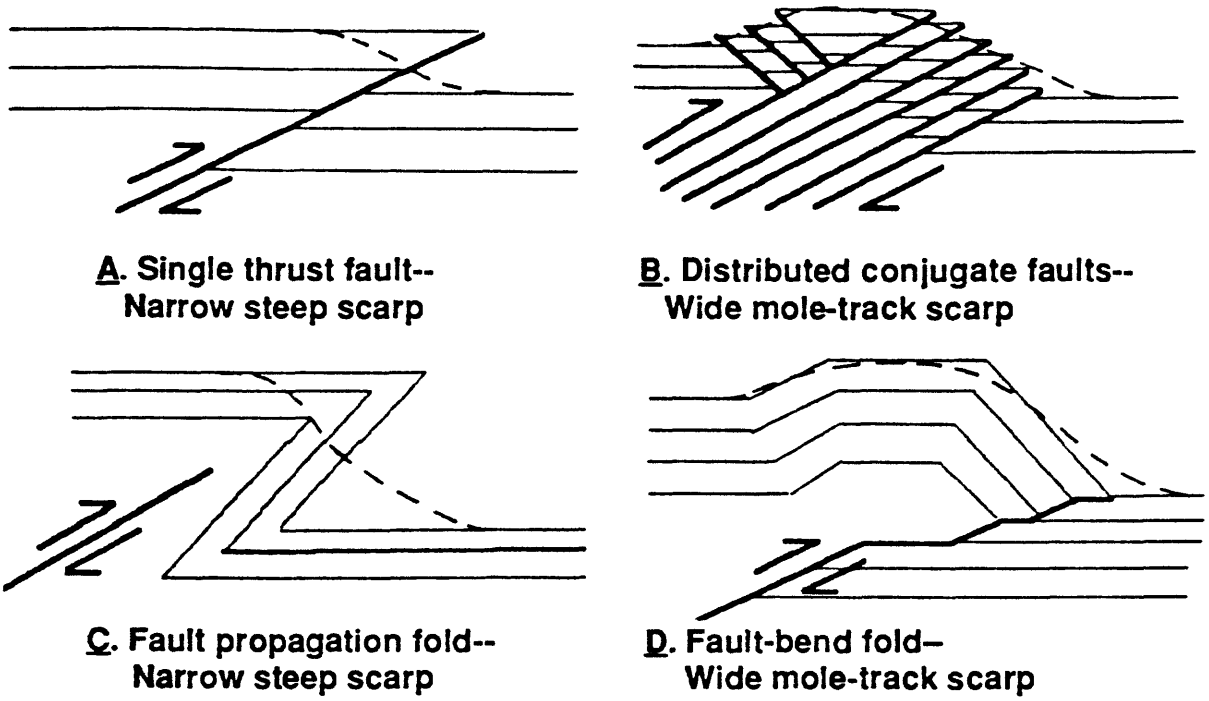

FIGURE 2 -- Schematic diagram of near-surface structural styles for thrust faults in coastal northwestern California and generalized characteristics of the resulting scarps. Heavy lines indicate faults with arrows to show sense of slip; fine lines indicate bedding.

surface are also narrow and steep, and promote strong scarp-colluvial processes. Overturning of the lower limb during coseismic growth of fault-propagation folds buries the previous interseismic colluvial sheet and initiates a new cycle of scarp colluviation (fig. 3). Scarps formed across broadly distributed conjugate slip surfaces and open fault-bend folds are wide with gentle slopes and frequently have mole-track or ridge-and-swale forms. Individual slip events produce incremental growth of the scarp. Subsequent sedimentation may unconformably onlap the scarp and folded near-surface sediments, preserving strata-bracketed evidence of the fault-line folding event.

Special depositional micro environments favor preservation of recognizable single-event paleoseismic relationships for broad scarps with low initial scarp-slope angles (fig. 2*B* and 2*D*). In such cases the stratigraphic and structural evidence of a paleoseismic event is best developed where deposition across the surface trace of the thrust involves processes associated with water surfaces, low-gradient fluvial systems, or other depositional settings in which well-bedded, nearly horizontal strata are deposited. To record and preserve multiple events and allow discrimination of individual events, sedimentation must be relatively constant and strata must accumulate at rates near the vertical separation rate on the fault. When these conditions are met, individual coseismic slip events are recorded as angular onlapping

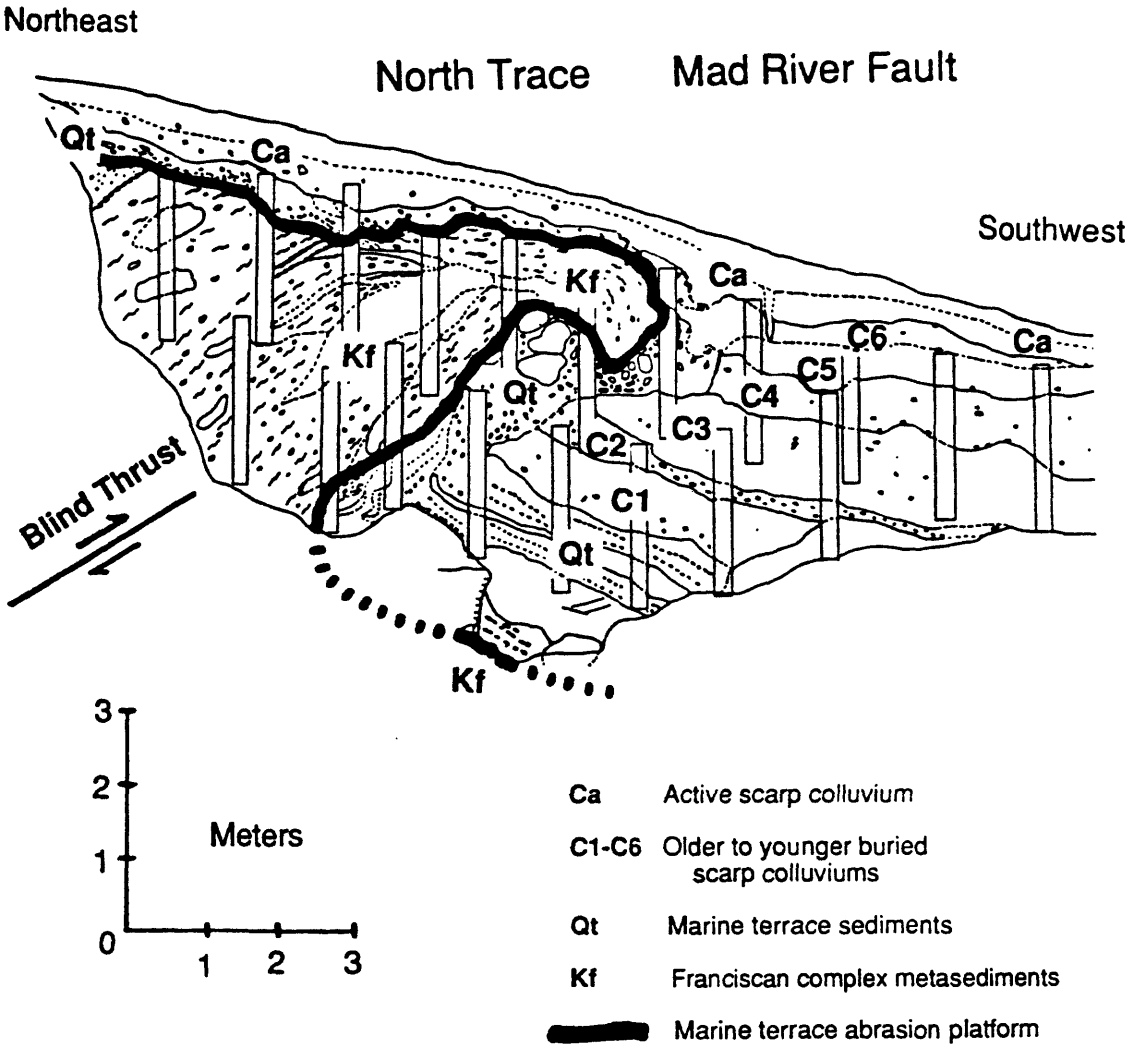

FIGURE 3. -- Portion of a trench log across the northern splay of the Mad River fault near McKinleyville, Humboldt County, Calif. At this location the fault is expressed as a well defined scarp that offsets a late Pleistocene marine terrace. The trenching showed the scarp is composed of a sharp overturned anticline with six scarp-derived colluvial wedges and associated buried soils below the overturned fold limb. The colluvial wedges are interpreted to result from coseismic slip on a shallow, blind thrust and sudden growth at the surface of the fault-propagation fold. Following each displacement, the scarp colluvium downslope from the fold crest was covered by a sheet of new colluvium eroded from the scarp above the fold. Each colluvial event quickly regraded the scarp profile and a weak soil developed during interseismic times. Trenches across the scarp 200 meters to the north revealed a sharply defined low-angle thrust fault similar that in figure 1.

strata with greater vertical separation of older deposits. Stratigraphically bracketed fault tips or truncated fault strands also may record individual slip events in such settings.

Where the coseismic fault slip is concentrated on a single fault or a few closely spaced slip surfaces (fig. 2,*A*), or where shallow blind thrusts propagate to the surface as tight overturned folds (fig. 2,*C*), steeper scarps form which favors generation of scarp colluviums and overthrusting of colluvial wedges. The relations between the near-surface structure of the fault, scarp morphology, and the occurrence of several types of paleoseismic indicators on thrust faults is shown in Figure 4.

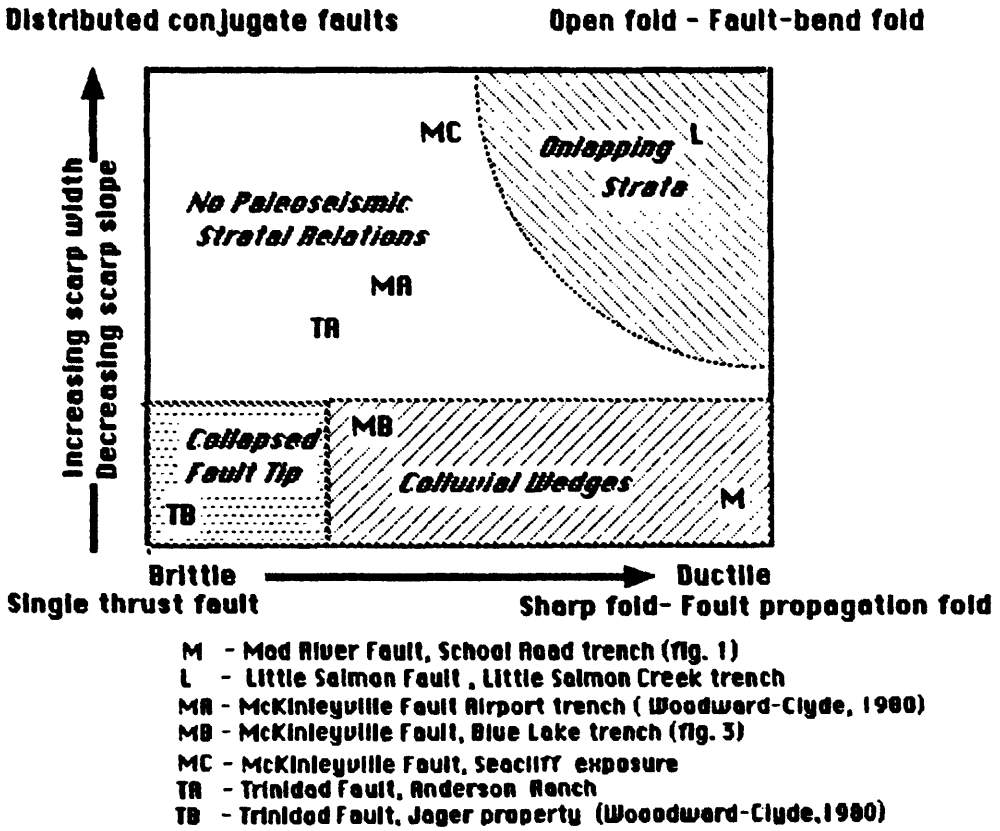

FIGURE 4. -- Relations between the style of deformation, structure, and scarp morphology for paleoseismic investigation of selected thrust faults in coastal northwestern California.

CONCLUSIONS

Criteria for recognizing individual paleoseismic events in compressional tectonic environments are varied and reflect the coseismic process and micro environment at the time of the earthquake. Large historic compressional earthquakes have produced paleoseismic indicators as a result of strong seismic shaking, tsunamis, uplift and subsidence, warping, folding, and surface-fault rupture. Similar features in the geologic record can be interpreted as resulting from individual paleoseismic events. Some paleoseismic relations result from tectonically controlled erosion and deposition and require special environments to form. Other relations, especially those associated with surface faulting, are the direct result of tectonic processes.

Paleoseismic relations usually show evidence of abrupt initiation, and commonly are bracketed by geologic features formed during quiescent interseismic intervals. The paleoseismic field relation is more informative if the amount and type of coseismic deformation from the paleoseismic event can be measured. Additional significance accrues if the age of the event can be determined. Presently, the data base for assessment of paleoseismic criteria in compressional tectonic environments is sparse. Particularly needed are studies, at the micro-stratigraphic and micro-geomorphic scale, of the effects of historic earthquakes in compressional environments. Similar detailed studies of the geologic record of active compressional structures and regions are also needed.

ACKNOWLEDGMENTS

Raymond (Bud) Burke shared responsibility for the trenching studies of northwestern California thrust faults and provided considerable insite concerning their paleoseismic interpretation. Kevin O'Dea, Greg Vick, Gilbert Craven, and Dave Lindberg also participated in the trenching and contributed valuable ideas and observations. John Parker and Ken Aalto reviewed a draft of the manuscript and made many helpful suggestions. The trenching investigation of northwestern California thrust faults was supported by a National Earthquake Hazard Reduction Program grant from the U.S. Geological Survey.

REFERENCES CITED

Abe, K., 1979, Size of great earthquakes of 1837-1974 inferred from tsunami data: Journal of Geophysical Research, v. 84, p. 1561-1568.

Adams, John, 1984, Active deformation of the Pacific Northwest continental margin: Tectonics, v. 3, p. 449-472.

Allen, C.R., 1987, Seismological and paleoseismological techniques of research in active tectonics, *in* Wallace, R. E., chairman, Active Tectonics: Washington, D.C., National Academy Press, p. 148-154.

Atwater, B.F., 1987, Evidence for great Holocene earthquakes along the outer coast of Washington state: Science, v. 236, p. 942-944.

Bartsch-Winkler, Susan, and Schmoll, H.R., 1987, Earthquake-caused sedimentary couplets in the upper Cook Inlet region, *in* Hamilton, T. D., and Galloway, J. P., ed., Geologic Studies in Alaska by the U.S. Geological Survey during 1986: U.S. Geological Survey Circular 998, p. 92-95.

Burke, R.M., and Carver, G.A., 1987, Soil development used as an indicator of fault scarp age and interseismic time, northwest California [*abs.*]: Geological Society of America Abstracts with Programs, v. 19, no. 7, p. 606.

Carver, G.A., and Burke, R.M., 1987, Late Pleistocene and Holocene paleoseismicity of the Little Salmon and Mad River thrust systems, N.W. California - Implications to the seismic potential of the Cascadia subduction zone [*abs.*]: Geological Society of America Abstracts with Programs, v. 19, no. 7, p. 614.

Davis, D.J., Suppe, John, and Dahlen, F.A., 1983, Mechanics of fold and thrust belts and accretionary wedges, Journal of Geophysical Research: v. 88, p.1153-1172.

Gordon, F.R., 1971, Faulting during the earthquake at Meckering, Western Australia--14 October 1968, *in* Recent Crustal Movements: Royal Society of New Zealand Bulletin 9, p. 85-93.

King, G.C.P., and Vita-Finzi, C., 1981, Active folding in the Algerian earthquake of 10 October 1980: Nature, v. 292, p. 22-26.

King, Geoffrey and Stein, Ross, 1983, Surface folding, river terrace deformation rate and earthquake repeat time in a reverse faulting environment, *in* The Coalinga, California, earthquake of May 1983: California Division of Mines and Geology Special Publication 66, p. 165-176.

Krinitzsky, E.L., 1974, State of the art for assessing earthquake hazards in the United States, Report 2, Fault assessment in earthquake engineering: Vicksberg, Mississippi, U.S. Army Corp of Engineers Waterways Experiment Station Miscellaneous Paper S-73-1, 88 p.

LaJoie, K.R., 1987, Coastal tectonics, *in* Wallace, R. E., chairman, Active Tectonics: Washington D.C., National Academy Press, p. 95-124.

Matsuda, T., Ota, Y., Ando, M., and Yonekura, N., 1978, Fault mechanisms and recurrence time of major earthquakes in southern Kanto district, Japan, as deduced from coastal terrac data: Geological Society of America Bulletin v. 89, p. 1610-1618.

Moore, J.C. and Silver, E.A., 1987, Continental Margin Tectonics-- Submarine Accretionary Prisms, *in* Heirtzler, J.R., ed., U.S. National Report to International Union of Geodesy and Geophysics 1983-1986 contributions in Tectonophysics: p. 1305-1312.

Nishenko, S.P., 1985, Seismic potential for large and great interplate earthquakes along the Chilean and southern Peruvian margins of South America-- A quantitative reappraisal: Journal of Geophysical Research v. 90, no. B5, p. 3589-3615.

O'Dea, K.M., Vick, G.S., Craven, G.F., and Lindberg, D.N., 1987, An analysis of deformation and surface expression of late Quaternary thrust faults, coastal northern California [*abs.*]: Geological Society of America Abstracts with Programs, v. 19, no. 7, p. 792.

Philip, H. and Meghraoui, M., 1983, Structural analysis and interpretation of surface deformations of the El Asnam earthquake of October 10, 1980: Tectonics, v. 2, no. 1, p. 17-49

Plafker, George, 1965, Tectonic deformation associated with the 1964 Alaska earthquake: Science, v. 148, no. 3678, p. 1675-1687.

Plafker, George and Kachadoorian, Reuben, 1966, Geologic effects of the March 1964 earthquake and associated seismic sea waves on Kodiak and nearby islands: U.S. Geological Survey Professional Paper 543-D, p. D1-D46.

Plafker, George and Savage, J., 1970, Mechanism of the Chilean earthquake of 1960--Implication for arc tectonics: Journal of Geophysical Research, v. 77, p. 901-925.

Plafker, George and Ruben, M., 1978, Uplift history and earthquake recurrences deduced from marine terraces on Middleton Island, Alaska, *in* Proceedings of Conference VI Methods and Identification of Seismic Gaps: U.S. Geological Survey Open-File Report 78-0943, p. 687-721.

Sims, J.D., 1975, Determining earthquake recurrence intervals from deformation structures in young sediments: Tectonophysics, v. 29, p. 141-152.

Slemmons, D.B., 1977, State of the art for assessing earthquake hazards in the United States, Report 6, Faults and earthquake magnitude: Vicksburg, Mississippi, U.S. Army Corps of Engineers Waterways Experiment Station Miscellaneous Paper S-73-1, 166 p.

Stein, R.S., 1983, Reverse slip on a buried fault during the 2 May 1983 Coalinga earthquake--Evidence from geodetic elevation changes, *in* The 1983 Coalinga, California earthquake: California Division of Mines and Geology Special Publication 66

Suppe, J., 1983, Geometry and kinematics of fault-bend folding: American Journal of Science, v. 283, p. 684-721.

Woodward-Clyde Consultants, 1980, Evaluation of the potential for resolving the geologic and seismic issues at the Humboldt Bay Power Plant Unit No. 3, unpublished report to Pacific Gas and Electric Company Inc.: Woodward-Clyde Consultants, San Francisco, Calif., p. C1-C129.

Yeats, R.S., 1983, Large-scale Quaternary detatchments in Ventura Basin, southern California: Journal of Geophysical Research, v. 88, p. 569-583.

_____ 1987, Active faults related to folding, *in* Wallace, R. E., chairman, Active Tectonics: Washington D. C. , National Academy Press, p. 63-79.

Yielding, G., Jackson, J.A., King, G.C.P., Sinvhal, C., Vita-Finzi, C. and Wood, R.M., 1981, Relations between surface deformation, fault geometry, seismicity, and rupture characteristics during the El Asnam (Algeria) earthquake of 10 October 1980: Earth and Planetary Science Letters, v. 56, p. 287-304.

RECOGNITION OF INDIVIDUAL PALEOSEISMIC EVENTS IN STRIKE-SLIP ENVIRONMENTS

BY

Thomas Rockwell
Department of Geology
San Diego State University
San Diego, California 92182

INTRODUCTION

Detailed analyses of laterally excavated, stratified, faulted sediments in trenches across strike-slip faults have yielded four morphostratigraphic criteria that are useful in recognizing and evaluating the relative timing of individual seismic events: (1) abrupt upward truncation of a fault strand or the level of faulting, (2) liquefaction phenomenon with associated unconformities or paleosurface features, (3) folding or dragging in the fault zone with associated unconformities, and (4) systematic and abrupt or stepped increases in displacement downsection (Sieh, 1978; 1984; Weldon and Sieh, 1984; Rockwell and others, 1986). The application of two or more of these criteria are usually sufficient for determining the relative timing of displacement events in a faulted section. Precise dating of events relies on the type and precision of the dating technique employed.

CRITERIA FOR THE DETERMINATION OF THE TIMING OF FAULTING EVENTS

Abrupt Truncation of a Fault Strand

Abrupt truncation is the clear, upward termination of a fault rupture in stratified sediments (fig. 1), the inference being that a rupture occurred, broke to the surface, perhaps produced a scarp, and was subsequently buried by younger sediments. Determining the age of the youngest faulted sediments and the oldest unfaulted sediments brackets the age of the event within the error limits of the dating technique (Sieh, 1978; 1984). Problems commonly arise when the third dimension is not taken into account. Most strike-slip surface ruptures produce en echelon or stepping patterns which, when considered in three dimensions, means that slip is being transferred from one surface-break segment to another (fig. 2). In the area of the step, there may be two or more breaks in the subsurface resulting from the one rupture event, but only one or two breaks at the surface since the termination of an individual rupture segment at the surface represents the location where the break begins cutting downsection as slip is transferred to an adjacent rupture segment. Thus a single two-dimensional exposure across a strike-slip fault, if poorly located, may expose multiple fault traces from a single rupture event that cut up to different

FIGURE 1.--Photograph of Dr. Kerry Sieh and the surface rupture of event R (circa 1100 A.D.) at Sieh's excavations at Pallet Creek on the San Andreas fault (see Sieh, 1978). Note the upward truncation of the fault trace by the youngest unfaulted peat. Dating of the oldest faulted and youngest unfaulted peats bracketed the timing of the earthquake.

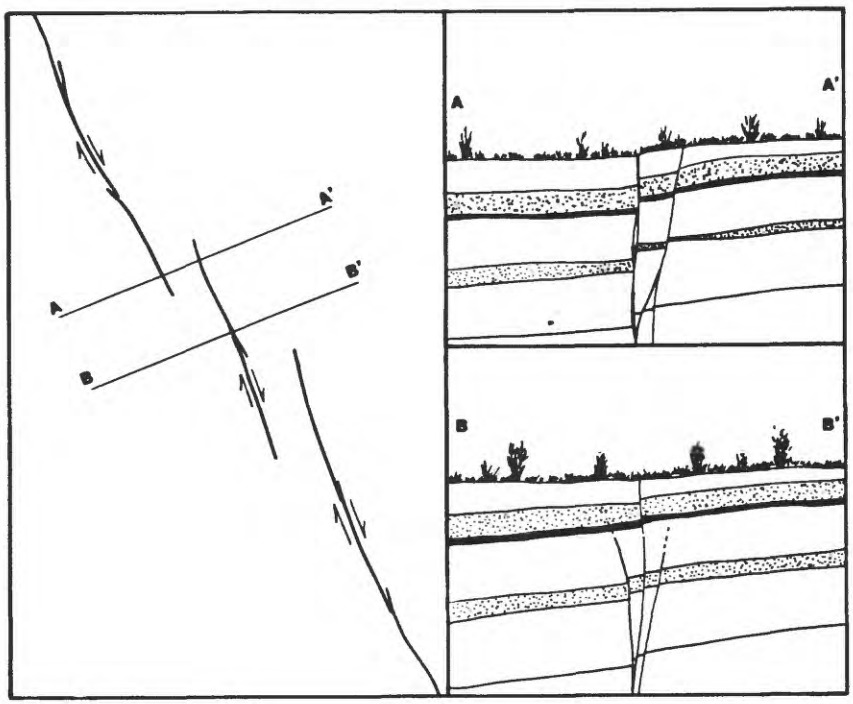

FIGURE 2.--Schematic map of a typical en eschelon surface-rupture pattern for a nearly pure strike-slip fault breaking through sediments (left figure). Cross-section A-A' shows a plausible pattern of faults in an exposure where there are two discrete surface traces. Section B-B' shows only one surface rupture but two subsurface ruptures. All of the ruptures formed at the same time due to transfer of fault slip across the step.

stratigraphic levels (B-B' in fig. 2). To identify this possibility, three-dimensional excavations within the fault zone are recommended to establish abrupt upward truncation of a rupture. To qualify, a rupture would have to maintain upward truncation at a specific stratigraphic level in sequential lateral exposures.

Liquefaction

Liquefaction is commonly produced by moderate and large magnitude earthquakes. Usually, establishing the source of the seismic shaking that produced the liquefaction feature is a problem. For instance, liquefaction of sag-pond sediments is possible by seismic slip on the fault that produced the sag pond or by movement on nearby seismogenic faults. Thus, liquefaction

alone is not a reliable criterion for recognizing individual events on a given fault. Nevertheless, it can be very valuable in conjunction with other kinds of evidence. In addition, some liquefaction features may be more useful than others in establishing whether or not the fault under study produced the apparently related features. Liquefaction within the fault zone resulting in the eruption of sand volcanoes or sandblows along the fault surface trace (fig. 3) is better evidence that a specific fault produced the liquefaction than, for instance, dewatering features in sediments removed some distance from the surface trace of the fault.

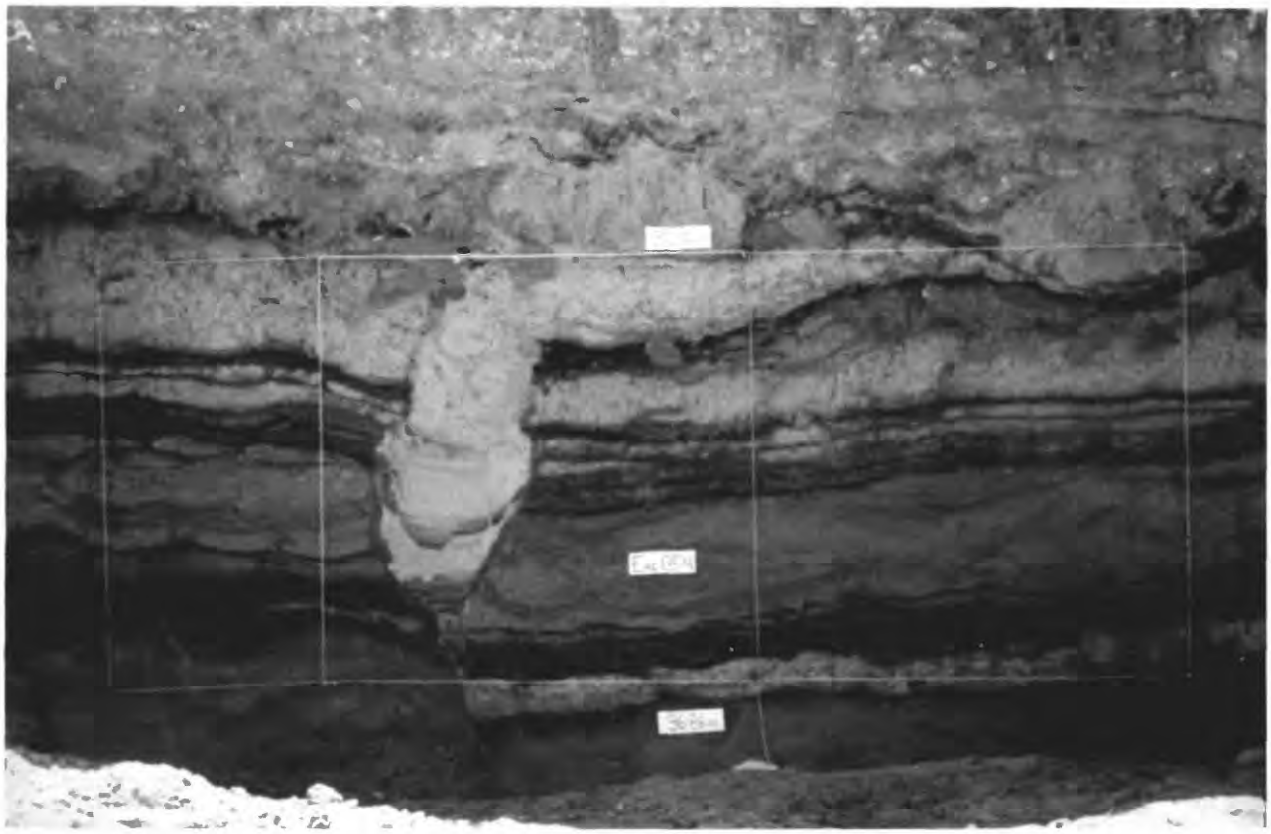

FIGURE 3.--Photograph of a sandblow injected along the rupture surface during an earhquake at Pallet Creek on the San Andreas fault (Photograph by Kerry Sieh).

Coseismic Folding and Drag

When present, vertical drag at the fault is easily recognized in horizontally stratified sediments (fig. 4). Usually, some vertical slip is locally present along strike-slip faults, especially where the fault makes a bend or step (Crowell, 1974). Many trenching studies that have yielded clear evidence

about the timing of prehistoric earthquakes were located in areas where sediments have been ponded in association with releasing fault jogs or bends and, thus, have local vertical components of slip (Rockwell and others, 1986; Clark and others, 1972). In these areas, bending or vertical drag may accommodate some of the vertical movement in unconsolidated sediments. Incremental increases in tilting with depth with associated onlapping statigraphic relationships (angular unconformities) (fig. 4) can indicate individual slip events.

Horizontal drag is much more difficult to recognize in horizontally stratified sediments but probably occurs if vertical drag is present. Paleomagnetism may be the best way to evaluate horizontal drag if the sediments carry a clean magnetic signal (Kerry Sieh and Steve Salyards, oral communication from work in progress, 1987).

Individual ruptures commonly end in folding and, in some cases, folding may be the dominant mechanism for strain accumulation in unconsolidated, fine-grained sediments (Sieh, 1984). Similar to the abrupt upward truncation of fault ruptures, upward truncation of folds or the sudden upward termination of a fold set with associated infilling by subsequent sedimentation or an unconformity can indicate the timing of slip events (Sieh, 1984).

Abrupt Downsection Increases in Slip

Assuming a fault has accumulated slip with time, stratigraphically lower, and therefore older, strata should display increasingly greater displacements. A creeping fault that cuts continously deposited sediments would probably show a gradual increase in displacement with increasing depth. A fault that releases accumulated elastic strain as individual, coseismic-slip events, however, should show abrupt downsection increases in slip at specific stratigraphic levels. These abrupt increases representing slip events should occur at the same levels, and therefore at the same time, as other indicators of paleoseismic events.

DISCUSSION AND CONCLUSIONS

In the above scenarios, two or more criteria should be used, when possible, to recognize and establish the timing of paleoearthquakes. If only the upward termination of a fault break is used, it should be clearly established in the third dimension that the break terminates at the same straigraphic level and is not simply cutting upsection or downsection as slip is transferred to another break.

When evidence from liquefaction features are used, care must be taken to determine whether or not the features can be confidently attributed to a specific fault. Folding with associated unconformities, like liquefaction features, may be excellent indicators of the timing of earthquakes but only if the

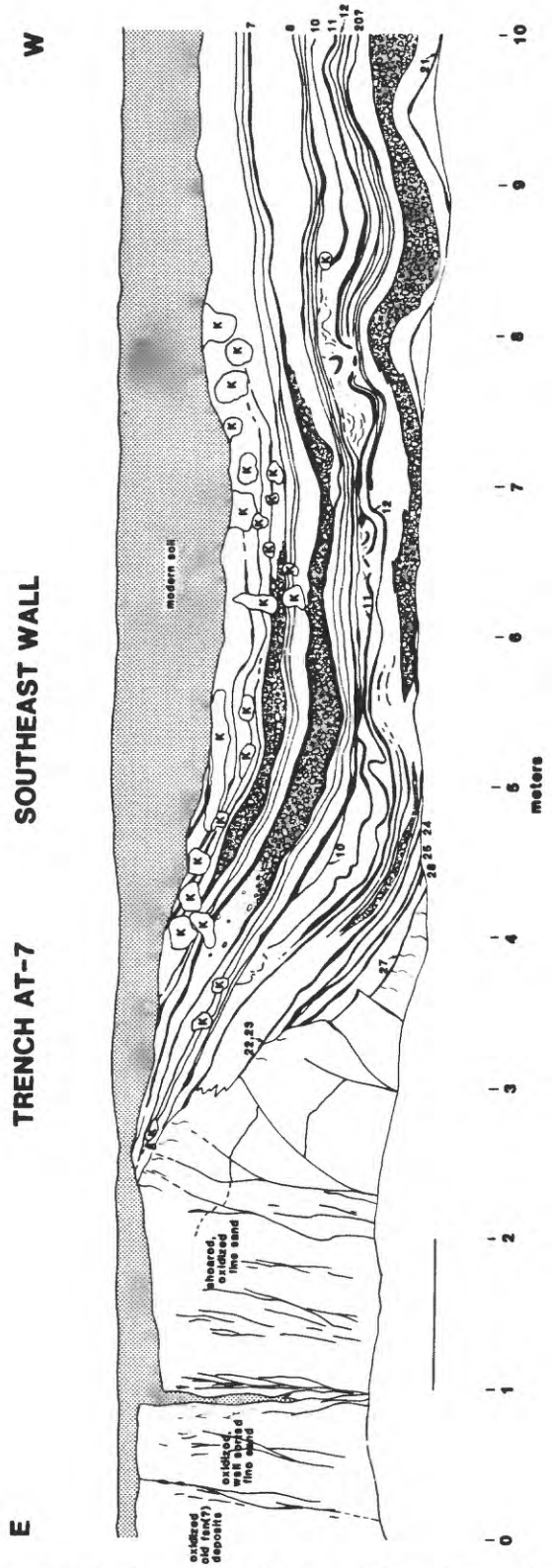

FIGURE 4.--Log of trench AT-7 from Glen Ivy Marsh along the Elsinore fault. The solid dark strata are peat layers. Note the severe folding and liquefaction of peats 10 and those below in the center part of the figure. The peats above peat 10 are less deformed. Also note that, from peat 10 downsection, the bed dips are steeper at the fault zone near the left side of the figure than they are in the overlying section.

folding can be directly related to slip on a specific fault or to other direct tectonic deformation. Soft-sediment slumping can produce folding and can be seismically triggered, but like liquefaction, it cannot always be attributed to a specific fault.

Abrupt increases in slip downsection, in association with any of the other criteria, can be the best evidence of timing of large earthquakes. Many moderate-sized events may be missed, however, if only a minor amount of slip was associated with each moderate-sized event, because the error in determining the amount of slip for large earthquakes can exceed the amount of slip in a moderate quake.

REFERENCES CITED

Clark, M.M., Grantz, A. and Rubin, M., 1972, Holocene activity of the Coyote Creek fault as recorded in sediments of Lake Cahuilla: U.S. Geological Survey Professional Paper 787, p. 112-130.

Crowell, J.C., 1974, Origin of late Cenozoic basins in southern California: in Dickenson, W.R., ed., Tectonics and sedimentation: Society of Economic Paleontologists and Mineralogists, Special Publication 22, p. 190-204.

Rockwell, T.K., McElwain, R.S., Millman, D.E. and Lamar, D.L., 1986, Recurrent late Holocene faulting on the Glen Ivy North strand of the Elsinore fault at Glen Ivy Marsh: in Ehlig, P., compiler, Neotectonics and faulting in southern California: Geological Society of America Fieldtrip Guidebook for the Cordilleran Section Meeting in Los Angeles, California, p. 167-175.

Sieh, K.E., 1978, Prehistoric large earthquakes produced by slip on the San Andreas fault at Pallet Creek, California: Journal of Geophysical Research, v. 83, p. 3907-3939.

Sieh, K.E., 1984, Lateral offsets and revised dates of large prehistoric earthquakes at Pallet Creek, southern California: Journal of Geophysical Research, v. 89, no. B9, p. 7641-7670.

Weldon, R. and Sieh, K.E., 1984, Holocene rate of slip and tentative recurrence interval for large earthquakes on the San Andreas fault, Cajon Pass, southern California: Geological Society of America Bulletin, v. 96, p. 793-812.

A FACIES MODEL OF COLLUVIAL SEDIMENTATION ADJACENT TO A SINGLE-EVENT NORMAL-FAULT SCARP, BASIN AND RANGE PROVINCE, WESTERN UNITED STATES

by

Alan R. Nelson[1]

Seismotectonic Section, D-1632
Engineering and Research Center
U.S. Bureau of Reclamation
P.O. Box 25007
Denver, CO 80225

[1]Present address:
Branch of Geologic Risk Assessment
U.S. Geological Survey, MS 966
P.O Box 25046
Denver, CO 80225

ABSTRACT

Inferring the magnitude and recurrence of paleoearthquakes from exposures of geologically young normal faults is difficult because the stratigraphy of colluvial sediments adjacent to faults is often complex. Facies models of colluvial sedimentation, which can be developed by comparing lithofacies in many exposures, are tools used in complex depositional environments to help understand the sedimentation history at a site. These tools are needed to improve the understanding of tectonic, pedologic, and slope processes near faults and the sequence of events on faults. A facies model of the sedimentary response to a single, 2.2-m surface-faulting event in coarse-grained alluvial sediments at a gently sloping site illustrates some common lithologic and stratigraphic relationships along normal faults in the Basin and Range. Lithofacies codes, adapted to colluvial sediments in this region, are used to describe the model.

INTRODUCTION

Geologic studies of the recent history of faults are one of the most successful approaches in earthquake-hazard research in the Western United States (Wallace, 1981). The most detailed data used to infer paleoearthquake magnitude and recurrence have come from trenching faults (for example, Clark and others, 1972; Sieh, 1978; Swan and others, 1980; McCalpin, 1982). Study of the stratigraphy in trench and natural fault exposures has advantages over morphologic studies of fault scarps (for example, Hanks and others, 1984) because exposed stratigraphic units usually record the number and relative size of surface-faulting events and, in many cases, trenching exposes datable material (for example, Sieh and Jahns, 1984; Nelson and VanArsdale, 1986; Machette, 1986). Unfortunately, the stratigraphy of deposits near young faults in the Basin and Range of the Western United States is often so complex or the record of events is so fragmentary that determining a detailed history of faulting is difficult--even in studies of the best exposures. Improved methods of interpreting fault exposures are needed if accurate earthquake-magnitude and recurrence values are to be obtained.

Most exposures of Quaternary faults show a complex stratigraphy. Some of this complexity is due to the fragmentary record produced by erosion of previously deposited units, but most of the complexity is the result of the variety of processes and process rates that influence slope-sediment transport and deposition near fault scarps. These processes and rates are affected by (1) changes in regional climate over time and altitude, (2) the magnitude, extent, and recurrence

interval of earthquakes producing surface ruptures (scarps) along range fronts, (3) surface rupture patterns and history, (4) site bedrock and surface-sediment lithology, (5) local geomorphology and aspect of a site, (6) soil development, and (7) fluvial or eolian deposition near the scarp.

In this paper I present a facies model of colluvial sedimentation adjacent to a single-event normal-fault scarp in the Basin and Range. The facies terminology and lithofacies codes used to describe the model are also introduced, but space limitations prevent a full discussion of these topics. Some of the lithofacies codes shown in figure 1 are not used here; the complete list of codes used by Nelson (1986) is shown to illustrate those features that are most important in describing lithofacies in the Basin and Range. Thorough discussion of these facies codes is reserved for a future publication.

SEDIMENTARY FACIES MODELS

The interpretation of many complex sedimentary environments has been made easier and more accurate by the development of facies models (Reading, 1978). Facies models are "...general summaries of a specific sedimentary environment..." (Walker, 1984). The summaries are based on detailed descriptions of lithofacies (grain size, bedding, sedimentary structures) and on studies of modern sedimentary processes. Models can be expressed in various formats (cross sections, block diagrams, graphs). A facies model "...must act 1) as a norm, for purposes of comparison, 2) as a framework and guide for future observations, 3) as a predictor in new geological situations, and 4) as an integrated basis for interpretation of the environment or system that it represents..." (Walker, 1984, p. 6). Facies models are widely used in fluvial and marine sedimentology (Reading, 1978) and are provoking reevaluation of some basic assumptions in fields such as glacial stratigraphy, which have tended to focus on chronology rather than sedimentary processes (Eyles and others, 1983; Karrow and others, 1984).

Although the term facies has been used in many ways, most geologists use the term in an objective, descriptive sense for a body of rock or sediment with specific characteristics (Middleton, 1978; Reading, 1978). A second, genetic use of the term facies simplifies discussion of colluvial lithofacies (discussed below). I use the term lithofacies in the abstract sense to describe the dominant characteristics of a group of lithologically similar bodies of sediment.

The development of facies models requires comparing lithofacies assemblages from many sites. Comparing lithofacies is relatively easy if standard symbols (codes) are used. Many authors have used the lithofacies codes of Miall (1977; 1978), which consist of a capital letter for the primary lithology followed by lower case letters describing the most characteristic internal features, to document fluvial facies relationships. Eyles and others (1983) modified these codes for use in glacial environments by adding a primary code (D) for diamict lithofacies, new internal-structure descriptors, and a few interpretive modifiers. Interpretive modifiers are placed in parentheses because they are not objective like the other code symbols (fig. 1); interpretive modifiers imply a particular genesis.

I have modified the codes of Eyles and others (1983) for use with small-scale colluvial, fluvial, and eolian deposits adjacent to fault scarps in the arid to semiarid Basin and Range of the Western United States (fig. 1). My codes are a shorthand notation designed to allow rapid visual assessment of facies relationships. The codes are not a substitute for the more detailed descriptions of color, grain size, structures, and contacts recorded during the mapping of any exposure (Eyles and others, 1983). My codes may also be useful in studies of colluvial facies in other geomorphic and climatic settings (for example, Mousinho de Meis and Da Silva de Moura, 1983; Watson and others, 1984).

COLLUVIAL FACIES

Colluvium is sediment found on and adjacent to slopes; it is usually an unconsolidated mixture of clay, silt, sand, and gravel, massive to poorly stratified, and poorly sorted (for

FIGURE 1.--Facies model of colluvial sedimentation adjacent to a hypothetical single-event normal fault scarp on a gently sloping, coarse, gravelly, fluvial terrace or alluvial fan. The scarp was produced by a single large earthquake (M = 6.5-7.5) during the early to middle Holocene in the arid to semiarid Basin and Range. This is one of the most common of many possible models for this depositional, climatic, and tectonic setting. Only major facies relationships are shown; most exposures of faults are more complex than the model. The lithofacies codes used in the model include the four primary lithofacies of Eyles and others (1983) with the addition of "R" for bedrock. Additional internal structure and interpretive modifier symbols and soil-horizon symbols (Guthrie and Witty, 1982) have also been added. Although some of the same letters are used as both lithologic and internal structure descriptors, position within the code symbol indicates the meaning. Where distinct subfacies within a unit are not separately delineated, code symbols for the unit are separated by commas. A, Cross section showing scarp in fluvial and soil units immediately after faulting, before any colluvial deposition. B, Cross section showing facies relationships after deposition of a colluvial debris wedge against the scarp. Proximal and distal debris wedge deposits are shaded. Lithofacies codes shown in A are not shown. C, Cross section showing present-day facies relationships after deposition of proximal and distal wash facies. Debris facies and wash facies are shaded. Lithofacies codes shown in A and B are not shown in C.

Explanation for Symbols

FAULTS AND FRACTURES

- Fault with measurable displacement
- Fracture

CONTACTS

- Sharp and distinct
- Gradual, but distinct
- Gradual and indistinct
- Faint
- Distinct lateral intertonguing (typically between subfacies)
- Gradual lateral intertonguing
- Uneroded free face of a fault
- Buried fault scarp

LITHOFACIES CODES

Main lithology	Lithologic or matrix modifier	Internal structure	Interpretive modifier	Soil horizon
G (gravel)	b=bouldery	s=stratified	(f)=dispersed fragments	A
D (diamicton)	p=pebbly	p=planar bedded	(r)=resedimented	BA
S (sand)	d=coarse	n=planar X-bedded	(s)=sheared	Bw=cambic B
F (fines)	f=fine sandy	t=troughs	(c)=current reworked	Bt=argillic B
R (rock)	s=silty	r=rippled	(e)=eolian additions	
	c=clayey	g=graded	(i)=infiltration of fines	
	k=CO3-rich	m=massive	(d)=deformed (in place)	
		x=matrix support	(b)=burrowed	
		c=clast support	(w)=highly weathered	
		i=clasts imbricated		
		h=horizontal lamination		
		l=loose		
		f=fractured		
		o=openwork (no matrix)		

[ ] = source lithology for colluvium
( ) = soil horizon
_ = modifier not used in this position
/ = both lithologies present in different parts of unit

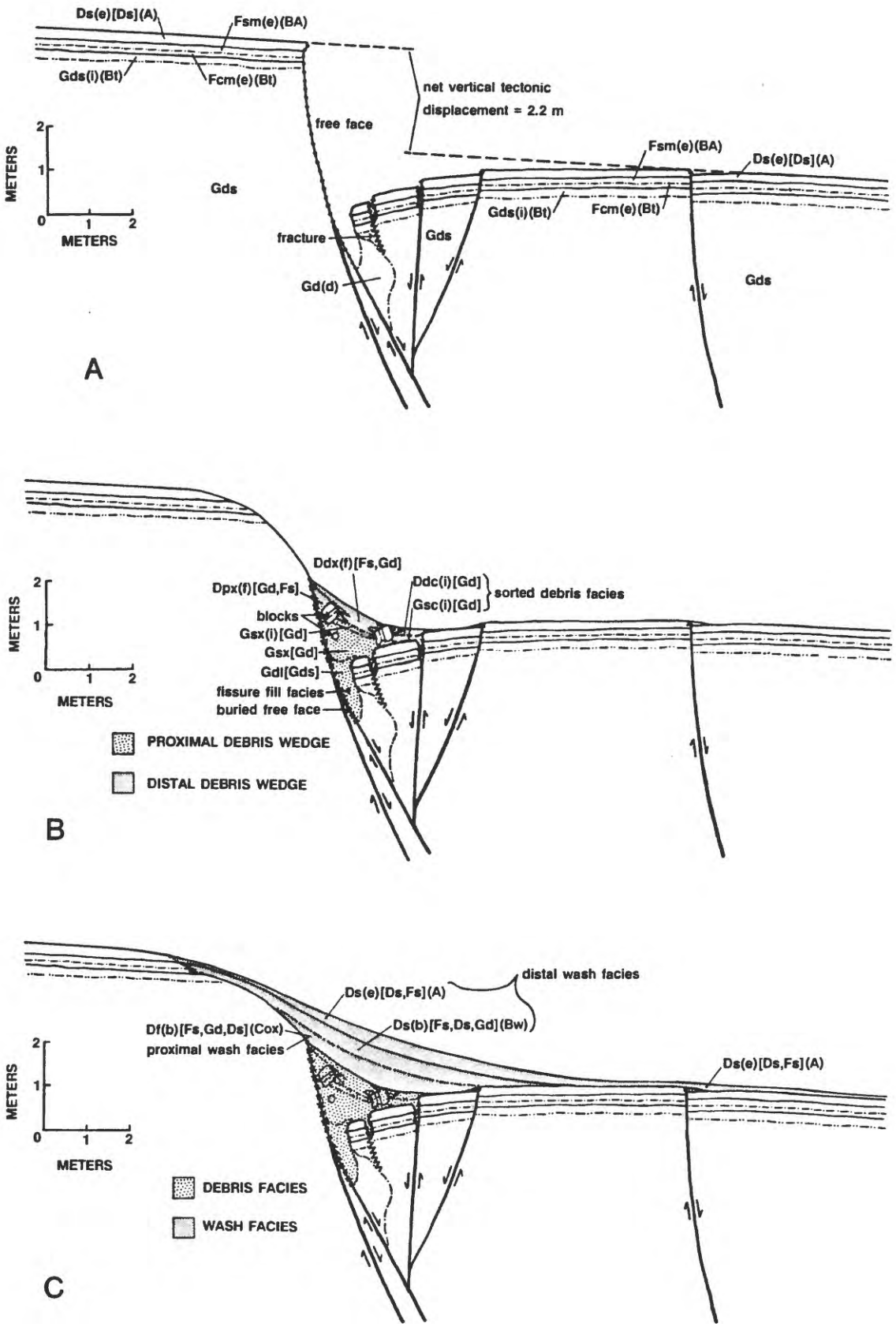
Ds(e)[Ds](A)
Fsm(e)(BA)
Gds(i)(Bt)
Fcm(e)(Bt)
net vertical tectonic
displacement = 2.2 m
free face
METERS
2
1
0
1
2
METERS
Gds
fracture
Gd(d)
Gds
Gds(i)(Bt)
Fcm(e)(Bt)
Fsm(e)(BA)
Ds(e)[Ds](A)
Gds
A
Ddx(f)[Fs,Gd]
Dpx(f)[Gd,Fs]
Ddc(i)[Gd]
Gsc(i)[Gd]
sorted debris facies
blocks
Gsx(i)[Gd]
Gsx[Gd]
Gdl[Gds]
fissure fill facies
buried free face
PROXIMAL DEBRIS WEDGE
DISTAL DEBRIS WEDGE
B
distal wash facies
Ds(e)[Ds,Fs](A)
Df(b)[Fs,Gd,Ds](Cox)
proximal wash facies
Ds(b)[Fs,Ds,Gd](Bw)
Ds(e)[Ds,Fs](A)
DEBRIS FACIES
WASH FACIES
C

example, Kwaad and Mucher, 1979; Imeson and others, 1980; Watson and others, 1984; Mills, 1987). Colluvium differs from some other genetic types of sediment in that its lithology is primarily a reflection of the lithology of its source (provenance) rather than a reflection of transport process.

The colluvial facies of concern here are those deposited adjacent to young normal fault scarps. In the Basin and Range, scarps are generally found near the base of fault-bounded mountain ranges (Gilbert, 1928; Wallace, 1978; Nakata and others, 1982). Rapid erosion of initial near-vertical scarps and the building of an adjacent wedge of colluvial debris forms moderately sloping scarps (25^{o}-40^{o}) that, with time, can degrade to slope angles of a few degrees (Wallace, 1977). The scarps are commonly developed in colluvium, alluvial-fan sediments, lake sediments, and stream alluvium. Scarps can be 0.1-80 m high, but most are between 1 and 10 m high.

Colluvial lithofacies can be discussed more easily if the term facies is used in a genetic sense. This use implies the process that produced a body of sediment, not the lithologic characteristics of the unit (Reading, 1978). Because colluvium can be derived from diverse lithologies and is transported only short distances, units of similar genesis often have different lithologies. Thus, terms are needed for colluvial units that were deposited by the same depositional processes and/ (or) may have the same relationship to tectonic features but that have different lithologies and so cannot be grouped into the same lithofacies. For example, proximal debris wedge is a genetic facies term for colluvium deposited mostly by gravity processes adjacent to a fault, but this facies could consist of coarse gravel or sandy silt. The genetic use of facies should be clearly distinguished from the objective, descriptive use of the term (by definition, the brackets around symbols in figure 1 indicate a colluvial genesis for that unit).

The recognition of soil development on previously deposited colluvial units is important in the correct genetic interpretation of lithofacies (Butler, 1959). A soil horizon may be coincident with all or part of a lithofacies or of a genetic facies. Lithofacies refers to the present lithology of a unit, not to its immediate post-depositional lithology. But soil development often alters the lithology of a unit. Recognition of soil development in a unit is part of the genetic interpretation of that unit, so identifying soil horizons is part of the process of distinguishing genetic facies. Soil-horizon symbols can be added to the facies codes to show the type of soil development in a unit (fig. 1).

Discussion of colluvial facies requires a consistent genetic facies terminology. Colluvial facies deposited either near the base of steep range-front slopes or adjacent to scarps in unconsolidated deposits can be divided into debris facies and wash facies, following process-oriented slope-morphology studies (for example, Young, 1972; Cooke and Warren, 1973; Wallace, 1977). Much of the material in scarp-associated debris facies is talus and the term talus is consistent with the term wash because both imply genesis. However, for consistency with the earlier literature and because some material in debris facies is often deposited by non-gravity-controlled processes the term debris is retained here.

Debris facies consist of blocks (>5 cm in diameter), fragments (2 mm to 5 cm in diameter), and minor amounts of fine-grained sediment deposited primarily by gravity-controlled processes. Blocks (including cobbles) can be released from a fault-scarp free face by falling (spalling), toppling, slumping, or sliding . Falling or toppling blocks frequently break into fragments on impact and slumping of the exposed free face often also produces fragments. Blocks of sediment on the debris wedge also weather into fragments. Although less important than gravity-controlled processes, wash processes also contribute sediment to the debris wedge. Thus, debris facies are usually mixed with and gradational with wash facies.

Wash facies are deposited predominantly by sheetwash, rill wash, and rainsplash (soilsplash) processes. Snowmelt may produce runoff that contributes sediment to wash facies. In some areas, eluviation of fines by throughflow, minor eolian deposition, and seasonal creep may contribute significant amounts of sediment to the units that I term wash facies. These sediments are included in wash facies because they are often difficult to distinguish from surface-wash-process sediments (Young, 1972). It is, however, important to try to distinguish

wash and creep deposits derived primarily from the fault scarp from similar deposits derived from slopes above the scarp (Ostenaa, 1984), and from fluvial and thick eolian beds deposited against the scarp.

In addition to genetic terms, positional terms are also useful in categorizing colluvial lithofacies. Proximal and distal refer to the relative distance from the scarp or fault; basal refers to the lower part of a wedge of colluvium adjacent to a fault.

A COARSE-SOURCE LITHOLOGY FACIES MODEL FOR A SINGLE-EVENT FAULT

Figure 1 is one of many possible facies models for colluvial sediments adjacent to young fault scarps in the arid to semiarid Basin and Range. The model is generalized from sediment characteristics and stratigraphic relationships in 35 exposures of normal faults in the eastern Basin and Range, and from studies of fault scarps produced by historic earthquakes throughout the Western United States (complete list of sources available from author). Most of the scarps marking these faults were produced by multiple, surface-faulting events; therefore, the facies relationships produced by an initial, single event are partly inferred. Unit dimensions, lithologies, and stratigraphic relationships in the model are typical of the fault exposures, but quantitative measurements of all units in these exposures have not yet been made. Many exposures are more complex than this model and no single exposure shows all facies exactly as they are shown in the model. However, as is the case with hillslope-morphology models (Small and Clark, 1982), more complex, detailed models are less widely applicable (Walker, 1984). By keeping the model simple I emphasize common colluvial facies patterns and the most significant units in interpreting fault displacement histories. This model provides a framework for the interpretation of normal fault exposures and forms a basis for developing more detailed models.

In the model, coarse, stratified, fluvial gravels (Gds in fig. 1) have been displaced by a range-bounding fault during a large earthquake forming a scarp about 2.5 m high. The gravels are mostly clast-supported and have a matrix that ranges from coarse sand to sandy silt. Typically, the gravels are alluvial-fan sediments deposited by streams issuing from a mountain front canyon, interbedded with occasional matrix-supported debris-flow deposits. However, the model also includes gravelly fluvial-terrace deposits along major stream valleys. In both cases, the gravels are usually capped by 0.3 to 1.0 m of loess (Fsm(e)(BA) on fig. 1A) and/or surface-wash colluvium (Ds(e)[Ds](A)) consisting of sandy or clayey silt; at older sites there is usually an argillic B horizon (Fcm(e)(Bt)) developed in the lower part of the fine-grained unit and the uppermost part of the gravel. The scarp in the gravels is far enough away from the mountain front or the valley side to be unaffected by wash processes on steep slopes.

Displacement of the gently-sloping ($<5^{\circ}$) fan or terrace is about 2.2 m. The fault, which dips about 65°-70° towards the basin at depth, ruptured the ground surface in a single, near-vertical (75°-90°) scarp. However, antithetic faulting and backtilting of the hanging wall block near the fault have increased the stratigraphic displacement at the fault to about 3.8 m. Typically, extensional stresses have produced a fissure at the base of the scarp which can be up to 0.7 m wide and several meters deep. Some of the antithetic fault blocks may be tilted and broken by small fractures (Gd(d) in fig. 1A).

The proximal debris wedge adjacent to the scarp often begins forming before the ground motion from the earthquake ceases (fig. 1B). If the gravels have a loose, sandy matrix, then a wedge forms quickly by slumping of the least-consolidated units and by spalling of clasts. In this case, the lithology of the basal part of the wedge will be almost identical to that of the loose gravels in the free face. However, if the gravels are more coherent, the wedge will form much more slowly, primarily by spalling of individual fragments and clasts, with an increasing wash contribution from the top of the scarp. In either case, the basal part of the proximal debris wedge will tend to have more clasts and a coarser matrix than the upper part (Gsx[Gd] in fig. 1B); these clasts usually have no preferred orientation. Blocks of finer, more-consolidated sediment (usually, pieces of A and B soil horizons from the top of the scarp) can be deposited throughout the wedge. However, blocks tend to occur above the coarsest, basal part of the

wedge because it usually takes longer for coherent blocks to break free from the free face than it does for the basal part of the proximal debris wedge to form.

If a fissure forms at the base of the scarp, then blocks and fragments of the proximal debris will fill the fissure (fissure-fill facies, fig. 1B). Because fissures fill rapidly with coarse gravelly debris, a jumbled, open-work gravel with little matrix sediment is often deposited. Infiltration of fines from younger overlying units usually fills the pore spaces in these gravels, but complete filling can take thousands of years. Fissure-fill facies are often confused with sheared sediment in fault zones; studies of clast fabrics (McCalpin, this volume) or micromorphological methods may be of use in distinguishing fissure fill from sheared sediments (for example, Low and others, 1982).

As soon as a proximal debris wedge has accumulated, falling and sliding clasts on the wedge become better sorted. Smaller clasts and fragments often lodge against the upper side of larger blocks. Clasts that reach the distal part of the debris wedge are sorted into thin, clast-supported wedges at the toe of the larger debris wedge (sorted-debris facies) (Gsc(i)[Gd] in fig. 1B). Sorting of clasts on the debris wedge is most effective when the clasts are rounded and the surface of the debris wedge is steep. If well-developed soils are found near the crest of the scarp, eroded fragments of argillic B soil horizons may also accumulate on the distal portions of the wedge. Non-equidimensional clasts on the wedge tend to be aligned parallel with the surface of the wedge. Elongate clasts oriented perpendicular to the slope are more common than clasts oriented across the slope in the distal facies of the debris wedge. Field observations suggest that the long axes of elongate clasts usually point downslope if they have fallen or slid but not rolled, and across the slope if they have rolled. Armoring of the wedge by coarse fragments has also been noted (Wallace, 1977). Where contrasting lithologies are exposed in the free face, an inversion of these stratigraphic units can often be identified by the lithology of fragments in the debris wedge (for example, McCalpin, this volume).

Over a period of weeks to decades, wash processes gradually begin to make important contributions to the debris wedge as the scarp free face erodes, producing a distal debris wedge. This gradual change from almost entirely gravity-controlled processes to partly wash-controlled processes produces a generally fining-upward sequence in the wedge. Even though clasts and blocks of sediment still fall onto the wedge and roll down it as they are released from the free face, wash processes now help move them downslope or deposit fine sediments around them. The sources of the fine sediments are the soil and loess units typically found in the upper part of the free face, dust, and fine-grained sediment from above the scarp. Even when a free face tends to erode back by block toppling and sliding rather than by clast spalling and wash erosion, wash processes will deposit sediments around the blocks. These processes produce distal debris-wedge facies that contain more debris than wash sediments; these facies are characteristic of the upper and distal parts of the debris wedge.

For example, in figure 1B in the upper part of the distal debris wedge, a pebbly diamiction with matrix support (Dpx(f)[Gd,Fs]) is deposited against what is left of the free face. However, in the center of the wedge, a similar diamicton contains cobbles (Ddx(f)[Fs,Gd]) because cobbles tend to roll farther than pebbles. Both distal debris-wedge facies also contain fragments (f) of a soil horizon eroded from near the top of the scarp. Along the distal part of the debris wedge, where there is usually a break in the slope of the scarp, rolling and sliding clasts are concentrated in a sorted-debris facies. The sorted-debris facies is a clast-supported diamicton that has received some of its present-day matrix silt by infiltration from overlying units (Ddc(i)[Gd]). All three colluvial-diamicton facies are derived from the faulted gravels (Gds), but the matrix-supported units are also partially derived from the fine-grained units (Fs) near the scarp crest. The relative amount of sediment contributed to the colluvial units from these two different lithologic sources changes down the wedge ([Gd,Fs] compared with [Fs,Gd]). In most cases, fines from the distal debris wedge infiltrate into the upper parts of the underlying proximal debris wedge (Gsx(i)[Gd]).

Once the lower part of the free face has been buried by the proximal wedge and the upper part has been eroded, deposition is dominated by wash processes. Wash facies are usually mixtures of sand, silt and clay, and are classified as diamictons in this code. Proximal wash

facies (Df(b)[Fs,Gd,Ds](Cox) on fig. 1C) tend to be sandier than distal wash facies, but all parts of the wash wedge usually fine upward. Clasts and fragments are dispersed in wash facies, but form only a minor component of these deposits. The rate of deposition of wash facies is much lower than the rate of debris facies deposition; therefore, eolian deposition, wash deposition from above the scarp, burrowing, and soil development influence the lithology of wash facies much more than they influence debris facies. In figure 1C, neither wash facies has a large enough eolian component to require the interpretive modifier (e), but both facies are partly derived from units above the scarp that may include loess, as shown by the Ds component within the square brackets of the code for each facies. Both wash units have also been burrowed by rodents ((b), fig. 1C) and the surface soil has developed in these units (soil-horizon symbols in parentheses following the brackets).

Wash processes and eolian deposition will eventually erode the scarp crest and infill the footslope to the point where a topographic step no longer exists. In the arid to semiarid Basin and Range, at least many tens of thousands of years are needed for a scarp of this height to disappear, but rates vary greatly depending on factors such as the rate of eolian influx. At flat sites where soils are cemented by carbonate, scarps can persist for hundreds of thousands of years (for example, Nelson and Weisser, 1985). Frequently, a former scarp may be marked by a vegetation contrast due to greater available moisture in the thick, fine-grained wash facies covering the former footslope. Usually, however, later surface-rupturing earthquakes with recurrences of thousands to tens of thousands of years (Wallace, 1984; Schwartz and Coppersmith, 1984; Machette, 1986; Crone and others, 1987) produce additional displacement at sites such as those modeled in figure 1.

CONCLUSIONS

The coarse-grained source, single-event model is the first facies model of colluvial sedimentation adjacent to fault scarps. Other models are needed for faults in less coarse-grained lithologies, and wherever climate, site, or tectonic factors produce significant differences in sedimentation patterns or rates. Facies models for composite scarps are especially needed because most scarps are the product of multiple fault events. Using the models should make interpreting fault exposures easier and more accurate. More importantly, the models will help provide the detailed, site-specific data needed to determine earthquake recurrence relationships on individual faults and to understand the fault rupture and propagation process in near-surface deposits.

ACKNOWLEDGMENTS

Many ideas presented here are the result of discussions with Dean Ostenaa, Tim Sullivan, Dave Schwartz, Jim McCalpin, Mike West, Tony Crone, Lucy Piety, Lucy Foley, Larry Anderson, Fred Hawkins, Carol Krinsky, and Ed Baltzer. West, Foley, Sullivan, McCalpin, and Piety provided unpublished data. Earlier versions of a manuscript from which this summary was taken benefited from comments by Tony Crone and Emily Taylor, and a thorough, perceptive review by John Whitney. Comments by Steve Personius and Lucy Piety substantially improved this paper.

REFERENCES

Butler, B.E., 1959, Periodic phenomena in landscapes as a basis for soil studies: C.S.I.R.O. Australia, Soil Publication 14, 20 p.

Clark, M.M., Grantz, Arthur, and Rubin, Meyer, 1972, Holocene activity of the Coyote Creek fault as recorded in sediments of Lake Cahuilla: U.S. Geological Survey Professional Paper 787, p. 112-130.

Cooke, R.U., and Warren, A., 1973, Geomorphology in deserts: University of California Press, Berkeley, California, 394 p.

Crone, A.J., Machette, M.N., Bonilla, M.G., Lienkaemper, J.J., Pierce, K.L., Scott, W.E., and Bucknam, R.C., Surface faulting accompanying the Borah Peak earthquake and segmentation of the Lost River fault, central Idaho: Bulletin of the Seismological Society of American, v. 77, p. 739-770.

Eyles, Nicholas, Eyles, C.H., and Miall, A.D., 1983, Lithofacies types and vertical profile models-An alternative approach to the description and environmental interpretation of glacial diamict and diamictite sequences: Sedimentology, v. 30, p. 393-410.

Gilbert, G.K., 1928, Studies of Basin and Range structure: U.S. Geological Survey Professional Paper 153, 89 p.

Guthrie, R.L., and Witty, J.E., 1982, New designations for soil horizons and layers and the new Soil Survey Manual: Soil Science Society of America Journal, v. 46, p. 443-444.

Hanks, T.C., Bucknam, R.C., Lajoie, K.R., and Wallace, R.E., 1984, Modification of wave-cut and faulting-controlled landforms: Journal of Geophysical Research, v. 89, no. B7, p. 5771-5790.

Imeson, F.J., Kwaad, F.J.P.M., and Mucher, H.J., 1980, Hillslope processes and deposits in forested areas of Luxembourg, in, Cullingford, R.A., Davidson, D.A., and Lewin, J., eds., Timescales in geomorphology: Chichester, UK, John Wiley, p. 31-42.

Karrow, P.F., Dreimanis, Aleksis, Kemmis, T.J., and Hallberg, G.R., 1984, Discussion--Lithofacies types and vertical profile models; an alternative approach to the description and environmental interpretation of glacial diamict and diamictite sequences: Sedimentology, v. 31, p. 883-890.

Kwaad, F.J.P.M., and Mucher, H.J., 1979, The formation and evolution of colluvium on arable land in northern Luxembourg: Geoderma, v. 22, p. 173-192.

Low, A.J., Douglas, L.A., and Platt, D.W., 1982, Soil-pore orientation and faults: Soil Science Society of America Journal, v. 46, p. 789-792.

Machette, M.N., 1986, History of Quaternary offset and paleoseismicity along the La Jencia fault, central Rio Grande rift, New Mexico: Bulletin of the Seismological Society of America, v. 76, p. 259-272.

McCalpin, J.P., 1982, Quaternary geology and neotectonics of the west flank of the northern Sangre de Cristo Mountains, south central Colorado: Colorado School of Mines Quarterly, v. 77, no. 3, 97 p.

Miall, A.D., 1977, A review of the braided river depositional environment: Earth Science Reviews, v. 13, p. 1-62.

Miall, A.D., 1978, Lithofacies types and vertical profile models in braided rivers-- A summary, in, Miall, A.D., ed., Fluvial sedimentology: Canadian Society of Petroleum Geologists Memoir 5, p. 597-604.

Middleton, G.V., 1978, Facies, in Fairbridge, R.W., and Bourgeois, J., eds., Encyclopedia of sedimentology: Stroudsburg, Pennsylvania, Dowden, Hutchinson and Ross, p. 323-325.

Mills, H.H., 1987, Variation in sedimentary properties of colluvium as a function of topographic setting, Valley and Ridge Province, Virginia: Zeitschrift fur Geomorphologie, v. 31, no. 3, p. 277-292.

Mousinho de Meis, M.R., and Da Silva de Moura, J.R., 1984, Upper Quaternary sedimentation and hillslope evolution--Southeastern Brazilian Plateau: American Journal of Science, v. 284, p. 241-254.

Nakata, J.K., Wentworth, C.M., and Machette, M.N., 1982, Quaternary fault map of the Basin and Range and Rio Grande rift provinces, Western United States: U.S. Geological Survey Open-File Report 82-579, 2 plates, scale 1:2,500,000.

Nelson, A.R., 1986, Use of lithofacies codes in paleoseismological studies of normal faults in unconsolidated sediments [abs.]: Geological Society of America Abstracts with Programs, v. 18, no. 2, p. 163.

Nelson, A.R., and Weisser, R.R., 1985, Late Quaternary faulting on Towanta Flat, northwestern Uinta Basin, Utah, in, Picard, M.D., ed., Geology and energy resources, Uinta Basin, Utah: Salt Lake City, Utah, Utah Geological Association Publication 12, p. 147-158.

Nelson, A.R., and VanArsdale, R.B., 1986, Recurrent late Quaternary movement on the Strawberry normal fault, Basin and Range--Colorado Plateau transition zone, Utah: Neotectonics, v. 1, p. 7-37.

Ostenaa, D.A., 1984, Relationships affecting estimates of surface fault displacements based on scarp-derived colluvial deposits [abs.]: Geological Society of America Abstracts with Programs, v. 16, no. 5, p. 327.

Reading, H.G., 1978, Sedimentary Environments and Facies: Oxford, UK, Blackwell Scientific Publications, 557 p.

Schwartz, D.P., and Coppersmith, K.J., 1984, Fault behavior and characteristic earthquakes: Examples from the Wasatch and San Andreas faults: Journal of Geophysical Research, v. 89, no. B7, p. 5681-5698.

Sieh, K.E., 1978, Prehistoric large earthquakes produced by slip on the San Andreas fault at Pallett Creek, California: Journal of Geophysical Research, v. 83, no. B8, p. 3907-3939.

Sieh, K.E., and Jahns, R.H., 1984, Holocene activity of the San Andreas fault at Wallace Creek, California: Geological Society of America Bulletin, v. 95, no. 8, p. 883-896.

Small, R.J., and Clark, M.J., 1982, Slopes and Weathering: Cambridge, UK, Cambridge University Press, 112 p.

Swan, F.H., III, Schwartz, D.P., and Cluff, L.S., 1980, Recurrence of moderate to large magnitude earthquakes produced by surface faulting on the Wasatch fault zone, Utah: Bulletin of the Seismological Society of America, v. 70, no. 5, p. 1431-1462.

Wallace, R.E., 1977, Profiles and ages of young fault scarps, north-central Nevada: Geological Society of America Bulletin, v. 88, p. 1267-1281.

Wallace, R.E., 1978, Geometry and rates of change of fault-generated range fronts, north-central Nevada: U.S. Geological Survey Journal of Research, v. 6, p. 637-650.

Wallace, R.E., 1981, Active faults, paleoseismology, and earthquake hazards in the western United States, in, Simpson, D.W., and Richards, P.G., eds., Earthquake prediction--An international review: Washington, D.C., American Geophysical Union, Maurice Ewing Series 4, p. 209-216.

Wallace, R.E., 1984, Patterns and timing of late Quaternary faulting in the Great Basin province and relation to some regional tectonic features: Journal of Geophysical Research, v. 89, no. B7, p. 5763-5769.

Walker, R.G., 1984, General introduction--Facies, facies sequences, and facies models, in, Walker, R. G., ed., Facies models [Second edition]: Geoscience Canada Reprint Series 1, Geological Association of Canada, p. 1-9.

Watson, A., Price Williams, D., and Goudie, A.S., 1984, The palaeo-environmental interpretation of colluvial sediments and palaeosols of the Late Pleistocene hypothermal in southern Africa: Palaeogeography, Palaeoclimatology, Palaeoecology, v. 45, p. 225-249.

Young, Anthony, 1972, Slopes: Edinburgh, Oliver and Boyd, 288 p.

APPLICATION OF MARINE-TERRACE DATA TO PALEOSEISMIC STUDIES

by

George Plafker
U. S. Geological Survey
Menlo Park, California 94025

ABSTRACT

Emergent marine terraces formed by coseismic uplift along many tectonically active coastlines provide useful data on the age and relative magnitude of major paleoseismic events. In a gross sense, such data can be used to forecast seismotectonic-uplift events. Coseismic terraces form most commonly in zones of tectonic compression and are best developed on actively growing anticlines within these zones. Terraces formed by coseismic uplift generally occur within about 70 m above present sea level and are likely to be less than about 7,000 yrs old; a few possible Pleistocene coral-reef terraces at higher elevations may have formed by coseismic uplift.

INTRODUCTION

Along many tectonically active coastlines, earthquake-related episodic uplift has produced sequences of elevated strandlines that can be used for paleoseismic interpretations. Major earthquakes related to subduction zones have been known to produce both emergent and submergent strandlines in Alaska, Japan, New Zealand, and a number of Pacific islands (figs. 1 and 2). Both

FIGURE 1.-- Aerial view of southern windward end of Middleton Island at high tide showing the second highest terrace (II) at an elevation of about 36 m and the 1964 terrace. The 1964 terrace, between the highest tides and the base of the sea cliff, formed by approximately 3.4 m of uplift during the 1964 earthquake. The three intervening terraces have been removed from this part of the island by pre-1964 erosion. White specks are seagulls. View is towards the southeast and was taken at about high tide. Photo by George Plafker, 1965.

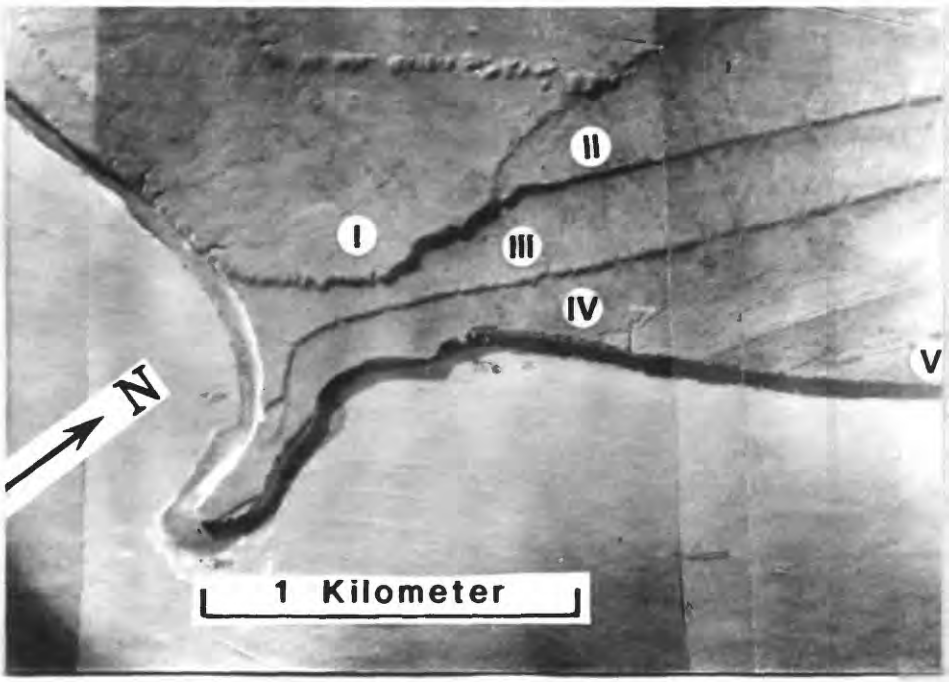

FIGURE 2. -- 1947 vertical aerial mosaic of southeastern end of Middleton Island showing the 5 pre-1964 marine terraces formed by 5-7 m coseismic uplift steps since emergence of the island about 4,900 yrs B.P. (see fig. 7A for elevations and ages). Terraces I through IV are mainly cut into bedrock, whereas terrace V is formed mainly on a wedge of gravels that thicken towards the northeast (right).

constructional- and destructional-strandline features may be preserved, but it is the strandline features that are resistant to subsequent erosion, mainly constructional coral-reef terraces and wave-cut terraces, that are best preserved and most useful for paleoseismic studies. Less commonly, uplifted sequences of beach ridges and related constructional near-shore features may result from episodic uplift as near Katalla along the Gulf of Alaska margin (Plafker, 1969, fig. 37). Such features, however, have limited usefulness in paleoseismology because of one or more of the following reasons: (1) they may not be distinguishable from storm berms, (2) their position relative to sea level can not be accurately determined, and (3) they are not well preserved in the geologic record. As a consequence, this paper focuses on the application of marine-terrace data only for paleoseismic studies.

As used in this paper, "terrace" refers to both surf-cut and constructional terraces. A terrace consists of a platform that slopes gently seaward from the high-tide strandline or "beach angle" and it is backed by a sea cliff on the landward side. On any given terrace, the elevation of the beach angle may vary by a few meters, depending upon the tidal range and exposure to storm waves. Terrace width is primarily a function of the duration of sea-level stability relative to the land and (for wave-cut terraces) the resistance of the rock to erosion. Emergence (or submergence) of a terrace is the sum of tectonic uplift (or subsidence) of the land and eustatic sea-level change. Although emergence (or submergence) of shorelines may result from both tect-

onic and isostatic processes, it is the episodic tectonic displacements that are of primary interest for paleoseismic studies. In this paper, only the emergent strandlines are considered; coseismic submerged shorelines are discussed by Atwater (this volume).

QUATERNARY SEA-LEVEL FLUCTUATIONS

Glacioeustatic sea-level changes during the late Quaternary were characterized by a series of fluctuations from about present sea level to as much as 100 to 150 m below present sea level caused by the advance and retreat of continental glaciers (fig. 3). Sea level was at about 100-150 m below its

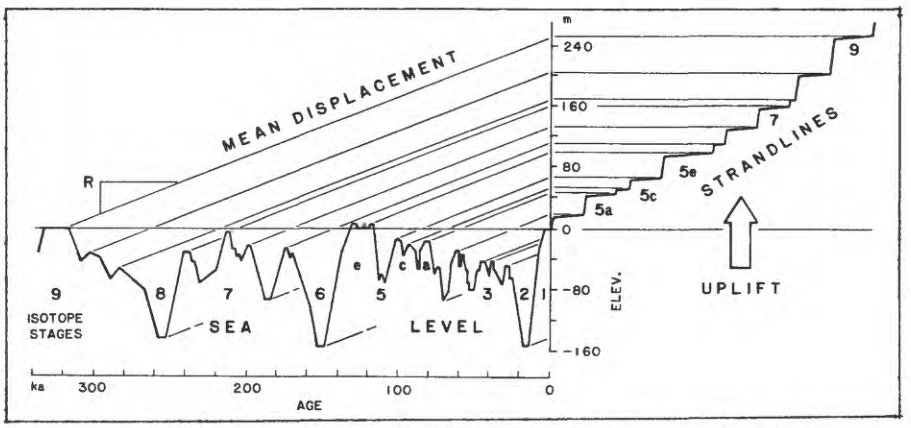

FIGURE 3. -- Quaternary sea-level fluctuations and origin of emergent strandlines (LaJoie, 1986). Emergent Pleistocene strandlines simult-aneously record tectonic uplift and major sea-level highstands. The rising coastline is a moving strip chart on which sea-level highstands are recorded sequentially as strandlines whose ages increase with altitude. The slope (R) of the diagonal line connecting each highstand to the altitude of its strandline is the average uplift rate. Sea-level curve modified from Chappell (1983); oxygen-isotope stages (1-9) from deep-sea cores (Shackleton and Opdyke, 1973).

present position during the last glacial maximum between 20 and 15 ka, and then rose at a rate of about 10 mm/yr to within 4-6 m of its present position by about 6.5 ka in response to retreat of the Wisconsinan ice sheets. Since about 5 ka, sea level has risen at an average rate of about 2 mm/yr to its present position. Because sea level is now close to its highest position in the past 336 ka, marine terraces above present sea level that formed during this time period (other than those related to transitory volcanic or glacio-eustatic processes) may be assumed to record coastal uplift--and are of interest for paleoseismic studies.

PLEISTOCENE TERRACES

Long-term crustal uplift along tectonically active coasts is expressed geomorphically by Pleistocene terraces deformed and uplifted to altitudes of hundreds of meters. These terraces formed mainly during the major eustatic sea-level highstands. At least 20 Pleistocene terraces have been correlated by Chappell (1983) with sea-level maxima between about 336 and 60 ka based on dating of marine coral terraces on New Guinea (fig. 3). Because of the long

time period, the Pleistocene terraces reach altitudes of several hundred meters even where average uplift rates are only a few mm/yr. Unfortunately, identification of coseismic terraces within erosional Pleistocene sequences is almost impossible because they are likely to be only 1-15 m high compared with the tens of meters for the eustatic terraces, and they are likely to be poorly preserved because of their considerable age. Some coral-reef terraces include well-preserved, small, abrupt steps that have been attributed by Chappell (1983) to coseismic uplift and show up as minor perturbations on the eustatic sea-level curve (fig. 3). The large errors inherent in techniques presently used to date Pleistocene terraces, which are older than the range of the radiocarbon dating method, preclude their use in obtaining meaningful data on recurrence intervals and short-term, average uplift rates. Consequently, they cannot be used in paleoseismologic studies and they will not be considered further in this paper.

HOLOCENE TERRACES

Tectonic Setting

Most Holocene marine terraces are located along tectonically active or convergent-transpressive plate margins and are related to growth of youthful anticlines (Hudson and others, 1976; Plafker and Rubin, 1978; LaJoie, 1986).

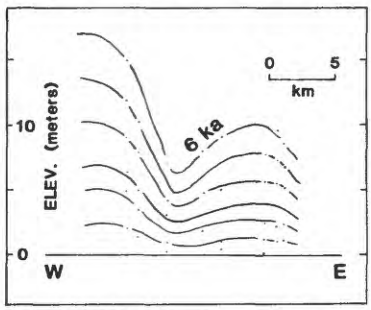

FIGURE 4. -- Tight folds recorded by Holocene strandlines on Wairarapa coast of North Island, New Zealand are of probable coseismic origin and indicate incremental folding. Highest (6-ka) strandline dated by graphical techniques. Modified from Wellman (1971).

In such areas, short-term crustal instability is expressed geomorphically by emergent Holocene marine terraces formed by uplift steps of 1-15 m and by crustal warps to maximum altitudes of about 70 m above sea level. The similarity between prehistoric Holocene terraces and terraces elevated during historic seismic events, most notably in Japan, New Zealand, Alaska, Chile, New Hebrides, and Mexico, suggests that all emergent Holocene terrace flights are mainly of coseismic origin (Fig. 5).

Uplift Rates

Worldwide data on the ages, altitudes, and average uplift rates for the better-studied late Pleistocene and Holocene strandline terraces have been compiled by LaJoie (1986) and Ota (1986). As may be expected, the highest tectonic uplift rates are above subduction zones along convergent plate boundaries. Zones of compression and uplift may also occur along transform plate

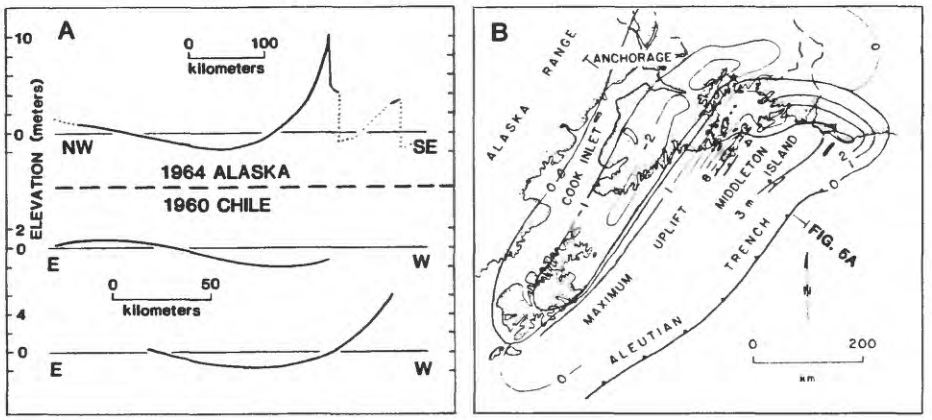

FIGURE 5. -- Coseismic crustal warps recorded by strandlines and illustrated by profiles. A, Profiles of deformed strandlines from historical coseismic events reveal broad crustal warps in the Gulf of Alaska (1964) and on the Chilean coast (1960). These profiles are not continuous but are defined by numerous points on highly irregular coastlines. Modified from Plafker (1972). B, 1964 strandline records subtle crustal warps associated with large megathrust earthquake in Gulf of Alaska. Isobase contours (in meters), represent lines of equal vertical crustal displacement. See A for profile of warped surface. Modified from Plafker (1972).

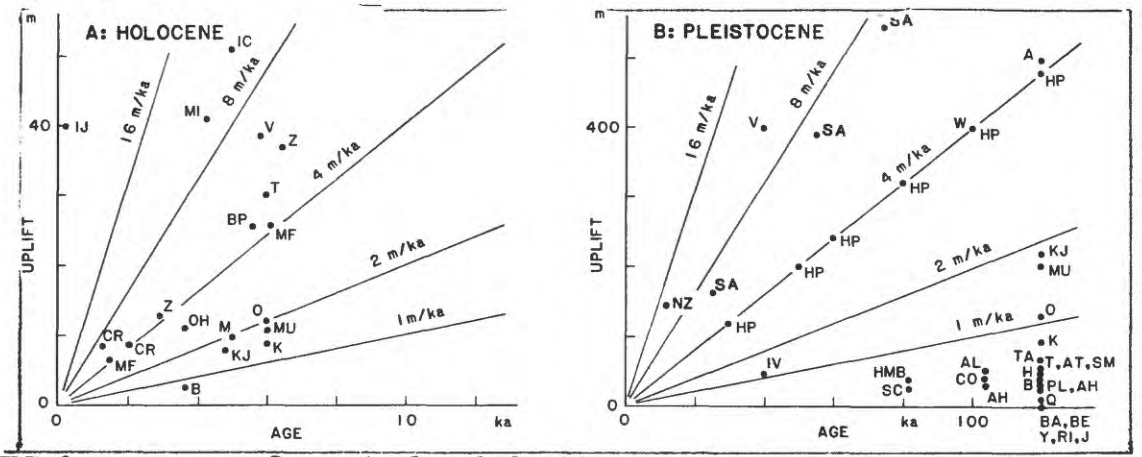

FIGURE 6. -- Rates of vertical uplift (data sources in LaJoie, 1986 except as otherwise noted). A, Holocene: IJ, Iwo Jima, volcanic uplift included for comparative purposes; CR, Crete; Z, Zagros; B, Bahrein; MI, Middleton Island; IC, Icy Cape; M, Makran; T, Turakirae; BP, Boso Peninsula; MF, Miller Flat; OH, Ocean House; V, Ventura; O, Osado; K, Kosado; MU, Muroto Peninsula; KJ, Kikai Jima. B, Pleistocene: NZ, New Zealand; V, Ventura; A, Arauco; HP, Huon Peninsula; W, Wairarapa; KJ, Kikai Jima; MU, Muroto; O, Osado; K, Kosado; HMB, Half Moon Bay; SC, Santa Cruz; RI, Royalty Islands; TA, Taanaki; T, Timor; AT, Atauro; H, Haiti; B, Barbados; AH, Arroyo Hondo; CO, Cojo; AL, Algeria; IV, Isla Vista; SM, Santa Monica; PL, Point Loma; J, Jamaica; BA, Bahamas; Y, Yucatan; BE, Bermuda; Q, Queensland; SA, Southern Alps, N. Z., Bull and Cooper (1986).

boundaries and local late Quaternary uplift rates as high as 11 mm/yr are

recorded at Ventura, Calif. (fig. 6A). Average late Holocene uplift rates recorded by terraces along tectonically rising coastlines are 2-10 mm/yr (fig. 6B), less than, or about equal to, the 10 mm/yr rate of sea-level rise before about 7 ka (fig. 3). As a consequence, Holocene terraces older than about 7 ka are submerged and only coastlines with average uplift rates more than 2 mm/yr for the interval 7 ka to present can be expected to be exposed above present sea level. Furthermore, the late Pleistocene sea-level fluctuations were such that strandlines younger than at least 30 ka--and possibly as much as 95 ka--would not be above present sea level (fig. 3). This results in a worldwide hiatus in the record of tectonically elevated strandlines for the interval from about 7-30 ka.

Holocene Terraces and Sea Levels

Ideally, a sequence of dated, emergent, Holocene terraces can provide a complete physical record of past earthquakes. Formation of such terraces requires average long-term average rates that are larger than the rate of Holocene sea-level rise (fig. 7). Preservation of an ideal sequence, however,

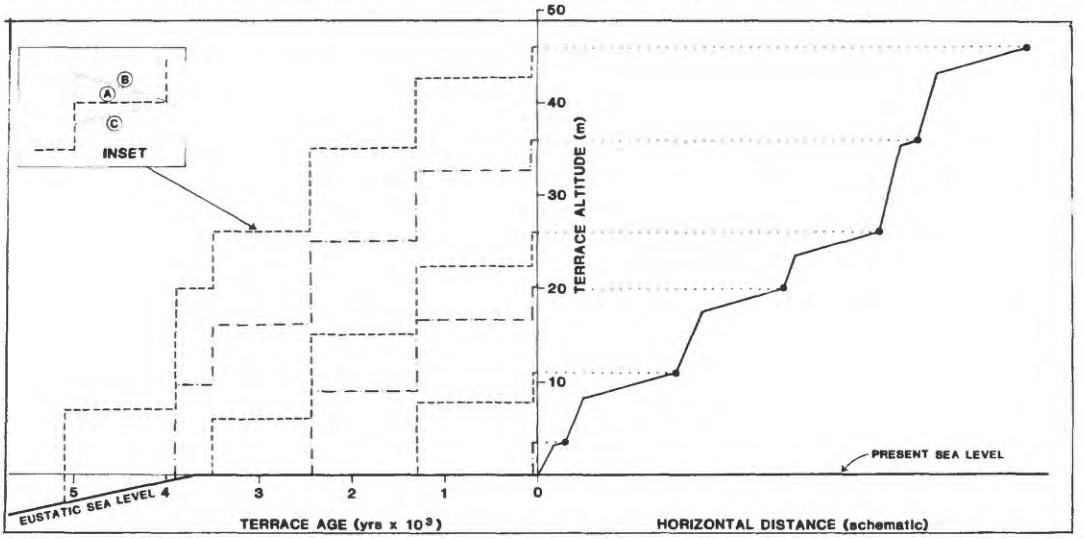

FIGURE 7. -- Holocene sea-level changes and origin of emergent Holocene strandlines (modified from LaJoie, 1986 and K.R. LaJoie, written comm., 1987). In contrast to Pleistocene strandlines, emergent Holocene strandlines represent discrete uplift events or, possibly, storm events, not sea-level fluctuations. The real uplift history of a given strandline terrace, shown in the left part of the diagram, is the algebraic sum of coseismic uplift, amount of sea-level rise since the terrace was formed, and any interseismic subsidence or uplift. Inset shows three alternative interseismic histories in which (A) indicates no change, (B) indicates interseismic subsidence, and (C) indicates interseismic uplift. Profile in right part of diagram shows strandline altitudes relative to present sea level. Note that average tectonic-uplift rates must be larger than eustatic sea-level rise rates for marine terraces to be exposed above present sea level. Sea-level curve shown is after Coleman and Smith (1964); it may vary slightly from region to region owing to minor geoidal distortions. Terrace data shown are for Middleton Island (fig. 8).

requires a fortuitous balance between uplift rate and erosion that is seldom achieved in nature so that the record is commonly incomplete due to removal of one or more terraces by wave erosion. For example, as shown in figure 2, the lower three pre-1964 terraces along the windward southern end of the Middleton Island have been eroded away leaving only half the uplift record intact, due to the high erosion rate and recurrence intervals as long as 1,350 yrs (Plafker and Rubin, 1978). Rigorous interpretation of the record of coseismic uplift requires data on the amount and sense of interseismic displacement that is seldom available.

Uplift History

Both the ages and altitudes of terrace strandlines or shore angles are required to reconstruct their uplift histories. Accurate dating, usually directly or indirectly by radiocarbon techniques, is required to determine earthquake periodicity. Dating of coseismic uplift events in erosional terraces can be done with <u>in situ</u> shelly material on the rock platform or driftwood in beach deposits on the platform; dating of constructional coral-reef terraces can be on coral or other calcareous organisms growing on the reef. For most erosional terraces, however, radiocarbon ages of the terrestrial organic material that began growing on the platform sometime after emergence are minimum terrace ages and do not directly date the time of uplift. Where both the altitudes and ages of terraces are known, it is possible to determine the coseismic uplift history, as illustrated for terrace sequences at Middleton Island and Icy Cape in the northern Gulf of Alaska (figs. 8 and 9). At Middleton Island, the vertical displacement of each uplift step

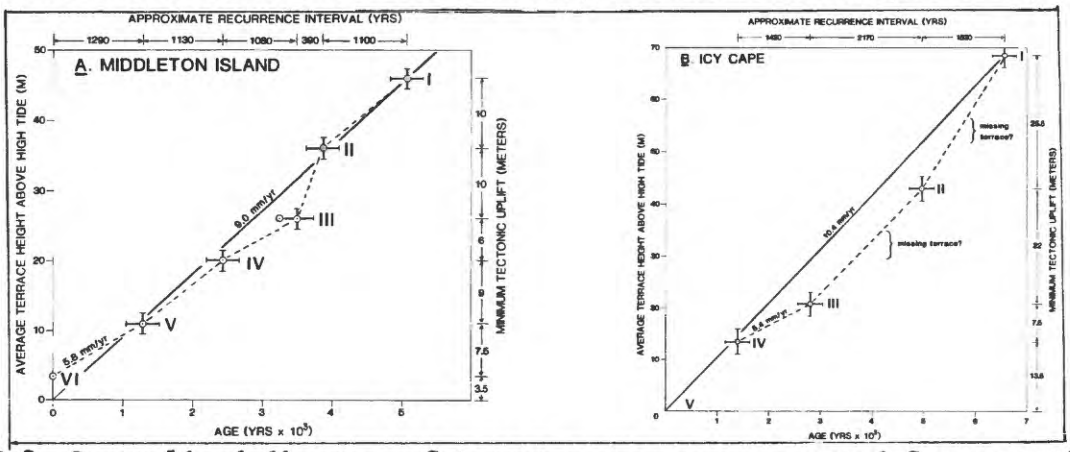

FIGURE 8. Generalized diagrams of terrace emergence corrected for eustatic sea-level rise and minimum tectonic uplift per event(s), versus terrace age and indicated recurrence interval in calendar years at Middleton Island <u>A</u> and Icy Cape <u>B</u> in the northern Gulf of Alaska (see fig. 9 for location). Terraces are identified by Roman numerals with the 1964 coseismic uplift at zero years (VI). Dashed lines indicate average uplift rate between terraces. Terrace elevations are the sum of altitude above present sea level and amount of eustatic sea-level rise since the terrace was formed plus-or-minus any interseismic displacements. Late Holocene eustatic sea-level corrections from Coleman and Smith (1964); radiocarbon years corrected to calendar years using data of Hassan and Robinson (1987) and Robinson (written comm., 1987). After Plafker (1986).

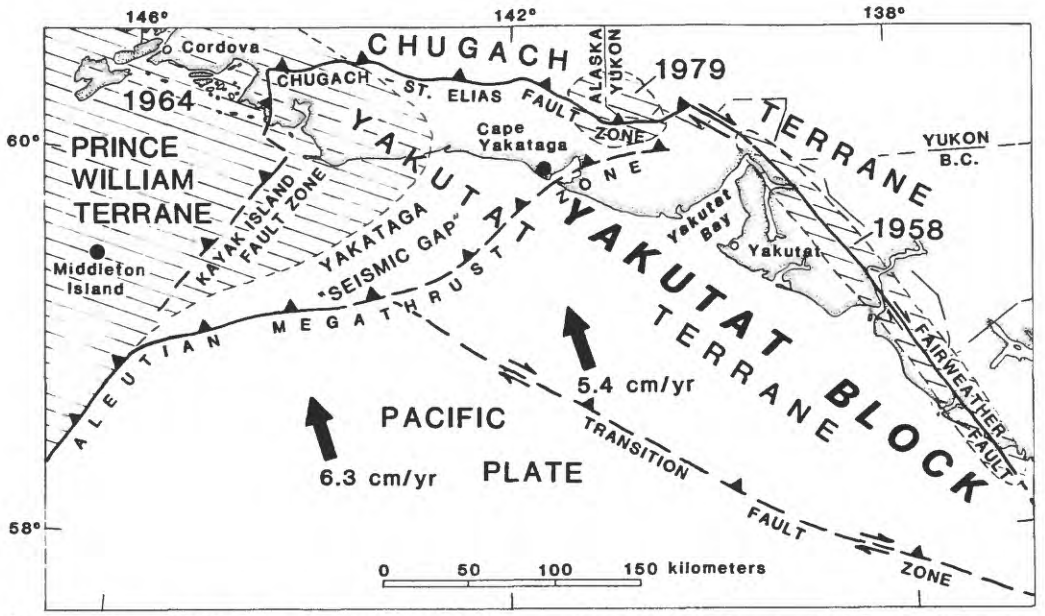

Figure 9. -- Simplified tectonic setting of the northern Gulf of Alaska showing relationship of the Middleton Island and Icy Cape terrace sequences (heavy dots) to plate boundaries and major faults (heavy lines) and the focal regions of the 1964 Alaska, 1958 Lituya, and 1979 St. Elias earthquakes (patterned areas). Northward motion of the Pacific plate and Yakutat block relative to the North American plate at about 6 cm/yr results in dextral strike-slip on the Fairweather fault transform and convergence across a broad zone that extends northwestward from the Aleutian megathrust (Modified after Lahr and Plafker, 1980 and McCann and others, 1980).

ranges from about 3.5 to 9 m, and the time between steps is roughly 400-1,300 yrs. Although interseismic subsidence occurred over much of the region affected by coseismic deformation during the 1964 Alaska earthquake (Plafker and Rubin, 1967), there is nothing in the stratigraphic record to indicate whether the subsidence extended seaward to Middleton Island. At Icy Cape the record is complicated by a large isostatic component uplift due to rapid 20th century retreat of the nearby Guyot Glacier and by probable missing or unrecognized terraces older than 3 ka. At Icy Cape, the most recent uplift step was about 13.5 m (IV terrace) with an apparent recurrence interval on the order of 1,400 yrs between that event and the preceding one.

Marine Terraces and Earthquake Forecasting

For constant average uplift, seismic events recorded by Holocene terraces may follow a time-predictable or displacement-predictable pattern (Shimazaki and Nakata, 1980); if the period and size of uplift events are regular, both can be predicted for the next event. Large errors can result using this method unless individual events are dated independently because constant uplift rates cannot be assumed.

In detail, the average uplift rate may vary with time (fig. 8). In addition, the interseismic displacements may be significant, but can seldom be deduced from the geologic data. Thus, in the 1964 focal region, which includes Middleton Island, coseismic uplift may be followed by variable amounts

of interseismic subsidence (Plafker and Rubin, 1967; Plafker, 1986) and, in some places, all of the coseismic uplift (as much as 10 m) has been recovered between seismic events (George Plafker and K.R. Lajoie, unpublished data). Furthermore, at Icy Cape, crustal unloading by neoglacial retreat of the Guyot and Malaspina Glaciers during this century has resulted in a large isostatic component of uplift being superimposed on earthquake-related tectonic uplift steps (Plafker and others, 1981).

Terraces in the Gulf of Alaska and the "Yakataga Seismic Gap"

In most parts of the world, the history of terrace sequences is too poorly known to permit forecasting of future seismotectonic events. A possible exception is along the structurally complex plate boundary in the northern Gulf of Alaska where terrace data at both Middleton Island and Icy Cape are consistent with forecast of a seismotectonic event that should be accompanied by significant coseismic uplift at these two localities (fig. 9).

For the Middleton Island sequence, the average late Holocene uplift indicated by the slope of the dashed curve (fig. 8A) appears to decrease with time; it is 10.2 mm/yr between 4,900 and 1,350 yrs B.P., about 6.5 mm/yr from 2,390 to 1,350 yrs B.P. and it was only 2.6 mm/yr since 1,350 yrs B.P., including the 1964 uplift of 3.4 m. The uplift data for Middleton Island leads to the obvious conclusion that, if the uplift rate prior to 1,350 yrs ago has not decreased abruptly, another uplift step of about 4 m is required to make up the uplift deficit. Data from terraces at Icy Cape near the eastern end of the gap suggest that the next earthquake in that area may also be overdue because the time since the last uplift event is close to the 1,400-yr interval between the two youngest terraces (III and IV, fig. 8B).

The terrace data in the northern Gulf of Alaska were cited as the basis for a "prediction" for a tectonic earthquake along the plate boundary from the Middleton Island area eastward to the vicinity of Icy Bay (Plafker and Rubin, 1978; Plafker and others, 1981; and Plafker, 1986). The coastal part of this same region has been named the "Yakataga seismic gap" by seismologists because it is an area that has not experienced a major shallow earthquake in historic times (McCann and others, 1980; Lahr and Plafker, 1980). However, the exceptionally long recurrence intervals for major tectonic earthquakes along this part of the plate boundary indicated by the terrace data (400-1,500 yrs) clearly limits the value of the short historic earthquake record for forecasting future great seismotectonic events in such areas.

CONCLUSIONS

Marine terraces formed by episodic uplift can provide data on the age and relative size of paleoseismic events during the last 7 ka. Under the best circumstances, such data may be used to for probabilistic estimates of the likelihood of a future major subduction-zone earthquake on a time span of several tens to a few hundred years. It may be possible to refine such forecasts in the future with improvements in the precision of isotopic dating. Development of a capability for predicting subduction-zone events is especially critical because such earthquakes can cause significant local damage as well as generate tsunami waves with the potential for causing major coastal destruction far from the seismic source.

ACKNOWLEDGMENTS

I gratefully acknowledge the major contribution made to this paper by K.R. LaJoie who patiently helped me to understand the relationship between terrace sequences and their uplift/time path, provided several of the figures, and thoroughly reviewed the manuscript. Helpful technical reviews by Oscar J. Ferrians and William B. Bull significantly improved this paper.

REFERENCES CITED

Bull, W.B., and Cooper, A.F., 1986, Uplifted marine terraces along the Alpine fault, New Zealand: Science, v. 234, p. 1161-1300.

Chappell, J. M., 1983, A revised sea-level record for the last 300,000 years from Papua New Guinea: Search, v. 14, p. 99-101.

Coleman, J.M. and Smith, W.G., 1964, Late Recent rise of sea-level: Geological Society of America Bulletin, v. 75, no. 9, p. 833-840.

Hassan, F.A. and Robinson, S.W., 1987, High-precision radiocarbon chronometry of ancient Egypt and comparisons with Nubia, Palestine, and Mesopotamia: Antiquity, v. 61, p. 119-135.

Hudson, Travis, Plafker, George, and Rubin, Meyer, 1976, Uplift rates of marine-terrace sequences in the Gulf of Alaska: U.S. Geological Survey Circular 733, p. 11-13.

Lahr, J. C., and Plafker, George, 1980, Holocene Pacific-North American plate interaction in southern Alaska -- Implications for the Yakataga seismic gap: Geology, v. 8, p. 483-486.

LaJoie, K.R., 1986, Coastal tectonics, in Active Tectonics: Washington, D.C., National Academy Press, p. 95-124.

McCann, W.R., Perez, O.J., and Sykes, L.R., 1980, Yakataga gap, Alaska -- Seismic history and earthquake potential: Science, v. 207, no. 21, p. 1309-1314.

Ota, Yoko, 1986, Marine terraces as reference surfaces in late Quaternary tectonic studies -- Examples from the Pacific rim: Royal Society of New Zealand Bull. 24, p. 357-375.

Plafker, George, 1969, Tectonics of the March 27, 1964, Alaska Earthquake: U.S. Geological Survey Professional Paper 543-I, 74 p.

------1972, The Alaskan earthquake of 1964 and Chilean earthquake of 1960 -- Implications for arc tectonics: Journal of Geophysical Research, v. 77, no. 5, p. 901-925.

------1986, Geologic studies related to earthquake potential and recurrence in the "Yakataga seismic gap": U. S. Geological Survey Open File Report 86-92, p. 135-143.

Plafker, George, Hudson, Travis, Rubin, Meyer, and Dixon, K. L., 1981, Holocene marine terraces and uplift history in the Yakataga seismic gap near Icy Cape, Alaska, in Coonrad, W. L., ed., United States Geological Survey in Alaska: Accomplishments during 1980: U.S. Geological Survey Circular 844, p. 111-115.

Plafker, George, and Rubin, Meyer, 1967, Vertical tectonic displacements in south-central Alaska during and prior to the great 1964 earthquake: Journal Geosciences (Osaka City University), v. 10, art. 1-7, p. 1-14.

------1978, Uplift history and earthquake recurrence as deduced from marine terraces on Middleton Island, Alaska, in Proceedings of Conference VI, Methodology for identifying seismic gaps and soon-to-break gaps: U.S. Geological Survey Open-File Report 78-943, p. 687-721.

Shackleton, N.J., and Opdyke, N.D., 1973, Oxygen isotope and paleomagnetic stratigraphy of equatorial Pacific core V28-238: Quaternary Research, v. 3, p. 39-55.
Shimazaki, K., and Nakata, T., 1980, Time-predictable recurrence model for large earthquakes: Geophysical Research Letters, v. 7, p. 179-282.
Wellman, H.W., 1971, Holocene tilting and uplift on the White Rocks coast, Wairarapa, New Zealand: Royal Society of New Zealand Bulletin, v. 9, p. 211-215.

SUBDUCTION-EARTHQUAKE TELLTALES BENEATH COASTAL LOWLANDS

by

Brian F. Atwater
U. S. Geological Survey at Department of Geological Sciences
University of Washington AJ-20
Seattle, Washington 98195

Buried coastal lowlands can offer excellent geologic records of great subduction earthquakes. Great thrust earthquakes in subduction zones usually cause tectonic subsidence that involves more coast than does the accompanying uplift (Plafker, 1972; Ando, 1975; Herd and others, 1981). Coseismic subsidence of a coastal lowland can invite the rapid estuarine burial of the lowland. Such burial protects the lowland from erosion while entombing rooted stumps suitable for dating the earthquake (Ovenshine and others, 1976). Postseismic burial may also preserve anomalous bodies of sand--sheets deposited by tsunamis (Wright and Mella, 1963), blows resulting from liquefaction (Reimnitz and Marshall, 1965)--that independently suggest the occurrence of a large earthquake.

Coastal-lowland stratigraphy is gaining importance as a paleoseismic tool in subduction-zone regions. Reconnaissance of coastal-lowland stratigraphy recently yielded the first strong evidence that great Holocene earthquakes have occurred in the Pacific Northwest (fig. 1; Atwater, 1987). The paleoseismic interpretation of coastal-lowland stratigraphy is also under way in south-central Alaska (Combellick, 1986; Bartsch-Winkler and Schmoll, 1987) and in New Zealand (Hull, 1986).

At least five problems can limit the usefulness of coastal-lowland stratigraphy as a recorder of great subduction earthquakes.

1. At least in the Pacific Northwest, most of the telltale strata are exposed only at low tide (fig. 1) or must be observed piecemeal, in core samples (Atwater, 1987).
2. Organic horizons, the most conspicuous and easily dated parts of buried-lowland soils, can become faint and scarcely datable after decomposition in succeeding soils (fig. 2).
3. Radiocarbon ages lack the precision to prove regional synchrony of subsidence, which (probably to the hour or minute) is a hallmark of coseismic subsidence from great subduction earthquakes. Synchrony to the century can probably be inferred, however, from regional similarities in stratigraphic sequence (fig. 1) and in radiocarbon age (Atwater and others, in press). Additionally, synchrony to the year might be tested by means of dendrochronology (fig. 3).
4. The stratigraphic record of sudden tectonic subsidence can resemble the stratigraphic records of other catastrophes, particularly storms and floods. But at least in the Pacific Northwest, many non-tectonic alternatives can be tested conclusively in the field (Atwater, 1987).
5. The great-earthquake record in coastal-lowland deposits has never been calibrated against archival records of successive historical earthquakes. Such calibration could be attempted, however, in Chile and Japan.

REFERENCES CITED

Ando, Masataka, 1975, Source mechanisms and tectonic significance of historical earthquakes along the Nankai Trough, Japan: Tectonophysics, v. 27, p. 119-140.

Atwater, B.F., 1987, Evidence for great Holocene earthquakes along the outer coast of Washington state: Science, v. 236, p. 942-944.

Atwater, B.F., Hull, A.G., and Bevis, K.A., in press, Aperiodic Holocene recurrence of regional, probably coseismic subsidence in southwestern Washington state: EOS [Transactions, American Geophysical Union], v. 68.

Bartsch-Winkler, S.R., and Schmoll, H.R., 1987, Earthquake-caused sedimentary couplets in the upper Cook Inlet region, in Hamilton, T. D., and Galloway, J. R., eds., Geologic studies in Alaska by the U. S. Geological Survey during 1986: U. S. Geological Survey Circular 998, pr. 92-95.

Combellick, R.A., 1986, Chronology of late-Holocene earthquakes in southcentral Alaska--Evidence from buried organic soils in upper Turnagain Arm: Geological Society of America Abstracts with Programs, v. 18, p. 569.

Herd, D.G., Youd, T.L., Meyey, Hansjurgen, Arango C., J.L., Person, W.J., and Mendoza, Carlos, 1981, The great Turmaco, Colombia earthquake of 12 December 1979: Science, v. 211, p. 441-445

Hull, A.G., 1986, Pre-A.D. 1931 tectonic subsidence of Ahuriri Lagoon, Napier, Hawke's Bay, New Zealand: New Zealand Journal of Geology and Geophysics, v. 29, p. 75-82.

Ovenshine, A.T., Lawson, D.E., and Bartsch-Winkler, Susan, 1976, The Placer River silt--intertidal sedimentation caused by the Alaska earthquake of March 27, 1964: U. S. Geological Survey Journal of Research, v. 4, p. 151-162.

Plafker, George, 1972, Alaskan earthquake of 1964 and Chilean earthquake of 1960--Implications for arc tectonics: Journal of Geophysical Research, v. 77, p. 901-925.

Reimnitz, Erk, and Marshall, N.F., 1965, Effects of the Alaska earthquake and tsunami on recent deltaic sediments: Journal of Geophysical Research, v. 70, p. 1363-1376.

Wright, Charles, and Mella, Arnoldo, 1963, Modifications to the soil pattern of south-central Chile resulting from seismic and associated phenomena during the period May to August 1960: Bulletin of the Seismological Society of America, v. 53, p. 1367-1402.

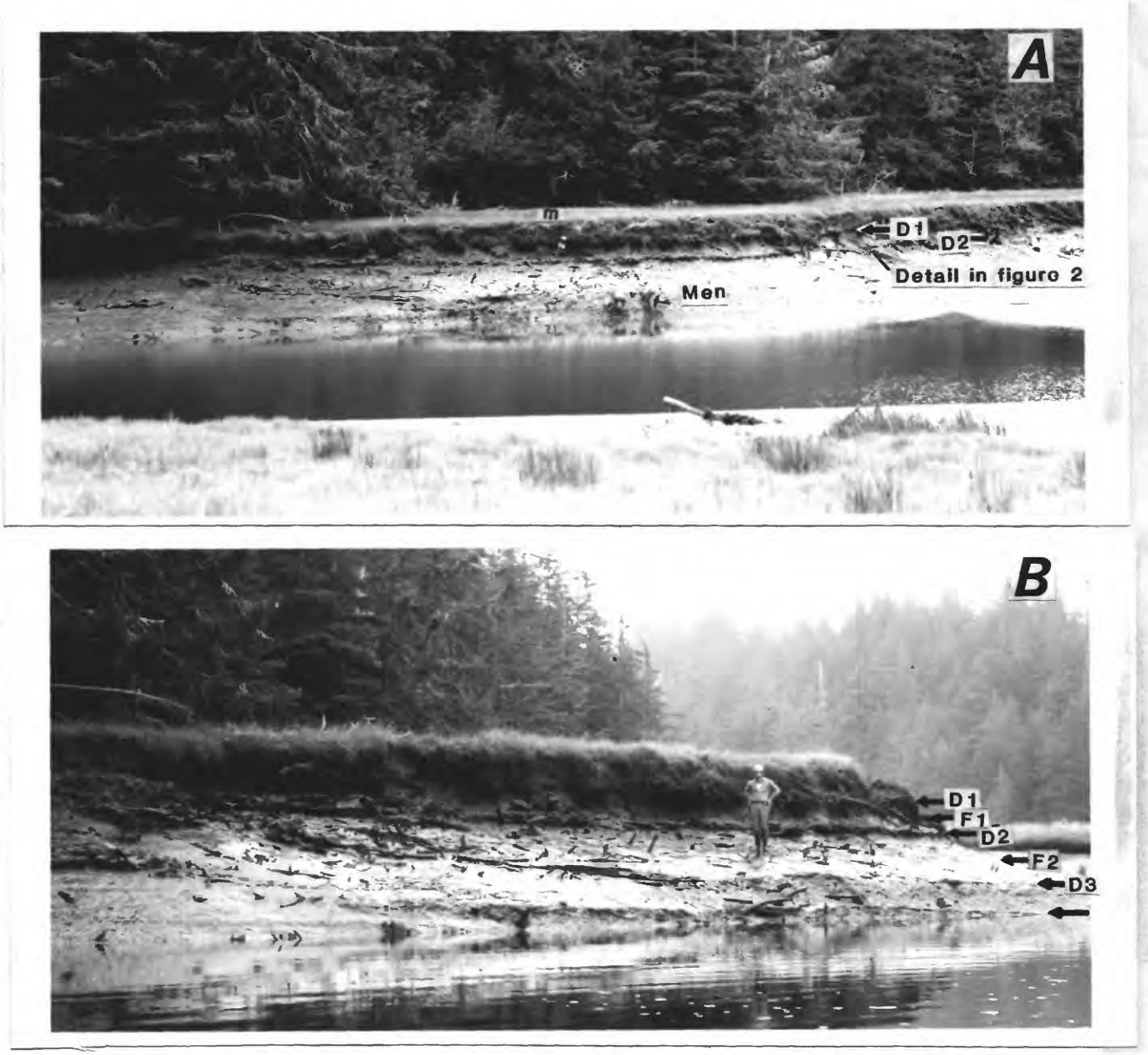

FIGURE 1.--Low-tide exposures of buried lowland soils (arrows) in southwestern Washington. The soils include a fivefold sequence in which three distinct soils (D1, D2, D3) alternate with two relatively faint soils (F1, F2; see fig. 2). In a coastal area at least 40 km long and wide, radiocarbon ages of these soils cluster near 300 (D1), 1600? (F1), 1700 (D2), 2700 (F2), and 3100 (D3) calibrated years before A.D. 1950 (Atwater and others, in press).
A, Outcrop along Niawiakum River (SW 1/4 of NE 1/4 sec. 10, T. 13 N, R. 10 W; Bay Center 7.5' quadrangle), a salt-water slough of Willapa Bay. Soil D2, having been abundantly wooded by Sitka spruce, is conspicuous from fossil roots that jut from the outcrop. The treeless modern tidal marsh (m) extends to the edge of the forested upland.
B, Left-hand part of outcrop shown in A. The lowermost buried soils dip away from the upland, probably because of differential settlement. Soil D1, though comparable to D2 in abundance of spruce roots, is mostly obscured by bank-dwelling plants of the modern tidal marsh.

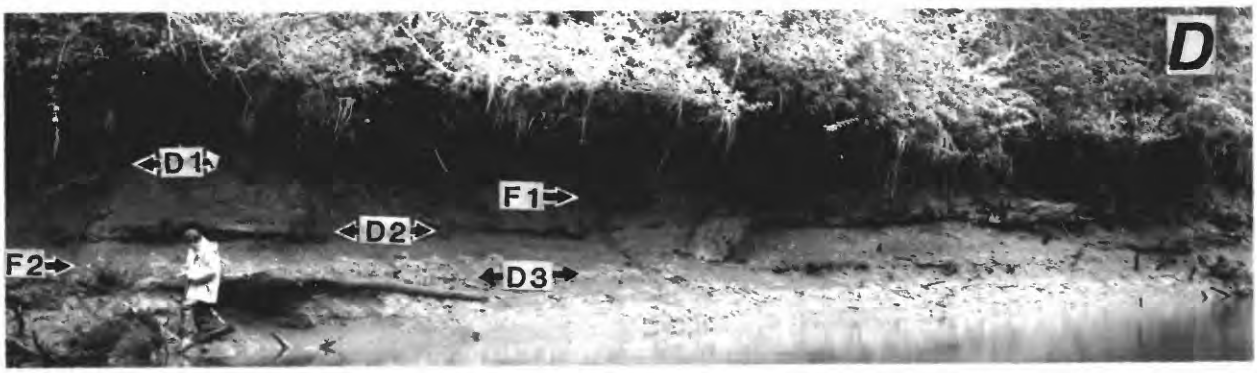

FIGURE 1 (continued).—C, Outcrop near mouth of Blue Slough (SW 1/4 of NE/4 sec. 19, T. 17 N, R. 8 W; Central Park 7.5' quadrangle), a mostly freshwater tidal stream in the Grays Harbor estuary. The woody fill of a shallow paleochannel (pc) crops out just left of the pilings. The modern tidal wetland supports Sitka spruce, crabapple, and red alder.
D, Left-hand part of outcrop shown in C. Jutting out behind the man's waist is the root of a spruce that lived on soil D3. Roots of a spruce that lived on soil F1 are visible in the middle of the photograph. Soil D1 is mostly obscured by the overhanging limbs of modern trees.

FIGURE 2.--Outcrop along Niawiakum River (see fig. 1A for location) showing soil that has been made faint by decomposition of most of its A or O horizon. The faint soil (F1) lies in a part of the succeeding soil (D1) where organic matter probably underwent oxidation before burial of D1. Aside from retaining the vestige of a dark-colored horizon, soil F1 remains evident because of a slight particle-size change across it; like the other buried soils in this outcrop, F1 culminates an upward fining sequence and is abruptly overlain by another such sequence. Both distinct soils (D1 and D2) abound in spruce roots. Water (at lower right) is about 2 m higher than when figures 1A and 1B were photographed. Shovel handle is 0.5 m long.

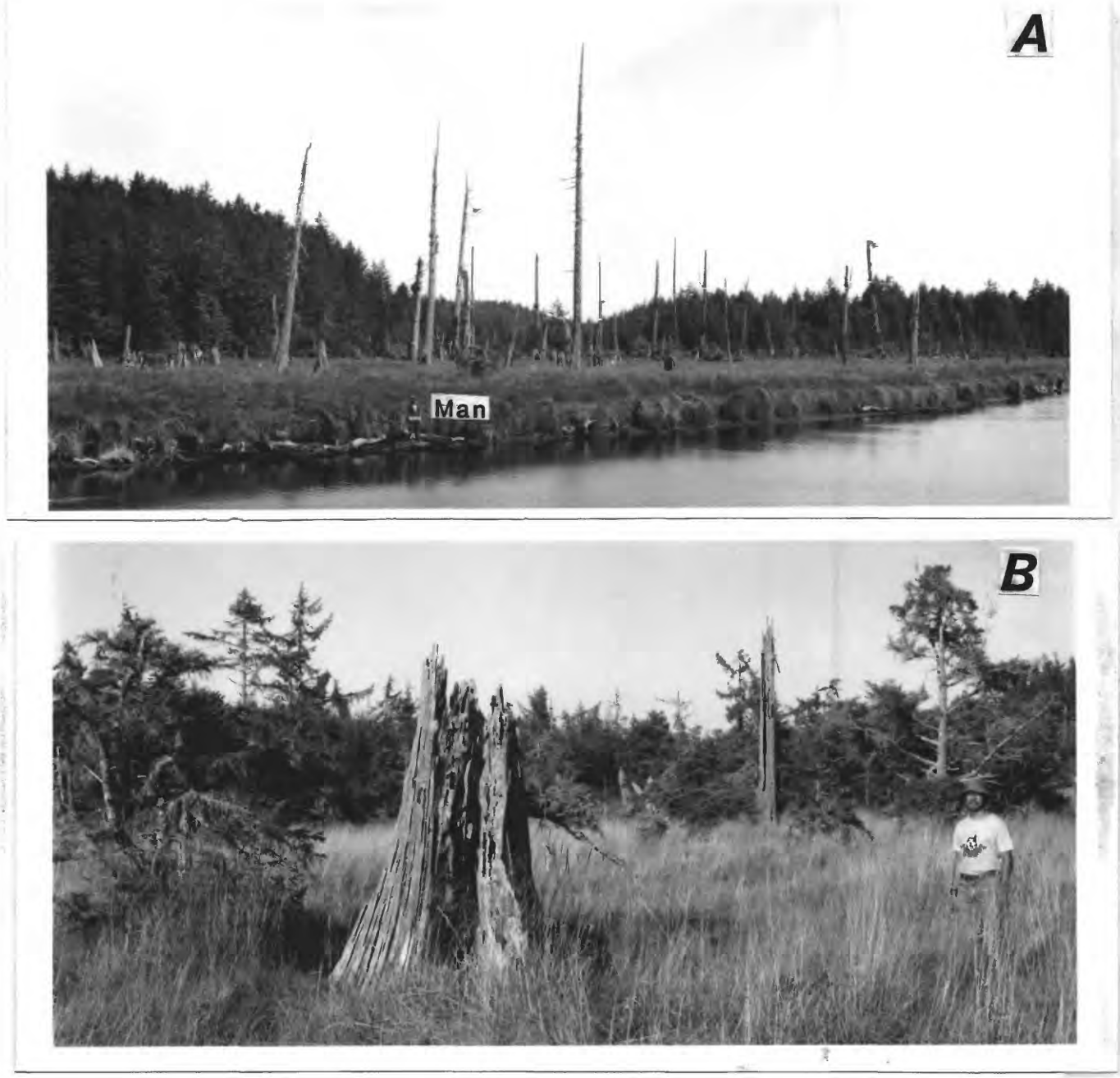

FIGURE 3.--Cedar snags rooted in the uppermost buried-lowland soil (D1; figs. 1, 2) in southwestern Washington. Cross-correlation of rings in these snags conceivably could reveal whether the cedars at both sites died during the same year, as should be the case if death resulted from the same jerk of coseismic subsidence.
A, Ghost forest in the Copalis River estuary (NW 1/4 of NE 1/4 sec. 22, T. 19 N, R. 12 W; Moclips 7.5' quadrangle). Site is now a brackish-water tidal marsh. The man stands on tree roots at the level of the soil in which the cedars are rooted.
B, Two snags along tidal reach of South Fork Palix River (SW 1/4 of NW 1/4 sec. 35, T. 13 N, R. 10 W; Nemah 7.5' quadrangle), a small tributary of Willapa Bay. The only conifer on the modern marsh is Sitka spruce much smaller in diameter than the cedar snags.

COSEISMIC FOLDING

by

Robert S. Yeats
Department of Geology
Oregon State University
Corvallis, Oregon 97331

ABSTRACT

Active convergent zones contain fold-and-thrust belts that deform a sedimentary wedge by low-angle thrusting and flexural-slip folding over a subjacent, more rigid basement. Flexural-slip folding occurs when a stack of stiff beds alternating with thin, less stiff layers is end-loaded, and these beds buckle by slip on mechanically weaker bedding surfaces. Upper layers slip over underlying layers toward anticlinal hinges and produce no stratigraphic separation unless there is a sequence overlying the flexural-slip fold with angular unconformity, and continued folding causes displacement of these younger deposits. Deformation also occurs due to bending moment within the stiffer flexed layers; normal faults and extension fractures form on the convex side of these layers, and reverse faults form on the concave side. Flexural-slip folds and the secondary faults that accompany them do not extend to seismogenic depths, and so these structures are not major producers of earthquakes. However, the folds are related to major faults, and these faults may be seismogenic; indeed, all historic examples of flexural-slip and bending-moment faulting accompanied earthquakes. In New Zealand, flexural-slip fault scarps facing up the depositional slope of outwash deposits now stranded on mesas are ungullied because the fault scarps formed instantaneously, defeating the drainage. Folds that are a result of fault displacement, with late Quaternary examples, include **drag folds** (Oak Ridge anticline and Santa Clara syncline, Ventura Basin), **fault-bend folds** (north-facing ramp on Salt Range thrust, Pakistan), **fault-propagation folds** (San Miguelito anticline, Ventura Basin), and **decollement folds** (Sulphur Mountain anticlinorium, Ventura Basin).

INTRODUCTION

The 1983 Coalinga, California, earthquake provided evidence that active folds may be the surface expression of buried seismogenic faults. Studies of active folds have been carried out in the Ventura Basin and the western and southern margins of the San Joaquin Basin, California, the fold belt of the Shinano River in northern Honshu, Japan, on the North Island and South Island of New Zealand, and the fold-thrust belts of the Potwar Plateau of northern Pakistan and the coastal plain of Taiwan. First, this paper considers the secondary faults that accompany flexural-slip folding. Then, because many folds are a result of

fault displacement, the relationship of folds to these faults is considered.

SECONDARY FAULTS ACCOMPANYING FOLDING

Flexural-Slip Faults

Much of the near-surface deformation in contractile regions is by flexural-slip folding, in which a stack of stiff beds alternating with thin, less stiff layers is end-loaded, and these beds buckle by slip on mechanically weaker bedding surfaces separating stiffer beds (Ramsay, 1967; Yeats and others, 1981; Yeats, 1986, 1987). Original layer thickness, unchanged except for the effects of compaction, remains constant across fold hinges. Layer-parallel slip accompanying these folds may produce slickensides that are perpendicular to the fold hinge. Upper layers slip over underlying layers toward anticlinal hinges and away from synclinal hinges. Slip is zero at fold hinges; on the limbs of folds, the amount of slip on bedding faults increases with maximum dip and with thickness of the flexed layer. Because such bedding faults, called **flexural-slip faults**, do not produce stratigraphic separation, they are not likely to be recognized unless there is a sequence overlying the flexural-slip fold with angular unconformity, and continued folding causes displacement of these younger deposits. Such deposits are cut by faults that are parallel to bedding in the folded sequence and upthrown toward the subjacent synclinal axis. The younger deposits may be tilted toward the synclinal axis so that their dip is in the same direction as the subjacent, more strongly folded beds (fig. 1A).

Flexural-slip faulting was first described by Suggate (1957) at Giles Creek in the Grey-Inangahua depression in the northwestern South Island, New Zealand (Yeats, 1986). A structural trough containing marine and nonmarine clastic strata as young as early Pleistocene in age was asymmetrically folded and faulted on its west side against the Paparoa Range. The folded strata are overlain with angular unconformity by glacial outwash gravels (Tophouse Formation) that form prominent surfaces above present river level (fig. 2). The gravels are tilted toward the axis of the subjacent syncline and are cut by faults that are upthrown toward the axis of the syncline and are parallel to bedding in the subjacent strata (fig. 3A). At Giles Creek, Suggate (1957) showed that fault scarps A, G, and H (not of flexural-slip origin) face east, down the depositional

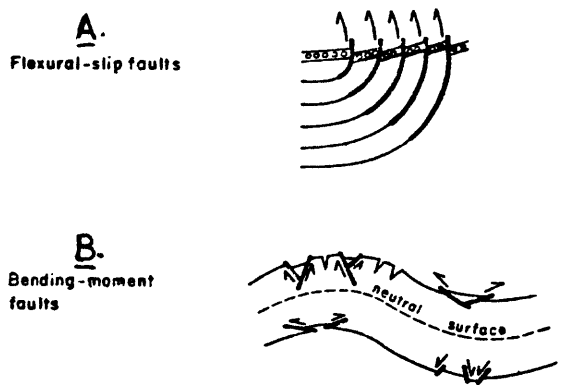

FIGURE 1.--Secondary faults related to folding: A, Flexural-slip faults. B, Bending-moment faults.

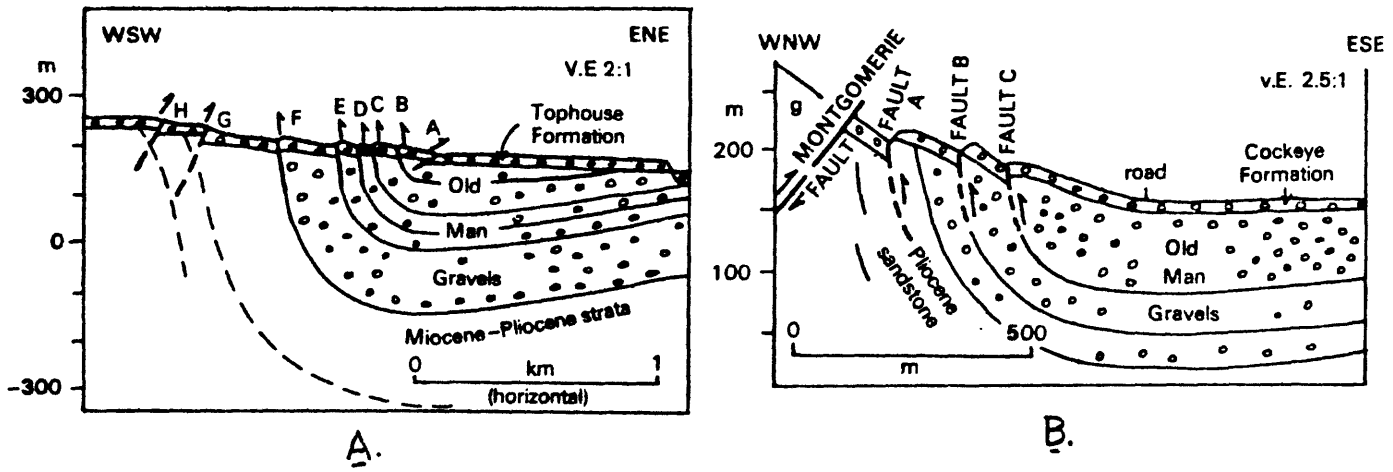

FIGURE 3.--Diagrammatic cross sections of flexural-slip fault scarps in Grey-Inangahua basin, New Zealand. A; Giles Creek scarps. Vertical exaggeration 2:1. Letter designation of scarps follows Suggate (1957). Cross section located on fig. 2. B; Blackball scarps, located at BB on inset to fig. 2, reinterpreted from Young (1963) by Yeats (1986). g: Greenland Group of Ordovician age.

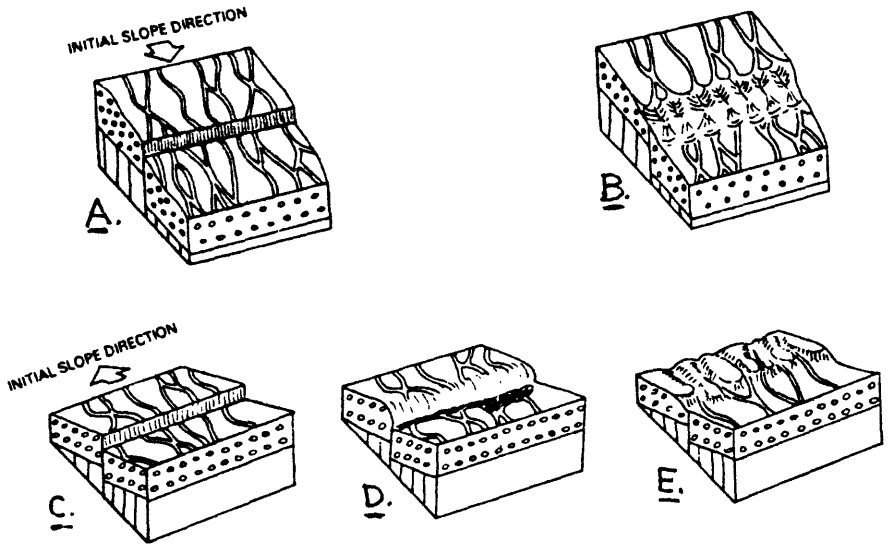

FIGURE 4.--Schematic diagrams of degradation of fault scarp facing upslope (A-B) versus downslope (C-E), from Yeats (1986). Scarp forms on glacial outwash surface which has been abandoned by major drainage, but old braided channels remain. A: fault scarp faces downslope; B: rills following old outwash channels flow across fault scarp, dissecting it. C: fault scarp, formed instantaneously (coseismically), faces upslope; D: rills, unable to cross new scarp, are collected by new drainage which flows along base of scarp. Alternatively, a pond forms at base of scarp. Crest of scarp becomes rounded. E: fault scarp forms by aseismic creep. Rills are able to maintain their courses across rising scarp, and scarp is dissected.

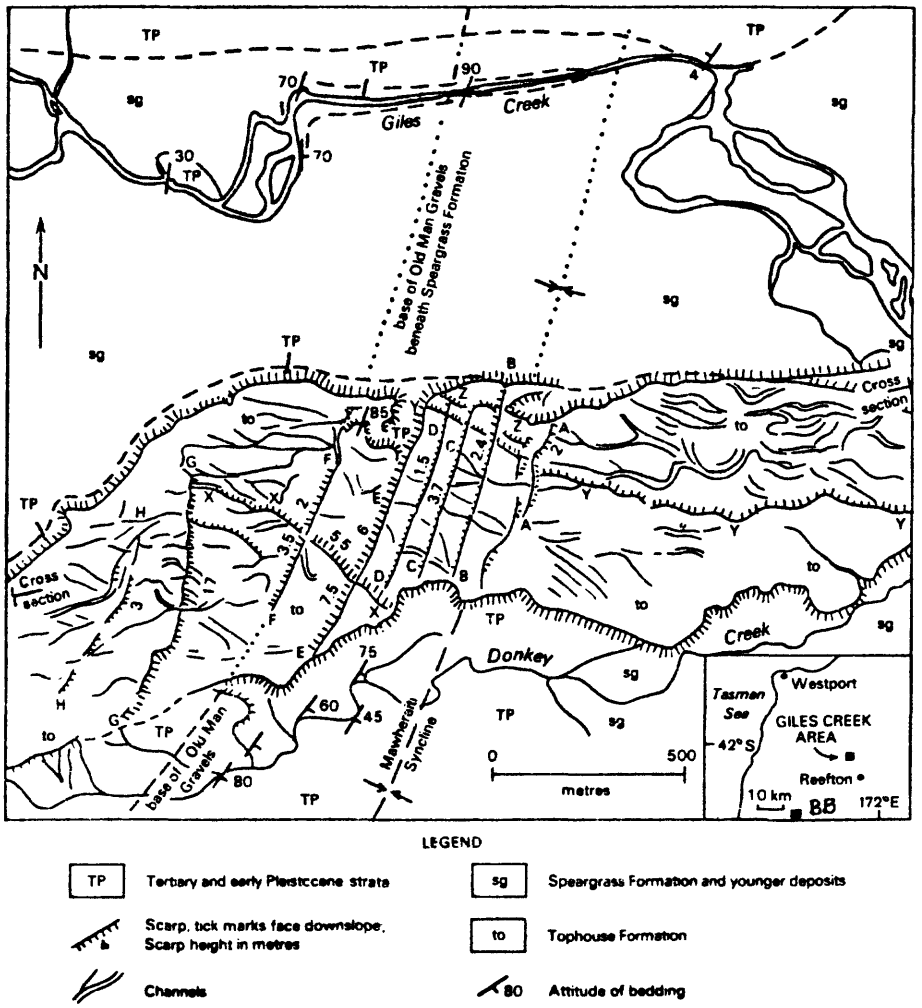

FIGURE 2.--Giles Creek, New Zealand scarps, modified from Suggate (1957) by Yeats (1986). Letter designation of scarps (A-H, X-Z) follows Suggate, although scarps X-Z are interpreted as stream-terrace risers, whereas Suggate mapped them as fault scarps. Scarp heights in meters are modified from Suggate (1957) by Yeats (1986). Cross section along line from lower left to center right is shown in fig. 3.

slope, whereas scarps B, C, D, E, and F face west, up the depositional slope (fig. 3A). The outwash surface on which the scarps are formed is grooved by braided channels which formerly carried outwash gravels of the Tophouse Formation eastward. The alluvial surface of the Tophouse Formation was abandoned in stages from south to north during flexural-slip faulting, such that the surface south of scarp X, a terrace riser, was abandoned first and the surface north of scarp Y was abandoned later

(Yeats, 1986). After abandonment of this surface altogether, the braided channels remained, but they now carry only the runoff derived from the outwash surface itself, whereas formerly they carried detritus from the Paparoa Range to the west.

The east-facing scarps (A, G, and H) are extensively gullied, whereas the west-facing scarps, particularly the largest ones (E and F), are not. For the most part, gullying of the east-facing scarps is due to rills occupying the former braided channels of the outwash surface (fig. 4A and B). The west-facing scarps are generally ungullied; instead, the rill drainage collects at the base of the scarps, forming small bogs or rivulets draining north toward Giles Creek (fig. 4C and D). The only gullies in the west-facing scarps are where scarp heights are relatively low, such as the southern part of scarps B and D. If the west-facing scarps formed by creep on flexural-slip faults, the rill drainage should be able to maintain itself across the slowly rising fault scarps (fig. 14E), just as it does when scarp height is very low, as at the southern parts of scarps B and D. However, the rill drainage is defeated by the scarps blocking its path, suggesting that the scarps formed instantaneously. Modification of the scarps consists of rounding of the scarp crest accompanied by downslope movement, producing a debris slope (terminology of Wallace, 1977). The wash slope of Wallace (1977) is removed by the small stream running along the base of the scarp.

Similar relations are observed to the south at Blackball, where three flexural-slip fault scarps formed on the west limb of a syncline in subjacent strata (Young, 1963; Yeats, 1986; fig. 3B). The largest scarps, A and B, are ungullied, whereas the small scarp C, with an apparent throw of only one meter, is gullied. The larger scarps, 12 and 5 meters, respectively, defeated the rill drainage, but the smallest one was not high enough to defeat drainage which reestablished itself over the scarp during peak runoff. Uphill-facing scarps at Orcutt and Timber Canyons, Ventura Basin, California (Yeats and others, 1981) are gullied by erosion because peak runoff on alluvial fans draining the range to the north is enough to overcome a fault scarp even if it forms instantaneously, during an earthquake.

Bending-Moment Faults

Deformation within a stiffer, flexed layer may be treated as bending an elastic plate around a fold axis. If the plate is bent by equal and opposite moments applied at its ends, the convex side is lengthened and placed in tension, and the concave side is shortened and placed in compression, producing a couple or bending moment. Between that portion of the plate in compression and that portion in tension, there is a neutral surface on which there is neither compression nor tension. The strain within a bent plate is approximately proportional to the distance from the neutral surface and inversely proportional to

the radius of curvature of the plate. On the convex surface, the minimum principal compressive stress (σ_3) is tangent to the plate surface but perpendicular to the axis of bending, whereas on the concave surface, the maximum principal compressive stress (σ_1) has this orientation. If the neutral surface lies within the plate, the deviatoric stress (σ_1-σ_3) is zero at the neutral surface and maximum at the convex and concave surfaces. If the plate is structurally isotropic and homogeneous, and folding is upright, initial rupture above the yield stress will be by extension fractures or normal faults at the convex surface and by reverse faults at the concave surface (fig. 1B). Dating such faults where they are observed in trenches or natural exposures dates the fold to which they are related (for examples, see Yeats, 1986, 1987). These are not known to form as growth faults but instead form in discrete faulting episodes, suggesting that the fold itself forms in jerky episodes rather than smoothly and aseismically.

FOLDS RELATED TO FAULTS

Flexural-slip faults and bending-moment faults are secondary faults that do not extend to seismogenic depths, and the flexural-slip folds that control them do not extend to seismogenic depths either, so these structures themselves are not major producers of earthquakes. However, the folds may be controlled by major faults, and these faults may be seismogenic. Indeed, there are no known examples of flexural-slip faults or bending-moment faults that formed aseismically. Therefore, these folds and their accompanying minor structures provide useful information about adjacent seismogenic faults that might otherwise not be obtained (Stein and King, 1984). There are several geometric possibilities. (1) the fold is in the footwall of an adjacent reverse fault, as in the Grey-Inangahua basin of New Zealand and the Santa Clara syncline in the Ventura basin of California, (2) the fold overlies a fault at depth, as demonstrated for the 1983 Coalinga earthquake (Stein and King, 1984), and (3) the fold is in the hanging wall of an adjacent reverse fault, as in the 1980 El Asnam earthquake.

Suppe (1985) recognized four kinds of folds that are a direct result of fault displacement: **drag folds**, **fault-bend folds**, **fault-propagation folds**, and **decollement folds**.

Drag folds exhibit asymmetry appropriate to the sense of displacement on the adjacent fault and respond to frictional drag on strata that are cut by the fault. The axial surface of a drag fold tends to be parallel to the fault, but other properties such as the mechanical properties of the folded beds also affect the orientation of the axial surface. In determining total displacement across a fault zone, it is important to include the effects of drag folding as well as fault displacement because both are near-surface, low-seismic expressions of reverse

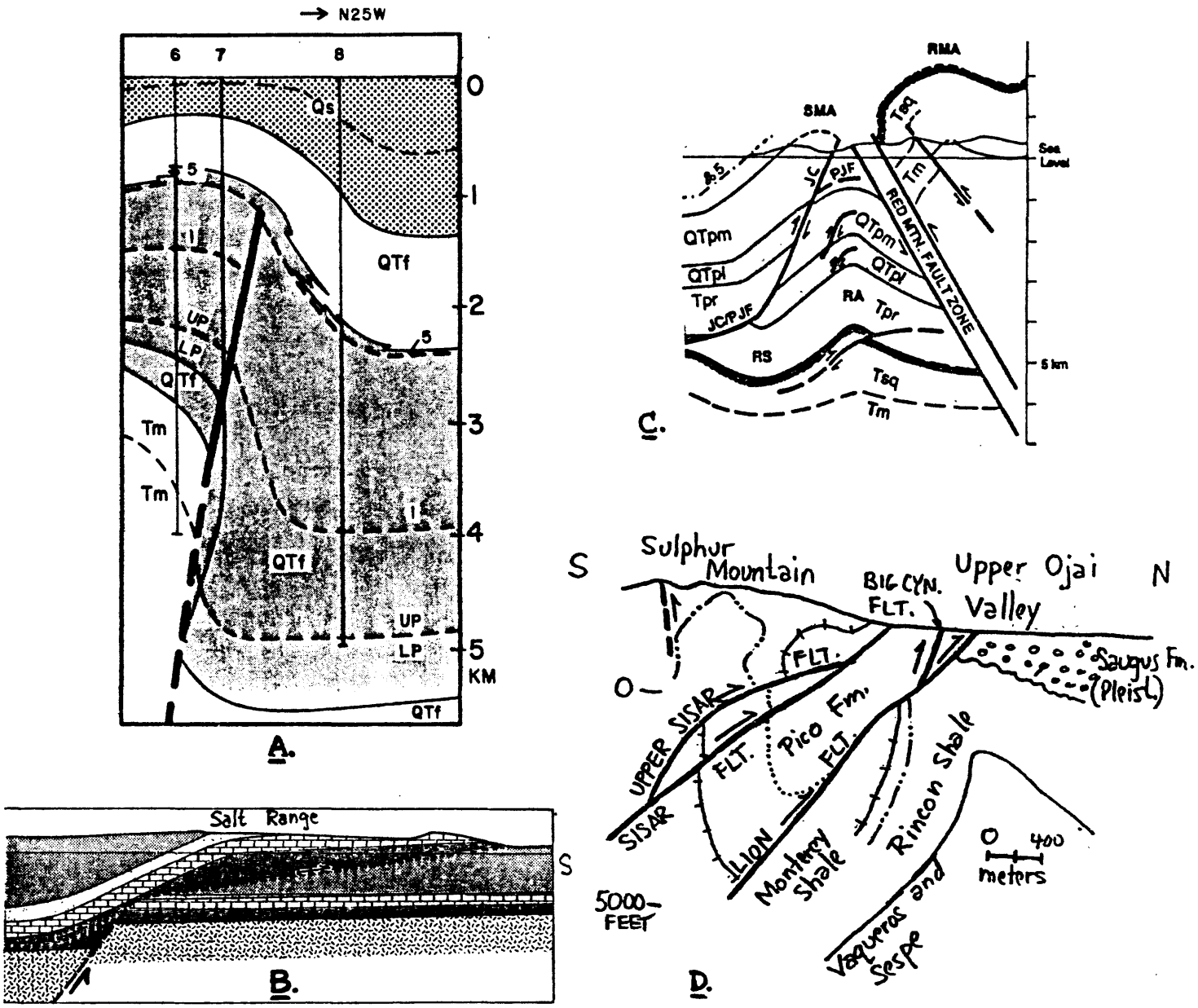

FIGURE 5.--Folds related to faults: A. Drag fold related to Oak Ridge fault, from Yeats and others (1981). Qs, Quaternary Saugus Formation; QTf, Pliocene-Pleistocene Fernando Formation; Tm, Miocene Modelo Formation; 5, 1, and UP/LP identify microfaunal horizons.

B. Fault-bend fold on north flank of Salt Range, Pakistan, after Lillie and others (1987).

C. Fault-propagation fold (San Miguelito anticline, SMA) related to Padre Juan fault (PJF), after Grigsby (1986). JC, Javon Canyon fault.

D. Decollement fold: Sulphur Mountain anticlinorium overlying Sisar fault system, after Huftile (in press and written commun., 1987). Pico, Monterey, and Rincon Formations are ductile strata that have been folded disharmonically over Vaqueros and Sespe Formations, stiffer strata that dip homoclinally southward, resulting in excess bed length of the overlying folded strata with respect to the Vaqueros and Sespe Formations.

faulting in high-strength rocks at depth in the seismogenic zone. An example is shown in fig. 5A of the Oak Ridge fault in the Ventura Basin, taken from Yeats and others (1981). In the example, vertical separation by faulting of Horizon 1 in the QTf unit is 750 m, but by including the drag folding of this horizon, particularly as expressed in the footwall block, the total vertical separation of this horizon is 2,500 m. This figure divided by the cosine of the fault-dip angle gives the component of fault slip at depth in the line of section.

Fault-bend folds are formed because fault surfaces are not planar in the direction of slip. Movement across a nonplanar fault surface must produce deformation of one or both blocks adjacent to the fault or cause the fault itself to break through one of the blocks to produce a straighter trace in the direction of slip (as the Sisar fault has done in fig. 5D). Fault-bend folds are most common in the hanging walls of faults, either in tilting of strata toward the surface of a listric normal fault or in bending of strata as they override a thrust surface characterized by ramps. These folds are produced by bending rather than by frictional drag. In northern Pakistan, the Salt Range thrust brings platform strata southward over Precambrian basement that has been previously block-faulted (Lillie and others, in press). One of these block faults in the Salt Range faces north, and the thrust plate has bent upward to override the block fault, producing the topographic north flank of the central Salt Range (fig. 5B).

Fault-propagation folds form ahead of the tip of a propagating fault. During the process of folding, a limb may fail, and the resulting fault will propagate toward the surface. Stratigraphic separation across the fault decreases to zero as the fault tip is approached, and an increasing amount of displacement is taken up by folding. In the Ventura basin, the San Miguelito anticline is a fault-propagation fold related to the subjacent Padre Juan fault (Grigsby, 1986; fig. 5C). The Padre Juan fault ramps upward from Miocene shale across Pliocene and Pleistocene turbidites as the Red Mountain fault is approached. Separation across the fault diminishes upsection as more displacement is taken up by the fold, and near the surface where the fault flattens, separation is near zero. The example is complicated by the fact that the near-surface trace of the Padre Juan fault has been folded into an orientation of lower shear stress, and a new fault, the Javon Canyon fault, has broken through to the surface and displaced Holocene terrace deposits (Sarna-Wojcicki, in press).

Decollement folds form in the hanging-wall block of a low-angle thrust fault and show a shortening in the hanging wall with respect to the unyielding footwall. When cross sections of decollements are retrodeformed, it is revealed that the beds in

the hanging wall are too long for the unyielding footwall that they were originally assumed to overlie. This kinematic problem must be resolved in the footwall; the decollement fault must produce the same shortening in the footwall at depth as it does in the hanging wall near the surface, otherwise, the cross section does not balance. An example is the Sisar fault system in the Ventura basin, in which bed lengths of weak Miocene strata in the hanging-wall block are 6.1 km longer than bed lengths in underlying stiffer strata (Huftile, in press and written commun., 1987; fig. 5D). Huftile resolved the bed length problem by making the Sisar fault a frontal fault of the Oak Ridge fault, which takes up the excess bed length of the footwall fault at depth.

ACKNOWLEDGMENTS

This work has been supported by contracts with the Earthquake Hazards Reduction Program of the U.S. Geological Survey, by Oregon State University and the New Zealand Geological Survey, and by the petroleum industry in the form of graduate-student support and well data.

REFERENCES CITED

Grigsby, F.B., 1986, Quaternary tectonics of the Rincon and San Miguelito oil fields area, western Ventura basin, California: MS thesis, Oregon State University, Corvallis.

Huftile, G.J., in press, A retrodeformable cross section across the central Ventura basin, California: EOS, Transactions, American Geophysical Union.

Huftile, G.J., 1987, Thin-skinned thrusting, retrodeformable cross-sections, and oil accumulation of the Upper Ojai Valley area, Ventura County, California: MS thesis, Oregon State University, Corvallis, in prep.

Lillie, R.J., Johnson, G.D., Yousuf, M., Zamin, A.S.H., and Yeats, R.S., in press, Structural development within the Himalayan foreland fold-and-thrust belt of Pakistan, in Beaumont, C. and Tankard, A.J., eds., Basins of Eastern Canada and Worldwide Analogs: Canadian Society of Petroleum Geologists Special Volume.

Ramsay, J.G., 1967, Folding and Fracturing of Rocks: New York, McGraw-Hill, 568 p.

Sarna-Wojcicki, A.M., in press, Recurrent Holocene displacement on the Javon Canyon fault: U.S. Geological Survey Professional Paper 1339.

Stein, R.S. and King, G.C.P., 1984, Seismic potential revealed by surface folding--1983 Coalinga, California, earthquake: Science, v. 224, p. 869-872.

Suggate, R.P., 1957, The geology of Reefton subdivision: New Zealand Geological Survey Bulletin n.s. 56, 146 p.

Suppe, J., 1985, Principles of Structural Geology: Englewood Cliffs, N. J.,Prentice-Hall, 537 p.

Wallace, R.E., 1977, Profiles and ages of young fault scarps, north-central Nevada: Geological Society of America Bulletin, v. 88, p. 1267-1281.

Yeats, R.S., 1986, Faults related to folding with examples from New Zealand: Royal Society of New Zealand Bulletin 24, p. 273-292.

Yeats, R.S., 1987, Active faults related to folding, in Active Tectonics: National Academy Press, p. 63-79.

Yeats, R.S., Clark, M.N., Keller, E.A., and Rockwell, T.K., 1981, Active fault rupture in southern California--Ground rupture versus seismic shaking: Geological Society of America Bulletin, part I, v. 92, p. 189-196.

Young, D.J., 1963, A faulted and tilted late Pleistocene terrace near Blackball: New Zealand Journal of Geology and Geophysics, v. 6, p. 721-724.

IDENTIFICATION AND GEOLOGIC CHARACTERISTICS OF EARTHQUAKE-INDUCED LIQUEFACTION FEATURES

by

Stephen Obermeier
U.S. Geological Survey
Reston, Virginia 22092

ABSTRACT

Classes of liquefaction-induced features that are commonly associated with an earthquake origin include (1) sand blows, (2) lateral-spread landslides, and (3) sediment intrusions such as sand dikes and sills. All these classes of features have been identified by the author in highly variable geologic settings, ranging from marine deposits in coastal South Carolina to fluvial deposits in the New Madrid seismic zone. Liquefaction in both geographic areas typically originated in sandy deposits containing little or no clay. Criteria for interpreting an earthquake origin have been developed for many combinations of geologic, topographic, and ground-water conditions.

INTRODUCTION

The surface expression of earthquake-induced liquefaction features is highly dependent on the local geologic setting. This paper discusses the types of features, primarily sand blows, that formed on level ground in two very different geologic settings, one in which the parent sediments have a marine or near-marine origin (coastal South Carolina) and one in which the parent sediments have a fluvial origin (New Madrid seismic zone). The diverse types of sand blows and the controls on their formation became apparent during field studies recently conducted to locate regions subjected to strong earthquake shaking, as indicatd by the presence of liquefaction-induced features. In coastal South Carolina, field studies focused on sand blows of very late Pleistocene to Holocene age, as well as features caused by the 1886 Charleston earthquake. In the New Madrid seismic zone, the search was largely restricted to sand blows caused by the 1811-12 earthquakes. In both areas features of non-earthquake origin occur that might be confused with earthquake-induced features. Geologic criteria have been developed by which the eathquake-induced features can be distinguished.

EARTHQUAKE-INDUCED FEATURES AND CRITERIA FOR ESTABLISHING ORIGIN

Sand Blows

Sand blows are of two types: craterlets or vented-sand volcanoes (Obermeier and others, 1986). A craterlet is a hole at the ground surface created when liquefied sand vents to the surface and moves aside the surface material, usually soil. After venting, a hole, commonly 1 to 3 m wide and 1 m deep, remains at the ground surface. The craterlet subsequently fills with adjacent material. A characteristic stratigraphic arrangement of sediments is present, which represents various phases of flowage from and subsequent filling of the crater. The outflow phase is represented by sediments in the

lower part of the crater, which are graded according to size and density. The upper part of the crater contains sediments of the filling phase, which began after flowage stopped. The filling phase is represented by thin beds of surficial sediments washed into the crater. All craterlets that we have found are filled, and no evidence of craterlets is present on the ground surface.

Craterlets are the most common type of sand blow in the marine sediments of coastal South Carolina. Craterlets generally formed along the flanks or crests of late Quaternary beach ridges (Peters and Herrmann, 1986). The craterlets occur where a cover, generally less than 1 m thick, of clay-bearing or humate-rich soil overlies clean (that is, containing no silt or clay) sand. (In some places the sand beds contain abundant friable and porous shells, whose earthquake-induced collapse could have caused liquefaction.) In areas topographically lower than beach deposits, where surficial materials contain more clay, the sand blows are expressed as vented-sand volcanoes, similar to those of the New Madrid seismic zone described below.

In the New Madrid seismic zone, vented-sand volcanoes are the most common type of sand blow. Thousands of sand blows produced by the 1811-12 earthquakes can be recognized easily on airphotos and on the ground surface. These sand blows are constructional cones, 0.5-1 m high, and 15-60 m in diameter. Throughout most of the 1811-12 meizoseismal zone, a 2-10 m thick clay cap overlies a thick deposit of clean, medium-grained sand. Beneath the central, highest part of the sand blow, the clay cap is shattered by intruded sand. The intruded sand contains stratigraphic characteristics indicating flowage. The surficial constructional cone becomes both finer-grained upward and shows evidence of flowage away from a central vent system.

Criteria for interpreting an earthquake origin to features that appear to be either the craterlet or vented-sand volcano type of sand blow generally have four elements:

1. The features have sedimentary characteristics that are consistent with an earthquake-induced liquefaction origin: that is, they show evidence of (a) an upward directed, strong hydraulic force that was (b) suddenly applied, and (c) of short duration.
2. The features are in ground-water settings (that is, areas of low relief) where suddenly applied, strong hydraulic forces of short duration could not be reasonably expected except from earthquake-induced liquefaction. In particular, it can be demonstrated that it is extremely unlikely that springs, caused by regional or local ground-water conditions, caused the features.
3. The features are clustered geographically at sites less than a few kilometers apart, in similar geologic and ground-water settings.
4. The features have characteristics that are consistent with historically documented observations of earthquake-induced liquefaction.

Considerable reliance has been placed on the fourth element for interpreting an earthquake origin in coastal South Carolina and the New Madrid seismic zone. If, however, the first three criteria are unequivocally satisfied outside these geographic areas, an earthquake origin can still be ascertained in areas that have not had historic earthquakes.

Artesian springs (non-earthquake) are the most likely source of liquefaction-induced features at many places. However, in coastal South Carolina, sand blows are commonly located near or along the crests of broad, ancient beach ridges, where it would have been impossible to have had artesian springs. In the New Madrid seismic zone, deep rivers that cut the fluvial

sediments would have prevented artesian conditions at most places within the past few thousand years. Other possible origins for ground disruption that must be eliminated to ascertain an earthquake origin include penecontemporaneous dewatering structures, landslides, fillings in root holes, ground disruption by thrown trees, and liquefaction by wave-action.

At some places, it is not possible to determine whether earthquakes or artesian springs produced craterlets or vented-sand volcanoes on the basis of sediment relations near the surface. The origin of some of these features is uncertain where springs could have formed, such as on the flanks of beach and point bar deposits, more than a few meters below their crests.

Lateral Spreads

An earthquake origin can be deduced at some places by the presence of lateral-spread landslides (that is, lateral spreads) on very low slopes (about 0.5-5 percent). Lateral spreads are basically large slabs of nonliquefied material that move downslope atop a liquefied stratum of large areal extent. Liquefaction by artesian springs over such a large areal extent is extremely unlikely in the ground-water and geologic settings in coastal South Carolina and the New Madrid seismic zone. Where slab movements are large (meters), reverse shears commonly form along the toe, and grabens form along the head.

In coastal South Carolina, small downslope movements (interpreted to be caused by "incipient" lateral spreads) can cause reverse shears through unliquefied sediments along the base of a crater. The shears are on the downslope side, and the offset is generally only a few centimeters. The reverse shearing is normally traceable into the liquefaction source sand bed for a very short distance, perhaps only a meter or so. Shortly after entering the source sand bed, the shear follows the bedding and cannot be traced. For such small shear movements, no upslope detachment structures appear to have formed.

Lateral spreads whose movements were large enough to form narrow, open fissures were apparently quite common during the 1886 earthquake, according to historical accounts (Peters and Herrmann, 1986). However, structures that unequivocally were once narrow open fissures have not been located in recent field studies. Features that possibly were wide (>1 m), open fissures have been identified, however, and are similar to filled craterlets in vertical cross section, except the edges of the craters show evidence of having been pulled apart laterally and the crater is filled with sediments having cut-and-fill relations, which indicates that a small, weakly flowing stream occupied the open fissure.

In the New Madrid earthquakes of 1811-12, large lateral spreads were commonplace near streams and terrace scarps. Many of the lateral spreads along streams were much larger (order of magnitude) than historical landslides caused by rapid drawdown of streams. This large size diffference, coupled with widespread distribution, permits assigning a probable earthquake origin. Lateral spreads with toes along terrace scarps, far from streams, would also appear to have an earthquake origin.

Dikes and Sills

In both coastal South Carolina and the New Madrid seismic zone, earthquake-induced liquefaction has formed numerous dikes and sills. An earthquake origin can be interpreted if springs, wave action, and penecontemporaneous deformations can be eliminated as source mechanisms.

ADDITIONAL CRITERIA FOR ESTABLISHING AN EARTHQUAKE ORIGIN

Where geologic studies of near-surface sediment relations are inadequate for determining if liquefaction was earthquake-induced, it should be possible at some places to decide the origin based on mechanical properties and piping (that is, tube-erosion) properties of source sand beds. The mechanical properties (as determined by tests such as the Standard Penetration Test or cone penetrometer) may show if earthquake-induced liquefaction was mechanically possible. Piping studies in the field may be useful to determine if very weak artesian conditions could have formed craterlets or vented-sand volcanoes.

FEATURES OF NON-EARTHQUAKE ORIGIN

In both coastal South Carolina and the New Madrid seismic zone, many other types of features produced by weathering superficially appear to be liquefaction-induced. Chemical and physical weathering in South Carolina has produced what seems to be shattered ground, white surficial sand sheets, and intrusions of clean sand connected to vents (Gohn and others, 1984). White sand sheets connected to vent-like features were interpreted as expulsions of liquefied sand by Gohn and others (p. 12), but subsequent mineralogical data have led to the conclusion that they are weathering features unrelated to liquefaction. This misinterpretation illustrates that geochemical and pedological studies may be required to resolve the question of origin.

Features in the New Madrid seismic zone that easily could be misinterpreted as having an earthquake origin include (1) "mima mounds", and (2) sand exposed along the crests of point-bar deposits which have had a thin surficial clay cap eroded off, thereby exposing underlying sand. Mima mounds are surficial sand and silt mounds of unknown, but nonearthquake origin, and can be distinguished from vented-sand blow deposits by the absence of vents (Fuller, 1912).

AGES OF LIQUEFACTION FEATURES

Craterlets formed in at least three widely separated times of strony earthquake shaking during the Holocene near Charleston, South Carolina (Weems and others, 1986). Highly accurate ages have been obtained from C^{14} analysis of small sticks (limbs) that fell into the open craters soon after initial formation. Less accurate ages have been obtained from relations between roots that pre-dated and post-dated initial formation of craters and from ages of soil clasts that fell into craters.

In general, it is difficult to get narrow constraints on the age of vented-sand volcanoes because of the poor conditions for preserving woody matter.

REFERENCES CITED

Fuller, M.L., 1912, The New Madrid earthquake: U.S. Geological Survey Bulletin 494, 119 p.

Gohn, G.S., Weems, R.E., Obermeier, S.F., and Gelinas, R.L., 1984 Field studies of earthquake-induced liquefaction-flowage features in the Charleston, South Carolina, area, preliminary report: U.S. Geological Survey Open-File Report 84-670, 26 p.

Obermeier, S.F., Jacobson, R.B., Powars, D.S., Weems, R.E., Hallbick, D.C., Gohn, G.S., and Markewich, H.W., 1986, Holocene and late Pleistocene (?) earthquake-induced sand blows in coastal South Carolina: Proceedings of the Third U.S. National Conference on earthquake engineering, Earthquake Engineering Research Institute, v. 1, p. 197-208.

Peters, K.E., and Herrmann, R.B., 1986, First-hand observations of the Charleston eathquake of August 31, 1886, and other earthquake materials: South Carolina Geological Survey Bulletin 41, 116 p.

Weems, R.E., Obermeier, S.F., Pavich, M.J., Gohn, G.S., Rubin, M., Phipps, R.L., and Jacobson, R.B., 1986, Evidence for three moderately large prehistoric Holocene earthquakes near Charleston, S.C.: Proceedings of the Third U.S. National Conference on earthquake engineering, Earthquake Engineering Research Institute, v. 1, p. 3-13.

LANDSLIDES AS INDICATORS OF PREHISTORIC EARTHQUAKES

by

David K. Keefer
U.S. Geological Survey
Menlo Park, California 94025

Landslides are among the most common geomorphic effects of seismic shaking. Landslides have been reported from historical earthquakes at least as small as magnitude 4.0, and many large historical earthquakes have triggered tens of thousands of landslides over areas of thousands of square kilometers. A recent study of historical earthquakes identified 14 types of earthquake-induced landslides (Keefer, 1984), but the use of landslide deposits as indicators of prehistoric seismic events is complicated by the fact that all of these types of landslides also occur under nonseismic conditions.

Potential studies using landslide deposits as paleoseismic indicators are of two main types. The first is intensive analysis of a particular landslide deposit to determine whether the landslide could reasonably have occurred without seismic shaking. The second is the mapping of the distribution of large numbers of contemporaneous landslide deposits and the determination of whether the numbers, types, and relative abundances of the different types of landslides are more likely due to seismic shaking than to some other regional event such as a severe storm.

The first type of study requires a detailed geologic and geotechnical evaluation of the landslide, including a slope-stability analysis. Such an analysis requires reconstruction of the pre-landslide geometry of the source, strength testing of the material, and reliable estimation of the ground-water conditions at the time of failure. If the slope-stability analysis indicates that the source slope was stable under the least favorable nonseismic conditions that are reasonable, then seismic shaking can be inferred as the probable triggering cause.

An example of this type of analysis is described by Jibson (1985), who studied a large, complex block slide and a large earth flow on the Mississippi River bluffs near New Madrid, Mo. He concluded that the bluffs that produced these landslides were stable under all reasonable estimates of nonseismic conditions but became unstable when subjected to the estimated shaking produced by the 1811-12 New Madrid earthquakes. Similar detailed analyses of landslides in areas where the seismic history is unknown could suggest the occurrence of a prehistoric earthquake. However, the use of these analyses in paleoseismic studies is limited by the need for relatively complete and precise data on the pre-failure conditions.

At least one type of landslide that is very common during earthquakes but is seldom triggered by nonseismic events is liquefaction-induced lateral spreads on gentle slopes (as gentle as 0.3^{o}) in sandy flood plain sediments. Even with flood-plain lateral spreads, however, a detailed analysis is necessary to eliminate any potential nonseismic cause.

The second type of study involves identifying contemporaneous landslides over a region of some size and differentiating landslide distributions probably caused by earthquakes from those probably due to other causes. For example, the most abundant landslides in the sample of historical earthquakes studied by Keefer (1984) were rock falls, rock slides, and disrupted soil

slides. These landslides are more likely to be triggered in large numbers by an earthquake than by a storm. Thus, the presence of many contemporaneous deposits of landslides of these types over a large region suggests a prehistoric seismic event. Major impediments to studies of this second type are the difficulty in accurately dating large numbers of landslide deposits and the fact that deposits of many of the landslides triggered by a prehistoric earthquake may have been destroyed by subsequent erosion.

Under ideal circumstances, however, some indications of the size of a prehistoric seismic event may be derived from landslide distributions using magnitude-distance, magnitude-area, and shaking intensity relations for landslides of various types such as developed by Kuribayashi and Tatsuoka (1975), Youd (1977), Youd and Perkins (1978), Adams (1980), Keefer (1984), Wilson and Keefer (1985), and Keefer and Wilson (1987?). In one example of a paleoseismic study using such relations, Adams (1981) inferred from a distribution of landslide-dammed lakes in the Lake Matiri area of New Zealand that a magnitude 7.4 earthquake had occurred there in approximately A.D. 1650. The use of these relations in paleoseismic studies is limited partly by the scatter in the data sets from which they are derived.

The simultaneous occurrence of large numbers of landslides has the potential for delivering a large volume of sediment to rivers and lakes. In some cases, the occurrence of numerous landslides and, thus, a prehistoric earthquake may be inferred from the study of sedimentation in flood-plain or lacustrine environments. Examples of such studies and some discussion of their limitations are given by Bapat (1985) and Doig (1986).

Whereas landslide deposits have been used in so far only a few paleoseismic studies--notably those of Adams (1980, 1981) and Jibson (1985)--significant potential exists for their future use. The limitations discussed above may be minimized by combining regional and analytical studies. The regional studies could determine the distribution of landslide deposits and provide estimates of their relative ages from the degree to which their features have been modified by erosion; slope-stability analyses and absolute dating of one or a few representative deposits could be used to infer whether the landslides were seismically triggered and, if so, when the triggering occurred. More accurate and precise paleoseismic studies using landslides may also be possible as dating techniques are refined and as more detailed geologic studies are carried out in seismically active areas.

REFERENCES CITED

Adams, J., 1980, Contemporary uplift and erosion of the Southern Alps, New Zealand: Geological Society of America Bulletin, v. 91, no. 1, Part II, p. 1-114.

Adams, J., 1981, Earthquake dammed lakes in New Zealand: Geology, v. 9, no. 5, p. 215-219.

Bapat, A., 1985, The phenomenon of seismosedimentation: Proceedings, International Workshop on Alluvial River Problems, 2nd, Roorkee, India, 1985, University of Roorkee, p. 47-52.

Doig, R., 1986, A method for determining the frequency of large-magnitude earthquakes using lake sediments: Canadian Journal of Earth Sciences, v. 23, no. 7, p. 930-937.

Jibson, R. W., 1985, Landslides caused by the 1811-1812 New Madrid earthquakes: Stanford, Calif., Stanford University Ph.D. Dissertation, 232 p.

Keefer, D. K., 1984, Landslides casued by earthquakes: Geological Society of America Bulletin, v. 95, no. 4, p. 406-421.
Keefer, D. K., and Wilson, R. C., [1987?], Predicting earthquake-induced landslides, with emphasis on arid and semi-arid environments, in Sadler, P. M., and Morton, D. M., eds., Landslides in a semi-arid environment: studies from the inland valleys of southern California: Riverside, Calif., University of Calif., 44 p. [in press].
Kuribayashi, E., and Tatsuoka, F., 1975, Brief review of liquefaction during earthquakes in Japan: Soils and Foundations, v. 15, no. 4, p. 81-92.
Wilson, R. C., and Keefer, D. K., 1985, Predicting areal limits of earthquake-induced landsliding, in Ziony, J. I., ed., Earthquake hazards in the Los Angeles region--An earth science perspective: U.S. Geological Survey Professional Paper 1360, p. 317-345.
Youd, T. L., 1977, Discussion of "Brief review of liquefaction during earthquakes in Japan" by Eiichi Kuribayashi and Fumio Tatsuoka, 1975, (in Soils and Foundations, v. 15, no. 4, p. 81-92): Soils and Foundations, v. 17, no. 1, p. 82-85.
Youd, T. L., and Perkins, D. M., 1978, Mapping liquefaction-induced ground failure potential: American Society of Civil Engineers, Journal of the Geotechnical Engineering Division, v. 104, no. GT4, p. 433-446.

HIGH-RESOLUTION SHALLOW-REFLECTION TECHNIQUES

by

Kenneth W. King and Robert A. Williams
U.S. Geological Survey
Denver, Colorado 80225

Considerable advances been made in high-resolution shallow-reflection techniques during the past 3 yr. An important result of the research has been to identify certain engineering parameters, and to identify and map structures in shallow, unconsolidated sediments. The use of high-resolution shallow seismic-reflection (HRSR) techniques has proven to be a useful tool for identifying and mapping shallow structures that are important in paleoseismic studies. However, the primary purpose of HRSR research has been to help determine important engineering properties of the materials within the upper 100 m of the Earth's surface. Medvedev (1965) showed that the potential for amplification of earthquake ground motions increases as the impedance contrast between the subsurface layers increases, provided that all other parameters are constant. The interval thickness, and shear and compressional velocities are important parameters in the study of site or ground-motion response.

The goal of the HRSR study is to use both shallow P- and S-wave reflection data to produce reflection profiles that show the subsurface structure, and to indicate some of the engineering parameters of the subsurface soils. The P- and S-wave profiles allow interpretation of more geological information than the use of P or S waves alone. It is possible to determine Poisson's ratio as a function of depth when the P- and S-interval velocities are determined. A second goal of the shallow-reflection study is to resolve the thickness of unconsolidated beds to within approximately 0.5 m. Widess (1973) indicated that resolution of "thin beds" by reflection techniques is theoretically limited to about one-eighth wavelength. The 0.5-m resolution goal can be obtained in unconsolidated sedimentary layers where the interval velocities range from 300 to 1,200 m/s if the reflected waves are in the 180- to 300-Hz frequency band.

The basic equipment used in this research is an Input/Output DHR 2400 seismic-recording system. The DHR 2400 is a 24-channel, digital seismic system employing an 11-bit plus sign-bit analog-to-digital (A/D) converter which uses 0.25-ms sampling rate, and has a wide range of source inputs and analog filters. The general technique uses a modified rifle or shotgun as the seismic source, pre-A/D filtering, and 0.5- to 2-m geophone spacing. The seismic source is generally a 12-gauge shotgun which fires a 28-g lead slug vertically into the ground. The DHR 2400 system has a 24,000-byte digital memory which allows the "summing" of repetitive seismic-source inputs. Summing increases inphase low-amplitude reflected wavelets and cancels random seismic noise. We have found that summing the signals of two to five repeated "shots" (source inputs) reduces random seismic noise, enhances the reflected wavelets, and minimizes the cost and time of fieldwork.

We use a minimum of eight-fold common-reflection midpoint stacking (CDP) with an average of twelve-fold stacking on the main target area by using a 24-summed-geophone input with a "push-on, pull-off" array-moving technique. The

ability to use only 100- to 300-Hz frequencies and the increased coherency of twelve-fold common-reflection midpoint stacking of two to five summed-input sources givea us the necessary high-frequency resolution to map velocity contrasts within unconsolidated sediments in the 20- to 500-ft-depth range.

The digital field data are processed on a VAX 11/780 computer. The data are edited, sorted into CDP gathers, and plotted in preliminary form. The CDP gathers are analyzed with constant-velocity search procedures and stacked to give the final two-way traveltime versus horizontal-distance format. The field and processing techniques were used to map several profiles in the Denver and Wasatch Front area.

Figure 1 shows the different target-depth tuning possibilities with the HRSR techniques. The general target depths and thicknesses vary from 20 to 60 ft at the Denver Federal Center, 75 to 160 ft at Liberty Park, and 220 to 1,000 ft at the Salt Lake International Airport (fig. 1A, B, C). The effective target zone generally appears to become thicker with increased subsurface depths because the resolution also decreases with depth.

Figure 1A shows a 240-Hz reflector at a 20-ft depth and a 180-Hz reflector at approximately 54-ft depth. Figure 1A shows no reflection with a two-way traveltime greater than 40 ms due to the interference of the arrivals with the ground coupled air wave, the tuning of the surface geophone array, and the low signal-to-noise ratio of the deeper reflections. The profile is derived from a twelve-fold CDP with a 2-ft geophone spacing and 2-ft shot interval. The data were filtered with a 140-Hz highpass filter. In this example, the geophone shot arrays, and method of operation and analysis were not tuned to reflections less than approximately 75 ft or deeper than 160 ft. Figure 1C is a profile from a twelve-fold CDP, 30-ft geophone spacing and shot interval with a 80-Hz highpass filter. The profiles displayed in figure 1 indicate generally horizontally bedded siltstones, clays, and sands. The slight depression shown on figure 1A proved through drilling to be a 2-ft depression in a silty sand lens. The subsurface bedding at Liberty Park and Salt Lake International Airport is due to very flat lying lake sediment.

Figure 2 indicates some of the shallow subsurface structures that can be detected and mapped by the HRSR methods. Figure 2A is a profile perpendicular to and across the East Bench fault in Salt Lake City. The profile shows the main fault offsetting the alluvial section and several other faults with some block rotation. The profile also shows a general dip of the alluvium of approximately 5° to the west. Figure 2B shows a domed or rotated gravel-sand bed which has a channel cut approximately 8 ft into it. The gravel-sand bed pinches out at the west end of the profile. Figure 2C shows three voids at approximately 40-ft depth where coal has been removed. The profile shows an example of a classic "bright spot", except that the reflected wavelets are at a much higher frequency (210 Hz) than the normal gas/oil exploration "bright spots". These examples show that HRSR methods, with proper field techniques and analysis, can be an effective tool for mapping detailed structure within an unconsolidated sediment wedge.

It is apparent from HRSR studies that the general reflection techniques developed for investigation of site response can be applied to mapping shallow structures in unconsolidated sediments. The only modifications needed to use HRSR methods in mapping layers within shallow unconsolidated materials are to extend the surface lines horizontally and to limit the target or section to be mapped in the vertical plane. The parameters for obtaining good, shallow, high-resolution reflections are extremely site dependent; therefore, a "walk-

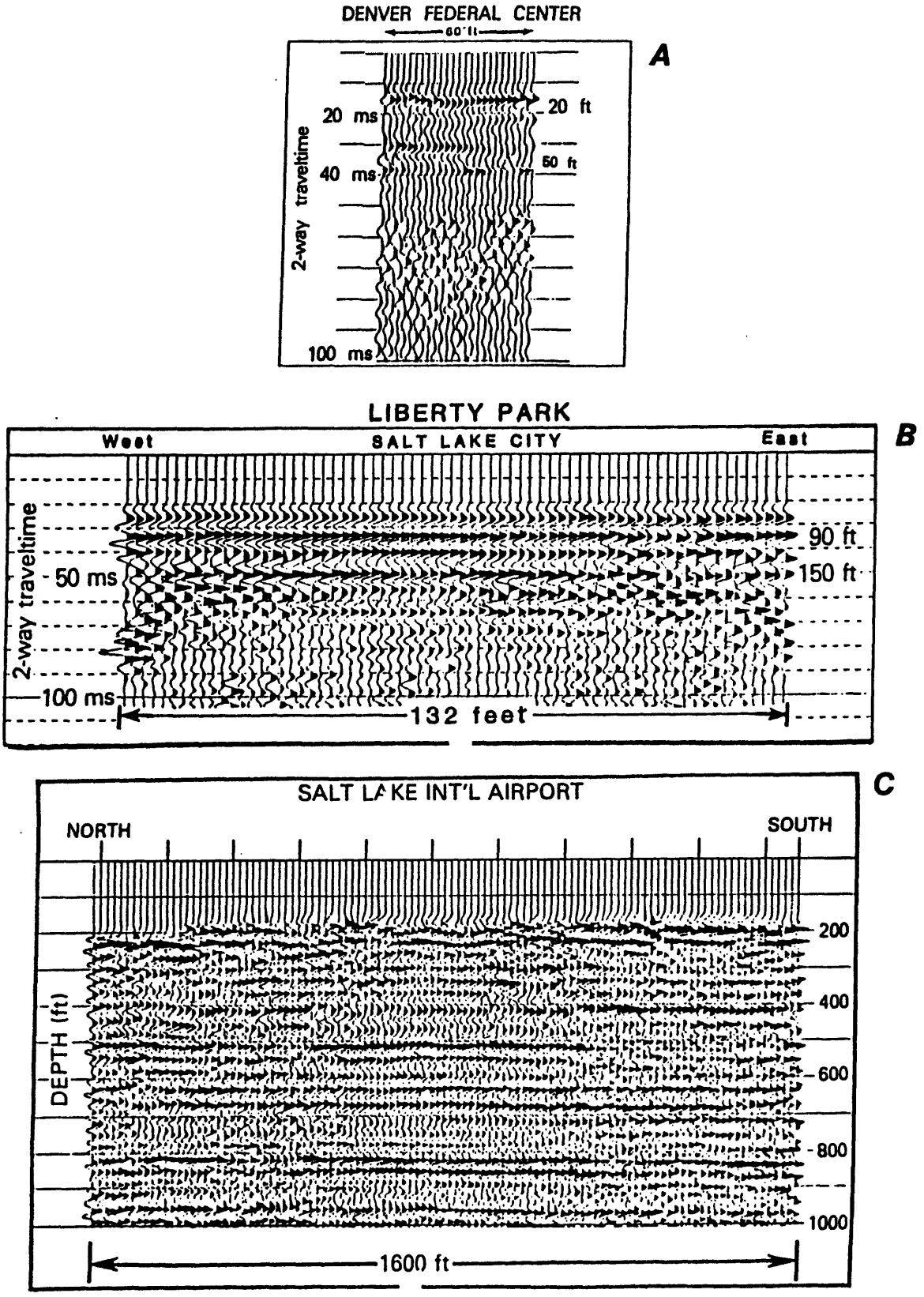

FIGURE 1.--Velocity reflection profiles showing depths-traveltimes to subsurface reflection zones. A, approximately 20-60 ft; B, approximately 90-180 ft; C, approximately 220-1,000 ft. (Profile A is from the U.S. Government Federal Center near Denver, Colorado; profiles B and C are from sites in Salt Lake City, Utah.)

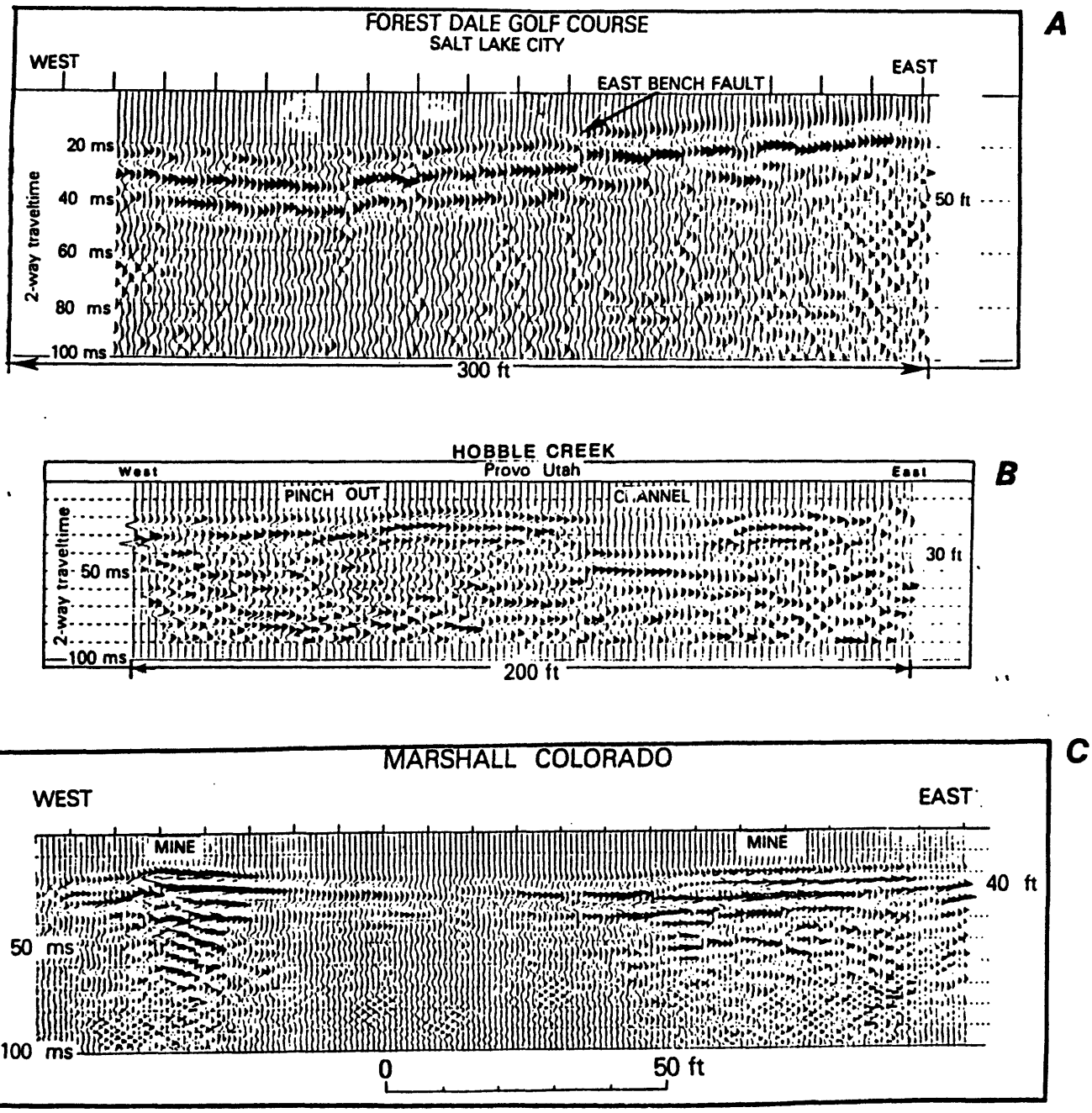

FIGURE 2.--Velocity reflection profiles indicating subsurface structure: A, faults; B channel and pinch-out; C, subsurface tunnel. (A, across the East Bench fault in Salt Lake City, Utah; B, from near Hobble Creek, south of Provo, Utah; C, from an area of coal mining near Marshall, Colorado.)

away" or a preliminary velocity analysis is necessary before starting routine field-data acquisition. The interval velocities, depth of target, and thickness of the target layers dictate the necessary source frequency input (thereby the type of source), source array, offset distances, geophone array design, and recording parameters. Our research has limited the array designs and methods to those that are compatible to use in urban areas. For example, sparkers, poppers, and explosives as input seismic sources have not been used; whereas, hammers, weight drops, vacuum guns, modified rifles, and modified shotguns have been used as energy sources for this study. Also, since we are not generally afforded long, open spaces in urban areas to run profiles, we do not generally run split-spread type of reflection lines which are usually used for deeper reflection investigations. The HRSR method should be an aid to mapping or detecting structure in the subsurface depths of 20-200 ft.

REFERENCES CITED

Widess, M.B., 1973, How thin is a thin bed?: Geophysics, v. 38, p. 1176.

Medvedev, S.V., 1965, Engineering seismology: National Technical Information Services, Springfield, Va., NTIS No. TT65-50011, 260 p.

SUMMARY OF DISCUSSION SESSION: RECOGNITION OF PALEOSEISMIC EVENTS IN THE GEOLOGIC RECORD

by

Anthony J. Crone
U.S. Geological Survey
Denver, Colorado 80225

Session Chairman: Randall W. Jibson, U.S. Geological Survey
Panel Members: Dean Ostenaa, U.S. Bureau of Reclamation
David P. Russ, U.S. Geological Survey
Robert S. Yeats, Oregon State University
T. Leslie Youd, Brigham Young University

Preserving the evidence of prehistoric earthquakes in the geologic record relies on a fortuitous balance between erosion and deposition. The nature and characteristics of the deposits in the record commonly depends on the specific type of tectonic environment (normal, reverse, or strike-slip faulting). Good, complete records of paleoseismic events are not ubiquitous. To obtain useful, quantitative data, paleoseismologists must study faults in three dimensions which means using all available techniques including mapping, trenching, and geomorphology. Even then, we may not recognize all of the prehistoric events because the geologic record may be incomplete or the stratigraphic evidence is extremely subtle or obscure. We have the basic expertise and tools to identify and characterize individual events, but in progressively older deposits, interpreting multiple events is hampered by poorer preservation and a greater likelihood of postdepositional modification.

Some scientists are skeptical about how well paleoseismologic data can be used to define fault segmentation, or how accurately specific events can be correlated along a fault. The uncertainties associated with dating individual events and the incompleteness of the geologic record increase the difficulty of these tasks. The great diversity of geomorphic and geologic features associated with different tectonic environments further complicates the problem. Reliable paleoseismologic interpretations must be based on multiple kinds of data from several sites. Ideally, trenching and a complete local geomorphic analysis should be conducted at each site. Furthermore, we must understand of the behavior of the fault from both a local and regional perspective.

Paleoseismic studies (particularly trenching) have been very successful at identifying large-magnitude faulting events particularly in normal faulting environments. However, there is doubt about our ability to recognize and accurately interpret stratigraphic relations produced by moderate-magnitude events. The stratigraphy exposed in trenches across many normal faults commonly indicates surface displacements of 1½-2 m. However, is there subtle evidence of smaller-magnitude events in the geologic record that we have not yet recognized? Because of this, have we seriously underestimated the hazards posed by potentially damaging, moderate-magnitude (M 6-7) events in some areas? Our studies tend to be biased towards investigations of large earthquakes on major faults and, as a result, we may not be evaluating the risk contributed by seismogenic features that can produce moderate-magnitude events. Earthquake hazard assessments treat the scenario of a large earthquake once every several hundred years very differently than a moderate earthquake every couple of decades. The potential damage from a moderate-

sized earthquake in the Los Angeles basin might be as extensive as the damage from a major earthquake on the San Andreas fault. (Editor's note: This concern was substantiated six months after the workshop by the damage caused by the M=5.9 Whittier Narrows earthquake on October 1, 1987.)

An important goal of future studies in paleoseismology should be to define our ability to identify moderate-magnitude events in the geologic record. To accomplish this, we need to study the geologic effects of historic earthquakes with magnitudes in the 6-6.5 range. At present, we do not know if we can identify a 20- or 40-cm-high scarp in the stratigraphic record and be sure that it is the product of an earthquake. We are faced with the reality that small features are more difficult to identify and less likely to be preserved in evolving landscapes for long periods of time. By studying moderate-magnitude historic events, we can establish the limits of our resolution and assess the chances of preserving relatively small features in the geologic record.

The people who use and apply paleoseismic data hope or expect that paleoseismologists can correlate individual faulting events along segments of faults. Successful correlations relies on good, high-resolution age control, and commonly, radiocarbon dating is the main source of that control. Scientists are concerned about the lack of standardization and non-reproducibility of dates by different laboratories. Without standardized quality control for radiocarbon dates, we may never have the resolution needed to precisely correlate events which will define the extent of prehistoric ruptures, thus providing information for hazard assessments.

Our resolution for dating past earthquakes is not only affected by the resolution of the dating techniques, but also by the amount of information preserved in the geologic record. In some depositional environments, high sedimentations rates produce a nearly complete annual record; in other environments, low rates leave large gaps in the record which may encompass the time of a significant seismic event. This variability in sedimentation rates means that in some places we may be able to resolve events spaced 100 years apart, whereas, elsewhere three events within a 1,000-year time span may appear as one event in the stratigraphic record. Thus, to a degree, we are constrained by geologic processes which establish the limits of our resolution. Seismologists and others that use paleoseismic data must recognize these inherent limitations.

Many interpretations in paleoseismology rely on one or two critical dates, yet we all realize that even the best determinations on the best samples can yield erroneous ages. Cross-checking these critical dates by using multiple dating techniques will identify errors and increase confidence in our interpretations. Unfortunately, the funding for most paleoseismic studies does not offer the luxury of dating critical datums with several techniques. A scientist with funding for five dates is likely to date five different stratigraphic horizons rather than get replicate dates on one datum because of the value of having age control throughout the stratigraphic section. Funding agencies should recognize the importance of cross-checking age determinations and encourage researchers to confirm the age of critical samples. Good age control is an essential component of any paleoseismologic study.

Hazard mitigation relies not only on identifying past earthquakes, but it also requires information on the size of those events. The conventional method for assigning magnitudes to prehistoric events is to determine the maximum displacement at a site and compare that displacement with the displacement from historic events of known magnitude. We must remember that

typically trenches are located where there is the best hope for finding dateable material, and not where the displacement is the greatest. Also, the amount of displacement can vary ten-fold or more in short distances along strike and many paleoseismic studies acquire detailed data only at one point. Thus, magnitudes of prehistoric earthquakes must be regarded only as estimates that contain significant uncertainties.

The indirect evidence of prehistoric earthquakes such as sand blows in the eastern United States and subsidence features in the Pacific Northwest can be useful indicators of large-magnitude earthquakes, but this evidence must be interpreted very cautiously because similar features can be generated by non-seismic processes. Earthquakes in these areas probably have long recurrence intervals of many hundreds to several thousands of years. Have we fully considered all of the alternate, non-seismic explanations for these features? Could a 1,000-year hurricane or a 5,000-year flood produce comparable features? Some scientists urge us to imagine the effects of natural climatic events that we have never seen and visualize how these events might be represented in geologic record. In contrast, others feel that major climatic events would leave clear, recognizable features in the geologic record that would be obvious in detailed studies. For example, large storms might significantly increases the sediment influx in a basin and produce a single, thick, flood deposit. Likewise, major individual climatic events might leave a visible record in tree rings.

Tree-ring analysis applied to paleoseismology is a two-stage process. First, dendrochronologist must establish a control chronology which defines the tree-ring pattern for trees not affected by prehistoric earthquakes. Next, with the control chronology as a guide, dendrochronologist can try to identify tree-ring anomalies that might be the result of prehistoric events. In some respects this two-step process is a liability because dendrochronologists are forced to spend half their time determining "normal" growth patterns in undisturbed areas. Even then, in the undisturbed areas, there is always the concern about the effects of major climatic events modifying the "normal" pattern. As a result, a dendrochronologist must discriminate between the effects of several different kinds of signals including those produced by ancient earthquakes.

Using landslides a indirect evidence of paleoseismic events demands extreme caution because we know that major storms (100- or 500-year storms) can trigger thousands of landslides. Based on our experience in northern California, it seems that most storm-induced landslides are debris flows and mudflows, whereas, the 1906 San Francisco earthquake generated mainly lateral spreads in fluvial sediments and rockfall. Before landslides can be used as a paleoseismic indicator, we must thoroughly document the kind and extent of landslides caused by historic events under a variety of conditions. We can then apply these calibrated studies to prehistoric events.

With proper calibration, landslides might provide some information on the magnitude of prehistoric earthquakes. The studies of historic events must include examples from different geologic environments where we can correlate the type and concentration of landslides with variables such as rock type, earthquake magnitude, and the distance from the causative fault. In an ideal case, well calibrated relationships between earthquakes and the kinds of landslides may help identify prehistoric events.

Like landslides, liquefaction features may be valuable indicators of prehistoric earthquakes. However earthquake-induced liquefaction features must also be carefully calibrated using historic events if we hope to make any inferences about the magnitude of the causative events. Some recent studies

has attempted this kind of calibration. The results are encouraging enough to suggest that we may eventually be able to estimate moment magnitudes of prehistoric events to possibly to within one quarter of a magnitude unit. Because numerous local and regional factors affect the susceptibility of deposits to liquefy, calibration studies must be conducted in each specific region.

For hazard evaluation purposes, liquefaction and landslide studies have one major advantage over trenching studies of a specific fault. Liquefaction and landslide studies indicate how frequently severe shaking occurred at a particular site regardless of the causative fault. Trenching results are site specific and apply only to a particular fault. In a region where there are several potentially seismogenic faults, liquefaction and landslide studies may provide better information on the severe-shaking hazard than site specific studies.

QUATERNARY SLIP-RATES AND COSEISMIC DEFORMATION

RELATIVE RATES OF LONG-TERM UPLIFT OF MOUNTAIN FRONTS

by

William B. Bull
Geosciences Department
University of Arizona
Tucson, AZ, 85721

ABSTRACT

Base-level processes at mountain range-basin junctions include the interdependent geomorphic processes of stream-channel downcutting (cd), piedmont aggradation (pa), piedmont degradation (pd): each base-level process is dependent on the relative uplift at the mountain front (u). The four processes influence hillslope and valley morphologies, and the thickness and loci of alluviation and the topography in the basins. Examples of common base-level interrelations are:

$$\text{active alluvial fan} -- \Delta u/\Delta t \geq \Delta cd/\Delta t + \Delta pa/\Delta t$$
$$\text{incised alluvial fan} -- \Delta u/\Delta t < \Delta cd/\Delta t > \Delta pd/\Delta t$$
$$\text{undissected pediment} -- \Delta u/\Delta t << \Delta cd/\Delta t = \Delta pd/\Delta t$$

(where Δt is the time interval of interest)

These equations also define classes of landforms that have been affected by different relative rates of Quaternary tectonic activity. When compared to inactive terrains, the landforms of tectonically active terrains (for similar total relief, climate, and rock type) have more convex ridgecrests, steeper footslopes, narrower and steeper valleys, less sinuous mountain-piedmont junctions, and thick accumulations of alluvium and minimal soil-profile development on the piedmonts adjacent to the mountain fronts. Thus regional studies of fluvial systems are the basis for mapping classes of Quaternary tectonic activity. The resulting tectonic-activity maps should provide insight about long-term paleoseismicity, which structures are active, and the potential for future earthquakes. The method works for the normal, reverse, and strike-slip faults of the Basin and Range Province and the Coast and Transverse Ranges of California, and for fault-bounded mountain fronts in humid New Zealand.

INTRODUCTION

Landforms can be used in an intuitive or qualitative sense to assess the degree of tectonic activity of a terrain. A straight mountain-piedmont junction may coincide with a linear structural feature such as an active fault. Residual knobs of bedrock protruding

above a piedmont adjacent to a sinuous mountain front suggest a dominance of erosional retreat and tectonic quiescence of the former range-bounding fault zones. By examining all elements of the stream and hillslope subsystems, one should be able to detect the effects of either continuous or pulsatory uplift of range-bounding, piedmont, or internal structures during the late Quaternary.

This article describes a quantitative geomorphic approach to tectonic analysis that emphasizes identification of processes that are responsible for changes in landscape relief. These base-level processes are interrelated and used to define tectonic-activity classes of mountain fronts that are bounded by faults and folds. Characteristics of landforms associated with mountain fronts are used to distinguish between tectonic-activity classes. Some landforms are more sensitive than others to the effects of base-level fall, which provides investigators options as to the time span they wish to examine for a particular study (Fig. 1).

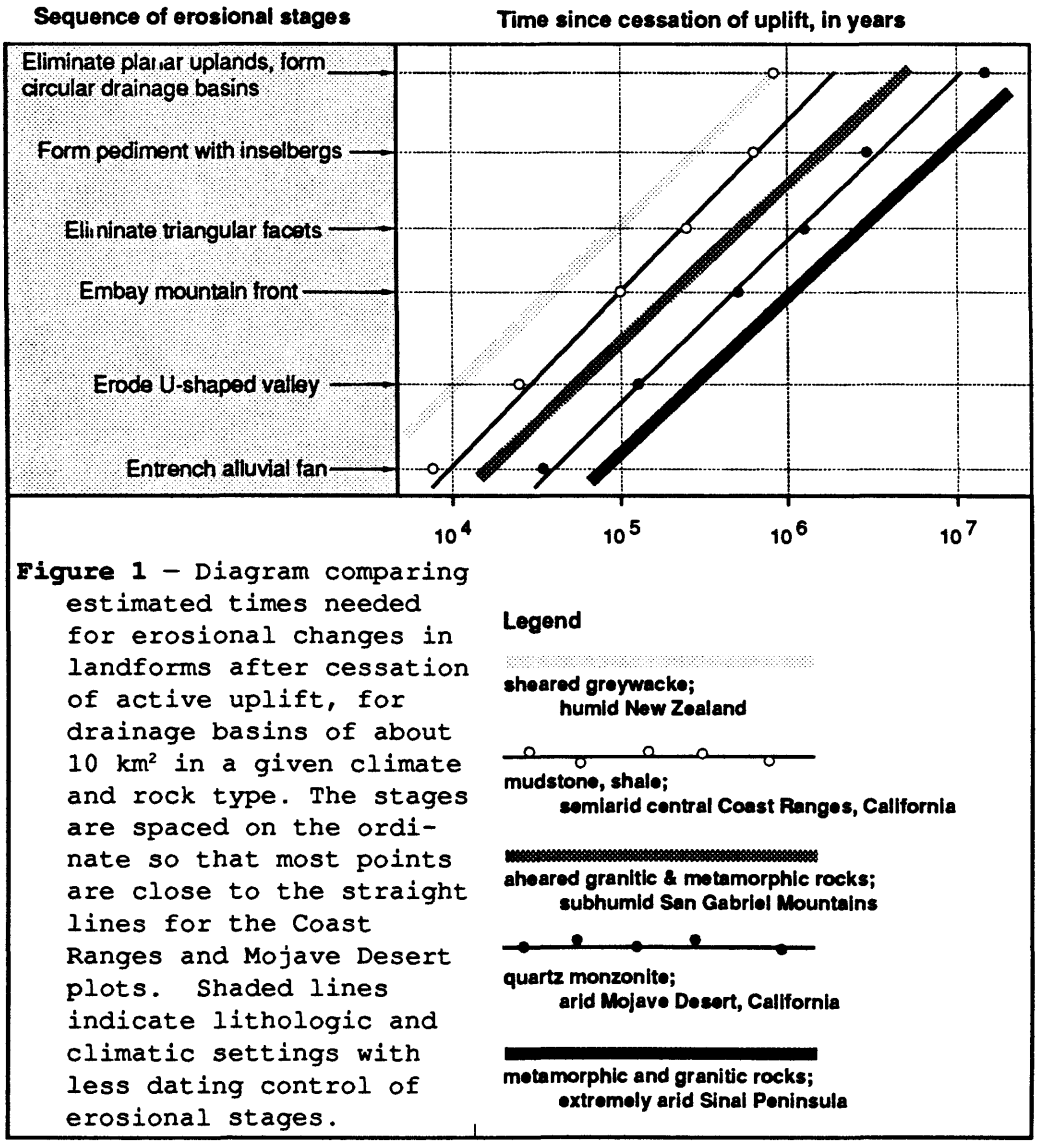

Figure 1 – Diagram comparing estimated times needed for erosional changes in landforms after cessation of active uplift, for drainage basins of about 10 km² in a given climate and rock type. The stages are spaced on the ordinate so that most points are close to the straight lines for the Coast Ranges and Mojave Desert plots. Shaded lines indicate lithologic and climatic settings with less dating control of erosional stages.

TIMESPANS NEEDED TO ERODE LANDFORMS

Hills and streams continue to change after uplift of mountains has ceased; the times needed to erode different types of landforms range from 10^3 to 10^7 yr. After assumed cessation of uplift, the time needed to erode the sequence of landforms noted on the left side of figure 1 is controlled by resistance to erosion and amounts of materials to be removed to create a given landform. Only a short time is needed for the concentrated power of a stream to remove a small volume of unconsolidated deposits and erode a fanhead trench. In contrast, long time spans are needed to consume the last vestiges of an uplifted planar surface. Such escarpment retreat is accomplished by gradual weathering of bedrock and slow hillslope erosional processes, and the volume of rock to be removed is large. Erosion rates also vary with changes in climate by at least two orders of magnitude.

Radiometric ages allow some rough estimates of the times needed for erosion of landforms in the Mojave Desert and the central Coast Ranges of California. Granitic and metamorphic rocks predominate in the Mojave Desert, and soft mudstone and sandstones predominate in the Coast Ranges. The Mojave Desert and Coast Range plots on figure 1 are separated by approximately an order of magnitude of time. The sheared granitic and metamorphic rocks of the semiarid to subhumid Transverse Ranges occupy an intermediate position between the plots for the Mojave Desert and the Coast Ranges. One extreme in the sequence of landscape development would be the easily eroded greywacke and schist of humid New Zealand, and the other extreme would be the massive plutonic rocks of the extremely arid Sinai Peninsula.

Earth scientists may use the concepts outlined in figure 1 to study the landforms whose time span of formation is of most interest. Studies of whether or not uplift is still occurring at maximum rates may emphasize the amount and age of fanhead trench development. Many earthquake hazard studies concentrate on the rates, magnitudes, and locations of earth deformation during the past several hundred thousand years. This article focuses on such an intermediate time span and will emphasize long-term processes such as embayment of mountain-piedmont junctions and downcutting of montain valleys.

THE MODEL

Fault-bounded mountain fronts have landscape assemblages that record the interactions between uplift and erosion. Uplift rates are partially offset by denudation and the resulting landforms vary as a function of the ratio of uplift rate to denudation rate. Rapid uplift of resistant materials results in straight mountain-piedmont junctions, narrow V-shaped valleys with steep longitudinal profiles, and truncated spur ridges with well defined triangular facets. Slow uplift of soft materials results in embayed sinuous mountain-piedmont junctions, broad U-shaped valleys with gentle longitudinal profiles, and highly degraded spur ridges (Bull, 1973, 1984a; Bull and McFadden, 1977).

Class of Relative Tectonic Activity	Relative Uplift Rate	Typical Landforms Piedmont	Mountain
Active			
Class 1A - maximal	$\Delta u/\Delta t \geq \Delta cd/\Delta t + \Delta pa/\Delta t$	Unentrenched alluvial fan	V-shaped cross valley profile in bedrock
1B	$\Delta u/\Delta t \geq \Delta cd/\Delta t + \Delta pa/\Delta t$	Unentrenched alluvial fan	U-shaped cross valley profile in alluvium / soft rock
Class 2 - rapid	$\Delta u/\Delta t < \Delta cd/\Delta t > \Delta pd/\Delta t$	Entrenched alluvial fan	V-shaped valley
Class 3 - slow	$\Delta u/\Delta t < \Delta cd/\Delta t > \Delta pd/\Delta t$	Entrenched alluvial fan	U-shaped valley
Class 4 - minimal	$\Delta u/\Delta t < \Delta cd/\Delta t > \Delta pd/\Delta t$	Entrenched alluvial fan	Embayed mountain front
Inactive			
Class 5A	$\Delta u/\Delta t << \Delta cd/\Delta t > \Delta pd/\Delta t$	Dissected pediment	Dissected pediment embayment
5B	$\Delta u/\Delta t << \Delta cd/\Delta t = \Delta pd/\Delta t$	Undissected pediment	Pediment embayment
5C	$\Delta u/\Delta t << \Delta cd/\Delta t < \Delta pd/\Delta t$	Undissected pediment	May have characteristics of active landscape

Figure 2 - Classification of Quaternary relative tectonic activity of mountain fronts. Classes 1A, 3, and 5B are illustrated in figure 3. (t, time; u, uplift; cd, channel downcutting with the mountains; pa, piedmont aggradation; pd, piedmont degradation). From Bull, 1984a.

These diagnostic landforms are easily recognized in the field or on maps and images, and form the basis for classes of tectonic activity in figures 2 and 3. The inequalities describe classes of relative uplift that may be used as a reconnaissance tool to identify those mountain fronts that have been subject to base-level fall during the last 0.1 - 1 Ma. Structural, lithologic, and topographic variation along a mountain-front escarpment are the basis for identification of segmentation of individual mountain fronts — those tectonic units with different styles, magnitudes, and rates of uplift. About 60 segments of mountain fronts have been identified along the south side of the San Gabriel Mountains near Los Angeles, Calif. (Bull, 1978, and fig. 7).

The model not only recognizes the influence of uplift on all parts of the landscape, but also includes the applied concept that the recent tectonic history of geologic structures in a fluvial system may be evaluated by study of its' landforms. The equations of figure 2 – the heart of the model–purposely define interrelations that can be readily defined in the field. Examples of tectonically sensitive landforms are the sinuosity of the mountain-piedmont junction and the state of valley downcutting as represented by the ratio of valley-floor width to valley height. Rates of tectonic uplift can be computed for mountain fronts where rates of erosion and deposition are known. For any region, classes of tectonic activity of mountain fronts can be identified to help solve the problems of earth scientists, engineers, and planners. The model of tectonic-activity classes of mountain fronts is an important paleoseismic tool. It complements the invaluable data about the locations, depths, magnitudes, and frequencies of earthquakes provided by seismologists, and the input about timing and magnitudes of fault ruptures provided by trenching of fault zones and diffusion-equation modeling of fault scarps.

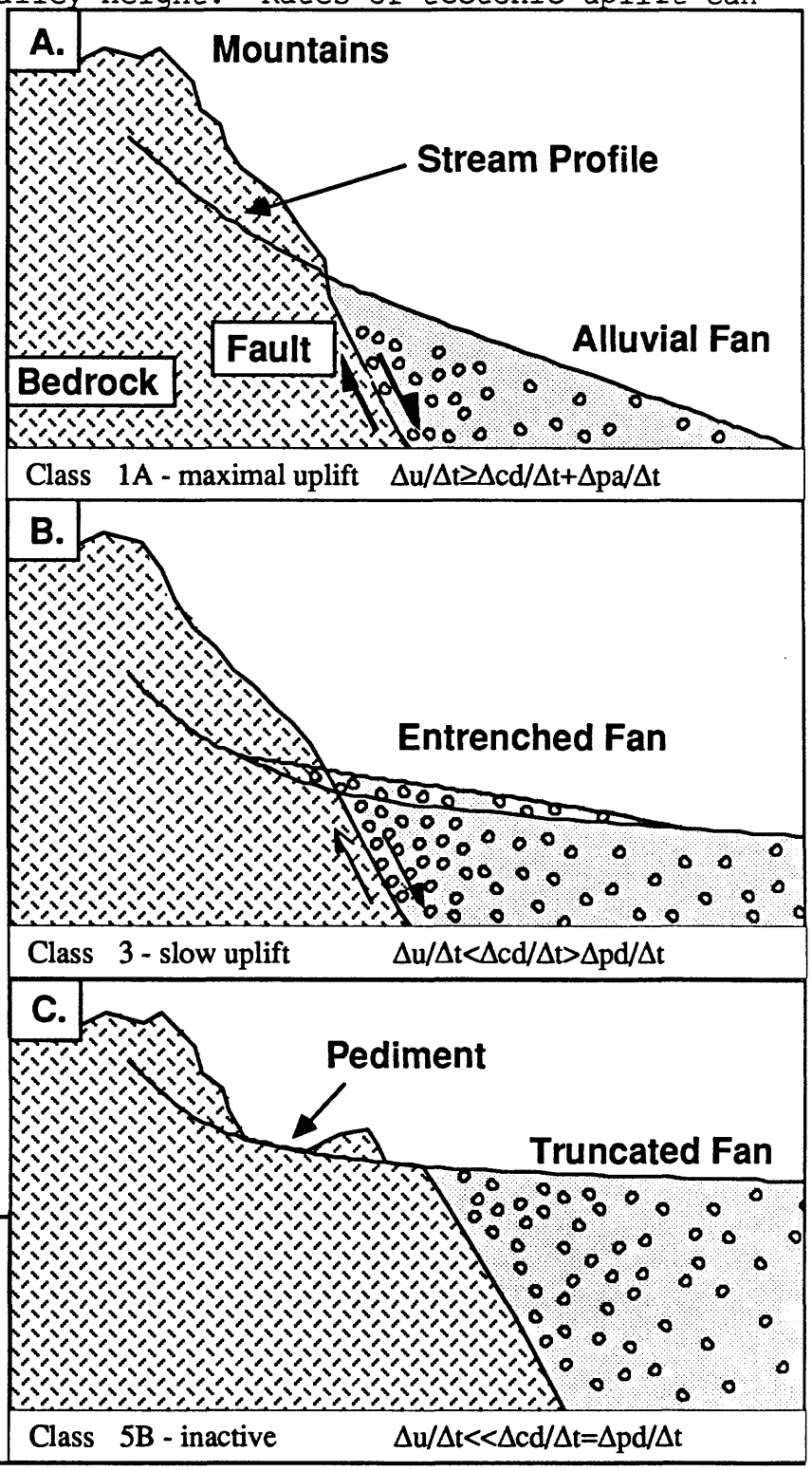

Figure 3 – Sketches of longitudinal profiles of fluvial systems showing the landform associations typical of different relative uplift rates. Classes are described in figure 2. (from Bull, 1984a).

t = time
u = uplift
cd = channel downcutting with the mountains
pa = piedmont aggradation
pd = piedmont degradation

soil-profile characteristics. Full-glacial climates were much different than Holocene climates; a contrast that has resulted in differences in pedogenesis that are reflected in their respective soil-profile characteristics.

In a rough sense, the five tectonic-activity classes may be thought of as representing five orders of magnitude of uplift rates. Previous studies in the Death Valley region (Hooke, 1972; Smith, 1976), the Transverse Ranges (Matti and others 1982) and Coast Ranges of California (W.B. Bull, unpublished data 1987) suggest that in arid and semiarid regions rates of uplift associated with class 1 mountain fronts commonly are on the order of 1 - 5 m/1,000 yr. Class 2 uplift rates appear to be an order of magnitude less, roughly 0.5m/1,000 yr. Class 3 rates may be assigned a rate of approximately 0.05m/,1,000 yr, and class 4 mountain fronts are almost tectonically inactive, perhaps having uplift rates on the order of 0.005m/1,000 yr. More rapid rates are necessary in humid regions to maintain a given tectonic-activity class because of the relatively greater stream channel downcutting rates of large perennial streams. Along the Alpine and Hope faults in New Zealand, class 2 mountain fronts are present even though uplift rates are 3 - 8 m/1,000 yr.

The model as applied to the south side of the San Gabriel Mountains of southern California is shown in figure 7. More than 60 mountain fronts have been assigned one of the five classes of figure 2. Those parts of the range-bounding fault that have been most active during the late Quaternary are north of the San Fernando Valley, and west of the San Jacinto and San Andreas faults. The range-bounding thrust faults have migrated southward, and the outermost fault has been the most active at fronts 5, 7, 9, 16, 18, 19, 20, 23, and 28. Holocene fault scarps are common along class 1 fronts but are not present along class 3 and class 4 fronts.

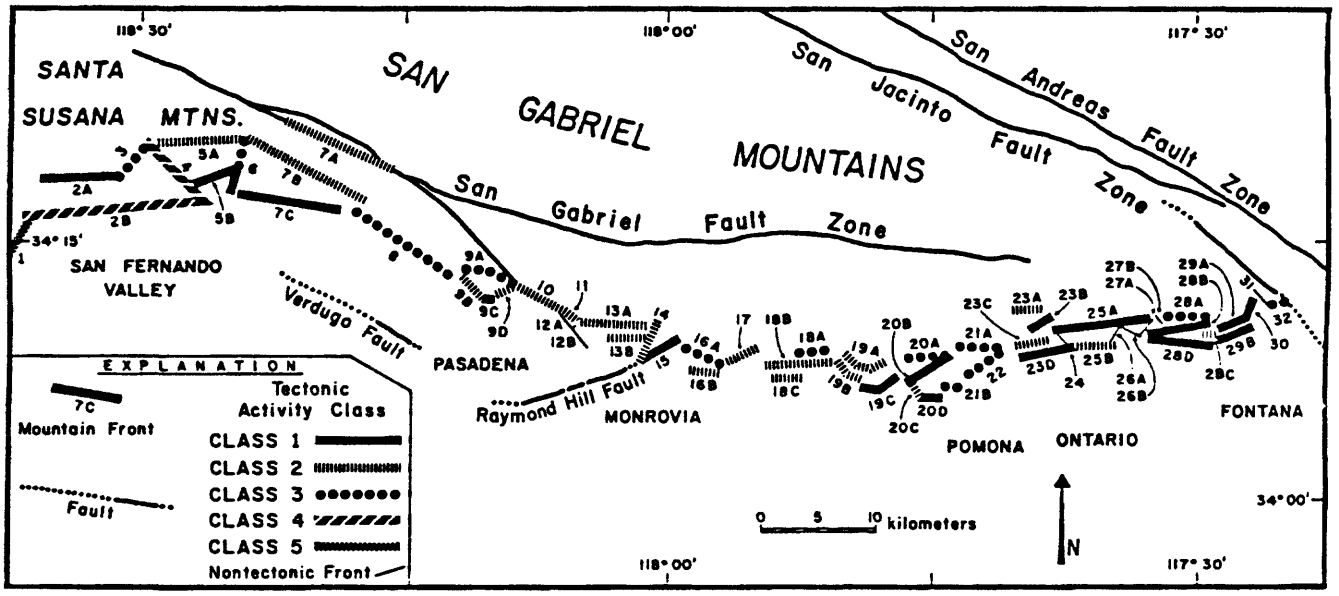

Figure 7 – Relative tectonic activity classes for thrust faulted mountain fronts along the south side of the San Gabriel Mountains of southern California. The classes are illustrated in figures 1 and 2 (from Bull, 1978).

Fluvial aggradation (pa) and degradation (cd and pd), as well as uplift (u) should be considered as local base-level processes that change altitudes of points along streams for each mountain-front segment. The five interrelations of base-level processes of figure 2 describe tectonically active, moderately active, and inactive landscape assemblages. The diagrammatic sketch of figure 3A depicts the situation where either continued stream-channel downcutting within the mountains or additional fanhead aggradation tends to promote entrenchment of the fanhead by the trunk stream issuing from the mountains. Fan deposits will continue to accumulate next to the mountain-piedmont junction only as long as the uplift rate equals or exceeds the sum of the other two base-level processes. An example of a class 1 mountain front is shown in figure 4. Pedimentation associated with relative tectonic inactivity is depicted in figure 3C. The three inequalities of class 5 in figure 2 describe three types of pediments; class 5C is not common. A view of an undissected pediment is shown in figure 5, and figure 6 shows the topography of an arid landscape that has not been subject to a tectonic base-level fall for millions of years. The mountain-piedmont junction (including the inselberg outliers) is extremely sinuous (a sinuosity value of about 10) instead of being straight as a range-bounding fault (a sinuosity value of about 1). The valley floors are very broad relative to the

Figure 4 – Unentrenched alluvial fans along the east side of the Sinai Peninsula, Egypt. The rapid aggradation of these fans, and other landforms of the landscape assemblage, is described by the class 1 equation of figure 2. The steep mountains have narrow valley floors and a moderately low sinuosity of the mountain-piedmont junction (fig. 16 from Bull, 1977a).

Figure 5 – View of pedimented landscape southeast of the Harquahala Mountains of western Arizona. Denudation rates have greatly exceeded uplift for millions of years; bedrock spur ridges have been degraded to a scattering of inselbergs rising above the beveled bedrock of the adjacent pediment (fig. 11.7A, from Bull, 1984b).

heights of adjacent ridgecrests; the ratios of valley-floor width to valley height are 10 to 100. For a class 1 front they would be less than 1. Landforms associated with intermediate rates of uplift are described by figure 3B. Aggradation may occur upstream from the mountain-piedmont junction in response to aggradation-induced base-level rise on the fanhead and the diagnostic piedmont landform is the presence of a fanhead that has been entrenched for more than 10,000 yrs.

Not all entrenched alluvial fans are described by the inequality for class 2 mountain fronts. Short term (100 - 1,000 yrs) climatic changes, perhaps combined with human impacts, have resulted in temporarily entrenched fanheads (Bull, in press). Class 1 fans are defined as being unentrenched or as being entrenched for less than 10,000 yrs. Permanently entrenched fans (class 2) are regarded as being entrenched for more than 10,000 yrs. Most Pleistocene alluvial surfaces can be readily distinguished from Holocene surfaces by their

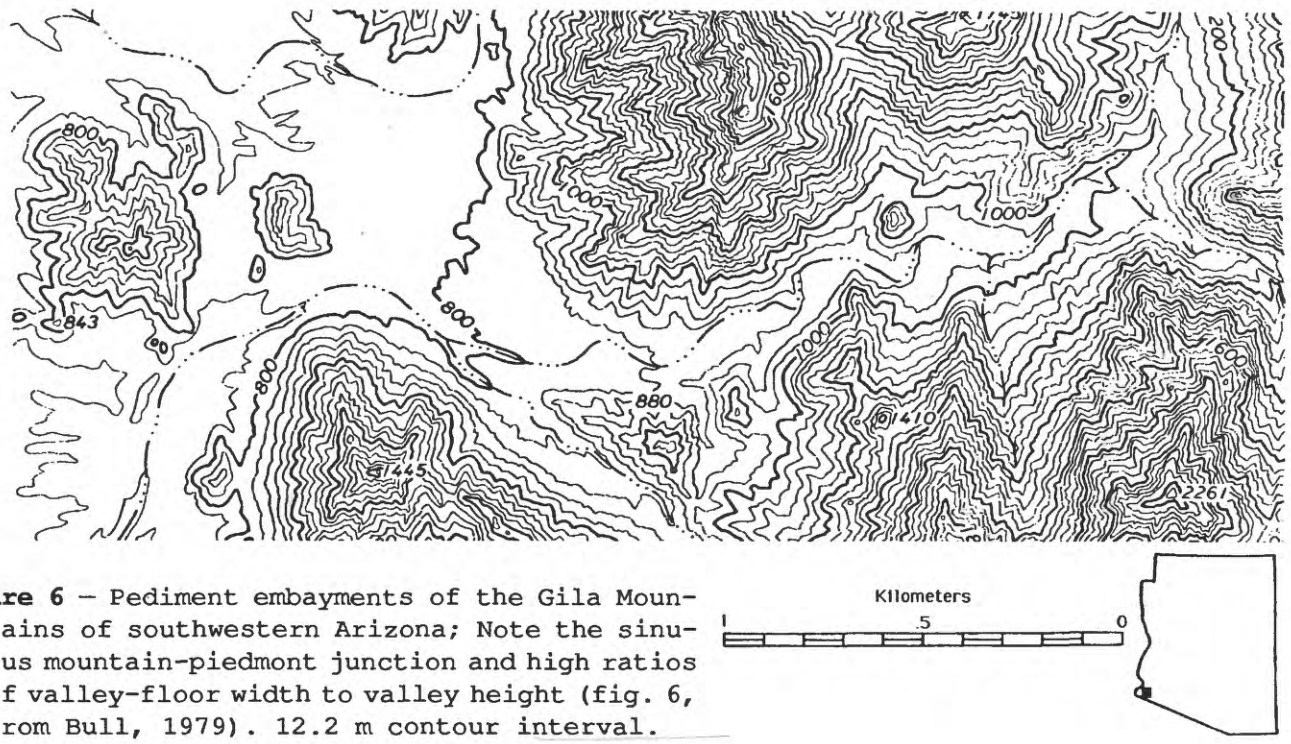

Figure 6 – Pediment embayments of the Gila Mountains of southwestern Arizona; Note the sinuous mountain-piedmont junction and high ratios of valley-floor width to valley height (fig. 6, from Bull, 1979). 12.2 m contour interval.

Advantages

The simple model described above is quite useful. The landform characteristics that define each of the five classes of tectonic activity are readily identified by quantitative and qualitative descriptions that are available from map, aerial photograph, and field studies. Descriptions of class 1 landscapes do not require knowledge of the times of initial uplift, and factors such as climate variations do not have to be taken into account in the relative classification. The model can be used in reconnaissance appraisals of large regions when three groups of classes are used (classes 1, 2-4, and 5 such as in the abstract), or for more detailed studies where presumed greater seismic risk dictates the use of five classes (figure 7). The resulting maps of relative Quaternary activity of the faults of a region are a convenient paleoseismic tool in communicating with engineers and planners and for comparison with spatial distributions of historical seismicity.

Needed Future Research

An important objective of future work would center on upgrading the model to be quantitative instead of relative comparisons. Such an improvement would require a much better understanding of the roles of spatial variations in lithology and structure, and of temporal and spatial variations in climate, on rates of denudation relative to a wide range of uplift rates. Radiometric dating at a few sites permits estimates of stream-channel downcutting and piedmont aggradation for class 1 fronts. Such examples should be regarded as calibration sites for obtaining a better understanding of the roles of nontectonic variables in landform evolution. The need for better understanding of lithologic and climatic control of tectonic-activity classes has a parallel in diffusion-equation modeling of fault scarps where the same independent variables are acknowledged as largely determining rates of fault-scarp degradation (Dodge and Grose, 1980; Pierce and Colman, 1986). Fortunately most fault scarps studied in the Western United States are in sandy gravels of semiarid piedmonts. Lithologic and climatic controls on mountain-front denudational processes are more varied and complex than for piedmont scarps.

Tectonically active mountain ranges commonly have more than one active fault zone. Mountain fronts, therefore, need to include landscapes associated with internal and piedmont fault zones as well as with range-bounding faults. Different emphases and types of landforms may have to be used to analyse piedmont, range-bounding, and internal faults. Strike-slip fault movement is not a base-level change that affects sensitive stream gradients of fluvial systems. Fortunately, offsets and bends in strike-slip faults create local areas of compression and extension (Crowell,1974). The resulting secondary faults and folds can be used to evaluate the tectonic-activity classes, even where lateral slip rates greatly exceed vertical slip rates.

REFERENCES CITED

Bull, W.B., 1973, Local base-level processes in arid fluvial systems [abs.]: Geological Society of America Abstracts with Programs, v. 5, p. 562.

_____ 1977a, The alluvial-fan environment: Progress in Physical Geography, v. 1, p. 222-270.

_____ 1977b, Tectonic geomorphology of the Mojave Desert, California: U.S. Geological Survey Contract Report 14-08-001-G-394; Menlo Park, California, 188 p.

_____ and McFadden, L.D., 1977, Tectonic geomorphology north and south of the Garlock fault, California: in Doehring, D.O. ed.: Geomorphology in Arid Regions, Proceedings 8th Annual Geomorphology Symposium, State University New York at Binghamton, p. 115-137.

_____ 1978, Geomorphic tectonic activity classes of the south front of the San Gabriel Mountains, California: U.S. Geological Survey Contract Report 14-08-001-G-394; Menlo Park, Calif., 100 p.

_____ 1979, Threshold of critical power in streams: Geological Society of America Bulletin, v. 90, p. 453-464.

_____ 1984a, Tectonic geomorphology: Journal of Geological Education, v. 32, p. 310-324.

_____ 1984b, Alluvial fans and pediments of southern Arizona: in Smiley T. L.,. Nations J. D,. Pewe T. L, and. Schafer J. P, eds.: Landscapes of Arizona, Lanham, Md, University Press of America, Chapter 11, p. 229-252.

_____ in press, Backfilling and entrenchment of valley floors by discontinuous ephemeral streams; in Geomorphic responses to climatic change, Chapter 6: New York, Oxford University Press.

Crowell, J. C. 1974, Origin of late Cenozoic basins in southern California: in Dickinson W. R., ed.: Tectonics and Sedimentation, Society of Economic Paleontologists and Mineralogists Special Publication 22, p. 190-204.

Dodge, R. L., and Grose, L. T., 1980, Tectonic and geomorphic evolution of the Black Rock fault, northwestern Nevada: in Andrise P. C., compiler: Earthquake hazards along the Wasatch-Sierra Nevada frontal fault zones, U. S. Geological Survey Open-File Report 80-801, p. 494-508.

Hooke, R. L., 1972, Geomorphic evidence for late Wisconsin and Holocene tectonic deformation, Death Valley, California: Geological Society of America Bulletin, v. 58, p. 2073-2098.

Matti, J. C., Tinsley, J. C., Morton, D. M., and McFadden, L. D., 1982, Holocene faulting history as recorded by alluvial stratigraphy within the Cucamonga fault zone -- A preliminary view, in Late Quaternary pedogenesis and alluvial chronologies of the Los Angeles and San Gabriel Mountains areas, southern California and Holocene faulting and alluvial stratigraphy within the Cucamonga fault zone -- A preliminary view: Guidebook for field trip 12, Cordilleran Section Meeting of the Geological Society of America, April, 1982, p. 29 - 44.

Pierce, K. L., and Colman, S. M., 1986, Effect of height and orientation (microclimate) on geomorphic degradation rates and processes, late-glacial terrace scarps in central Idaho: Geological Society of America Bulletin, v. 97, p. 869-885.

Smith, R. S. U., 1976 Late Quaternary pluvial and tectonic history of Panamint Valley, Inyo and Mono Counties, California: Pasadena Calif., California Institute of Technology Ph.D. dissertation, 295 p.

TEMPORAL AND SPATIAL SEGMENTATION OF PLIOCENE-QUATERNARY FAULT RUPTURE ALONG THE WESTERN SANGRE DE CRISTO MOUNTAIN FRONT, NORTHERN NEW MEXICO

by

Christopher M. Menges

Department of Geology
University of New Mexico
Albuquerque, NM 87131

ABSTRACT

The morphology of a 1200-m-high bedrock mountain front in the Rio Grande rift of northern New Mexico demonstrates the persistence through Pliocene-Quaternary time of temporal and spatial patterns of late Quaternary rupture along the range-bounding fault zone. Variations in fault-scarp morphology and displaced geomorphic surfaces suggest that several latest Pleistocene and Holocene ruptures are nonuniformly distributed along a 50- to 70-km-long section of fault scarps. These scarps display a complex geometric segmentation pattern of 4 primary segments 15-20 km in length, each containing two to three 5- to 10-km-long subsegments. The central to south-central part of a subsegment or segment is defined by a narrow zone of single- to double-strand fault scarps commonly at the base of a reentrant in the range front. The confined rupture patterns typically change along strike into more complex zones of mixed piedmont fault scarps and multiple bedrock fault splays that bound structural benches. These diffuse terminations of subsegments or segments preferentially occur at salients and (or) abrupt deflections in the mountain front. The base of the mountain front at salients typically rises between 100 m and 400 m in average elevation as it enters adjacent reentrants. Morphologic age estimates from height-slope regressions and diffusion modeling of fault scarps suggest that: (1) a mid- to early-Holocene rupture may have extended 30 to 50 km across three primary segments of the range-bounding fault; and (2) a late- to mid-Holocene rupture may have occurred on one 6-10 km long subsegment. These two rupture lengths are associated with average vertical displacements of 1.2 m and 0.8 m, respectively, which suggest different scales of paleoearthquakes with estimated magnitudes of 6.9-7.1 (multiple segment) and 6.5-6.7 (single subsegment only).

This time-space segmentation of the fault zone influences the morphology of larger-scale tectonic landforms such as facets and spurs which have developed in the adjacent bedrock escarpment over longer Quaternary time spans. Basal triangular facets above the central parts of subsegments or segments have greater relief and size, steeper mean slopes, fewer benches, less dissection, and thicker colluvial mantles, compared to facets at adjacent subsegment boundaries. Similar morphologic patterns characterize the overall profiles of the larger facet-spur systems of the range-front. These patterns

extend upwards at least as high as a prominent mid-escarpment bench that correlates with a 4.3 Ma basalt overlying a bench at the northern end of the range crest. The subsegment containing the morphologically-youngest fault scarps also coincides with an unusually high, steep, and undissected set of basal facets, and the greatest amount of post-Pliocene vertical displacement, as estimated from the elevation of the mid-escarpment bench above correlative basalts in the adjacent basin. These collective relationships suggest that the cumulative rates and amounts of vertical displacements since mid-Pliocene time may increase by a factor of 1.5 to 2 near the south ends of some primary segments of the range-bounding fault.

INTRODUCTION

A critical geologic element in paleoseismic studies is accurately characterizing the seismogenic behavior of tectonically-active fault zones in time and space (for example, National Research Council, 1986). Many recent investigations of historic and late Quaternary fault scarps highlight the importance of factors such as fault segmentation, characteristic earthquakes, uniform versus nonuniform slip rates, and temporal grouping of surface ruptures in the Quaternary seismic activity of large range-bounding faults in the Basin and Range province of the Western United States (Schwartz and Coppersmith, 1984, 1986; Slemmons and Depolo, 1986; Crone and others, 1987; Wallace, 1987). These concepts are important in the evaluation of seismic source parameters such as the length, amount, and frequency of individual surface ruptures, which in turn form the bases for estimating the magnitudes of paleoearthquakes.

There is an obvious need to establish the degree to which segmentation and slip patterns indicated by late Quaternary fault scarps persist over longer time intervals in the Quaternary. These factors gain importance in studies of scarps located at the base of high mountain fronts that have formed over long periods of faulting, especially given the growing evidence for long recurrence intervals of 10^4 to 10^5 yrs between individual ruptures on many faults (Scott and others, 1985; McCalpin, 1982; Pearthree and Calvo, 1987). Statistical analyses of some large-scale geologic and geomorphic characteristics of the Wasatch mountain front suggest that certain fault segments persist over long time intervals (Mayer and Maclean, 1986; Maclean, 1985; Wheeler and Krystinik, 1987). Yet it is still not clear to what extent, and over what time intervals, various scales of fault segmentation influence the form and evolution of mountain front landforms such as bedrock facets and spurs.

This paper summarizes a study of the tectonic geomorphology of a major boundary escarpment of the northern Rio Grande rift and provides information on time-space patterns of segmentation on the range-front fault zone (Menges, 1987a, 1987b, unpub. data; Menges and Wells, 1987). In this study I defined the segmentation patterns and paleoseismicity in late Quaternary fault scarps along the base of the mountain front; the rupture patterns of the basal fault scarps were then compared with morphometric analyses of landforms along the range front that record longer time intervals of faulting and landscape evolution on the order of 10^5 to 10^6 yrs.

Study Area

The study area is a 70-km-long section of the bedrock mountain front that forms the western structural boundary of the Sangre de Cristo Mountains between Taos and the New Mexico-Colorado border (fig. 1). This prominent topographic escarpment trends north-south and slopes westward with 500-1200 m of local relief. The highest summits reach altitudes of 3700 m above the adjacent basalt flows, basin fill, and piedmont alluvial fans of the southeastern San Luis Basin at 2000- to 2700-m-altitudes (Upson, 1939; Lambert, 1966).

Bedrock lithologies in the study area include Precambrian granitic and mafic gneisses and schists overlain and intruded by mid- to late- Tertiary volcanic and plutonic rocks (Reed and others, 1983; Reed, 1984). Most of the volcanic rocks are related to the formation of the Questa caldera and Latir volcanic field in late Oligocene time (Lipman and others, 1986). Paleozoic sediments are exposed south of the study area in the mountain front adjacent to the town of Taos.

Several characteristics of this mountain front make it suitable for neotectonic analyses. A complex but well-defined normal fault zone along the base of the main bedrock escarpment is marked along much of its length by discontinuous fault scarps of Holocene to mid-Pleistocene age that offset piedmont alluvium and (or) alluvial- or colluvial-mantled bedrock. Most scarps are located at, or slightly basinward of ($\leq$0.5 km), the base of the mountain front. The range-front escarpment has a well-developed suite of erosional landforms, including triangular facets, spur ridgecrests, drainage basins, and range crest summits, that are characteristic of tectonically active mountain fronts in the Basin and Range province (Wallace, 1978; Mayer, 1986).

Mid-Pliocene basalt flows with a 4.3-Ma K-Ar date are locally preserved on the north end of the range crest near the Colorado border (fig. 2; Lipman and others, 1986). These rocks are correlated with the 3-5 Ma Servilleta basalts of the Taos Plateau volcanic field that outcrop extensively throughout the Rio Grande gorge and are interbedded with basin fill in the shallow subsurface of the San Luis Basin (Lipman and Mehnert, 1979; Lipman and others, 1986; Summers and Hargis, 1984). Thus the elevation difference between the basalt flows on the range crest and those in the adjoining basin are an approximate measure of the cumulative vertical offset along the range-front fault zone since mid-Pliocene time.

LATE QUATERNARY RUPTURE PATTERNS

Geometric Segmentation of Fault Scarps and Related Features

Figure 2 is a detailed summary of fault scarps and associated features along the mountain front. This map is based on photointerpretation of aerial photography field mapping at eight sites on the mountain front. Geomorphic and structural data on the map portray the spatial distribution of late-Quaternary rupture along the fault zone. These data, listed in order of decreasing reliability, include: (1) piedmont fault scarps and low-relief bedrock fault benches, (2) the basal topographic junction of the main set of triangular facets; and (3) a few fault zones in the lower bedrock escarpment

FIGURE 1.--Location of study area in the southern Sangre de Cristo Mountains near Taos. Large box in center outlines the part of the range-bounding fault zone and adjoining mountain front included in this study. Solid heavy lines delimit the northern part of the range front studied in detail; heavy dashed lines enclose the southern section examined in reconnaissance. Abbreviations are: Rio Grande gorge (RG); Sangre de Cristo Mountains (SdC); and southern San Luis Valley (SLV). Northern limit of map coincides with the Colorado (CO) and New Mexico (NM) border. (Adapted from composite Landsat image; New Mexico Geological Society, 1982.)

---

that generally strike parallel to and mimic the geometry of the other tectonic landforms along the base of the range front. Most of these latter fault zones lie at the base of well-defined topographic steps with significant down-to-the-basin relief.

The complex rupture pattern inferred from these data varies in geometry and geomorphic position along the range front. Along some sections, evidence for late Quaternary faulting is confined to a narrow zone at or slightly basinward of (<100 m) the base of the bedrock escarpment. Rupture is these confined zones (type A) is characterized by either a single fault scarp or slope break (for example, ER- FS, fig. 2A), or, more commonly, by two subparallel to slightly branching scarps that define a narrow alluvial- or colluvial-mantled bedrock bench at the base of the main system of triangular facets (e.g., UR-FS or LA-FS, fig. 2). The relatively narrow simple type A pattern of basinward-facing scarps and benches typically changes along strike into more complex and broader patterns of surface rupture (type B). Type B faulting is distributed among one or more piedmont fault scarps located up to 1 km basinward from fault splays that bound structural benches at the base of the main bedrock escarpment (for example, SU-FS, CPB-FS, and SCB-FS, fig. 2A).

These two types of fault geometries are not randomly distributed along the mountain front, but alternate in a pattern suggesting several scales of spatial or geometric segmentation in fault rupture. The total length of the mountain front between Taos and the Colorado border may be subdivided into four primary geometric segments (labeled 1 to 4 in fig. 2); each segment is 15-20 km in length, although only the northern two and one-half segments are in the specific 50-km section of the mountain front studied in detail. The boundaries of primary segments are defined by complex zones of type B rupture that enclose the narrow simpler type A patterns of faulting comprising most of the segment. The simplest and most pronounced development of the latter geometry occurs near the southern ends of these segments; rupture geometry generally increases irregularly in width, and in topographic and structural complexity northward along each primary segment (fig. 2).

Most of the boundaries between primary fault segments also coincide with major changes in the geology and (or) gross morphology of the mountain front (fig. 2). These include one or more of the following: (1) abrupt transverse jumps in the base of the mountain front that typically step 1-2 km to the right; (2) major salients or deflections in the average trend of the range front; (3) broad ($\geq$1-2 km) subhorizontal benches in the mountain front that are bounded by internal and external (that is, range-bounding) bedrock escarpments exceeding 100-200 m in height; (4) large gaps or sections of low range-front summits; and (5) major structures and (or) lithologic contacts in the range block oriented transverse to the mountain front.

Rupture patterns within primary fault segments contain considerable internal variation along strike that may be used to subdivide each segment into two to four subsegments with 5-10 km lengths. The centers of subsegments are narrow type A zones of simple rupture that are bounded to either side by more complex type B fault patterns. Thus subsegments resemble segments in geometry, although the geometric variation is smaller and less distinct at subsegment scales. The boundaries of most subsegments are not associated with the major discontinuities or changes in the mountain front that commonly occur at segment boundaries (see above).

The internal rupture patterns of fault segments and subsegments also coincide with pronounced changes in the relative position and elevation of the base of the mountain front. The narrow type A zones of segments and subsegments typically occur in reentrants in the mountain front, whereas type B boundaries form on adjacent salients or promontories in the range front (fig. 2). Mountain-front salients are commonly 100-400 m lower in elevation

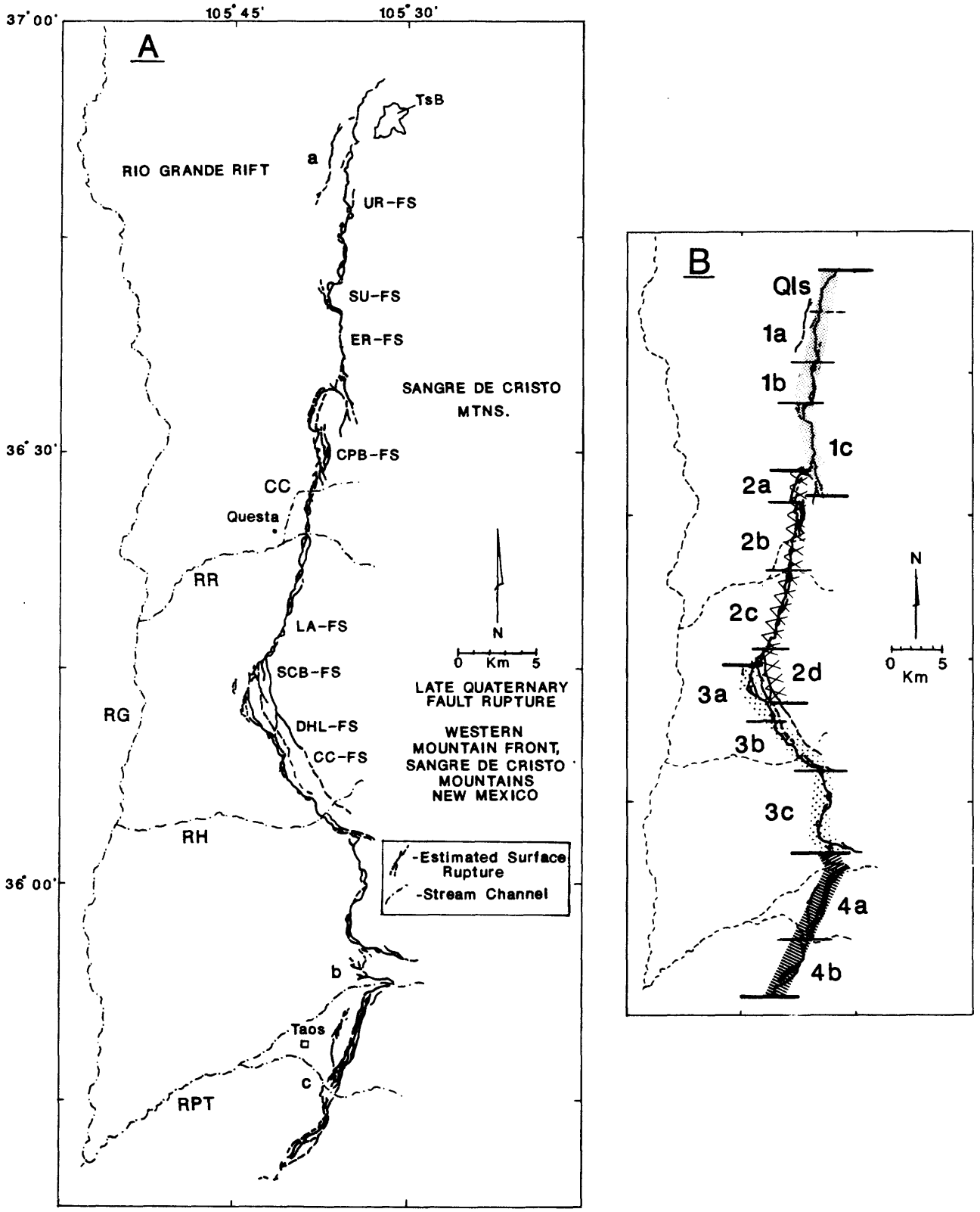
A
37° 00'
105° 45'
105° 30'
36° 30'
36° 00'
TsB
a
RIO GRANDE RIFT
UR-FS
SU-FS
ER-FS
SANGRE DE CRISTO MTNS.
CPB-FS
CC
Questa
RR
LA-FS
SCB-FS
RG
DHL-FS
CC-FS
RH
b
Taos
c
RPT
N
0 Km 5
LATE QUATERNARY FAULT RUPTURE
WESTERN MOUNTAIN FRONT, SANGRE DE CRISTO MOUNTAINS NEW MEXICO
-Estimated Surface Rupture
-Stream Channel
B
Qls
1a
1b
1c
2a
2b
2c
2d
3a
3b
3c
4a
4b
N
0 5
Km

FIGURE 2.--Map of late Quaternary rupture pattern along the range-bounding fault zone of the Sangre de Cristo Mountains interpreted from selected geomorphic and structural features along the mountain front. A: Map of fault rupture estimated from fault scarps, the basal topographic junction of the mountain front, and selected bedrock faults considered to be part of the boundary fault zone (defined in text). Mapping based on interpretation of aerial photographs and fieldwork at eight sites (labeled in capitol letters, that is, UR-FS). Three sites identified as a, b, and c are from Machette and Personius (1984). Abbreviations for rivers: Rio Grande gorge (RG), Red River (RR), Cabresto Creek (CC), and Rio Hondo (RH). TsB is an outcrop of Pliocene basalt (Servilleta basalts of Lipman and others, 1986) on the north end of the range front. B: Map of geometric segmentation patterns based on variations in the features presented in figure 2A (see text for details). Four primary segments are bounded by the heavy lines and are indicated by numbers 1-4; subsegments are outlined by fine lines and labeled with combination of lower-case letters and numbers.

---

than adjacent reentrants (fig. 3). Thus adjacent subsegments and segments tend to produce distinct lateral and vertical shifts in the base of the mountain front that generally increase in scale southward along a given segment. The average elevation of the base of the mountain front also increases irregularly to the south along most segments, until the range front abruptly deflects or drops in altitude across the boundary to the next segment to the south (figs. 2, 3).

Amount and Timing of Late Quaternary Rupture along Fault Scarps

The length and displacement of a surface rupture are critical parameters in magnitude estimates. Thus, it is important to establish the extent to which various segments and subsegments are linked in a given rupture event, and whether individual segments or subsegments behave as independent seismic sources. Constraints on the timing, size, and length of rupture associated with each segment or subsegment are needed to adequately address these questions.

Late Quaternary fault scarps were studied on six subsegments of the three primary segments that comprise the northern two-thirds of the range-front fault zone (fig. 2). Field studies consisted of: (1) measuring rod and level profiles of undissected fault scarps; (2) measuring the displacement of late Quaternary surfaces across fault scarps; and (3) using soil development to estimate the ages of displaced surfaces. Approximate ages are estimated from correlations with local and regional soil chronosequences (e.g., McCalpin, 1982; Kelson, 1986; Wesling and McFadden, 1986).

I determined scarp heights and the amounts of vertical offset across fault scarps using the graphical techniques of Machette and Personius (1984). These reconstructions indicate that both single-rupture and composite (multiple superimposed ruptures) fault scarps occur at most study sites. The most recent surface rupture produces a slightly steeper section in the profiles of composite fault scarps. The height and amount of offset typically increases in composite fault scarps formed in older geomorphic

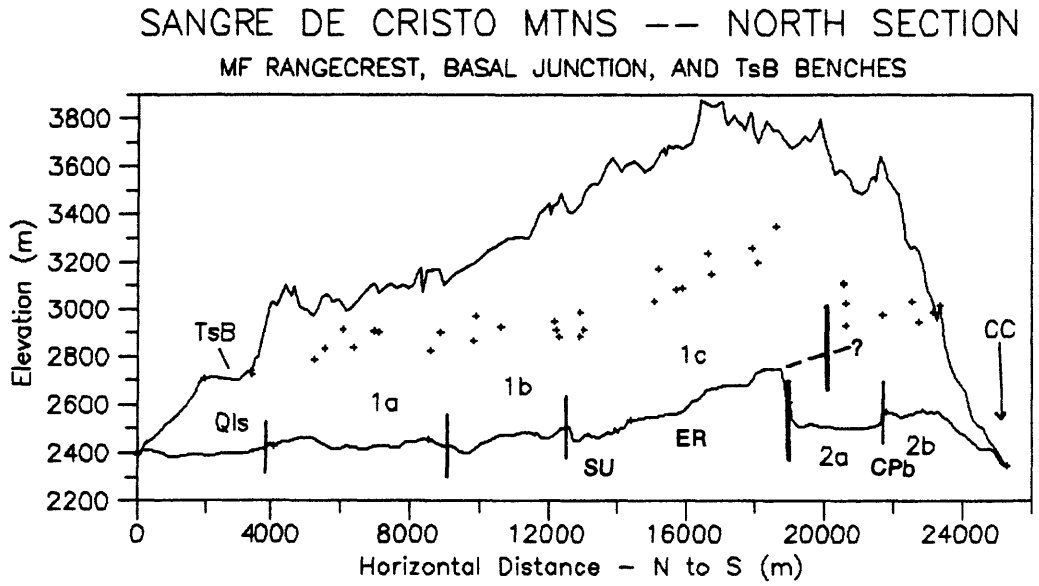

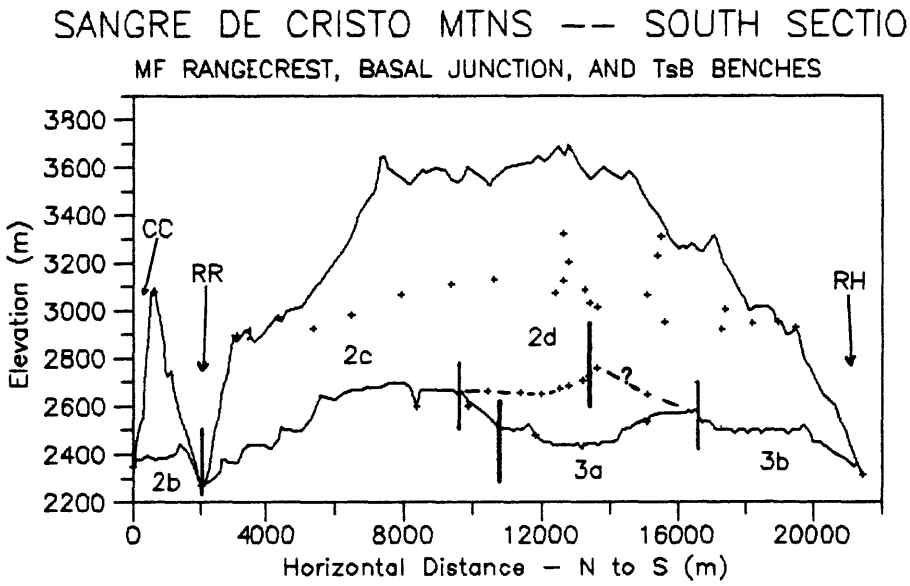

FIGURE 3.--Plot of elevation of range crest, base, and selected benches of the mountain front of the western Sangre de Cristo Mountains, subdivided into sections north and south of Cabresto Creek (CC). Altitudes from 1:100,000 and 1:24,0000 scale maps, and are projected approximately perpendicular to the mountain front into a common vertical plane (5.4X vertical exaggeration). Crosses indicate the projected positions of a set of prominent topographic benches at mid-escarpment levels on most facet-spur systems that correlate with Pliocene basalt flows (TSB) at the north end of the range crest (see text for details). Alphanumeric labels refer to segments and subsegments of figure 2B, with heavy and fine

vertical lines indicating approximate segment and subsegment boundaries, respectively. Dashed horizontal lines indicate projected altitudes of the base of interior mountain fronts, that is, large escarpments above subhorizontal bedrock benches within the main bedrock mountain front. Qls: areas of Quaternary landslides that bury range-front fault beneath basalt flows (TsB) of figure 2A. Other symbols are river abbreviations of figure 2A.

---

surfaces. In some cases, the height and offset of large composite scarps may be underestimated by 10-30 percent because colluvial wedges bury the original surface at the base of the scarp.

The profiles provide data for morphologic age estimates of the most recent rupture at each site. I applied two types of morphologic analyses to fault-scarp profiles that were subdivided according to individual site and small groups of two to four sites.

The first analysis is a linear regression of log-scarp-height versus maximum-slope-angle, following the procedures of Bucknam and Anderson (1979) and Machette and Personius (1984). Regressions were fitted to profiles of both single-rupture and composite fault scarps, but the age estimate of the most recent rupture was derived from height-angle data of either single-rupture scarps or the steepest sections of composite faults scarps.

The second morphologic analysis consisted of diffusion modeling of slope degradation (Nash, 1980, 1984; Colman and Watson, 1983; Mayer, 1984; Andrews and Hanks, 1985). I applied this method to 20 single-rupture fault scarps using the finite difference solution of Nash (1984, 1987), which is sensitive to both variations in the initial form of the scarp and the diffusivity constant used to calculate scarp ages. I statistically incorporated inherent analytical uncertainties using a modal histogram technique adapted from Mayer (1984). I constructed a composite age histogram for sets of scarps by successively stacking the range in age estimates derived for each scarp by using several initial morphologies and three different diffusivity constants (from Nash, 1984; Pierce and Colman, 1986). The median value and modal peak in the histogram provide general composite age estimates for the group of scarps.

Fault Scarp Heights and Vertical Offsets

The profiles of both single-rupture and composite fault scarps from all sites indicate that scarps from the most recent rupture average 2.2 m high with a mean of 1.2 m of vertical surface offset. The cumulative height and vertical displacements of composite scarps on upper Pleistocene alluvial surfaces of probable Bull Lake age (approximately 120 to 200 Ka) average 5.6 m and 3.6 m, respectively, although these may be minimum estimates because of partial burial. The largest composite scarps displace older geomorphic surfaces of probable mid-Pleistocene age, and reach maximum heights of 12-15 m and vertical surface offsets of 9-10 m.

Scarp heights and offsets are generally consistent at a given site, and there are no significant differences in these scarp parameters among the various sites along the mountain front, with the possible exception of scarps located on subsegment 1c (ER-FS and SU-FS, fig. 2). and on the northern end of subsegment 3a (SCB-FS, fig. 2). The two sites on subsegment 1c have somewhat

lower values in the mean heights (1.7 m) and displacements (0.8 m) of the single-rupture scarps. Site ER-FS also contains 5-6-m-high, composite fault scarps in upper Pleistocene alluvium with a weaker soil than is typical at similar sites along the range front. Fault scarps at site SCB-FS on the boundary of subsegment 3a are unusually high and degraded, and lack the steeper slope sections ($\geq$20° on scarps exceeding 5 m high) that occur on most fault scarps along the range front.

Estimated Ages of Most Recent Rupture along Fault Scarps

The combined morphologic estimates from all sites indicate a probable latest Pleistocene to Holocene age for the most recent rupture on this part of the range-bounding fault. The Latir section of the range front to the north of Cabresto Creek (CC, fig. 2) has the best evidence of Holocene rupture. However, the diffusion modeling, and somewhat less clearly, the regression analyses of scarp morphologies suggest a more complicated pattern with three distinct age ranges for the most recent rupture distributed among various fault segments and subsegments (figs. 2, 4): (1) the youngest rupture of late- to mid-Holocene age (median age (Md): 2.5-3.0 Ka) restricted to scarps on subsegment 1c only, (2) a slightly older rupture of mid- to early-Holocene age (Md: 5-6 Ka) found on scarps at sites on five subsegments of three primary fault segments, and (3) one or more latest Pleistocene ruptures (Md: 12-13 Ka) detectable only on more degraded piedmont fault scarps at the northern ends of three of the primary fault segments.

The morphologic age estimates are not precise enough to determine whether the fault scarps at the sites in age groups (1) or (2) formed in one simultaneous event, or whether they record smaller magnitude events clustered in a relatively short time interval. The age difference between groups (1) and (2) is probably near the resolution of the morphologic analyses (Knuepher and Turko, 1987); however, nonparametric Mann-Whitney tests do indicate that all three age groups are statistically distinct at a 97.5 percent significance level. Assuming that there are three distinct age groups of scarps, the morphologic data do not indicate whether the youngest faulting on subsegment 1c was superimposed on slightly older Holocene scarps, or filled a rupture gap between intermediate-age Holocene scarps located to either side (fig. 4).

General Patterns of Surface Rupture and Paleoseismicity

The spatial distribution of these age estimates suggest several possible patterns and scales of surface rupture may have occurred on the youngest set of fault scarps in the study area.

1) One small discrete rupture with a relatively small vertical displacement of 0.8 m is restricted to a single subsegment.
2) One large rupture, or several smaller ruptures, is evident on at least three of the four primary fault segments. This suggests that a large coseismic event with a total length of 30-50 km and average vertical displacements of 1.2 might have ruptured across several subsegment and segment boundaries.
3) There is a notable lack of any Holocene ruptures at site SCB-FS (figs. 2, 4) or at three sites from Machette and Personius (1984) (sites a, b, and c, figs. 2, 4). Piedmont fault scarps at these sites are located basinward

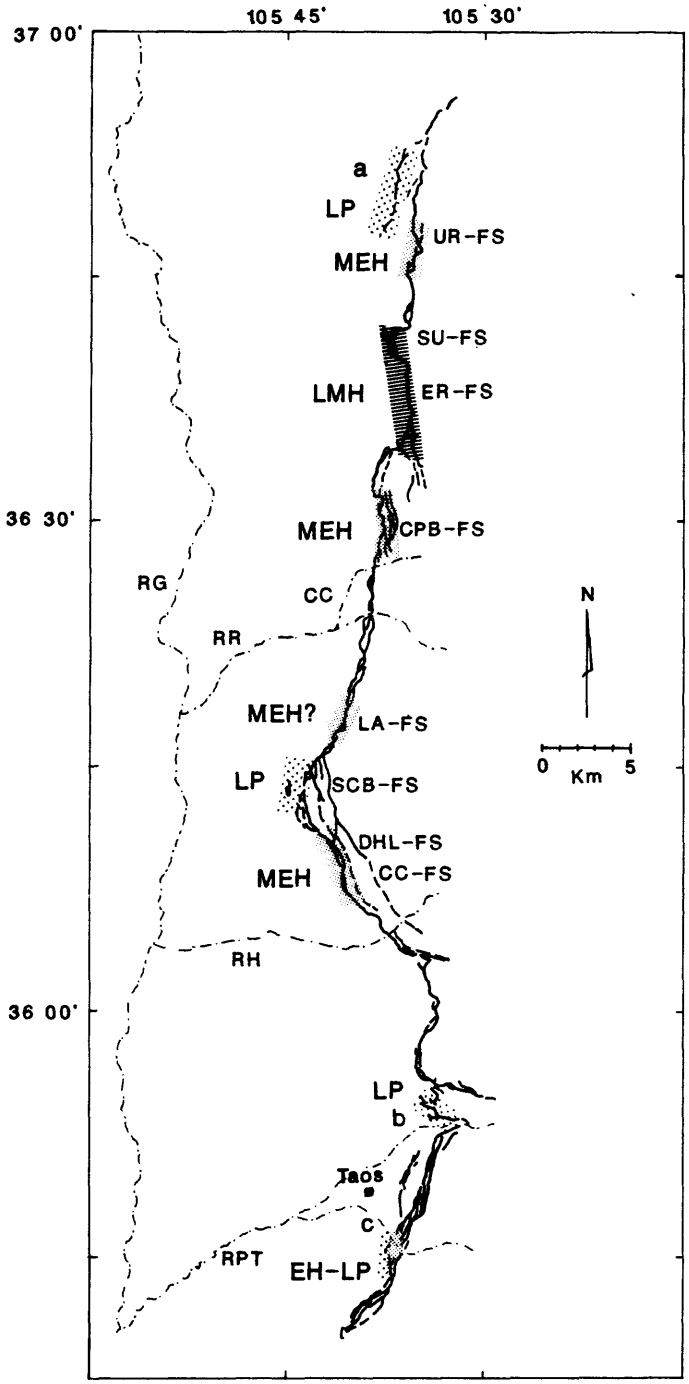

FIGURE 4.--Map of the distribution of estimated morphologic ages for the most recent single-event fault scarps along the range-bounding fault zone. Data for estimates include: a) combined diffusion modeling and regression analyses at sites identified by capital letters (for example, UR-FS); and b) regression analyses of piedmont fault scarps at sites a,b, and c, from Machette and Personius (1984). Morphologic age estimate are consistent with stratigraphic constraints on the age of most recent rupture. General age categories for sections of the fault zone with patterned strips are: LP-latest Pleistocene, MEH-middle to early Holocene, LMH-late to middle Holocene, EHLP-early Holocene to latest PLeistocene.

from prominent salients or low parts of the range front that coincide with the northern boundaries of three of the four primary segments. These gaps in Holocene fault scarps may mark persistent gaps or zones of less frequent rupture and (or) smaller displacements located at the boundaries of major segments. Crone and others (1987) describe similar gaps in surface rupture associated with the 1983 Borah Peak earthquake, as well as earlier Holocene events, that correlate with the proposed boundaries between major segments of the Lost River fault in Idaho.

These rupture patterns have obvious implications for interpreting late Quaternary paleoseismicity along the mountain front of the southern Sangre de Cristo Mountains. The contrasting scales in coseismic rupture imply at least two magnitudes of earthquakes. Surface ruptures less than 1 m in size confined to a 6-10-km-long subsegment would be associated with earthquakes of estimated magnitudes of 6.5-6.7 and 6.1-6.3, using rupture-size-magnitude regressions of Slemmons (1977) and moment-magnitude relationships of Hanks and Kanamori (1979), respectively. These same techniques suggest paleoearthquake magnitudes of 6.9-7.1 and 6.7-6.9 for 30-50-km-long ruptures with 1.2 m vertical displacement that extend across several primary fault segments.

Unfortunately, the fault scarp analyses do not tightly constrain the timing of the various coseismic ruptures. The cumulative displacement of the older geomorphic surfaces suggests generally recurrence intervals of 10^4 at most sites, but these data do not indicate the relative frequency of the two scales of late Quaternary ruptures. However, the general rate inferred above is compatible with better constrained recurrence intervals of 10^4 yr (more specifically, 10-50 Ka) inferred by McCalpin (1982) for the section of the Sangre de Cristo Mountains range-bounding fault to the north near Alamosa, Colorado. McCalpin's estimates are based on the offset relationships of radiometrically dated surficial deposits in several trenches across the fault zone.

PERSISTENCE OF FAULT-SCARP SEGMENTATION THROUGH PLIOCENE-QUATERNARY TIME

An important question in evaluating the paleoseismicity of this fault zone is the persistence of the late Quaternary segmentation pattern through longer Pliocene-Quaternary time intervals. Therefore I systematically analyzed selected erosional landforms and stratigraphy of the mountain front that record patterns of long-term deformation along the boundary fault (Menges, 1987a,b; unpub. data; Menges and Wells, 1987). I also examined the concurrent effects of such nontectonic variables as bedrock lithology, piedmont dissection related to downcutting along the Rio Grande, climatic change, and general processes of hillslope dissection and aggradation on landform morphology .

Basal Triangular Facets

These analyses indicate that major characteristics of the basal set of triangular facets more closely correspond to their position relative to fault segments and subsegments than to other geologic variables and geomorphic processes (fig. 5). For example, facets along the relatively narrow zones of faulting in the central parts of subsegments display greater local relief between base and apex, greater average size and slope area, steeper mean slope angles ($\geq$20°-22°), fewer facet benches, less-developed internal drainages,

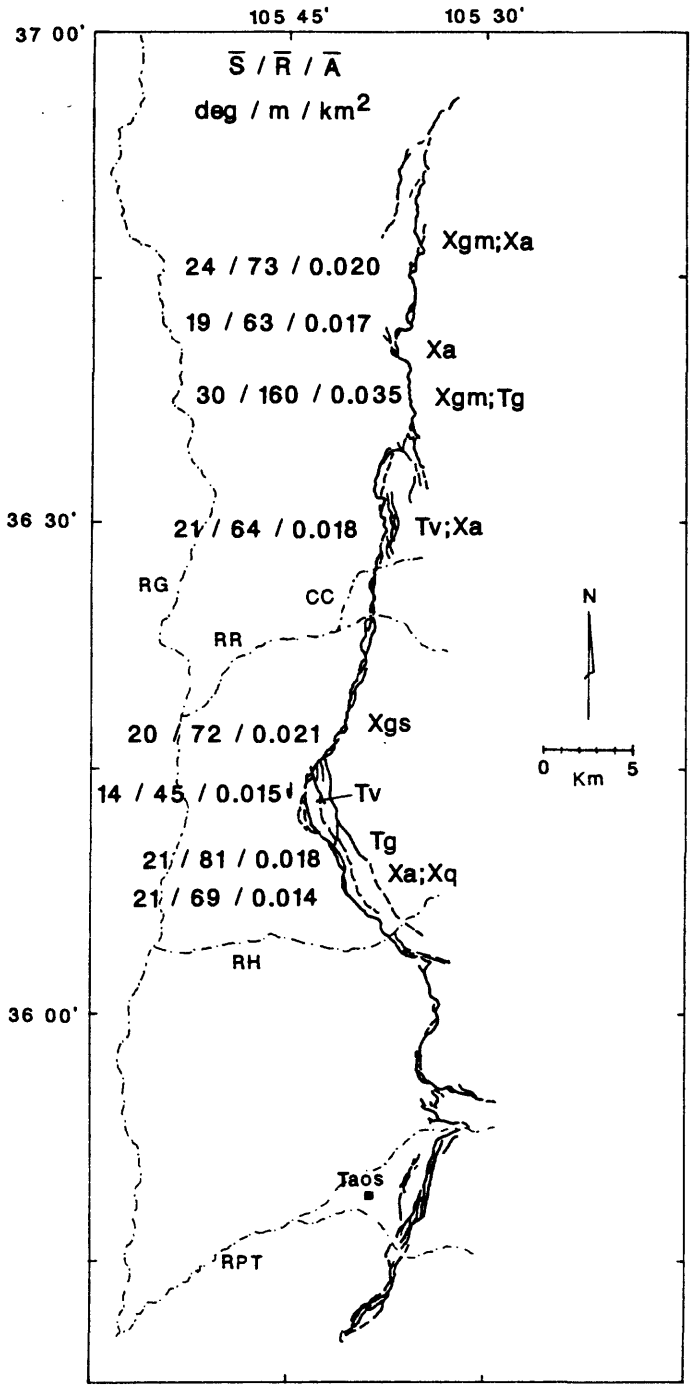

FIGURE 5.--Map showing variations in selected morphologic characteristics of basal facets along the mountain front, relative to fault segmentation and dominant bedrock lithology. Numbers on left are means (n = 4 to 20) of three morphometric parameters of basal facets at same sites as figures 2 and 4. Parameters, listed from left to right are: (1) site average of the mean slope angles ($\bar{S}$, in degrees) for field profiles of selected undissected basal facets, (2) mean local relief ($\bar{R}$, in m) of all basal facets at each site from 7.5-minute topographic maps with 40 ft contours, and (3) mean facet area ($\bar{A}$, in sq km), measured with planimeter on same facets and maps as (2) above. Dominant bedrock lithologies of facets at sites are listed on right (from Reed, 1984, and Reed and others, 1983): Precambrian granitic gneisses-Xgm, amphibolitic gneisses and schists-Xa, granites-Xg, and quartzites-Xq; and Tertiary granites-Tg, and volcanic rocks-Tv.

and thicker colluvial mantles, compared to facets adjoining the more complex rupture patterns at subsegment or segment boundaries (figs. 2, 5). These morphologic patterns are especially pronounced on facets near the south end of the primary segments, and the largest, steepest, and least dissected facets occur on subsegments with independent fault scarp or stratigraphic evidence (discussed below) for increased amounts and rates of tectonic activity (for example, subsegments 1c or 2c; figs. 4, 5, 6). The morphologies of facets with similar rock types likewise vary with position relative to the boundary fault, indicating the subordinate role of bedrock relative to tectonic activity in controlling the large-scale characteristics of facets. Variations in rock type primarily affect the matrix texture and gravel size of colluvium and the amount and pattern of bedrock outcrops.

The effects of nontectonic variables complicate the tectonically-induced patterns of facet morphology at some places. For example, the average slopes of facets at the northernmost site (fig.2) are slightly steeper on felsic gneisses compared to other less resistant rock types such as amphibolites. Also, deep incision of the piedmont near the south end of the study area causes increased dissection of the mountain front, which in turn produces relatively small basal facets in that area.

Topographic Profiles of the Full Escarpment

I measured the topographic profiles of 15 facet-spur systems on the full mountain-front escarpment from USGS quadrangle maps. The profiles show morphologic variations that, like the basal facets, correlate with the specific position relative to segmentation patterns of the boundary fault zone (fig. 6). In general, the morphologic patterns of a set of basal facets characterize the overall vertical profile of the larger facet-spur system of the range front. For example, the lower part of the facet-spur profile above the interior of subsegment 1c (ER-FP, fig. 6) is generally steeper and more convex-upwards, and contains fewer and less pronounced benches, relative to profiles of the escarpment at adjacent subsegment or segment boundaries (CPB-FP and LSU-FP, fig. 6). Similar spatial variations occur in the gross morphology of basal facets at these three sites as well (fig. 5; see above). These patterns extend vertically upwards along facet-spur systems to at least the elevation of a prominent set of mid-escarpment benches that correlate with Pliocene basalt flows at the north end of the range front (see below; benches (B) identified in fig. 6).

Correlation of Pliocene (TsB) Benches

The long-term segmentation patterns of the range-front fault can be determined in another manner by measuring the deformation of a Pliocene surface fortuitously preserved along much of the mountain front. As noted previously, gently eastward-tilted 4.3-Ma basalt flows are locally preserved above a low-relief surface at the northern end of the range block (TsB in figs. 2, 3). The basalts and underlying surface are correlated along the range front to the south with a series of prominent topographic benches at upper- to mid-escarpment levels in most facet-spur systems (fig. 6). Figure 3 depicts the positions of these benches relative to the base and the range crest of the mountain front; all three surfaces or datums have been projected

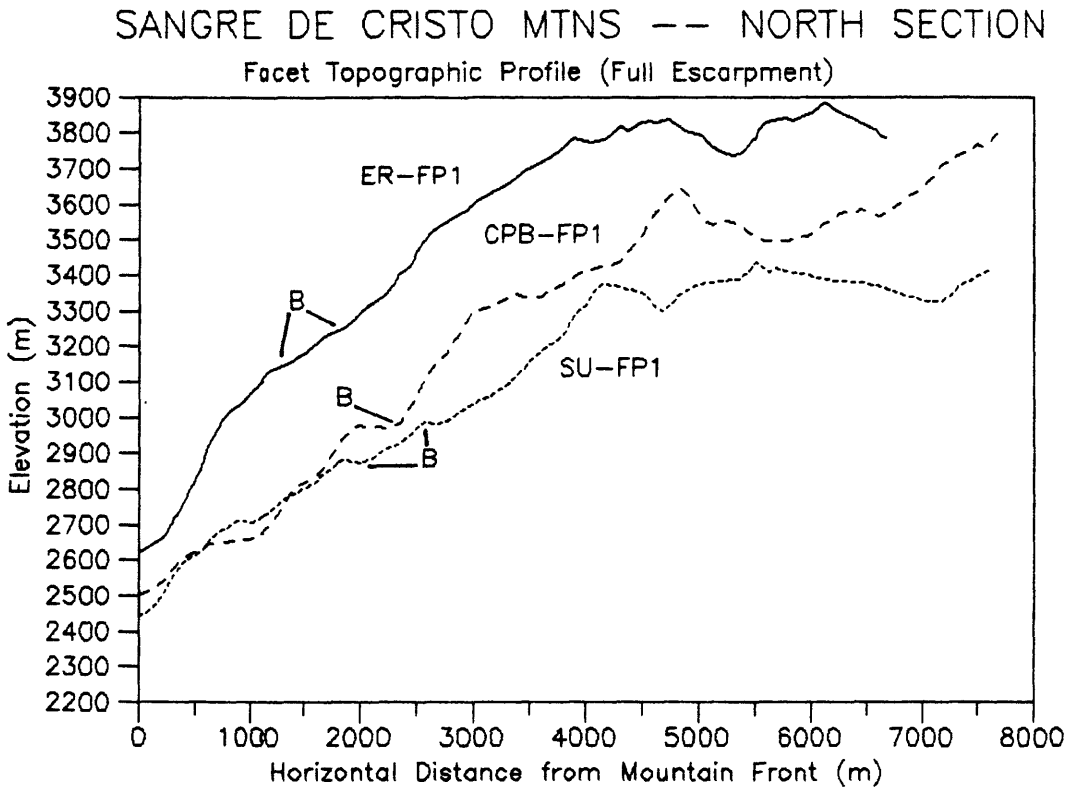

FIGURE 6.--Three topographic profiles of the full mountain-front escarpment from 7.5-minute topographic maps. Profiles begin on piedmont below base of mountain front and extend upslope along facet-spur systems to range crest. Profiles extend upwards from three sites used in fault-scarp and facet studies that are located at the northern boundary and interior of subsegment 1c (SU-FP and ER-FP, respectively, figs. 2, 5) and at the northern end of subsegment 2a (CPB-FP). B marks the position of mid-escarpment benches correlated with the Pliocene basalts at the north end of the range crest (discussed in text).

---

westward approximately perpendicular to the average trend of the mountain front into a common vertical plane.

The average altitude of the escarpment benches in this projection closely mimics the elevation patterns and gradients of the range crest, as well as the base of the mountain front, which approximates the trace of the zone of surface rupture along the range-bounding fault zone. The parallelism in the elevation of the TsB benches and the basal junction is especially striking along subsegments 1c and 2a (figs. 2, 3). The steep rise in altitude of the bench across subsegment 1c, relative to the position of similar basalts in the subsurface of the adjacent piedmont, suggests a sharp increase in cumulative offset southward from approximately 700 m to 975 m. This is followed by an even more abrupt drop in elevation and decrease in offset (to 755 m) across the boundary between segments 1 and 2.

These analyses indicate a strong correlation among many diverse landforms in those characteristics that best reflect patterns of tectonic activity along

the range-front fault. For example, subsegment 1c contains fault scarps with the youngest morphologic age estimates, the steepest, largest, and least dissected set of basal facets, an unusually convex, unbenched and steeply-sloping escarpment profile, and the highest elevations of the Tsb bench (figs. 4, 5, 6). The correspondence among tectonic landform parameters at this and other parts of the range front strongly suggests that many of the more prominent segmentation patterns, including those developed at subsegment scales, have persisted over the 4 millon year interval of deformation recorded by the TsB benches.

SUMMARY AND CONCLUSIONS

Morphometric analyses of fault scarps and bedrock landforms of the western mountain front of the Sangre de Cristo Mountains near Taos suggest several time-space patterns in coseismic rupture along the boundary fault zone. These complexities have potential significance for short- and long-term estimates of the paleoseismicity along this major rift-bounding fault zone, and they may have applications to other tectonically-active faults bounding large mountain fronts in the Basin and Range province. Among the more important interpretations from this study are:

1) Variations in the pattern of fault scarps and the morphology of the base of the range front define several scales of geometric segmentation along the 70 km-long section of boundary fault zone in the study area. These include four primary fault segments averaging 15-20 km in length, each composed of two to three subsegments 5-10-km long. These segments and subsegments are defined by systematic variation in geomorphic and structural criteria, including the width and complexity of the zone of late Quaternary surface rupture, its position on the piedmont relative to the mountain front, and alternating changes in the altitude of the base of the mountain front that correspond to reentrants and salients in the range front.
2) Morphologic analyses of fault scarps at eight sites suggest that Holocene rupture is present along most of the range-bounding fault zone. The main exceptions are relatively degraded piedmont scarps of probable latest Pleistocene age at the northern ends of primary fault segments. Variations in the morphologic age estimates of the most-recent single-rupture fault scarps suggest several scales of Holocene surface rupture, including one mid- to early-Holocene event with an average 1.2 m vertical offset that probably extended 30-50 km across several primary segments, and a smaller (0.8 m average offset) and younger late- to mid-Holocene event confined to a single subsegment 6-10 km long. These data suggest that surface rupture on the fault may be associated with two different sizes of earthquakes with estimated magnitudes of 7.1-6.9 and 6.5-6.7, respectively.
3) The morphology of bedrock landforms along the mountain front suggest that many of the segmentation patterns indicated by late Quaternary fault scarps have persisted over Pliocene-Quaternary time spans. Many of the major characteristics of basal triangular facets--including average size and slope steepness, the degree of internal dissection, the number and size of facet benches, and the thickness of colluvial mantles--correlate better with the position of the facet relative to fault subsegments/segments than other nontectonic variables such as bedrock lithology and piedmont dissection. Most of these morphologic properties characterize the overall topographic profile of the composite system of facet and spurs in the range-front

escarpment. The morphologic characteristics of basal facets extend up to at least the level of a prominent set of mid-escarpment benches that correlate with 4.3 Ma basalt flows. Projections of the probable Pliocene benches along the range front are remarkably parallel with the altitudes of both the range crest and the base of the mountain front. All three elevation datums generally rise abruptly to the south along the southernmost subsegments of fault segments.

Many geomorphic patterns of the range front may reflect large-scale variations in the net displacement and structural geometry of the range-front fault zone. The estimated cumulative offset and the average displacement rates of the TsB bench increase southward along the two northern fault segments; for example, the amount and rate of post-Pliocene vertical displacements increase from 500 m to 975 m and 115 m/m.y. to 225 m/m.y. to the south along segment 1. These variations correlate with position relative to subsegments of the boundary fault. There is a only a gradual southward increase in the inferred offset of the Tsb bench along the northern subsegments of any primary segment; however variations in the geometry of the basal fault zone do produce changes in the morphology of adjacent bedrock facets. Estimated displacements typically increase abruptly to maximum values along the south-central part of the southernmost subsegment of the fault segment. Perhaps this long-term differential offset along fault segments accumulates in part from more frequent ruptures on the southern subsegments, similar to the small isolated late Holocene event inferred for subsegment 1c.

ACKNOWLEDGMENTS

I would like to acknowledge financial support from the following sources that funded parts of the dissertation fieldwork: a Challenge Scholarship grant from the Office of Graduate Studies at the University of New Mexico, funds provided by the New Mexico Bureau of Mines and Mineral Resources, the 1986 New Mexico Geological Society Fellowship, and a 1986 Mackin and general grant-in-aid from the Geological Society of America. This manuscript has benefitted from reviews by L.D. McFadden and A.J. Crone. Many other friends and associates have substantially contributed to some of the data collection and (or) ideas presented herein, including J. Hawley, J. Callender, Y. Enzel, B. Harrison, P. Drake, K. Kelson, and J. Wesling. However I assume ultimate responsibility for the interpretations presented in this article.

REFERENCES CITED

Andrews, D.J., and Hanks, T.C., 1985, Scarp degraded by linear diffusion--Inverse solution for age: Journal of Geophysical Research, v. 90, no. B12, p. 10,193-10,208.

Bucknam, R.C., and Anderson, R.E., 1979, Estimation of fault-scarp ages from a scarp-height--slope-angle relationship: Geology, v. 7, p. 11-14.

Colman, S.M., and Watson, Ken, 1983, Ages estimated from a diffusion equation model for scarp degradation: Science, v. 221, p. 263-265.

Crone, A.J., Machette, M.N., Bonilla, M.G., Lienkaemper, J.J., Pierce, K.L., Scott, W.E., and Bucknam, R.C., 1987, Surface faulting accompanying the Borah Peak earthquake and segmentation of the Lost River fault, central Idaho: Bulletin of the Seismological Society of America, v. 77, no. 3, p. 739-770.

Hanks, T.C., and Kanamori, Hiroo, 1979, A moment magnitude scale: Journal of Geophysical Research, v. 84, p. 2348-2350.

Kelson, K.I., 1986, Long-term tributary adjustments to base-level lowering, northern Rio Grande rift, New Mexico: Albuquerque, New Mexico, University of New Mexico, M.S. thesis, 211 p.

Knuepher, P.L.K., and Turko, J.M., 1987, Limits to distinguishing ruptures on adjacent fault segments from scarp degradation modeling (Abs.): Geological Society of America Abstracts with Programs, v. 19, no. 7, p. 730.

Lambert, P.W., 1966, Notes on the late Cenozoic geology of the Taos-Questa area, New Mexico, in, Northrop, S.A., and Read, C.B., eds., New Mexico Geological Society Guidebook, 17th Field Conference Guidebook, p. 43-50.

Lipman, P.W., and Mehnert, H.H., 1979, The Taos Plateau volcanic field, northern Rio Grande rift, New Mexico, in, Riecker, R.E., ed., Rio Grande rift--Tectonics and magmatism: Washington D.C., American Geophysical Union, p. 289-311.

Lipman, P.W., Mehnert, H.H., and Naeser, C.W., 1986, Evolution of the Latir volcanic field, northern New Mexico, and its relation to the Rio Grande rift, as indicated by potassium-argon and fission track dating: Journal of Geophysical Research, v. 91, no. B6, p. 6329-6345.

Machette, M.N., and Personius, S.F., 1984, Map of Quaternary and Pliocene faults in the eastern part of the Aztec 1 X 2 quadrangle and the western part of the Raton 1 X 2 Quadrangle, northern New Mexico: U.S. Geological Survey Miscellaneous Field Studies Map MF-1465-B, scale 1:250,000, with text, 20 p.

Maclean, A.G., 1985, Quaternary segmentation of the Wasatch Fault zone, Utah, as studied by morphometric discriminant analyses: Miami, Ohio, Miami University, M.S. thesis, 200 p.

Mayer, Larry, 1984, Dating Quaternary fault scarps formed in alluvium using morphologic parameters: Quaternary Research, v. 22, p. 300-313.

_____1986, Tectonic geomorphology of escarpments and mountain fronts, in, Active tectonics: National Research Council, Washington D.C., National Academy Press, p. 125-135.

Mayer, Larry, and Maclean, A., 1986, Tectonic geomorphology of the Wasatch Front, Utah, using morphologic discriminant analysis--Preliminary implications for Quaternary segmentation of the Wasatch fault zone

[abs.]: Geological Society of America Abstracts with Programs, v. 18, no. 2, p. 155.

McCalpin, J.P., 1982, Quaternary geology and neotectonics of the west flank of the northern Sangre de Cristo Mountains, south-central Colorado: Colorado School of Mines Quarterly, v.77, no. 3, 97 p.

Menges, C.M., 1987a, Time-space segmentation of late-Quaternary rupture along the western Sangre de Cristo mountain front, north-central New Mexico [abs.]: Geological Society of America Abstracts with Programs, v. 19, no. 5, p. 321.

_____1987b, The form and evolution of bedrock facet hillslopes along the tectonically-active mountain front of the western Sangre de Cristo Mts, northern New Mexico [abs.]: Geological Society of America, Abstracts with Programs, v. 19, no. 7, p. 770.

Menges, C.M., and Wells, S.G., 1987, Late Quaternary fault scarps, mountain front landforms, and Plio-Quaternary rupture segmentation along a range-front normal fault zone, Sangre de Cristo Mtns, New Mexico [abs.]: Geological Society of America Abstracts with Programs, v. 19, no. 7, p. 770-771.

Nash, D.B., 1980, Morphologic dating of degraded normal fault scarps: Journal of Geology, v. 88, p. 353-360.

_____1984, Morphologic dating of fluvial terrace scarps and fault scarps near West Yellowstone, Montana: Geological Society of America Bulletin, v. 95, p. 1413-1424.

_____1987, SLOPEAGE program, v. 2.1: Cincinatti Ohio, Fenneman-Rich Geomorphic Laboratories, Department of Geology, University of Cincinatti.

National Research Council, 1986, Active tectonics: Washington D.C., Studies in Geophysics, National Academy Press, 266 p.

New Mexico Geological Society, 1982, New Mexico Highway Geological Map: New Mexico Geological Society in cooperation with New Mexico Bureau of Mines and Mineral Resources, scale 1:1,000,000.

Pearthree, P.A., and Calvo, S.S., 1987, The Santa Rita fault scarp--Evidence for large-magnitude earthquakes with very long recurrence intervals in the Basin and Range province of southeastern Arizona: Bulletin of the Seismological Society of America, v. 77, p. 97-116.

Pierce, K.L., and Colman, S.M., 1986, Effect of height and orientation (microclimate) on geomorphic degradation rates and processes, late-glacial terrace scarps in central Idaho: Geological Society of America Bulletin, v. 97, p. 869-885.

Reed, J.C., Jr., 1984, Proterozoic rocks of the Taos Range, Sangre de Cristo Mountains, New Mexico, in, Baldridge, W.S., Dickerson, P.W., Riecker,

R.E., and Zidek, J., eds., New Mexico Geological Society Guidebook, 35th Field Conference, p. 179-185.

Reed, J.C., Lipman, P.W., and Robertson, J.E., 1983, Geologic map of the Latir Peak and Wheeler Peak Wildernesses and Columbine-Hondo Wilderness Study Area, Taos County, New Mexico: U.S. Geological Survey Miscellaneous Field Studies Map MF-1570-B, scale 1:50,000.

Schwartz, D.P., and Coppersmith, K.J., 1984, Fault behavior and characteristic earthquakes--Examples from the Wasatch and San Andreas fault zones: Journal of Geophysical Research, v. 89, no. B7, p. 5681-5698.

_____1986, Seismic hazards--New trends in analysis using geologic data, in, Active tectonics: Research Council, Washington D.C., National Academy Press, p. 215-230.

Scott, W.E., Pierce, K.L., and Hait, M.H., Jr., 1985, Quaternary tectonic setting of the Borah Peak earthquake, central Idaho: Bulletin of the Seismological Society of America, v. 75, p. 1053-1066.

Slemmons, D.B., 1977, State-of-the-art for assessing earthquake hazards in the United States, Report 6: Faults and earthquake magnitude: Miscellaneous Paper, U.S. Army Corps of Engineers, S-73-1, 129 p.

Slemmons, D.B., and Depolo, C.M., 1986, Evaluation of active faulting and associated hazards, in, Active Tectonics: National Research Council, Washington D.C., National Academy Press, p. 45-62.

Summers, W.K., and Hargis, L.L., 1984, Hydrologic cross section through Sunshine Valley, Taos County, New Mexico, in, Baldridge, W.S., Dickerson, P.W., Riecker, R.E., and Zidek, J., eds., New Mexico Geological Society Guidebook, 35th Field Conference, p. 245-248.

Upson, J.E., 1939, Physiographic subdivisions of the San Luis Valley, southern Colorado: Journal of Geology, v. 47, p. 721-736.

Wallace, R.E., 1978, Geometry and rates of change of fault-generated range-fronts, north-central Nevada: U.S. Geological Survey, Journal of Research, v. 6. no. 5, p. 637-650.

_____1987, Grouping and migration of surface faulting and variations in slip rates on faults in the Great Basin province: Bulletin of the Seismological Society of America, v. 77. no. 3, p. 868-876.

Wesling, J.R., and McFadden, L.D., 1986, Pleistocene and Holocene glacial chronology for the glacial deposits in the southernmost Sangre de Cristo Mountains, New Mexico [abs.]: Geological Society of America Abstracts with Programs, v. 18, no. 5, p. 422.

Wheeler, R.L., and Krystinik, K.B., 1987, Persistent and nonpersistent seismic segmentation of the Wasatch fault zone, Utah [abs.]: Geological Society of America Abstracts with Programs, v. 19, no. 5, p. 342.

THE EFFECT OF ACTIVE TECTONICS ON ALLUVIAL RIVERS

by

S.A. Schumm

Department of Earth Resources
Colorado State University
Fort Collins, CO 80523

ABSTRACT

Experimental and field studies of alluvial rivers indicate that active tectonics has an effect on river morphology. In its simplest form active uplift will change the slope of an alluvial valley floor, thereby decreasing slope above the uplift and increasing slope below the uplift. Alluvial rivers respond to the change in valley slope by aggradation and degradation as well as by a change in sinuosity or by a change from a meandering to a braided pattern.

RESPONSE OF ALLUVIAL RIVERS

Experimental Studies

Alluvial rivers adjust their morphology in response to changes of valley-floor slope, which can be the result of bedrock controls tributary sediment contribution, localized aggradation or active tectonics, (Schumm, 1986; Schumm and others, 1987, p. 251-277). Experimental studies, that were carried out in a flume with a floor that could be deformed by hydraulic jacks, show the nature of river response to uplift and subsidence (Ouchi, 1985; Jin and Schumm, 1987).

Experimental studies of braided channels show incision and terrace formation below an uplift axis and aggradation, bar formation, and overbank flooding above an uplift axis. Experimental studies of meandering channels show an increase in sinuosity and meander wavelength below an uplift axis, and meander cutoffs and overbank flooding above an uplift axis.

In addition to the primary valley-floor deformation by active tectonics and the secondary channel response to this deformation, there are third-order effects beyond the area of deformation. For example, deposition upstream from the axis of uplift can progress further upstream beyond the area of active deformation. This means that the uplift is acting as a dam, and unless erosion on the steeper downstream side of the uplift produces sufficient sediment to compensate, erosion will occur downstream beyond the limits of deformation. However, it is more likely that the reduced sediment load will accelerate erosion on the steeper reach, and when this increased load moves downstream, aggradation results.

As a result of the uplift more resistant materials may appear in the channel as it degrades. Resistant alluvium or bedrock will confine the channel and retard meander shift and bank erosion. The result should be deformed or compressed meanders upstream and a change of meander character at the contact (figs. 1 and 2).

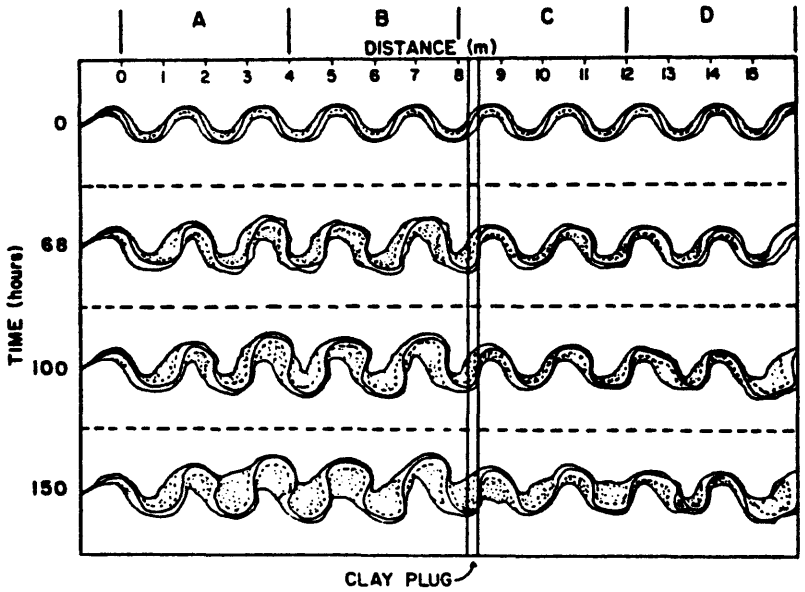

FIGURE 1.—Effect of a clay outcrop on channel pattern. Flow is from left to right in 15 m flume (from Jin and Schumm, 1987). Changes in sinuosity and amplitude are shown in figure 2.

Alluvial channels are sensitive indicators of change, but they also adjust to changes of hydrology and sediment load as well as to active tectonics. Therefore, it may be difficult to determine the cause of channel change when, in fact, human activities have altered both discharge and sediment load during historic time. Pattern change alone is not sufficient evidence for active tectonics, rather it is one bit of evidence that must be supported with other morphologic evidence and/or surveys that provide clear evidence of deformation. In many areas the evidence will be circumstantial. Nevertheless, anomalous reaches that are not related to artificial controls or to tributary influences may reasonably be assumed to be the result of active tectonics until proved otherwise.

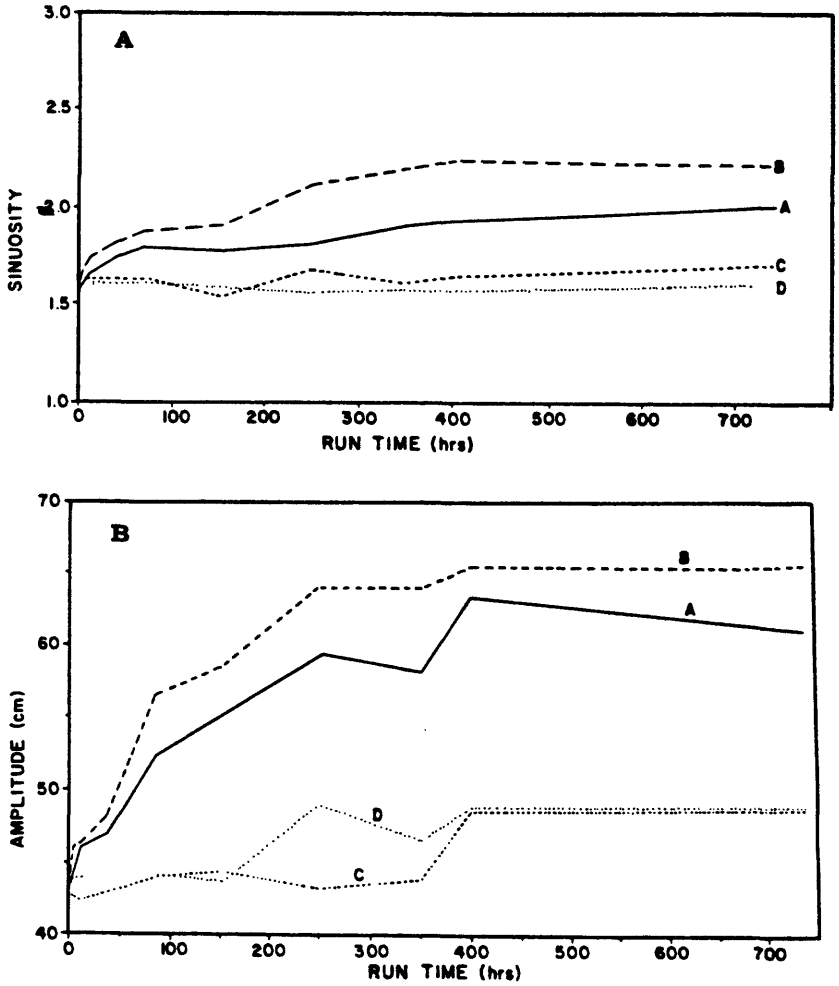

FIGURE 2.--Effect of clay outcrop (fig. 1) on channel sinuosity (A) and meander amplitude (B) (from Jin and Schumm, 1987). Channel patterns are shown in figure 1.

Field Studies

Streams crossing the Monroe Uplift in northeast Louisiana, southeast Arkansas, and western Mississippi show upwarping of valley profiles, and changes in channel depth, sinuosity, and channel slope associated with the uplift (fig. 3). Similar changes occur along streams crossing the active Wiggins Uplift in southeastern Louisiana and southern Mississippi (Burnett and Schumm, 1983). The Mississippi River crosses the Lake County, Monroe, and Wiggins Uplifts and its valley-floor profile is deformed at these locations; however, the morphologic response of the river is complicated by the influence of bedrock (Gregory and Schumm, 1987).

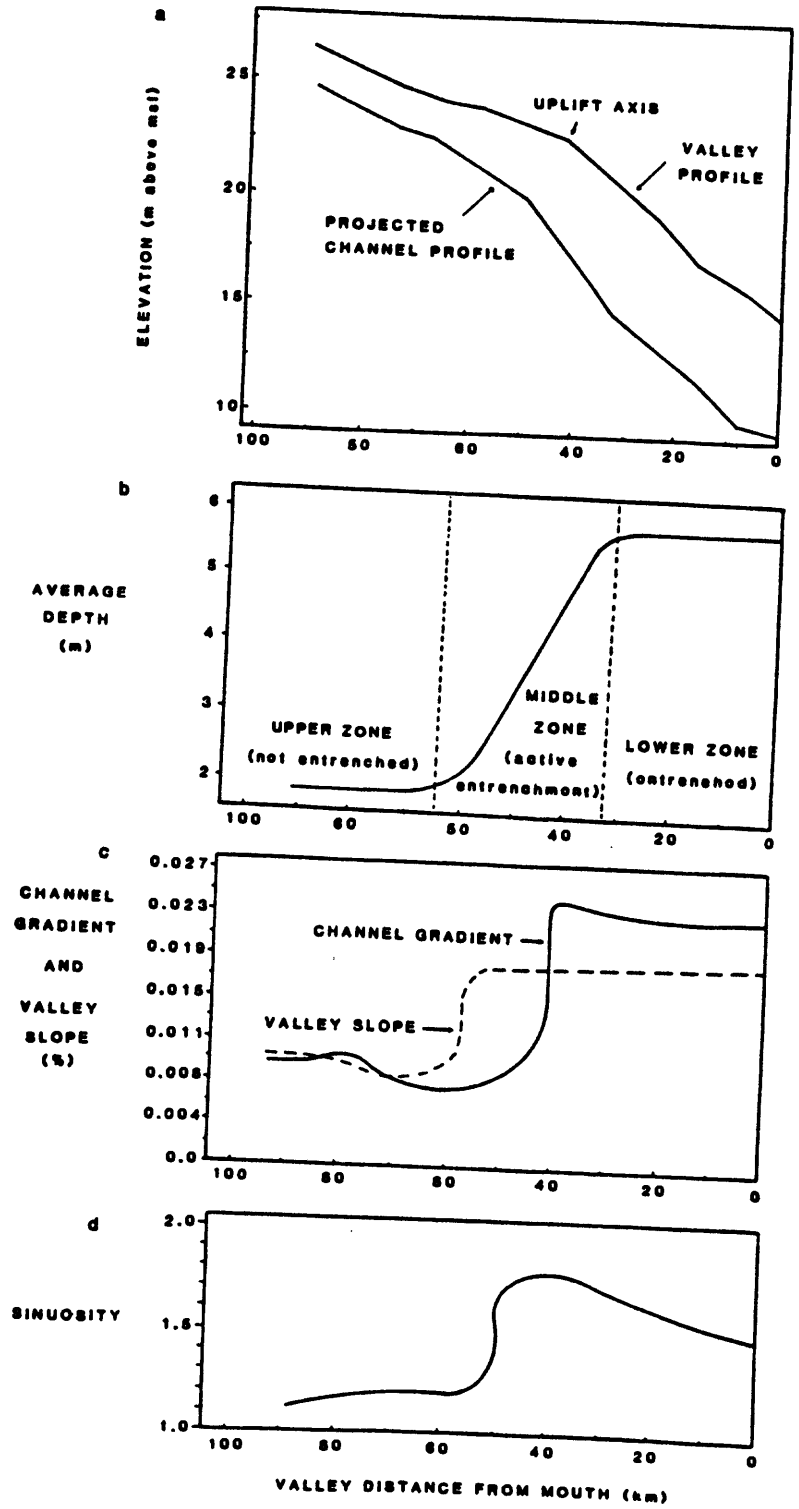

FIGURE 3.—Change of channel morphology associated with uplift, Big Colewa Creek, Louisiana (from Burnett and Schumm, 1983).

DISCUSSION

If some alluvial rivers are presently adjusting to active tectonics, this must be considered to be an additional explanation for river instability. This has practical significance, because river navigation can be affected by aggradation and the development of bars. Bank erosion, incision, and pattern change can impact on riparian land use and cause loss of valuable structures (bridges, loading docks) as well as agricultural land and homes. The frequency of overbank flooding will be increased in reaches of aggradation and reduced gradient. Changes in the frequency of overbank flooding will change the position of "ordinary high water", which is a legal boundary, and this may lead to confusion and litigation.

ACKNOWLEDGMENTS: Support for this research was provided by National Science Foundation, Grant EAR 8518375

REFERENCES CITED

Burnett, A.W. and Schumm, S.A., 1983, Active tectonics and river response in Louisiana and Mississippi: Science, v. 222, p. 49-50.

Gregory, D.I. and Schumm, S.A., 1987, The effect of active tectonics on alluvial river morphology, in Richards K.S., (ed.), Rivers: Wiley and Sons, Chicester, in press.

Jin, Desheng and Schumm, S.A., 1987, A new technique for modelling river morphology, in Richards, K.S. (ed.), River Channel Dynamics: Wiley and Sons, Chichester, in press.

Ouchi, Shungi, 1985, Response of alluvial rivers to slow active tectonic movement: Geological Society of America Bulletin, v. 96, p. 504-515.

Schumm, S.A., 1986, Alluvial river response to active tectonics: in Active tectonics: Washington, D.C., U.S. National Academy Press, p. 80-94.

Schumm, S.A., Mosley, M.P. and Weaver, W.E., 1987, Experimental fluvial geomorphology: New York, Wiley and Sons, 413 p.

CHANGES IN LONG-TERM VERSUS SHORT-TERM SLIP RATES IN AN EXTENSIONAL ENVIRONMENT

by

Michael N. Machette
U.S. Geological Survey
Denver, Colorado 80225

INTRODUCTION

Quaternary faulting in the Basin and Range province and Rio Grande rift of the Western United States shows nonuniform patterns of activity in time and space. Recent detailed studies of several major faults suggest that temporal clustering and spatial migration of faulting are patterns common to individual fault zones as well as the to the region as a whole.

Only recently have there been enough data collected from major normal faults in extensional environments to document changes in long-term versus short-term slip rates. For example, during the past decade 49 trenches have been excavated across the Wasatch fault zone of Utah (see table 1, Machette and others, 1987). Interpretation of the relations between tectonically derived colluvium, buried soils, and faulted deposits, combined with about 60 radiocarbon dates, has enabled workers to constraint the times of the most recent faulting events, of prior faulting events, and the lengths of quiescent intervals between faulting events (recurrence intervals). Detailed mapping of Quaternary deposits along 250 km of the 330-km-long Wasatch fault zone has yielded estimates of the *average* slip rates since the middle Pleistocene (past 150-250 ka). In this case, comparison of slip rates for short (15 ka) and intermediate (150 ka) time intervals reveal a 5-10 fold increase in average slip rate (Machette and others, 1987).

For the region as a whole, most syntheses of time-space distributions of young faulting are handicapped by a lack of precise short-term records: for example, a well-dated record of multiple faulting events on a large numberof faults during the Holocene. With the exception of recent (yet still unpublished) data from the Wasatch fault zone, I am not aware of any other normal faults in the Western United States for which the timing of three or more consecutive faulting events is well constrained; thus, it is hard to distinqush between *bona fide* changes in slip rate and natural variability in slip rates (see following discussion of apparent patterns of fault movement). Nevertheless, slip rates determined from detailed studies of trenches, tectonic geomorphology and Quaternary geology, compared with rates determined from isotopic studies of uplifted fault blocks suggest that nonuniformity is typical of slip patterns for normal faults in the Basin and Range province (Wallace, 1987) and Rio Grande rift (Machette, 1987)--the two largest tracts of extensional terrain in the United States.

This nonuniformity is manifest in several ways. Most obvious is temporal clustering of historic surface faulting in seismic zones or belts, such as the Central Nevada Seismic Belt (see Wallace, 1987). Another type of temporal clustering (or preferential focusing) is marked by consecutive rupture events on a single fault or fault zone, whereas adjacent faults remain inactive for considerable time. This pattern is typical where paleoseismic activity has been concentrated on faults with high slip rates, such as those associated with the transition zones between major geologic provinces such as the Colorado Plateaus, Basin and Range and Sierra Nevada, and along the Rio Grande rift. On a longer time span, nonuniform patterns of faulting are seen as migrating zones of active deformation, such as mountain building episodes on the regional scale. Finally, on a purely temporal scale, dramatic changes may occur in short-term (1,000-10,000 yr) slip rates relative to intermediate- (100,000's yr) and long-term (1,000,000's yr) slip rates on individual faults or fault zones.

PROBLEMS WITH SLIP-RATE DETERMINATIONS

To assess evidence for changes in slip rates, one must appreciate the type and scale of problems associated with determining slip rates on normal faults (much of this discussion applies to other types of faults). However, some of the problems noted below are a direct result of the block uplift and basin subsidence that typify of an extensional tectonic setting. Inherent in this setting is a tendency to bury tectonically derived colluvial deposits that are the stratigraphic record of faulting. This setting is distinctly different from that of strike-slip faults where evidence of faulting commonly is laid out conveyor-belt style on opposing sides of the fault. One advantage of normal faults is that uplifted blocks (mountain ranges) may record long histories of faulting, both geomorphically and geologically. The history and rate of uplift may be interpreted from erosional benches perched upon the range or from faceted spurs cut on the bedrock front of a range (Menges, this volume). Research on interpreting these types of tectonic record is just beginning in a quantitative sense and qualitative studies of tectonic geomorphology, as championed by Bull (1984, this volume) have not been utilized fully in studies of paleoseismology. Most of the data for very long-term (that is 5-10 m.y.) uplift rates has come from fission-track studies of apatite or zircon extracted from basement rock now exposed in uplifted ranges (Naeser and others, 1983; Parry and Bruhn, 1986). Fission-track data commonly record the initiation of uplift and thus perhaps the onset of extensional faulting, but rarely yield evidence of intermediate- or long-term changes in slip rates.

Values of two parameters are needed to calculate a valid slip rate: fault displacement and time between successive rupture events. However, we may not have exact values for these parameters and must substitute values of similar parameters. For example, surface offset (S, fig. 1), which may or may not compensate for near- and far-field deformation, is the most common proxy for the amount of vertical displacement on normal faults. In some cases, scarp height (H, fig. 1) is the only indicator of net displacement.

For elapsed time between rupture events, often we can obtain minimum-limiting dates from charcoal in unfaulted materials (overlapping alluvium or fault-scarp colluvium) and (or) maximum-limiting dates from the faulted materials (that is, from a buried A horizon or charcoal from faulted materials). Consider the following example of typical dating control as illustrated in figure 1. Charcoal from the middle of a colluvial wedge is dated at 1000 yr B.P. (sample 2 in fig. 1). The charcoal is younger than the faulting by tens to hundreds of years, the time needed to accumulate the colluvial wedge. For a maximum age limit, assume that a soil that formed prior to faulting (sample 4, fig.1) is buried by colluvium on the downdropped fault-block. The soil yields an age of 1500 yr B.P., but because the organic matter in the soil requires time to accumulate (perhaps 200-400 yr), the 1500 yr age reflects the sum of the mean residence age (MRT) of the organic matter (perhaps 100-300 yr at the time of burial) plus the time since the soil was buried by fault-scarp colluvium. On the basis of these dates one should argue that faulting occurred before 1000 yrs B.P. and after 1500 yr B.P. (or perhaps after 1300-1400 yr B.P. if one considers the MRT of the buried soil). In this hypothetical but traditionally well-contrained case, the time window for faulting is as large as 500 yr (1000 to 1500 yr B.P.) irrespective of analytical errors in radiocarbon dates. (The analytical errors associated with ^{14}C dates of 500-1500 yr are commonly 50 to 100 yr or more, and unreported laboratory errors may exceed this.) By using geologic and soil relations, the window for most probable time of faulting could be narrowed to 1100-1300 yr B.P. (a 200 yr window). This example and published data show that the times of faulting rarely are well contrained (that is, within several hundred years for Holocene events), thus recurrence intervals also are poorly constrained. As illustrated in figure 1, dates that most closely approximate the time of faulting come from material in two stratigraphic positions: (1) the proximal-basal (oldest) part of a colluvial wedge (sample 3) or (2) the proximal portion of the downdropped surface (sample 4), which is the first part buried by colluvium.

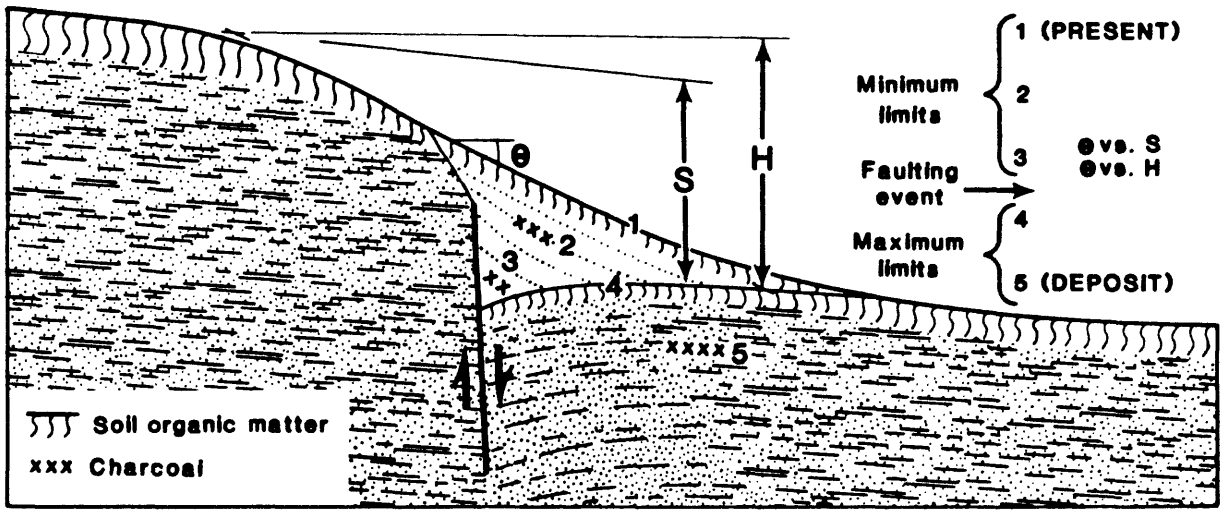

FIGURE 1.--Hypothetical cross section of a faulted deposit showing potential sampling locations (small numbers) and common contraints on the time of faulting. The symbols *0*, S, and H indicate maximum scarp-slope angle, surface offset, and scarp height, respectively. Estimates of scarp age are commonly based on empirical models or diffusion-equation models of *0* versus H or S.

CUMULATIVE SLIP RATES THROUGH TIME AS A RESULT OF LARGE CYCLIC CHANGES IN SLIP RATE

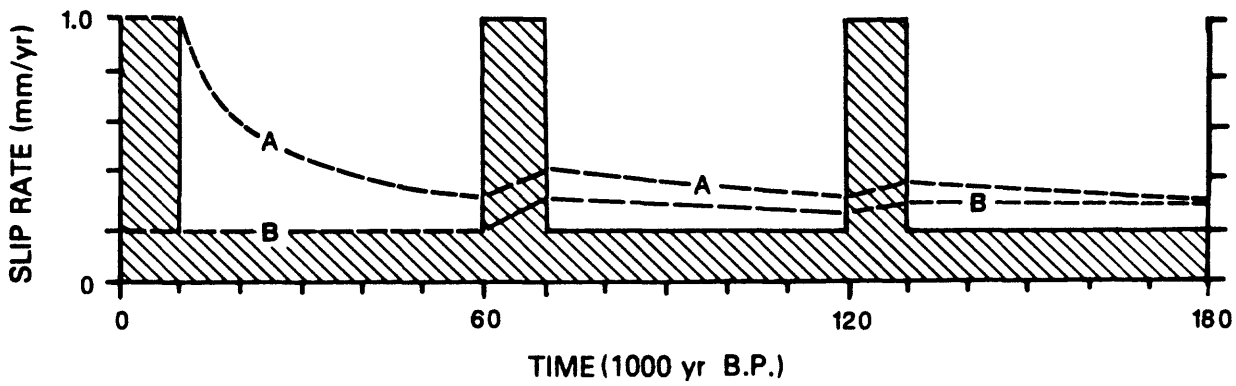

FIGURE 2.--Hypothetical *average* slip rates through time. Model is based on 5X change in slip rate: high rate (1.2 mm/yr) during short intervals (10,000 yr) and low rate (0.2 mm/yr) during long intervals (50,000 yr). Line A--rates if most recent interval is high; line B--rates if most recent interval is low..

In the worse cases of control on time of faulting, the age of a faulted surface (or deposit) is inferred from correlation with nearby dated features (or materials). If the correlation is correct, one still only has a maximum time limit. Trenches often expose datable materials, but usually they are not deep enough to unravel a long tectonic record. In addition, trenches are dangerous to excavate and can be expensive and time consuming, and thus often are not feasible. In urban areas the best sites might not be available and in arid regions datable materials usually are sparse. Considering the practical and scientific limitations on determining time of faulting and displacement, most calculated slip-rate values are approximations; they should be reported as a range of values based on uncertainties in displacement and recurrence interval, perhaps with a favored (most probable?) value based on geologic considerations.

The time interval for which slip rates are calculated can be a critical factor in comparisons of slip rate. For example, Gardner and others (1987) show that comparisons of slip rates for vastly different lengths of time (that is, intervals that vary by 4 or 5 orders of magnitude) can indicate an apparent 5-10X increase in rate solely from inherent time-dependent relations. However, when comparing Quaternary slip-rates over intervals of 10,000 yr versus 100,000 yr (one order of magnitude), this factor should not cause more than a 2X change in apparent rates.

Long intervals (that is, 100,000's yr) tend to dampen (average) large changes in slip rate, whereas short intervals tend to emphasize recent slip rates (fig. 2) whether they are high or low. For example, lines A and B in figure 2 illustrate the average slip rates through time that result from a model of cyclic, large-scale (5X) changes in slip rate (that is, tectonic episodes). From this illustration, you can see that after a fault has passed through at least one full cycle of slip rate change (0-60,000 yr B.P. in fig. 2), slip rates for intervals that encompass multiple cycles will be little influenced by the presence or lack of a recent episode of high slip rates (compare lines A and B in fig. 2). Thus, if there is evidence of a recent and large change in slip rate, one should be cautious of interpretating slip rates over intervals shorter than one full cycle.

The age of deposits which record net slip across normal faults is also a factor in calculation of slip rates. For example, assume that a 150 ka alluvial fan records 30 m of slip from numerous faulting events. If one simply uses the age of the deposits and the net slip, you get a slip rate of 0.2 mm/yr. However, this value is a *minimum average rate* because faulting may have started well after deposition the alluvium and because the most recent event may have been well in the past. If 50,000 yr is encompassed by these two periods of quiescence, then the average slip between the oldest and youngest recorded events would be 0.3 mm/yr (30 m/100,000 yr), or 50 percent higher than previously calculated. In addition, if faulting events are clustered into tectonic episodes as shown in figure 3, then slip rates could range widely if the datums (faulted deposits) happen to sample or miss these tectonic episodes.

Thus, one must look closely at the types of data used to calculate slip rates, the intervals for comparisons of slip rate, and the apparent changes indicated by such comparisons.

EXAMPLES OF CHANGES IN SLIP RATE THROUGH TIME

There are several good examples of both temporal and spatial changes in slip rate from the Basin and Range province. The first example involves Neogene tectonism along the Snake River Plain in the northeastern Basin and Range province. Scott and others (1985) show that range-front faulting and block uplift (associated with very high slip rates) propagated eastward along and outward from the southern margin of the Snake River Plain during the past 15 Ma in response to eastward migration of the Yellowstone hotspot. The wave of tectonism that formed the basins and ranges adjacent to the Snake River Plain lasted about 2 m.y. in each range (Pierce and Scott, 1986) and resulted in deformation that is progressively younger eastward between ranges and southward within ranges.

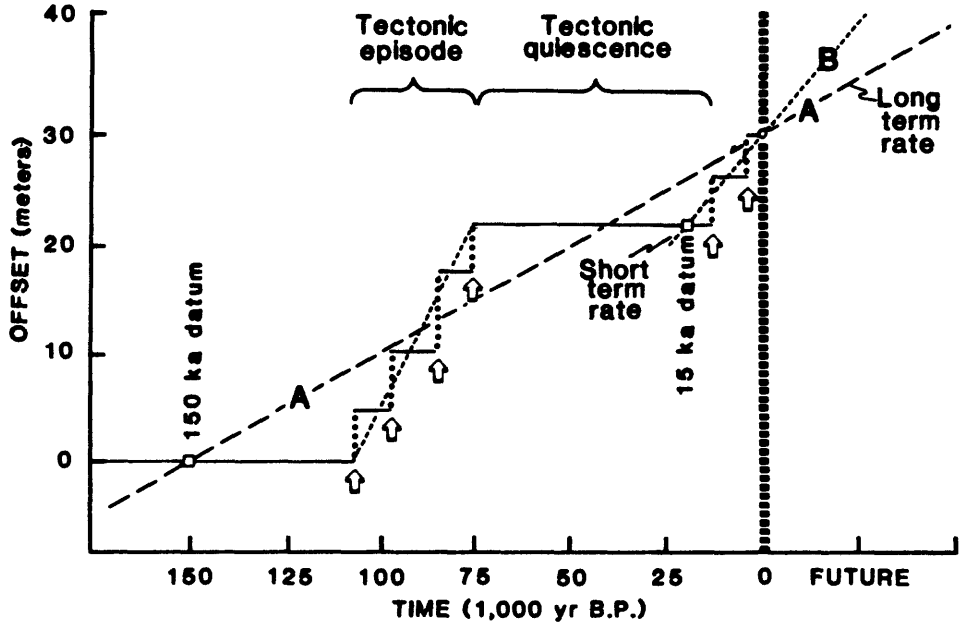

FIGURE 3.--Calculations of slip rates through time illustrating the effects of age of faulted datum, window of slip rate calculation, and cyclic patterns (temporal clustering or tectonic epidoses) of fault activity. Line A indicates a long-term slip rate of 0.2 mm/yr calculated from age of older datum (150 ka) and 30 m of net offset. Line B indicates a short-term slip rate of 1.5 mm/yr calculated from age of younger datum (15 ka) and 10 of net offset.

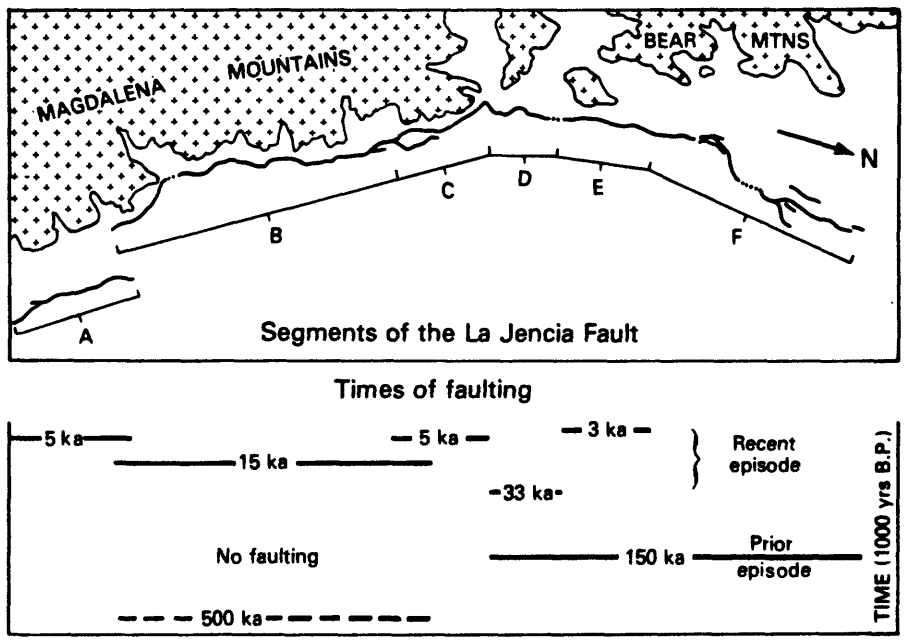

FIGURE 4.--Map of the La Jencia fault, central New Mexico, showing segments and times of faulting since the middle Quaternary (modified from Machette, 1986). Capital letters identify segments of the fault.

To the southwest in the central Basin and Range, Wallace (1987) documented a similar spacial pattern of deformation. His study of tilted Miocene basalts that cap the crests of two adjacent ranges in Nevada shows that the ranges were formed by mountain-building episodes at distinctly different times, even though they are in nearly identical geologic environments. He found that during the past 10-14 m.y., the East Range was tilted early in its history whereas the adjacent Cortez Range was tilted significantly later. This disparate history is expressed as a prominent, sharp range front along the young Cortez Mountains, and a deeply embayed and eroded range front along the older East Mountains. These two examples from the Basin and Range province show that mountain building (a long-term process) can be nonuniform in time and space, even within fairly small areas such as subprovinces.

The age of movement and distribution of Quaternary faults in the Basin and Range province suggest that temporal grouping of surface faulting events is common. Bucknam and others (1980) show that the province can be divided into areas that have different times of the most recent surface faulting. This regional zonation of paleoseismic activity is a product of migration of faulting through time, wherein large areas are tectonically active while adjacent areas remain relatively inactive. Similar patterns of paleoseismic zonation are being recognized in the Rio Grande rift of New Mexico (Machette, 1987) through a systemmatic reconnaissance mapping of Quaternary faults.

The Central Nevada Seismic Belt illustrates short-term temporal clustering of seismic activity. The seismic belt is characterized by a concentration of historic, large-magnitude earthquakes each of which formed long surface ruptures on an average of once every 15-20 yr. The pattern of rupturing suggests that the belt is being sequentially filled by faulting events (Wallace, 1984, 1987). If and when rupturing is completed by filling the two remaining seismic gaps in the belt, activity might shift to another major fault zone in the region or reactive a paleoseismic belt that is not now active. In fact, Pearthree and Demsey's (1987) study of prehistoric fault scarps of the Central Nevada Seismic Belt suggests that individual faults have recurrence intervals of several thousand years.

The La Jencia fault is a major range-bounding fault on the west margin of the Rio Grande rift in central New Mexico. This fault shows a pattern of late Quaternary seismicity that is similar to the currently active Central Nevada Seismic Belt--that is, one of a tectonic episode marked by clustering of rupture events on segments of a fault. Trenching along this fault reveals a long history of quiescence that was terminated by sequential rupture of six segments during the past 33 ka (Machette, 1986). Prior to the most recent episode of faulting, individual fault segments were inactive for periods of 100,000 yr or more (fig. 4). Filling of unruptured segments along the fault was completed in the past 3-5 ka with rupturing along three discrete segments. Five or six discrete paleoearthquakes of estimated magnitude 7 occurred along the fault over an interval of about 30,000 yr, thus the average recurrence interval during the recent tectonic episode is 5000-7500 yr. Some major faults in the rift have recurrence intervals of only 20,000-30,000 yr, but more commonly the intervals are as much as 100,000 yr (Machette, 1987). The recent flurry of activity on the La Jencia fault is striking when compared to evidence for Holocene movement on only nine other faults in the Rio Grande rift of New Mexico.

CHANGES IN LONG-TERM VERSUS SHORT-TERM SLIP RATES

There are but a few well-dated fault histories that permit accurate analyses of changes in slip rate. In addition, slip rates derived from faults that have cyclic patterns of tectonism as shown in figures 2 and 3 can lead to erroneous interpretations of tectonic activity. Nevertheless, the differences in slip rate recorded over short, intermediate, and long intervals on some faults reflect real changes in rates of movement. Dating of Holocene surface ruptures along the Wasatch fault zone (see Schwartz and Coppersmith, 1984; Machette and others, 1987) and estimates of net slip recorded in 12-15 ka and 150-250 ka deposits along the fault zone suggest as much as a 5-10 fold increase in average slip rate during the past 15 ka (fig. 5; Machette and others, 1986, 1987). Holocene slip rates are typically 1-2 mm/yr, but evidence from some sites

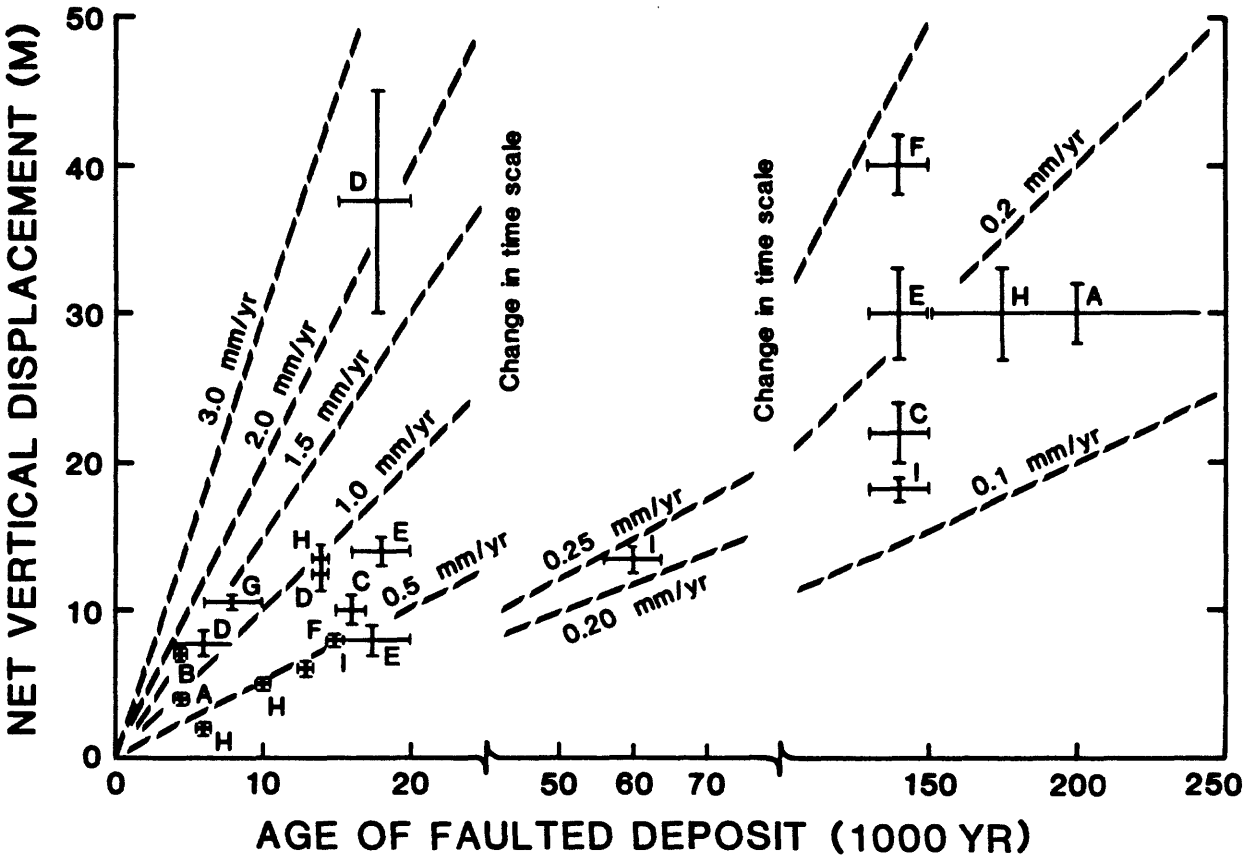

LOCATIONS OF SLIP-RATE DETERMINATIONS

A-- Gardner Creek, Nephi segment, Wasatch fault zone
B-- North Creek, Nephi segment, Wasatch fault zone
C-- Santaquin Valley, Nephi segment, Wasatch fault zone
D-- Hobble Creek, Spanish Fork segment, Wasatch fault zone
E-- Dry Creek, American Fork segment, Wasatch fault zone
F-- Big and Little Cottonwood Creeks, Salt Lake City segment, Wasatch fault zone
G-- Kayswille, Weber segment, Wasatch fault zone
I -- Granger fault, West Valley fault zone (Keaton and others, 1987)

FIGURE 5.--*Average* slip rates determined for the Wasatch and West Valley fault zones, Utah, over three time spans. Letters indicate locations listed in the table; matching letters (A, C, E, F, H, and I) show evidence for large temporal changes in slip rate. Vertical and horizontal bars indicate range in probable amount of slip and age of faulted deposits. Slip rates are shown by dashed lines. Note changes in horizontal time scale and thus slip rates versus slope on the graph. (Modified from Machette and others, 1987, fig. 5).

along the fault zone suggests that slip rates between 12 ka and 15 ka might have exceeded 4 mm/yr. In contrast, the average rates recorded by the older (150-250 ka) deposits are only 0.1-0.3 mm/yr. This large increase in average slip rate could be related to tectonic cycles and (or) to the catastrophic draining of Lake Bonneville, which occurred about 15 ka. Overflow and inci-sion of the lake's sill at Red Rock Pass dropped the level of Lake Bonneville as much as 100 m: this drop was accompanied by rapid isostatic rebound of the Bonneville basin. Further draw-down of the lake to near-present level occurred by about 11 ka and was accompanied by more rebound. This rebound--upward flexing of the earth's crust--may have stimulated extension on the Wasatch fault zone--the primary structure separating the Colorado Plateaus and Middle Rocky Mountains provinces from the Basin and Range province.

APPARENT PATTERNS OF SLIP (EXTENSION)

As previously mentioned, patterns of slip rates must be interpreted carefully. To illustrate some of these cares, let us consider a model of rupturing on segments of a fault zone that is driven by a process that assigns the next rupture to a randomly chosen segment regardless of which segment ruptured last (fig. 6). Although faulting is not a random processes, their driving mechcanisms might be deterministic processes complex enough to create a record indistiguishable from that of a random process. The parameters selected are similar to values determined by Schwartz and Coppersmith (1984) for the Wasatch fault zone: they include a fault zone having 5 segments and one faulting event every 400 yr (*overall* recurrence interval, ri) somewhere on the zone. The average recurrence interval for each individual segment (RI) should average 2000 yr. The timing of movement on individual segments was dictated by a random number sequence (n=1-5) that was allowed run for 38 iter-ations (equivalent to 15,000 yr).

Figure 6 shows the result of this modeling process. This process resulted in several interesting, albeit artificial, patterns of fault movement and estimates of recurrence intervals. Data for the Holocene (past 10 ka) are tabulated in the right-hand column of figure 6, although values for the past 15 ka are not much different. First of all, the number of events (shown by black bands) on any one segment varies from 4 to 7, whereas the average should be 5 (25 events in 10 ka on 5 segments). Secondly, on two segments the most recent event (MRE) exceeds 2 ka, the value one would expect if segments filled in an orderly manner. Thirdly, the *average* of recurrence intervals on individual segments (RI) varies from as little as 1300 yr to as much as 2300 yr (on 3 segments) and individual recurrence intervals range from 400 yr to 5600 yr. If this model were allowed to run for many recurrence intervals, the long term averages of number of earthquakes and RI would stablize about their expected values. Nevertherless, this example illustrates the degree of temporal and spacial variability that can occur and interpretations that might drawn from patterns of faulting. For example, the occurrence of some clusters and laterally sequential patterns might lead one to draw inappropriate conclusions about the processes responsible for generating earthquakes. It also shows how unreliable inter-pretations of slip-rate patterns and faulting-mechanisms can be if you only have 2 or 3 dated faulting events (a 6 ka record in this example). However, some of the simulated patterns are strikingly similar to patterns evolving for segments of the Wasatch fault zone (Machette and others, 1987).

CONCLUSIONS

The several examples mentioned here illustrate spacial and temporal patterns of faulting in the Basin and Range province and Rio Grande rift, two large extensional terrains of the United States. Nonuniformity of faulting seems to typify the Quaternary and temporal clustering and spacial migration of faulting seem to be two processes that are wide-spread in the Western United States. At the present time, meaningful comparisons of changes in slip rate are severely handicapped by a paucity of high-quality data. Although few faults in the region have well-dated histories of movement, recent trenching efforts are producing excellent results. Finally, the disparity between short- and intermediate-term slip rates on some faults demands that cyclic episodes of faulting occur on some major faults in extensional environments.

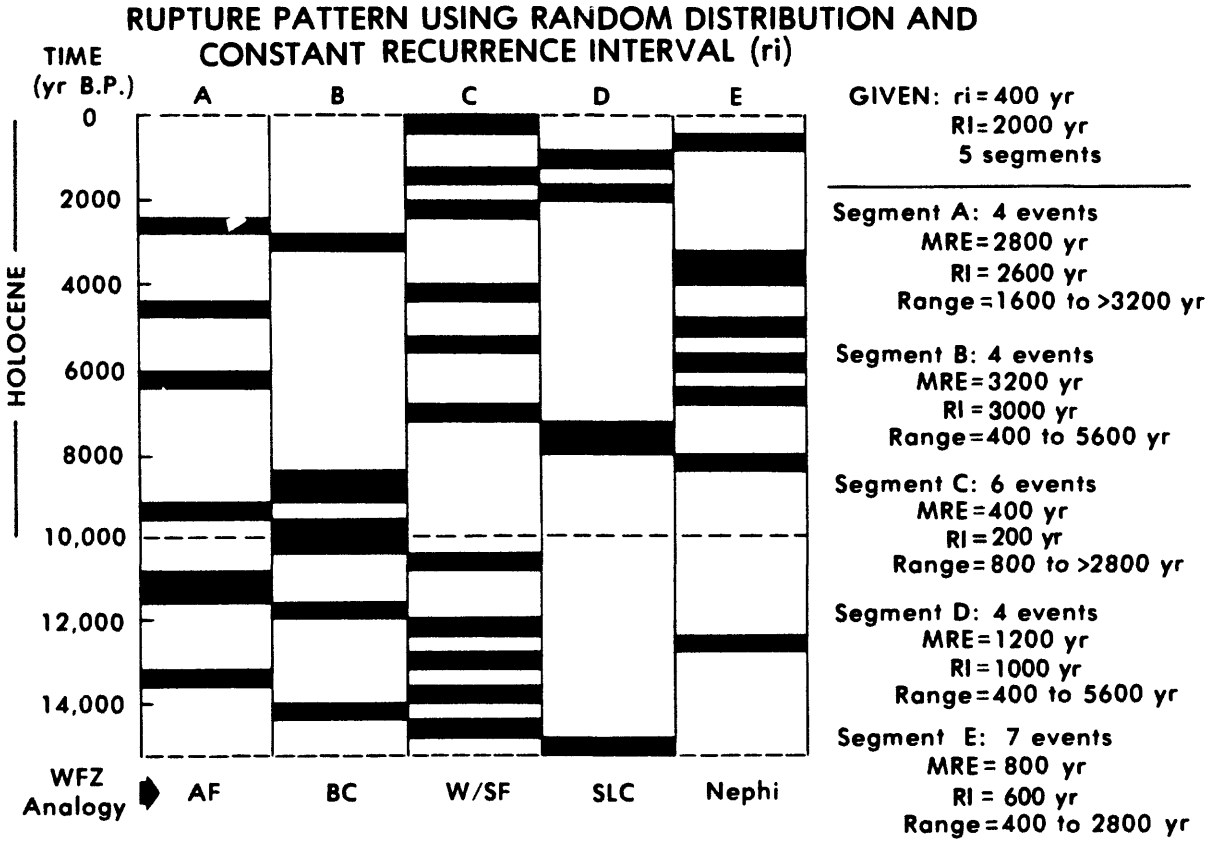

FIGURE 6.--Simulated patterns of faulting that result from a random distribution of fault activity on five hypothetical segments of a fault zone. Black bands indicate time intervals (400 yr long) in which faulting occurs. The right-hand column shows calculated values for the time of most recent faulting event (MRE), *average* recurrence intervals on segments (RI), and *overall* recurrence interval (ri) for the whole fault zone. Also shown are segments of the Wasatch fault zone (WFZ) which have similar patterns of movement. These segments are AF-American Fork, BC-Brigham City, W/SF-Weber or Spanish Fork, SLC-Salt Lake City, and Nephi (see Machette and others, 1987, for definition and location of segments).

REFERENCES CITED

Bucknam, R.C., Algermissen, S.T., and Anderson, R.E., 1980, Patterns of late Quaternary faulting in western Utah and an application in earthquake hazards evaluation, *in* Proceedings of Conference X, Earthquake Hazards along the Wasatch and Sierra-Nevada frontal fault zones: U.S. Geological Survey Open-File Report 80-801, p. 299-314.

Bull, W.B., 1984, Tectonic geomorphology: Journal of Geological Education, v. 32, p. 310-324.

Gardner, T.W., Jorgensen, D.W., Shuman, G., and Lemieux, C.R., 1987, Geomorphic and tectonic process rates--Effects of measured time interval: Geology, v. 15, p. 258-261.

Keaton, J.R., Currey, D.R., and Olig, S.J., 1987, Paleoseismicity and earthquake hazards evaluation of the East Valley fault zone, Salt Lake City urban areas, Utah: Report to U.S. Geological Survey for Contract No. 14-08-0001-22048, March 6, 1987, 55 p., 33 p. appendix.

Machette, M.N., 1986, History of Quaternary offset and paleoseismicity along the La Jencia fault, central Rio Grande rift, New Mexico: Bulletin of the Seismological Society of America, v. 76, p. 259-272.

_____1987, Neotectonics of the Rio Grande rift, New Mexico: Geological Society of America Abstracts with Programs, v. 19, no. 7, p. 754.

Machette, M.N., Personius, S.F., and Nelson, A.R., 1986, Late Quaternary segmentation and slip-rate history of the Wasatch fault zone, Utah: Eos (Transactions, American Geophysical Union, v. 67, no. 44, p. 1107.

Machette, M.N., Personius, S.F., and Nelson, A.R., 1987, Quaternary geology along the Wasatch fault zone--Segmentation, recent investigations, and preliminary conclusions, in Hays, W.W., and Gori, Paula, eds., Assessment of Regional Earthquake Hazards and Risk along the Wasatch Front, Utah: U.S. Geological Survey Open-File Report 87-585, v. 1, p. A1-A72.

Naeser, C.W., Bryant, Bruce, Crittenden, M.C., Jr., and Sorensen, M.L., 1983, Fission-track ages of apatite in the Wasatch Mountains, Utah--An uplift study, in Miller, D.M., Todd, V.R., and Howard, K.A., eds., Tectonic and stratigraphic studies in the eastern Great Basin: Geological Society of America Memoir 157, p. 29-36

Parry, W.T., and Bruhn, R.L., 1986, Pore fluid and seismogenic characteristics of fault rock at depth on the Wasatch fault, Utah: Journal of Geophysical Research, v. 91, no. B1, p. 730-744.

Pearthree, P.A., and Demsey, Karen, 1987, Patterns of Holocene faulting and the rate of extension in central Nevada: Geological Society of America Abstracts with Programs, v. 9, no. 7, p. 802.

Pierce, K.L., and Scott, W.E., 1986, Migration of faulting along and outward for the track of thermovolcanic activity in the eastern Snake River Plain region during the last 15 m.y.: Eos (Transactions, American Geophysical Union), v. 67, no. 44, p. 1225.

Schwartz, D.P., and Coppersmith, K.J., 1984, Fault behavior and characteristic earthquakes--Examples from the Wasatch and San Andreas fault zones: Journal of Geophysical Research, v. 89, no. B7, p. 5681-5698.

Scott, W.E., Pierce, K.L., and Hait, M.J., Jr., 1985, Quaternary tectonic setting of the 1983 Borah Peak earthquake, central Idaho: Bulletin of the Seismological Society of America, v. 75, no. 5, p. 1053-1066.

Wallace, R.E., 1984, Patterns and timing of late Quaternary faulting in the Great Basin province and relation to some regional tectonic features: Journal of Geophysical Research, v. 89, no. B7, p. 5763-5769.

_____1987, Variations in slip rates, migration, and grouping of slip events on faults in the Great Basin province: Bulletin of the Seismological Society of America, v. 77, no. 3, p. 868-876

TEMPORAL CLUSTERING OF PALEOSEISMIC EVENTS ON THE OUED FODDA FAULT, ALGERIA

by

F.H. SWAN

Geomatrix Consultants
One Market Plaza
Spear Street Tower, Suite 717
San Francisco, California 94105

ABSTRACT

Paleoseismic investigations of the Oued Fodda fault, which experienced surface-fault rupture during the 10 October 1980 Algeria earthquake (M_s 7.3), indicate that the average recurrence interval based on the long-term geologic slip rate (past 10^5 years) is at least an order of magnitude longer than the intervals between recent surface-faulting events based on radiocarbon dating of faulted colluvial deposits. Evidence from trenches excavated across the 1980 surface rupture indicate there have been at least three and possibly four surface-faulting events on the Oued Fodda fault during approximately the past 1,500 years (including the 1980 earthquake). The ages of the three most recent events are well constrained. The most recent event occurred in 1980; the second-most-recent surface-faulting event occurred before 320 ± 220 ^{14}C yr B.P. and after 875 ± 240 ^{14}C yr B.P.; and the third-most-recent event occurred just prior to deposition of a layer containing charcoal dated at 875 ± 250 ^{14}C yr B.P. (that is approximately 900 years ago). The average interval between the three most recent surface-faulting events on the Oued Fodda fault has been approximately 450 years. The cumulative slip on the Oued Fodda fault was produced by relatively short episodes characterized by frequent displacements (surface-faulting events every few hundred years) separated by long periods of quiescence lasting several thousands to tens of thousands of years.

INTRODUCTION

The 10 October 1980 El Asnam (now Ech Cheliff), Algeria, earthquake (magnitude M_s 7.3) was generated by reverse slip on the Oued Fodda fault. The fault is a northeastward-striking reverse fault that dips 50 to 60 degrees to the northwest (fig.1). The earthquake, the associated surface rupture, and the geometry of the faulting have been investigated extensively and are described in numerous papers (for example Espinosa, 1980; Ambraseys, 1981, 1983; King and Vita-Finzi, 1981; Mahdjoub and others, 1981; Ouyed and others, 1981, 1983; Yielding and others, 1981; Cisternas and others, 1982; Ouyed and Hatzfield, 1982; Deschamps and others, 1982; and Philip and Meghraoui, 1983). Except for a brief reference in a paper by King and Vita-Finzi (1981), who postulate that one or two events similar to the 1980 earthquake may have caused the apparent warping of an alluvial terrace that they estimate to be about 500 years

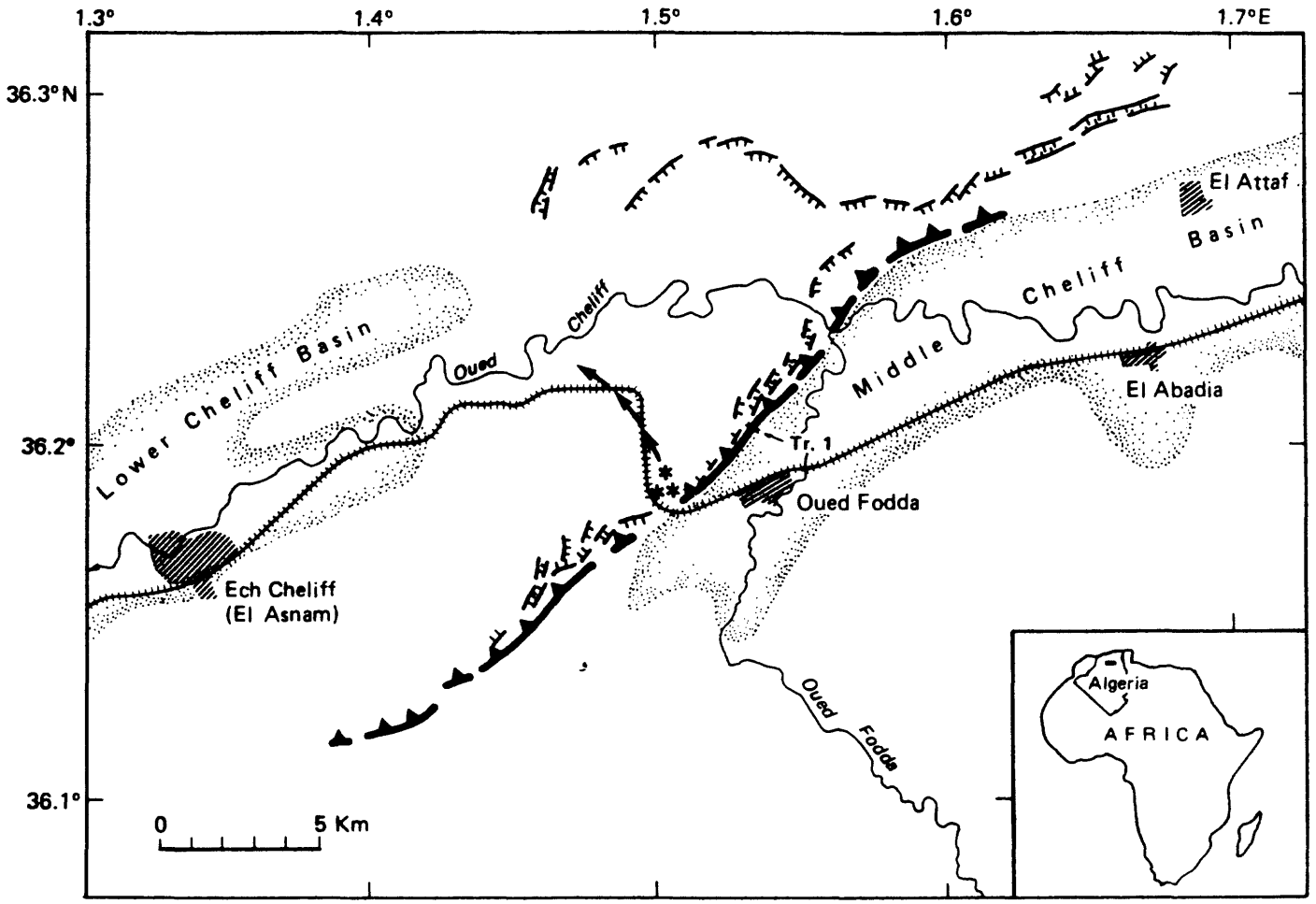

EXPLANATION

Outcrop of ancestral Oued Fodda gravel (*) and approximate location of paleochannel across fault/fold (arrows)

Tr. 1 Oued Fodda Trench No. 1

Primary thrust, teeth on hanging-wall side

Secondary normal fault, hachures on foot-wall side

Railroad

FIGURE 1. -- Location map showing generalized pattern of 1980 surface faulting along the Oued Fodda fault. Modified from Philip and Meghraoui, 1983.

little has been reported about the geologic evidence of paleoseismic events on the Oued Fodda fault.

Detailed paleoseismic investigations were conducted along the fault as part of a regional seismic microzonation study of the Ech Cheliff Region (Woodward-Clyde Consultants, 1984; Swan and others, 1984). Data from this study permit the comparison recurrence intervals based on long-term Quaternary strain rates to short-term estimates based on paleoseismic evidence observed in trenches excavated across the 1980 surface rupture. The data provide new information on the nature of the long-term seismic cycle and demonstrate the temporal clustering of large-magnitude earthquakes on this compressional fault.

RECURRENCE ESTIMATES BASED ON LONG-TERM SLIP RATE

At present, there are no well-dated Pleistocene marker horizons that can be used to determine the actual long-term rate of deformation on the Oued Fodda fault. Maximum limiting rates of deformation can be estimated based on: 1) an uplifted fluvial gravel deposited along an ancestral course of the Oued Fodda, and 2) the maximum cumulative displacement of a well-developed paleosol across the primary trace of the Oued Fodda fault.

West of the town of Oued Fodda, an ancestral channel of Oued Fodda crosses the Oued Fodda fault and adjacent anticline (fig. 1). Crossbedded alluvial gravels crop out in a roadcut on the north side of a beheaded valley near the axis of the anticline at a height of about 50 m above the present channel of Oued Fodda. The crossbedding indicates a northerly flow direction, and the composition of the gravels indicates a southern provenance similar to that of the modern alluvium along the present channel of Oued Fodda. The correlative gravels along the axis of the syncline to the southeast on the downthrown side of the Oued Fodda fault cannot be more than 50-100 m below the modern channel (that is the total thickness of the valley fill); the gravels could be much shallower. Therefore, the maximum vertical structural relief on this gravel deposit (both faulting and folding) across the Oued Fodda structure is 100-150 m.

The ancestral gravels are incised into and lie below Upper Pliocene (Vilafrancian ?) bedrock that underlies the anticline. Therefore, they are younger than 1.8 m.y. old. The gravels predate a well-developed paleosol that formed on a surface which is inset topographically below the paleochannel. The paleosol is probably about 100,000 years old (see below). Based on the stratigraphic position of the gravels and the regional geomorphic relationships, the gravels are probably closer in age to the red paleosol and are inferred to be between 500,000 and 750,000 years old. Using the maximum amount of structural relief on the ancestral gravels (less than or equal to 150 m) and their minimum inferred age (500,000 years), the maximum rate of vertical uplift (folding and faulting) is less than or equal to 0.3 mm per year.

Geodetic measurements along the railroad immediately south of this exposure indicate the vertical deformation due to both faulting and folding associated with the 1980 earthquake was 6 m; the northwestern side of the fault was uplifted 5 m, the southeastern side subsided 1 m (Ruegg and others, 1982). The displacement across the 1980 surface rupture

immediately north of the railroad was 1.65 m (that is vertical displacement on the primary reverse fault). If the ratio of vertical uplift on the fold to the vertical displacement on the fault during the 1980 earthquake (6 m versus 1.65 m or 3.6 to 1) is representative of past surface faulting events, the long term vertical slip rate on the Oued Fodda fault is less than or equal to 0.08 mm per year.

Extensive remnants of a well-developed red paleosol (Munsell soil color - 2.5 YR 4/6) are present locally on both the upthrown and downthrown sides of the fault along nearly the entire length of the fault. The paleosol occurs both as a relict soil at the surface and as a buried soil beneath younger Quaternary deposits. The soil is characterized by a well-developed textural B2t horizon that has continuous, well-developed clay films on the ped surfaces, and contains up to 20-30 percent clay, an increase of approximately 15-20 percent compared to the unweathered parent material. The paleosol ranges from about 1 m to more than 2 m thick. In many places, where the paleosol is at or near the ground surface, the paleosol is associated with a well-developed calcium carbonate horizon. The stage of carbonate accumulation (Gile and others, 1966) is typically stage-II, but stage-III development is common and stage-IV development was observed locally. Based on the geomorphic and stratigraphic position of the paleosol, the degree of weathering and soil-profile development, and the amount of erosion of the landscape subsequent to the soil's formation, the paleosol is probably as old as, or older than paleosols recognized worldwide that formed during the most recent major interglacial epoch (oxygen isotope stage 5 of Shackleton and Opdyke, 1973, 1976). This suggests a minimum age of approximately 100,000 years for the paleosol.

The distribution of the paleosol on both sides of the Oued Fodda fault indicates that the maximum cumulative vertical displacement across the fault since the soil was formed is less than or equal to about 10 m. Therefore, the average rate of vertical displacement is probably less than or equal to about 0.1 mm per year. This rate is consistent with the estimated long-term rate (vertical fault displacement) of less than or equal to 0.08 mm per year based on the uplifted ancestral Oued Fodda fluvial gravel.

The average return period for surface-faulting events similar to the 1980 earthquake can be calculated for the section of the fault east and north of Oued Fodda based on the long-term slip rate on the fault and the displacement per event data for this part of the fault. The vertical displacements on the primary reverse fault measured following the 1980 earthquake typically ranged from about 1.5 to 2.5 m along this part of the fault. If this range of displacement was characteristic of past events, a maximum slip rate of 0.1 mm per year suggests an average repeat time of 15,000-25,000 years.

Alternatively, the average repeat time can be calculated based on the moment rate. Based on an average fault dip of 55° (Deschamps and others, 1982) and assuming an average rate of vertical slip along the length of the fault of $\leq$ 0.1 mm per year (the vertical rate on the primary thrust near Oued Fodda) to 0.3 mm per year (the maximum limiting value for the rate of vertical deformation due to faulting and folding near Oued Fodda) gives an average long-term slip rate of $\leq$ 0.13-0.4 mm per year (dip

slip). The total length of the fault is 47 km (Woodward-Clyde Consultants, 1984). The fault width is estimated to be 15 km based on a maximum fault depth of 12 km and an average dip of about 55 degrees. Twelve kilometers is the average maximum depth of seismicity in the area (Ambraseys, 1981; Ouyed and others, 1981; Cisternas and others, 1982; Yielding and others, 1981). Following the procedure outlined in Brune (1968), these parameters yield a moment rate of $\leq 2.1 \times 10^{22}$ to 6.3×10^{22} dyne-cm per year. If all the displacement was produced by slip events of similar size to the 1980 earthquake, which had a seismic moment of 5×10^{26} dyne-cm, the average return period for this size event would be about 8,000 years to more than 24,000 years.

TIMING OF RECENT EVENTS BASED ON RESULTS OF TRENCHING

Trenches excavated across the 1980 surface rupture north of Oued Fodda (fig. 1) exposed faulted colluvial deposits containing small fragments of charcoal that have been dated using accelerator mass spectrometer techniques. A schematic log of Oued Fodda trench no. 1, showing the relationship of the faulting to the main depositional units and the locations of the dated radiocarbon samples, is presented in figure 2. Figure 3 summarizes the recent history of faulting and deposition reconstructed from the evidence in this trench.

There have been at least three and possibly four surface-faulting events on the Oued Fodda fault during approximately the past 1,500 years (including the 1980 earthquake), The fact that the cumulative vertical displacement of unit 1a (fig. 2) is greater than 5 m, which was the depth exposed in the trench, indicates that there were also earlier events at this location. The ages of the three most-recent events are well constrained (fig. 3). The most recent event occurred in 1980. The second-most-recent event occurred before 320 ± 220 ^{14}C yr B.P. and after 875 ± 240 ^{14}C yr B.P. The third-most-recent event occurred between 875 ± 240 ^{14}C yr B.P. and 960 ± 250 ^{14}C yr B.P., that is, approximately 900 years ago. Therefore, the average interval between the three most-recent large magnitude earthquakes produced by surface-fault rupture on the Oued Fodda fault has been approximately 450 years.

DISCUSSION OF RESULTS

The late Quaternary slip rate on the Oued Fodda fault is poorly constrained. Nonetheless, there is at least an order of magnitude difference between the recurrence intervals calculated on the basis of the long-term (late Quaternary) slip rate and the actual interval between the most recent series of events. Even if the ages assigned to the ancestral Oued Fodda gravel and the red paleosol are too old by a factor of 2 or 3, there would still be a marked contrast between the average long-term recurrence and the actual intervals between the recent events. It is more likely that the ages assigned to these features are too young. The paleoseismic data indicate that the cumulative slip on the Oued Fodda fault was produced by short episodes characterized by frequent displacements (surface-faulting events every few hundred years) separated by long periods of quiescence.

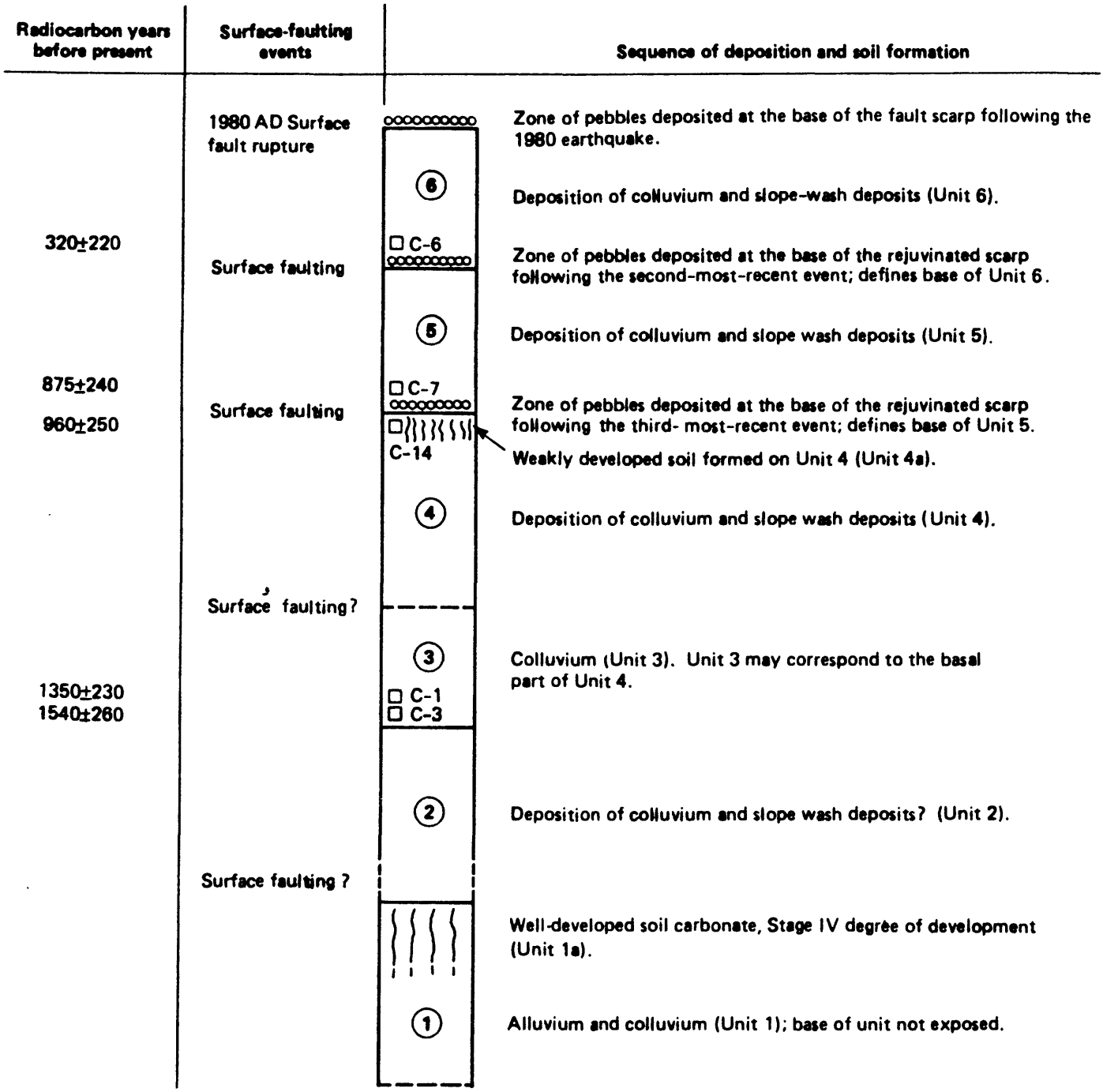

FIGURE 3. -- Sequence of faulting and deposition at Oued Fodda, Trench No. 1. Trench log is shown in figure 2.

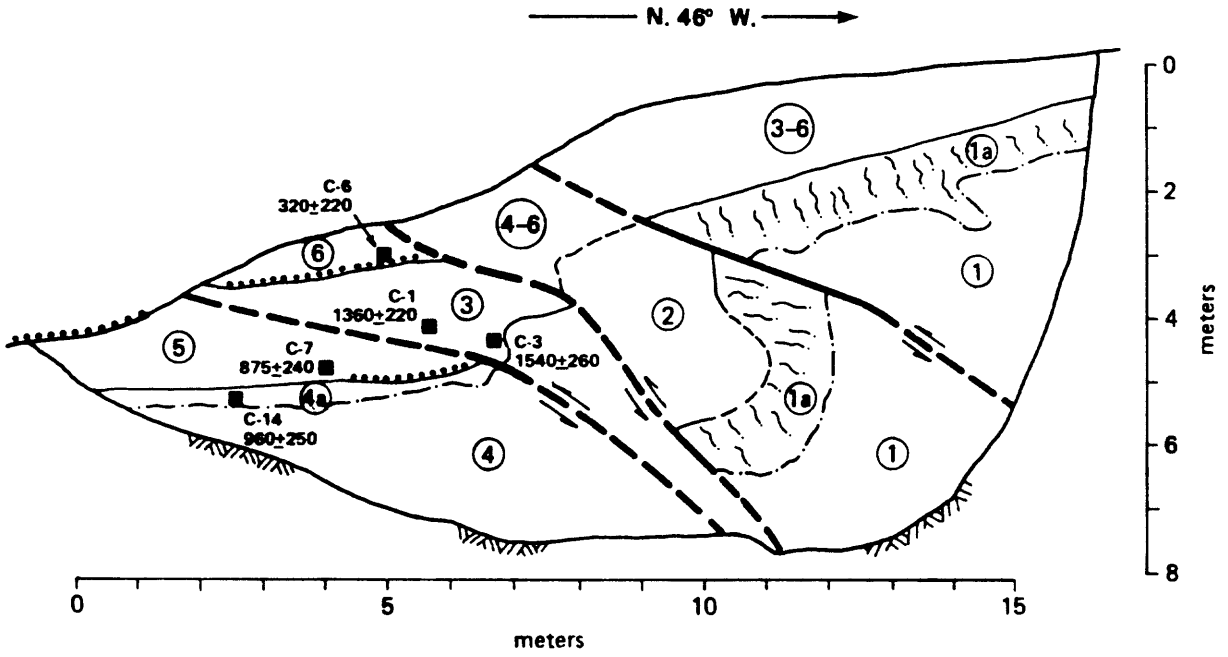

UNIT DESCRIPTION

6, 5, 4, 3, 2 — Recent colluvial deposits

1a — Soil carbonate

1 — Older alluvial and colluvial deposits

EXPLANATION

Depositional contact

Approximate lower boundary of buried soil

Fault

Pebble lines formed at base of fault scarp following the three most recent events

Radiocarbon sample number and age (^{14}C yr. B.P.)

FIGURE 2. -- Schematic log of Oued Fodda Trench No. 1.

There are no data on the actual duration of the quiescent periods between the active phases of the seismic cycle. If the cycles are uniformly spaced, the quiescent periods between the active phases on the Oued Fodda fault must last several thousands to tens of thousands of years.

Paleoseismic data in general and slip-rate data in particular are now being used extensively in the assessment of seismic hazards. The results of this study indicate the importance of understanding the late Quaternary history of faulting. In cases like the Oued Fodda fault, hazard assessment based only on long-term slip rate data would grossly underestimate the hazard. In other cases, where a fault may be in the dormant phase of the cycle, use of long-term slip rate data may overestimate the hazard. On the other hand, ignoring the long-term behavior of the fault in these cases and focussing only on the recent history of faulting, could result in the failure to consider faults that may be potentially active and might pose a serious hazard.

There have been too few studies to tell if temporal clustering of events is a common characteristic of Quaternary active faulting. Perhaps it is more common to certain tectonic environments; for example it may be more common to interplate regions or it may be more characteristic of dip-slip faults compared to strike-slip faults. I suspect the phenomena is much more common then current literature on fault behavior would indicate. The phenomena is almost universally ignored in seismic-hazard analyses, mostly because it is difficult to quantify and it requires a more complex hazard model. Recognition of temporal clustering of surface-faulting earthquakes on a fault has important implications to both deterministic hazard assessments (definition of active faults) and probabilistic assessments (earthquake recurrence models). Detailed paleoseismic studies of specific faults in a variety of tectonic environments that focus on both the long-term (middle to late Pleistocene) and the recent (late Holocene) history of faulting will lead to a better understanding this aspect of fault behavior.

ACKNOWLEDGMENTS

This paper is based on data collected as part of a regional seismic microzonation study conducted by Woodward-Clyde Consultants, Lausanne, Switzerland for the Organisme de Controle Technique de la Construction (CTC), Alger, Algeria. The geological field studies were conducted by J.R. Wagner, M. Genoud, D. El Foul, A. Boudiaf, and the author. Preparation of this paper was funded by Geomatrix Consultants, Inc.

REFERENCES CITED

Ambraseys, N.N., 1981, The El Asnam (Algeria) earthquake of 10 October 1980--Conclusions drawn from a field study: Quarterly Journal of Engineering Geology, v. 14, p. 143-148.

------ 1983, Le Tremblement de Terre d'El Asnam le 10 October 1980, Actes des Journees Scientifiques sur le Seisme d'El Asnam du 10.10.80, Alger, 15-16 Juin 1981: Organisme National de la Recherche Scientifique, Alger, Algeria, p. 14-55.

Brune, N.J., 1968, Seismic moment, seismicity and rate of slip along major fault zones: Journal of Geophysical Research, v. 73, p. 777-784.

Cisternas, A., Dorel, J., and Gaulon, R., 1982, Models of the complex source of the El Asnam earthquake: Bulletin of the Seismological Society of America, v. 72, pp. 2245-2266.

Deschamps, A., Guademer, Y. and Cisternas, 1982, The El Asnam, Algeria, earthquake of 10 October 1980--Multiple-source mechanism determined from long-period records: Bulletin of the Seismological Society of America, v. 72, p. 1111-1128.

Espinosa, A.F., 1981, The Algerian earthquake of October 10, 1980: A preliminary report, Earthquake Information Bulletin, v. 13, no. 1, p. 23-33.

Gile, L.H., Peterson, F.F., and Grossman, R.B., 1966, Morphological and genetic sequences of carbonate accumulation in desert soils: Soil Science, v. 101, p. 347-360.

King G.C.P., and Vita-Finzi, C., 1981, Active folding in the Algerian earthquake of 10 October 1980: Nature, v. 292, p. 22-26.

King, G., and Yielding, G., 1984, The evolution of a thrust fault system-processes of rupture initiation, propagation and termination in the El Asnam (Algeria) earthquake: Geophysical Journal of the Royal Astronomical Society, v.77, p. 915-933.

Mahdjoub, Y., Kireche, O., and Saaddallah, A., 1981, Etude des deformations au sol cuasees lors du seisme du 10.10.80 a El Asnam Place dans le contexte technique alpin et neogene, le Seisme d'el Asnam du 10 October 1980: Geosciences, Bulletin des Sciences de la Terre, no. 1, p. 18-58 (in French).

Ouyed, M. and Hatzfeld, D., 1981 Etude de microseismicite en Algeria du Nord, Le Seisme d'El Asnam du 10 October 1980: Geosciences, Bulletin des Sciences de la Terre, no. 1, p. 2-17 (in French).

Ouyed, M., Meghraoui, M., Cisternas, A., Deschamps, A., Dorel, J., Frechet, J., Gaulon, R., Hatzfeld, D., and Philip, H., 1981, Seismotectonics of the El Asnam earthquake: Nature v. 292, p. 26-31.

Ouyed, M., Yielding, G., Hatzfeld, D. and King, G.C.P., 1983, An aftershock study of the El Asnam (Algeria) earthquake of 1980: Geophysical Jouranl of the Royal Astronomical Society, v. 73, p. 605-639.

Philip, H., and Meghraoui, M., 1983, Structural analysis and interpretation of the surface deformation of the El Asnam earthquake of 10 October 1980: Tectonics, v. 1, p. 17-49.

Ruegg, J.C., Kasser, M., Tarantola, A., Lepine, J.C. and Chouikrat, B., 1982, Deformation associated with the El Asnam earthquake of 10 October 1980--Geodetic determination of vertical and horizontal movements: Bulletin of the Seismological Society of America, v. 72, p. 2227-2244.

Shackleton, N.J., and Opdyke, N.D., 1976, Oxygen-isotope and paleomagnetic stratigraphy of Pacific core V28-239 late Pliocene to latest Pleistocene, in Cline, R.M., and Hays, J.D., eds., Investigation of Late Quaternary Paleoceonography and Paleoclimatology: Geological Society of America Memoir 145, p. 449-464.

Swan F.H., Youngs, R.R., Power, M.S., El Foul, D., and Boudiaf, A., 1984 Characterization of earthquake sources and assessment of seismic hazards in the Ech Cheliff Region, Algeria: Conference Internationale Sur la Microzonation Seismique, 10-12 October 1984, Ech Cheliff, Algeria, v.1, p. 393-428.

Woodward-Clyde Consultants, 1984, Seismic microzonation of Ech Cheliff Region, Algeria: Final report submitted to Organisme de Controle Technique de la Construction Ministere de l'Urbanisme de la Construction et de l'Habitat, Algero, Algeria, 6 volumes, 810 p.

Yielding, G., Jackson, J.A., King, G.C.P., Sinvhal, H., Vita-Finzi, C., and Wood, R.M., 1981, Relations between surface deformation, fault geometry, seismicity, and rupture characteristics during the El Asnam (Algeria) earthquake of 10 October 1980: Earth and Planetary Science Letters, v. 26, p. 287-304.

CHANGES IN HOLOCENE SLIP RATES IN STRIKE-SLIP ENVIRONMENTS

by

Peter L.K. Knuepfer

Department of Geological Sciences
State University of New York at Binghamton
Binghamton, NY 13901

ABSTRACT

Detailed studies from sites along the San Jacinto and San Andreas faults in California, and the Awatere and Hope faults in New Zealand all either suggest or strongly indicate that rates of slip across strike-slip faults can be variable over time-scales of several thousand to a few tens of thousands of years. Such nonuniformity is best illustrated by examining incremental slip rates along a fault--that is, slip rates over an interval of the whole time period considered, rather than an average slip rate for the entire time-period studied. Nonuniformity can be recognized only when numerous displaced reference lines and/or geomorphic surfaces can be studied at a site, and if the techniques for estimating ages of the offset features have adequate resolution. Uncertainties in correlation of reference features across the fault, displacement measurements, and age estimates all must be factored into any argument for nonuniform slip. In each of the studies cited, the fault-slip data are subject to varying interpretations, and in some cases the nonuniform interpretation is less likely than a uniform slip rate. However, incremental slip rates at the Charwell River on the Hope fault range from > 55 mm/yr from 11 ka to 3.9 ka to < 5 mm/yr for the last 3.9 ka, and incremental slip rates on the Coyote Creek fault of the San Jacinto fault zone range from 1.4-2.0 mm/yr in the early and middle Holocene to as much as 5 mm/yr in the last few hundred years. Thus it is clear that slip-rate variability is a real phenomenon on at least some strike-slip faults. If nonuniform slip is present, detailed paleoseismicity studies must be placed into a longer-term context to know how representative activity of the last thousand or few thousand years is with respect to longer term seismic activity and how useful paleoseismic studies will be in predicting future rupture events.

INTRODUCTION

Detailed studies of slip across strike-slip faults increasingly are demonstrating evidence that, on many faults, slip rates are not uniform on time scales of several thousands to tens of thousands of years. That is, the rate of strain as measured by offset geomorphic surfaces is variable over time scales of thousands of years. Furthermore, detailed paleoseismic studies show that, while return times of surface ruptures can be placed within relatively confined recurrence intervals (Swan and others, 1980; Sieh, 1984), fault-slip events (that is, surface ruptures) do not follow a simple time- or slip-predictable model: the recurrence of surface ruptures is not uniform (although there generally is a high degree of regularity). Thus, "nonuniformity" is measured both on the time scale of recurrence intervals between major surface-faulting earthquakes and, in some cases, over time scales an order of magnitude or more longer than the average recurrence interval. The emphasis of this paper is on the evidence for nonuniform slip over what I will call "intermediate" time scales (to differentiate from long-term fault slip measured over millions of

years and the short-term nonuniformity of earthquake cycles)--several thousands of years. The discussion is restricted to faults with relatively high slip rates (at least several millimeters per year), for which the recurrence intervals typically are no more than several hundred to a thousand years.

The key to examining whether faults slip at uniform or nonuniform rates over time-intervals of several thousands to tens of thousands of years is to conduct high-resolution studies of fault-slip histories. By high-resolution studies, I mean examination of multiple offset geomorphic surfaces and features at a site or within a restricted region: numerous radiocarbon dates and (or) other methods of estimating ages of individual surfaces, and detailed analysis of displacements of each surface. The age differences of the surfaces ideally are larger than the average recurrence of slip events, but shorter than several thousand years. The most ideal sites are those at which surface ages span the full breadth of the Holocene and (or) latest Pleistocene, so that details of the displacement history can be deduced. While such sites are certainly not universal, several studies have produced such high-resolution analysis.

SLIP-RATE ESTIMATES AND THEIR UNCERTAINTIES

Estimates of slip rates across strike-slip faults require the matching of displaced geomorphic or geologic piercing points or reference lines, such as fluvial terrace risers (the escarpment from one terrace up to a higher and older terrace), abandoned stream channels, apices of alluvial fans, sedimentary facies changes, shoreline angles on marine terraces, etc., across the fault. Where displacements are relatively small, say a few meters to tens of meters, this generally can be accomplished readily. However, as piercing points are displaced progressively greater amounts, increasing uncertainty accompanies the correlation of features across the fault.

Interpretation of the displacements of faulted geomorphic reference lines also must be based on realistic geomorphic models of the formation of these features and their responses to tectonism. For example, the crests of glacial moraines preserve the fault displacement that has occurred since formation of the moraine, but the margins of a moraine may preserve less displacement if they have been trimmed by later erosion. The age of displacements preserved by the riser between one stream terrace and the next higher or lower terrace generally is the same as the age of the terrace surface below the riser, since a streambank usually continues to be subject to erosion as long as the river occupies the flood plain at its base (Ikeda and Yonekura, 1986; fig. 1). When a fault-rupture event produces a lateral displacement of the riverbank, it is removed very rapidly by most rivers unless the riverbank is on the inside of a meander bend or at some other location where it is protected from rapid undermining by fluvial erosion. Thus in most cases, only displacements that occur <u>after</u> a flood-plain level is abandoned and becomes a stream terrace are likely to be preserved by the riser above that terrace. In some cases, it is possible that not all displacement of a riverbank was removed prior to abandonment and downcutting to a new flood plain (Lensen, 1964); in these cases, determinations of slip rate by correlating a terrace riser with the age of the terrace below the riser may be in error.

The other critical information in determining fault-slip rates is the age of the displaced surface. Direct dating of deposits within an offset geomorphic surface by radiometric means is the most common (and generally most precise)

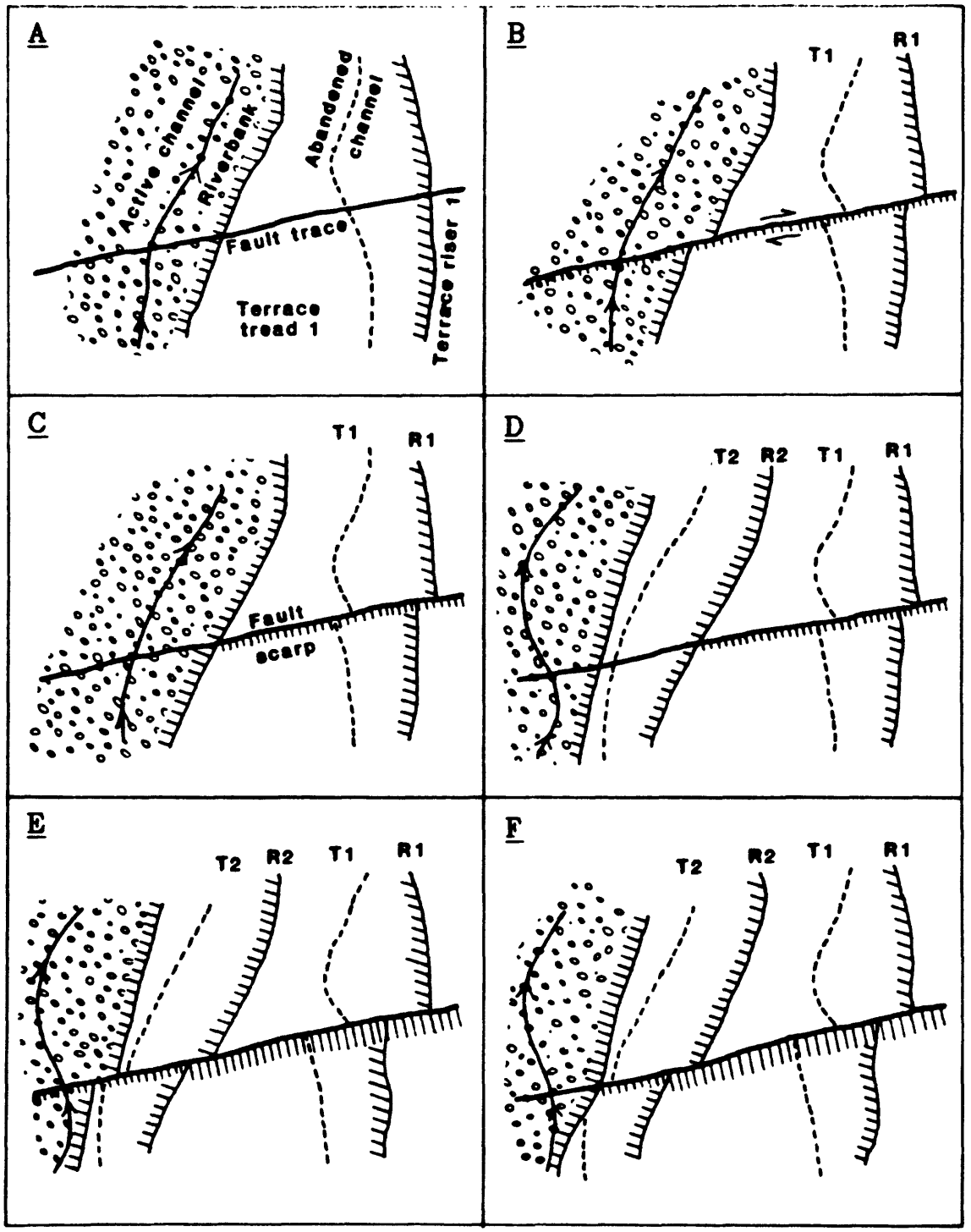

FIGURE 1. Hypothetical development of a faulted terrace sequence. A terrace tread and flood plain (A) are offset by a slip event (B). The river erodes its bank, removing the displacement (C). After a downcutting episode forms a second terrace (D), another faulting event displaces the sequence (E). Continued trimming leads to the preservation of displacement from two events on terrace 1 (preserved in riser 1), one event on terrace 2, and no displacement of the bank below terrace 2 (F).

means of age estimation. However, most radiometric dating techniques utilize materials deposited below the surface that preserves the offset across the fault. Commonly, more than one date is obtained from a stratigraphic sequence, and the age of the surface is estimated assuming uniform sedimentation rates. However, unless the offset feature can somehow be dated directly, the age estimate for the offset is necessarily uncertain. Furthermore, in most instances no materials that are suitable for radiometric dating are found, so indirect age-estimation techniques, such as quantitative soils analyses (e.g. Harden and Matti, in press), are utilized. The use of soils and other weathering phenomena, such as rock-weathering rinds (Knuepfer, in press), has both advantages and disadvantages over radiometric techniques. The principal advantage is that these techniques allow direct estimation of the age of the geomorphic surface being used as the reference line: soil development and weathering proceed systematically after a geomorphic surface has formed (unless, of course, subsequent geomorphic or depositional processes alter the surface). The principal disadvantages involve complexities of the weathering process and the difficulty of adequately calibrating rates of soil-forming and rock-weathering processes to use them as quantitative age estimation techniques.

The displacements and ages of individual geomorphic surfaces are combined to produce slip rates since formation of individual geomorphic surfaces. The uncertainties in those slip rates occur from three sources: the obvious uncertainties associated with the age estimate and the field measurement of displacement, and the more complicated uncertainty associated with the relation of timing of formation of geomorphic surfaces to timing of fault-slip events. If two terraces formed within a few hundred years of each other and no surface-rupture event occurred between them, then the older terrace will imply a lower slip rate than the younger only because the recurrence interval is longer than the terrace-formation interval. Such a result may lead to an incorrect interpretation that slip rates have changed, when in fact the slip rate may be constant. Thus caution must be taken in interpreting individual displacement histories. For this reason, the greater the number of geomorphic surfaces that can be utilized in a study of slip rates and their variations, the better.

Slip-rate data commonly are reported by listing the average rate of slip since formation of a reference line. Thus, an author might report a slip rate of 20 mm/yr since 14 ka (1 ka = 1000 yr) and a rate of 15 mm/yr since 20 ka. However, variations like these in slip rate can be examined better by considering the slip data graphically. Displacement-time diagrams are a common representation of fault-slip data; an example from the San Andreas fault is shown in figure 2. These diagrams generally involve plotting the age of the offset feature, with its uncertainty, against the displacement and its uncertainty. A further way to describe variations in slip rates is to compute incremental rates--the rate of slip for an increment of time. This is particularly feasible for those studies in which numerous reference lines are established and multiple-time increments can be defined. Using the displacement-time diagrams, time increments during which fault slip occurred at a more-or-less constant rate are defined. These kinds of diagrams are used in the following discussions.

NONUNIFORM SLIP RATES IN THE HOLOCENE AND LATEST PLEISTOCENE

During the past 10 yrs, several studies of slip rates across strike-slip faults have yielded evidence indicating (or at least permitting the interpretation of) nonuniform slip during the Holocene and (or) latest Pleistocene.

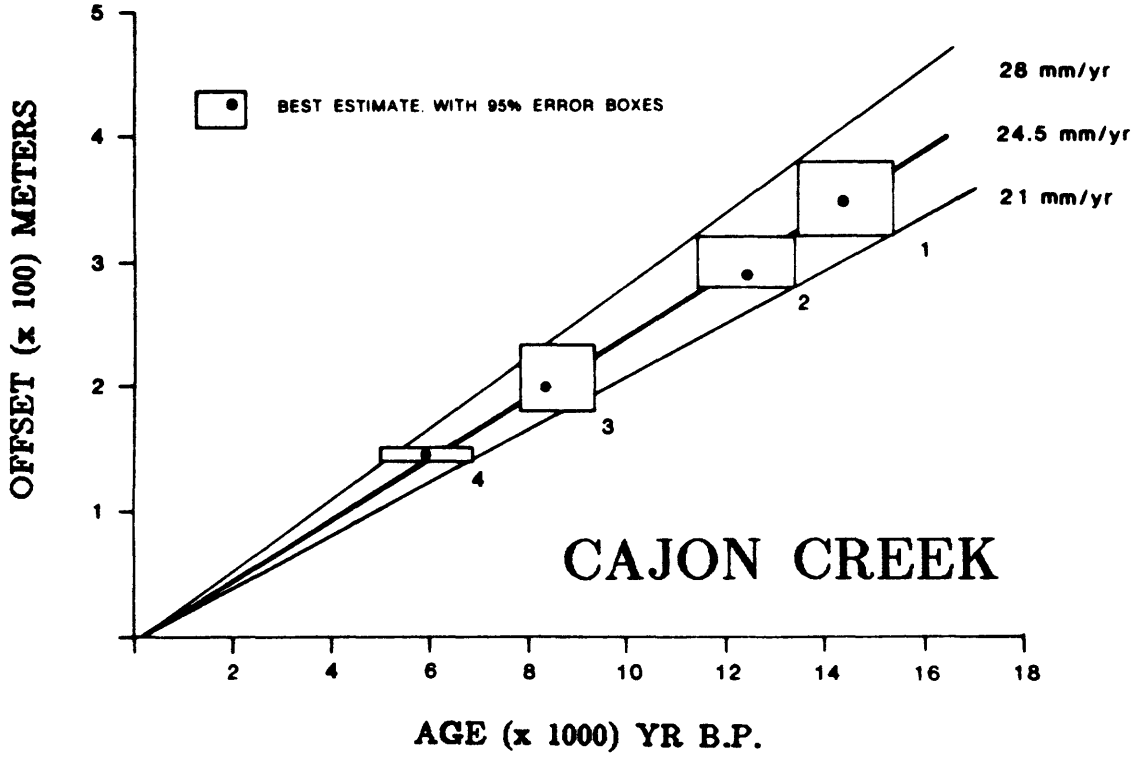

FIGURE 2. Displacement-age diagram for latest Pleistocene slip across the San Andreas fault at Cajon Creek (from Weldon and Sieh, 1985).

These include studies of the San Andreas and related faults in California, and the Alpine fault and related faults in New Zealand.

San Andreas and Related Faults

San Jacinto Fault

One of the first studies indicating time-varying slip rates on the order of thousands of years was that of Sharp (1981) for the San Jacinto fault in the Imperial Valley of California. He found that the late Holocene slip rate along the Coyote Creek fault of the San Jacinto fault zone twice the early Holocene rate, based on measured offsets of a young deposit of Lake Cahuilla (about 400 yr old) and a mid-Holocene buried stream channel (fig. 3). The age of the Lake Cahuilla deposit is bracketed by a radiocarbon date on plant debris in the offset stratigraphic horizon (point A in fig. 3) and the likely minimum age of the Lake Cahuilla shoreline (point B, fig. 3). Radiocarbon dating of the deposits within a mid-Holocene stream channel (point D, fig. 3) and the deposits truncated by that channel (point E, fig. 3) provide maximum and minimum estimates of the age of the displaced channel, which provides a piercing point across the fault. The latest Holocene slip rate inferred from the Lake Cahuilla datum is 2.8-5.0 mm/yr for 250-500 yr (perhaps little more than one or two recurrence intervals). The incremental rate from 5-7 ka until 0.4 ka is 1.4-2.0 mm/yr. In this case, the apparent change in slip rate may result from the very short time period from Lake Cahuilla to the present (it may be comparable

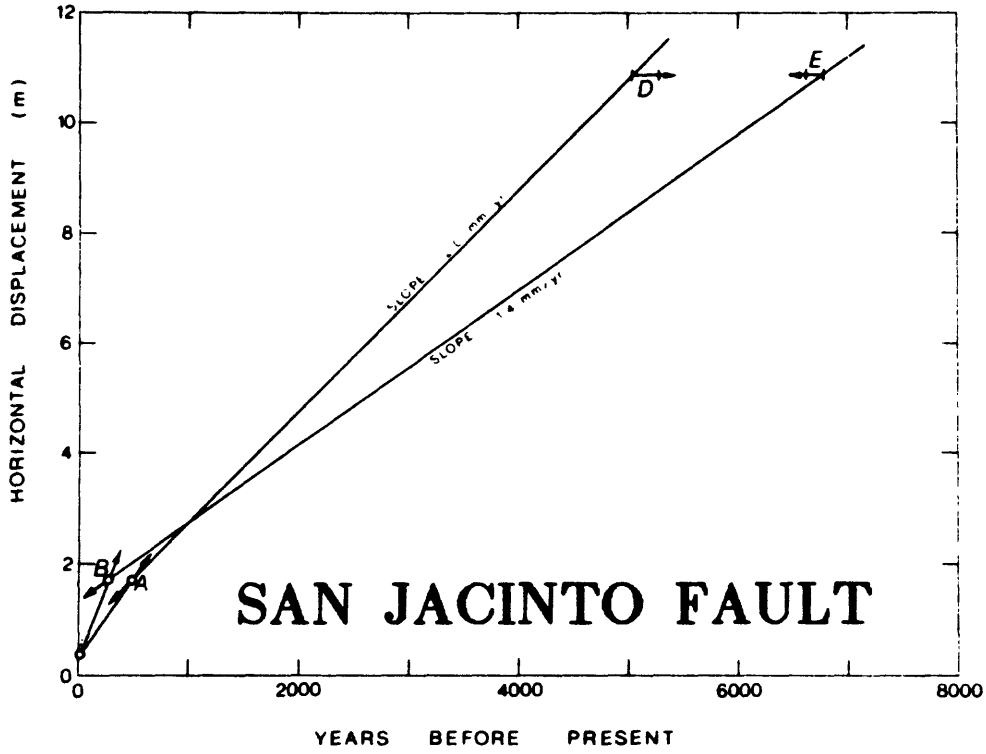

FIGURE 3. Displacement-age diagram for Holocene slip across the Coyote Creek trace of the San Jacinto fault (from Sharp, 1981).

to the recurrence interval) rather than a change in tectonic slip rates. In contrast, T. Rockwell (oral commun., 1987) obtained a uniform slip rate farther north across the entire San Jacinto fault zone.

San Andreas Fault

Published and unpublished studies of progressive displacements across the San Andreas fault in southern and south-central California have yielded conflicting data and interpretations on uniformity or nonuniformity of slip rates in the Holocene and latest Pleistocene. The data sets include studies at Wallace Creek (Sieh and Jahns, 1984) and Cajon Creek (Weldon and Sieh, 1985), and near San Gorgonio Pass (Harden and Matti, in press).

Wallace Creek

Sieh and Jahns (1984) studied in detail the latest Quaternary slip across the San Andreas fault at Wallace Creek in the Carrizo Plain of south-central California. The late-Holocene slip rate was determined from the offset of the modern channel of Wallace Creek: the 128-m offset and constraining radiocarbon ages from deposits into which the channel was incised. This data point--128 m in approximately 3,700 yr--is shown as point A in figure 4. An alluvial fan (whose basal sediments are dated at 13,250 yr) offset from its source near Wallace Creek also was studied by Sieh and Jahns (1984). The age of the fan surface is not actually known, because the charcoal is buried by 1.3 m of fan

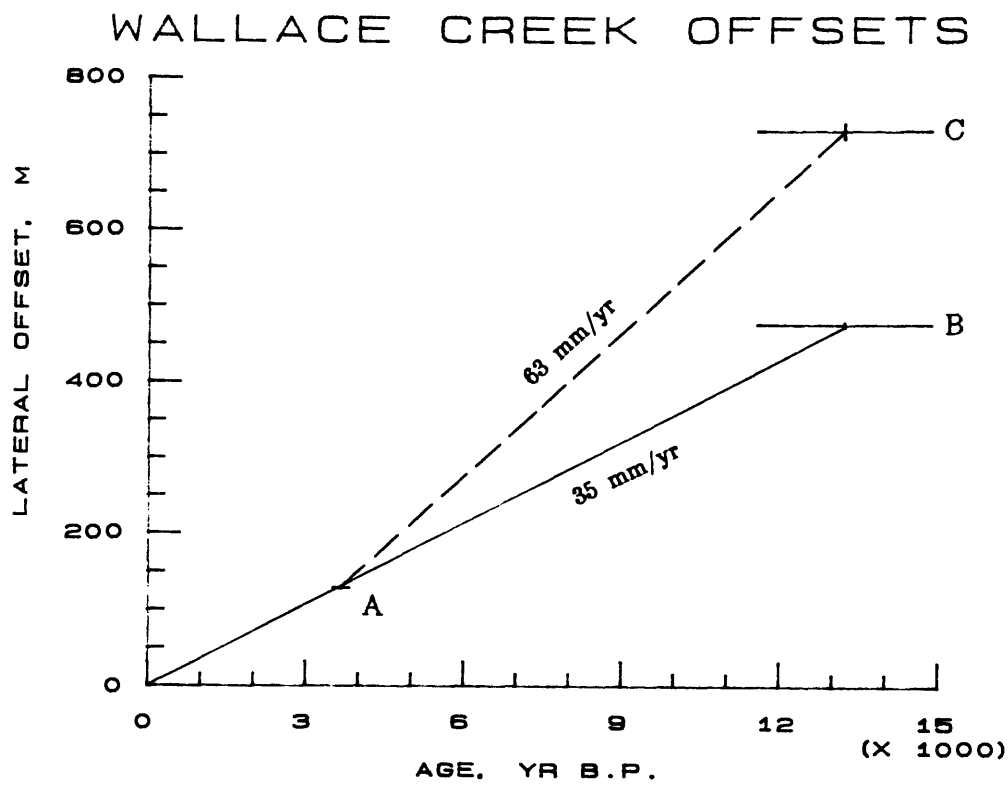

FIGURE 4. Displacement-age diagram for latest Pleistocene slip across the San Andreas fault at Wallace Creek. Data compiled from Sieh and Jahns (1984). The solid line (joining A and B) indicates their preferred interpretation of the field relations.

deposits, so the fan is some age younger than 13,250 yr. Sieh and Jahns (1984) argued that the lack of pedogenic development, weathering, or bioturbation between the three stratigraphic units comprising the fan deposit argue for very rapid deposition. They offer three possible interpretations of sources and corresponding amount of displacement of the fan: Wallace Creek, suggesting an offset of 128 m; four small gullies, suggesting an offset of some 475 m (corresponding to point B on fig. 4); and a single larger gully, suggesting an offset of some 730 m (point C on fig. 4). The first interpretation implies no slip between 13,250 yr and 3,700 yr, and is considered very unlikely. The second interpretation implies a slip rate of about 35 mm/yr between 13,250 and 3,700--in other words, uniform slip throughout the Holocene. The third interpretation implies an incremental early-mid Holocene slip rate of 63 mm/yr. The second interpretation was preferred by Sieh and Jahns (1984) because of the topography of the beheaded fan and the uniformity of the derived slip rates. However, the uncertainty of both the fan surface age and the displacement mean that nonuniform slip may have occurred at Wallace Creek.

Cajon Creek

Weldon and Sieh (1985) showed even more convincing evidence of uniform Holocene slip rates across the San Andreas fault at Cajon Creek. They studied stream terraces of Cajon Creek near Cajon Pass that are offset by the San Andreas fault. Radiocarbon dating of the Cajon Creek terraces document uniform slip of about 25 mm/yr since 16 ka (fig. 2). However, some of the displacement

measurements at this site are uncertain due to the shallow angle with which piercing points (i.e. terrace risers) intersect the fault and difficulties in correlation across the fault. Recent re-examination of the older terraces suggests that the average slip rate since 16 ka may be only about 17 mm/yr (D.P. Schwartz, oral commun., 1987)--implying a low latest Pleistocene incremental slip rate and nonuniform slip over increments of several thousand years.

Yucaipa

Harden and Matti (in press) have conducted detailed studies of alluvial fans progressively offset across the active trace of the San Andreas fault west of San Gorgonio Pass. Using soil development calibrated to well-studied chronosequences from elsewhere in California, they estimated ages of three alluvial fans. Displacements were determined by matching fan apices back to source canyons. Best-estimate rates are 19-26 mm/yr for the last 14 ka, 21 mm/yr for the last 30 ka, and 10-11 mm/yr for the last 100 ka. The implied incremental rates are only around 7 mm/yr for the interval 30-100 ka, and 15-22 mm/yr for the interval 14-30 ka. Although uncertainties are higher for both the displacements and the age estimates than in the other studies previously cited, these data give a strong indication of nonuniform slip across the San Andreas fault.

Alpine Shear System, New Zealand

The right-lateral faults of the Alpine shear system in the northern South Island, New Zealand, progressively displace sequences of latest Quaternary stream terraces, all latest glacial and post-glacial in age. Many of the sequences have been mapped in detail by New Zealand geologists, but due to the lack of datable materials they had assumed that slip rates have remained uniform throughout the post-glacial period (Lensen, 1968). Studies of weathering-rind thickness and soil morphologic and chemical changes (calibrated to sites of known, radiocarbon-dated, age) at several of these sequences, however, has allowed estimation of ages of individual terraces (Knuepfer, in press), leading to detailed histories of fault slip in post-glacial times. Because few materials for radiocarbon dating were found from the gravelly stream terrace deposits studied in New Zealand, ages of individual terraces were estimated by calibrating rates of weathering-rind growth and rates of change of soil morphology and chemical distributions at sites of known (radiocarbon-dated) age and applying these calibration data to sites of unknown age. Uncertainties of the ages obtained from these techniques range from an estimated 5 to 20 percent for the weathering-rind data to 15 to 50 percent for the soil data (Knuepfer, in press). The oldest surfaces examined have ages of 15-20 ka and right-lateral displacements of as much as 400 m.

Most of the sites I studied in New Zealand exhibit evidence of changes of slip rates in the Holocene that cannot readily be explained by uncertainties in the fault-slip or age-estimation data nor by the relationship of intervals between various geomorphic surfaces and recurrence intervals of rupture events as postulated above. Two of these sites, which exhibit the most spectacular changes in slip rates, are considered in some detail in the following paragraphs: the Saxton River terraces on the Awatere fault, and the Charwell River terraces on the Hope fault (fig. 5).

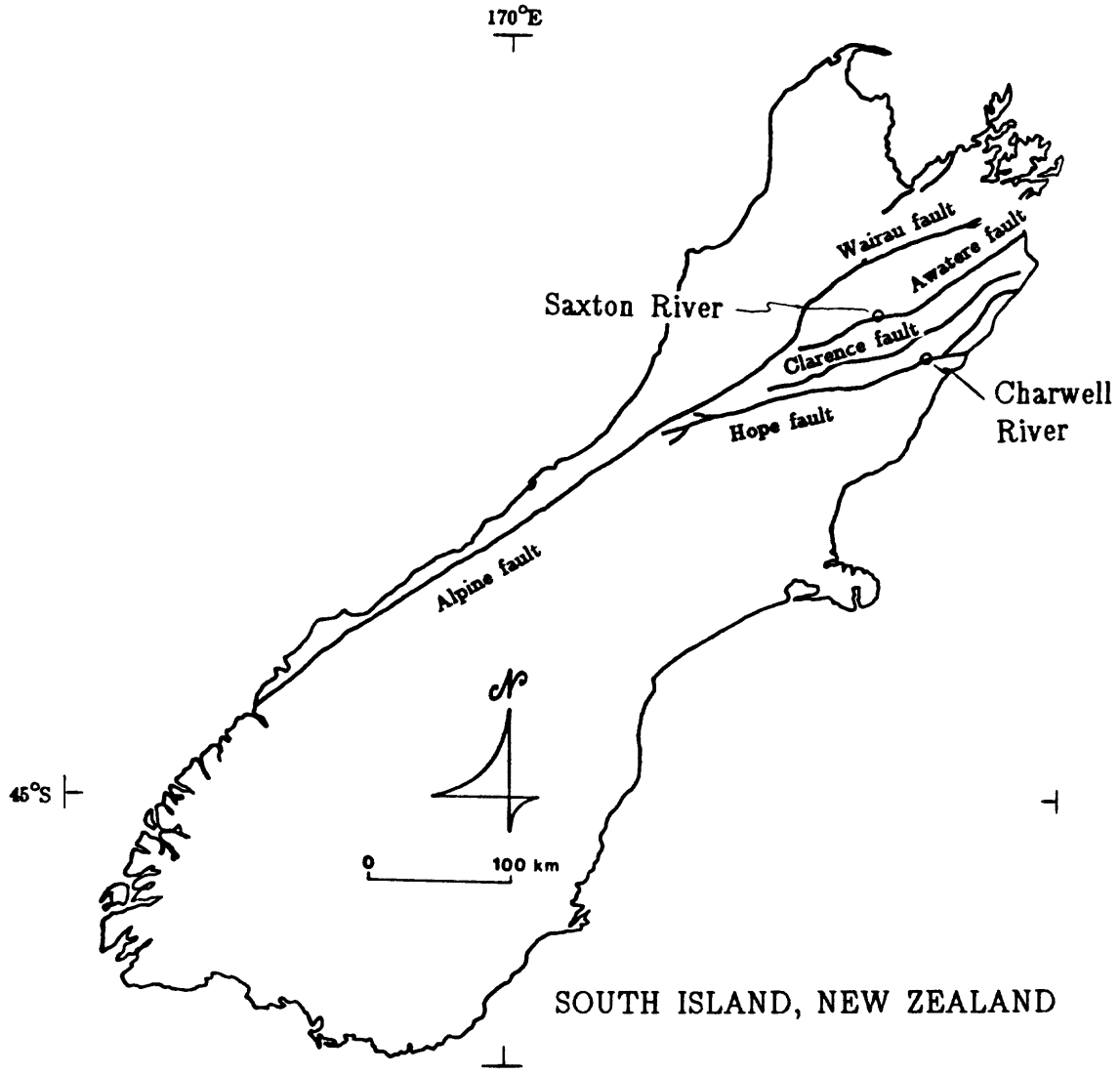

FIGURE 5. Location map of the Alpine shear system, South Island, New Zealand, showing Saxton River and Charwell River study sites.

Saxton River

The Awatere fault displaces a sequence of five terraces at the Saxton River where the river enters an intermontane alluvial plain just south of the fault. The sequence on the east bank was mapped by Lensen (1973) and in more detail by Blick (unpublished data) and field-checked for this study. Weathering-rind and soil data were obtained for each of five terraces, and these provide the data for the displacement-time diagram of figure 6.

Average slip rates computed for each terrace range from 6.9 (+2.6, -1.6) mm/yr for Terrace 1 (66±5 m offset in 9500±2000 yr) to 4.0 (+2.7, -1.6) mm/yr for Terrace 5 (8±2 m in 2000±500 yr). In fact, only one rupture event has displaced the youngest terrace, and Lensen (1973) suggests that it occurred in 1848. At Saxton River, then, the slip rate is consistent from the beginning of the Holocene (about 10 mm/yr incremental rate) until about 3 ka but, in the late Holocene, slip probably has occurred only during one historic earthquake.

Charwell River (Hope Springs Eternal)

A sequence of at least 11 stream terraces is preserved immediately downstream of the Hope fault at the southwest bank of the Charwell River. Most of the terraces can be correlated with terrace remnants preserved immediately upstream of the fault. Knuepfer and Bull (in prep.) discuss the site in detail; their results are summarized here.

Lateral displacements of the Charwell River terraces are difficult to determine for several reasons: (1) lack of extent of terrace remnants on the upstream, upthrown side of the fault, (2) a graben in the central part of the site, which disrupts continuity of terrace risers into the fault zone, (3) a young fan burying parts of high terrace remnants upstream of the fault, and (4) apparent meander-bend river cutting nearly along the fault trace in the lower terrace area. Detailed surveying of the terraces and studies of weathering and soil characteristics of terrace remnants on both sides of the fault form the basis for the displacement measurements recorded in figure 7. Age estimates were obtained for seven of the terraces from weathering-rind and soil studies; a young alluvial fan that is displaced 6.3±0.3 m right-laterally has a maximum age of 770±52 yr from a radiocarbon date on charcoal buried 0.5 m below the fan surface (Knuepfer, in press). This fan apparently has been displaced by only one rupture event, and the lowest fluvial terrace about 3.9 ka in age preserves a similar displacement.

The data from Charwell River display the most pronounced change in lateral slip rates of any of the sites I studied in New Zealand. However, the displacement data are only moderately reliable, because of the graben within the fault zone and the poorly preserved terrace remnants upstream of the fault that make correlations of terraces across the fault uncertain. Yet even if the displacement measurements are in error by a factor of two, which is unlikely, the late-Holocene lateral-slip rate (only 1.3 mm/yr for the last 3.9 ka from data displayed in fig. 7) remains at least an order of magnitude less than the incremental early-mid Holocene rate (about 55 mm/yr from 11 ka to 3.9 ka).

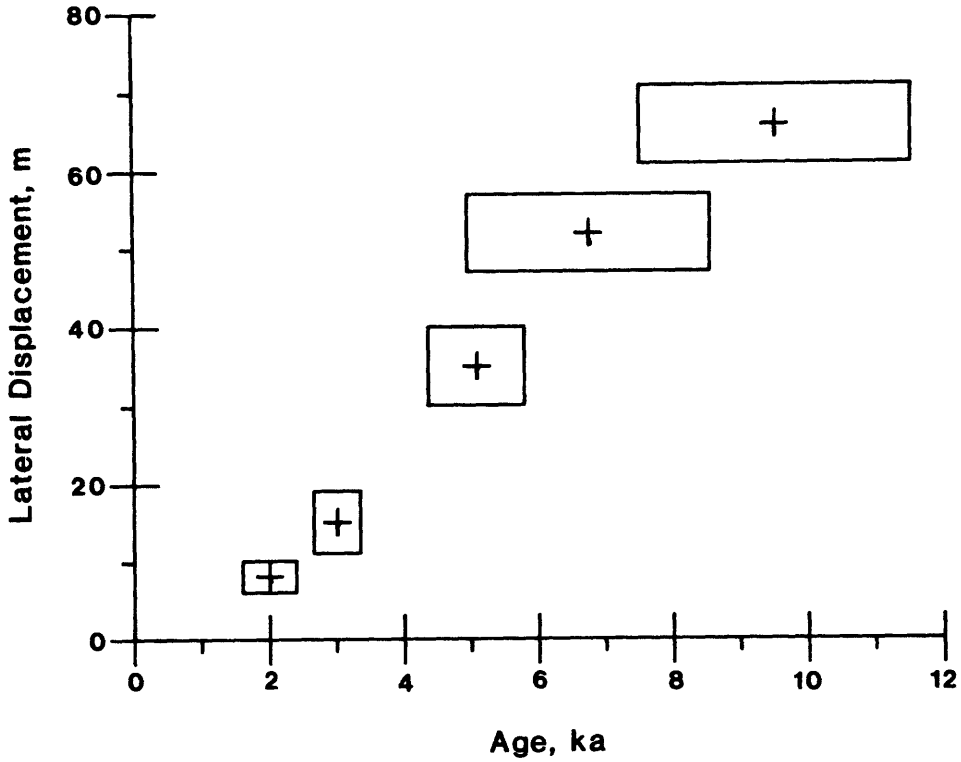

FIGURE 6. Displacement-age diagram for Holocene lateral slip across the Awatere fault at Saxton River. Note the sharp change in apparent slip rate in the latest Holocene. Boxes define error limits of age and amounts of displacement.

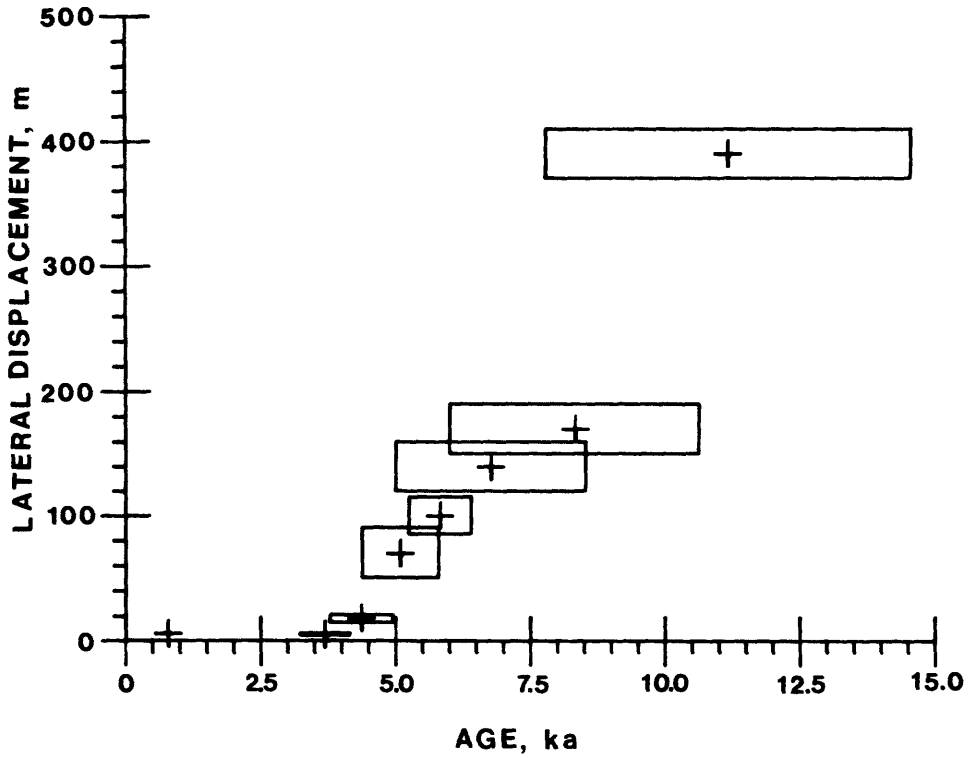

FIGURE 7. Displacement-age diagram for latest Pleistocene slip across the Hope fault at Charwell River. The two youngest surfaces appear to be displaced by only one fault rupture event (perhaps in 1888, certainly within the last few hundred years). Boxes define error limits of age and amounts of displacement.

DISCUSSION

Detailed studies from sites along the San Jacinto, San Andreas, Awatere, and Hope faults all either suggest or strongly indicate that rates of slip across strike-slip faults can be variable over time-scales of several thousand to a few tens of thousands of years. Each of the studies is subject to varying interpretations, and in some cases the nonuniform interpretation is less likely than a uniform slip rate. Nonetheless, it is clear that slip-rate variability is a real phenomenon on at least some strike-slip faults. This implies a non-uniformity to fault behavior that can be extremely important in paleoseismicity studies. If nonuniform slip is present, detailed paleoseismicity studies must be placed into a longer term context to know how representative activity of the last thousand or few thousand years is with respect to longer term seismic activity and how useful paleoseismic studies will be in predicting future rupture events. For example, a detailed paleoseismology study along the Hope fault in New Zealand would suggest few slip events during the last few thousand years (if my interpretations of the displacement history are correct), leading to an assessment of long recurrence intervals. However, a similar study in the early Holocene would have indicated short recurrence and high hazard. Thus, interpretations of paleoseismic data must be made in the context of the uniformity or nonuniformity of slip on the fault.

REFERENCES CITED

Harden, J.W., and Matti, J.C., in press, Holocene and late Pleistocene slip rates on the San Andreas fault in Yucaipa, California, using displaced alluvial-fan deposits and soil chronology: Geological Society of America Bulletin.

Ikeda, Y., and Yonekura, N., 1986, Determination of late Quaternary rates of net slip on two major fault zones in central Japan: Bulletin of the Department of Geography, University of Tokyo, no. 18, p. 49-63.

Knuepfer, P.L.K., in press, Estimating ages of late Quaternary stream terraces from analysis of weathering rinds and soils: Geological Society of America Bulletin.

Lensen, G.J., 1964, The general case of progressive fault displacement of flights of degradational terraces: New Zealand Journal of Geology and Geophysics, v. 7, p. 864-870.

Lensen, G.J., 1968, Analysis of progressive fault displacement during downcutting at the Branch River terraces, South Island, New Zealand: Geological Society of America Bulletin, v. 79, p. 545-555.

Lensen, G.J., 1973, Guidebook for excursion A10: Christchurch, New Zealand, Field Trip Guide, 9th Congress, International Union for Quaternary Research, 76 p.

Sharp, R.V., 1981, Variable rates of late Quaternary strike slip on the San Jacinto fault zone, southern California: Journal of Geophysical Research, v. 86, p. 1754-1762.

Sieh, K.E., 1984, Lateral offsets and revised dates of large prehistoric earthquakes at Pallett Creek, southern California: Journal of Geophysical Research, v. 89, p. 7641-7670.

Sieh, K.E., and Jahns, R.H., 1984, Holocene activity of the San Andreas fault at Wallace Creek, California: Geological Society of America Bulletin, v. 95, p. 883-896.

Swan, F.H., III, Schwartz, D.P., and Cluff, L.S., 1980, Recurrence of moderate to large magnitude earthquakes produced by surface faulting on the Wasatch fault, Utah: Bulletin of the Seismological Society of America, v. 70, p. 1431-1462.

Weldon, R.J., II, and Sieh, K.E., 1985, Holocene rate of slip and tentative recurrence interval for large earthquakes on the San Andreas fault, Cajon Pass, southern California: Geological Society of America Bulletin, v. 96, p. 793-812.

PALEOSEISMIC SLIP AT REVERSE FAULTS

by

Alan G. Hull
Department of Geological Sciences
University of California
Santa Barbara, California 93106

ABSTRACT

The recent history of reverse and thrust faults can be determined by careful application of established techniques of tectonic geomorphology and interpretation of trench exposures. Variation in coseismic slip at sinuous and short fault traces which are quickly modified by erosion introduces large errors to the estimation of rupture dimensions and earthquake magnitude. Surface faulting is not always produced in large (>M=7) thrust earthquakes, and future studies must improve the integration of geological estimates of coseismic elevation change with seismicity and geophysical modelling.

INTRODUCTION

Active thrust and reverse faults are an important source of elastic strain energy and their coseismic movements have been responsible for some of the most damaging historic earthquakes. Most of the techniques developed for seismic-hazard analysis have been in regions of strike-slip and normal-slip fault movement. However, most of the commonly used geologic and geomorphological techniques, with some modification, have been used to determine the style and rate of reverse-fault and thrust-fault activity. This note reviews the general characteristics of the surface and near-surface expression of active reverse and thrust fault scarps and the techniques that can be used in the study of past activity. Some directions for further study, particularly in regions where fault scarps are absent or not preserved, are suggested.

GEOMORPHOLOGY

The presence of a shallow-dipping fault plane near the base of steep-sided mountain ranges, makes the initial recognition of reverse-fault and thrust-fault traces difficult because of active slope processes, stream degradation, and(or) alluvial-fan aggradation (Sawa 1980, Beanland and others., 1986). Fault scarps are often sinuous and short (fig.1). Commonly the deformation zone ranges from 10 m to 5 km width and contains multiple scarps, those scarps most easily recognized are often nearest the range front and upthrown in the opposite sense to the master fault at depth (Ikeda, 1983). Scarp morphology is highly variable and depends on the nature of the surficial materials

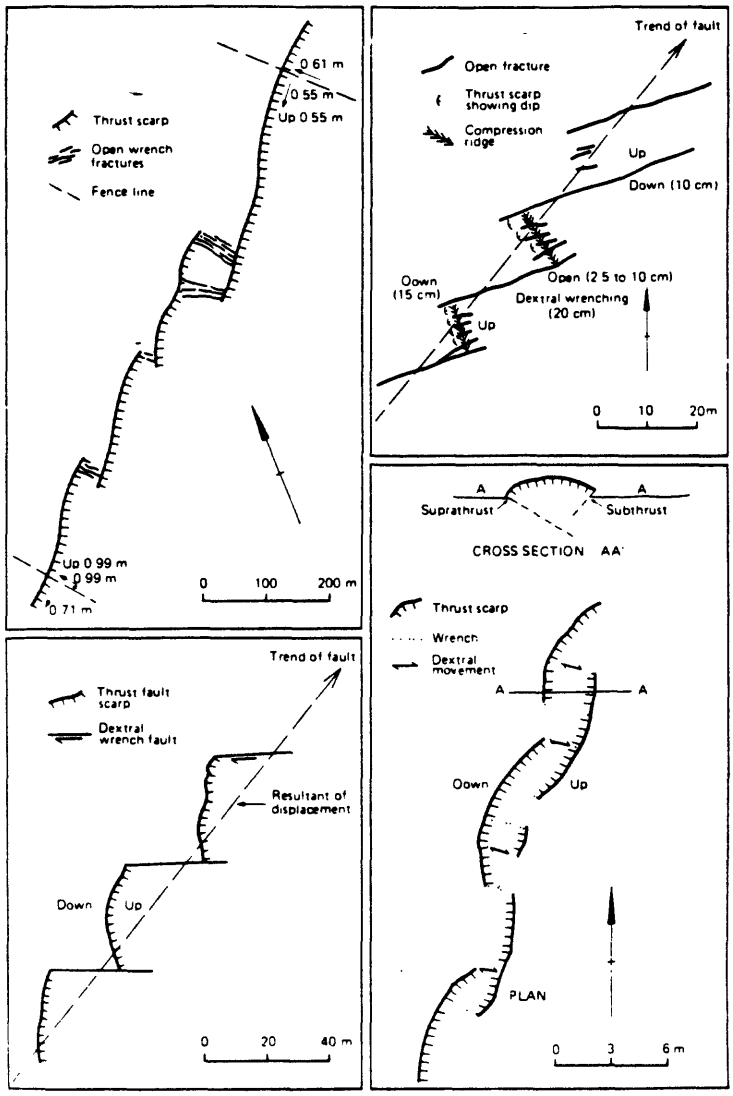

FIGURE 1.--Map showing variation in fault traces produced during October 1968, Meckering earthquake, Western Australia. Fault rupture occurred on a ground surface of low relief providing ready recognition of tectonic features. A typical reverse-fault trace pattern of *en echelon* thrust scarps separated by strike-slip faults is apparent. Note the presence of "pop up" structures in the bottom right diagram (from Gordon and Lewis, 1980).

(fig. 2) and the orientation of the scarp with respect to the principal axis of horizontal compression (Gordon and Lewis, 1980). Fault-scarp preservation is often poor, even after short periods of time (fig. 3) because scarps oversteepen existing slopes.

Locating active reverse faults may be best accomplished with the aid of high-quality, low sun-angle aerial photography. Large-scale topographic maps (1:500 scale, if available) supplemented by detailed surface profiles can further define the extent of the deformation zone and reduce the threshold of minimum scarp height recognition to within 0.5 m.

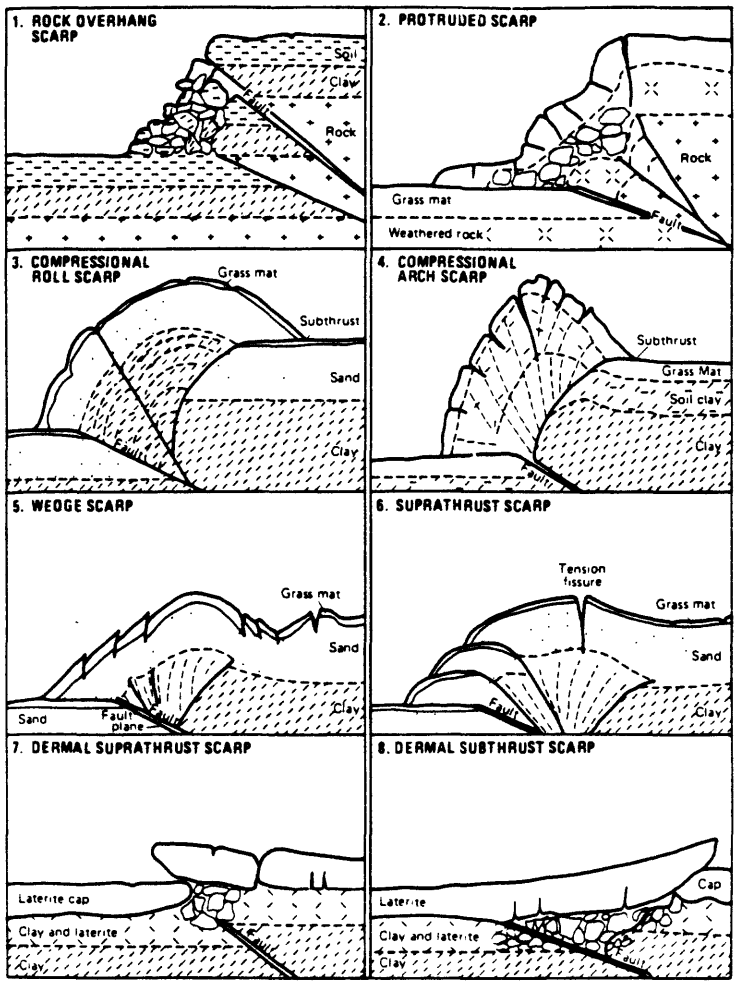

FIGURE 2.--Cross sections of thrust-fault scarps produced in the October 1968, Meckering earthquake. The degree of folding is related to the thickness and moisture content of the near surface materials, the greatest folding developed in the more plastic clay. Fault-trace variability increases where scarps develop on existing slopes (from Gordon, 1971).

TRENCHING INVESTIGATIONS

Trenching of active fault traces has proven a valuable tool to assess the nature and timing of surface-fault rupture. It is particularly useful in the study of dip-slip faults as the dominant movement is vertical. Interpretation from trenching data for the amount of coseismic movement at active reverse and thrust faults is subject to potential errors from the following:

1. Wide variations in the measured values of an individual slip event occur along fault strike. Trenches 20 m apart and

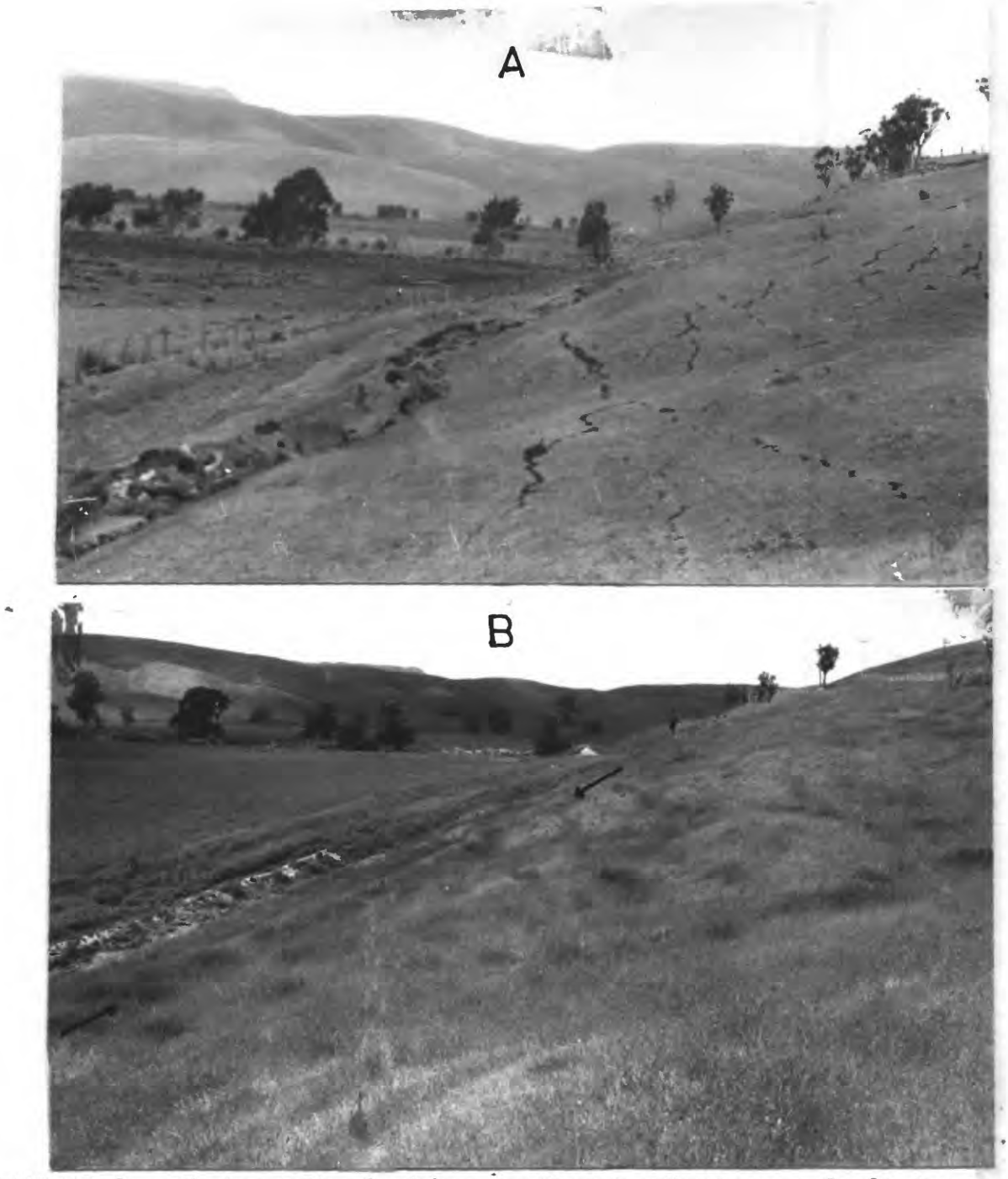

FIGURE 3.--Photographs looking southwest of reverse-fault trace produced in February 1931, Hawke's Bay earthquake, New Zealand. A, photograph taken immediately following the earthquake showing a compressional roll breaking the ground surface near the base of the existing fault scarp. Tension fractures are well developed in the hanging wall and extended up to 1 km farther northwest. B, photograph showing the same locality in November 1984 with the fault trace (arrowed) barely recognizable as a result of agricultural modification. The presence of an active-fault trace was not recognized prior to 1931.

across the same fault have shown single bed displacement values that vary by 20 percent (Officers of the New Zealand Geological Survey, 1983). These data are consistent with observations from coseismic faulting (fig. 2) and suggest that many more trenches may be necessary to determine the amount of coseismic slip than would be required at strike-slip faults. The distribution of slip across a number of subparallel fault traces has been observed in all historic fault movements, but it remains uncertain whether past faulting events had this same distribution. Uncertainty about the past slip distribution across the fault zone requires assumptions about the total slip for each earthquake event. Slip per event data are necessarily average values and make questionable the correlation of fault slip and length with earthquake magnitude.

2. Large-scale drag folds with amplitudes that exceed half the total vertical separation, and associated small scale secondary, reverse and normal faults are common. Trenches may require extension to determine reliable values for bed and geomorphic surface separations (Beanland and others, 19°3)
3. Rapid development of fault scarps promotes degradation of the hanging wall deposits. Truncation of bedding and deposition of younger beds on the footwall block severely limit correlation across the fault, preventing the recognition of multiple events and perhaps, in the case of large single events, the recognition of the maximum displacement value for that event.
4. The dip of fault planes often shallows toward the ground surface so that subhorizontal fault planes can become unrecognizible, particularly in well-sorted sand and silt layers (fig. 4).
5. Lack of suitable datable material to determine the absolute age of individual events.
6. Only the net amount of fault slip is recorded in the geologic record. Any interseismic movement that can occur in the same or opposite sense to that which occured during the faulting event, will affect the final estimate of earthquake size. However, along strike variations in slip probably exceed those from any interseismic movement.

With careful site selection, trench exposures can be interpreted to determine the approximate amount and timing of coseismic fault movement (fig. 5).

FOLDING

Surface faulting may be only a minor part of the surface deformation associated with coseismic reverse or thrust faulting at depth. Deformation is rarely confined to the narrow zone of surface faulting, and uplift and downwarping can affect large areas (>1000 km^2) without significant surface rupture (Plafker,

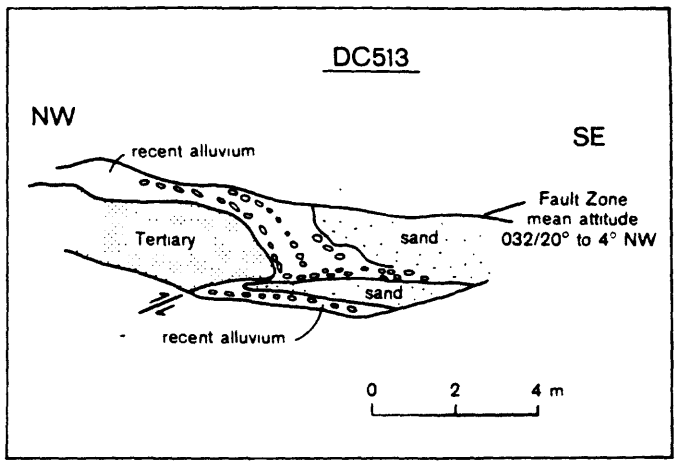

FIGURE 4.--Sketch of trench across trace of Dunstan fault, New Zealand, showing marked shallowing of the fault plane within 3 m of the ground surface. The fault plane becomes subhorizontal at the sand-alluvium contact and cannot be traced through the sand to the ground surface (from Beanland and others, 1986).

1969). Ground surface movement from past earthquakes can be determined by the analysis of the geomorphological and stratigraphic record. Subhorizontal datums such as marine and lacustrine shorelines, fluvial and alluvial-fan surfaces, and cultural features can reveal the major patterns of surface deformation. Stratigraphic studies in enviroments such as estuaries and shallow lakes can often be interpreted to determine the amount of sudden vertical tectonic movements (Hull, 1986; Atwater, 1987). Considerable speculative interpretation is often required, however, to link data from a wide area, the major limitations arising from the uncertainties of dating and the non-tectonic causes of sudden enviromental change.

FUTURE DIRECTIONS

Future studies of active thrust and reverse faults should focus in the following areas:

1. Documentation of historic events. The relationship between surface fault rupture and large earthquakes is still poorly known for thrust and reverse events. A number of studies of large thrust and reverse faulting events have been carried out in the last 20 years (for example, Gordon, 1971; U.S. Geological Survey Staff, 1971; Berberian, 1979; Yeilding and others, 1981; Stein and King, 1984) but there is a need to understand better the relationship between earthquakes and fault displacement from other, less well studied historic earthquakes. In many regions good data already exists but the

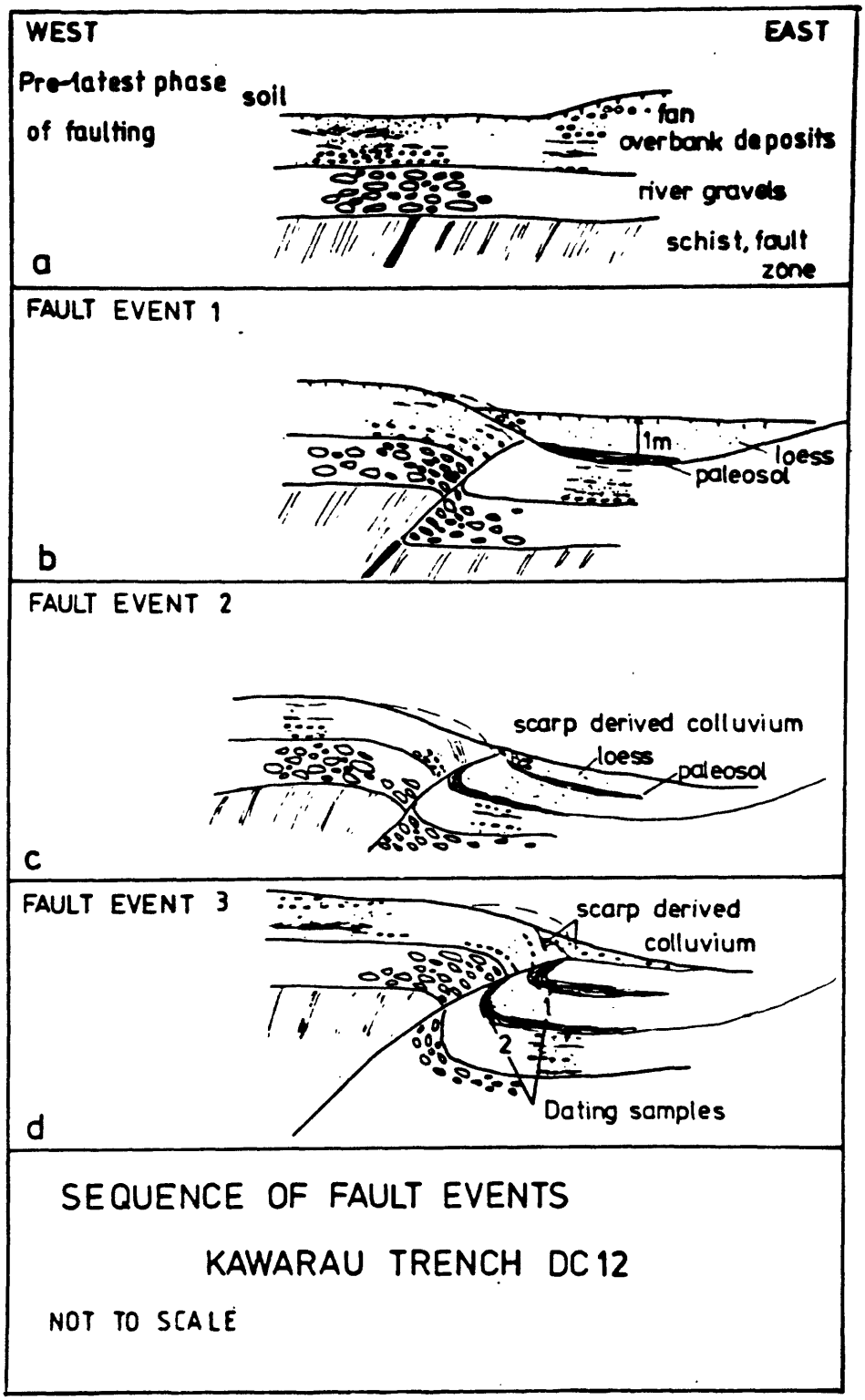

FIGURE 5.--Sequence (a-d) of three fault displacements established from buried soils exposed in a trench across a trace of the Kawarau fault, South Island, New Zealand (from Beanland and Fellows, 1984).

seismological and geologic data require integrated interpretation.

2. Analyses that correlate fault slip and rupture area to earthquake magnitude require further extension to relate tectonic uplift and downdrop, without surface faulting, to earthquake magnitude. Fault dislocation modelling using geologically determined surface movement may be able to assess the size of earthquakes in regions without significant surface -fault rupture. The geological data can come from further studies of the distribution of uplifted Holocene marine terraces, fluvial systems affected by sudden elevation changes, and coastal enviroments subjected to subsidence.

ACKNOWLEDGMENTS

I thank the conference organisers for their invitation to participate in this important meeting. Brian Atwater, Sarah Beanland and Rick Sibson provided valuable comments on early drafts. Financial support from a New Zealand National Research Advisory Council Postgraduate Fellowship is acknowledged.

REFERENCES

Atwater, B.F., 1987, Evidence for great Holocene earthquakes along the outer coast of Washington state: Science, v. 236, p. 942-944.

Beanland, S., Hull, A G., Thomson, R., 1983, Trenching investigations of the Dunstan Fault--Appendix 2, Seismotectonic hazard evaluation of the Clyde dam site, New Zealand Geological Survey Report EG 375, 40 p.

Beanland, S. and Fellows, D.L., 1984, Late Quaternary tectonic deformation in the Kawarau River area, Central Otago: New Zealand Geological Survey/EDS Immediate Report 84/019, 6 p.

Beanland,S., Berryman, K.R., Hull, A.G., Wood, P.R., 1986, Late Quaternary deformation at the Dunstan Fault, Central Otago, New Zealand: Royal Society of New Zealand Bulletin 24, p. 293-306

Berberian, M., 1979, Earthquake faulting and bedding thrust associated with the Tabas-e-Golshan (Iran) earthquake of September 16, 1978: Bulletin of the Seismological Society of America, v. 69, no. 6, p. 1861-1889.

Gordon, F. R., 1971, Faulting during the earthquake at Meckering, Western Australia--14 October 1968: Royal Society of New Zealand Bulletin 9, p. 95-96.

Gordon, F.R and Lewis, J.D., 1980, The Meckering and Calingiri earthquakes October 1968 and March 1970: Geological Survey of Western Australia, Bulletin 126, 229 p.

Hull, A.G., 1986, Pre-A.D. 1931 tectonic subsidence of Ahuriri Lagoon, Napier, Hawke's Bay, New Zealand: New Zealand Journal of Geology and Geophysics v. 29, p 75-82.

Ikeda, Y., 1983, Thrust front migration and it's mechanism--Evolution of intraplate thrust fault systems:

Bulletin of the Department of Geography, University of Tokyo, v. 15, p. 125-159.
Officers of the Geological Survey, 1983, Seismotectonic hazard evalution of the Clyde dam site: New Zealand Geological Survey Report EG 375, 170 p.
Plafker, G., 1969, Tectonics of the March 27, 1964 Alaska earthquake: U.S.Geological Survey Professional Paper 543-I, 174 p.
Sawa, H., 1980, Active faults in western and southern margin of the Kofu Basin, central Japan: Geographical Review of Japan, v. 54, p 473-492.
Stein, R., and King, G.P.C.,1984, Seismic potential revealed by surface folding: 1983 Coalinga, California, earthquake: Science, v. 224, p. 869-872.
U.S.Geological Survey Staff, 1971, Surface faulting: Geological Survey Professional Paper 733, p. 55-76.
Yeilding, G.A., Jackson, J.A., King, G.C.P., Sinvhal, H., Vita-Finzi, C., Wood, R.M., 1981, Relations between surface deformation, fault geometry, seismicity, and rupture characteristics during the El Asnam (Algeria) earthquake of 10 October 1980: Earth and Planetary Science Letters, v. 56, p. 287-304.

MIGRATION OF HISTORICAL EARTHQUAKES, CENTRAL JAPAN

by

Eikichi Tsukuda

Geological Survey of Japan
Higashi 1-1-3, Yatabe, Tsukuba, 305 Japan

ABSTRACT

Faults for historical intraplate earthquakes during the past 1,200 yrs in central Japan are discussed in this paper. Recent excavation surveys of active faults, and reexamination of hazard distribution and surface deformation at the time of historical earthquakes have provided some well-constrained data that we have used to identify faults for historical events and their space-time relationships.

In the Kinki district, starting from the earthquake of 1510 on the eastern marginal thrust faults of Osaka Basin, earthquakes of 1596, 1662, 1812, and 1854 occurred and migrated generally eastward. On the other hand, in the Chubu district, the 1586 earthquake on the Atera fault was followed by the 1779 earthquakes and two 1858 earthquakes. In this case, earthquakes migrated generally northwestward. Then, the great Mino-Owari earthquake (M=8.0) occurred in the manner of connecting those two major migration ends.

On the basis of the above mentioned migration history and the interpretation of earthquakes during the period 8 to 15 century, I designated four "Potential seismic zones" or precaution fault zones surrounding the previously active area. Those are named as Median Tectonic Line seismic zone, Itoigawa-Shizuoka Tectonic Line seismic zone, Central Japan Alps seismic zone, and Noto Peninsula seismic zone, which has experienced no destructive earthquakes in our history and is now in a state of very low seismicity.

INTRODUCTION

Trench excavation surveys have been conducted widely in Japan to identify paleoseismic events on faults (fig. 1). These studies were very successful (Tsukuda and Yamazaki, 1984; Tsukuda, 1985) and should be carried out more extensively because there is no alternative way and there are many active faults with no geologic information on activity and previous events.

For the evaluation of the near-future earthquake potential, Matsuda (1977) proposed the elapsed ratio (E) expressed by ratio of t to recurrence interval R, where t is a length of time elapsed without large earthquakes up to the present. Faults of E (t/R)>0.5 are designated as "precaution faults". In this case, it is very important to recognize and date the most recent event on the fault. Fortunately, we have an excellent data set of historical earthquakes (Usami, 1975), and the date of the most recent event for some faults may be constrained well by referring to the catalogue.

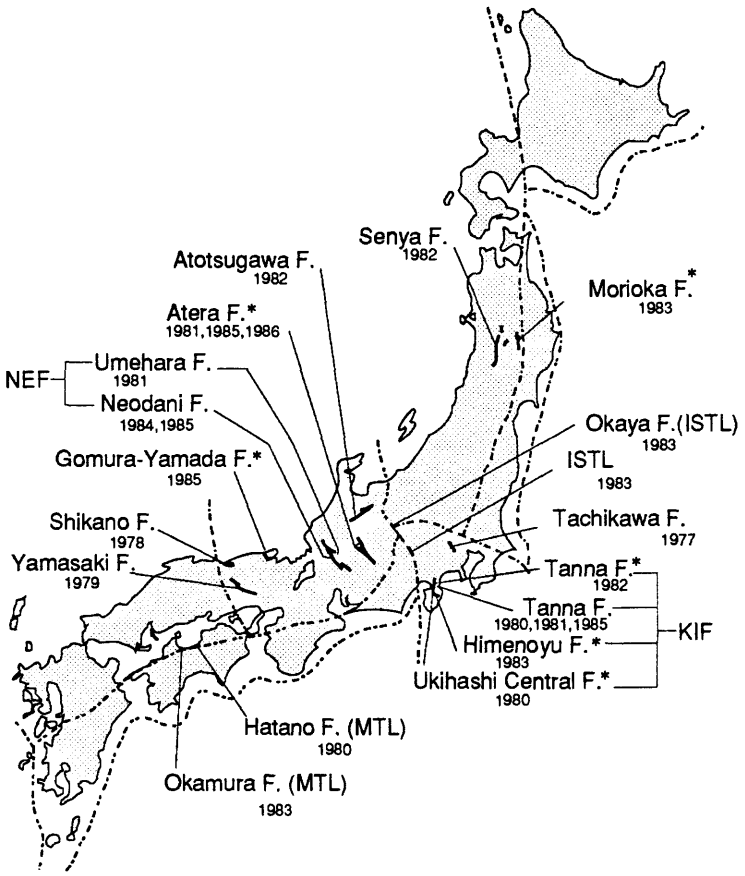

FIGURE 1. -- Excavation survey of active faults in Japan through the end of 1986. Faults (F) marked by * were mainly surveyed by Geological Survey of Japan. ISTL: Itoigawa-Shizuoka Tectonic Line; KIF: Kita-Izu Fault System; MTL: Median Tectonic Line; NEF: Nobi(Mino-Owari)Earthquake Fault System.

It is also important to identify the fault or fault segment associated with historical earthquakes in order to reveal a space-time relationship of faulting in our historical time. On the basis of recent studies, the migration behavior of historical destructive earthquakes is discussed in this paper. It may give us some idea on segmentation of faults, and the interaction of segments and seismogenic processes. It may also provide a clue to predict a future occurrence of earthquakes in the fault system of central Japan.

TECTONIC SETTING AND ACTIVE FAULTS OF CENTRAL JAPAN

The area discussed in this paper is located in the marginal zone of the Eurasian plate and

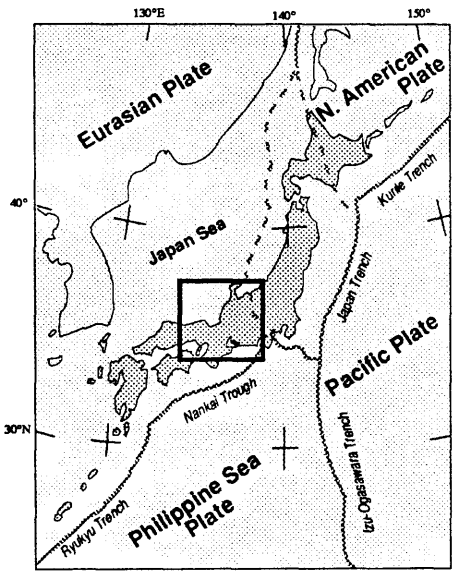

FIGURE 2. -- Plate tectonic setting in and around Japan. Active faults in the rectangular area are discussed in this paper.

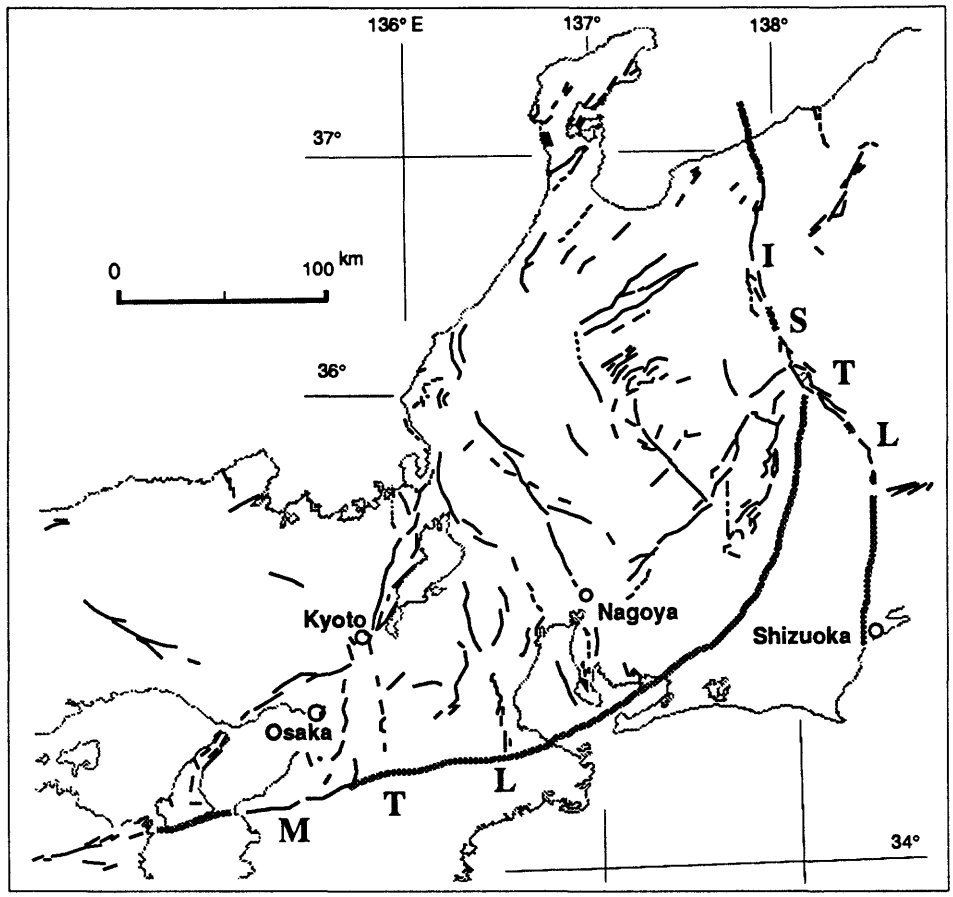

FIGURE 3. -- Active faults in central Japan compiled from 1/500,000 Neotectonic maps of Geological Survey of Japan. Active faults are most densely distributed in this area. MTL; Median Tectonic Line, ISTL; Itoigawa-Shizuoka Tectonic Line.

belongs to the tectonic province known as the inner zone of southwest Japan (fig. 2). This area includes two major tectonic lines, the Median Tectonic Line (MTL) and Itoigawa-Shizuoka Tectonic Line (ISTL). ISTL has recently been referred to the boundary fault between the North American plate and Eurasian plate. This area is divided into two districts; the Chubu in the east and the Kinki in the west.

Active faults are most densely distributed in central Japan (Matsuda, 1981; Kakimi, 1983; fig. 3). Generally speaking, north-south-trending faults are thrust faults, northwest - southeast are left-lateral slip faults and northeast - southwest are right-lateral slip faults. Maximum compressional stress obtained from conjugate sets of strike-slip faults is oriented east-west. It is the same direction as P-axis of shallow earthquakes (Ando and others,1979; Wesnouskey and others, 1982). Regional averages of the rates of crustal shortening and horizontal compressive strain are calculated at 6.7 mm/yr and 2.6 x 10^{-8}/yr, respectively from 400-yr record of seismicity by Wesnousky and others (1982).

STUDY OF HISTORICAL EARTHQUAKES

Owing to geologic excavations and interdisciplinary work with seismologists and archae-

ologists, the study of historical earthquakes in Japan is being advanced. Recent studies of earthquakes in 1510, 1586, and 1662 are reviewed as follows:

Earthquake of 1510

Sangawa (1986) investigated the detailed topography of Konda-yama tumulus (burial mound, 430 m long) in the eastern end of Osaka plain. This tumulus is said to be built for the Emperor Ohjin in the fourth or fifth century. He found that the tumulus was deformed by the Konda fault of 4 km long. Vertical displacement is measured 1.8 m, which may represent an historic destructive event. He concluded the event was the earthquake of 1510 (fig. 4b) because there was no other destructive earthquake in eastern Osaka plain in our history.

Magnitude (M) for the earthquake is calculated as 7.1 from the equation M = (logD+4.0)/0.6 (Matsuda, 1975; 1977). D (meter) is the surface displacement accompanying an earthquake. The long-term vertical slip rate (S) of 0.25-0.4 m/10^3 yr for the Konda fault is obtained from terrace-deformation analysis. Then, recurrence interval (R) is estimated at 5,000 - 7,500 yrs from the equation logR = 0.6M-(logS+4.0) (Matsuda, 1977).

Empirically speaking, the surface faulting for the earthquake of magnitude 7.1 extends at least 20 km. Therefore, it is very possible that the eastern marginal thrust faults of Osaka Basin, composed of the Konda fault and Ikoma fault, generated the earthquake of 1510 (fig. 5).

Earthquake of 1586

The great earthquake of 1586 affected almost the entire area of the Chubu and Kinki districts. The magnitude is estimated at 7.9 - 8.1 and the epicenter is located in the northwest border of Gifu prefecture by Usami (1975). Because it occurred in the mountainous area and it was a time of war, the earthquake fault had not been well identified in spite of the magnitude of the earthquake.

The Atera fault, which dissects central Japan with a northwest-southeast strike and a length of 70 km, is one of the most active faults in Japan. The fault shows left-lateral slip and a vertical component with the northeast side up. Lateral-slip rate is estimated to be about 3-5 m/10^3 yr (Sugimura and Matsuda, 1965). The Atera fault was designated as one of the precaution faults (Matsuda, 1981) because it was believed that there was no historic activity on the fault and more than half of its recurrence interval had elapsed. Therefore, the Geological Survey of Japan chose the Atera fault as one of our main study fields and five excavation surveys have been conducted along the fault since 1981 (Tsukuda and Yamazaki, 1984; Awata and Tsukuda, 1986; fig. 1). Estimated dates of previous events and recurrence intervals are summarized in figure 6. The latest four events an average recurrence interval of 1,700 yrs. The date of the most recent event could not be well constrained by excavation surveys because of artificial modification near surface, but it is very possible that this event occurred historically. Dai-itokuji, a temple on the fault, is reported to have collapsed completely during the 1586 earthquake. En echelon fractures still remain covered by thick forest near the temple. There is a legend that the 1586 earthquake made a pond, which is a wet mud field now and is explained as a sag pond on the fault. These geological and historical observations strongly suggest the Atera fault moved during the earthquake of 1586.

TABLE 1. -- Intraplate earthquakes, A.D. 715 to present, of magnitude greater than or equal to 6.4 in central Japan(fig..4A and 4B). Cat.No. is Usami's (1975) catalogue number.

No.	Cat.No.	Date	Mag.	Location (Earthq. Name)	Long.	Lat.
1	005	7/4/715	6.4	Tenryu river	137.9	35.1
2	006	7/5/715	6.7	Mikawa	137.4	34.8
3	007	5/18/734	7.0	Kii	136.1	34.3
4	008	6/5/745	7.9	Mino	136.6	35.5
5	009	6/9/762	7.4	Mino, Hida, Shinano	137.3	35.6
6	012	8/11/827	6.7	Kyoto	135.6	34.9
7	014	?/?/841	6.7	Matsumoto	138.0	36.2
8	019	7/10/863	7.0	Echu-Echigo	138.1	37.1
9	020	8/3/868	7.1	Harima, Yamashiro	134.8	34.8
10	027	8/26/887	7.4	N. Shinano	138.1	36.6
11	031	5/22/938	6.9	Kyoto	135.8	34.8
12	032	7/22/976	6.7	Yamashiro, Omi	135.8	34.9
13	033	1/30/1038	6.7	Kii, Koyasan	135.6	34.3
14	035	12/1/1070	6.4	Yamashiro, Yamato	135.8	34.8
15	042	8/13/1185	7.4	Omi, Yamashiro, Yamato	136.1	35.3
16	050	2/24/1317	6.7	Kyoto	135.8	35.1
17	051	12/5/1325	6.7	Northern Omi	136.1	35.6
18	064	5/13/1449	6.4	Yamashiro, Yamato	135.75	35.0
19	067	6/19/1494	6.4	Nara	135.7	34.6
20	069	1/28/1502	6.9	SW Echigo	138.2	37.2
21	070	9/21/1510	6.7	Settsu, Kawachi	135.6	34.6
22	078	1/18/1586	8.1	Hida, Mino (Tensho)	136.8	36.0
23	082	9/5/1596	7.25	Kyoto, Settsu	135.75	34.85
24	087	11/26/1614	7.7	Echigo-Takada	138.0	37.5
25	099	11/23/1640	6.7	Kaga-Taiseiji	136.2	36.4
26	115	6/16/1662	7.8	Yamashiro, Omi	136.0	35.25
27	121	2/1/1662	6.4	W. Echigo	138.2	37.1
28	159	4/28/1714	6.4	Omachi	137.8	36.7
29	163	8/22/1718	6.4	Shinano, Ina	137.9	35.3
30	184	3/26/1751	6.4	Kyoto	135.4	35.0
31	185	5/20/1751	6.6	Echigo, Ecchu	138.1	37.1
32	218	6/29/1799	6.4	Kaga	136.6	36.6
33	229	8/2/1819	7.4	Ise, Mino, Omi (Hikone)	136.3	35.2
34	236	8/19/1830	6.4	Kyoto	135.7	35.0
35	238	5/27/1833	6.4	W. Mino	136.6	35.5
36	248	5/8/1847	7.4	Nagano(Zenkoji)	138.2	36.7
37	254	7/9/1854	7.6	Iga-Ueno, Yokkaichi	136.0	34.75
38	268	4/9/1858	6.9	Kaga, Echizen(Hietsu)	137.2	36.5
39	269	4/9/1858	6.9	Kaga, Echizen	136.3	36.2
40	279	3/6/1864	6.4	Harima, Tamba	134.8	35.0
41	300	10/28/1891	8.0	Mino, Owari (Nobi)	136.4	35.6
42	376	8/14/1909	6.8	N. Nagahama(Anegawa)	136.3	35.4
43	418	11/11/1918	6.5	(Omachi)	137.88	36.45
44	438	5/25/1925	6.8	(Tajima)	134.8	35.7
45	445	3/7/1927	7.5	(N. Tango)	135.1	35.6
46	503	9/10/1943	7.4	(Tottori)	134.2	35.5
47	507	1/13/1945	7.1	(Mikawa)	137.0	34.7
48	515	6/28/1948	7.3	(Fukui)	136.2	36.1
49	526	3/7/1952	6.8	(Off Taiseiji) Ishikawa Pref.	136.20	36.48
50	551	8/19/1961	7.0	E. Fukui Pref.(Kita-Mino)	136.77	36.02
51	556	3/27/1963	6.9	Wakasa bay	135.77	35.78
52	568	8/3/1966 ~	6.4	(Matsushiro)	138.2	36.5
53	591	9/9/1969	6.6	(C. Gifu pref.)	137.04	35.47
54		9/14/1984	6.8	(W. Nagano pref.)	137.56	35.82

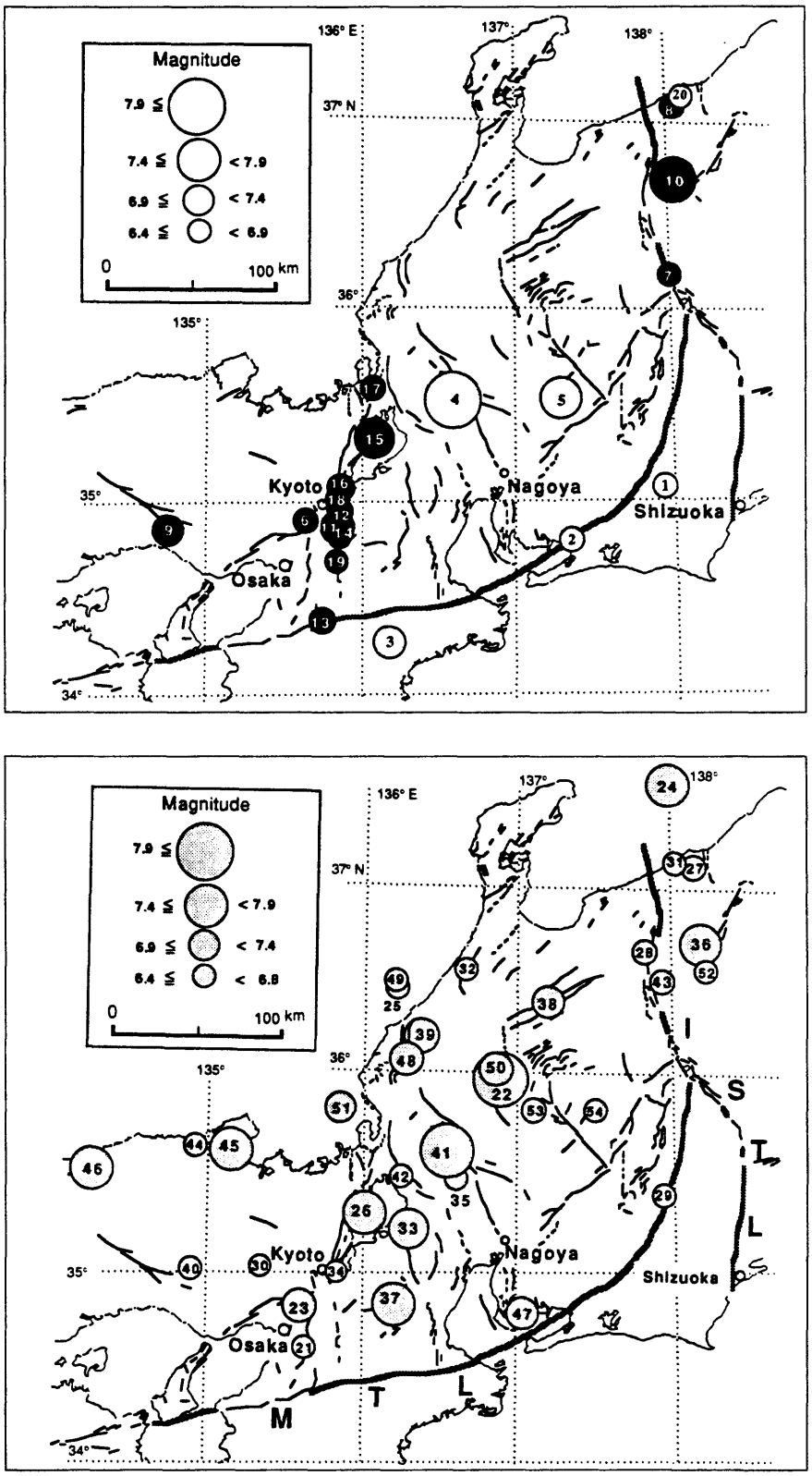

FIGURE 4. -- Historical intraplate earthquakes in central Japan of M ≥ 6.4 during the period 715 - 1500 (fig. 4A), 1500 - 1986 (fig. 4B). The dark symbols of figure 4A indicate the events during the period 800-1500. The radius of the epicenter symbol is proportional to the magnitude of the event. Numbers in or adjacent to symbols correspond to table 1.

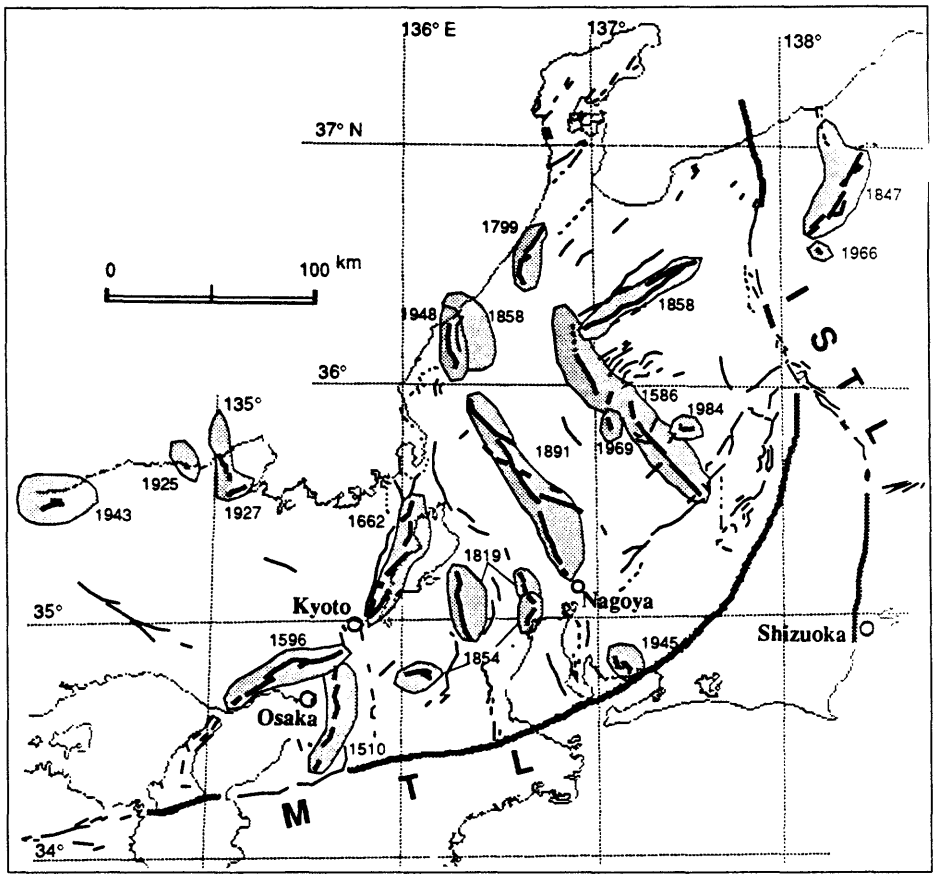

FIGURE 5. -- Faults for historical events during the period 1510 to present. Numbers are dates for earthquakes.

The area of severe damage from the earthquake extended northwest of the Atera fault, where a number of landslides were reported. This is the reason why the epicenter is located there. This may suggest that the Ohara and Miogo faults northwest of the Atera fault moved at the same time. It means that the total fault length for the 1586 earthquake would be estimated at about 85 km.

Earthquake of 1662

The epicenter of 1662 earthquake (M=7.8) is located in Biwa lake. The western coast region of the lake suffered severe damage and it is reported that a significant area of the coast had been submerged into the lake. Sangawa and Tsukuda (1986b) investigated ancient picturesque maps for comparison with present topography. The detailed bathymetric map shows the ancient main road is now below the water. The tectonic depression from the earthquake was estimated at about 2-3 m.

Fault scarplets near the coast that cut the terrace dated younger than 5,700 yr B. P. show 2.0-2.7 m of vertical displacement, the amount of which is comparable to the depression. The submerged zone was recognized along the entire coast of Biwa lake. The length of surface-fault

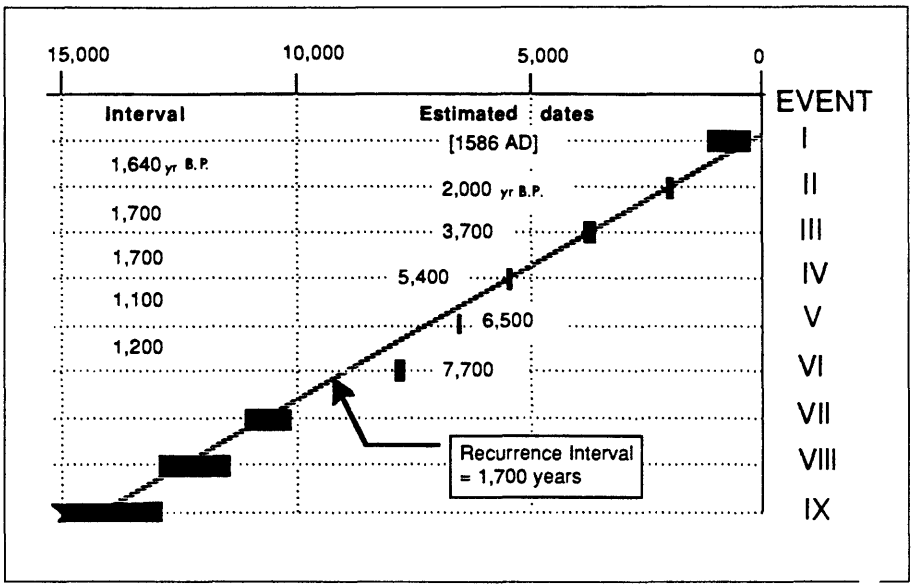

FIGURE 6. -- Estimated date and recurrence interval of events on the Atera fault. Width of black rectangles indicates uncertainity in timing of each event.

rupture is expected more than 50 km for the earthquake of magnitude 7.8. Accordingly, we concluded that the 1662 earthquake was caused by the movement of the western marginal fault system of Biwa lake, which is composed of en echelon thrust faults and is responsible for development of Biwa lake basin.

The event prior to the 1662 earthquake is estimated to be about 3000 yr.B.P. from the analysis of sand dikes in the archaeological excavation site near the coast (Sangawa and Tsukuda, 1986a).

EARTHQUAKE MIGRATION IN CENTRAL JAPAN

Paleoseismological studies mentioned above lead to a migration sequence of destructive large earthquakes from the 16th century to the present. Faults for earthquakes during this period (fig. 4B) are shown in figure 5 and migration behavior described below is illustrated in figure 7.

In the Kinki district, the 1596 earthquake (M=7.25) occurred after the faulting (1510) on the eastern margin of Osaka basin. Umeda and others (1984) indicated the activation of the Arima-Takatsuki line in the historical time by the existence of earthquake traces impressed on the Yayoi-age (B.C. 3c - A.D. 3c) dwelling site in the western portion of the fault. Recently geologic evidence of faulting between 15- and 17-century layers was found during archaeological excavation near the eastern end of the fault. These data strongly suggest the 1596 earthquake was caused by Arima-Takatsuki line, which is the northern margin of Osaka basin. After that the earthquake on the western marginal faults of Biwa lake occurred in 1662. Then, the Hikone

earthquake (M=7.4) occurred in 1819. Faults for Hikone earthquake have not been identified geologically yet. But, the seismic intensity map for the earthquake (fig. 229-1 of Usami, 1975) indicates the western marginal thrust faults of the Suzuka mountains were activated paired with the Yoro fault. The Iga-Ueno earthquake (M=7.6) occurred in 1854. The Kizugawa fault is identified as the earthquake fault by Yokota and others (1976). Seismic intensity map (fig. 254-2 of Usami, 1975) suggests the Kuwana and Yokkaichi faults were activated at the same time.

On the other hand, in the Chubu district, the Kaga earthquake (M=6.4) of 1799 occurred north of the 1586 rupture zone (Atera fault). Sangawa (1986) indicated the thrust fault (Morimoto fault) in Kanazawa caused this earthquake. The earthquake (M=6.9) of 1858 occurred on the Atotsugawa fault (Matsuda, 1966; Research Group for Excavation of the Atotsugawa Fault, 1983). Two hours later, another earthquake (M=6.9) occurred east of Fukui. The fault for this earthquake is not identified.

The Mino-Owari earthquake of 1891 (M=8.0, Matsuda, 1974) occurred after these events. It seems that the occurrence of this Mino-Owari earthquake is closely related to the earthquake migration in the Kinki and Chubu districts. Near both ends of the Mino-Owari earthquake faults ruptured in 1945 (Mikawa earthquake) and 1948 (Fukui earthquake).

DISCUSSION

Earthquake data from before the 16 century have more uncertainties (fig. 4A). However, it is easy to recognize the earthquake clustering from 827 to 1487 in Kyoto-Nara area, which is supposed to have occurred on north-south-trending faults (Miki, 1980; 1983). I call it "Kyoto-Nara seismic zone". It is very interesting that most of the earthquakes in this period were generated in this seismic zone except for earthquakes Nos.7, 8 and 10, which are located on or east of Itoigawa-Shizuoka Tectonic Line, and No. 9 which occurred on the Yamasaki fault (Okada and others,1980). After this seismic period, the 1510 earthquake occurred and the eastward migration began.

The earthquake (M=7.9) in 745 was thought to be the previous event of the Mino-Owari earthquake (Matsuda, 1977), but it is not identified by excavation survey (Disaster Prevention Research Institute, 1983). The most possible candidate would be the Yanagase-Suzuka fault zone. No geologic information on the previous events on this fault zone are not reported. The earthquake (M=7.0) in 734 is located south of the Median Tectonic Line where is no active fault. It may be relocated to the southern segments of the Yanagase-Suzuka fault zone.

The earthquake (M=7.4) in 762 was thought to be the most recent event of the Atera fault. But, there is no geologic and historic evidence (Awata and Tsukuda, 1986). It may be the event on the Hachiman fault between the Mino-Owari earthquake fault and the Atera fault.

Consequently, it appears that almost every major fault of inner central Japan has broken during our historical time.

Earthquake clustering or seismic chain reaction appears to have occurred in fault zones in several areas. These include the Kyoto-Nara area, the Mikawa and Fukui earthquakes after the Mino-Owari earthquake, the Kanto-Izu district (Matsuda, 1981) and the Kitayuri thrust system of Tohoku district (Awata and Kakimi, 1985). This seismic chain reaction can be one of the characteristics of faulting in intraplate Japan. Migration described in the previous section might be seen as a kind of chain reaction.

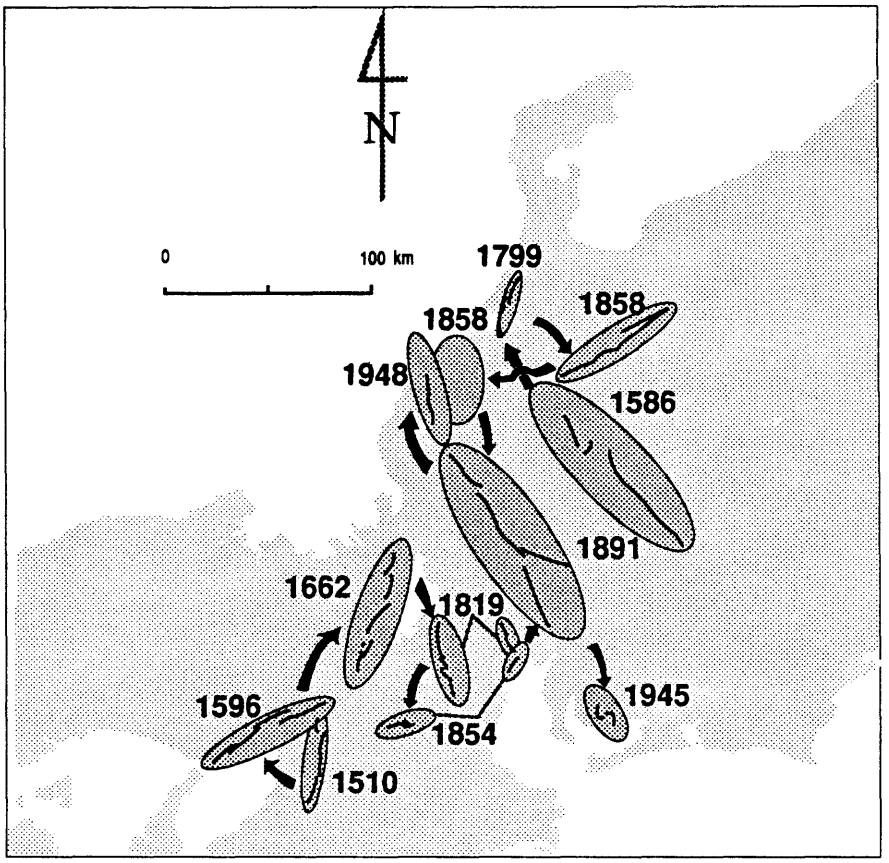

FIGURE 7. -- Migration of faulting in central Japan from earthquake 21 to 41 of table 1. Numbers are dates of the event. Before the earthquake of 1510, there was earthquake clustering along the faults of Kyoto and Nara area, which is east of 1510 faults and west of 1662 faults (figs. 4A and 5).

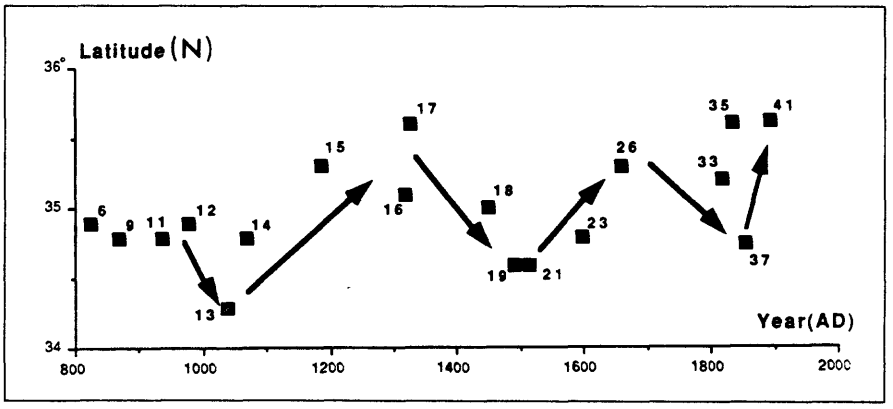

FIGURE 8. -- North-south oscillation of epicenters from earthquake 6 to 41 of table 1 in Kinki district.

North-south epicentral oscillation since the 9th century in Kinki is shown in figure 8, which was superimposed on general eastward earthquake migration. This north-south oscillation is also recognized on earthquakes since 1586 in Chubu. Yoshida (1987) indicates the southward migration of recent earthquakes (Nos. 50, 53, 54 of table 1) after the Fukui earthquake in 1948.

Wesnousky and others (1982) showed that the rate of seismic moment release in central Japan calculated from the seismicity data during the past 400 yrs is in good agreement with the rate obtained from the late Quaternary average slip rates of active faults. They concluded that the rate and mode of deformation in central Japan has been steady during the late Quaternary. This suggests that the activity in historical time, which may look exceptionally high, will continue in the near future as well.

It is interpreted that most of major faults inside of central Japan have moved during the period of the past 1,200 yrs as discussed above. It is recognized by geological observations that an active fault in central Japan causes "characteristic earthquakes" (Schwartz and Coppersmith, 1984) with a long recurrence interval. A seismic chain reaction or clustering is expected in seismotectonic zones in intraplate Japan. With this view, I designate four "potential seismic zones" (fig. 9), which have almost the same meaning as precaution fault of criterion 1 in Matsuda (1981). Potential seismic zones are characterized by low seismicity at present, no historic major events and tectonic significance.

Median Tectonic Line (MTL) seismic zone: the right-lateral slip rate and recurrence interval of MTL is estimated 5-10 m/10^3 yr by Okada (1980) and 600-1,300 yr B.P., respectively. The most recent event of MTL is obtained as A.D. 510±200 from the excavation survey (Disaster Prevention Research Institute, 1985).

Itoigawa-Shizuoka Tectonic Line (ISTL) seismic zone: ISTL is a major tectonic boundary as well as MTL. The most recent event is estimated as 1,700-2,500 yr B.P. at Okaya site (Research Group for the Okaya fault, 1984), and 1,000-1,400 yr B.P. at Fujimi site (Miyoshi and Research Group for the Itoigawa-Shizuoka Tectonic Line, 1984) by excavation survey in the central segments of this zone. The recurrence interval is estimated at about 2,500±500 yrs in northern segment.

Central Japan Alps (CJA) seismic zone: characterized by thrust faults on both fronts of CJA. The Inadani fault system belongs to this seismic zone.

Noto Peninsula seismic zone: characterized by very short dip-slip faults with low seismicity.

SUMMARY AND CONCLUSIONS

According to recent progress of paleoseismology, I described the long-term seismic behavior in central Japan from the 8th century to the present. Some of the active faults in this area are at present being investigated and much more detailed studies are required. It is, however, hard to avoid pointing out the following conclusions:

1. After the earthquake of 1510 on the eastern marginal faults of Osaka plain, destructive earthquakes in 1596, 1662, 1819 and 1854 migrated to the east. In the Chubu district the 1586 earthquake on the Atera fault are followed by 1799 and two 1858 earthquakes migrating to northwest. The Mino-Owari earthquake in 1891 occurred, connecting termination ends of those two major migrations.

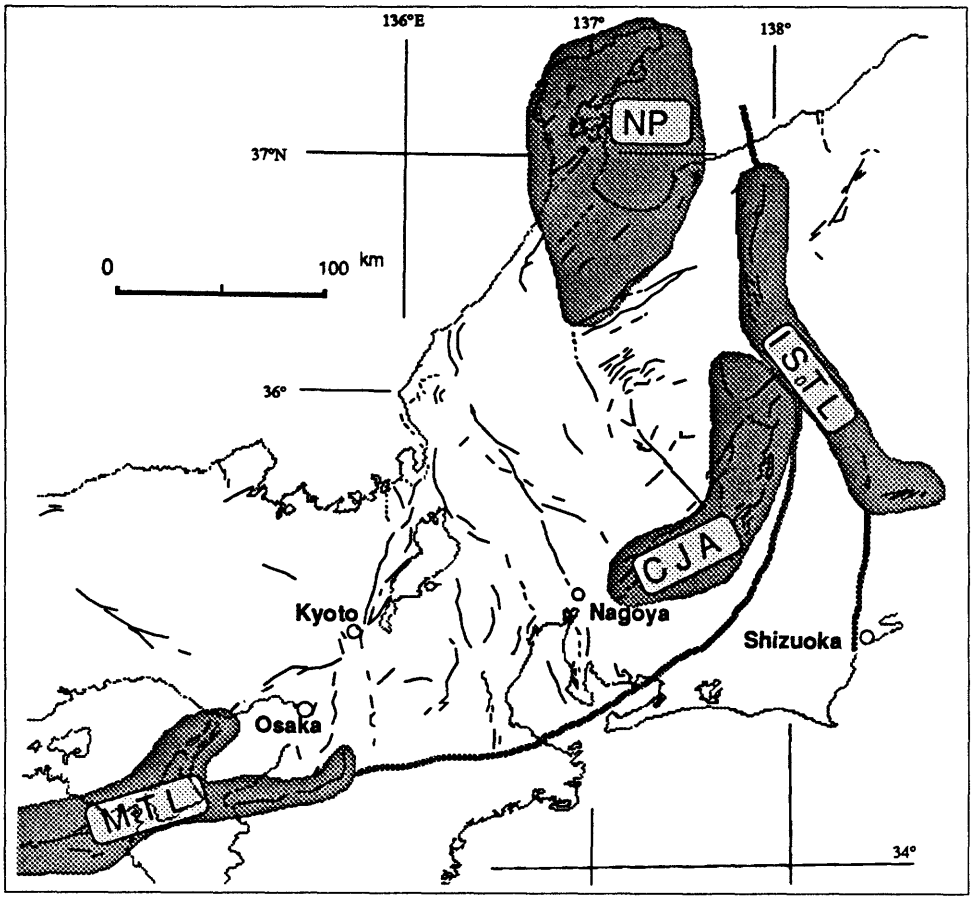

FIGURE 9. -- Major potential seismic zones surrounding the core of central Japan which had been active during the past 1,200 yrs. MTL: "Median Tectonic Line seismic zone"; CJA: "central Japan Alps seismic zone"; ISTL: "Itoigawa-Shizuoka Tectonic Line seismic zone"; NP: "Noto peninsula seismic zone".

2. It is very possible that earthquakes for 8-15 centuries occurred on faults that did not break since the 16th century.
3. The north-south oscillation of epicenters is recognized.
4. Outside of the core region of central Japan in which major faults have ruptured in our historic time, four potential seismic zones are designated by low seismicity, no historic major events, and tectonic characteristics.

I understand these are a kind of working hypotheses suggesting future contributions of geologic studies for this area.

Acknowledgements

I am indebted to my colleagues of the seismotectonic research section of the Geological Survey of Japan, especially to Drs. Akira Sangawa, Haruo Yamazaki, Yasuo Awata, and chief, Yoshihiro Kinugasa for their frequent discussions. I thank Dr. David P. Schwartz for reading the manuscript and for his helpful suggestions.

REFERENCES CITED

Ando, M., Matsuda, T. and Abe, K., 1973, Stress field of the upper crust in the Japanese island: Seismological Society of Japan, Program and abstracts, p. 51. (in Japanese)

Awata, Y. and Kakimi, T., 1985, Quaternary tectonics and damaging earthquakes in northwest Honshu: Earthquake Prediction Research, v. 3, p. 231-251.

Awata, Y. and Tsukuda, E., 1986, Recent activity of the Atera fault — from excavation surveys of Kashimo, Tsukechi, Sakashita and Yamaguchi: Proceeding of the second Atera fault symposium, Sakashita-cho Educational Committee, p. 1-11. (in Japanese)

Disaster Prevention Research Institute, 1983, Trenches across the trace of the 1891 Nobi earthquake faults: Reports of Coordination Committee for Earthquake Prediction, v. 29, p. 360-367. (in Japanese)

_____ 1985, Exploratory trenching survey of the Median Tectonic Line: Reports of Coordination Committee for Earthquake Prediction, v. 33, p. 446-454. (in Japanese)

Kakimi, T., 1983, Regional interrelation between active faults and destructive earthquakes on land in Japan: Bulletin Geological Survey of Japan, v. 34, p. 295-309. (in Japanese with English abstract)

Matsuda, T., 1966, Lateral displacement of Atotsugawa fault, Japan: Special Bulletin Earthquake Research Institute, University of Tokyo, 13, p. 85-126. (in Japanese)

_____ 1974, Surface faults associated with Nobi (Mino-Owari) earthquake of 1891, Japan: Special Bulletin Earthquake Research Institute, University of Tokyo, v. 13, p. 85-126. (in Japanese)

_____ 1975, Magnitude and recurrence interval of earthquakes from a fault: Journal of Seismological Society of Japan, v. 28, p. 269-282. (in Japanese with English abstract)

_____ 1977, Estimation of future destructive earthquakes from active faults on land in Japan: Journal Physics of Earth, v. 25, suppl., p. S251-S260.

_____ 1981, Active faults and damaging earthquakes in Japan — macroseismic zoning and precaution fault zone, *in* Simpson, D. W., and Richards, P.W., (eds) Earthquake prediction — An International review: Washington D.C., American Geophysical Union, Maurice Ewing Series 4, p. 279-289,

Miki, H., 1980, Ultra-long-term Prediction of earthquakes— Lecture notes for the memory of late Prof. Tamaki: Kyoto Science Research Association, v. 14, p. 10-27. (in Japanese)

_____ 1983, Long-term prediction of earthquakes in western Honshu, Japan: Journal Seismological Society of Japan, v. 36, p. 180-186. (in Japanese with English abstract)

Miyoshi, M. and Research Group for the Itoigawa-Shizuoka Tectonic Line, 1984, Trenching survey of Itoshizu Line active faults system, Program and Abstracts, Quaternary Research, v. 14, p. 115. (in Japanese)

Okada. A., 1980, Quaternary faulting along the Median Tectonic Line of southwest Japan: Memoir of Geological Society Japan, v. 18, p. 79-108.

Okada. A., Ando, M., and Tsukuda, T., 1980, Trenches across the Yamasaki fault in Hyogo prefecture: Reports of Coordinate Committee for Earthquake Prediction, v. 24, p. 190-194. (in Japanese)

Research Group for Active Faults of Japan, 1980, Active faults in Japan, sheet maps and inventories: Tokyo,University of Tokyo Press, 363p. (in Japanese)

Research Group for the Atotsugawa Fault, 1983, Trenching excavation across the Atotsugawa fault: The Earth Monthly, no. 5, p. 335-340. (in Japanese)

Research Group for the Okaya fault, 1984, The trenching study for the Itoshizu Tectonic Line at Okaya area in 1983: Reports of Coordinate Committee for Earthquake Prediction, v. 32, p. 363-372. (in Japanese)

Sangawa, A., 1986, Fault displacement of the Kondayama tumulus caused by earthquake: Journal of Seismological Society of Japan, v. 32, p. 423-434. (in Japanese with English abstract)

Sangawa, A., and Tsukuda, E., 1986a, Evidence of earthquake recognized at Kitoge-Nishikaido ruins, Imazu-cho,Takashima-gun, Shiga prefecture: Seismological society of Japan, Program and Abstracts, no. 2, p. 136. (in Japanese)

_____ 1986b, Active faults on the west coast of Biwa lake and submergence of coastal zone by the earthquake of 1662 (Kanbun 2): Seismological society of Japan, Program and Abstracts, no. 2, p. 137. (in Japanese)

Schwartz, D. P., and Coppersmith, K. J., 1984, Fault behavior and characteristic earthquakes — Examples from the Wasatch and San Andreas fault zones: Journal of Geophysical Research, v. 89, p. 5681-5698.

Sugimura, A., and Matsuda T.,1965, Atera fault and its displacement vectors: Geological Society of America Bulletin, v. 81, p. 2875-2890.

Tsukuda, E. and Yamazaki H., 1984, Excavation survey of active faults for earthquake prediction in Japan — with special reference to the Ukihashi central fault and the Atera fault: Geological Survey of Japan Report, no. 263, p. 349-361.

Tsukuda, T., 1985, Long-term seismic activity and present microseismicity on active faults in southwest Japan: Earthquake Prediction Research, v. 3, p. 253-284.

Umeda, Y., Murakami, H., Iio, Y., Cho, A., Ando, M., and Daicho, A., 1984, Earthquake traces impressed on the Yayoi-age dwelling site: Journal of Seismological Society of Japan, v. 37, p. 465-473. (in Japanese with English abstract)

Usami, T., 1975, Descriptive catalogue of disastrous earthquakes in Japan : Tokyo, University of Tokyo Press, 327p. (in Japanese)

Wesnousky, S. G., Scholz, C. H., and Shimazaki K., 1982, Deformation of an island arc — Rates of moment release and crustal shortening in intraplate Japan determined from seismicity and Quaternary fault data: Journal of Geophysical Research, v. 87, p. 6829-6852.

Yokota, S., Shiono S., and Yashiki, M., 1976, Earthquake fault of Iga-ueno: Chikyu Kagaku, v. 30, p. 54-56. (in Japanese)

Yoshida, A., 1987, Characteristic pattern in the space-time distribution of large shallow earthquakes: Tectonophysics., v. 136, p. 283-297.

GEODETIC DEFORMATION AND PALEOSEISMOLOGY

Robert Reilinger
Earth Resources Laboratory
Department of Earth, Atmospheric, and Planetary Sciences
Massachusetts Institute of Technology
Cambridge, MA 02139

ABSTRACT

Three examples from the Western U. S. are presented in which short-term geodetic deformation shows a close relationship to longer term deformation as revealed by topographic/structural relief. In the Imperial Valley of southern California, earthquake deformation (coseismic and postseismic) has a very similar spatial pattern to topographic relief within the complex transition zone between the Imperial and San Andreas faults. The relationship between long-term tectonic subsidence in this area and earthquake deformation suggests that currently active fault systems are very young relative to the age of the Imperial Valley or that activity has been episodic on these faults throughout this period. In the Pacific Northwest, considerable uncertainty persists as to the spatial and temporal character of ongoing deformation, although there appears to be some similarity between ongoing coastal tilting measured geodetically and tilting indicated by deformed marine terraces. While this similarity has been interpreted to indicate aseismic subduction, the question of a possible future large subduction earthquake in this area remains unresolved. Comparisons between earthquake deformation measured geodetically and structural relief in the Basin and Range province suggest that large interearthquake movements must occur in such normal-fault environments. These movements apparently involve broad regional uplift. Such uplift has been measured directly in the vicinity of the 1959 Hebgen Lake earthquake. Modeling suggests that postseismic viscoelastic relaxation and strain accumulation in an elastic lithosphere overlying a viscoelastic asthenosphere are possible physical mechanisms to generate these interseismic movements. These mechanisms may be the contemporary expression of the processes responsible for the generally high elevation of the Basin and Range province.

INTRODUCTION

Geodetic observations have played a major role in our understanding of the earthquake process. Traditionally, geodetic measurements made before and after major earthquakes have provided information on surface deformation produced by the earthquake (coseismic), information that has been critical for deducing the geometry of the earthquake-generating fault and the nature of slip on the fault. Among other things, such geodetic observations were instrumental in the development of the elastic-rebound hypothesis of earthquake generation (Reid, 1910) and in the solidification of the plate tectonics hypothesis (Savage and Hastie, 1966; Plafker and Savage, 1970).

The long history of geodetic observations that is being developed in a number of seismically active regions is beginning to reveal the nature of the more subtle deformations which occur between major earthquakes. The earthquake deformation cycle (fig. 1) provides a conceptual framework for understanding many of these observations (Thatcher, 1984); interseismic deformations apparently reflect postseismic adjustments and the slow accumulation of strain energy leading up to the next earthquake. It is the

imperfect balance between the release and accumulation of strain within the seismic cycle that produces the permanent deformation that is revealed by the geologic record (fig. 1). The relationship between the historic deformation that can be measured directly with geodetic methods and longer-term deformation indicated by geologic structure provides the link between geodetic measurements and paleoseismology.

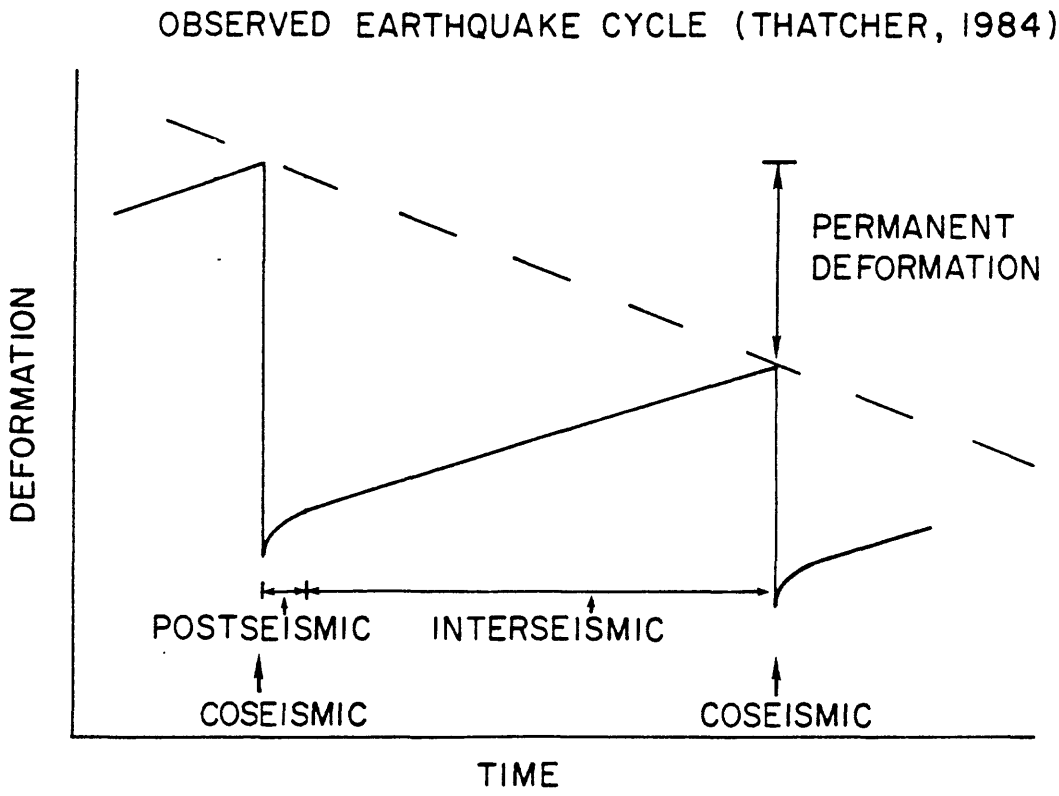

FIGURE 1. --Idealized earthquake deformation cycle (from Thatcher, 1984).

The importance of permanent deformation in the earthquake deformation cycle and the associated implications for estimating earthquake repeat times from geodetic measurements, has been expounded by Thatcher (1984) primarily on the basis of observations from Japan. King and Vita-Finzi (1981), Jackson and McKenzie (1983), Stein (1985), Stein and Barrientos (1985), and Reilinger and Kadinsky-Cade (1985) have utilized geodetic and geologic observations in the vicinity of large intraplate, dip-slip earthquakes to investigate the relationship between geologic structure and earthquake deformation and to estimate earthquake repeat times. In the simplest sense, if the amount of permanent deformation from a single earthquake and the total geologic deformation (for example, topographic or basement relief) are known, it is possible to estimate the number of earthquakes required to develop the existing structure. Information on the age of the structure will then provide an estimate of the average earthquake repeat time. Of course, this is a gross over

simplification and involves a number of assumptions which are difficult to verify and, in at least some cases, are likely incorrect. For example, this reasoning assumes that earthquakes occurring over long periods of time each produce the same permanent deformation, that earthquake activity is roughly uniform in time (versus episodic), and that erosional/depositional processes are known or can be neglected. In spite of these difficulties, these relationships, and the ideas they have given rise to, provide a conceptual framework for beginning to apply geodetic and geologic observations to the earthquake prediction problem. In addition, it may be possible to investigate some of the above assumptions with paleoseismic techniques.

This paper describes a number of examples of the relationship between short (geodetic) and longer (geologic) term deformation from the Western United States and considers possible consequences for earthquake processes (for example, earthquake recurrence, mountain building, etc.). Examples include a region of complex strike-slip deformation along the southernmost segment of the San Andreas fault (Imperial Valley), a region of possible ongoing subduction along the Pacific Northwest coast of Washington and Oregon, and normal faulting in the Basin and Range.

STRIKE-SLIP FAULTING AND TOPOGRAPHIC/STRUCTURAL RELIEF

Many previous studies relating earthquake deformation to topography and geologic structure have involved dip-slip earthquakes. Such earthquakes are dominated by vertical surface movements and thus have a large effect on topography. However, spatially coherent vertical movements are also associated with strike-slip faulting (for example, Chinnery, 1961; Bilham and Williams, 1985; Reilinger and Larsen, 1986), and these vertical movements provide important information on the faulting process. Many of these vertical movements are transient in nature; the coseismic movements are canceled by the postseismic and interseismic movements (or by coseismic movements for earthquakes along adjacent segments of the fault). In these cases, no topography will develop as a result of faulting. On the other hand, some vertical movements associated with strike-slip faulting appear to continue in the same sense throughout the earthquake cycle, and therefore impact topographic and geologic structure. Both types of vertical movements have been recorded by geodetic measurements in the Imperial Valley.

Figure 2 shows the location of three leveling routes crossing the Imperial fault (fig. 2A) and elevation changes in relation to topography along these routes (figs. 2B,C,D). The two approximately east-west routes cross relatively simple sections of the Imperial fault (roughly linear fault segments characterized by predominantly strike-slip behavior) while the north-south route crosses the complex region of intense seismic activity connecting the Imperial and San Andreas faults (Brawley seismic zone: BSZ). Elevation changes along the east-west route crossing the fault near El Centro (fig. 2C) include the coseismic period for the 1940 M = 7.1 earthquake on the Imperial fault, the postseismic period for this event and the coseismic period for the 1979 M = 6.6 earthquake. Examination of figure 2C indicates that the roughly sinusoidal deformation centered on the Imperial fault during the 1940 coseismic period is approximately reversed during the postseismic period. Reilinger (1984) has suggested that this behavior results from coseismic, right-lateral slip along the fault south of the leveling route and postseismic, right-lateral slip north of the route. The important point is that the movements approximately cancel, leaving no net effect on topography. Hence, there is no clear relation between topography and earthquake deformation (however, note that the region just

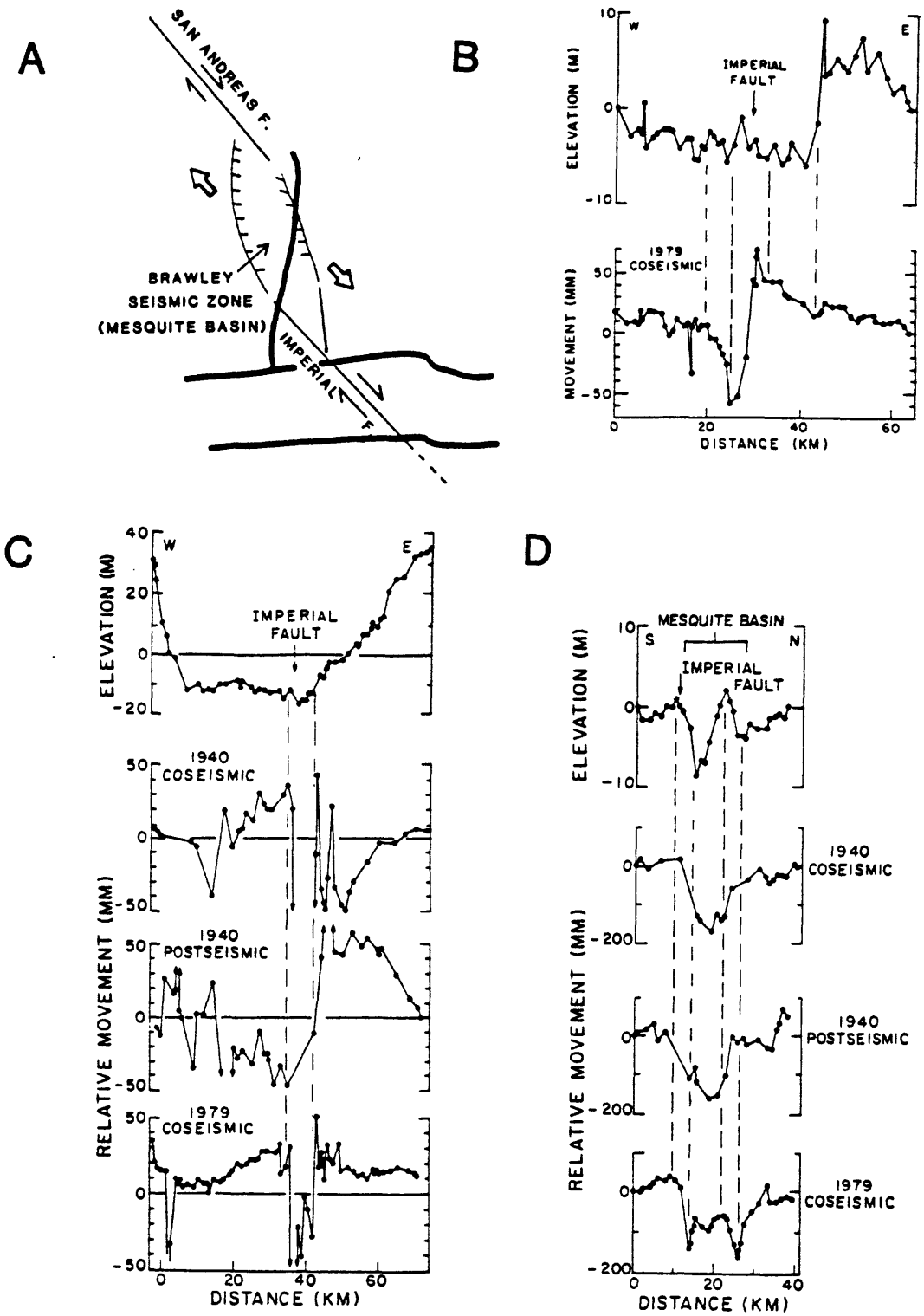

FIGURE 2. --A, Map of portion of the Imperial Valley showing the location of leveling routes (heavy lines) crossing the Imperial fault-Brawley Seismic Zone. B, Elevation changes and topography along route crossing southern end of Imperial fault. C, As B for route crossing central part of the Imperial fault. D, As b for route crossing Brawley seismic zone.

east of the Imperial fault marked by dashed vertical lines in figure 2C shows a continuous history of subsidence and corresponds to the lowest part of the Imperial Valley). Similarly, the route crossing the southern end of the fault shows large sinusoidal motions centered on the fault which are not reflected in the topography (fig. 2B). These movements have been attributed to right-lateral strike-slip along the Imperial fault north of the leveling route (Reilinger and Larsen, 1986). Future slip on the fault south of the route (postseismic creep or another earthquake) should, according to our interpretation, cancel these 1979 coseismic movements. In contrast, the route crossing the BSZ indicates a continuous history of subsidence including 1940 coseismic and postseismic movements, and the 1979 coseismic movements (fig. 2D). This region of historic subsidence corresponds to the Mesquite basin, an area which is topographically lower than its surroundings. In fact, there is a remarkably close correlation between the 1979 coseismic movements and topographic relief within the basin (fig. 2D). This relationship suggests that topography results, at least in part, from the accumulated deformation from many prehistoric earthquakes along the Imperial-Brawley fault system. By comparing the deformation associated with one earthquake to topographic relief, it should be possible to estimate the number of similar earthquakes required to generate the existing topography.

A major problem with trying to quantitatively relate earthquake deformation to topographic relief for this case concerns the poor constraints on erosion and deposition rates for this area. In a region of unconsolidated sediments such as the Imperial Valley, erosion rates could very likely be comparable to rates of tectonic deformation. This problem is avoided by considering basement deformation. While the detailed configuration of the basement is not well known beneath the Mesquite basin, some information is available from seismic refraction measurements (Fuis and others, 1984). The refraction data indicate roughly 700 m of basement relief across the basin. From the geodetic observations, earthquakes on the Imperial-Brawley system produce about 15 cm coseismic and 15 cm postseismic subsidence (fig. 2D). Assuming 30 cm subsidence per earthquake suggests that 2,300 earthquakes similar to the 1940 event are required to produce the observed basement relief. Initial formation of the Imperial Valley is believed to have begun about 4 m.y. B.P. (Fuis and others, 1982). Assuming more or less uniform activity on the Imperial fault during this period suggests a recurrence time of about 2,000 yrs for 1940-type events. This result finds some support from trenching studies along the Imperial fault recently undertaken by R.V. Sharp of the U.S. Geological Survey (USGS). Trenching near the United States-Mexico border indicated no fault offset other than that from the 1940 and 1979 events for many meters of sediment. About halfway down through the section Sharp obtained an age of 700 yrs. Near the bottom of the trench, Sharp documented an unconformity below which the offset shows a significant increase. Although the age is uncertain, 2,000 yrs is reasonable given estimated deposition rates. Thus, the results obtained from analysis of the geodetic data appear to support those obtained through independent methods by Sharp (the trenching results were provided by G. Fuis of the USGS).

The very long recurrence time suggested by the analysis described above raises a number of important questions. For one, there have been two major historic earthquakes on the Imperial fault, the 1940 and 1979 events. This has led some investigators to suggest a recurrence time of 40 yrs for this fault (Sykes and Nishenko, 1984). However, the 1979 event was considerably smaller than the 1940 earthquake and may well have been a kind of aftershock (Reilinger, 1984). If the 1979 event was an aftershock, then it is necessary to redetermine the estimate of recurrence time. Considering the 1940 and 1979

earthquakes as one "event", total basement subsidence per event is about 40 cm. Seven hundred meters of relief then requires roughly 1,750 events yielding a recurrence time of about 2,300 yrs. This is not significantly different from the previous estimate and does not alter the main conclusions.

A more difficult question concerns the missing plate motion. A 2,000-yr recurrence time with roughly 5 m of slip per event implies an average slip rate of about 2.5 mm/yr. This is more than an order of magnitude less than the estimated Pacific-North American plate rate during the last 4 m.y. This would appear to imply that other faults in the Imperial Valley must, over the long term, accommodate much of the plate motion. However, the Imperial fault is, at present, clearly the locus of the large majority of seismic activity. This appears to imply that the current concentration of activity on the Imperial fault is ephemeral and that activity may shift to other faults in the future.

It is possible that the trenching results are in error and that a 40-yr recurrence time is appropriate for the Imperial fault (Sykes and Nishenko, 1984). A 40 year recurrence time with about 2.5 m of slip per earthquake (half that for the 1940 plus 1979 events) yields a slip rate of 6 cm/yr, not significantly different from the long-term plate rate. However, assuming a 40-yr recurrence time implies that the roughly 2,000 earthquakes required to produce the basement relief in the Mesquite basin would occur in only 80,000 yrs. This is much younger than the age of the Imperial Valley and would appear to require that other fault systems have accommodated the plate motion in the past. In support of this interpretation, a number of other lines of geophysical and geological evidence have been interpreted to indicate a young age for the Imperial-Brawley fault system (for example, Fuis and others, 1982; Lachenbruch and others, 1985).

While it is not presently known which, if either, of these interpretations is correct, this work raises some important questions relevant to both earthquake prediction and the nature of the physical processes responsible for the structural evolution of the Imperial Valley and similar areas, questions that can be addressed through integrated studies of geodetic, geophysical, and geologic (paleoseismology) observations.

ACTIVE SUBDUCTION ALONG THE OREGON-WASHINGTON COAST?

Considerable interest has been focused on the Pacific Northwest during the past few years because of the potential for a large thrust earthquake in this area (for example, Heaton and Kanamori, 1984). Plate tectonic reconstructions indicate that the Juan de Fuca plate has been subducted beneath the North American plate at an average Quaternary rate of 3-4 cm/yr (Riddihough and Hyndman, 1976). However, there have been no historic interplate earthquakes to confirm present-day subduction. In fact, focal mechanisms for small earthquakes in the Puget Sound region, within the overriding North American plate, indicate north-south compression (Crosson, 1972) rather than the N 60° E compression which would be expected from plate convergence.

Analysis of historic geodetic leveling and tide-gauge data indicates contemporary east-west tilting along the northwest coast of the United States from the Olympic Peninsula of Washington to southern Oregon (fig. 3) (Ando and Balazs, 1979; Reilinger and Adams, 1982). By analogy with contemporary deformation in Japan, Ando and Balazs (1979) suggested that tilting in Washington resulted from aseismic subduction of the Juan de Fuca plate. Reilinger and Adams (1982) and Adams (1984) presented evidence that contemporary tilting along the Pacific Northwest coast is accumulating at rates comparable to the long- term averages (~10,000 yrs) inferred from tilted

marine terraces. Figure 3 shows the elevations of a number of these terraces plotted versus distance from the coast. This consistency over vastly different time intervals was taken as evidence that at least part of the plate convergence is occurring aseismically. On the other hand, Savage and others (1981) reported horizontal strain measurements from Washington State and Vancouver Island which they interpret in terms of elastic strain accumulation. They further demonstrated that observed tilting was consistent with simple models of elastic strain accumulation and suggested that large thrust earthquakes should be expected in this area (it was this study that raised much of the current concern regarding a large thrust earthquake in this area). Conversely, Adams (1984) points out that horizontal shortening does not necessarily represent elastic strain accumulation, but could result from folding of the upper plate (he points out, however, that this would require that the plate interface is at least partially coupled). More recently, Crosson (1986) has questioned the robustness of the strain measurements reported by Savage and others (1981). While Savage and others (1986) defend their original interpretation, they state that "no additional strain accumulated in the 1979-85 interval" (Savage and others, 1986, pg. 7560). Furthermore, Prescott and others (1986) report that

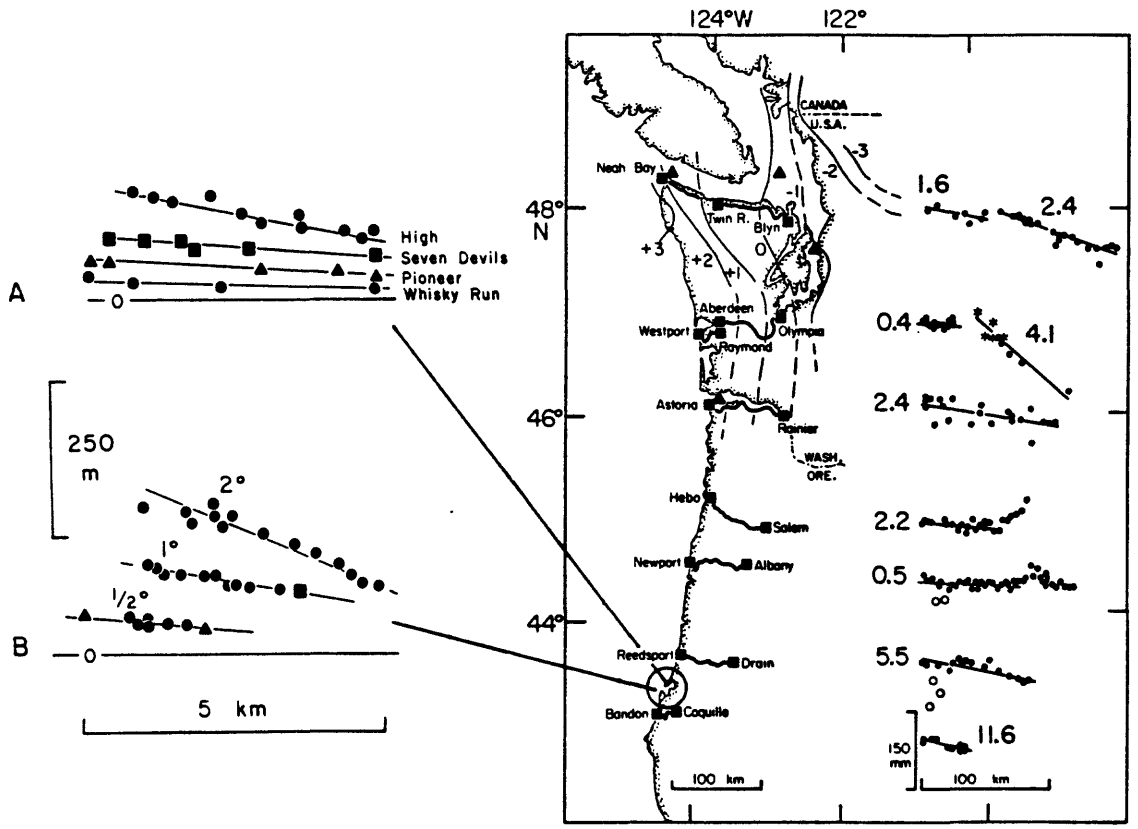

FIGURE 3. --Location of east-west leveling routes in coastal Oregon and Washington and elevation change-distance plots relative to arbitrary zero points for each line. Numbers near plots give tilt rates (units = 10^{-8}/yr). Contours give elevation change (mm/yr) from leveling and tide gauge data in the Olympic Peninsula according to Ando and Balazs (1979). From Reilinger and Adams, 1982. Terrace elevation (left) plotted versus distance from the coast (from Adams, 1984).

the most recent strain measurements in western Washington (1982, 1983, 1986) are not consistent with simple elastic models of subduction of the Juan de Fuca plate beneath North America. They note that the expected N 60° E contraction could be masked by a systematic error in dilatation of perhaps 0.1 ppm/yr. This magnitude error is, however, roughly equal to the expected signal.

As indicated by the previous discussion, there is considerable uncertainty regarding the nature of contemporary deformation along the Pacific Northwest coast. This together with the similarity between long-and short-term tilt rates, the lack of seismicity at the location of the possible interface thrust zone, and the predominance of north-south compression from focal mechanisms in the Puget Sound region, demonstrate that the question of a possible thrust earthquake in this area remains unresolved. However, continued geodetic monitoring, and ongoing studies of Quaternary deformation and other evidence of prehistoric earthquake activity (for example, Adams, 1984; Atwater, 1987), hold considerable promise for delineating earthquake risk along this section of the coast in the near future.

NORMAL FAULTING IN THE BASIN AND RANGE PROVINCE

During the past few years, a number of important geodetic data sets have become available which are relevant to the nature of faulting and interseismic deformation in the Basin and Range and presumably other normal fault environments. In this section, I consider the implications of two of these data sets for the long-term evolution of Basin and Range structures.

Perhaps the most detailed geodetic information on coseismic movements for a normal-fault earthquake is that for the M=7.0, 1983 Borah Peak, Idaho, earthquake. Stein and Barrientos (1985) utilized these data to convincingly argue that slip on a high-angle, planar fault was responsible for this earthquake, and, by analogy, that similar faults (as opposed to listric faults) are the primary *active* structures in the Basin and Range.

Figure 4A shows observed (dots) and modeled (line) coseismic elevation changes along a leveling route traversing the epicentral area of the Borah Peak earthquake (from Stein and Barrientos, 1985). The modeled planar fault is shown in cross-section in relation to the main shock (focal mechanism shown) and aftershocks in the figure 4B, and a simplified geologic cross-section is given in figure 4C. As indicated by figure 4A, coseismic deformation consisted predominantly of subsidence of the Thousands Springs Valley with relatively minor uplift of Borah Peak (subsidence is more than five times uplift). In fact, this imbalance is a general characteristic of normal faulting (note that listric faulting produces even more subsidence relative to uplift). In contrast, the geologic cross-section in figure 4C indicates that overall basin subsidence is roughly equal to the overall uplift of the adjacent mountain range (for example, the offset of Tev). The obvious implication of the discrepancy between coseismic deformation and long-term deformation is that the basin and range structure is not simply the result of the accumulated deformation from many earthquakes on this fault through geologic time. Other deformational processes with magnitudes comparable to coseismic deformations must contribute to the development of the observed basin and range structure. Within the context of the earthquake deformation cycle, these other deformational processes can be considered as part of the "interearthquake" phase of deformation.

Some indication of the spatial pattern of interearthquake deformation can be obtained by comparing observed coseismic and long-term deformation. Examination of the cross sections in figure 4 indicates that a broad uplift of the

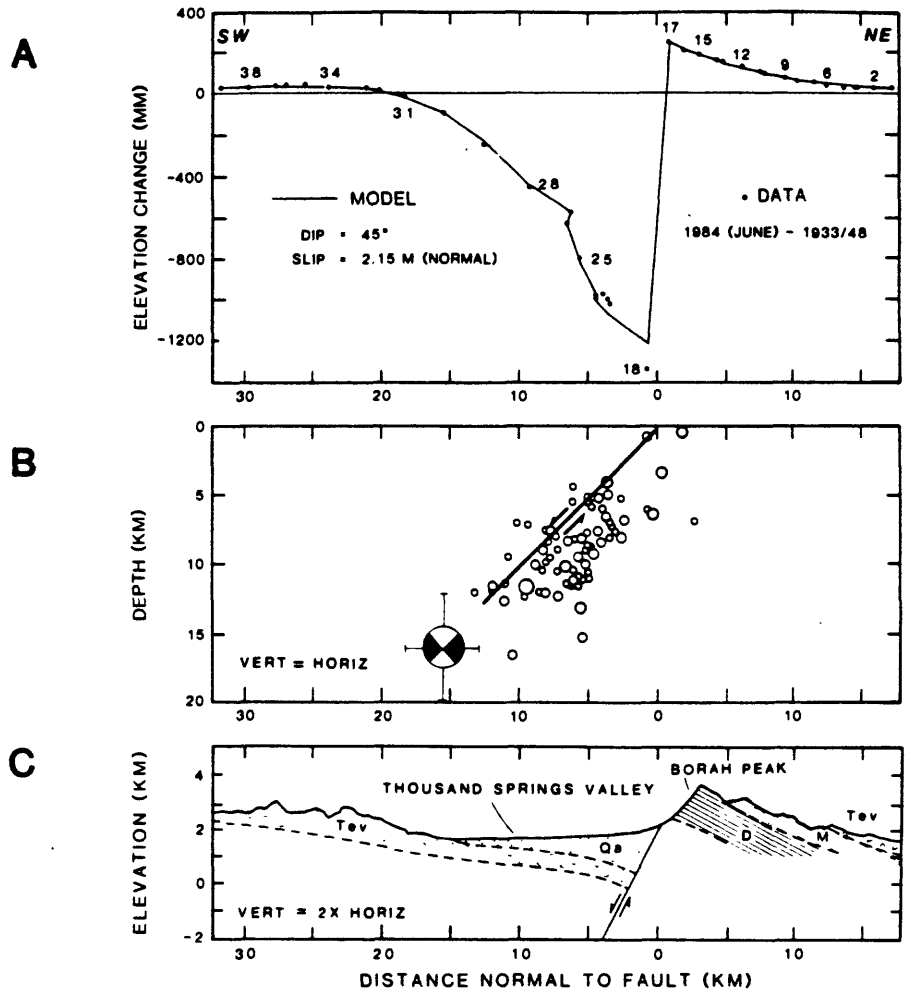

FIGURE 4. --A: Observed (dots) and modeled (line) elevation changes from leveling line crossing the Borah Peak earthquake fault. B: Cross-section showing main shock (focal mechanism), aftershocks and fault model for earthquake. C: Simplified geologic cross-section. From Stein and Barrientos (1985).

downdropped basin and adjacent range will, in combination with coseismic deformation, roughly produce the long-term deformation.

Both observational evidence and theoretical modeling support broad uplift during the interearthquake deformation phase for normal-fault events. Geodetic observations throughout a broad region surrounding the site of the M=7.3 1959 Hebgen Lake, Montana earthquake, a major normal-fault event in the Basin and Range, revealed a pattern of broad regional uplift roughly centered on the zone of intense coseismic subsidence (fig. 5). Reilinger (1986) interpreted this deformation, as well as the large horizontal strains observed following the earthquake (Savage and others, 1985), as resulting from postseismic viscoelastic relaxation for the 1959 earthquake, using a model proposed by Thatcher and others (1980) (fig. 5). The relevant point is that both the observed and theoretical deformation involve broad uplift of the epicentral region, a pattern that is very similar to that proposed for the Borah Peak event on the basis of the relationship between observed coseismic deformation and geologic structure.

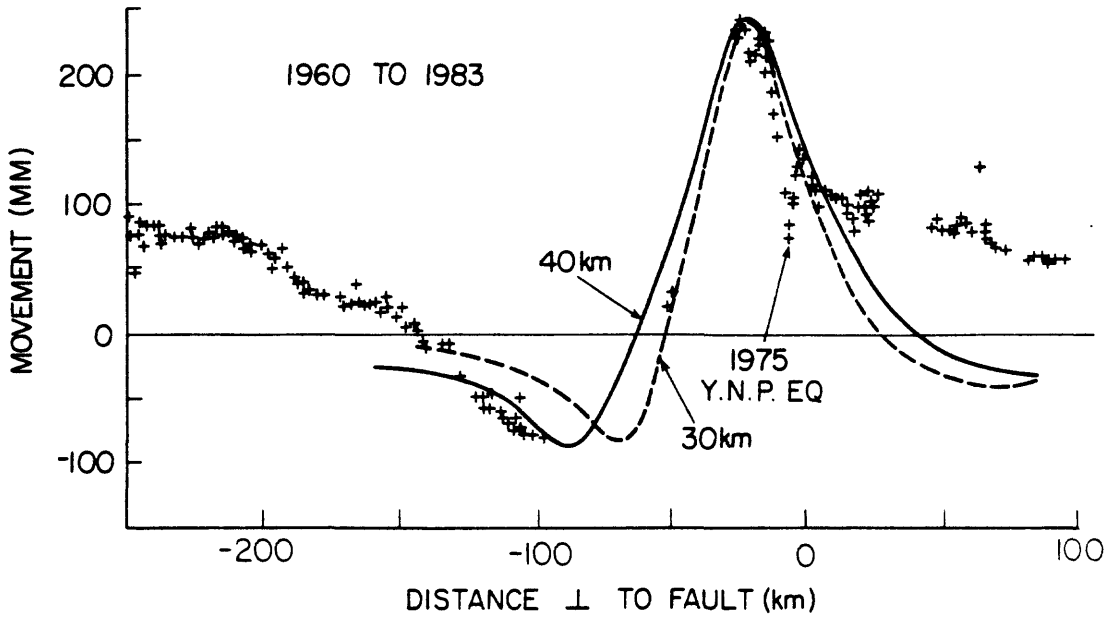

FIGURE 5. --Observed (+) and modeled elevation changes for postseismic uplift following the Hebgen Lake, Montana earthquake. Model involves postseismic viscoelastic relaxation (modified from Reilinger, 1986). 1975 Y.N.P. EQ is the location of the 1975, M6.1 earthquake in Yellowstone National Park.

While the pattern of vertical uplift observed after the Hebgen Lake earthquake has the proper shape, the amplitude of uplift due to postseismic viscoelastic relaxation is not sufficient to counter the large coseismic subsidence. The estimated total uplift due to viscoelastic relaxation for the Hebgen Lake earthquake is about 40 cm (Ward, 1986). In contrast, as much as 6.7 m of subsidence was observed near the Hebgen Lake fault (with ~ 0.5 m uplift of the foot wall) and over 3 m of subsidence occurred throughout an area of roughly 400 km^2 (Myers and Hamilton, 1964). It therefore appears necessary that the pattern of broad postseismic uplift extends into the strain accumulation phase. Given the long recurrence time for earthquakes in the Basin and Range (on the order of a few thousand years; Wallace, 1981) and the rapid rate of postseismic uplift observed (> 1 cm/yr; fig. 5), uplift during the strain accumulation phase will necessarily occur at a much slower rate than that during the postseismic phase. Doming during the strain accumulation phase is consistent with the theoretical results of Koseluk and Bischke (1981) who report on models of strain accumulation for normal fault earthquakes in an elastic layer over a viscoelastic half-space. These models predict broad uplift in the vicinity of the impending fault rupture.

The overall interpretation described above--namely, counteracting the large coseismic deformation by rapid postseismic adjustment grading into strain accumulation in order to produce the observed structural relief, is consistent with the behavior predicted by the observed earthquake deformation cycle (fig. 1).

An interesting corollary of interseismic uplift concerns the effect on fault dip. The peak in uplift after the Hebgen Lake earthquake lies roughly 20 km south (downdip) of the fault outcrop (fig. 5). This deformation pattern will therefore tend to uplift the deeper segment of the fault more than the shallower part, thereby rotating the fault toward the horizontal. After sufficient rotation (that is, a sufficient number of earthquakes), the fault may cease

to be active and a new, steeper fault may develop. A process of this type, perhaps in conjunction with the geometric constraints discussed by Jackson and McKenzie (1983), might explain the presence of shallow, low-angle listric faults on seismic reflection records while major earthquakes apparently occur on through-going planar faults.

CONCLUSIONS

In addition to the site specific implications for earthquake recurrence and structural evolution for the areas described above, the following generalizations are suggested:

(1) The earthquake deformation cycle provides a useful framework for investigating the relationship between short-term (geodetic) and long-term (geologic/topographic) deformation.

(2) The established relationship between earthquake deformation and topographic relief, even in predominantly strike-slip environments, indicates that topography can reflect detailed fault behavior.

(3) While there is often a clear relationship between coseismic deformation and long-term deformation, the differences between the spatial patterns and rates of deformation over these time scales require large (similar amplitude to coseismic) postseismic and/or interseismic movements. Comparison of the coseismic and permanent deformation patterns provides direct, quantitative information on the character of these interearthquake movements.

(4) Models involving postseismic viscoelastic relaxation in the asthenosphere and strain accumulation acting on an elastic layer over a viscoelastic half-space can account for many of the salient features of the required interearthquake deformation.

While problems concerning errors and nontectonic influences in geodetic measurements continue, there is no doubt that these data have provided critical information for earthquake research. The progress made in estimating possible errors in historic measurements, the development and deployment of new and improved geodetic techniques, and on going efforts to monitor deformation in areas of past and possible future earthquake activity, promise to maintain these measurements as an important element of future investigations into the nature of earthquake processes.

ACKNOWLEDGMENTS

Much of the discussion regarding deformation in the Imperial Valley was taken from unpublished work done in collaboration with Shawn Larsen. I am grateful to Sara Brydges for editing the manuscript. The research reported here was supported in part by USGS Grant 14-08-0001-G1337 and NSF Grants EAR-8608496 and EAR-8618705.

REFERENCES

Adams, J., 1984, Active deformation of the Pacific northwest continental margin: Tectonics, v. 3, p. 449-472.

Ando, M., and Balazs, E.I., 1979, Geodetic evidence for aseismic subduction of the Juan de Fuca plate: Journal of Geophysical Research, v. 84, p. 3023-3027.
Atwater, B.F., 1987, Evidence for great Holocene earthquakes along the outer coast of Washington state: Science, v. 236, p. 942-944.
Bilham, R., and Williams, P., 1985, Sawtooth segmentation and deformation processes on the southern San Andreas fault, California: Geophysical Research Letters, v. 12, p. 557-560.
Chinnery, M.A., 1961, The deformation of the ground around surface faults: Bulletin Seismological Socety America, v. 51, p. 355-372.
Crosson, R.S., 1972, Small earthquakes, structure, and tectonics of the Puget Sound region: Bulletin Seismological Socety America, v. 62, p. 1133-1171.
Crosson, R.S., 1986, Comment on "Geodetic strain measurements in Washington" by J.C. Savage, M. Lisowski, and W.H. Prescott: Journal Geophysical Research, v. 91, p. 7555-7557.
Fuis, G.S., Mooney, W.D., Healey, J.H., McMechan, G.A., and Lutter, W.J., 1982, Crustal structure of the Imperial Valley region: U.S. Geological Survey Professional Paper 1254, p. 25-50.
Fuis, G.S., Mooney, W.D., Healy, J.H., McMechan, G.A., and Lutter, W.J., 1984, A seismic refraction survey of the Imperial Valley region, California: Journal Geophysical Research, v. 89, p. 1165-1189.
Heaton, T.H., and Kanamori, H., 1984, Seismic potential associated with subduction in the Northwest United States: Bulletin Seismological Society America, v. 74, p. 933-941.
Jackson, J., and McKenzie, D., 1983, The geometrical evolution of normal fault systems: Journal Structural Geology, v. 5 p. 471-482.
King, G.C.P., and Vita-Finzi, C., 1981, Active folding in the Algerian earthquake of 10 October 1980: Nature, v. 292, p. 22-26.
Koseluk, R.A., and Bischke, R.E., 1981, An elastic rebound model for normal fault earthquakes: Journal Geophysical Research, v. 86, p. 1081-1090.
Lachenbruch, A.H., Sass, J.H. and Galanis, S.P., 1985, Heat flow in southernmost California and the origin of the Salton Trough: Journal Geophysical Research, v. 90, p. 6709-6736.
Myers, W.F., and Hamilton, W., 1964, Deformation accompanying the Hebgen Lake earthquake of August 17, 1959: U.S. Geological Survey Professional Paper 435, p. 55-98.
Plafker, G., and Savage, J.C., 1970, Mechanism of the Chilean earthquakes of May 21 and 22, 1960: Geological Society America Bulletin, v. 81, p. 1001-1031.
Prescott, W.H., Savage, J.C., Lisowski, M., and King, N., 1986, Crustal strain, *in*, National Earthquake Hazards Reduction Program, Summaries of Technical Reports: v. XXIII, U.S. Geological Survey Open-File Rep. 87-63, p. 235-239.
Reid, H.F., 1910, The mechanics of the earthquake, *in*, The California Earthquake of April 18, 1906: Rep. of the State Earthquake Investigation Commision, Publication No. 87, II, Carnegie Inst., Wash., D.C., 192 p.
Reilinger, R., and Adams, J., 1982, Geodetic evidence for active landward tilting of the Oregon and Washington coastal ranges: Geophysical Research Letters, v. 9, p. 401-403.
Reilinger, R.E., 1984, Coseismic and postseismic vertical movements associated with the 1940 Imperial Valley, California earthquake: Journal Geophysical Research, v. 89, p. 4531-4537.

Reilinger, R.E. and Kadinsky-Cade, K., 1985, Earthquake deformation cycle in the Andean back arc, western Argentina: Journal Geophysical Research, v. 90, p. 12701-12712.
Reilinger, R., 1986, Evidence for postseismic viscoelastic relaxation following the 1959 M = 7.5 Hebgen Lake, Montana, earthquake: Journal Geophysical Research, v. 91, p. 9488-9494.
Reilinger, R., and Larsen, S., 1986, Vertical crustal deformation associated with the 1979 M = 6.6 Imperial Valley, California earthquake: Implications for fault behavior: Journal Geophysical Research, v. 91, p. 14,044-14,056.
Riddihough, R.P. and Hyndman, R.D., 1976, Canada's active western margin-The case for subduction: Geoscience Canada, v. 3 p. 269-278.
Savage, J.C., and Hastie, L.M., 1966, Surface deformation associated with dip-slip faulting: Journal Geophysical Research, v. 71, p. 4897-4904.
Savage, J.C., Lisowski, M., and Prescott, W.H., 1981, Geodetic strain measurements in Washington: Journal Geophysical Research, v. 86, p. 4929-4940.
Savage, J.C., Lisowski, M., and Prescott, W.H., 1985, Strain accumulation in the Rocky Mountain states: Journal Geophysical Research, v. 90, p. 10,310-10,320.
Savage, J.C., Lisowski, M., and Prescott, W.H., 1986, Reply: Journal Geophysical Research, v. 91, p. 7559-7560.
Stein, R.S., 1985, Evidence for surface folding and subsurface fault slip from geodetic elevation changes associated with the 1983 Coalinga, California, earthquake: U.S. Geological Survey Open-File Rep., 85-44, p. 225-253.
Stein, R.S., and Barrientos, S.E., 1985, Planar high-angle faulting in the Basin and Range: Geodetic analysis of the 1983 Borah Peak, Idaho, earthquake: Journal Geophysical Research, v. 90, p. 11,355-11,366.
Sykes, L.R., and Nishenko, S.P., 1984, Probabilities of occurrence of large plate rupturing earthquakes for the San Andreas, San Jacinto, and Imperial faults, California, 1983 - 2003: Journal Geophysical Research, v. 89, p. 5905-5927.
Thatcher, W., Matsuda, T., Kato, T., and Rundle, J., 1980, Lithospheric loading by the 1896 Riku-u earthquake, northern Japan: Implications for plate flexure and asthenospheric rheology: Journal Geophysical Research, v. 85, p. 6429-6435.
Thatcher, W., 1984, The earthquake deformation cycle, recurrence, and the time-predictable model: Journal Geophysical Research, v. 89, p. 5674-5680.
Wallace, R.E., 1981, Active faults, paleoseismology, and earthquake hazards in the western United States, *in*, Simpson, D.W., and Richards, P.G., eds., Earthquake prediction: An international review, Maurice Ewing Series 4, American Geophysical Union, Washington, D.C., p. 209-216.
Ward, S.N., 1986, A note on surface volume change of shallow earthquakes: Geophysical Journal Royal Astronomical Society, v. 85, p. 461-466.

SUMMARY OF DISCUSSION SESSION: QUATERNARY SLIP RATES AND COSEISMIC DEFORMATION

by

Anthony J. Crone
U.S. Geological Survey
Denver, Colorado 80225

Session Chairman: Thomas K. Rockwell, San Diego State University
Panel Members: Malcolm M. Clark, U.S. Geological Survey
N. Timothy Hall, Earth Science Associates
Michael J. Rymer, U.S. Geological Survey
Roy J. Shlemon, Shlemon and Associates
Ross S. Stein, U.S. Geological Survey

Recent studies in paleoseismology suggest that are dramatic variations in long-term slip rates compared to short-term slip rates. The long-term rates usually encompass time spans of tens to hundreds of thousands of years and are based on displacement of geologic datums. In comparison, short-term slip rates reflect deformation that spans decades to several thousand years, and are based on geodetic and geologic data. Evidence supporting changes in long-term versus short-term slip rates can be found in strike-slip settings (the South Island of New Zealand), extensional settings (the Wasatch fault zone, Utah), and compressional settings (El Asnam, Algeria). The data we have accumulated to date is scanty, but suggestive of substantial rate changes. Further studies need to confirm if these apparent changes are real, and if such changes are typical or atypical. Obviously, substantial changes in long-term versus short-term slip rates would have a major impact on assessing seismic hazards.

There is a difference of opinion about how accurately geologic slip rates represent the seismic hazards. One viewpoint considers geologic rates to overestimate the hazards because geologic features record both coseismic displacements, and aseismic creep and postseismic slip. The creep and postseismic slip components are not associated with any severe shaking, and therefore, is not a true seismic hazard. The opposing view considers geologic rates to underestimate the hazards because localized folding and ductile deformation in unconsolidated sediments adjacent to fault zones can lead to erroneously low estimates of the total slip. Furthermore, seismologic and geodetic models of historic events indicate that coseismic slip at depth is usually greater than the displacement measured on geologic features at the surface. For example, geodetic data suggests that perhaps half of the uplift associated with the 1959 Hebgen Lake, Montana earthquake is coseismic and half is aseismic. Hopefully, future research will better define how accurately surface deformation recorded by geologic features reflects the actual fault slip at depth.

The amount of surface deformation and associated distortion can vary greatly in different tectonic environments and between adjacent sites. For example, the left-lateral reverse slip of the 1971 San Fernando earthquake produced surprisingly little surface deformation. In contrast, extensive surface deformation is very common along normal faults, and in many places, it is related to changes in fault geometry. Antithetic faults scarps, grabens, and backrotation typically produce about twice the apparent displacement at the main scarp compared to the actual displacement after compensating for

these effects. It is relatively easy to compensate for most of the excess deformation along normal faults. For strike-slip faults, the situation is more complicated and more variable. In places on the Garlock fault, long linear features are completely undeformed as the approach the fault; at the fault, they are abruptly offset a distance of 80 m. At the other end of the spectrum, distributed strain from left slip along the Las Vegas Valley shear zone has produced a large oroclinal bend of regional proportions that can be identified from paleomagnetic data.

Additional paleoseismic studies will allow geologists to more accurately characterize the surface deformation associated with faults in different tectonic environments, and help them determine how site characteristics influence the nature of the deformation. Ultimately, better understanding of the characteristics of surface deformation will help us evaluate the quality of individual slip rate measurements at different sites in different tectonic environments. If a geologic slip rate is consistent with a rate determined from other kinds of data, such as geodetic data, our confidence in the geologic rate increases; congruent data assures one of being on the right track, but, we should remember that the rates from both data sets could be incorrect. Such is the nature of science in general because we usually rely on consistency to support our interpretations.

An important outgrowth of our studies to characterize surface deformation is that we now have better data on the dimensions of the zones of brittle and ductile deformation across fault zones. These data are important guides for zoning and planning commissions to use when establishing development regulations. An valuable future contribution would be to upgrade these deformation data and identify the site conditions that enhance or confine the extent of the surface deformation in different tectonic environments.

Recent studies show that strain can be distributed in rocks in a variety of ways. Some basic principles of rock mechanics permit speculation that coseismic strain release is primarily confined to discrete faults coseismic, whereas, immediately after a seismic event, strain is released by distributed shear. In one example, field observations suggest that slip in a 1-km-wide zone of pervasively shattered granite is concentrated at one edge rather than being distributed throughout the body of shattered rock. At the other extreme, in the eastern Sierras, a large kink-band, kilometers across, apparently formed through permanent strain bending in the brittle regime without evidence of a central shear zone.

Several reasonable explanations are available to explain the apparent changes in long-term versus short-term slip rates. The changes may simply result from a temporal clustering of earthquakes in which lengthy periods of quiescence are interrupted by relatively short episodes of intense activity. For example, recurrence data from El Asnam, Algeria favor an interpretation of several events spaced perhaps a few centuries apart followed by a period of inactivity tens or possibly hundreds of thousands of years long. We are beginning to find similar evidence of temporal clustering in some normal faulting environments. What we perceive as an apparent change in slip rate may simply be an artifact of the relatively short time window we are observing within a much longer seismic cycle. If long-term seismic cycles are real, seismic hazard assessments require that we characterize the cycle, determine its length, and know where we are within the cycle. However, even if we can establish that a given fault has experienced cyclic behavior in the past, we cannot be sure that the next cycle will follow the same pattern

The natural variability in recurrence intervals of different segments on a fault can produce an apparent temporal clustering. Using random numbers to

model the timing and sequence of earthquakes on a segmented fault yielded several temporal patterns that, if documented in the geologic record, would probably be interpreted as clustered events. Thus some apparent clustering might develop randomly on faults that have a uniform slip rate.

Apparent temporal clustering can also be explained by a contagion effect This effect develops when a major earthquake relaxes the strain on one segment of a fault, but increases the strain on an adjacent segment. The increased strain causes an earthquake on the adjacent segment within a relatively short period of time. This event then loads other segments, and the continuation of this contagious process results in a natural temporal clustering. Such a clustering does not necessarily indicate complicated or variable rates of tectonic deformation, that is, the contagion process does not require the accumulating strain to be "turned on" and "turned off".

A fundamental question to be addressed in paleoseismology is whether randomness and unpredictability typifies fault behavior, or if the behavior is controlled by physical properties of faults and by strain accumulation rates. In the latter case, monitoring physical properties may help predict future behavior. Conceptually, it is easier to imagine random behavior in an intraplate setting versus an interplate setting. In interplate environments, one can envision strain-loading moving from one fault to another throughout a relatively large region. In interplate environments, it seems intuitively more difficult to move the loading around to numerous faults because usually, there are only a few major faults or fault systems at plate boundaries.

Logically, the spatial and temporal distribution of earthquakes must be directly related to the accumulation of crustal stresses over time and space. We may be able to explain the sequence of historical earthquakes in the central Nevada seismic belt in terms of a particular pattern of shifting stress from one segment of the belt to another, but we have no basis for being sure that the pattern we observe now will be exactly repeated in the future. So there is certainly some irreducible randomness in the system. Perhaps the critical issue is not whether this strain accumulation occurs randomly, but whether we can collect enough data on spatial and temporal patterns to actually model the fault behavior. With sufficient data, we may be able to identify local and regions patterns and determine if a uniform or nonuniform pattern typifies fault behavior.

The numerous trenches that are excavated for building-site evaluations across the United States every day. These trenches are a major source of potentially valuable but unexploited paleoseismic data. Many of these trenches are open only long enough (commonly one day) for a cursory inspection, and are not available for detailed studies. However, some of these trenches may offer opportunities to confirm important stratigraphic relationships that can be applied elsewhere, or they may provide material for dating movements on important faults. Often the construction schedules to develop a building site do not permit the time needed to process and date samples. Nevertheless, geologists involved in paleoseismology should examine these trenches when possible and collecting pertinent samples, even if funds are not available to date the samples. Quaternary dating specialists note that improvements in both standard techniques (for example, TAMS, thermoluminescence, and uranium disequilibrium) and in new, promising techniques, such as photo-stimulated luminescence and He^3 accumulation from cosmic bombardment may permit dating samples in the future that are undateable today. Therefore, paleoseismologists should collect and properly store potentially important samples.

MODELING FAULT-SCARP DEGRADATION:

KNOWNS, UNKNOWNS, AND PERSPECTIVES ON THE PROBLEMS

SOURCES OF ERROR IN MORPHOLOGIC DATING OF FAULT SCARPS

by

Larry Mayer
Department of Geology
Miami University
Oxford, Ohio 45056

ABSTRACT

Diffusion modeling of alluvial fault-scarp degradation enables researchers to estimate the age of faulting, but the precision of these estimates is affected by geologic processes, measurement error, and model error. Use of linear diffusion models as part of a procedure to estimate scarp age should therefore incorporate, as much as possible, estimates of precision. Simple statistical descriptions of error are difficult because the the sources of error are sometimes inseparable from model deficiencies.

INTRODUCTION

Methods used for dating, such as isotopic ratios of radioisotopes, incorporate the uncertainties of the precision of the age estimate along with the age estimate. If morphologic dating procedures are to be used as a serious tool for dating fault scarps, they should be structured to permit the determination of precision or confidence in the age estimate.

Morphologic dating is based on the observation that fault scarps degrade in a systematic (Bucknam and Anderson, 1979) and predictable (Nash, 1980) fashion as a function of time. More precisely, the degradation of fault scarps can be modeled using solutions to the linear-diffusion equation (for example, Nash, 1980; Colman and Watson, 1984; Hanks and others, 1984) or nonlinear diffusion (Andrews and Bucknam, in press). These models have been successful in as much as they have explained much of the variation in scarp morphology for the wave-cut scarps formed by Lake Bonneville, which were abandonned about 15 ka (Scott and others, 1983) and for fault scarps, of similar or younger age (Nash, 1980; Hanks and others, 1984; Mayer, 1984; Hanks and Wallace, 1985; Pierce and Colman, 1986; Hanks and Schwartz, 1987); though some older scarps have been studied as well (Mayer, 1984; Pearthree and Calvo, 1987).

"Dating" a fault scarp in this discussion refers specifically to the application of such models to estimate the age of a fault scarp. Error, therefore refers to variations in model-derived age estimates that are unrelated to actual fault-scarp age. This type of error is observed either as a bias in the age estimates for a scarp of a given age or as scatter around a model age. In the latter case, error is equivalent to uncertainty in a

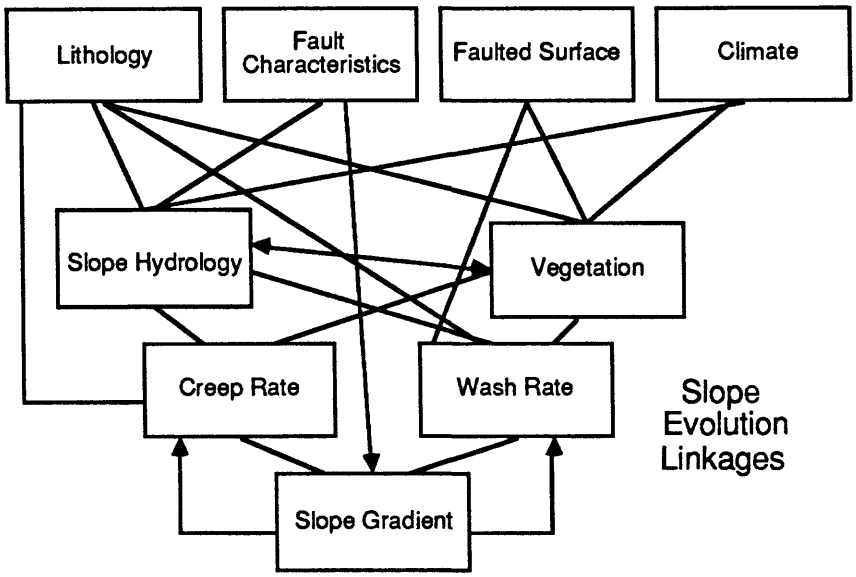

FIGURE 1.-- Diagram illustrating the geologic processes and their respective linkages that affect scarp degradation.

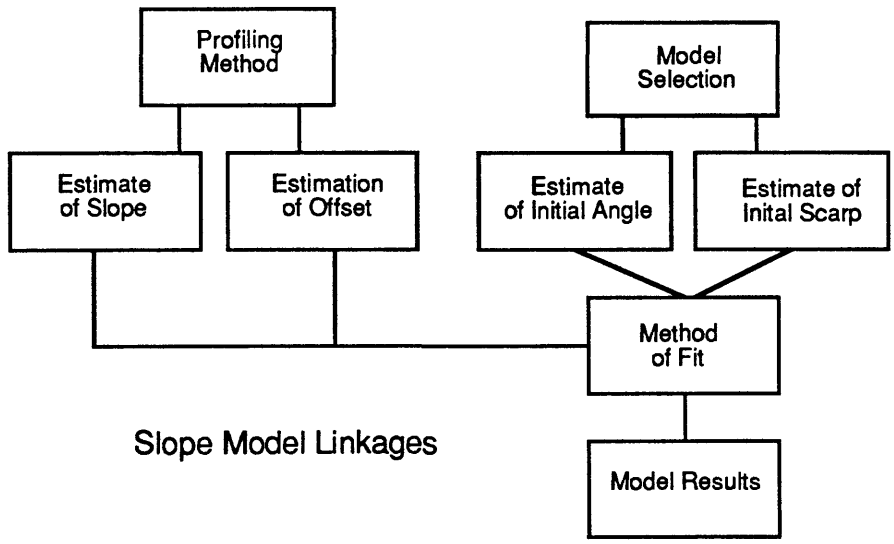

FIGURE 2.-- Diagram illustrating the steps in fitting a scarp profile to a model to estimate scarp age.

statistical sense. Sources of error may be categorized as measurement, geologic, or model. To understand the entry points of error in morphologic dating, it is useful to visualize the linkages between the geologic processes affecting the evolution of a fault scarp (fig. 1) and the sequence of steps used to fit the the diffusion model to a measured profile or group of scarp-angle versus offset data pairs (fig. 2). Unfortunately, some of these linkages are understood either in general terms of slope processes or merely in an intuitive sense.

EFFECT OF GEOLOGIC PROCESSES

Four or more independent or interdependent variables, other than time, affect the evolution of fault scarps (fig. 1). Lithology, broadly signifying the type of material faulted, its weathering and geotechnical characteristics (such as cohesiveness, angle of internal friction, and particle-size distribution) affects the rate of degradation in a complex fashion. Along the Pitaycachi fault in northern Sonora, a scarp that formed in 1877 varies in angle from vertical to about 25°, depending on the material faulted.

The characteristics of the fault itself, including the multiple-scarp formation (for example, Borah Peak Fault scarp), backtilting of the downthrown block towards the fault (for example, Wasatch fault), antithetic faulting and graben formation (for example, Lost River fault, Pitaycachi fault), initial angle of the fault scarp, and offset (all faults), directly or indirectly affect the evolution of the scarp by forming its initial starting conditions. Repeated faulting creates composite fault scarps whose morphology, and hence morphologic age, reflects a combination of the individual faulting events. Recognition of composite faulting may be difficult; however, scarp width may be helpful as a discriminator (fig. 3).

The nature of the faulted surface affects subsequent scarp degradation in several ways. The easiest effect to account for is that resulting from different slopes of the faulted surface (the "far-field" slope in the terminology of Hanks and others, 1984). That slope, b, is directly parameterized in equation 21 of Hanks and others (1984, with a correction noted in Andrews and Hanks, 1985). Less obvious effects include the rate of material transport that exists on the faulted surface, say an alluvial-fan surface. This rate may be small or large relative to the rate of material transport on the upper (erosional) portion of the fault scarp but it is completely unaccounted for in the diffusion model which equilibrates at the (far-field) slope of the faulted surface. An example of the effect of such transport was found on the Pitaycachi fault scarp. A part of the fault scarp is completely armored by a hydrothermal spring deposit of slickensided quartz. Though the armor prevented the scarp itself from degrading, a wedge of sediments is accumulating at the base of the scarp. The source of these sediments was the faulted surface above the scarp and not the scarp itself. Similar situations may occur when the faulted material is bedrock mantled

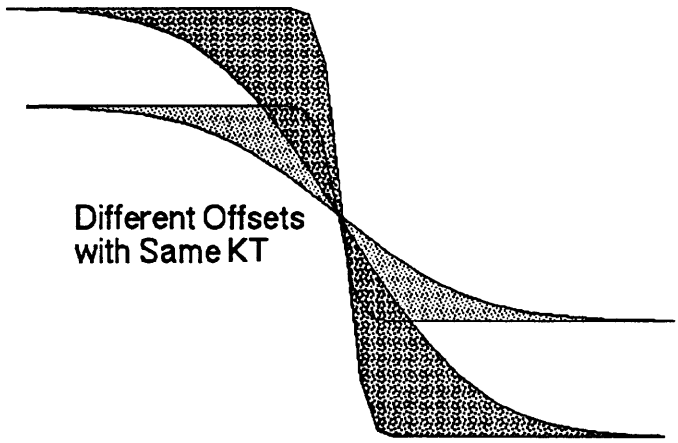

FIGURE 3.-- Cartoon of two scarps (shown with different patterns) with different offsets. Though offset directly affects scarp slope, scarp width is a function only of scarp age. Scarp widths for a given scarp age should therefore be similar and, thus, be dissimilar for scarps formed by repeated faulting of different ages alluvial surfaces. There should also be consistency between age estimates based on scarp angle and scarp width. **k** is the diffusivity used in linear diffusion modeling and **t** is time. Scarps with the same **kt** value are morphologically equivalent in age.

by a veneer of sediment (such as pediments). If one accepts that upscarp material transport has an effect on apparent morphologic degradation, then the relation between the strike of the fault scarp and the strike of the faulted surface will also have an effect on scarp degradation. Scarps that parallel the topographic contours of the faulted surface receive the most upscarp derived material while those at a high angle to the contours will receive less.

Climate is believed to affect the rates of scarp degradation but no work on fault scarps has suggested that small variations in climatic variables may actually affect the form controlling processes of scarp degradation. Perhaps the work of Pierce and Colman (1986) on the effect of scarp aspect and the associated microclimatic variations on high scarps is suggestive of this latter possibility.

MEASUREMENT ERROR

Fault-scarp dating techniques are based on the morphology of the scarp in profile. Model profiles may then be fit individually to scarp profiles or to a group of scarp-angle versus offset data pairs. The scarp profile is surveyed in the field using such methods as (1) laying an adjustable length stadia rod on the ground and measuring its slope (Bucknam and Anderson, 1979)

(2) transit and rod (3) tape, rod and level or (4) some other surveying method commonly used for surveying slope profiles. The users of each method have their own ways of dealing with vegetation, bioturbation mounds, or other obstructions to measuring a scarp profile. However, it is important to recognize that each technique introduces some amount of measurement error. Repeated measurement of profiles allows one to estimate the amount of measurement error. Without making repeated measurements, it is impossible to distinguish between real variation in morphology and measurement artifacts. Repeated measurement of an historic fault scarp (Mayer, 1984) resulted in measurements of 27.3° ±1.1° (mean ± one standard deviation) for the expandable rod technique while for a fixed rod technique, maximum scarp angles were 26.6° ±1.9°. The standard deviation for the 2.5 m high scarp was ±0.15 m for the expandable rod technique (Mayer, 1984). Variation such as this does not appreciably affect age estimates for very young scarps, but can have severe effects on age estimates derived from very old scarps (say >30 ka).

In addition to the measurement error associated with profiling, there is an error associated with estimating offset. This latter error can be due to the limits of graphical renderings of a scarp profile from which offset is measured, or may be related to real uncertainty about what constitutes the present upper and lower surfaces of the original faulted surface. Generally, such ambiguity does not exist for very young single-rupture fault scarps that cut gently sloping fan surfaces. However for steeper fan surfaces or those which are themselves dissected or complicated by aggradation from nearby fans, measuring offset from topography alone may be imprecise.

MODEL ERROR

Model error refers to variation seen as either systematic or random variation in the morphology of fault scarps that remains unexplained by the diffusion model. Consider, for example, the fit of model to data shown on figure 4. One model fits the high scarps and tends to consistently underestimate the lower scarps. The second model fits the lower data but systematically overestimates the higher scarps. *Ad hoc* methods of dealing with this systematic error have involved changing the initial conditions (initial scarp angle) to achieve better empirical fit between model and data (for example, Hanks and others, 1984). Another source of variation may come from different methods of fitting a model to the data. When fitting a model to individual profiles, should we minimize the squared error in the x or y direction? Should we use least squares methods and minimize sums-of-squares or use a goodness of fitness test (Kolmogorov-Smirnov or Chi-Square) and minimize the test statistic? These questions are yet unanswered though they may influence the selection of model parameters.

The effect of offset on apparent diffusivity (in the simple linear-diffusion model) is the clearest example of systematic departure of model from data. This problem, discussed by various

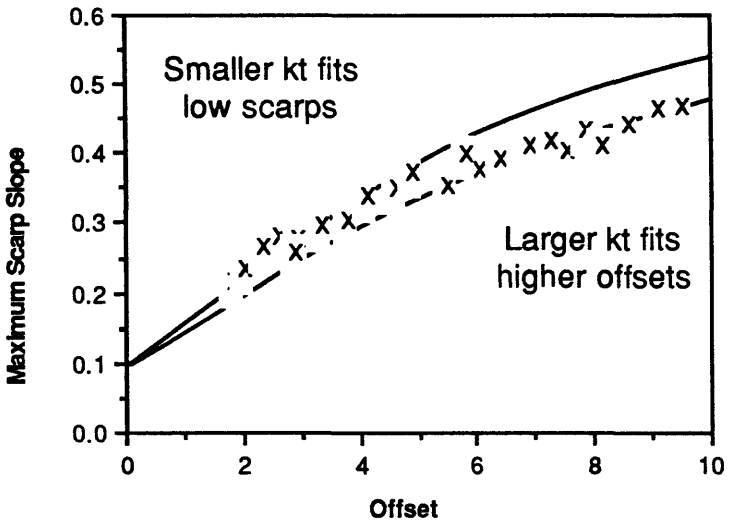

FIGURE 4.-- Cartoon illustrating systematic departures from a linear-diffusion model. The two curves represent the solution for two different values of **kt**, the upper curve having a smaller **kt** than the lower curve. The smaller **kt** fits the lower scarps better than the higher ones, while the larger **kt** fits the higher scarps better than the lower ones.

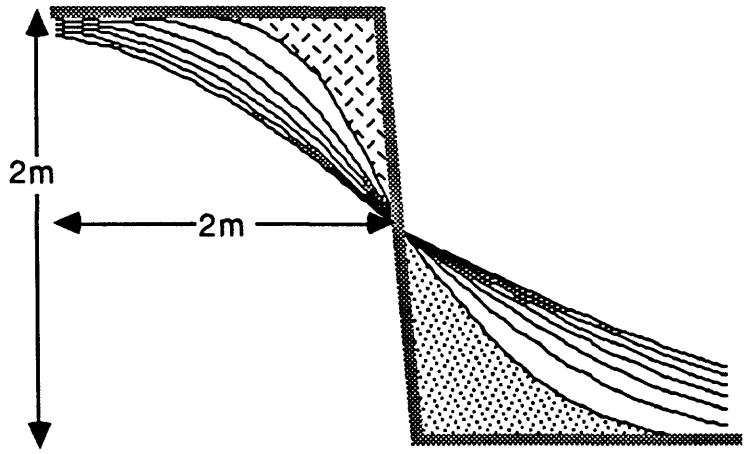

FIGURE 5.-- Diagram showing the evolution of a fault scarp where the erosion (the left part of the scarp) is proceeding at half the rate of deposition (the part on the right). The diagram was produced using a diffusivity twice as large on the depositional side as on the erosional side.

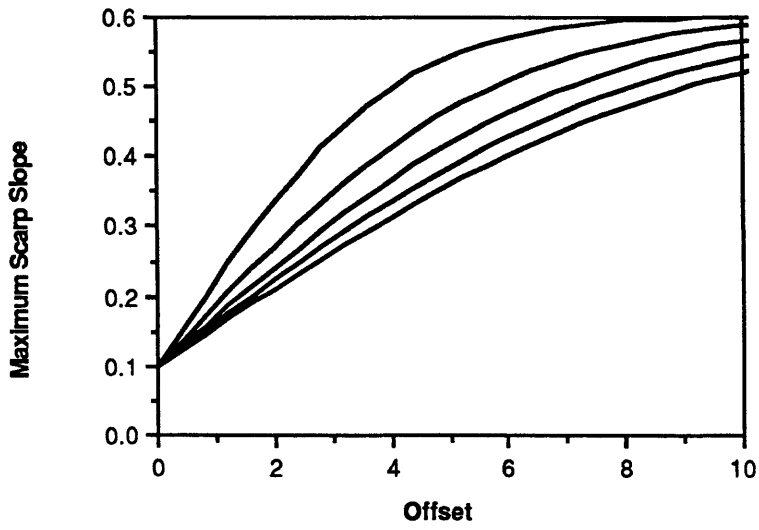

FIGURE 6.-- Graphs showing relation between offset (2a) and maximum scarp slope predicted by the diffusion model for kt=5,10,15,20,25 m^2 (from upper to lower curves, using same parameters as Hanks and others, 1984, figure 12, α=0.6, b=0.1).

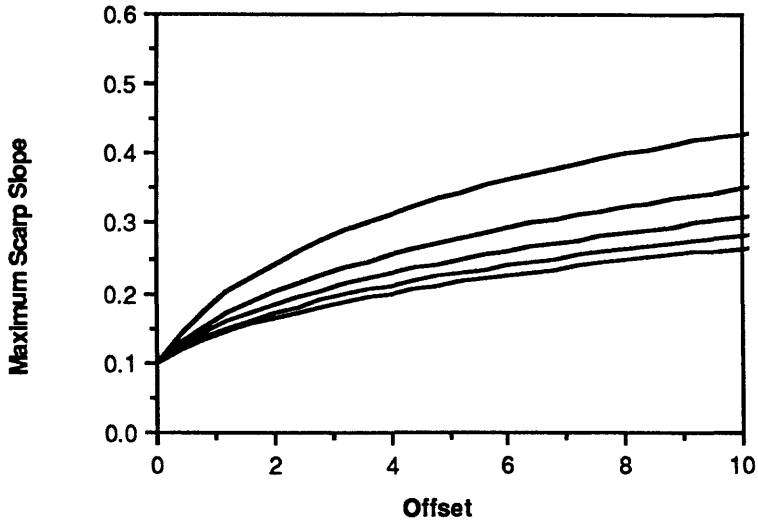

FIGURE 7.-- Graph showing relation between offset and maximum scarp slope predicted by the diffusion model with diffusivity directly proportional to offset for **kt***=5,10,15,20,25 m^2 (from upper to lower curves [where **kt=kt*+kt***(2a) and α=0.6, b=0.1].

authors (Mayer, 1984; Pierce and Colman, 1986; Andrews and Bucknam, 1987; various authors, this volume) simply reflects the biased (or autocorrelation of residuals) fit between offset and scarp-angle data, and diffusion models. Simply stated, for a given age, higher scarps appear to degrade more rapidly than lower ones; that is, they appear to have a larger diffusivity. The answer to this contradiction may not be unique for all scarps, but if it is, then a new form of the diffusion model (or other model) will be required. Bearing in mind that several very reasonable alternative explanations for this phenomenon have already been proposed, I will only mention one heretofore unstudied possibility. The possibility that the erosional and depositional portions of the scarp may be degrading at different rates may partially explain the so-called height effect. The depositional part of the scarp evolves as material is transported from the erosional and upscarp locations. Thus it is not unlikely to see more material deposited at the base of the scarp than is eroded from the scarp crest. This scenario does not apply to every scarp; many of us have seen total erosion apparently balanced by total deposition. Figure 5 shows the effect of unequal erosion and deposition.

The amount of error in age estimates resulting from the height effect is related to the apparent dependency of diffusivity on offset. To illustrate the range of possibilities, two families of curves where constructed (figs. 6 and 7). Comparison of these figures illustrates that scarps with small offsets have similar maximum slope angles even if the dependency of **k** on offset is real. Only very high scarps appear to have severe departures from a diffusion model with a constant **k**.

CONCLUDING REMARK

Morphologic dating of fault scarps using diffusion models continues to provide a useful, quick and simple method for estimating the timing of fault movements. However, those applying the method should attempt to determine tghe precision of age estimates and the sources of non-age-related variation in age estimates. Perhaps in a manner analogous to reporting an age range base on counting statistics used in isotopic dating, scarp ages should include measurement error. In addition, a statement as to the confidence of the morphology-derived age would be helpful. Use of a limited range in offset in dating may also alleviate some of the problems associated with attempting to compare dates from scarps with very different heights. At the same time however, this alternative may reduce the data set available for morphologic description and reduce the confidence in discriminating scarp ages.

REFERENCES

Andrews, D.J., and Bucknam, R.C., in press, Fitting degradation of shoreline scarps by a model with nonlinear diffusion: Journal of Geophysical Research.

Andrews, D.J., and Hanks, T.C., 1985, Scarps degraded by linear diffusion -- Inverse solution: Journal of Geophysical Research, v. 90, p. 10,193-10,208.

Bucknam, R.C., and Anderson, R.E., 1979, Estimation of fault scarp ages from a scarp-height-slope-angle relationship: Geology, v. 7, p. 11-14.

Colman, S.M., and Watson, Ken, 1983, Ages estimated from a diffusion-equation model for scarp degradation: Science, v. 221, p. 263-265.

Hanks, T.C., Bucknam, R.C., Lajoie, K.R., and Wallace, R.E., 1984, Modification of wave-cut and faulting controlled landforms: Journal of Geophysical Research, v. 89, p 5771-5790.

Hanks, T.C., and Wallace, R.E., 1985, Morphologic analysis of the Lake Lahontan and beachfront fault scarps, Pershing County, Nevada: Bulletin of the Seismological Society of America, v. 75, p. 835-846.

Mayer, Larry, 1984, Dating Quaternary fault scarps in alluvium using morphological parameters: Quaternary Research, v. 22, p. 300-313.

Nash, D.B., 1980, Morphological dating of degraded normal fault scarps: Journal of Geology, v. 88, p. 353-360.

Pearthree, P.A., and Calvo, S.S., 1987, The Santa Rita fault zone--Evidence for large magnitude earthquakes with very long recurrence intervals, Basin and Range province of southeastern Arizona: Bulletin of the Seismological Society of America, v. 77, p. 97-116.

Pierce, K.L., and Colman, S.M., 1986, Effect of height and orientation (micro-climate) on geomorphic degradation rates and processes, late-glacial terrace scarps in central Idaho: Geological Society fo America Bulletin, v. 97, p. 869-885.

Scott, W.E., McCoy, W.D., Shroba, R.R., and Rubin, Meyer, 1983, Reinterpretation of the exposed record of the last two cycles of Lake Bonneville, Western United States: Quaternary Research, v. 20, p. 261-385.

LIMITS AND CONSTRAINTS OF THE DIFFUSION EQUATION IN MODELING GEOLOGICAL PROCESSES OF SCARP DEGRADATION

by

Steven M. Colman
U.S. Geological Survey
Woods Hole, MA 02543

ABSTRACT

Diffusion-equation models for scarp degradation have recently received much attention and have provided considerable information about the age and morphology of scarps. However, use of the model to estimate scarp ages is subject to several constraints that are associated with at least three major classes of assumptions used in formulation of the model. These limitations are related to (1) the effect of environmental variables such as lithology and climate, (2) uncertainties about boundary conditions, and (3) the validity of the rate transport equations used in the model. The last of these limitations is perhaps the most serious, and it appears that the linear transport-rate assumption used in many models applies only in special circumstances. However, this limitation is also an opportunity to learn more about the rates and mechanisms of slope processes in general through modeling of scarp morphology.

INTRODUCTION

Recent research on fault scarps and wave-cut scarps has shown that their morphology progressively changes with time. Descriptive work has shown that fault scarps proceed through a sequence of predictable morphological changes (Wallace, 1977). Scarps are created with steep faces, called free faces, that vary in steepness from vertical to as little as 50^{o} (Wallace, 1977). The free face is rapidly removed by slumping and other mass-movement processes, leading to a relatively planar profile at the angle of repose (commonly 33^{o}-35^{o}). This process appears to take from a few tens to perhaps a thousand years in the western United States (Wallace, 1977, 1980; Crone and Machette, 1984). The scarp then degrades by creep, slope wash, and other processes and becomes progressively gentler and more rounded at the crest and base.

Measurements of scarp morphology have shown empirically that the maximum scarp angle decreases with age and increases with scarp height (Bucknam and Anderson, 1979; Mayer, 1984; Sterr, 1985; Machette, 1986). Regression lines that relate maximum scarp angle to the logarithm of scarp height generally form a set of subparallel lines whose relative positions are systematically related to the ages of the fault scarps (Bucknam and Anderson, 1979). The position of the regression line for a scarp changes with time as the maximum scarp angle for a given height decreases. See Pierce and Colman (this volume, fig. 1) for an example.

The texture, cohesion, and other lithologic properties of the deposits on which scarps are formed obviously affect the rates at which they degrade. Many of the scarps that have been studied in the western United States are formed on deposits of a similar character: coarse, poorly sorted, weakly

consolidated, sandy, fan gravel. No major effect of lithologic variables on rates of scarp degradation has been documented among these deposits. However, Dodge and Grose (1980) noted much higher degradation rates in clay compared to gravel. Nash (1984) suggested that differences in degradation rates among different areas were partly due to differences in grain size. Colman (in press) documented higher apparent rates in noncohesive sand than in poorly sorted, slightly cohesive fan gravel. McCalpin (1982) noted that departures from the regression lines of scarp angle against the logarithm of scarp height correlated with the modal clast size on the scarp.

Differences in climate and associated vegetation between areas also have a major affect on rates of scarp degradation, although direct comparisons of scarps in different climates are lacking. Pierce and Colman (1986) have shown that slope aspect (compass orientation) has a significant bearing on rates of scarp degradation. The major differences in rates between north-facing and south-facing scarps, which amount to a factor of 5 for scarps 10 m high, are due to differences in microclimate. Because most of the scarps that have been studied have experienced major climatic fluctuations, scarps of different ages in the same area commonly have experienced different average climates. Machette (1986) has suggested that, all else being equal, average degradation rates for Holocene and late Pleistocene scarps may vary by a factor of 3-4.

THE GENERAL DIFFUSION-EQUATION MODEL AND LINEAR DIFFUSION

Much recent work has focused on mathematical models of scarp degradation and ages estimated from such models (Nash 1980a, b, 1984; Colman and Watson, 1983; Mayer, 1984; Hanks and others, 1984; Andrews and Hanks, 1985; Pierce and Colman, 1986; Andrews and Bucknam, in press). These studies have shown that degradation of scarps with time can be modeled by a diffusion-type equation, and provide a theoretical basis for the empirical maximum-scarp-angle versus log-height relation first developed by Bucknam and Anderson (1979). Most of these diffusion-equation models, whether solved numerically (Nash 1980a, b, 1984) or analytically (Colman and Watson, 1983; Mayer, 1984; Hanks and others, 1984; Andrews and Hanks, 1985; Pierce and Colman, 1986) assume that transport rates are directly proportional to slope and incorporate a single, constant rate coefficient that integrates the effects of lithology, climate, and other environmental factors that affect rates of scarp degradation.

Modeling scarp degradation as a diffusion process depends on three fundamental geomorphic elements: (1) the boundary conditions, including the initial configuration of the scarp, (2) the continuity equation, and (3) the transport-rate equation. The continuity equation, which generally applies to the scarps that have been studied, typically is not a problem in the models. Appropriate boundary conditions for the models, particularly the initial scarp angle, are a matter of some discussion, but differences resulting from assumed boundary conditions generally can be tested and should be resolvable. By far the weakest link in the models is our understanding of the geomorphic processes that act on the scarps and the transport rates that apply to these processes.

A general diffusion-equation model for scarp degradation is summarized in table 1. For age calculations, specific solutions of the general model have commonly been chosen by assumption or by calibration of the model for special boundary conditions or processes. The mass-transport equations used in these models generally assume that the mass-transport rate is a linear

proportion of the slope, $y/_x$ (table 1). Although these specific solutions are valid and produce useful age information, their application is limited to situations in which the chosen assumptions, processes, and boundary conditions hold. However, difficulties may arise when rate constants that have been calibrated for one set of scarps are transferred to another set, which may have different conditions or be influenced by a different mix of slope processes.

TABLE 1.--Geomorphic processes and diffusion-equation models

1.	Transport equation.....	$S = -K(x,t)\ (y/_x)$
2.	Continuity equation.....	$y/_t = -S/_x$
3.	Diffusion equation..... (combining 1 and 2)	$y/_t = /_x\ K(x,t)\ y/_x$

x = horizontal distance; y = vertical distance; S = mass-transport rate; K(x,t) = mass-transport function

In particular, it is becoming increasingly clear that the assumption of a linear mass-transport rate is not valid in all cases. As table 2 indicates, a wide variety of transport-rate equations have been suggested for different slope processes. A linear transport-rate ($S = k_0\ y/_x$) is probably appropriate for some types of scarps, especially creep-dominated ones located in heavily vegetated areas or in very porous materials. However, recent work has also shown that some scarps are affected by processes such as sheetwash and gullying, for which transport rates are not simple linear functions of slope (table 2). Pierce and Colman (1986) have documented a systematic departure of scarp morphology from the predictions of the diffusion-equation model in some arid and semi-arid areas. Specifically, the apparent rate coefficient increases linearly with scarp size. The departure appears to be due to the effect of slope wash or other processes whose transport rates are not a simple, linear function of slope angle, as required by the diffusion-equation model with a constant rate coefficient. Finally, Andrews and Bucknam (in press) found that a cubic transport-rate equation fit data for Lake Bonneville and Lake Lahontan shoreline scarps better than several other types of equations, including the linear one.

Even if the form of the nonlinear transport-rate equations for different processes were known, difficulties would arise because various processes act in different relative proportions on different scarps. The complexity of possible transport-rate equations is not a serious problem for diffusion-equation models; although exact solutions may not be feasible, finite-difference methods should provide solutions for most conceivable models. The most pressing need is for work, including experimental, direct-observation, and historical studies, to defined the mass-transport rates that apply to different processes on scarps with different slopes, climates, and lithologies.

Even for simple slope processes with known mass-transport equations, rate constants are known to vary with factors such as climate and scarp materials. Some data are now available to assess the variation in rates with these variables. However, very little is known about changes in the form or in the rate constants for mass-transport functions over time (table 2). Considering the magnitude of changes in climate and vegetation in recent geologic time, variations in time may be as important as present spatial variations.

CONCLUSIONS

The diffusion-equation model of scarp degradation has been extremely useful in understanding scarp morphology and in providing age estimates for scarps. However, at present, the model has many limitations. The effects of variations in climate and lithology have long been recognized, but the effect of climatic history is underappreciated or ignored.

It is becoming increasingly clear that the assumption of transport rates that are a linear function of slope is a simplification that applies in only certain situations. Not only do many slope processes have nonlinear transport rates, but most scarps are affected by several different slope processes in different relative proportions. Despite the limitations that these factors impose on use of the diffusion-equation model to estimate the ages of scarps, the situation provides major research opportunities: scarp-morphology data combined with diffusion-equation modeling offer a new approach to a more complete understanding of general slope processes and their rates. Such knowledge is a key to progress in other fields such as paleoseismicity and tectonic geomorphology.

TABLE 2.--Transport-rate equations and diffusion-equation solutions
[Modified from Pierce and Colman (1986) and references therein, with additional information from Trofimov and Moskovkin (1984) and Andrews and Bucknam (in press).]

Process	Transport rate, K(x)	Diffusion-equation solution[1]
Mass movement.....	None	None.
Creep.....	$k_0 x^m (y/ x)^n$; m=0, n=1 $k_0 (y/ x)$	Exact: $y/ t = k_0 \ ^2y/ x^2$ Fourier series.
Cohesion-limited creep.	$k_0 x^m (y/ x)^n$; m=0, n>1	Finite difference.
Solifluction.....	$k_0 x^m (y/ x)^n$; m=0, n=1	Exact: $y/ t = k_0 \ ^2y/ x^2$ Fourier series.
Rain splash.....	$k_0 x^m (y/ x)^n$; m=0, n=1-2	Exact: $y/ t = k_0 \ ^2y/ x^2$ Fourier series (for n=1).
Sheetwash.....	$k_0 x^m (y/ x)^n$; m=0.3-1.0 n=1.3-2	Finite difference.
	$(k_0+k_1x) (y/ x)$	Fourier-Bessel series.
Sheetwash with gullying.	$k_0 x^m (y/ x)^n$; m=1-2 n=1.3-2	Finite difference.
Sheetwash with infiltration.	$(k_0+k_1x+k_2x^2) (y/ x)$	Fourier-Legendre series.
River flow.....	$k_0 x^m (y/ x)^n$; m=2-3, n=3	Finite difference.
Power-law creep or turbulent overland flow.	$k_0 (y/ x)^n$; n=3	Finite difference.

Process	Transport rate, K(t)	Diffusion-equation solution
All	Unknown	Finite difference.

[1]Cases where exact or series solutions exist also can be solved by finite-difference methods.

REFERENCES CITED

Andrews, D.J., and Bucknam, R.C., in press, Fitting degradation of shoreline scarps by a model with nonlinear diffusion: Journal of Geophysical Research.

Andrews, D.J., and Hanks, T.C., 1985, Scarp degraded by linear diffusion--Inverse solution for age: Journal of Geophysical Research, v. 90, no. B12, p. 10,193-10,208.

Bucknam, R.C., and Anderson, R.E., 1979, Estimation of fault-scarp ages from scarp-height--slope-angle relationship: Geology, v. 7, p. 11-14.

Colman, S.M., in press, Morphology and age of fault scarps in the Rio Grande rift, south-central Colorado: Colorado Geological Survey Bulletin.

Colman, S.M., and Watson, Ken, 1983, Diffusion-equation model for scarp degradation: Science, v. 221, p. 263-265.

Crone, A.J., and Machette, M.N., 1984, Surface faulting accompanying the Borah Peak earthquake, central Idaho: Geology, v. 12, p. 664-667.

Dodge, R.L., and Grose, L.T., 1980, Tectonic and geomorphic evolution of the Black Rock fault, northwestern Nevada, in Andrise, P. C., compiler, Earthquake hazards along the Wasatch - Sierra Nevada frontal fault zones, U.S. Geological Survey Open-File Report 80-801, p. 494-508.

Hanks, T.C., Bucknam, R.C., Lajoie, K.R., and Wallace, R.E., 1984, Modification of wave-cut and faulting-controlled landforms: Journal of Geophysical Research, v. 89, no. B7, p. 5771-5790.

Machette, M.N., 1986, History of Quaternary offset and paleoseismicity along the La Jencia fault, central Rio Grande rift, New Mexico: Bulletin of the Seismological Society of America, v. 76, p. 259-272.

Mayer, Larry, 1984, Dating Quaternary fault scarps formed in alluvium using morphologic parameters: Quaternary Research, v. 22, p. 300-313.

McCalpin, J.P., 1982, Quaternary geology and neotectonics of the western flank of the northern Sangre de Cristo Mountains, south-central Colorado: Colorado School of Mines Quarterly, v. 77, 97 p.

Nash, D.B., 1980a, Morphological dating of degraded normal fault scarps: Journal of Geology, v. 88, p. 353-360.

_____1980b, Forms of bluffs degraded for different lengths of time in Emmet County, Michigan: Earth Surface Processes and Landforms, v. 5, p. 331-345.

_____1984, Morphologic dating of fluvial terrace scarps and fault scarps near West Yellowstone, Montana: Geological Society of America Bulletin v. 95, p. 1413-1424.

Pierce, K.L., and Colman, S.M., 1986, The effect of height and orientation on the geomorphic degradation rates and processes, late-glacial terrace scarps in central Idaho: Geological Society of America Bulletin, v. 97, p. 869-885.

Sterr, Horst, 1985, Rates of change and degradation of hillslopes formed in unconsolidated materials--A morphometric approach to date Quaternary fault scarps in western Utah, USA: Zeitschrift fur Geomorphogie, v. 29, p. 315-333.

Trofimov, A.M., and Moskovkin, V.M., 1984, Diffusion models of slope development: Earth Surface Processes and Landforms, v. 9, p. 435-453.

Wallace, R.E., 1977, Profiles and ages of young fault scarps, north-central Nevada: Geological Society of America Bulletin, v. 88, p. 1267-1281.

_____1980, Degradation of the Hebgen Lake fault scarps of 1959: Geology, v. 8, p. 225-229.

EFFECT OF HEIGHT AND ORIENTATION (MICROCLIMATE) ON DEGRADATION RATES OF IDAHO TERRACE SCARPS

by

Kenneth L. Pierce[1] and Steven M. Colman[2]

[1] U.S. Geological Survey, Denver, CO,
[2] U.S. Geological Survey, Woods Hole, MA

ABSTRACT

Analysis of late-glacial terrace scarps in central Idaho demonstrate the importance of two factors not recognized in previous quantative studies of scarp degradation. First, degradation-rate coefficients calculated by a linear diffusion model increase with scarp height. This relationship shows that downslope transport rates are not solely determined by the first power of the slope. Slopewash has been observed to erode rills on these scarps and could explain the increasingly higher rate coefficients for the higher (and longer) scarps. Second, scarp orientation and associated microclimatic differences have a large effect on degradation rates. The effect increases with height such that, for scarps 2 m high, south-facing ones degrade three times as fast as north-facing ones, whereas for scarps 10 m high, south-facing ones degrade five times faster than north-facing ones.

INTRODUCTION

Scarps formed in unconsolidated materials become gentler with time. Such scarps may be formed by faulting, wave erosion, stream undercutting, or excavations by man. In the last decade, the progressive degradation of such scarps has been studied quantitatively (see Colman, this volume; and Nash, this volume). Such studies have been done mostly out of a desire to date fault scarps and thereby date the most recent displacement and associated earthquake on a given fault.

Bucknam and Anderson (1979) showed that for a given age scarp, the maximum scarp-angle increases approximately linearly with the log of the scarp height. They also showed that, for a given scarp height, the maximum scarp-angle diminishes systematically with scarp age. Subsequent studies, drawing on models using the linear-diffusion equation, have focused on the numerical relation between the morphology and age for scarps of fault, terrace, or wave-cut origin (see Colman, this volume, for summary).

Terrace scarps on adjoining alluvial fans in the Lost River Valley of central Idaho were last undercut and abandoned in late glacial time, about 15,000 yrs ago (Pierce and Colman, 1986). These scarps are formed in noncohesive sandy gravel mantled by a thin loess. These scarps are all about the same age, but differ in both their heights and their orientations. This report summarizes the effects of scarp height and scarp orientation on degradation rates: a more complete discussion is in Pierce and Colman (1986).

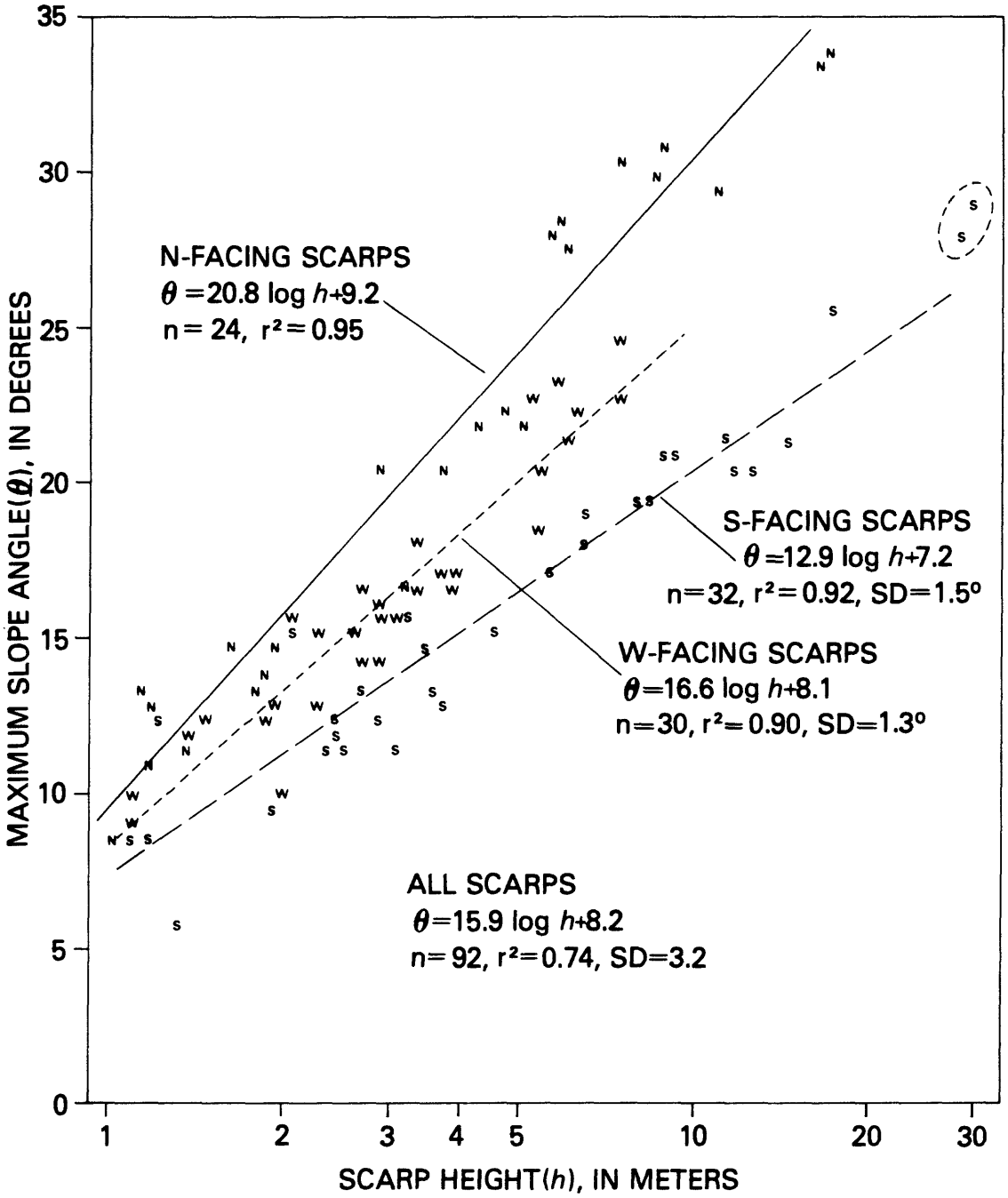

FIGURE 1.--Plot of maximum scarp angle (θ) against log of scarp height (h), for Idaho terrace scarps facing north (N), south (S), and west (W). For 3-m-high scarps, south-facing ones have degraded to maximum angles about 6^{o} less than north-facing ones. For regression analyses, n = number of scarps in a group, r^2 = coefficient of determination adjusted for degrees of freedom, and SD = standard deviation of the y values about the regression line. The two highest south-facing scarps (circled) are excluded from regression analyses, because they may be younger than the others (see Pierce and Colman, 1986).

DISCUSSION

Figure 1 plots maximum slope-angle against log of scarp height in the format of Bucknam and Anderson (1979) for north-, west-, and south-facing Idaho terrace scarps. For each orientation group, maximum slope-angle increases linearly with log of height. This relation is strong with coefficients of determination between 90 and 95 percent. A dependence on compass orientation is also clear: for 3-m-high scarps, the maximum slope-angle on south-facing scarps is about 3° lower than for west-facing scarps, which in turn is about 3° less than north-facing scarps.

The linear diffusion-equation model assumes that the transport rate is simply a linear function of slope. Consequently, scarp height (or length) should have no effect on the rate coefficient, c. To examine this assumption, we analyzed the group of west-facing Idaho scarps. In contrast to north-facing and south-facing scarps, west-facing ones have essentially constant solar insolation regardless of scarp slope. We assumed a starting angle of 33.5° for the diffusion-equation model both because some scarps in the data set measured as steep as $33\ 1/4^{\circ}$ and because the angle of repose in the sandy gravel in which the scarps were cut is at least 33.5° (Pierce and Colman, 1986, p. 872-873)

Idaho terrace scarps show a height effect in addition to that modeled by the linear diffusion equation (figs. 2 and 3). Rather than being constant, the rate coefficient calculated by a linear-diffusion model shows a more than a one to one dependence on height (c^*/h has a slope of 1.54). As a check on this unexpected finding, we made a similar analysis of the Lake Bonneville shoreline scarps and found a nearly identical dependence on height (figs. 2 and 3). Both sets of data clearly indicate that the degradation of these scarps is not adequately modeled by the linear-diffusion equation. Consequently, the key assumption of this diffusion-equation model--that transport rates for the various processes involved are solely a linear function of slope--is incorrect.

This discrepancy with the diffusion-equation model may be because of transport by slopewash, which has been observed to form rills on the scarps and which is associated with sediment transport rates which are a non-linear function of slope (Carson and Kirkby, 1972). The effectiveness of slopewash increases as the length of slope increases (see Colman, this volume). The effectiveness of slopewash therefore tends to increase on the higher and longer scarps. The dependence on height might also be explained if transport rate is proportional to more than the first power of the slope expressed as a tangent (Pierce and Colman, 1986, p. 882). For Bonneville and Lahontan shoreline scarps, D. J. Andrews and R. C. Bucknam (in press) found this height effect could be explained by a nonlinear, cubic diffusion-equation model in which the transport rate is proportional to the third power of the slope (expressed as a tangent).

South-facing Idaho terrace scarps degrade faster than north-facing ones. Diffusion-equation analysis (linear model) shows the apparent degradation-rate coefficient increases much more with height for south-facing than north-facing scarps (fig. 4). The slope of the regression line for south-facing scarps is more than seven times that for north-facing scarps (fig. 4). Solar insolation increases with the more southerly orientation. For south-facing scarps, it increases with slope, whereas for north-facing scarps, it decreases. Scarps with high values of solar insolation are drier

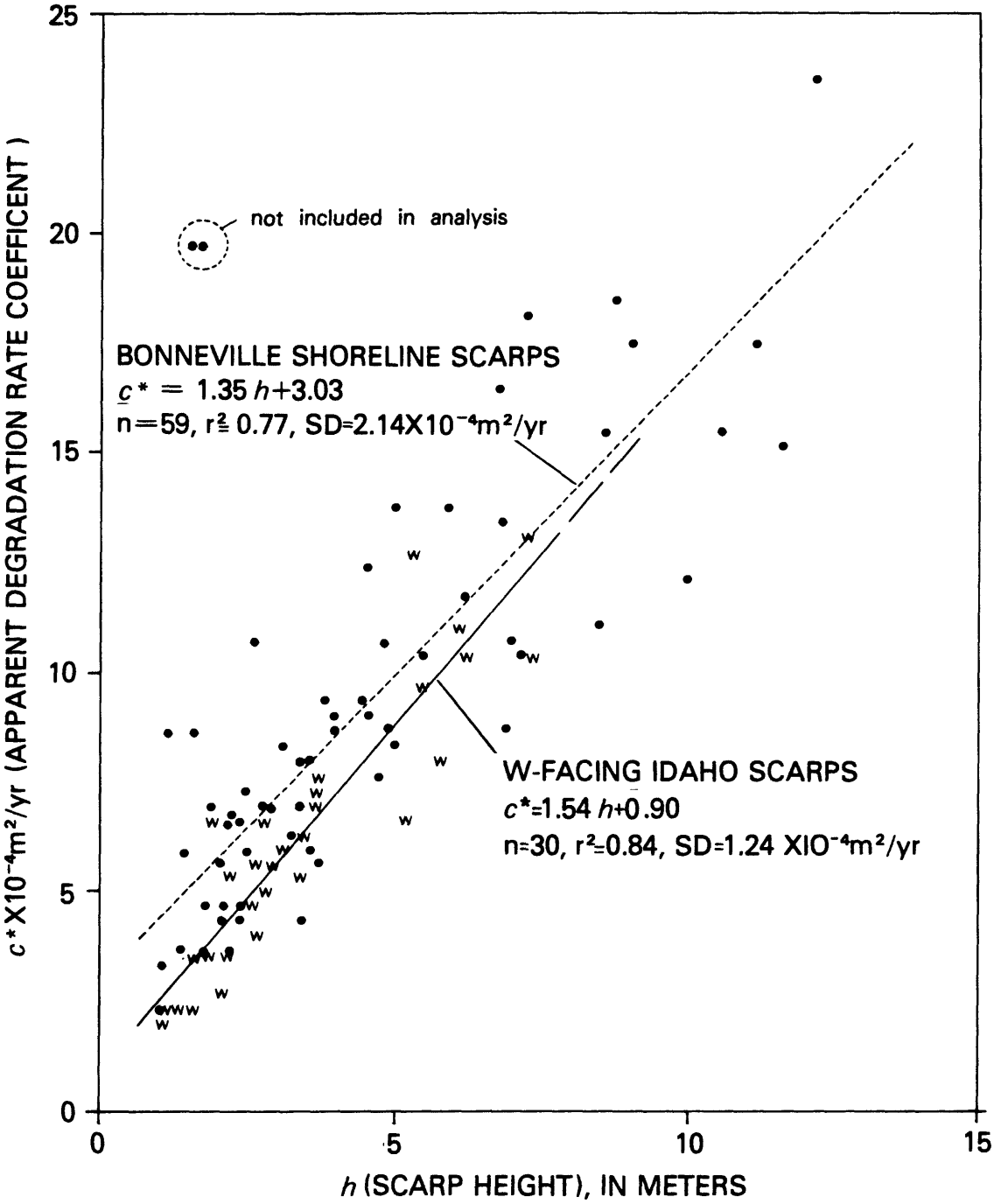

FIGURE 2.--Dependence of the apparent degradation rate coefficient (c*) on h for west-facing Idaho scarps. Also shown are Lake Bonneville shoreline scarps that face west or east (solid dots). For Bonneville shoreline scarps, calculations of c* use "surface offset" rather than height to account for the effect of fan slopes above and below the scarps (Bonneville data from R. C. Bucknam, written commun., 1983).

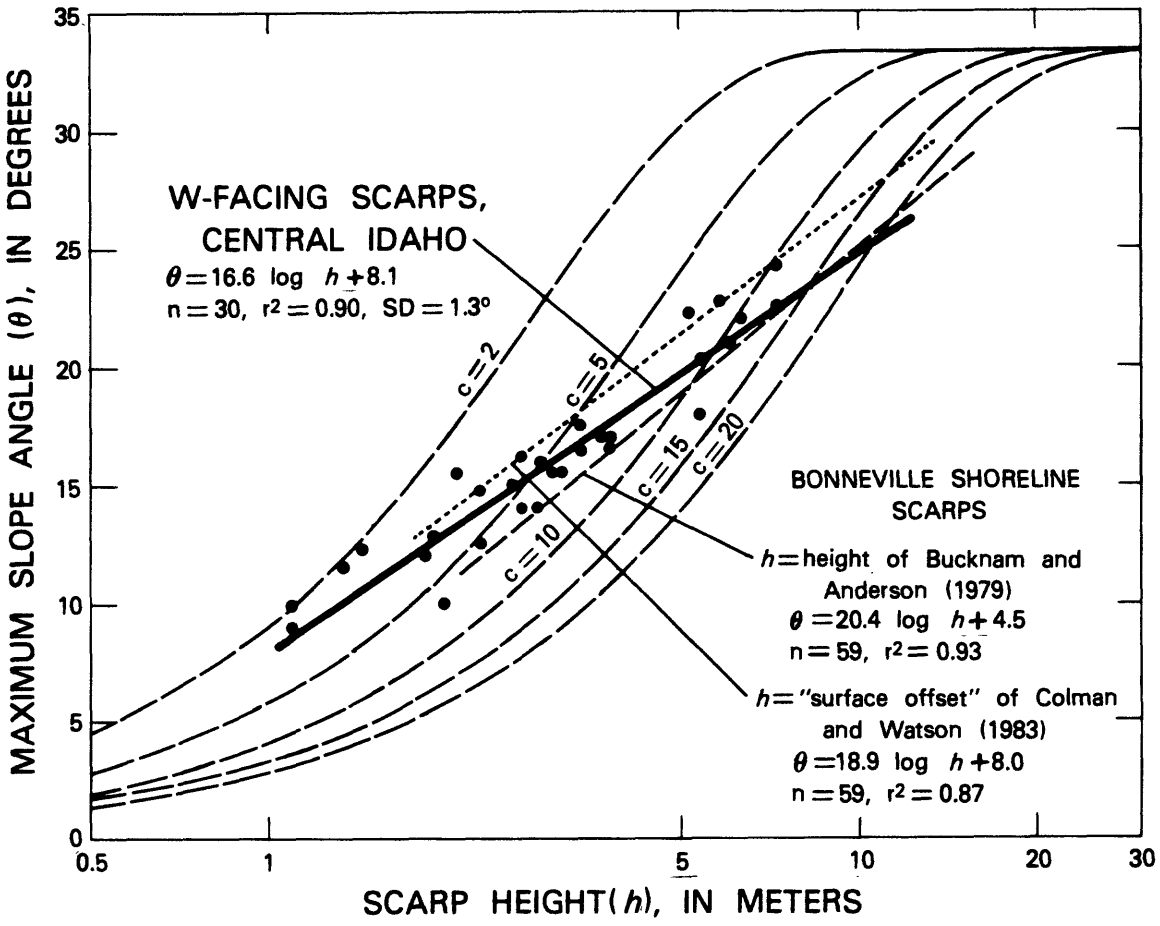

FIGURE 3.--Plot in format of Bucknam and Anderson (1979) showing departure of west-facing Idaho terrace scarps (dots) from constant values of c shown by dashed, curved, lines. The five degradation-rate coefficients are for a 15,000-yr-old scarp, and c is in the units 10^{-4} m^2/yr. West-facing Idaho scarps define the regression line (heavy line) that transects constant values of c, although they are subparallel at the lower end. A similar increase occurs for the Bonneville shoreline scarps shown by short- and long-dashed regression lines (Bonneville data from R.C. Bucknam, written commun., 1983).

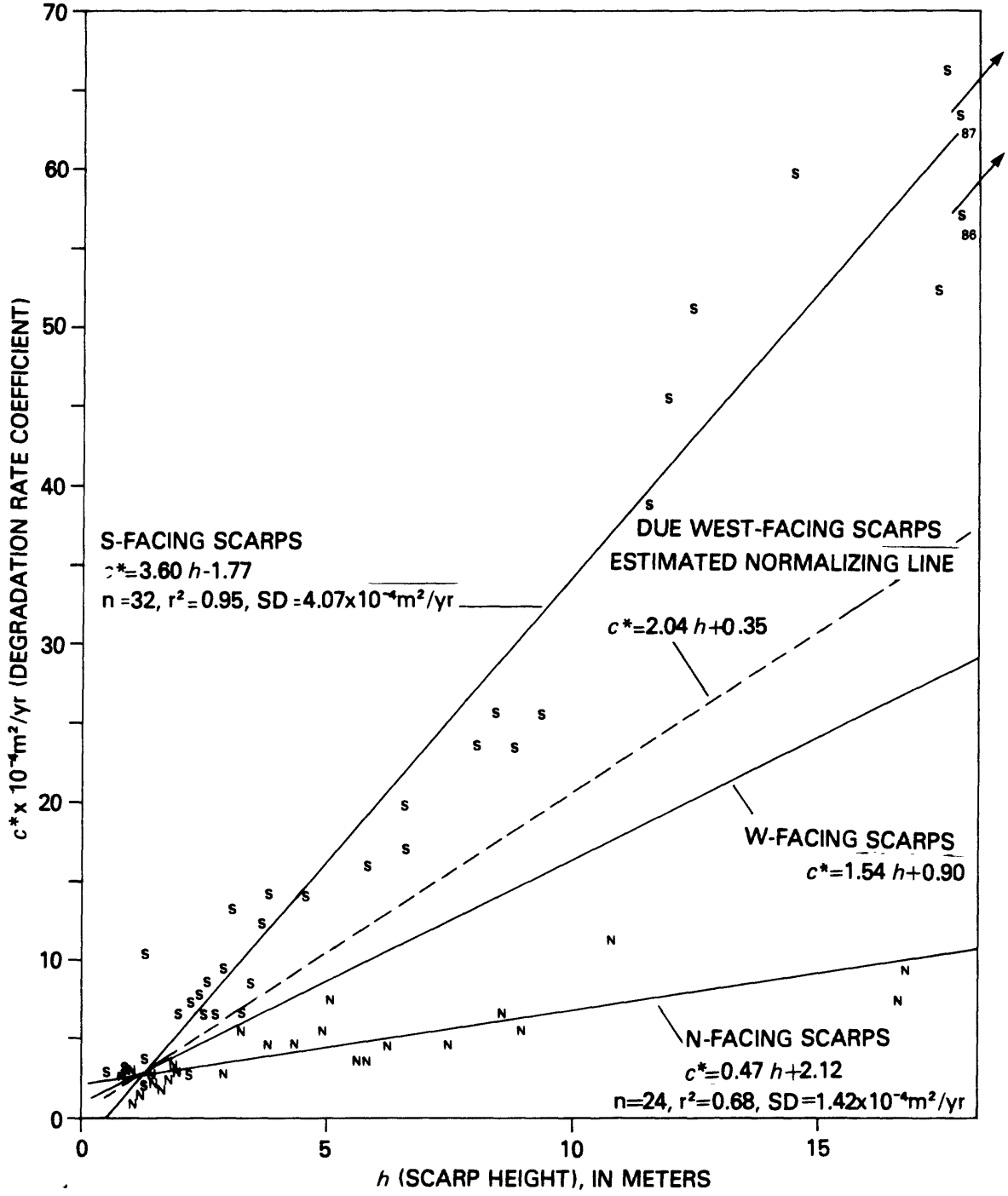

FIGURE 4.--Plot showing greater degradation-rate coefficients (c*) on south-facing terrace scarps (S) than north-facing ones (N). The apparent degradation-rate coefficient c* increases much more with h for south-facing than north-facing scarps. This difference results from the fact that, for south-facing scarps, solar isolation increases with increasing surface inclination, whereas, for north-facing scarps it decreases (see Pierce and Colman, 1986, fig. 8). Data for west-facing scarps is not shown.

and less vegetated and experience more freeze-thaw cycles (see discussion in Pierce and Colman, 1986).

For scarps in semiarid and perhaps in other environments, age estimates using a linear-diffusion model should account for the height effect shown in figures 2 and 3. An example is shown in table 1 for diffusion-equation calculation of the age of the Drum Mountains fault scarps for heights of 2 and 5 meters. Data from the Drum Mountains fault scarps (R.C. Bucknam, written commun., 1983) yield a regression equation of $tc^* = 1.16\ h + 2.69$. These scarps are in the same area as the Bonneville shoreline scarps and face either east or west, as do also the Bonneville scarps. Hence the dated Bonneville shoreline scarps (Scott and others, 1983) can be used for calibration. Table 1 outlines calculations for 2- and 5-m-high scarps. The 5-m scarp has nearly twice the rate coefficient of the 2-m-scarp, but both heights result in nearly identical ages of just under 9,000 yrs. This age is consistent with geologic estimates of age as early Holocene, based on relations to Lake Bonneville and on relative soil development. An age of 9,000 yrs is about twice that of previous diffusion-equation-model estimates that did not account for this height effect in linear-diffusion models (see discussion and references in Pierce and Colman, 1986).

TABLE 1.--Age estimates of Drum Mountains, Utah, fault scarps based on comparison with Bonneville shoreline scarps of the same height

Scarp height (offset in meters)	Location	tc^* m^2	c^* $10^{-4}m^2/yr$	t yrs
2 m	Bonneville.....	8.6	[1]5.7	15,000
"	Drum Mountains.....	5.0	[2]5.7	[2]8,800
5 m	Bonneville.....	14.7	[1]9.8	15,000
"	Drum Mountains.....	8.5	[2]9.8	[2]8,700

[1]Calculated using known age (t) of 15,000 yr (Scott and others, 1983).
[2]Calculated assuming the same c^* as Bonneville shoreline scarps.

REFERENCES CITED

Andrews, D.J., and Bucknam, R.C., in press, Fitting degradation of shoreline scarps by a model of nonlinear diffusion: Journal of Geophysical Research.

Bucknam, R.C., and Anderson, R.E., 1979, Estimation of fault-scarp ages from a scarp-height--slope-angle relationship: Geology, v. 7, p. 11-14.

Carson, M.A., and Kirkby, M.J., 1972, Hillslope form and process: London, England, Cambridge University Press, 475 p.

Colman, S.M., and Watson, Ken, 1983, Ages estimated from a diffusion equation model for scarp degradation: Science, v. 221, p. 263-265.

Pierce, K.L., and Colman. S.M., 1986, Effect of height and orientation (microclimate) on geomorphic degradation rates and processes, late-glacial terrace scarps in central Idaho: Geological Society of America Bulletin, v. 97, p. 869-885.

Scott, W.E., McCoy, W.D., Shroba, R. R., and Rubin, Meyer, 1983, Reinterpretation of the exposed record of the last two lake cycles of Lake Bonneville, Western United States: Quaternary Research, v. 20, p. 261-285.

REEVALUATION OF THE LINEAR-DIFFUSION MODEL FOR MORPHOLOGIC DATING OF SCARPS

by

David Nash

Department of Geology
University of Cincinnati
Cincinnati, Ohio 45221-0013

ABSTRACT

A simple diffusion model in which the downslope flux of debris is assumed to be proportional to gradient predicts the general pattern of degradation of terrace scarps underlain by alluvium. On some higher scarps, however, the model predicts more rounding of the basal concavity and crestal convexity than is observed. In addition, for at least some scarps known to be the same age, there is a strong positive correlation between the age determined by morphologic dating and the height of the scarp. Although neither problem necessarily invalidate the model, they suggest that a thorough theoretical and experimental examination be made of the model's basic assumptions.

INTRODUCTION

Morphologic dating of a hillslope involves matching its profile with a profile produced by a calibrated model that accurately describes the degradation of that hillslope. Before a hillslope can be dated in this way, an initial morphology for its profile must be assumed, an appropriate model must be selected, and that model must be calibrated for local conditions (for example, climate, aspect, and underlying material). Transport-limited hillslopes, those on which more material is loosened and available for transport than the transportational processes are capable of removing, are observed to degrade by progressive rounding of the basal concavity and crestal convexity. This pattern of degradation can be closely matched by a simple diffusion model in which the rate of change in elevation at a point on a hillslope is proportional to the curvature of the hillslope at that point. The model predicts the observed rounding of the basal concavity and crestal convexity. The simple diffusion model also explains Bucknam and Anderson's (1979) observation that the gradient of the midsection of a low scarp decreases faster than that of a higher scarp.

The study reported here was undertaken to determine the influence various factors have on the calibration of the simple diffusion model. At the time the study was undertaken, there was substantial evidence that the model was valid for describing the degradation of transport-limited hillslopes and that the primary limitation to its use in morphologic dating of scarps produced by normal faulting was the necessity for having a nearby scarp of known age with which to calibrate the model for local conditions. Late-glacial fluvial terrace scarps in Wyoming, Montana, and Idaho were profiled to determine the effect factors such as underlying geology, aspect, vegetation cover, and climate have on model calibration.

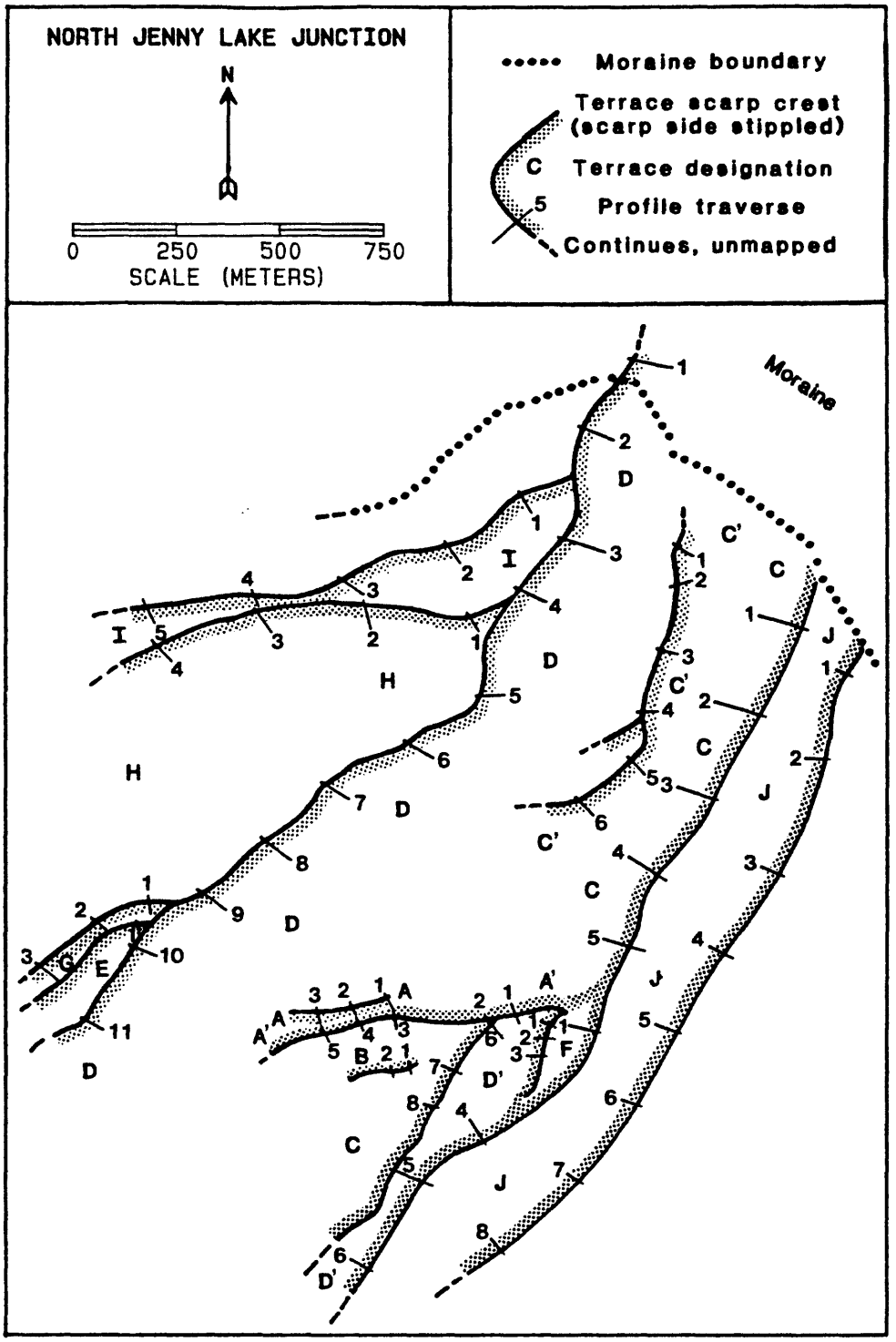

FIGURE 1. Terrace scarps cut by an outwash channel of the Jackson Lake phase of glaciation by the Snake River glacial lobe near Jenny Lake Junction in Grand Teton National Park. Numbered lines indicate locations at which the profiles shown in figures 8 and 9 were measured.

The study concentrated on a set of scarps at a site in the vicinity of the Jenny Lake Turnoff in Grand Teton National Park (fig. 1). The scarps are underlain by a virtually cohesionless outwash of predominantly highly rounded chert cobbles. The scarps formed during what Pierce and Good (1986) name the Jackson Lake phase of glaciation by the Snake River glacial lobe. K.L. Pierce (oral commun., 1985) believes the sequence of terraces were cut rapidly sometime between 15,000 and 20,000 yrs ago when glacial ice advanced to the southern margin of the Jackson Lake basin.

Along their length, each of the terrace scarps varies in aspect and, to a lesser extent, in their cover of vegetation and the grain size distribution of the underlying outwash. Even if all of the scarps where not formed simultaneously, a single scarp can be assumed to be nearly the same age along its length. Variations in the age determined by morphologic dating of profiles taken from different places along the length of the same scarp were at first presumed to be caused by problems with calibrating the model rather than deficiencies in the model itself. If all of the scarps were not formed simultaneously, they must have formed successively as the channel incised into the outwash so scarps whose bases are at successively lower elevations are successively younger (that is, scarps in fig. 2 are successively older from J to A).

The ages the terrace scarps from the Jenny Lake Junction site determined by morphologic dating range over more than an order of magnitude and are unrelated to the order in which they formed. Even more disturbing, the study finds the same strong correlation between morphologic age and scarp offset (the perpendicular distance separating the scarp base and crest), H, as found by Pierce and Colman (1986). The effect of offset on the calibration of the diffusion model is so profound that the influence of all other factors is trivial by comparison. In addition, a comparison between the observed scarp profile and the best-fit model profile for terrace scarps with large offsets ($H > 20$ m) shows consistent differences. In view of these unexpected problems, should the simple diffusion model for hillslope degradation be used for morphologic dating?

SIMPLE DIFFUSION MODEL

G. K. Gilbert (1877) observed that debris moves downslope as a rate which is a function of gradient.

> "...erosion is favored by declivity [gradient]. Where the declivity is great the agents of erosion are powerful; where it is small they are weak; where there is no declivity they are powerless. Moreover it has been shown that their power increases with declivity in more than simple ratio."

He further observed that water and debris are conserved as they move downhill.

> "Every slope is a member of a series, receiving the water and waste of the slope above it, and discharging its own water and waste upon the slope below."

These two observations form the basis of the simple diffusion model. In this model, however, contrary to Gilbert's assertion, the debris is assumed to be a simple linear function of gradient.

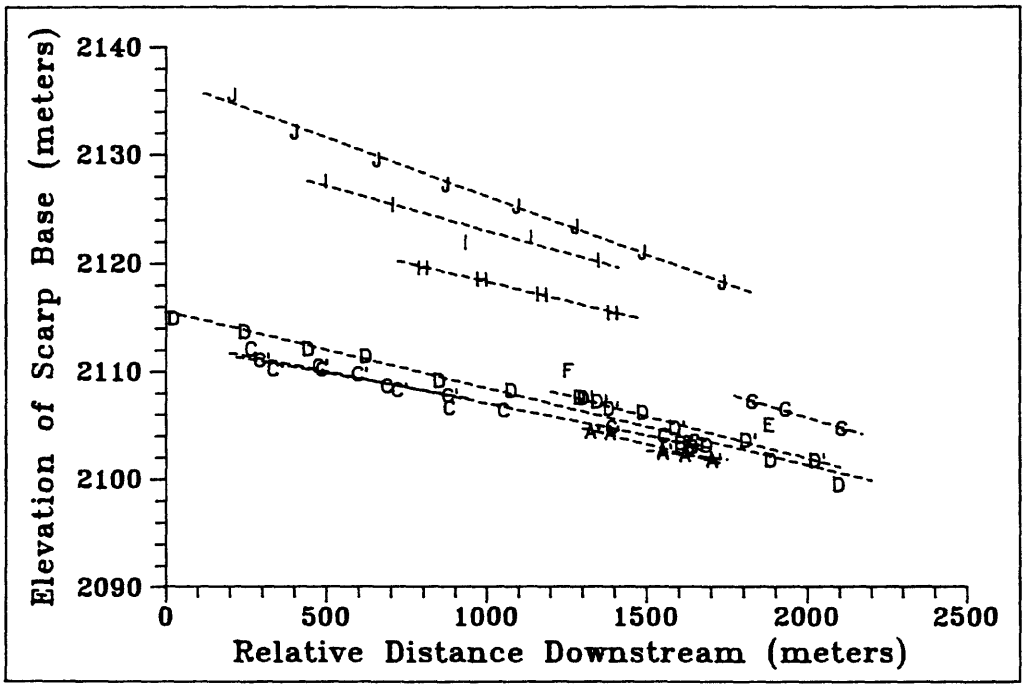

FIGURE 2. Elevation of the bases of profiles marked in figure 1 plotted against their downstream distance from the Jackson Lake moraine.

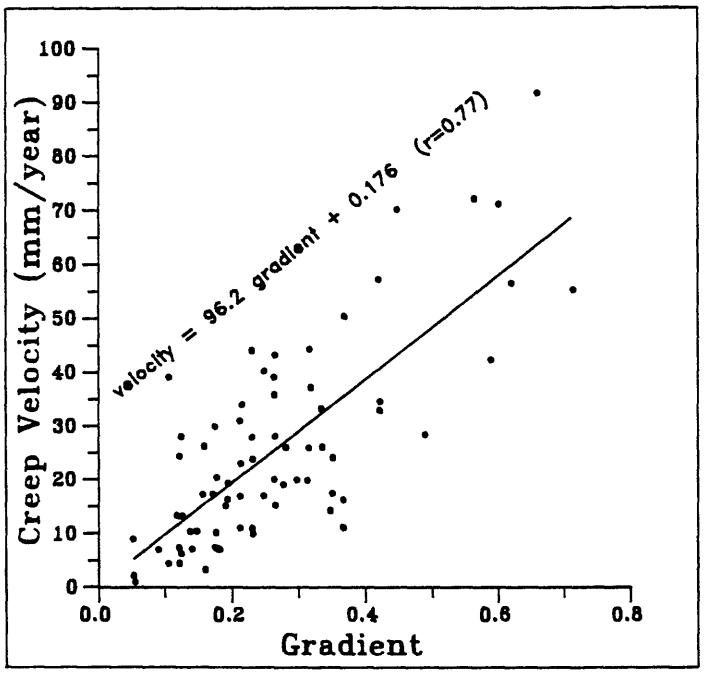

FIGURE 3. Creep velocity observed over a 7-yr period on shale hillslopes in western Colorado plotted against hillslope gradient (modified from Schumm, 1967).

Downslope Debris Flux

Is the volumetric rate of debris transport (volume of debris per length of contour or L^2/T), q, a linear function of gradient...

$$q = -c \frac{\partial y}{\partial x}, \qquad (1)$$

where c is a constant proportionality (generally referred to as diffusivity), and x and y are the horizontal and vertical coordinates respectively? Although a convincing theoretical argument can be made that q should be proportional to the force of gravity acting tangentially to the surface (proportional the sine of the slope-angle) if the debris is rheologically similar to a Bingham model or to an alternate expansion-contraction creep model, there is little experimental data.

Schumm (1967) observed the velocity at which marked fragments creeped downslope over a 7-yr period on a shale hillslope in western Colorado. The creep velocity can be fit fairly closely (r = 0.77) with a linear function (fig. 3) but this velocity is not the same as q. If it is assumed that the thickness of the creeping debris mantle is not a function of gradient, then Schumm's data supports equation 1. Although it is quite possible that the thickness of the debris mantle is independent of gradient, it should not be assumed a priori. Field studies of debris flux are badly needed.

Downslope Conservation of Debris

If equation 1 is valid and if c is not a function of gradient or position (x), volumetric conservation of debris demands

$$\frac{\partial y}{\partial t} = c \frac{\partial^2 y}{\partial x^2}, \qquad (2)$$

where t is time and assuming the density of the debris prior to removal is the same as its density after deposition. Numerous analytical and numerical techniques have been developed to determine the value of tc that most closely matches the observed slope profile. For this study, a numerical technique implemented by a computer program, SLOPEAGE, is used (the program runs on IBM or IBM-compatible PC's and is available free from the author). SLOPEAGE can determine tc for a profile having either a horizontal or sloping base and crest (sometimes referred to as the far-field slope).

SHORTCOMINGS OF THE SIMPLE DIFFUSION MODEL

Scarp Height Effect

The simple diffusion model closely predicts the observed pattern of scarp degradation. It also explains Bucknam and Anderson's (1979) observation that the midsection gradient of low scarps decreases faster than the gradient of higher scarps underlain by the same material. Assuming a scarp is of the same age along its length, tc, the scarp age multiplied by diffusivity, should be independent of scarp offset. Despite the lower midsection gradients of the

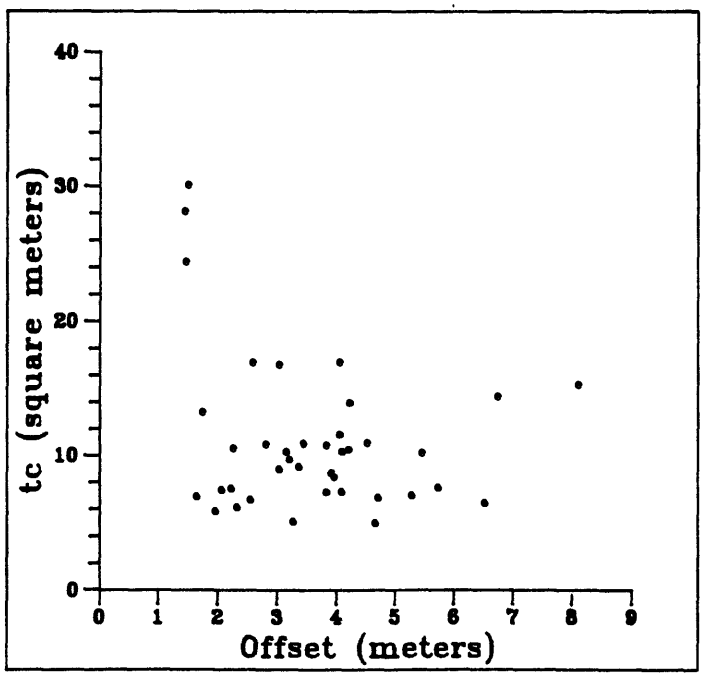

FIGURE 4. tc values calculated for profiles of the Drum Mountain fault scarps in western Utah plotted against scarp offset. A slope-angle of 33.5° is assumed for the initial midsection (profile data courtesy of R.C. Bucknam, USGS, Denver).

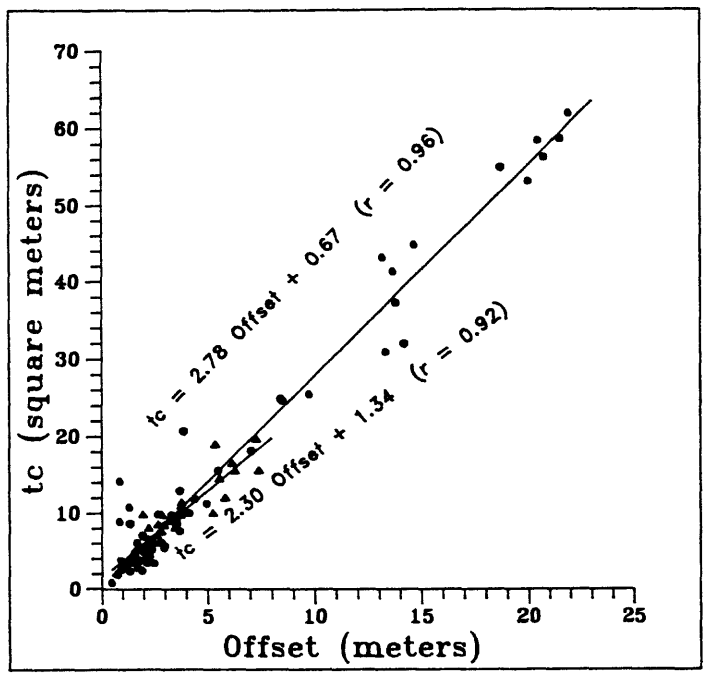

FIGURE 5. There is a strong positive correlation between age calculated by morphologic age based on the simple diffusion model and scarp offset. This correlation is observed both for west-facing terrace scarps measured by Pierce and Colman (1986) in central Idaho (triangles) and for terrace scarps at the Jenny Lake Junction site (dots). An initial midsection slope-angle of 33.5° is assumed for the Jenny Lake site scarps.

lower scarps, the values of tc derived with the diffusion model are independent of offset for Bucknam and Anderson's data from the Drum Mountain fault scarps in western Utah (fig. 4). In a study of terrace scarps in central Idaho, however, Pierce and Colman (1986) find a strong, linear correlation between tc and offset (fig. 5). A nearly identical relationship between tc and offset is found for the scarps at the Jenny Lake Junction site (figs. 5 and 6). Even if all of the scarps did not form simultaneously, tc increases with offset for a single scarp (for example, scarp C in fig. 6).

To examine the influence factors other than offset have on tc and to compare values of c collected from other areas, tc values for scarps at the Jenny Lake Junction site are adjusted for an equivalent scarp with a 5-m offset, tc_5:

$$tc_5 = tc + 2.78\ (5 - \text{offset}). \qquad (3)$$

There are at least four possible explanations for why tc increases with offset:

1) The simple diffusion model is invalid.

2) c increases linearly with offset.

3) Higher scarps are more likely to initially have consisted of two or more smaller scarps.

4) The initial slope-angle of higher scarps is lower than for lower scarps.

The validity of the diffusion model and alternate models will be discussed later. The other possible explanations are discussed below.

c Increases Linearly with Offset

The offset of a scarp may influence the microclimate on its face. At the Jenny Lake Junction site, higher scarps are commonly more heavily vegetated and are more disturbed by grazing animals than are lower scarps. As Pierce and Colman (1986) note, however, microclimate is also quite sensitive to scarp aspect; they find a strong relation between aspect and tc for scarps in central Idaho. Despite the fact that aspect strongly effects soil moisture, soil temperature, vegetation cover, etc., tc_5 is apparently unaffected by aspect at the Jenny Lake Junction site (fig. 7).

High Scarps are likely to Initially Consist of Two or More Smaller Scarps

A terrace scarp is formed by lateral migration of a cutbank that commonly undercuts higher terraces. The higher terrace surface is often not completely removed resulting in a stepped scarp face consisting of two or more smaller scarps. As they degrade, stepped scarps will be smoothed-out and otherwise be indistinguishable from unstepped scarps of the same height except they will appear much older (Nash, 1984; Andrews and Hanks, 1985). The greater a scarp's offset, the more terrace surfaces it is likely to have undercut and thus is more likely initially to have been stepped. It would seem unlikely,

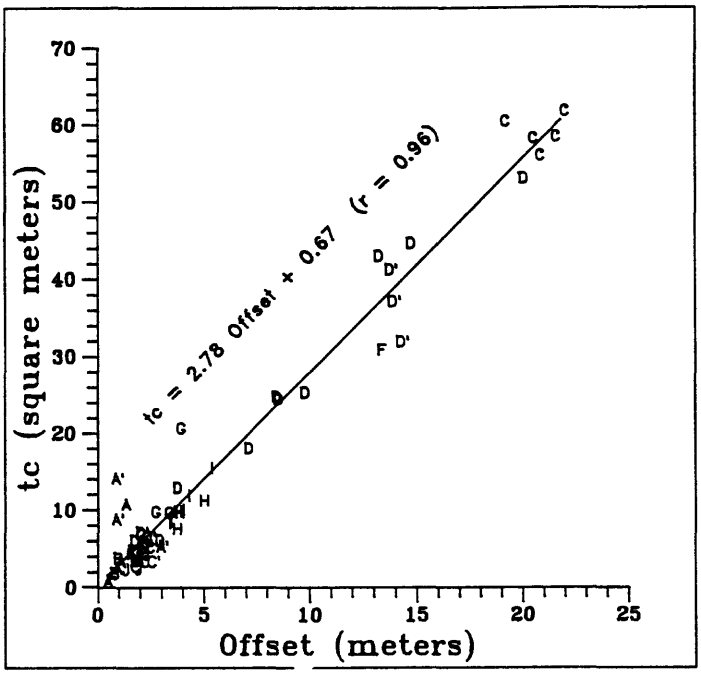

FIGURE 6. tc calculated for scarps in the Jenny Lake site using the simple diffusion model with an assumed initial midsection slope-angle of 33.5° plotted against scarp offset. Data points are marked with the scarp letter labels used in figures 1 and 2.

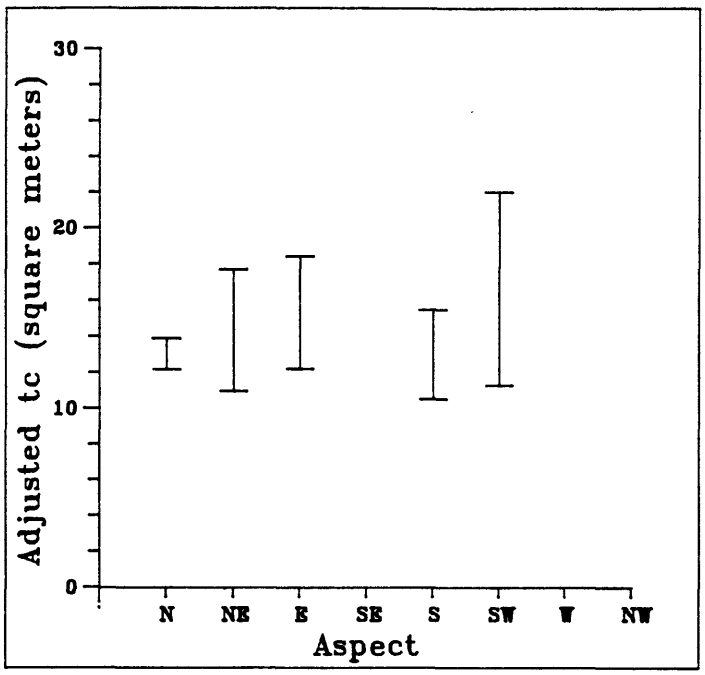

FIGURE 7. There is no apparent affect of scarp aspect on tc_5 (tc adjusted for a scarp with a 5-m offset) calculated by the simple diffusion model using an initial midsection angle of 33.5°.

however, that the number of steps would increase linearly to give the relationship between tc and offset seen in figure 6.

Higher Scarps Have a Lower Initial Gradient Than Lower Scarps

Scarps are assumed to have had a simple initial morphology consisting of a straight base and crest separated by a midsection at the angle of repose of the underlying material. The angle of repose is assumed to be independent of offset. Observations of active cutbanks in cohesionless material find the gradient on the debris apron at the base of higher scarps is lower than that at the base of lower scarps (Carson, 1977). As the free face ravels and is progressively buried by the debris apron; however, the average height of drop decreases and presumably the gradient of the scree surface would increase to ultimately equal the gradient of the scree at the base of initially low scarps.

If the relationship between tc and offset in figure 6 were to be accounted for by a progressively lower initial slope-angle for higher scarps, and if the initial slope-angle of a 5-m-high scarp were 33.5°, it would be necessary for the initial slope-angle of a 20-m-high scarp to be 26°. Observations of 20-m-high active cutbanks along the Snake River found no basal scree slopes with angles less than 30°. It is perhaps possible that a larger scree apron "settles" more than a smaller scree aprons to produce a lower gradient.

Differences Between Observed and Predicted Profiles

At high vertical exaggerations, the profiles predicted by the diffusion model are seen to systematically deviate from the observed scarp profile (fig. 8). For high scarps, the model predicts a lower curvature for the basal concavity and crestal convexity than is observed. This lower than predicted curvature may again indicate a fundamental problem with the simple diffusion model. It is possible, however, to duplicate the observed curvature of the basal concavity and crestal convexity by lowering the gradient assumed for the initial midsection. If an initial midsection slope-angle of 26° is assumed for a 20-m-high scarp, a much better fit between the observed and predicted midsection is achieved.

ALTERNATE MODELS

D.J. Andrews (USGS, Menlo Park) proposes a model in which the debris flux at a point on a scarp profile is proportional to the cube of the gradient at that point,

$$q = c(\partial y/\partial x)^3 \qquad (4)$$

(oral commun., 1987). With volumetric conservation of debris,

$$\frac{\partial y}{\partial t} = \frac{\partial(c(\partial y/\partial x)^3)}{\partial x} . \qquad (5)$$

Although the physical basis of equation 4 is unclear, the profiles predicted by equation 5 using an initial midsection slope-angle of 33.5° fit the curva-

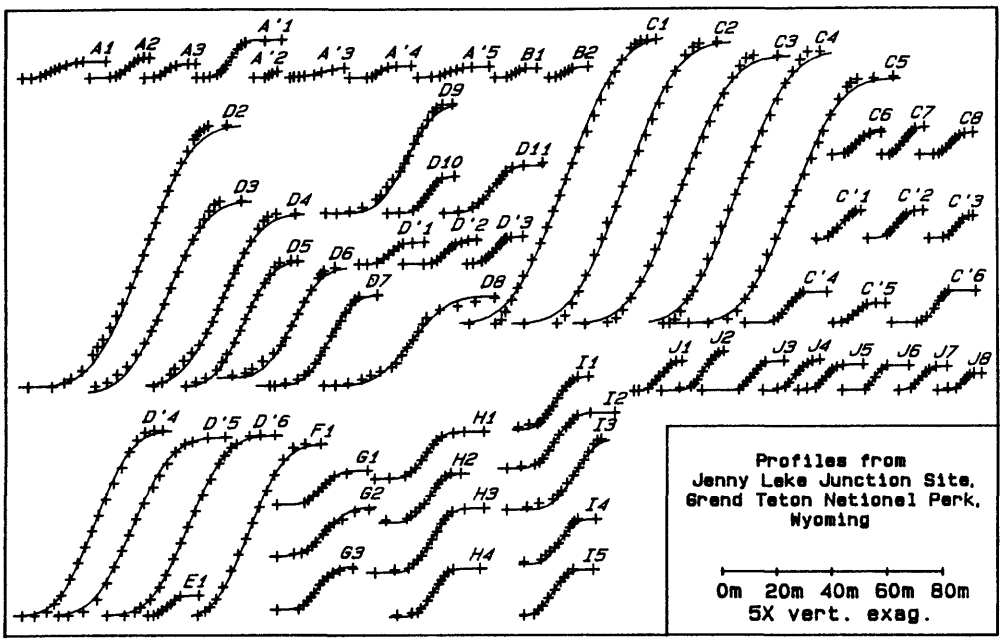

FIGURE 8. Observed profiles (+'s) from terrace profiles at the Jenny Lake Junction site with the best-fit model profile using the simple diffusion model and an midsection angle of 33.5°. For high scarps, the basal concavity and crestal convexity of the model profile is more rounded than the observed profile. Location of profiles is shown in figure 1.

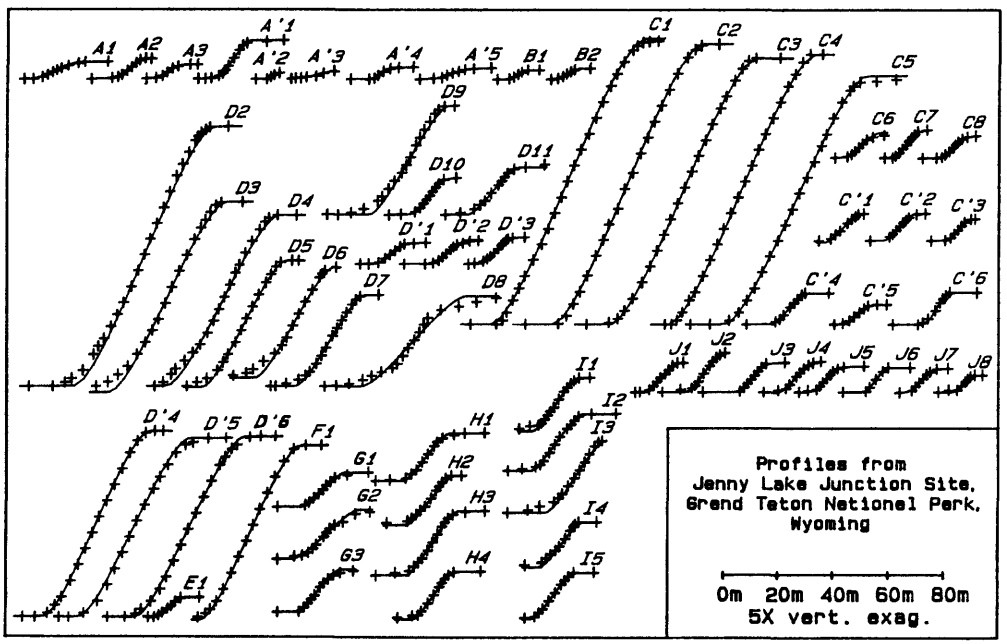

FIGURE 9. Observed profiles (+'s) from terrace profiles at the Jenny Lake Junction site with the best-fit model profile assuming the debris flux is proportional to the cube of the gradient and using an initial midsection angle of 33.5°. This model matches the curvatures of the crestal convexity and basal concavity better than the simple diffusion model. Location of profiles is shown in figure 1.

tures of the basal concavity and crestal convexity better than the simple diffusion model (fig. 9). As with the simple diffusion model, the tc value for the best-fit model profile predicted by equation 5 for the Jenny Lake Junction scarps increases with increasing scarp offset (fig. 10).

A number of other models have been proposed for modeling the debris flux (see Pierce and Colman, 1986 for a summary of some of these models). Many of the models are of the form

$$q = f(x, \partial y/\partial x). \qquad (6)$$

Models in which q is only a function of gradient produce symmetric profiles from symmetric initial profiles (an equal amount of material is removed from the crestal convexity as is deposited at the basal concavity). Models in which q is also some function of x will produce asymmetric profiles from initially symmetric scarps.

An average of 24±52 percent more material is deposited than is removed from the Jenny Lake Junction scarps. K.L. Pierce (written commun., 1987) notes that the balance between the volume of material deposited and removed may change systematically with orientation (fig. 11, depositional surplus is defined as the percent by which the volume of material deposited at the scarp base exceeds the volume of material removed from the scarp crest). Given the very high standard deviation of these data, it can not be statistically demonstrated (95 percent confidence) that the volume of material removed differs from the volume of material deposited. I therefore concluded that, at least for the Jenny Lake Junction terrace scarps, models based on q being some function of x are inappropriate.

CONCLUSIONS

It is clear there are serious problems with morphologic dating using a simple diffusion model. Although adjusting tc values for an equivalent 5-m-high scarp is a short term solution for comparing tc between different areas, it avoids basic questions about initial scarp morphology, the validity of the simple diffusion model, and c. A better fit to the observed profiles from the Jenny Lake Junction site can be achieved with the Andrews' model (eq. 5) in which transport rate increases with declivity "...in more than a simple ratio" but there is no theoretical or observational basis for equation 4.

A dating technique proposed by Nash (1980) can be used for morphologic dating if either equations 2 or 5 are appropriate (fig. 12). Andrews (oral commun., 1987) notes that if q is some function of gradient alone, then maximum slope-angle of a scarp midsection is some function of tc/H^2. Therefore, two scarps having the same initial slope-angle that have degraded to the same slope-angle must have the same value for tc/H^2. If maximum slope-angle is plotted against scarp offset for two different aged scarps, a and b, a horizontal line intersects the two curves at offsets of H_a and H_b respectively but

$$t_a c_a / H_a^2 = t_b c_b / H_b^2. \qquad (6)$$

Therefore

$$(t_a c_a)/(t_b c_b) = H_a^2/H_b^2. \qquad (7)$$

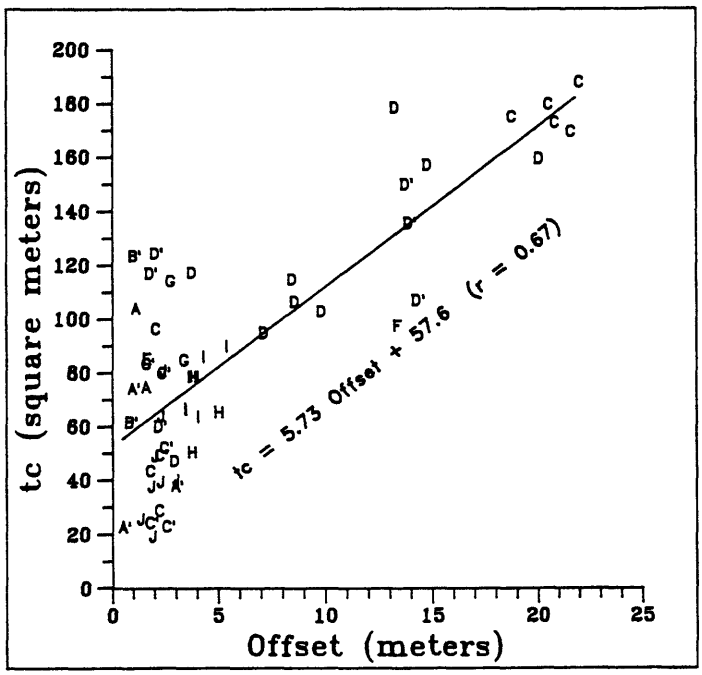

FIGURE 10. There is a correlation between offset and values of tc calculated for the Jenny Lake Junction scarps assuming q is proportional to the cube of the gradient that is similar to, but not as strong as, the correlation in figure 6.

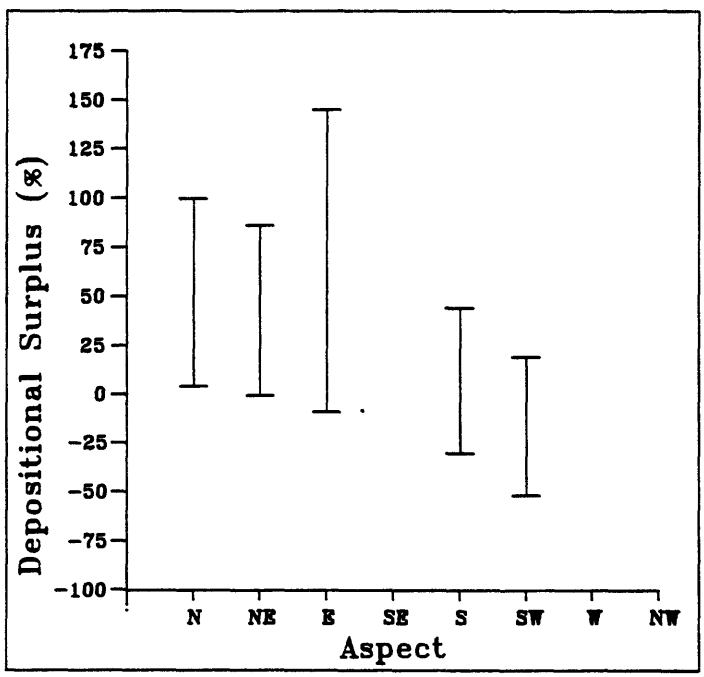

FIGURE 11. Depositional surplus plotted against scarp aspect. If the scarp is symmetric, the depositional surplus is 0 percent.

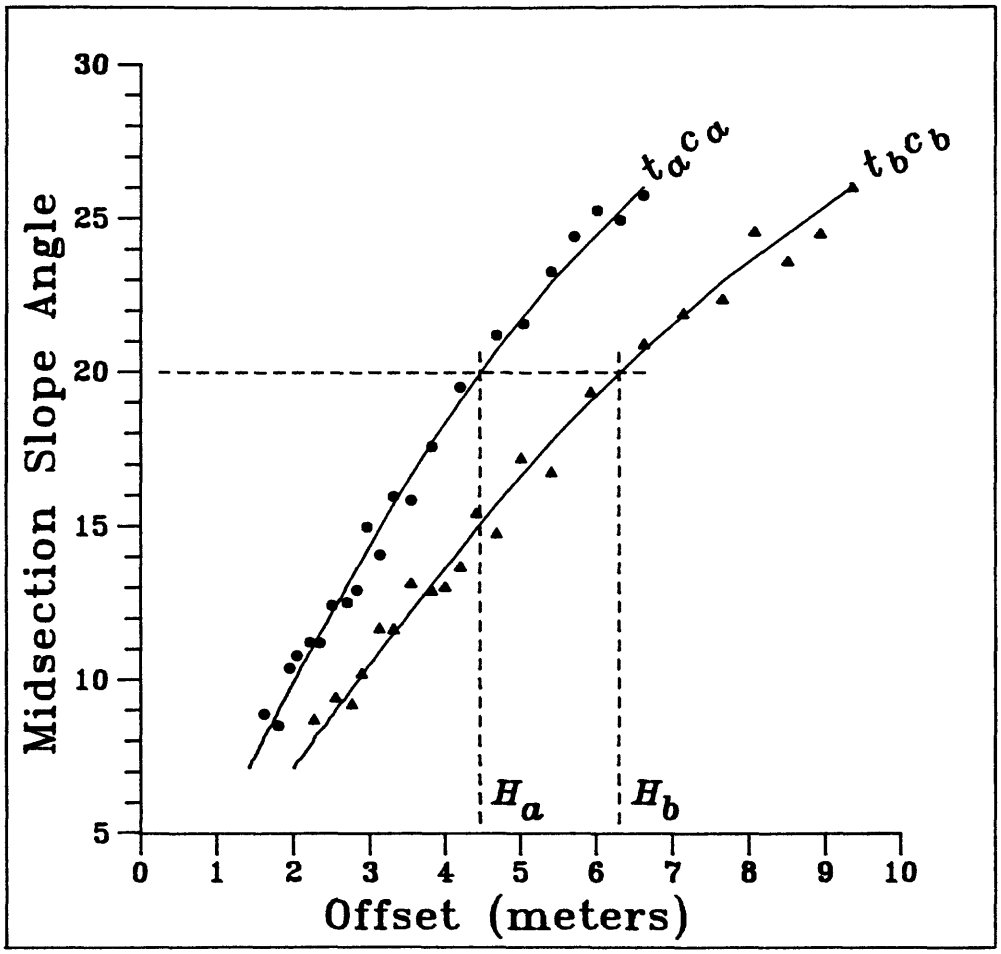

FIGURE 12. If debris flux is some function of gradient alone, then maximum midsection slope-angle is a unique function of tc/H^2. Therefore, if the maximum midsection slope-angle is plotted against H for two scarps (a and b) having different values for tc, a horizontal line will intersect both curves at a point where they both have the same value of tc/H^2 so $t_a c_a / t_b c_b = H_a^2 / H_b^2$.

Whether or not the simple diffusion model continues to be used in the future, the principle of morphologic dating is valid; hillslopes do go through a consistent change in morphology as they degrade with time. Future research should concentrate on examining the simple diffusion model "from the ground up" starting with a very careful experimental study of the functional relationship between debris flux and climate, gradient, and material. If a new model is necessary, it should have a firm theoretical and experimental basis. The effect of scarp offset and underlying material on the repose angle of the debris apron should also be examined in detail.

ACKNOWLEDGMENTS

The study of the Jenny Lake Junction site was funded by U.S. Geological Survey Contract Number 14-08-0001-21960. Jim Beaujon is thanked for his capable assistance in the field and for preparing figure 1. I have benefited from discussions with Joe Andrews, Tom Hanks, Larry Mayer, and Bob Wallace. I am particularly indebted to Ken Pierce and John Good for their help and advice with the fieldwork and for their subsequent suggestions and observations.

REFERENCES CITED

Andrews, D.J., and Hanks, T.C., 1985, Scarp degraded by linear diffusion--Inverse solution: Journal of Geophysical Research, v. 90, p. 10193-10208.

Bucknam, R.C., and Anderson, R.E, 1979, Estimation of fault-scarp ages from a scarp-height-slope-angle relationship: Geology, v. 7, p. 11-14.

Carson, M.A., 1977, Angle of repose, angles of shearing resistance and angles of talus slopes: Earth Surface Processes, v. 2, p. 363-380.

Gilbert, G.K., 1877, Geology of the Henry Mountains: U.S. Geographical and Geological Survey of the Rocky Mountain Region, 160 p.

Nash, D.B, 1980, Morphologic dating of degraded normal fault scarps: Journal of Geology, v. 88, p. 353-360.

Nash, D.B., 1984, Morphologic dating of fluvial terraces scarps and fault scarps near West Yellowstone, Montana: Geological Society of America Bulletin, v. 95, p. 1413-1424.

Pierce, K.L., and Colman, S.M., 1986, Effect of height and orientation (microclimate) on geomorphic degradation rates and processes, late-glacial terrace scarps in central Idaho: Geological Society of America Bulletin, v. 97, 869-885.

Pierce, K.L., and Good, J.D., 1986, Quaternary Geologic Setting of Archaeological Sites, Jackson Lake, Wyoming--A Preliminary Report Concerned Mostly with the Lawrence Site: Unpublished preliminary report for U.S. Bureau of Reclamation

Schumm, S.A., 1967, Rates of surficial creep on hillslopes in western Colorado: Science, v. 155, p. 560-561.

FAR-FIELD SLOPES AND THE NATURE OF GENERAL DIFFUSION MODELS OF SCARPLIKE LANDFORMS IN WEAKLY CONSOLIDATED TERRAINS

by

Thomas C. Hanks and D. J. Andrews
U.S. Geological Survey
Menlo Park, CA 94025

ABSTRACT

The principal conclusion of this paper is that the far-field slope has a first order effect on model age determinations of scarplike landforms in weakly consolidated terrains. Observationally this can be demonstrated in two ways, using the Bonneville and Lahontan shoreline scarps as separate and combined data sets. Use of the reduced scarp slope, $\tan\theta_s - b$, where θ_s is the maximum scarp angle and b is the far-field or fan slope, instead of $\tan\theta_s$ alone as the measure of scarp slope (i) measurably reduces separation between the two data sets induced by different average fan slopes for the two data sets and (ii) significantly reduces scatter in the slope-offset plot for both the separate and combined data sets. Theoretically, the argument can be put even more strongly, at least within the range of linear diffusion and nonlinear diffusion models we consider here together with a mathematical transformation of the empirical approach of Bucknam and Anderson (1979): when one correctly takes into account the far-field slope, one will basically get the same age determination no matter which of these models one uses; conversely, without accounting properly for the effect of far-field slope, one is virtually guaranteed to get an erroneous age determination, no matter which model is used.

INTRODUCTION

Quantitative analysis of the detailed morphology of late Quaternary wave-cut and faulting-controlled landforms is a young but vigorous field of study at the present time, appealing to several geomorphological, geological, and geophysical interests, and the accumulating evidence for nonlinear material transport down the scarp face presents some interesting problems in applied mathematics as well. Moreover, such studies have attracted much attention from a large community of scientists and engineers interested in the cause and effect of earthquakes, given the potential such studies hold for easy dating of earthquakes occurring before the short instrumental and historical records.

Observationally, this science has its origins in Wallace (1977), who noted that fault scarps standing at a steeper slope must imply a younger age, all other factors (of which, in general, there are many) being equal. Bucknam and Anderson (1979) formalized this notion with scarp-slope angle (θ_s)/scarp height ($2H$) plots. (Figure 1 graphically defines the morphologic parameters of interest to this study, and table 1 defines these and others in words.) In particular, they showed that the Drum Mountains fault scarps stood at greater θ_s at the same $2H$ than did nearby shoreline scarps of ancient Lake Bonneville. Thus, the fault scarps were younger than the shoreline scarps, which was known from separate

TABLE 1.—Definitions of Mathematical Symbols

a	=	half of the surface offset $2a$ (fig. 1)
b	=	far-field or fan slope
H	=	half of scarp height $2H$ (fig. 1)
t	=	time, or age before present in kiloanni (ka)
$u(x,t)$	=	relative elevation as function of one spatial dimension x and t
α	=	tangent of the angle of repose
κ	=	mass diffusivity, m^2/ka
θ_f	=	far-field or fan-slope angle (fig. 1), $\theta_f = \tan^{-1} b$
θ_s	=	scarp-slope angle (fig. 1), $\theta_s = \tan^{-1} (\partial u/\partial x\|_{x=0})$

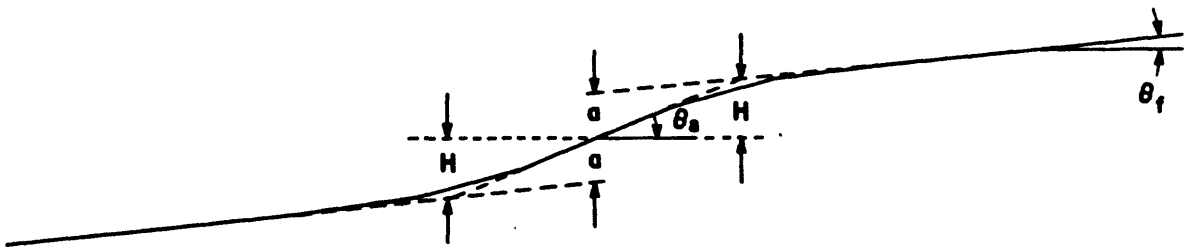

FIGURE 1.—Geometry of a fault or shoreline scarp, mostly after Bucknam and Anderson (1979). See also table 1 for definitions of these and other terms used in the text.

geologic constraints, but it was difficult to say by how much in this strictly empirical approach.

The application of linear diffusion-equation mathematics has provided absolute ages for many late Quaternary scarplike landforms. Briefly, this approach returns the product κt from the scarp profiles or morphologic parameterizations of them. The trick is to know separately something about κ, and this information generally comes from well-dated high stands of sea level or glacial lakes.

Because the ages of the shoreline scarps of Lakes Bonneville and Lahontan at the last glacial highstands are well known, because these features are widespread through the Basin and Range province, and because this province is a rich hunting ground for students of late Quaternary fault scarps in weakly consolidated terrains, the determination and application of the Bonneville and Lahontan κ's have figured prominently in those studies of late Quaternary, weakly consolidated landform modification for which diffusion-equation mathematics supply the model calculations (for example, Nash, 1980; Hanks and others, 1984; Hecker, 1985; Hanks and Wallace, 1985; Zhang and others, 1986; Hanks and Schwartz, 1987; and Andrews and Bucknam, 1987). It is worthwhile remembering, however, that only some average value of κt is rendered from this approach, and κ may be a strong—and nonlinear—function of time, climate, and, worse still, the morphology itself.

These studies, together with many others employing the strictly empirical approach of Bucknam and Anderson (1979), for example, Machette (1982), Mayer (1982, 1984), Pierce and Colman (1986), and Pearthree and Calvo (1987), have left three important issues as yet unresolved, and these provide the central themes of this study. First, what role does the far-field slope really play in these processes, and what effect does it have on model ages? In the Bucknam and Anderson (1979) approach, for example, scarp-slope angle is considered without regard to the angle or slope of the surface on which the scarp sits, but the mathematics of linear diffusion, at least, tell us that it is not $\tan\theta_s$ that counts in age determinations but the reduced scarp slope $\tan\theta_s - b$. Second, there is enough evidence now to suggest the reality of nonlinear transport laws and thus the importance of nonlinear diffusion equations (Hanks and others, 1984; Pierce and Colman, 1986; Andrews and Bucknam, 1987). How do we formulate this nonlinearity and what effect will it have on model ages? Finally, very little has been said about the physical processes by which mass might "diffuse" down the face of some scarplike landform, and we find here a strong coincidence between an empirically derived nonlinear transport law and a transport law based on frictional sliding of particles when excited by kinetic energy incoming from above.

As many of our readers know, these are matters the two of us have argued about for more than a year, often sharply and as recently as the meeting from which these proceedings derive. This paper represents, among other things, our own meeting of minds on these issues in July of 1987.

Scarp slopes can be expressed in terms of $2a/L$, so scarp slopes or scarp-slope angles can be written in terms of the single variable $2a/\sqrt{\kappa t}$ or, more conveniently, $(2a)^2/\kappa t$.

$$\theta_s = g\left(\frac{(2a)^2}{\kappa t}\right) . \tag{7}$$

To illustrate the use of equation (7), we plot in figure 2 49 pairs of θ_s and $2a$ data for the Bonneville shoreline scarps, in the semilogarithmic plot favored by Bucknam and Anderson (1979). This set of data includes only the east- and west-facing profiles, and we also use here the height measure $2a$ instead of $2H$ as used in Bucknam and Anderson (1979). The relation between $2a$ and $2H$ is (Hanks and others, 1984)

$$2a = 2H\left(1 - \frac{\tan\theta_f}{\tan\theta_s}\right) . \tag{8}$$

Equation (8) says $2a \simeq 2H$, so long as θ_f is small compared to θ_s. Especially for the smaller scarps with smaller scarp-slope angles, this is not always the case.

The data of figure 2 are well fit by the straight line

$$\theta_s = (16.6^\circ \pm 1.0^\circ)\log(2a) + (9.5^\circ \pm 0.6^\circ) , \tag{9}$$

the result of a regression analysis of θ_s in degrees on $2a$ in meters. θ_s, obviously, cannot be larger than the initial slope angle, perhaps 30° to 35°, nor smaller than the fan-slope angle θ_f, typically 5° for the Bonneville shoreline scarps.

The form of equation (7) consistent with equation (9) is

$$\theta_s = A\log\left(\frac{(2a)^2}{\kappa t}\right) + C , \tag{10}$$

where we now assume, at least implicitly, that some (but unknown) sort of slope-dependent diffusive mechanisms have something to do with the nature and form of figure 2.

Expanding equation (10) into

$$\theta_s = 2A\log 2a - A\log t + B \tag{11}$$

allows us to bury κ in the constant B. Finally, differentiating equation (11) with respect to t and taking $2A = 16.6^\circ$ from equation (9),

$$d\theta_s = -Ad(\log t) = -0.43Ad(lnt) = -3.6\,dt/t \tag{12a}$$

or

GENERAL DIFFUSION EQUATIONS AND DIMENSIONLESS FORMS

With respect to one spatial dimension x, we suppose that mass goes downhill at a rate $\dot{M}$ given by a general function of slope $\mathcal{S} = \partial u/\partial x$

$$\dot{M} = -\mathbf{K} f(\mathcal{S}) \, . \tag{1}$$

In equation (1), $\mathbf{K}$ is a constant of proportionality that allows $f(\mathcal{S})$ to be a dimensionless function of the dimensionless variable slope. We require $f(\mathcal{S})$ to be positive for positive $\mathcal{S}$ and negative for negative $\mathcal{S}$ so that the leading minus sign ensures that the net flux of mass is downhill. This suggests that $f(\mathcal{S})$ should be an odd function of slope, to avoid the awkwardness of absolute values, and in a later section we assume one to exist in the form of a Taylor series expansion

$$f(\mathcal{S}) = a_1 \mathcal{S} + a_3 \mathcal{S}^3 + a_5 \mathcal{S}^5 + \ldots \tag{2}$$

and explore this form retaining the linear and cubic terms.

In differential form, conservation of mass is written

$$\rho \frac{\partial u}{\partial t} dx = \frac{-\partial \dot{M}}{\partial x} dx \, , \tag{3}$$

and equations (1) and (3) can be combined to write

$$\frac{\partial u}{\partial t} = \kappa \frac{\partial}{\partial x} \left[f\left(\frac{\partial u}{\partial x} \right) \right] \tag{4}$$

where $\kappa = \mathbf{K}/\rho$ has the units of diffusivity, m^2/ka being those for this line of work.

Solutions $u(x,t)$ of equation (4) can be related to dimensionless solutions $u'(x',t')$ with unit offset and $\kappa' = 1$ by the scaling

$$u = Lu', \quad x = Lx', \quad t = Tt' \, , \tag{5}$$

provided that all initial conditions (the initial profiles) are geometrically similar (that is, they possess the same angle of repose and far-field slope b) and that T is related to L by

$$T = L^2/\kappa \, . \tag{6}$$

This scaling is invariant for any choice of $f(\mathcal{S})$ consistent with equation (1), again because $f(\mathcal{S})$ is a dimensionless function of a dimensionless variable. This would not be the case, say, had we expressed the transport law in terms of $2a$ or $2H$.

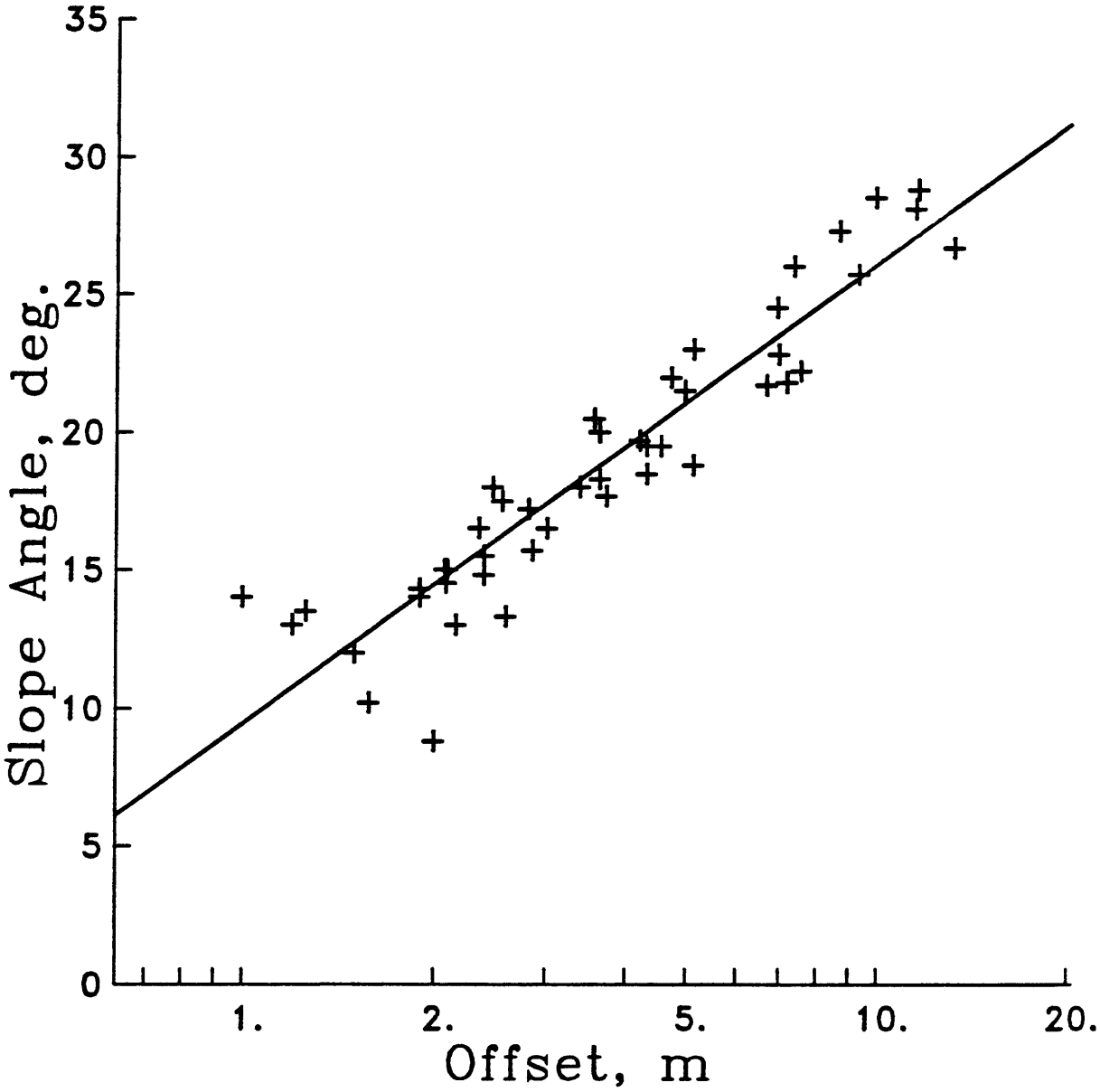

FIGURE 2.—θ_s *vs.* log $(2a)$ for 49 Bonneville shoreline scarps, a subset of the 61 available data (fig. 5) that includes only east- and west-facing scarps. The straight line is a least-squares fit to the data, the algebraic relation being equation (9).

$$\frac{dt}{t} = -0.28\, d\theta_s \ , \tag{12b}$$

which allows us to estimate the time rate of change of scarp-slope angle without knowing anything about κ or anything about $f(\mathcal{S})$ other than what we choose to infer from the data themselves, in the case here equation (9). In words, equation (12b) says that a 1° change in θ_s from some present value corresponds to a 28 percent change in age from its present value.

In fact, this is a curious result, that $td\theta_s/dt$ is constant, not depending on scarp slope. It seems intuitively obvious that the steeper slopes will change their shape more rapidly with time, at any time. Remembering, however, that the simple scaling arguments that have led us to equation (12b) depend on the assumption that all profiles began with geometrically similar shapes, it is time to explore in more detail the effect of variable b, both in the data themselves and on the model age determinations.

THE EFFECT OF FAR-FIELD SLOPE

In their application to fault-scarp degradation in weakly consolidated terrains, the mathematics of linear diffusion are precise about the effect of far-field slope. Briefly, one is motivated to work in terms of the reduced scarp slope, $\tan\theta_s - b$, rather than scarp slope, $\tan\theta_s$ ($\simeq \theta_s$, in radians), because of the following forms

$$\tan\theta_s - b = \frac{a}{\sqrt{\pi\kappa t}} \tag{13}$$

and

$$\tan\theta_s - b = (\alpha - b)\, erf\left[\frac{a/(\alpha - b)}{2\sqrt{\kappa t}}\right] \ . \tag{14}$$

Equations (13) and (14) are solutions to the linear, homogeneous diffusion equation with constant coefficient κ (Hanks and others, 1984), where $erf(v)$ is the error function of argument v; equation (13) supposes the scarp initially stood vertically, and equation (14) is the solution for an initial morphology at the angle of repose. Either of these solutions tells us that it is $\tan\theta_s - b$ that counts in the age determinations, not $\tan\theta_s$ alone.

To explore this matter of age dependence on θ_f, we invert equations (13) and (14) in terms of the dimensionless age quantity $t' \equiv \kappa t/(2a)^2$,

$$t' = \left[2\sqrt{\pi}\,(\tan\theta_s - b)\right]^{-2} \tag{13'}$$

and

$$t' = \left[4\,(\alpha - b)\, erf^{-1}\left(\frac{\tan\theta_s - b}{\alpha - b}\right)\right]^{-2} \ , \tag{14'}$$

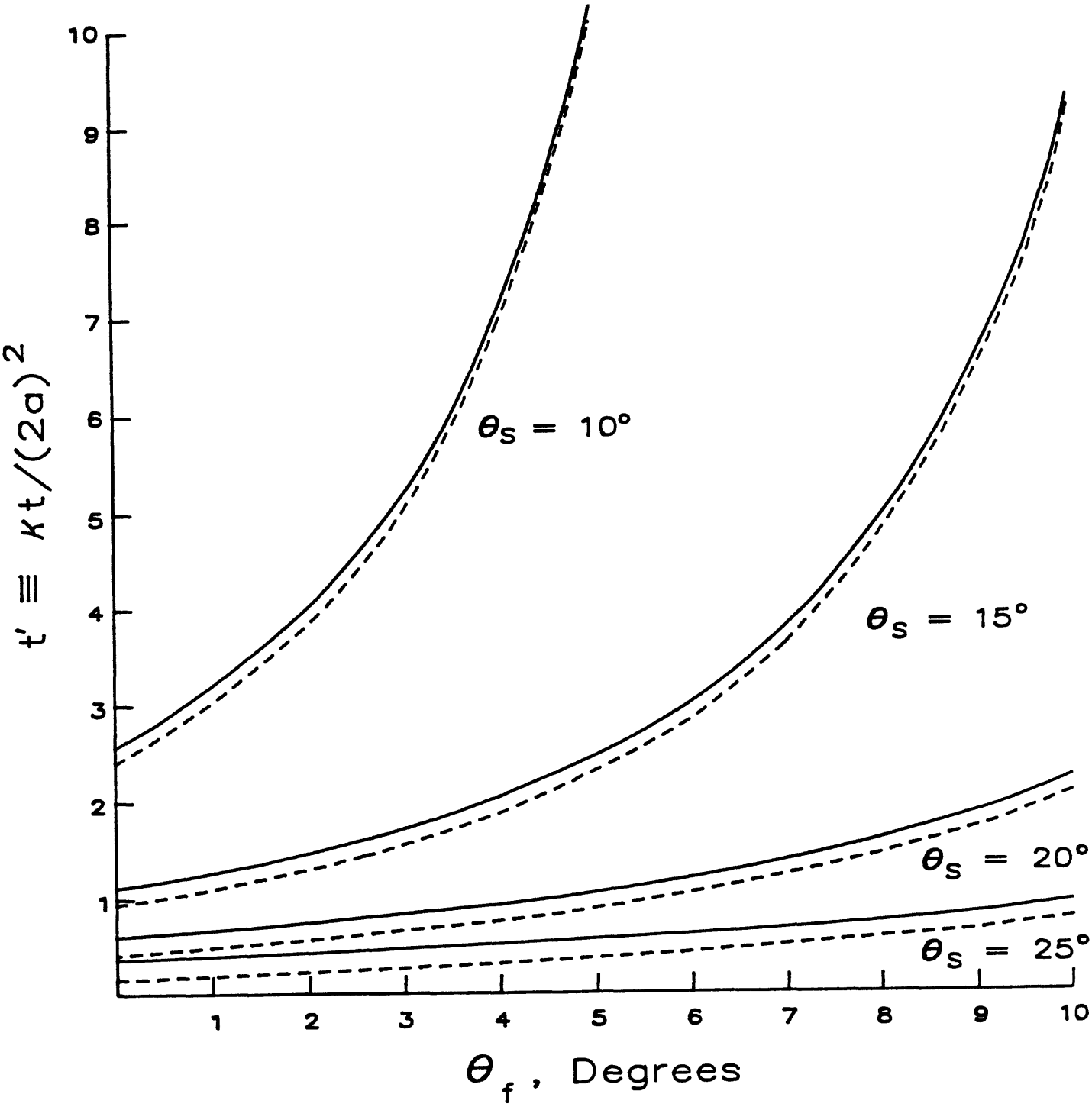

FIGURE 3.—Evaluations of equation (13′) (solid lines) and equation (14′) (dashed lines), t' as a function of $\theta_f (= \tan^{-1} b)$ for four choices of θ_s. See text for discussion.

and plot t' as a function of $\theta_f = \tan^{-1} b$ in figure 3, for four choices of θ_s and a fixed value of $\alpha - b = 0.5$.

In figure 3, it is plain that for any combination of θ_s and θ_f such that $\theta_s - \theta_f \leq 10°$, t' depends strongly on θ_f, and this dependence becomes singular as $\theta_s \rightarrow \theta_f$. It can also be seen here that initial morphology makes little difference in terms of t' determinations except at small $t'(\leq 1)$, corresponding, roughly, to $\theta_s - \theta_f \geq 15°$. This is because the less steep scarps have lost memory of their initial shape (see Hanks and Schwartz, 1987, fig. 5, but note t' as defined there is $\kappa t^2/a^2$, whereas we use $t' = \kappa t/4a^2$ here).

Figure 4 is the θ_f distribution for all 61 Bonneville profiles, reproduced from the inset of figure 11 of Hanks and others (1984). The median value is between 5° and 6°, with a reasonable expectation of finding any value between 2° and 9°. If linear diffusion has anything to do with the present form of the Bonneville shoreline scarps, it is clear from figure 3 that not correcting for the average or median θ_f will introduce a substantial age bias, and not correcting for individual values will introduce a substantial age scatter since the bulk of the Bonneville θ_s values are less than 20° (fig. 5*A*).

Within the confines of the linear-diffusion model, then, we can say that the effect of far-field slope on the resulting age determinations is, in general, important and often times dramatic. This is not to say, however, that we have proved that the linear-diffusion model is the correct way to approach this problem, even to first order. In fact, we will never be able to prove such a case, but there are ways to explore whether or not we are going in the right direction.

At the present time, there are 61 $(\theta_s, 2a, b)$ triples available for Lake Bonneville shoreline scarps (Bucknam and Anderson, 1979; Hanks and others, 1984) and 32 more for Lake Lahontan (Hanks and Wallace, 1985; Hecker, 1985). The Bonneville and Lahontan shoreline scarps are of very similar age, they have experienced very similar climates since their formation in the latest-Pleistocene, and they can be found to cut very similar, weakly consolidated, alluvial fans that abound in the Basin and Range. Thus the Bonneville and Lahontan shoreline scarps should look a lot alike, and they do; indeed, Hanks and Wallace (1985) found them to be indistinguishable from one another, if the effects of variable $2a$ and b are accounted for according to the dictates of linear diffusion.

With respect to the separate and combined $(\theta_s, 2a, b)$ data sets for Bonneville and Lahontan, we can ask two questions. Can we reduce if not eliminate a separation of the two populations in the $\tan\theta_s - 2a$ space that might (and does) exist because of different average θ_f's ($\simeq$5 1/2° for Bonneville, 3 1/2° for Lahontan) by using $\tan\theta_s - b$ as the dependent variable? Secondly, can we reduce the scatter in either or both populations by using $\tan\theta_s - b$ instead of $\tan\theta_s$ on the slope-offset plot? If the answer to *both* of these questions is yes, it would seem that linear diffusion, at least as a first approximation, is indeed a consistent way of proceeding.

In figure 5, then, we show these two representations of these two data sets, $\tan\theta_s$ *vs.* $2a$ in figure 5*A* and $\tan\theta_s - b$ *vs.* $2a$ in figure 5*B*; the solid symbols are for Bonneville,

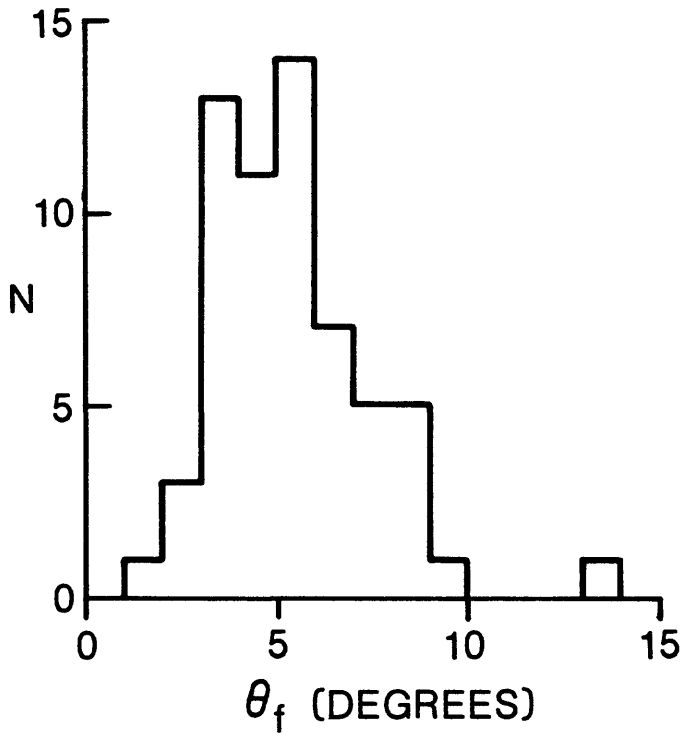

FIGURE 4.—Distribution of the Bonneville shoreline scarps with respect to θ_f. N is counted according to 1° bins of θ_f.

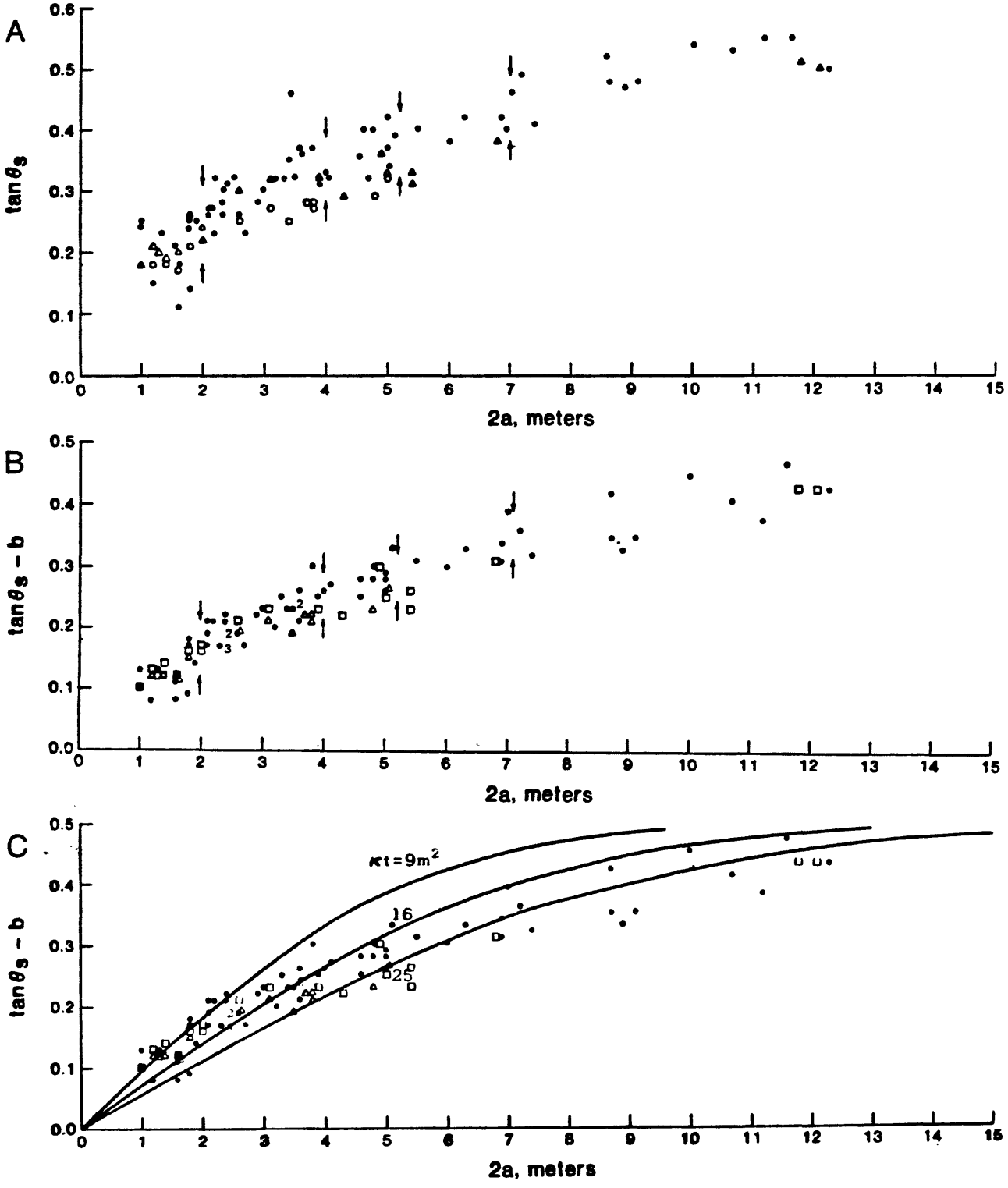

FIGURE 5.—(*A*), $\tan\theta_s$ *vs.* $2a$ data for Bonneville (solid circles) and Lahontan (open symbols) shoreline scarps; (*B*), the reduced scarp slope representation, $\tan\theta_s - b$ *vs.* $2a$, for the same data; (*C*), evaluations of equation (14) for $(\alpha - b) = 0.5$ and the indicated values of κt superimposed on the reduced scarp slope plot (*B*).

open ones for Lahontan. In figure 5*A*, there is in fact a separation of the Bonneville from the Lahontan data that largely disappears in figure 5*B*, although a subset of 11 Lahontan points in the range 3 1/2 $\leq 2a \leq$ 5 1/2 m are uniformly low in the latter plot. Moreover, it is easily discernible that the "full-range" scatter in $\tan\theta_s - b$ (fig. 5*B*) is less than the scatter in $\tan\theta_s$ (fig. 5*A*). The distance between the facing vertical arrows at $2a$ = const are meant to indicate this, being 5° to 6° in the $\tan\theta_s$ *vs.* $2a$ plot and 4° in the $(\tan\theta_s - b)$ *vs.* $2a$ plot. This 4° of "full-range" scatter in the $(\tan\theta_s - b)$ *vs.* $2a$ plot corresponds, approximately, to a standard deviation of about 1°, which includes both measurement error and "real-Earth" variations. That the form of these shoreline scarps, in the eyes of at least six different beholders, should be this well-behaved is nothing short of astonishing. Finally, figure 5*B* also suggests that $(\tan\theta_s - b)$ goes smoothly to zero as $2a \rightarrow 0$; this common-sense constraint is an important one, insofar as it allows us to consider the origin as a real data point.

Figure 5 also indicates, however, that linear diffusion is not the whole story, insofar as the present morphology of these scarps is concerned. The model calculations in figure 5*C*, where the data come as a replot of figure 5*B*, are based on an evaluation of equation (14) for $(\alpha - b) = 0.5$ and three choices of κt, as indicated. Clearly, κt (which is to say κ) increases with increasing $(\tan\theta_s - b)$ and/or $2a$, sure evidence of nonlinear diffusive processes.

A NONLINEAR DIFFUSION MODEL

To deal with the nonlinear behavior apparent in figure 5*C*, but in the context that linear diffusion is to be the first-order approximation, we return to equation (4)

$$\frac{\partial u}{\partial t} = \kappa \frac{\partial}{\partial x}\left[f\left(\frac{\partial u}{\partial x}\right)\right] \tag{4}$$

and take $\kappa f(\mathcal{S})$, $\mathcal{S} = \partial u/\partial x$, to be of the form

$$\kappa f(\mathcal{S}) = \kappa(\mathcal{S} + \frac{a_3}{a_1}\mathcal{S}^3 + \dots)\,. \tag{2}$$

In effect, we are assuming the transport law to be a dimensionless, odd function of slope alone, one that we can represent as a Taylor series expansion about $\mathcal{S} = 0$. Dimension is provided by the leading constant κ, we choose $f(\mathcal{S})$ to a dimensionless function of a dimensionless variable to preserve scaling invariance, we choose $f(\mathcal{S})$ to be an odd function of slope to eliminate sign problems, and we retain only the first two terms of the expansion. Then equation (4) becomes

$$\frac{\partial u}{\partial t} = \kappa \frac{\partial^2 u}{\partial x^2} + \kappa \frac{a_3}{a_1}\frac{\partial}{\partial x}\left(\frac{\partial u}{\partial x}\right)^3 \tag{15}$$

or

$$\frac{\partial u}{\partial t} = \left[\kappa + 3\kappa_3\left(\frac{\partial u}{\partial x}\right)^2\right]\frac{\partial^2 u}{\partial x^2} \tag{15'}$$

where $\kappa_3 = \kappa a_3/a_1$. For small slopes, equation (15′) reduces to the homogeneous diffusion equation with constant coefficients, that is, linear diffusion.

Our first choice for the transport law (eq. 2) comes from figure 5*C*, where the quantity κt (where $t = 14.5$ ka for the Bonneville data) can be seen to increase from about 10 m^2 at small slopes to ~25 m^2 at slopes near 0.5, and a guess that $a_3/a_1 = 5$. Then

$$\frac{\kappa f(\mathcal{S})}{\mathcal{S}} = 0.69\,(1 + 5\,\mathcal{S}^2)\,. \tag{16}$$

This form is used in equation (4) which is then solved with the finite-difference techniques described in Andrews and Hanks (1985). From these calculations, we obtain θ_s *vs.* $2a$ for the 49 Bonneville data of figure 2 as shown by the curved line in figure 6*A*, where the data and the straight line (eq. 9) are reproduced from figure 2. A least-squares fit of these data to the form (eq. 16), where the leading constant is adjustable but the ratio 5 is held fixed yields the curved line in figure 6*B* and the result

$$\frac{\kappa f(\mathcal{S})}{\mathcal{S}} = 0.48\,(1 + 5\,\mathcal{S}^2)\,. \tag{17}$$

Finally, an inversion of all 49 profiles to this form using, in addition, the inversion techniques described in Andrews and Hanks (1985), again with the ratio 5 held fixed, yields the curved line in figure 6*C* and the result

$$\frac{\kappa f(\mathcal{S})}{\mathcal{S}} = 0.46\,(1 + 5\,\mathcal{S}^2)\,, \tag{18}$$

in any meaningful way the same as equation (17).

The term in the brackets of equation (15′) allows us to estimate the effective (but now slope-dependent) κ or product κt. With $\kappa = 0.46$ m^2/ka and $a_3/a_1 = 5$ from equation (18) and $t = 14.5$ ka, we obtain $\kappa t = 6.7$ m^2 at $\mathcal{S} = 0$, 16 m^2 at $\mathcal{S} = 0.3$, and 32 m^2 at $\mathcal{S} = 0.5$. These are surprisingly close to the three choices of κt used for model calculations in figure 5*C*, given their appropriate ranges of validity. In detail, this coincidence is fortuitous, we think, because while we believe the linear term to be well-determined the cubic coefficient (a_3/a_1) is much less so. We shall take up sensitivity studies of this parameter at a later date.

Andrews and Bucknam (1987) have described a frictional-sliding transport model for which the function $\kappa f(\mathcal{S})$ is written

$$\kappa f(\mathcal{S}) = \frac{\kappa \mathcal{S}}{1 - (\mathcal{S}/f)^2}\,, \tag{19}$$

where f is the coefficient of friction. The basic physics here involve exciting a particle of weight mg with kinetic energy E. If projected upslope, this particle will travel a

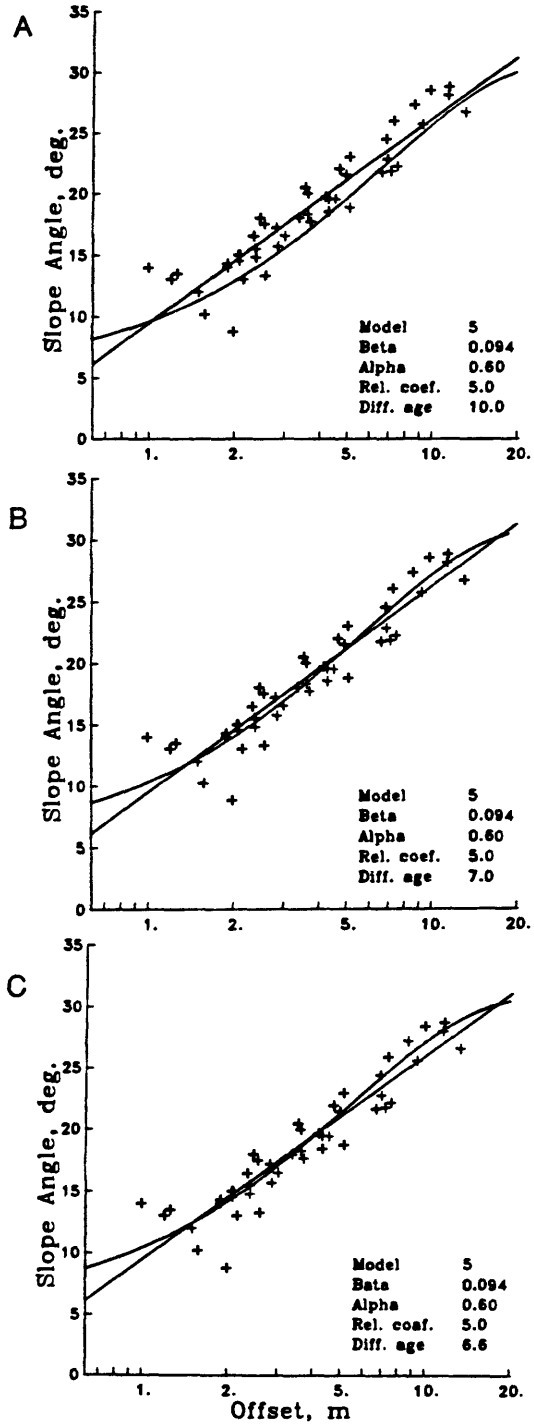

FIGURE 6.—Nonlinear diffusion models compared to the Bonneville data and straight line fit of figure 2.

A. $\kappa f(\mathcal{S})/\mathcal{S} = 0.69\ (1 + 5\mathcal{S}^2)$
B. $\kappa f(\mathcal{S})/\mathcal{S} = 0.48\ (1 + 5\mathcal{S}^2)$
C. $\kappa f(\mathcal{S})/\mathcal{S} = 0.46\ (1 + 5\mathcal{S}^2)$

distance $(E/mg)/(f\cos\theta + \sin\theta)$, but if projected downslope it will travel the greater distance $(E/mg)/(f\cos\theta - \sin\theta)$, where θ is the slope angle. The details are worked out in Andrews and Bucknam (1987), but of interest here is the very close coincidence between the functions $\kappa f(\mathcal{S})$ as expressed in equation (18), the empirical guess, and equation (19) with $\kappa = 0.61$ m^2/ka and $f = 0.75$. These forms are shown in figure 7 together with the linear model specified by $\kappa f(\mathcal{S}) = 1.1\,\mathcal{S}$ with 1.1 in units of m^2/ka, the preferred Bonneville κ of Hanks and others, 1984. The physics implicit in equation (19) are so simple as to defy any real significance to the coincidence between equations (18) and (19). Nevertheless, it may well be true that within this coincidence is the embryo of a physical understanding of the actual processes that shape and reshape these landforms.

SUMMARY AND CONCLUSIONS

The basic point of this paper is shown graphically in figure 8: when one properly takes into account the far-field slope one will basically get the right age determination no matter what model one uses (of the three considered here), but without accounting properly for θ_f one is virtually guaranteed to get an erroneous age estimate no matter what model is used. At least qualitatively, one could (and we did) guess that θ_f does have a first-order effect on age determination, but figure 8 emphasizes this so definitely and dramatically to surprise us both.

Figure 8, in essence, is a variation on the theme of figure 3, but here we use θ_s on the abscissa and θ_f as a parameter. Moreover, the ordinate in figure 8 is $t/(2a)^2$, not $\kappa t/(2a)^2$ as in figure 3, because somewhat different κ's are used or are implicit in the models expressed in figure 8. The first of these models is the finite-slope linear-diffusion model (solid curves), basically an evaluation of equation (14′) with $\kappa = 1.1$ m^2/ka and $\alpha = 0.6$ to obtain $t/(2a)^2$ as a function of θ_s, for three choices of θ_f: 0°, 5°, and 10°. The models represented by the long-dashed lines take the transport law of equation (18) and the computational apparatus of Andrews and Hanks (1985) to calculate $t/(2a)^2$ as a function of θ_s, for the same three choices of θ_f. Finally, the short-dashed line is derived from the semilogarithmic fit of θ_s to $2a$ for the Bonneville data (eq. 9 and fig. 2). We assume this is valid at the average Bonneville $\theta_f \simeq 5°$, and this seems to be the case to the extent it is much the same as the linear and the linear-plus-cubic diffusion models for $\theta_f = 5°$.

All of these calculations, of course, are fundamentally keyed to the Bonneville data (and to a lesser extent the Lahontan data) through parameter selection that, in the end, has the models "fit" the data; it is important, then to recognize where these data lie in the space of figure 8. With respect to θ_s, figure 2 and figure 5*A* reveal that θ_s lies almost exclusively between 10° and 30°. In fact, $12° \leq \theta_s \leq 25°$ is the range for most of the observations. With respect to $t/(2a)^2$ and $t = 14.5$ ka for the Bonneville data, all scarps with $2a \geq 2$ m will sit at $t/(2a)^2 \leq 3.6$ ka/m^2 in figure 8; this again is most of the data, but a small number of $1 \leq 2a \leq 2$ m points will be at larger $t/(2a)^2$ in figure 8, at $10° \leq \theta_s \leq 15°$.

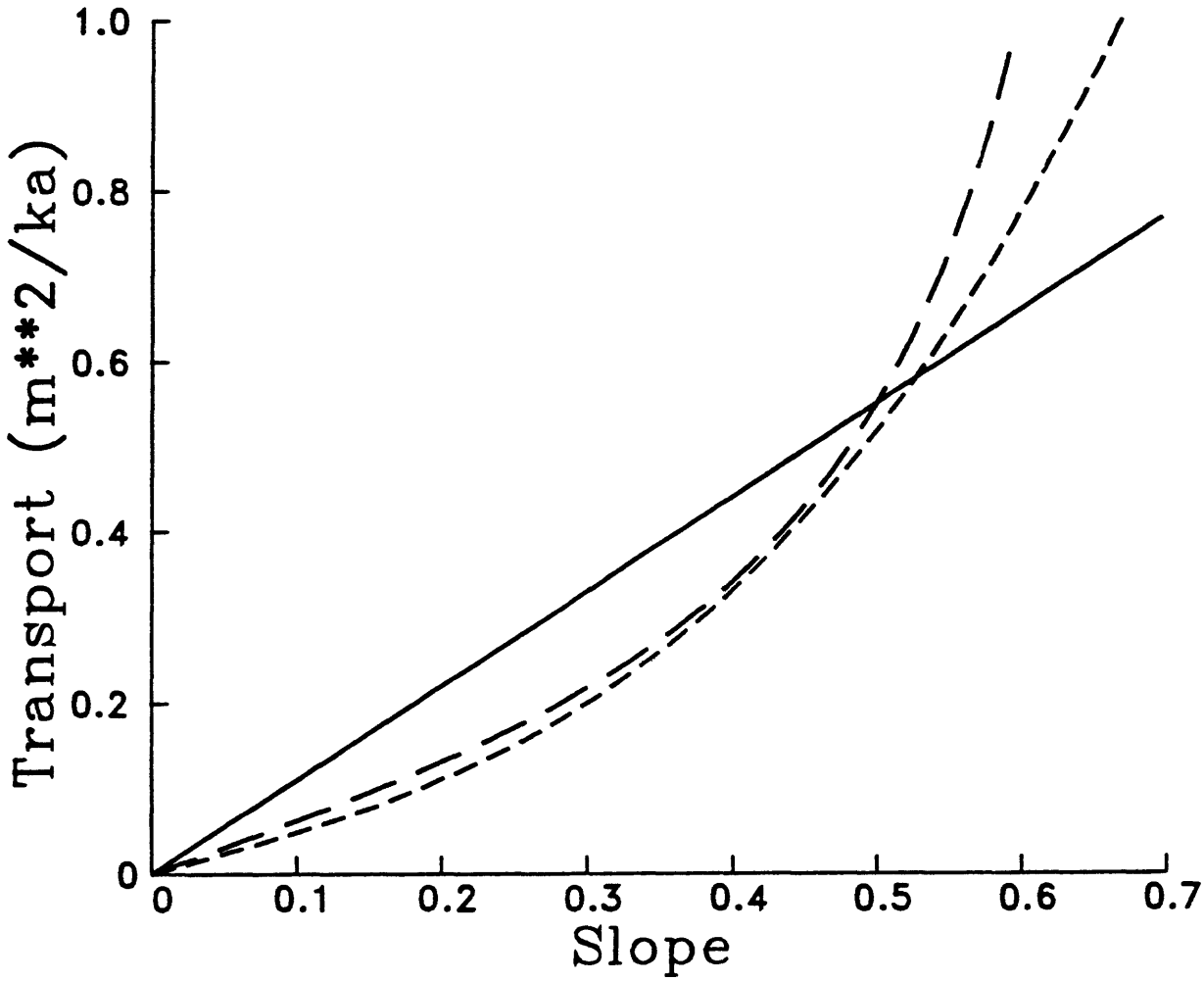

FIGURE 7.—Three transport laws, $\kappa f(\mathcal{S})$. Solid curve: linear transport, $\kappa f(\mathcal{S}) = \kappa \mathcal{S}$, $\kappa = 1.1\text{m}^2/\text{ka}$. Short-dashed curve: linear-plus-cubic transport, $\kappa f(\mathcal{S}) = \kappa(1 + 5\mathcal{S}^2)\mathcal{S}$, $\kappa = 0.46$ m^2/ka (eq. 18). Long-dashed curve: frictional sliding transport, $\kappa f(\mathcal{S}) = \kappa \mathcal{S}/(1 - (\mathcal{S}/0.75)^2)$, $\kappa = 0.61$ m^2/ka (eq. 19).

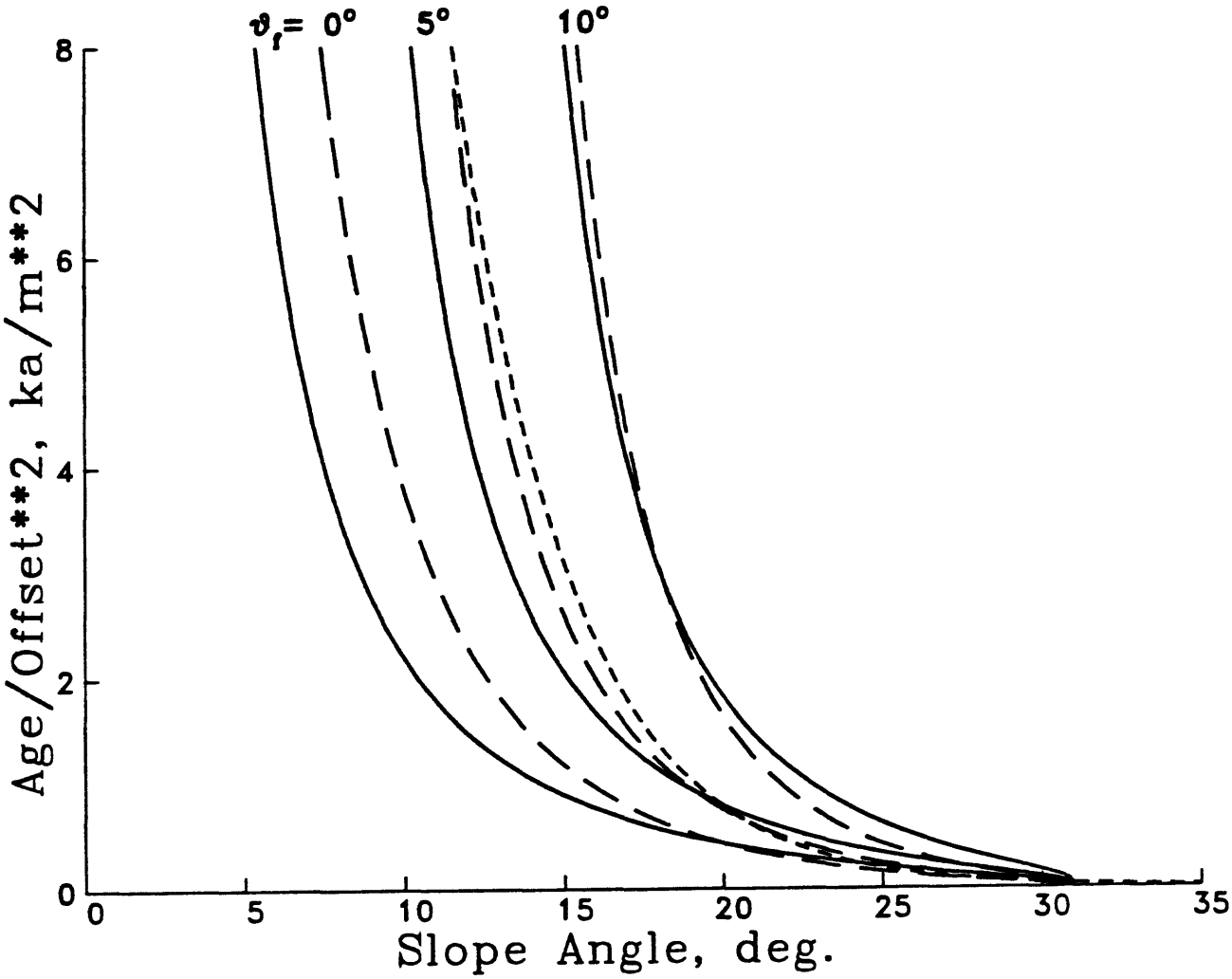

FIGURE 8.—Age (t) divided by square of offset $(2a)^2$ plotted against scarp-slope angle (θ_s). Solid curves: linear model with $\kappa = 1.1$ m^2/ka. Long-dashed curves: linear-plus-cubic model with $\kappa = 0.46$ m^2/ka. Each of these models is evaluated for three values of θ_f: 0°, 5°, and 10°. Short-dashed curve: equation (9), the best fitting $\theta_s - \log(2a)$ straight line to the Bonneville data in figure 2 is transformed to this space with $t = 14.5$ ka, the age of the Bonneville shoreline scarps.

With these data constraints in mind, $12° \leq \theta_s \leq 25°$ and $t/(2a)^2 \leq 3.6$ ka/m^2 as the general rule, one can see that differences in the model predictions are fairly nominal, 50 percent or less except when $t/(2a)^2$ gets very small, *provided* that one has specified the correct θ_f. Without knowing θ_f, however, figure 8 says that in general it is a hopeless exercise to get any age control at all. Take, for example, $\theta_s = 15°$, a typical Bonneville slope angle. If $\theta_f = 0°$, $t/(2a)^2 \simeq 1$ ka/m^2 for either the linear or the linear-plus-cubic models; if $\theta_f = 5°$, $t/(2a)^2 \simeq 2.5$ ka/m^2 for either of these two models or for the semilogarithmic fit; if, however, θ_f is 10°, $t/(2a)^2$ goes through the roof, being greater than 10 ka/m^2 for either the linear or linear-plus-cubic models. On the other hand, when one knows what θ_f to use, $t/(2a)^2$ differences due to different models are small to trivial in these ranges of θ_s and $t/(2a)^2$.

Finally, it is worth noting that the constraints on θ_s and $t/(2a)^2$ for the Bonneville data will, in general, be much the same for all latest-Pleistocene and Holocene scarps in weakly consolidated terrains. If, for example, fan slopes are typically 3° to 5° and if one needs a scarp with angle 3° to 5° greater than this to even know it's there (so that it casts a shadow on a low sun-angle photograph, say), it may be anticipated that one would hardly ever collect data at $\theta_s \leq 5°$ and would not collect much at $\theta_s \leq 10°$. This is typical of all the data sets of which we are aware. For dating purposes, what happens at $\theta_s \leq 10°$ would thus seem to be an irrelevant issue, but it is important to recognize also that control on the transport law at $\theta_s \leq 10°$ is virtually nonexistent because of this same lack of data. At the other extreme, $\theta_s \geq 25°$, one can be virtually guaranteed that the scarp is very young ($\leq$1 ka) or is very big ($2a \geq 10$ m) or both, in any case yielding small values of $t/(2a)^2$ where all models converge irrespective of θ_f. But one should not expect to learn too much at $\theta_s \geq 25°$ and small $t/(2a)^2$ since for these conditions the basic assumptions of the diffusion-equation representation are open to question. Nevertheless, depending on the value of $2a$, one can often say with some confidence, that is model-independent, that a scarp is younger than a certain age, and this can be important information in earthquake recurrence-interval studies.

REFERENCES CITED

Andrews, D. J., and Hanks, T. C., 1985, Scarp degraded by linear diffusion: inverse solution for age: *Journal Geophysical Research*, v. 90, p. 10193–10208.

Andrews, D. J., and Bucknam, R. C., 1987, Fitting degradation of shoreline scarps by a model with nonlinear diffusion: *Journal Geophysical Research*, v. 92, in press.

Bucknam, R. C., and Anderson, R. E., 1979, Estimation of fault-scarp ages from a scarp-height–slope-angle relationship: *Geology*, v. 7, p. 11–14.

Hanks, T. C., Bucknam, R. C., Lajoie, K. R., and Wallace, R. E., 1984, Modification of wave-cut and faulting-controlled landforms: *Journal Geophysical Research*, v. 89, p. 5771–5790.

Hanks, T. C., and Schwartz, D. P., 1987, Morphologic dating of the pre-1983 fault scarp on the Lost River fault at Doublespring Pass Road, Custer County, Idaho: *Bulletin Seismological Society America*, v. 77, p. 837–846.

Hanks, T. C., and Wallace, R. E., 1985, Morphologic analysis of the Lake Lahontan shoreline and Beachfront fault scarps, Pershing County, Nevada: *Bulletin Seismological Society America*, v. 75, p. 835–846.

Hecker, S., 1985, Timing of Holocene faulting in part of a seismic belt, west-central Nevada: University of Arizona, Tucson, M.S. thesis, 42 pp.

Machette, M. N., 1982, Quaternary and Pliocene faults in the La Jencia and southern part of the Albuquerque–Belen basins, New Mexico: Evidence of fault history from fault-scarp morphology and Quaternary geology, *Field Conference Guidebook New Mexico Geological Society*, v. 33, p. 161–170.

Mayer, L., 1982, Quantitative tectonic geomorphology with applications to neotectonics of northwestern Arizona: Univ. of Arizona, Tucson, Ph.D. thesis, 213 pp.

Mayer, L., 1984, Dating Quaternary fault scarps formed in alluvium using morphologic parameters: *Quaternary Research*, v. 22, p. 300–313.

Nash, D. B., 1980, Morphologic dating of degraded normal fault scarps: *Journal Geology*, v. 88, p. 353–360.

Pearthree, P. A., and Calvo, S. S., 1987, The Santa Rita fault zone: evidence for large magnitude earthquakes with very long recurrence intervals, Basin and Range province of southeastern Arizona., *Bulletin Seismological Society America*, v. 77, p. 97–116.

Pierce, K. L., and Colman, S. M., 1986, Effect of height and orientation (microclimate) on geomorphic degradation rates and processes, late-glacial terrace scarps in central Idaho: *Geological Society America Bulletin*, v. 97, p. 869–885.

Wallace, R. E., 1977, Profiles and ages of young fault scarps, north-central Nevada, *Geological Society America Bulletin*, v. 88, p. 1267–1281.

Zhang, B., Liao, Y., Guo, S., Wallace, R. E., Bucknam, R. C., and Hanks, T. C., 1986, Fault scarps related to the 1739 earthquake and seismicity of the Yinchuan graben, Ningxia Huizu Zizhiqu, China, *Bulletin Seismological Society America*, v. 76, p. 1253–1287.

SUMMARY OF DISCUSSION SESSION: MODELING FAULT-SCARP DEGRADATION-- KNOWNS, UNKNOWNS, AND PERSPECTIVES ON THE PROBLEMS

by

Anthony J. Crone
U.S. Geological Survey
Denver, Colorado 80225

Session Chairman: R. Ernest Anderson, U.S. Geological Survey
Panel Members: D. Joseph Andrews, U.S. Geological Survey
Steven M. Colman, U.S. Geological Survey
Thomas C. Hanks, U.S. Geological Survey
Larry Mayer, Miami University
David Nash, University of Cincinnati
Kenneth L. Pierce, U.S. Geological Survey

At present, scarp morphology is of limited value as an numeric dating technique but is a useful tool for regional studies of fault scarps. Accurate numeric age estimates using scarp morphology are hampered by our poor knowledge of the specific processes and variables that affect scarp degradation. However, scarp morphology is an valuable regional reconnaissance tool that can be used to classify fault scarps into broad age categories (for example, late Holocene, early Holocene, late Pleistocene, middle Pleistocene). The morphologic data used for this age classification can be collected quickly and easily. The ability to classify the scarps in a region into broad age categories is very useful for probabilistic hazard assessments because these assessments rely on information about the spatial and temporal distribution of large earthquakes (which produce scarps) in a region.

Perhaps the single most important control on scarp degradation is the nature of the material in which the scarp is formed. Scarp-degradation models based on the diffusion equation emulate an idealized fault scarp formed in cohesionless material. The processes modeled by the diffusion equation begin to affect the scarp when the original near-vertical free face has ravelled to the angle of repose which may require a few hundred years. In reality, not all scarps are formed in the same materials and there are large morphologic variations along the strike of a single scarp. For example, the Pitaycachi scarp in northeast Sonora Mexico formed about 100 years ago and now has maximum slope angles that range from vertical to only 7-8°. This wide range in slope angles is a function of lithology, cementation, and cohesiveness (related to clay content) of the faulted materials. Attempts to quantify the effects of lithology on degradation of this scarp have been only partially successful. This example demonstrates the importance of lithologic control, and emphasizes the difficulty in isolating and compensating for this effect in scarp models.

Careful field observations are the best way to start to understand the processes and controls on scarp degradation. These observations should focus on determining the effects of material properties on scarp degradation, and documenting the processes that degrade a scarp. Some of the effects of material properties are obvious; for example, a scarp in basalt will not degrade the same as one in alluvial gravels or lacustrine muds. In some boulder and cobble gravels, fines are winnowed out, leaving a residual armor of large clasts that may retard the rate of scarp degradation. In deposits

with well developed soil horizons, calcic and argillic horizons can substantially reduce degradation rates. Freeze-thaw cycles probably play a major role in scarp degradation in some climatic settings. Recent studies show that slope aspect and vegetation are other important controls. These variables and others need to be examined individually and collectively through careful field studies because they all affect the diffusivity rates that used in modeling.

An alternative to process-oriented studies is an empirical approach which involves systematic studies of the morphologic evolution of single-event fault or terrace scarps of known ages. Ideally, this approach would include studies of different scarps that span the time range from late Holocene through much of the Pleistocene. These studies should also include scarps in a variety of climatic settings. To date, this empirical approach has been handicapped by a lack of well-dated scarps because, most of the prominent fault scarps in the United States are in the arid and semiarid western region where it is difficult to find datable material.

A important benefit of the empirical approach is that it would provide accurate measurements of diffusivity coefficients. Without reliable values for diffusivity coefficients, it is impossible to accurately estimate the numeric age of a fault scarps with the diffusion equation.

Multiple-event fault scarps are very common in the geologic record, but there have been virtually no attempts to date multiple-event fault scarps with degradation models. Modeling a partially degraded scarp that is rejuvinated by a younger event is extremely complex. The consensus of individuals working with scarp-degradation models is that dating the rupture events of multiple-event scarps will be very difficult. From empirical relationships, we can now reasonably estimate the time of faulting for some scarps formed by two rupture events of Holocene or latest Pleistocene age. With better morphologic data on older scarps, we may be able to extend these empirical estimates back to scarps tens of thousands of years old. For scarps produced by more than two events, the outlook is less promising.

page 361 follows

THE BEHAVIOR OF SEISMOGENIC FAULTS

EFFECTS OF FAULT HETEROGENEITY ON RUPTURE PROPAGATION

by

Richard H. Sibson

Department of Geological Sciences
University of California
Santa Barbara, CA 93106

ABSTRACT

Characteristic earthquake behavior along major fault zones suggests the presence of structures which control the nucleation and arrest of ruptures at specific sites. Within strike-slip systems especially, modern seismological techniques (strong ground-motion analyses, aftershock studies) are yielding important information on the starting and stopping sites for large ruptures, allowing correlation with major geometrical irregularities along the surface traces of the faults, or with variations in the depth of the seismogenic zone attributable to rheological heterogeneity.

Precision microearthquake studies along strike-slip faults show that jog and bend structures, apparently responsible for rupture arrest or perturbation, lie transverse to the direction of rupture propagation and extend throughout the seismogenic regime to depths of ~10 km. These structures are usefully classified as dilational or antidilational depending on the tendency for areal increase or reduction, respectively, associated with incremental deformation accompanying slip propagation. It is important to note a directivity effect in the case of isolated fault bends; incremental slip transfer around a bend to a differently oriented fault segment may involve dilation or compression across that segment depending on the direction of rupture propagation into the bend.

Nucleation sites for moderate to large ruptures show no obvious consistent relationship to surface irregularities, but there are some indications that they may correlate with regions of abnormally deep background microseismic activity along fault zones. On rheological grounds these would be expected to be zones of abnormally high shear resistance. However, major dilational fault jogs and bends appear to form preferential sites for rupture arrest. Because these structures also make good targets for trenching studies, this latter relationship has special significance for paleoseismology.

INTRODUCTION

The recognition of characteristic-earthquake behavior (Schwartz and Coppersmith, 1984) along many active faults, coupled with the increasing resolution of modern seismological data, has led recently to a growing interest in structural controls affecting the nucleation, propagation, and arrest of earthquake ruptures. These structural controls on earthquake

rupturing are important to seismic-hazard assessment because: (1) they determine the size of characteristic earthquakes; and, (2) they may act as localized radiators of high-frequency energy inducing strong ground motion during rupture perturbation and arrest.

Investigations have largely concentrated on strike-slip faulting because structural irregularities are then easily visible in map view and may be correlated with epicentral distributions. The effects of various structural irregularities on strike-slip earthquake ruptures have been considered by Bakun and others (1980, 1987), Segall and Pollard (1980), King (1983, 1987), Bakun and Lindh (1985), Bilham and Williams (1985), King and Nabelek (1985), Sykes and Seeber (1985), Sibson (1984, 1985, 1986), Scholz (1985), Barka and others (1987), Knuepfer and others (1987). This paper reviews some of the findings of these studies of particular relevance to paleoseismology. Many of the conclusions expressed here are at best, provisional, at worst, speculative, in the hope of provoking more critical analyses of the data base as it expands in the future.

STRUCTURAL HETEROGENEITY OF FAULT ZONES

Heterogeneity within crustal fault zones occurs over a tremendous scale range. Concepts of self-similar fault behavior (King, 1983) suggest, however, that the larger earthquakes, which are our main concern, are likely to be affected only by the larger heterogeneities. Thus, in considering the complex trace of a strike-slip rupture such as that shown in figure 1, we consider only the larger cross-strike irregularities which occur on scales of hundreds of meters to kilometers. Clearly, it is of prime importance to determine the critical size of irregularities capable of affecting these larger events. Two distinct classes of heterogeneity appear to influence rupture behavior: rheological heterogeneities affecting the depth of the seismogenic regime, and fault segmentation by structural irregularities transverse to the direction of rupture propagation.

Rheological Heterogeneity

In tectonically active continental crust, the base of the seismogenic regime as defined by background microearthquake activity generally lies at depths of 10-20 km, and appears to represent the transition from unstable frictional (FR) fault behavior to quasi-plastic (QP) shearing flow at the onset of greenschist metamorphic conditions (Sibson, 1983). Construction of composite rheological profiles of shear resistance versus depth suggest that the peak shear resistance should occur in the vicinity of the FR/QP transition (fig. 2). In this regard, it is notable that larger earthquake ruptures ($M>5.5$, say) generally nucleate toward the base of the seismogenic regime.

Detailed regional studies of microseismicity (for example, Sanders and Kanamori, 1984; Doser and Kanamori, 1986) have, however, shown considerable fluctuations in the maximum depth of activity along the strike of major active fault zones. From

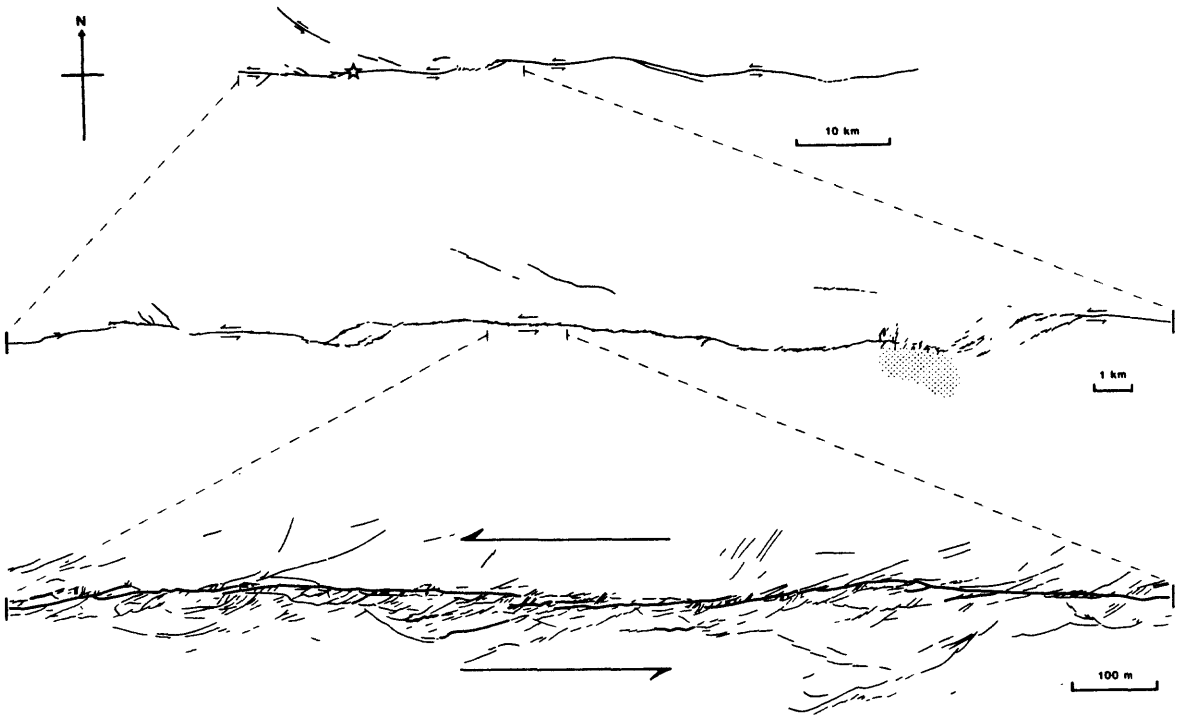

Figure 1.--Left-lateral rupture trace from the 1968 M_S7.2 Dasht-e-Bayaz earthquake, Iran (after Tchalenko and Berberian, 1975). Star indicates probable epicenter, stippling an area of sandblows.

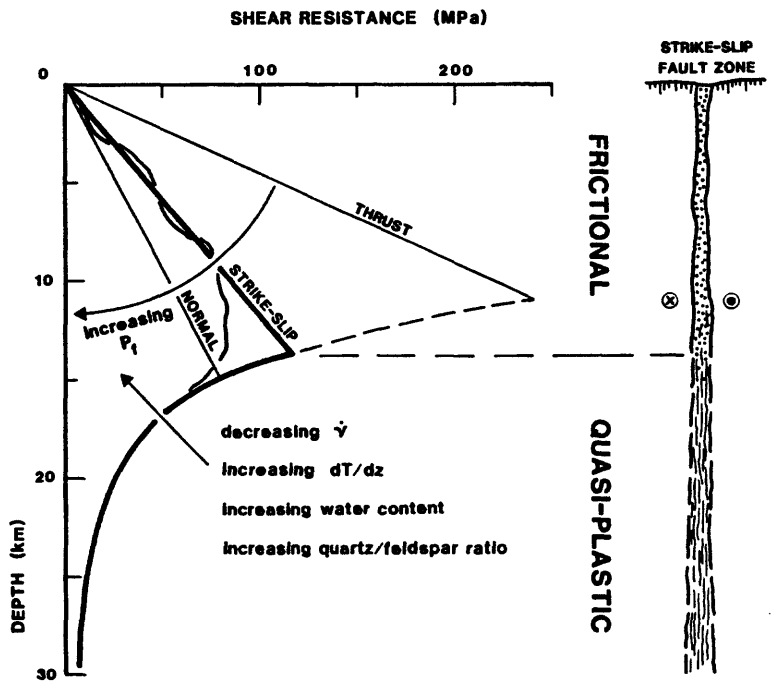

Figure 2.--Composite shear resistance profile for a simple fault model in quartz-bearing crust showing the perturbing effects of various parameters on the depth of the FR/QP transition (after Sibson, 1984).

rheological modeling, a likely expectation is that the deeper the seismogenic regime, the greater should be the value of peak shear resistance at the FR/QP transition. Thus it has been suggested (Sibson, 1984) that patches of deep microearthquake activity along fault zones may correlate with high-strength asperities which form potential nucleation sites for larger ruptures (fig. 3). Support for this hypothesis comes from the recognition of abnormally deep microseismicity in the anticipated preparation zone for the next Parkfield earthquake on the San Andreas fault (Poley and others, 1987), and from the deep patches of microseismicity at each end of the Anza seismic gap on the San Jacinto fault (Sanders and Kanamori, 1984). However, many more corroborative studies are needed before it can count as a ranking hypothesis.

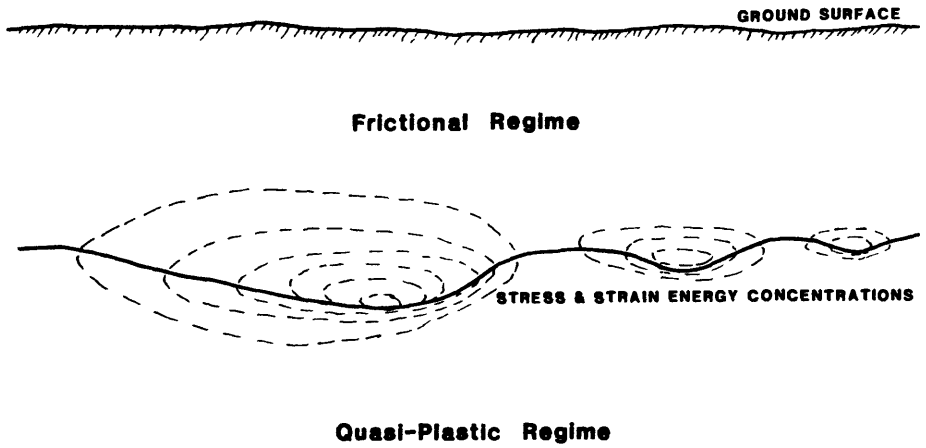

Figure 3.--Schematic diagram of fault surface illustrating stress and strain energy concentrations arising from irregularities in the depth of the FR/QP transition (after Sibson, 1984).

Fault Segmentation

The surface traces of large strike-slip earthquake ruptures are almost invariably segmented on cross-strike scales of hundreds of meters to kilometers (Wallace, 1973; Tchalenko and Berberian, 1975; Segall and Pollard, 1980). Precision aftershock studies suggest that in many instances these structural irregularities extend throughout the seismogenic regime to depths of ~10 km (Reasenberg and Ellsworth, 1982).

While composite structures and more complex 3-dimensional linkage structures undoubtedly occur, two main classes of irregularity transverse to the direction of rupture propagation may be recognized; fault jogs linking en echelon fault segments, and isolated fault bends (fig. 4). Within these two basic classes, the structures are usefully classified as <u>dilational</u> or <u>antidilational</u> depending on the tendency for areal <u>increase</u> or <u>reduction</u>, respectively, associated with incremental deformation accompanying slip propagation. From their geomorphic expression

(dilational jogs are associated with small pull-apart basins, antidilational jogs with "pop-up" structures), it is clear that many of these structures are transitory features that are bypassed from time to time as the fault zones readapt. At present, little hard data exists on their longevity though it is demonstrable that some irregularities have persisted through many rupture episodes for lengthy time periods (perhaps 10^4-10^5 yrs in some instances).

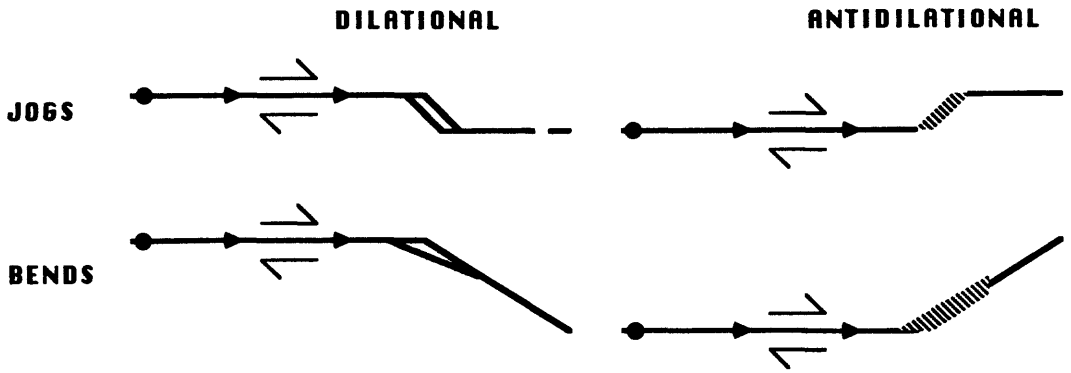

Figure 4.--Schematic representation of dilational and antidilational jogs and bends on a right-lateral strike-slip fault.

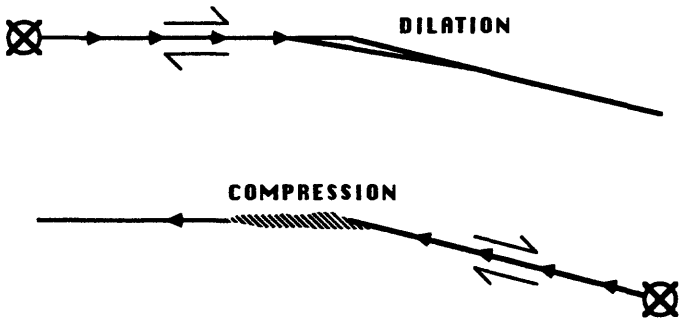

Figure 5.--Changing response of an isolated fault bend to rupture directivity.

Rupture Directivity and Isolated Fault Bends

A potentially important directivity effect is associated with isolated fault bends. Consider the single bend in a right-lateral fault illustrated in figure 5, and the problems of incremental slip transfer around that bend for ruptures propagating in opposite directions. For a rupture approaching from the left, incremental slip transfer at the rupture tip will tend to dilate the fault segment across the bend whereas for a rupture approaching from the right, the fault segment across the bend will experience increased compression.

OBSERVED EFFECTS

Rupture Nucleation

Bakun and others (1980), King and Nabelek (1985), and King (1987) have discussed structural controls on rupture initiation, finding some evidence for a correlation with fault jogs and bends. However, consistent correlations with structural features visible at the surface are by no means always apparent (Aki, 1987). Because the larger ruptures tend to initiate towards the base of the seismogenic zone, it seems probable that rheological as well as geometrical inhomogeneities play a key role in the nucleation process, as discussed above.

Rupture Interaction with Fault Jogs

More information is available on the structural controls effecting rupture perturbation and arrest, and a fairly consistent pattern is emerging. While antidilational jogs clearly perturb ruptures and form obstacles to both short- and long-term slip transfer along a fault, dilational fault jogs seem to play an especially important role as preferred sites for rupture arrest (Sibson, 1985; 1986).

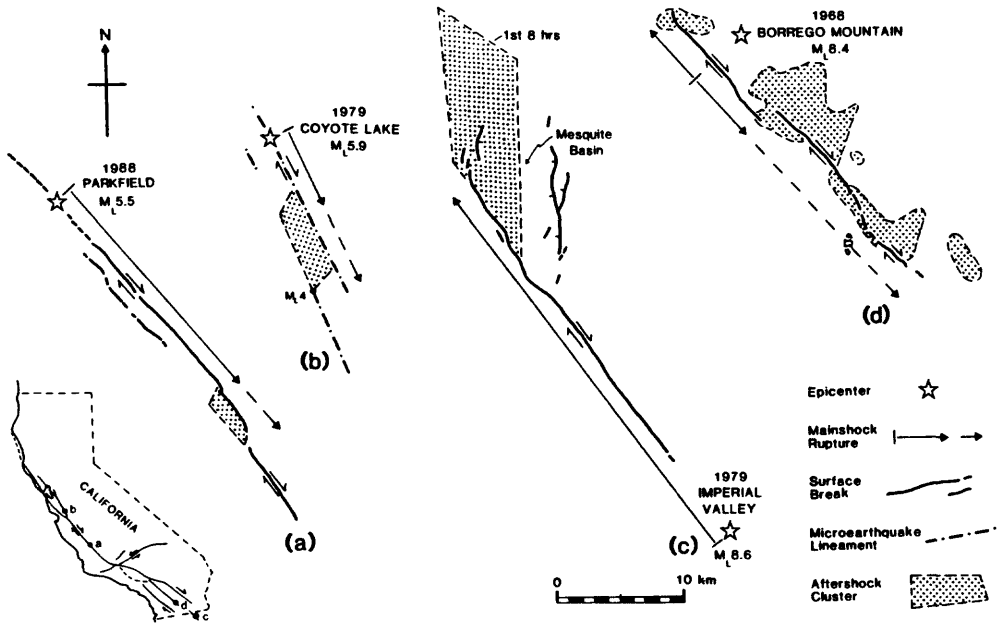

Figure 6.--Rupture interactions with fault jogs in the San Andreas fault system, California (after Sibson, 1986). Examples a, b, and c demonstrate rupture arrest at dilational fault jogs, d illustrates perturbation but non-arrest at an antidilational jog.

This is illustrated above for a series of recent ruptures within the San Andreas fault system (see also Sibson, 1987). Similar relationships have been observed along other major strike-slip

fault zones throughout the world (Barka and others, 1987; Knuepfer and others, 1987).

The preferential arrest of ruptures at dilational fault jogs is contrary to expectations from the quasi-static elastic analysis of en echelon fault segmentation (Segall and Pollard, 1980). However, rupture arrest at such sites is generally followed by delayed slip transfer to the en echelon fault segment with accompanying aftershock activity. Dilational fault jogs thus appear to behave as kinetic barriers which impede rapid slip transfer, but allow it to occur slowly. This time-dependent behavior is attributed to the difficulties of opening a linking extensional fracture mesh quickly in fluid-saturated crust (Sibson, 1985). Induced suctions, which oppose rapid slip transfer, scale with jog width. It appears that the minimum stepover width for arrest of a moderate ($5.5<M<6.5$) rupture at a dilational fault jog is about 1-2 km.

Aftershock Distributions

Aftershocks arise through readjustment of the wallrock to slip on an irregular main-shock rupture. Distinctly different patterns of aftershock activity are associated with dilational and antidilational jogs following rupture arrest or perturbation (fig. 6), but it is notable in both cases that the greatest concentrations occur in regions of inferred reduction in mean stress. For a dilational jog, the greatest reduction in mean stress occurs in the step-over region between en echelon fault segments. In the case of an antidilational jog, mean stress is reduced in areas flanking the jog but outside the main fault zone (Segall and Pollard, 1980). This accords with the suction mechanism for rupture arrest at dilational fault jogs, and with the hypothesis of Nur and Booker (1972), who account for the time-dependent decay of aftershock activity by restoration of fluid pressures in these regions of lowered mean stress.

Rupture Interaction with Isolated Bends

At present, there is little high-resolution seismological data on the interactions of ruptures with isolated fault bends. However, from the few (usually poorly documented) examples we have, some interesting but highly speculative conclusions may be drawn. The M6.8 Izu-Oshima earthquake in Japan involved right-lateral strike-slip rupturing on a largely offshore fault (Shimazaki and Somerville, 1979). The main-shock rupture propagated ~17 km from east to west to terminate at a dilational bend near the coast where the fault trend, as defined by a linear concentration of aftershock activity, changed by ~30° (fig.7).

Turning to the San Andreas fault, we may also consider effects associated with the two major historic ruptures. Right slip associated with the 1906 San Francisco earthquake drops from 3.4-4.4 m to 1.4-2.6 m in the vicinity of the ~9° bend in the fault trace at Black Mountain (Scholz, 1985; Thatcher and Lisowski, 1987)(fig. 8). Given the probable epicenter to the northwest, this bend would have behaved as an antidilational

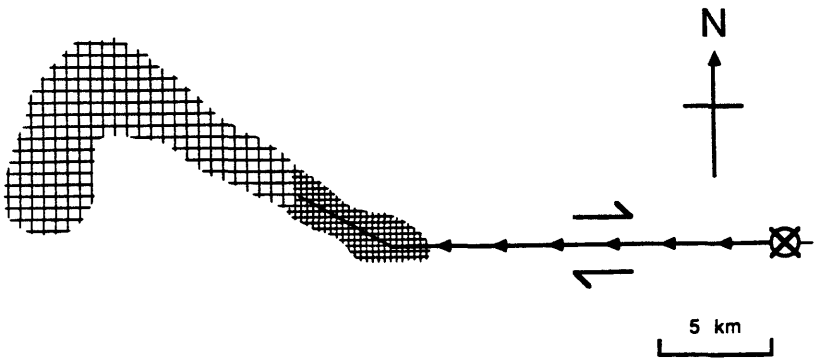

Figure 7.--Cartoon illustrating the seismotectonics of the 1978 M6.8 Izu-Oshima earthquake (after Shimazaki and Somerville, 1979). Star represents the main-shock epicenter, intensity of cross-hatching the concentration of aftershocks.

structure to a south-propagating rupture. Thus, while the rupture was clearly perturbed by the antidilational bend, propagation to the southeast continued for some 90 km. Note also the bowing-out of isoseismals in the immediate vicinity of the bend, presumably reflecting locally intense energy release from the perturbation.

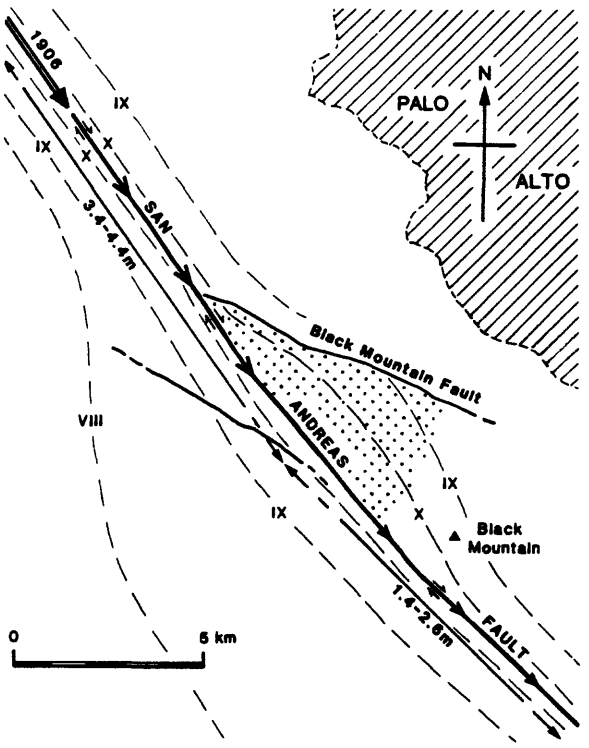

Figure 8.--Perturbation of the 1906 rupture at the Black Mountain bend (modified from Scholz, 1985). Dashed lines are Rossi-Forel isoseismals.

Similar effects may be noted in the case of the 1857 rupture through the "Big Bend" of the San Andreas fault (fig. 9). From the probable occurrence of foreshocks in the Parkfield area

(Sieh, 1978a), it seems likely that the rupture propagated north-to-south, in which case the prominent ~25° bend at the southern end of the Carrizo Plain would likewise have acted as an antidilational structure. A major reduction in slip occurred in the vicinity of the bend (Sieh, 1978b), but rupturing again continued southward for an additional 200 km.

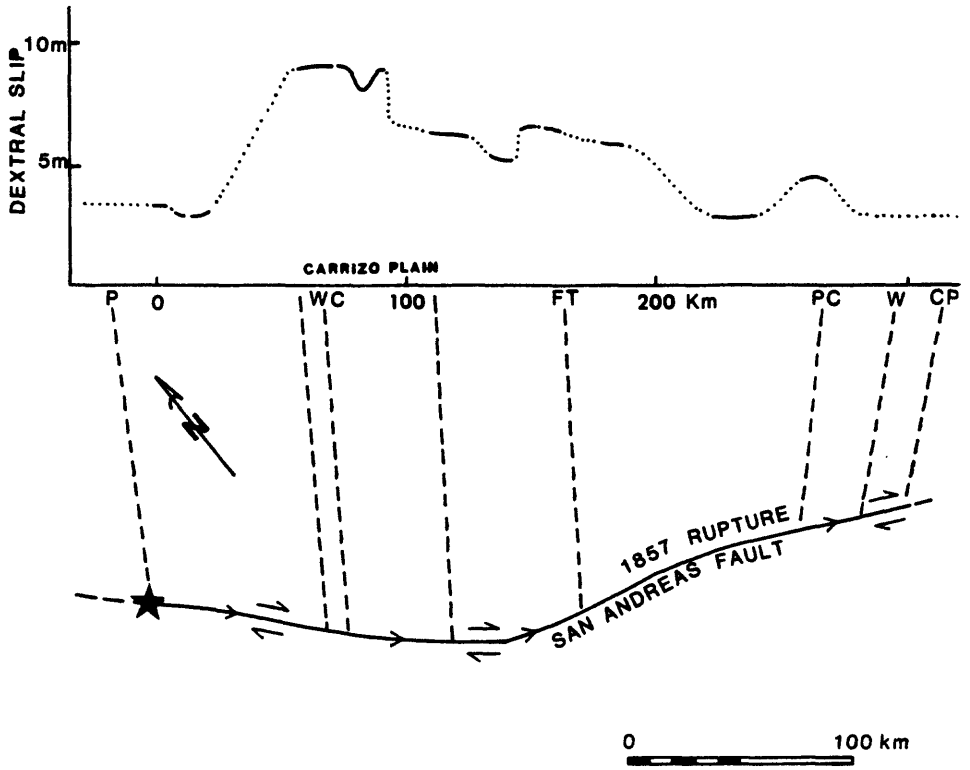

Figure 9.--Slip distribution associated with the 1857 rupture on the San Andreas fault (after Sieh, 1978b). Localities: P = Parkfield; WC = Wallace Creek; FT = Fort Tejon; PC = Pallet Creek; W = Wrightwood; CP = Cajon Pass.

Thus on this admittedly scanty information it appears that, as with fault jogs, dilational bends may present greater obstacles to rupture propagation than antidilational bends. Since the response of a bend to incremental slip transfer depends on the direction of rupture propagation, this raises the intriguing possibility that such structures may act as "one-way valves", allowing rupture propagation in one direction but not the other. This could help explain the paleoseismic evidence from the 1857 rupture trace for only three large-slip events over the past thousand years at Wallace Creek, north of the bend, compared with six smaller-slip events over the same time period in the segment south of the bend (Weldon and Sieh, 1985). North-to-south propagating ruptures, though perturbed, would replicate the 1857 event, but south-to-north propagating "catch-up" ruptures would be arrested at the bend which to them would act as a dilational structure.

IMPLICATIONS FOR PALEOSEISMOLOGY

The recognition that dilational fault jogs and bends act as preferential sites for rupture perturbation and arrest has important implications for paleoseismic studies because small pull-apart basins associated with these structures form particularly good sites for trenching investigations. On the plus side, locally intensified ground shaking associated with rupture deceleration can be expected to trigger liquefaction and sedimentation events, leaving a clear paleoseismic signal from each earthquake. Slip measurements made in the vicinity of such structures are unlikely, however, to be representative of the rupture trace as a whole. Moreover, interpretative difficulties may arise if ruptures from adjacent fault segments are terminating in the same jog (fig.10). Particular care may therefore be needed interpreting the paleoseismic record in the vicinity of such structures.

Figure 10.--Cartoon illustrating dextral strike-slip ruptures propagating from opposite directions to terminate in the same dilational fault jog (DJ).

DISCUSSION

From the viewpoint of paleoseismic studies, I emphasize again that many of the ideas presented here are preliminary and speculative. Additional multidisciplinary work is clearly needed on all aspects of fault jog and bend behavior. With time, the accumulation of seismological and geodetic data on rupture interactions with fault irregularities will substantiate or negate many of the issues raised here. One important goal will be more accurate definition of the critical jog or bend dimensions capable of causing rupture arrest. Understanding the mechanical response of fault jogs and other irregularities will require detailed knowledge of their internal structure. Work on fault-hosted hydrothermal mineral deposits exposed by mining suggests they may provide valuable information on the internal structure of dilational fault jogs in particular (Sibson, 1987). Combined structural-geomorphic studies along active fault zones are also needed to explain how fault irregularities develop, and what factors control their longevity in a particular configuration.

ACKNOWLEDGMENTS

I thank the organizers for the invitation to attend the Albuquerque Paleoseismology Workshop. Research leading to this publication was supported by the National Science Foundation, Grant Number EAR86-17445.

REFERENCES CITED

Aki, K., 1987, How to find the nucleation point of an earthquake faulting: Seismological Research Letters, v. 58, p. 32.

Bakun, W.H., King, G.C.P., and Cockerham, R.S., 1987, Seismic slip, aseismic slip, and the mechanics of repeating earthquakes on the Calaveras fault, California: in, Das, S., Boatwright, J., and Scholz, C.H., eds., Earthquake source mechanics: American Geophysical Union Monograph 37 (Maurice Ewing 6), p. 195-207.

Bakun, W.H., and Lindh, A., 1985, The Parkfield, California, prediction experiment: Science, v. 229, p. 619-624.

Bakun, W.H., Stewart, R.M., Bufe, C.G., and Marks, S.M., 1980, Implication of seismicity for failure of a section of the San Andreas Fault: Seismological Society of America Bulletin, v. 70, p. 185-201.

Barka, A.A., Kadinsky-Cade, K., and Toksoz, M.N., 1987, North Anatolian fault geometry and earthquake activity: Seismological Research Letters, v. 58, p. 31.

Bilham, R., and Williams, P., 1985, Sawtooth segmentation and deformation processes on the southern San Andreas Fault, California: Geophysical Research Letters, v. 12, p. 557-560.

Doser, D.I., and Kanamori, H., 1986, Depth of seismicity in the Imperial Valley region (1977-1983) and its relationship to heat flow, crustal structure, and the October 15, 1979, earthquake: Journal of Geophysical Research, v. 91, p. 675-688.

King, G.C.P., 1983, The accommodation of large strains in the upper lithosphere of the earth and other solids by self-similar fault systems--The geometrical origin of b-value: Pure and Applied Geophysics, v. 121, p. 761-815.

_____1987, Speculations on the initiation and termination processes of earthquake rupture and its relation to morphology and geological structure: Pure and Applied Geophysics, v. 124, p. 567-586.

King, G.C.P., and Nabelek, J., 1985, Role of fault bends in the initiation and termination of earthquake rupture: Science, v. 228, p. 984-986.

Knuepfer, P.L.K., Bamberger, M.J., Turko, J.M., and Coppersmith, K.J., 1987, Characteristics of the boundaries of historical surface fault ruptures: Seismological Research Letters, v. 58, p. 31.

Nur, A., and Booker, J.R., 1972, Aftershocks caused by pore-fluid flow: Science, v. 175, p. 885-887.

Poley, C.M., Lindh, A.G., Bakun, W.H., and Schulz, S.S., 1987, Temporal changes in microseismicity and creep near Parkfield, California: Nature, v. 327, p. 134-137.

Reasenberg, P., and Ellsworth, W.L., 1982, Aftershocks of the Coyote Lake, California, earthquake of August 6, 1979--A detailed study: Journal of Geophysical Research, v. 87, p. 10,637-10,655.

Sanders, C.O., and Kanamori, H., 1984, A seismotectonic analysis of the Anza seismic gap, San Jacinto fault zone, southern California: Journal of Geophysical Research, v. 89, p. 5873-5890.

Scholz, C.H., 1985, The Black Mountain asperity--Seismic hazard of the southern San Francisco peninsula, California: Geophysical Research Letters, v. 12, p. 717-719.
Schwartz, D.P., and Coppersmith, K.J., 1984, Fault behavior and characteristic earthquakes--Examples from the Wasatch and San Andreas fault zones: Journal of Geophysical Research, v. 89, p. 5681-5698.
Segall, P., and Pollard, D.D., 1980, Mechanics of discontinuous faults: Journal of Geophysical Research, v. 85, p. 4337-4350.
Shimazaki, K., and Somerville, P., 1979, Static and dynamic parameters of the Izu-Oshima, Japan earthquake of January 14, 1978: Seismological Society of America Bulletin, v. 69, p. 1343-1378.
Sibson, R.H., 1983, Continental fault structure and the shallow earthquake source: Journal of the Geological Society of London, v. 140, p. 747-767.
_____1984, Roughness at the base of the seismogenic zone--Contributing factors: Journal of Geophysical Research, v. 89, p. 5791-5799.
_____1985, Stopping of earthquake ruptures at dilational fault jogs: Nature, v. 316, p. 248-251.
_____1986, Rupture interaction with fault jogs, in, Das, S., Boatwright, J., and Scholz, C.H., eds., Earthquake source mechanics: American Geophysical Union Monograph 37 (Maurice Ewing 6), p. 157-167.
_____1987, Earthquake rupturing as a hydrothermal mineralizing agent: Geology, v. 15, p. 701-704.
Sieh, K.E., 1978a, Central California foreshocks of the great 1857 earthquake: Seismological Society of America Bulletin, v. 68, p. 1731-1749.
_____1978b, Slip along the San Andreas fault associated with the great 1857 earthquake: Seismological Society of America Bulletin, v. 68, p. 1421-1448.
Sykes, L.R., and Seeber, L., 1985, Great earthquakes and great asperities: Geology, v. 13, p. 835-838.
Tchalenko, J.S., and Berberian, M., 1975, Dasht-e-Bayaz fault, Iran--Earthquake and earlier related structures in bedrock: Geological Society of America Bulletin, v. 86, p. 703-709.
Thatcher, W., and Lisowski, M., 1987, Long-term seismic potential of the San Andreas fault south-east of San Francisco: Journal of Geophysical Research, v. 92, p. 4771-4784.
Wallace, R.E., 1973, Surface fracture patterns along the San Andreas fault, in, Kovach, R.L. and Nur, A., Proceedings of the Conference on Tectonic Problems of the San Andreas Fault System: Stanford University Special Publications in the Geological Sciences, v. XIII, p. 248-250.
Weldon, R.J., and Sieh, K.E., 1985, Holocene rate of slip and tentative recurrence interval for large earthquakes on the San Andreas fault, Cajon Pass, southern California: Geological Society of America Bulletin, v. 96, p. 793-812.

STRUCTURAL AND FLUID CHARACTERISTICS OF NORMAL FAULTS: SOME OBSERVATIONS AND APPLICATIONS TO SEISMOGENICS

by

Ronald L. Bruhn and William T. Parry
Department of Geology and Geophysics
University of Utah
Salt Lake City, Utah 84112

ABSTRACT

Rupture segments in normal fault zones are commonly linked by jogs in the fault trace that reflect changes in fault-zone attitude, branching of the zone into multiple strands, and changes in slip vectors. These zones of fault linkage form geometrical boundaries or "barriers" which affect the initiation, propagation and arrest of earthquake ruptures. Such structures may arise from several phenomena, including reorientation of stresses near zones of overlapping or offset fault sections, cross-faulting at the margins of discrete crustal blocks, and along-strike changes in downdip geometry of fault planes or in the level of decollement or "detachment".

Internally, the barriers consist of multiple sets of mutually interacting faults that also interact mechanically and chemically with crustal fluids. Presumably, the structure reflects the mode of origin and the evolutionary history of the barrier. Analyses of fluid inclusions and alteration-mineral assemblages in faulted rock provide information on the fluid-chemical and fluid-mechanical properties of rupture barriers that are fundamental to the generation of earthquake ruptures. Examples are cited from the Wasatch fault, Utah and Dixie Valley fault, Nevada.

A number of outstanding problems need to be addressed, both to maximize our knowledge of the effects of crustal structure and fluids in influencing rupture propagation, and in the creation of fault-zone models for hazards mitigation. Normal fault zones are structurally complex in three dimensions, perhaps best visualized as a "pleated or corrugated" curtain extending into the earth. This type of geometry has important implications for strong ground motion, but in most cases subsurface data from seismic-reflection profiles or deep wells are severely limited. Procedures for estimating the subsurface geometry of normal fault zones by better utilizing commonly available geological and geophysical data need to be developed, refined, and consistently applied in hazards mitigation studies. We have little understanding of the internal structure of most barriers, and how this structure is likely to influence ruptures propagating either (1) quasi-statically or (2) unstably (coseismic). The temporal persistence and mechanical consistency of barriers over several earthquake cycles is also open to question. Geometrical barriers are frequently positions of extensive hydrothermal alteration and spring activity in fault zones. Understanding the fluid-mechanical and fluid-chemical properties of the barriers and how these properties differ in the intervening sections of the fault zone remains a major challenge.

INTRODUCTION

Geometrical boundaries in fault zones affect the initiation, history of propagation, and arrest of earthquake ruptures (Aki, 1984, 1987; Schwartz and Coppersmith, 1984; King and Yielding, 1984; King and Nabelek, 1985). The origin of geometrical boundaries,

which are often referred to as "geometrical barriers" when discussed in terms of rupture propagation, their persistence over geological time and their effects on earthquake rupture propagation are fundamental problems in understanding seismogenics. Fluids will also affect rupturing, either through time-dependent pressure or chemical processes (Das and Scholz, 1981; Sibson, 1985, this volume).

Our purpose in this report is to share some of our ideas on the geometrical and fluid-mechanical properties of seismogenic normal faults. We wish to discuss some of our observations and methods of investigation that seem to hold promise for utilyzing structural geology and geochemistry in the study of fault systems. Consequently, it is not our purpose to provide a comprehensive review of the subject.

Presently, considerable effort is being directed at understanding the rupture segmentation of fault zones and how it relates to fault geometry (Sibson, this volume; Wheeler, this volume). We note that there is no apriori reason to expect a subdivision of a fault zone based on earthquake rupturing to be the same as that defined by fault-zone geometry. Thus, unless we specify *rupture segmentation* in the following discussion, we refer to *geometrical segmentation* of the fault zone. Geometrical boundaries in fault zones may originate from several processes, including (1) structural linking of laterally growing or overlapping fault sections, (2) cross-faulting reflecting inherited crustal structure or alternatively, strain accomodation at the margins of rotating crustal blocks, and (3) along-strike changes in the seismogenic depth extent of the fault zone, perhaps reflecting changes in rheological properties or the level of detachment (Susong and Bruhn, 1986). How these boundaries influence the flow of crustal fluids and earthquake rupture behavior is a fundamental topic in crustal seismogenics.

MODELING PLANAR NORMAL FAULTS

Fault Geometry

Fault zones are complex, perhaps best visualized in three dimensions as a "pleated or corrugated" curtain extending into the earth. This type of geometry has important implications for understanding and predicting the seismogenic properties of the fault zone, but by its very nature presents difficulty in modeling fault geometry. Seismic-reflection and well data are usually limited in areal extent, and if the dip of one part of the fault zone is determined by such means, it cannot be arbitrarily extrapolated into adjacent parts of the fault zone. Here we will discuss simple procedures to model normal fault zones that focus on the use of *along-strike* structural information that is supplemented with standard *across-strike* geological or geophysical data. These procedures consist of well-established techniques in structural geology and can be equally applied to reverse and strike-slip faults. They apply to planar faults, which appear to be common in fault zones that have generated large normal faulting earthquakes. A modification of the method is required to handle listric faults, and is not described here.

A three-dimensional model is constructed using the following procedural steps:

1. The zone is divided into rectilinear sections based on the geometry of the fault trace. These sections will intersect at geometrical boundaries formed by bends, branching, or en echelon offset of the trace.
2. The boundaries are classified as either geometrically cylindrical or noncylindrical.
3. The fault sections are grouped into geometrical segments that contain one or more cylindrical boundaries and are separated by non-cylindrical ones. Estimating the trend, plunge, and depth extent of the boundaries is a fundamental aspect of the work.

4. The dip of each fault section within a segment is then modelled if one can obtain the following type of information in addition to the strike of the fault sections as inferred from the trace of the fault zone:
    a. Dip of one fault section within the segment and trend of a cylindrical boundary.
    b. Trend and plunge of one of the cylindrical boundaries.
    c. Slip vector across the fault segment and trend of a cylindrical boundary.

This approach has several limitations. First, it is doubtful that an ideally "cylindrical" boundary exists, particualarly over any significant interval of geological time. Thus, one is faced with the subjective judgment of deciding if a cylindrical geometry is an appropriate approximation for a particular structural boundary within the fault zone.

The depth extent of a boundary is also a fundamental problem that has important implications for seismogenic properties of the fault zone. A non-cylindrical boundary may have limited depth extent. This is partly resolved by noting the lateral extent of cross faults or gravity anomalies marking hanging wall basin boundaries, that extend outward from the main fault zone. These features overlie the position of the boundary in the subsurface, and their lateral extent is then a direct expression of both the structural trend and depth extent of the boundary.

Slip Directions

Determining the orientation of a fault plane and slip vector at some point within a geometrical segment remains a persistent problem, that is often exacerbated by poor exposure of fault planes, and limited well or geophysical data. The slip direction is critical in classifying the boundaries as either conservative or nonconsevative with respect to rupture characteristics (King and Yielding, 1984).

Our work on the 1954 Dixie Valley earthquake rupture in Nevada suggests that a set of closely spaced extension fractures forms in the footwall during rupture propagation, and this fracture set may provide useful information on both the slip direction and attitude of the fault plane. This fracture set can be mapped in the footwall over almost the entire length of the rupture segment, while exposures of the fault plane occur only at a few, isolated places. Consequently, use of extension fractures to infer fault attitude or slip direction could prove extremely useful. Here we discuss the field observations and potential applications of this fracture system.

The pervasive set of extension fractures at Dixie Valley is concentrated within the footwall immediately adjacent to the rupture. Locally, the 1954 earthquake rupture cut into intensley fractured, granitic bedrock (Slemmons, 1957). The relationship between coseismic shearing on the main fault plane and fracturing in the adjacent rock can be directly demonstrated by field observation. For example, the fault zone is exposed at Big Box Canyon, in the central part of the 1954 rupture segment. There, fault breccia directly overlies the footwall granite (fig.1). The spacing between steeply east-dipping extension fracture planes (set #1 in fig. 1) is only a few centimeters, and these closely spaced fractures extend through the breccia and into the footwall for distances of several meters to several tens of meters. Thin, discontinuous shear planes that are subparallel to the main fault plane also extend into the footwall, and coexist with the penetrative extension fracture set.

The geometrical relationship between the extension fracture set and main fault plane is illustrated in figure 2. The angle between the extension fractures and main fault plane is ≈ 29°-37°, a value commonly observed in rock-deformation experiments. The slip direction on the main fault plane is defined by the intersection line between the fault plane and a great circle containing the pole to the extension fracture set and the pole to the fault

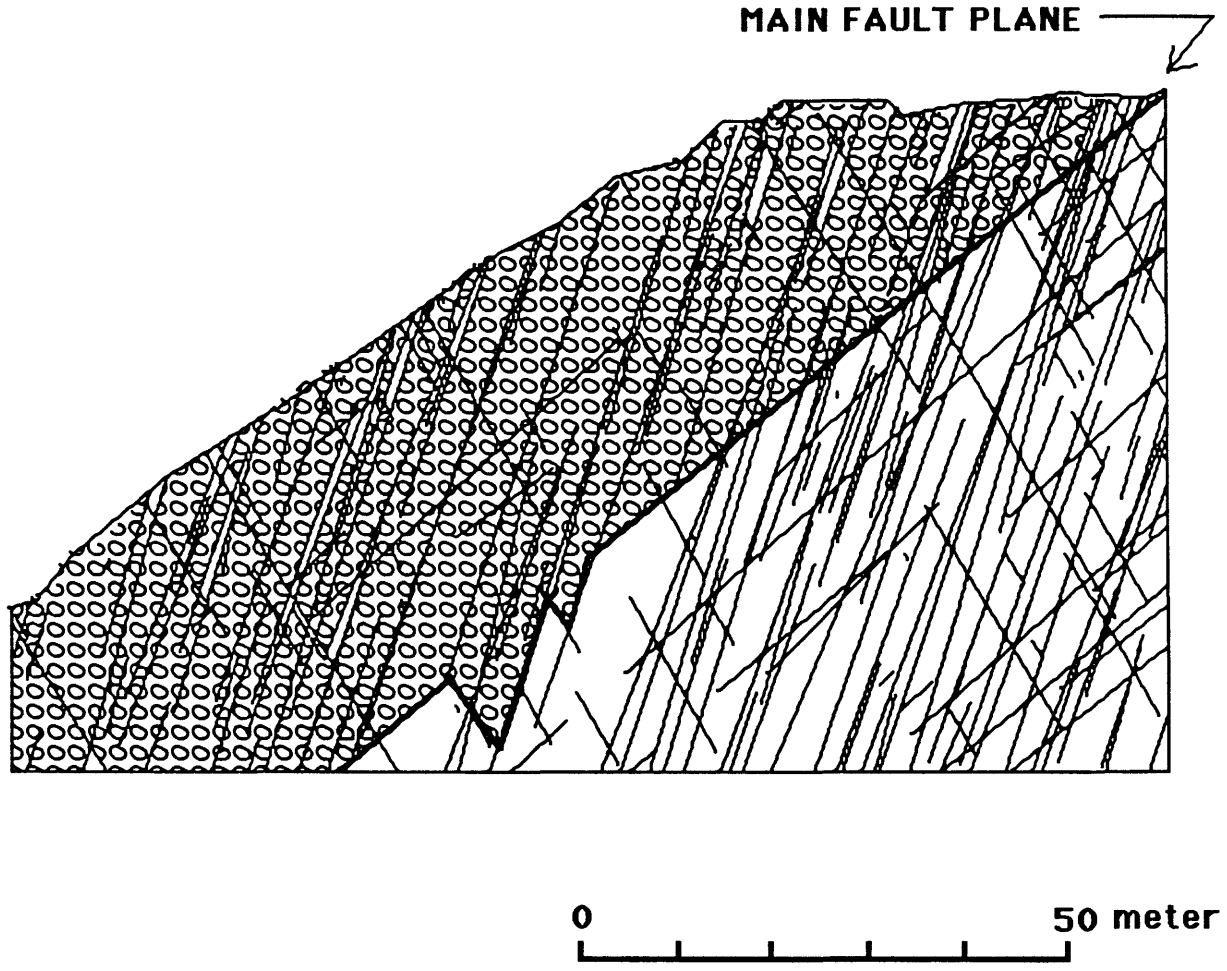

FIGURE 1: Schematic diagram of fracture sets of Dixie Valley fault zone, Nevada, at Big Box Canyon. View is to the south.

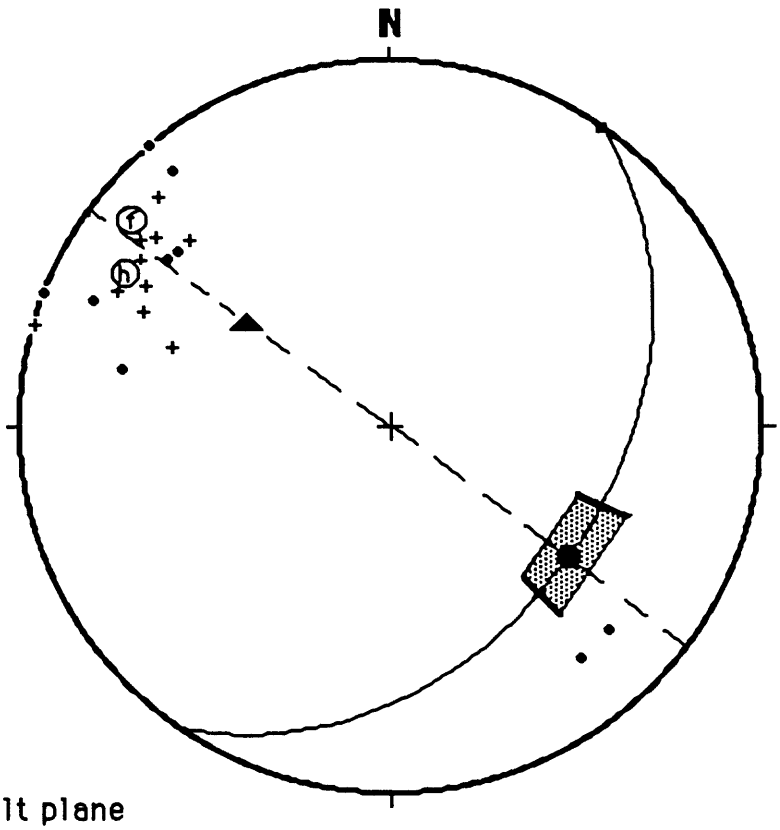

▲ Pole to fault plane

Fault plane with slip direction indicated by extension fracture set (black ball) and shaded area showing trends of grooves on fault plane

• Pole to extension fractures in footwall (n = 10)

+ Pole to extension fractures in hanging wall cataclasite (n = 10)

Ⓕ Average pole to footwall extension fractures

Ⓗ Average pole to hanging-wall extension fractures

FIGURE 2. Geometrical relationship of the extension fracture sets and the main fault plane for the Dixie Valley fault zone, Nevada, at Big Box Canyon. Sketch of the exposure is shown in Figure 1.

plane. Notice that this line lies within the field of independently determined slip vectors measured directly from grooving and striations on the fault plane (fig. 2) and agrees with the regional slip direction determined by Thompson and Burke (1973) by measuring many striated surfaces in the Dixie Valley fault zone.

These observations suggest a simple means for estimating both the dip and slip direction on a fault plane if one knows the orientation of the dynamic extension fracture set in the footwall and the strike of the fault plane. The former parameter can be measured directly in the field and the latter estimated from the trace of the fault zone. The first step is to plot the pole to the extension fracture set and strike line of the fault plane on a stereonet. The fault plane is then constructed as a great circle that has the known strike direction, a pole located at 30° to that of the extension fracture set, and the proper sense of dip for the fault zone. This simple method may prove extremely useful in studying other fault zones, where direct observations of the fault plane cannot be made because of erosion or surficial deposition.

Application of Modeling

A three-dimensional model of the zone linking the Salt Lake and American Fork rupture segments in the Wasatch normal fault zone, Utah is presented in figure 3 to illustrate the usefulness of such modeling in inferring potential seismogenic properties of fault zones. The orientations of the various fault sections comprising the linkage zone are presented in a structure contour map. We focus on two aspects of the fault zone that have important implications for inferring seismogenic properties. Namely, would the boundary act as a conservative or nonconservative barrier during rupture propagation, and if nonconservative would it be dilatant or antidilatant (see Sibson, 1985 and this volume). First, note that the fault zone is offset about 7 km to the east between the southern end of the Salt Lake segment and northern end of the American fork segment, along an east-trending normal fault that dips to the south. The prominent fault intersection (A) forms a "turtle back" structure within the fault zone that plunges to the west-southwest, while fault intersection zone (B) at the eastern end of the linkage zone plunges more steeply to the southwest. This geometry is by definition, non-conservative, in that the intersection lines A and B are not parallel; therefore the fault surface is not cylindrical. Furthermore, geological data suggest that the slip vector in the Salt Lake segment is either parallel to the trend of intersection line A, or possibly directed clockwise of line A by ≈ 30° (Zoback, 1983; Bruhn and others, 1987). Consider the first case, displacement parallel to line A would cause dilatancy in the vicinity of intersection line B, creating volumetric expansion, and perhaps tending to arrest seismic ruptures. If the slip vector is clockwise from the trend of intersection line A, the fault zone will be dilatant in the vicinity of both intersection lines. In either case, coseismic dilatantcy would increase the overall resistance of this linkage zone or "nonconservative" barrier to rupture propagation. This is a plausible rationale for the different Quaternary rupture history reported between the Salt Lake and American Fork rupture segments (Schwartz and Coppersmith, 1984). The inference is also supported by the presence of southwest-trending normal faults that cut the hanging wall above intersection lines A and B (see Bruhn and others, 1987). These faults indicate that the hanging wall has extended at a high angle to the intersection lines, consistent with large scale crustal dilatantcy within a non-conservative barrier.

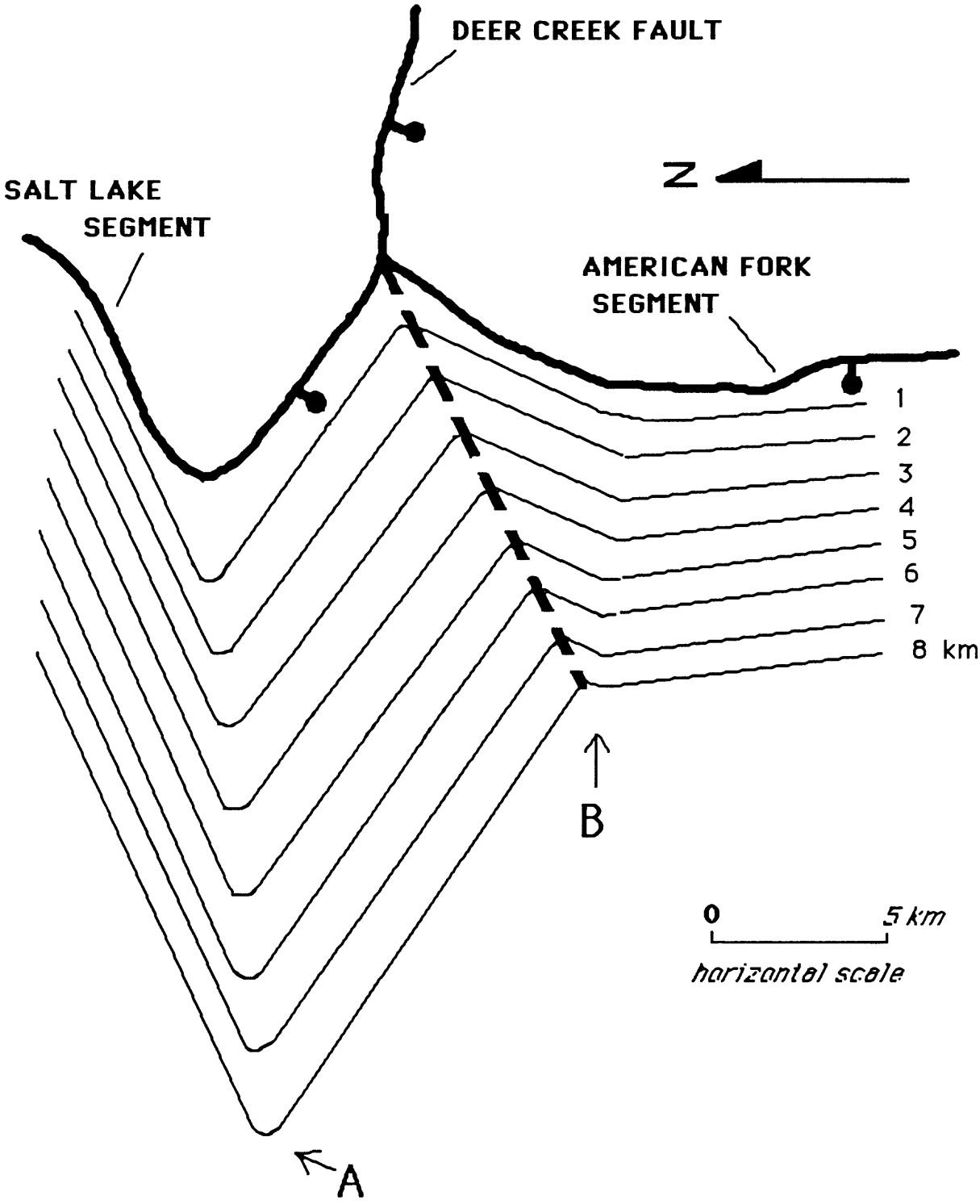

FIGURE 3. Structure contour map of faults and fault geometry near the boundary between the Salt Lake and American Fork segments of the Wasatch fault, Utah. Heavy solid lines are faults mapped on the surface; fine solid lines are contours of fault planes in kilometers.

PALEOFLUIDS IN SEISMOGENIC NORMAL FAULTS

Observations

Uplift and exhumation of the footwall during normal faulting exposes deformed rock that developed at depth within the fault zone. Studies of alteration minerals and fluid inclusions trapped in healed fractures provides a means of inferring the composition of fault-zone fluids at various pressure and temperature conditions. This information, when combined with study of textural properties of the fault rock, provides insight into the fluid-chemical and fluid-mechanical properties of faulting.

We have studied parts of two major, seismogenic fault zones--a rupture barrier at the southern end of the Salt Lake rupture segment of the Wasatch normal fault zone, Utah and the 1954 earthquake rupture in Dixie Valley fault zone, Nevada. Footwall rock composition is important in these studies, crystalline rocks containing alumino-silicate minerals provide a better record of chemical interaction of fluids with rocks during faulting than do sedimentary sequences. Syntectonic mineral assemblages in the granitic footwall rocks of both fault zones are, from highest to lowest temperature, biotite-actinolite-orthoclase, epidote-chlorite-calcite, quartz-sericite, zeolite-prehnite-clay, clay-calcite.

Systematic changes in fluid pressure and composition accompany the decrease in temperature and changes in alteration-mineral assemblages. Fluid inclusions from fault rock in the barrier at the southern end of the Salt Lake rupture segment (fig. 3, Parry and Bruhn, 1986) contains significant CO_2. The amount of CO_2 decreased as pressure of fluid entrapment decreased. Salinity varied between 2.0 and 17.3 wt percent NaCl equivalent. The maximum temperature recorded in fluid inclusions is 330 °C and the mode of fluid inclusion homogenization temperatures for CO_2 rich inclusions is 285 °C. Minimum fluid pressures estimated from the two-phase boundary curve in the phase diagram for CO_2, NaCl, and H_2O vary between near-lithostatic and hydrostatic values. These inclusions were trapped at depths as great as 11 km within the fault zone, near the frictional/quasi-plastic transition. Generation of high fluid pressures by time-dependent changes in permeability and porosity are augmented by the ionizable hydrogen provided by CO_2 hydrolysis. The hydrogen ion produced promotes reaction of H_2O with minerals in the host rock to produce chlorite, epidote, and sericite that fills fractures and replaces host-rock minerals. Later zeolite-prehnite-clay alteration is associated with fluid inclusions that are free of CO_2, have salinities between 2.0 and 16.0 wt percent NaCl equivalent, homogenize at a temperature mode of 100 °C and are presumed to have been entrapped at hydrostatic pressure at depths well above the frictional/quasi-plastic transition (Parry and Bruhn, 1986).

Hydrothermal alteration of granitic footwall rocks in the Dixie Valley fault zone includes replacement of igneous minerals and vein fillings of mineral assemblages listed above. Secondary fluid inclusions occur in healed fractures within hydrothermal quartz veins and calcite. Primary inclusions occur in quartz, calcite, and epidote. Prelimiary measurements show homogenization temperatures between 189° and 377 °C and salinites of 0.2-7.2 NaCl equivalent. One pair of liquid dominated and vapor-dominated inclusions suggests entrapment of a boiling fluid at 350 °C and pressure of ≈ 200 bars. Carbon dioxide is also an abundant constituent of the paleofluid in the Dixie Valley fault zone, but temperatures appear to be substantially higher at shallower depths than at the southern end of the Salt Lake segment of the Wasatch fault zone.

Implications for Seismogenic Properties

Fluid inclusions in the Wasatch fault zone homogenize near the same temperature at widely differing pressures, suggesting different fluid pressures and compositions at the same depth in the fault zone. A plausible explanation is that fluid pressures vary drastically between coseismic and interseismic periods. Coseismic fracturing may enhance fracture permeability within the fault zone, drastically reducing fluid pressures (see Sibson, 1985; this volume). Fluid-rock interaction in the interseismic period may result in renewed mineral precipitation, decrease of fault zone permeability, and increased fluid pressure until near lithostatic values are reached. Notably, chemical reactions and crack sealing would be augmented by a CO2-rich fluid like that observed in the fluid inclusions. The increased fluid pressures may of course lead to failure within the fault zone, initiation of a new rupture, and another abrupt decrease in fluid pressure.

On the Dixie Valley fault, chemical reactivity of fluids with rocks is enhanced by CO2, and by relatively high temperatures at shallow depths, such that fault rock may be converted to alteration minerals, particularly where fluid access is permitted at bends or jogs in the fault zone. Footwall rocks have been extensively altered to sericite and clay minerals in sections of the fault zone. Examples include parts of the footwall that are intensely altered and extend for up to 1 km along strike at the northern and southern ends of the 1954 rupture segment. Alteration of granitic host rock to phyllosilicate-rich catclasite may affect the rheology of the fault zone, leading to strain softening as feldspar is replaced by micaceous minerals. The significance of this chemical process relative to fluid-pressure transients caused by chemically induced crack-sealing cannot yet be evaluated.

These observations raise major questions concerning the manner in which fluids are transported into the fault zone, and the origin of fluid chemistry. Presently, we do not understand the relative importance of hanging-wall versus footwall recharge paths for fluid flow into the fault zones. The origin of CO2 in the fault fluids is also poorly understood, but this component is particularily important in driving mineralogical reactions that alter fault rheology.

SUMMARY

Fault-zone geometry and the mechanical and geochemical properties of fluids are key features controlling the seismogenic properties of fault zones. Crack and pore-space sealing by geochemical reactions at depth within the fault zone presumably increase fluid pressure. Chemical reactions may also remove asperities by grain boundary diffusion, chemically enhanced cracking, or alteration of the host rock to a phyllosilicate-rich assemblage during cataclasis, which in turn causes strain-softening and enhanced creep within parts of the fault zone (see Mitra, 1984). These processes may be particularly effective during rupture initiation. We note that such processes may occur at either dilatant or antidilatant boundaries. However, extensive coseismic fracturing in dilatant boundaries will favor the influx of reactive fluids over a large depth range within the fault zone. These sites may become the most extensively altered parts of the fault zone. Consequently, mapping of hydrothermal alteration, particularly in the footwalls of normal fault zones, provides evidence for the positions of paleo-geometrical boundaries. Careful dating of the hydrothermal assemblages and comparison of the spatial distribution of these paleo and contemporary geometrical boundaries will increase our understanding of the evolution of seismogenic faults and the role of geometrical segmentation in controlling rupture propagation.

REFERENCES CITED

Aki, K., 1987, How to find the nucleation point of earthquake faulting?: Seismology Research Letters, v. 58, p. 32,.

_____ 1984, Asperities, barriers, characteristic earthquakes and strong motion prediction: Journal of Geophysical Research, v. 89, p. 5867-5872.

Bruhn, R.L., P.R. Gibler, and W.T. Parry, 1987, Rupture characteristics of normal faults-An example from the Wasatch fault zone, Utah, in Coward, M.P., Dewey, J.F., and Hancock, P.L., eds., Continental Extensional Tectonics: Special Publication Geological Society London, p. 337-353.

Das, S., and Scholz, C.H., 1981, Theory of time-dependent rupture in the earth: Journal Geophysical Research, v. 86, p. 6039-6051.

King, G., and Yielding, G., 1984, The evolution of a thrust fault system-- processes of rupture initiation, propagation and termination in the El Asnam (Algeria) earthquake: Geophysical Journal Royal Astronomical Society, v. 77, p. 915-933.

King, G.C.P., and J. Nabelek, 1985, The role of bends in the initiation and termination of earthquake rupture--implications for earthquake prediction: Science, v. 228, p. 984-987.

Parry, W.T., and Bruhn, R.L., 1986, Pore fluid and seismogenic characteristics of fault rock at depth on the Wasatch fault, Utah: Journal Geophysical Research, v. 91, p. 730-744.

Mitra, G., 1984, Brittle to ductile transition due to large strains along the White Rock thrust, Wind River Moutains, Wyoming: Journal Structural Geology, v. 6, p. 51-61.

Schwartz, D.P., and Coppersmith, K.J., 1984, Fault behavior and characteristic earthquakes--examples from the Wasatch and San Andreas fault zones: Journal Geophysical Research, v. 89, p. 5669-5673.

Sibson, R.H., 1985, Stopping of earthquake ruptures at dilational fault jogs: Nature, v. 316, p. 248-251.

Slemmons. D.B., 1957, Geological effects of the Dixie Valley-Fairview Peak earthquake of December 16, 1954: Bulletin Seismological Society America, v. 47, p. 353-375.

Susong, D., and Bruhn, R.L., 1986, Structure of an earthquake rupture segment boundary in the Lost River fault zone, Idaho--implications for rupture propagation during the 1983 Borah Peak earthquake: [abs] EOS [Transactions of the American Geophysical Union] v. 67, p. 1107.

Thompson, G.A., and Burke, D., 1973, Rate and direction of spreading in Dixie Valley, Basin and Range Province, Nevada: Geological Society America Bulletin, v. 84, p. 627-632.

Zoback, M.L., 1983, Structure and tectonism along the Wasatch fault zone, Utah: Memoir Geological Society of America, v. 157, p. 3-27.

ACKNOWLEDGMENTS

Research supported by NSF grants EAR 8618250 & EAR 8420774 to R.L. Bruhn and W.T. Parry and American Chemical Society grant PRF # 17405-AC2-C to R.L. Bruhn.

BOUNDARIES BETWEEN SEGMENTS OF NORMAL FAULTS-- CRITERIA FOR RECOGNITION AND INTERPRETATION

by

Russell L. Wheeler
U.S. Geological Survey
Denver, Colorado 80225

ABSTRACT

Segments are defined as parts of a fault that tend to rupture independently of each other. On normal faults, a segment boundary exists where at least two large ruptures on the same side of the boundary have started or stopped. This can be determined from rupture zones of individual earthquakes, multiple-event scarps, and the structural record of cumulative slip deficits. Evaluation of bends and dilational jogs as possible segment boundaries requires considering the bend or jog in a plane that contains the slip vector. Then one sees that bends are not useful guides to segment boundaries on normal faults, and dilational jogs at hypocentral depths are hard to recognize from the Earth's surface. The likelihood of a particular segment boundary controlling future ruptures can be estimated by examining both young scarps and longer-term geological and geophysical records.

INTRODUCTION

Schwartz and Coppersmith (1984, p. 5687) referred to fault segments as parts of a fault "... that control the location and extent of rupture." Swan and others (1980, p. 1459-1460) noted that segments might behave either independently of each other or dependently, and could rupture piecemeal, individually, or with other segments. A definition that addresses these possibilities is that segments are parts of a fault or fault zone that tend to rupture independently of each other (Wheeler and Krystinik, in press). This definition is readily testable against geological and geophysical evidence along normal fault zones. "Independently" implies that rupture zones will tend not to cross boundaries into adjacent segments. Sometimes segments might rupture dependently, such as in large earthquakes that rupture two or more segments, or by contagion (Perkins, this volume).

The critical aspect of recognizing segmentation of a normal fault is identifying the boundaries between segments. This report describes criteria for recognizing segment boundaries. It also summarizes applications of the criteria (Wheeler and Krystinik, in press) to the Wasatch fault zone and to fault zones in the Basin-Range (the area of Basin-and-Range structure in the Western United States) that have experienced large, historic, normal-faulting earthquakes.

SEGMENT BOUNDARIES

Rupture Ends

Ends of rupture zones that are much too short (in map view) to break an entire segment will be scattered along the interior of the segment. The longer a rupture zone is, the more likely it is that one or both of its ends will coincide with a segment boundary. Rupture zones that span a segment will

tend to end at both of its boundaries. Segment boundaries will tend to limit the maximum rupture length and constrain the maximum earthquake size (Schwartz and Coppersmith, 1984), although for normal faults the association between rupture length and earthquake magnitude is weaker than for other fault types (Bonilla and others, 1984, p. 2391). In contrast, on an unsegmented fault rupture ends will be scattered along the entire fault. In the absence of contagion (Perkins, this volume), coincident rupture ends will be few, occurring by chance. Therefore, the key to recognizing segmentation is recognizing coincident rupture ends. Segmentation cannot be detected with a single rupture zone by itself.

In the Basin-Range there have been few large, historic earthquakes that can be used to identify rupture ends. Furthermore, our present geologic knowledge does not allow us to distinguish starting ends from stopping ends. For rupture zones on the same side of a possible boundary, at least two coincident ends are needed to identify the boundary (fig. 1A). It is preferable that the ends be of successive rupture zones. However, if the rupture zones are on opposite sides of the possible boundary, the pattern (fig. 1B) can form without segmentation: the first rupture would load the part of the fault to the left of the proposed boundary--only the loaded part of the fault would rupture later. The part of the fault that ruptured first would not be sufficiently loaded to rupture during the second event. Because starting and stopping ends cannot be distinguished, all possible arrangements of two rupture zones with coincident ends, the sequencing of the two ruptures, and propagation directions reduce to the two arrangements of figure 1. Therefore, to recognize a segment boundary we must identify at least two coincident ends of large rupture zones that are on the same side of the proposed boundary.

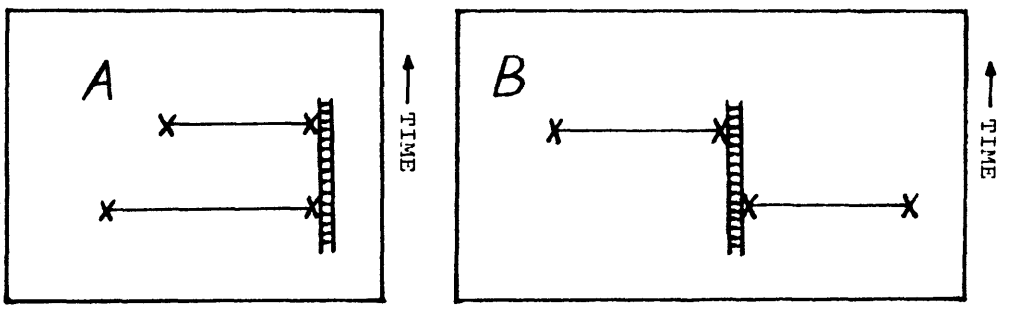

FIGURE 1.--Schematic partial history of rupture ends at proposed segment boundary. Vertical direction represents time progressing upward, and horizontal direction shows distance along fault zone in map view. Cross-hatched line shows location of proposed segment boundary. Horizontal lines with X's at ends show extent of rupture zone in map view. A, Two ruptures on same side of boundary. B, Ruptures on opposite sides.

To tell whether rupture ends coincide, rupture lengths should be large compared to boundary widths and locational uncertainties of rupture ends. In the fault zones of this report, boundaries are typically 5-15 km wide and segments are typically a few tens of kilometers long, so rupture zones that are used to identify the boundaries should break much or all of the adjacent segments. Documentation of shorter inferred segments, as on the La Jencia fault zone (Machette, 1986), requires better than average definition of rupture ends.

Slip Deficits

Slip drops to zero at both ends of a rupture zone. Slip measurements vary along strike for historic, normal-faulting earthquakes in the Basin-Range (Slemmons, 1957; Myers and Hamilton, 1964; Crone and Machette, 1984; Wallace, 1984), but overall slip is greatest near the centers of the surface ruptures and tapers to zero near the ends. Rupture ends produce slip deficits compared to the middles of rupture zones (King, 1986), and if ends of large ruptures tend to occur at segment boundaries, then over time, boundaries will develop cumulative slip deficits.

Structural Expressions of Cumulative Slip Deficits

The cumulative slip deficit at a segment boundary produces structural relief across the fault zone that is smaller than the relief produced along segment interiors. Several kinds of structures can accommodate the reduced structural relief, but buried and exposed bedrock ridges (figs. 2A, B), some fault-bounded, appear to be the most common (table 1). In the Wasatch fault zone the footwall ends of some bedrock ridges have dropped only partway down toward the structural elevations of the rest of the ridges and remain as fault-bounded salients (fig. 2B; locality 2, fig. 3A). At the Traverse Mountains boundary the footwall projects into the hanging wall as an unfaulted spur (locality 3, fig. 3A). The Hebgen Lake earthquake (fig. 3B) broke a young fault zone whose geometry is still evolving; therefore, this fault zone should not be used to infer the presence of long-lasting segment boundaries.

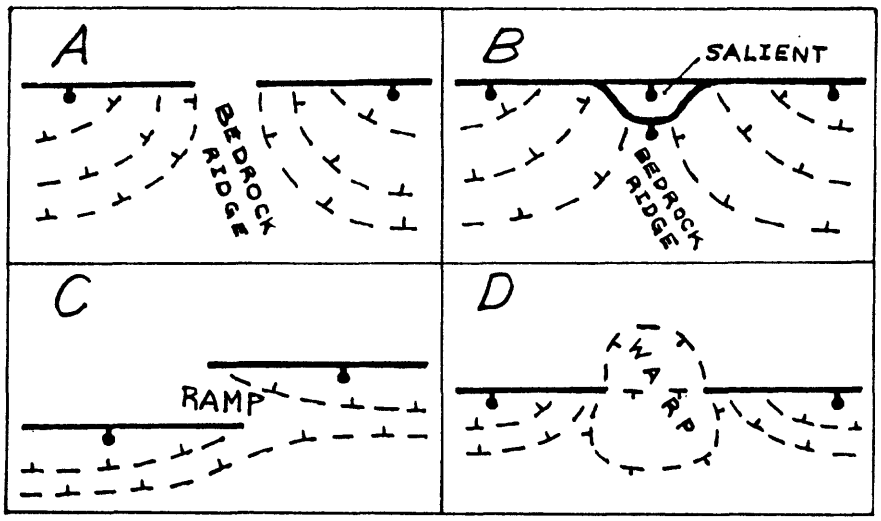

FIGURE 2.--Sketch maps of structural expressions of cumulative slip deficits at hypothetical segment boundaries on normal faults. Maps show main characteristics of four boundary geometries. Heavy lines show map traces of faults, bars and balls on downthrown sides. Footwalls have remained fixed. Dashed lines represent structure contours on a surface that was planar and horizontal before faulting, with tick marks pointing downslope.

The north and south ends of the 1954 Fairview Peak-Dixie Valley rupture zone (fig. 3C) and the north end of the 1915 Pleasant Valley rupture zone (locality 3, fig. 3E) lack enough evidence to support inferences about segment boundaries. The Pleasant Valley rupture zone steps right, across a ramp (fig. 2C; locality 2, fig. 3E) that was at least partly broken by a pre-1915 scarp (Wallace, 1984). With additional slip the two fault tips that overlap at the ramp, and any connecting faults, might link to form an irregular salient, as appears to have happened at the Payson salient (locality 4, fig. 3A; M.N. Machette, unpub. mapping, 1987). I found no examples of warps (fig. 2D) but they might develop as initial forms of bedrock ridges.

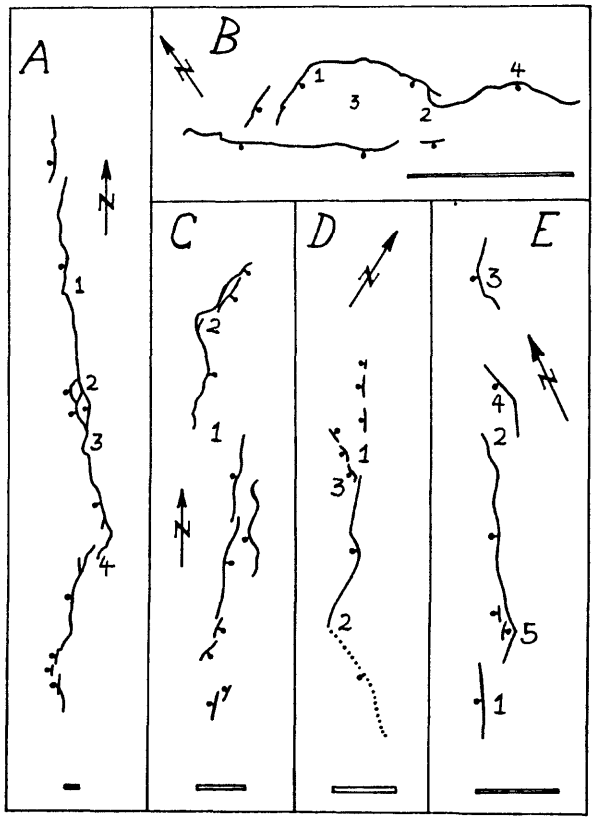

FIGURE 3.--Sketch maps of selected normal-fault zones in area of Basin-Range structure. Solid lines represent simplified fault traces, with bars and balls on downthrown sides. Dotted line in D shows selected prehistoric rupture trace. Open scale bars represent 10 km. Numerals identify localities referred to in text or tables. A, Wasatch fault zone, Utah, after Machette and others (in press). B-E, Surface ruptures from historic earthquakes. B, Hebgen Lake, Montana, 1959, after Myers and Hamilton (1964, plate 2); C, Fairview Peak-Dixie Valley, Nevada, 1954, after Slemmons (1957); D, Borah Peak, Idaho, 1983, after Crone and Machette (1984); E, Pleasant Valley, Nevada, 1915, after Wallace (1984).

The longer a segment boundary persists in time, the greater its cumulative slip deficit, and the greater the likelihood that it breaks. For example, the 1983 Borah Peak earthquake did not break the Willow Creek Hills boundary, but there are older scarps there (locality 1, fig. 3D). The Sou Hills boundary broke during the 1915 Pleasant Valley earthquake (locality 1, fig. 3E). The rupture zone of the 1903 Wonder earthquake broke the Pirouette Mountain boundary between Dixie and Fairview Valleys (locality 1, fig. 3C) and appears to have been mostly confined to the boundary (Slemmons and others, 1959). The 1903 break was reactivated in 1954 when the scarps north and south of the boundary apparently formed in separate earthquakes 4 min apart (Doser, 1986). Both segments and the boundary between them broke in the same earthquake sequence in 1954. Thus, boundaries can break by themselves, or during a single-segment earthquake, or as part of a runaway, multisegment earthquake.

RECOGNIZING RUPTURE ENDS

Single Earthquakes

Recognizing rupture ends is easiest for historic earthquakes, but in the Basin-Range most faults have not broken in historic times. For prehistoric earthquakes the ends of single rupture zones are the most useful features for identifying boundaries, but recognizing ends is uncertain. Our present ability to resolve details of prehistoric rupture zones generally precludes distinguishing the rupture zones of individual shocks in a prehistoric earthquake sequence. For example, the Fairview Peak and Dixie Valley earthquakes occurred 4 min apart, and we assume that the rupture zones of the two earthquakes are separated by the Pirouette Mountain boundary (locality 1, fig. 3C), but we do not know which scarps or parts of scarps are 4 min older than others. From geodetic modeling (Snay and others, 1985) it appears that the two earthquakes could have broken adjoining parts of a single fault zone at depth. Nearby, two earlier earthquakes occurred 7 weeks apart and broke overlapping parts of the Rainbow Mountain fault zone, sharing many individual scarps (Tocher, 1956). At Pleasant Valley in 1915, parts of the four main scarps (fig. 3E) might have formed in two large foreshocks, 5 and 7 hrs before the main shock (Wallace, 1984). In 1981 near Corinth, Greece, three normal-faulting earthquakes ruptured in turn from west to east along the same trend over 9 days (Jackson and others, 1982; Vita-Finzi and King, 1985). Each produced a zone of surface ruptures about 10-15 km long, and the zones were separated by gaps about 10 km long. Across the eastern gap the faulting changed dip and stepped across strike about 10 km, resembling some geometric aspects of the Pleasant Valley and Fairview Peak-Dixie Valley rupture zones (figs. 3C, 3E).

Seismologically these sequences are resolvable into their individual events or even subevents. However, the geologic record of each sequence will look like the record of a single earthquake. Given the limits of present relative and absolute dating methods, it is possible that unrelated Holocene earthquakes that occurred several centuries apart might also be interpreted as a single earthquake. This inability to distinguish closely timed earthquakes might obscure some segment boundaries because we might misinterpret the ends of separate rupture zones from different earthquakes (fig. 3C) as discontinuities in the rupture zone from a single earthquake (fig. 3E). Alternatively, discontinuities in the rupture zone from a single earthquake (as at locality 2 of fig. 3E) could be misinterpreted as spurious segment

boundaries. These examples demonstrate that two coincident rupture ends on the same side of a segment boundary is a minimum but not optimal criterion for identifying the boundary.

Multiple Earthquakes

Variations in initial scarp morphology, later erosional modification of scarps, and uncertainties in radiometric and geomorphic dating make it difficult to correlate scarps from some single earthquakes or earthquake sequences (for example, Crone and others, 1987, p. 761-766). For most multiple-event scarps, their single-event components cannot be correlated along the scarps. However, mapping, trenching, scarp-morphology analysis, and related methods might show that the ends of a multiple-event scarp formed by about the same number of surface ruptures, during about the same span of time, as did the middle of the scarp. Then one could suggest that at least a few of the individual events had coincident ends at the ends of the composite scarp.

Gravity data can help identify boundaries that have persisted through much or all of the evolution of a fault zone. The data can identify bedrock ridges that separate hanging-wall basins (figs. 2A, 2B) filled with comparatively low-density Cenozoic materials. The basins appear as gravity lows and the bedrock ridges as gravity saddles (Zoback, 1983). Each boundary of table 1 coincides with a gravity saddle, and some coincide with exposed bedrock ridges. Surface measurements of slip per earthquake can reach 2-10 m in the fault zones and rupture zones of figure 3. The greatest slip is in segment interiors, and slip diminishes toward the segment boundaries. Structural relief between the bedrock ridges and the adjacent hanging-wall basins is typically hundreds of meters to a kilometer. Each such slip deficit is the cumulative effect of the ends of hundreds of large ruptures, so that at least a few successive rupture ends must have coincided on each side of a gravity saddle. This coincidence fulfills the minimum criterion for identification of a segment boundary. However, the boundary might have affected only the early evolution of the fault zone, especially if the bedrock ridge is completely buried and separated from the footwall by a through-going fault with large accumulated slip. Accordingly, to demonstrate that a boundary at a gravity saddle still tends to control ruptures, at least one individual rupture zone or a multiple-event scarp should be shown to end there.

BENDS, JOGS, AND SLIP VECTORS

Experience with strike-slip faults drew attention to bends (King and Nabelek, 1985) and dilational jogs (Sibson, 1985) in mapped fault traces. These reports suggested that large ruptures are likely to start and stop at bends, and to stop at dilational jogs. Thus, bends and jogs could be segment boundaries. The observations and models of King and Nabelek (1985) and Sibson (1985) explain why bends can act as both asperities and barriers, and jogs as barriers. Contrary to some recent usage, neither model applies simply to normal faults.

Bends

Bends are important because of their inferred role as nonconservative barriers (King and Nabelek, 1985). Strike slip cannot occur around a bend without deforming one or both fault walls near the bend (King, 1983), thereby

forming a volume of intensely faulted rock, the process zone of King and Nabelek (1985). The fault network of the process zone renders the zone soft enough to absorb and disperse the energy of incoming rupture tips sufficiently to stop them. The process zone slips little, has high fracture toughness, and therefore is a likely starting place for the next large rupture. In this way bends could be segment boundaries.

All this occurs only because the plane in which the bend appears (map view for strike slip) contains the slip vector, so that the orientation of the vector is not conserved across the bend (King, 1983; hence the term "nonconservative"). (The slip vector differs from the direction of rupture propagation, which is not considered in this report.) In contrast, normal faulting involves dip slip down the axis of the bend, so the curved fault walls can slide freely downdip along each other instead of being forced past each other along strike. Slip does not occur around the bend, the orientation of the slip vector is conserved, and the bend that is seen in map view has no effect on large ruptures.

King and Nabelek (1985) showed six examples of the traces of strike-slip rupture zones that started near map-view bends of 5°-40° (one rupture tip also propagated through a bend of 26°). In contrast, the 1983 Borah Peak rupture tip started near a northeast-concave bend of about 55°, propagated northwestward, and stopped near a fork that produced a 45° bend for one branch (table 2, fig. 3D). Dewey (1987) showed geometrically that even at the 55° bend near the epicenter, the orientation of the slip vector could be conserved around the bend. For normal faults that dip 30°-60° with bends as sharp as 90°, calculations show that the line of intersection of both arms of the bent fault surface can plunge to within about 10° as steeply as the fault dips. If slip occurs down this intersection, the orientation of the slip vector is conserved around the bend. Therefore, in a normal fault the presence of a bend, however sharp, by itself is no indication of a nonconservative barrier or a segment boundary. This conclusion is borne out by sharpnesses of bends in historic rupture zones (table 2); the only two bends at which surface ruptures had ends are, if anything, less sharp than the average.

To demonstrate the presence of a nonconservative barrier, slip-vector orientations could be determined on both arms of the bend, either (1) seismologically from at least one rupture on each arm, (2) geologically from slickenlines on both arms (Bruhn and others, in press), or (3) from cultural features that were offset by historic ruptures. The slickenlines are presumed to be superimposed records of several past ruptures associated with earthquakes of indeterminate but variable magnitudes; many measurements are needed to overcome the scatter in slickenline orientations.

Direct observation of bends in a viewing plane that contains the slip vector is difficult on normal faults because such a plane would be vertical, and the pertinent bends would be at hypocentral depths, near the base of the brittle upper crust where large earthquakes nucleate (Das and Scholz, 1983). Seismic-reflection profiles that could detect bends at such depths are few and expensive. To show that a bend lies at, and only at, the proposed segment boundary would require at least three profiles, one at the bend and one on each arm. Then slip-vector orientations near the bend could be estimated geometrically, analogously to the approach of Bruhn and others (in press).

Jogs

Sibson (1985) suggested that dilational jogs can stop a propagating rupture tip, and modeled a jog as a network of permeable fractures in a fluid-

TABLE 1.--Persistent segment boundaries (Summarized from Wheeler and Krystinik, in press)

[Structural expression: BBR, buried bedrock ridge; EBR, exposed bedrock ridge; SA, fault-bounded footwall salient; FS, footwall spur. Number of rupture ends: Numerals give minimum numbers. Numerals in parentheses are for ends on same side of boundary. Most prehistoric ends are of multiple-event scarps, which each count as at least two ends. Ends for Wasatch fault zone are from Machette and others (in press)]

Boundary name and locality	Structural expression	Number of rupture ends	
		Prehistoric	Historic
Wasatch fault zone, Utah (fig. 3A)			
Pleasant View (1)	BBR, SA	4(2)	0
Salt Lake (2)	BBR, SA	4(2)	0
Traverse Mountains (3)	EBR, FS, SA	4(2)	0
Payson (4)	EBR, SA	4(2)	0
Fairview Peak-Dixie Valley, Nevada (fig. 3C)			
Pirouette Mountain (1)	EBR	4(2)	2(1)
Borah Peak, Idaho (fig. 3D)			
Willow Creek Hills (1)	EBR	4(2)	1(1)
Elkhorn Creek (2)	BBR	4(2)	1(1)
Pleasant Valley, Nevada (fig. 3E)			
Sou Hills (1)	EBR	4(2)	1(1)

TABLE 2.--Bends (fig. 3), ranked by sharpness

Figure	Locality	Bend[1] (degrees)	Trace length around bend[1] (km)	Sharpness (deg/km)
3E	4	60	1	60
3E	5	44	1	44
3C	2	75	2	38
3B	2	105	3	35
3B	3	310	9	34
3B	1	55	2	28
3D	3	45	2	[2]22
3B	4	40	2	20
3D	2	[3]55	[3]4	[2]14
3E	3	60	6	10

[1]Measured on maps cited in figure 3, except where stated otherwise.

[2]Bend at end of main rupture of Borah Peak earthquake. Other bends are not at rupture-zone ends (fig. 3).

[3]Measured on Dubois, Idaho, 1:250,000 topographic map.

saturated crust. Slip from an incoming rupture dilates the network faster than the surrounding fluid can inflow, inducing a localized suction force that opposes dilation. Sibson (1985) calculated that overcoming the suction force could drain enough energy from a moderate-sized earthquake to stop the propagating rupture tip at the jog.

As is the case for bends, pertinent jogs are those visible in a viewing plane that contains the slip vector. For strike slip this plane can be a map view, but for dip slip the plane must be a cross section. Because large earthquakes tend to nucleate at the base of the brittle upper crust and propagate upward, an analogy with Sibson (this volume, fig. 5) shows that dilational jogs will form where normal faults flatten downward, not where they steepen downward. For pure normal faults, jogs that are able to stop the tips of large ruptures will lie at least several kilometers deep. Such jogs will be hard to detect.

However, slip on normal-oblique faults could create observable evidence of buried dilational jogs that might be associated with the strike-slip component of the oblique faulting. An illustratively frustrating example is the 1983 Borah Peak earthquake, the best studied so far in the Basin-Range. Slip was left-normal at the ground surface (Crone and Machette, 1984) and at the hypocenter (Richins and others, 1987). The northwest end of the main surface rupture forks, with one branch striking west (fig. 3D). The largest cluster of aftershocks was about 5-12 km deep, in the southwest-facing angle between the western branch and the main surface rupture (Richins and others, 1987). By analogy with Sibson's (this volume, after Nur and Booker, 1972) suggestion for aftershocks on strike-slip faults, this aftershock cluster might reflect fluid flowing down a pressure gradient into a dilated jog at depth; the slowly rising fluid pressure in the jog would reduce the frictional strengths of subsidiary faults and allow them to slip to produce a sequence of aftershocks.

However, Boatwright (1985) found that the aftershocks with greatest stress drops tended to cluster in this same angle. The high stress drops might be related to decreased fluid pressure in a jog that had just been dilated by the main shock. The decreased fluid pressure would cause increased normal stresses on faults that might slip to produce aftershocks, and increased strengths of these faults. The highest stress drops would require the lowest fluid pressure, and would occur soonest after the mainshock. For the analogy with Sibson's suggestion to be consistent with the inference drawn from Boatwright's finding, the high-stress-drop aftershocks would have to be the first to occur in the angle, indicating dilation and a drop of fluid pressure preceding inflow of fluid. Unfortunately, the high-stress-drop aftershocks were not among the first to occur in the angle (Boatwright, 1985, table 2, fig. 11; Richins and others, 1987, fig. 11A). The inference that a dilational jog underlies the northwest end of the main rupture zone of the Borah Peak earthquake appears to be inconsistent with either the locations or the stress drops of the aftershocks.

Geodetic modeling indicated that the Borah Peak rupture zone extended from the surface down to the hypocentral depth of 14-16 km (Doser and Smith, 1985; Dewey, 1987) on the main part of the rupture zone, but only down to 6 km deep under the western branch (Barrientos and others, 1987). These different depths are consistent with an interpretation that a rupture-stopping dilational jog lies deeper than about 6 km beneath the western branch of the surface rupture. However, Wheeler and Krystinik (in press) interpreted the same evidence in terms of a nonconservative barrier. The two interpretations can be shown to be consistent with each other, but data are too few to demonstrate that either is correct.

In summary, the effect of dilational jogs on propagating normal-fault ruptures is likely to be difficult to identify, as shown by the Borah Peak earthquake.

PERSISTENCE OF SEGMENT BOUNDARIES

Evaluating seismic hazard for a segmented normal fault requires estimating whether a specific segment boundary is likely to control the next few large ruptures on either adjacent segment. This likelihood is greatest for boundaries that have controlled ruptures persistently in the past. Normal faults in the Basin-Range exhibit spatial and temporal grouping of ruptures, and variations of short-term slip rates about long-term average slip rates (Wallace, 1987; Machette, this volume). A simulation experiment showed that this grouping can arise randomly (Machette, this volume). More likely, the grouping arises from deterministic physical processes that are so complex and poorly understood that their results are indistinguishable from the effects of random processes.

On a fault with permanent segment boundaries, this variable behavior will affect only the time spans between ruptures (the simulation experiment used permanent boundaries). However, the variable behavior, and likely variations in the mechanical properties and shapes of different patches of fault walls that are successively juxtaposed, indicate that some segment boundaries might be nonpersistent, that is, they might control a few successive large ruptures but few or none before or after. Wheeler and Krystinik (in press) recognized four segment boundaries in the pre-Cenozoic geologic and geophysical record of the Wasatch fault zone. Machette and others (1986) recognized these four boundaries plus five others, all in the late Quaternary record. Wheeler and Krystinik (in press) suggested that the four boundaries recognized in the late Quaternary and pre-Cenozoic records are persistent, whereas the other five might be nonpersistent.

Possible Causes of Nonpersistent Boundaries

Although nonpersistent boundaries have not yet been identified, probably they exist on normal faults for three reasons. This probability is important because coincident ends of a few young ruptures can identify a segment boundary but cannot demonstrate its persistence. (Sibson (this volume) observed that many bends and jogs on strike-slip faults are transitory.)

1. Nonpersistence is inherent in segmentation, because eventually any segment boundary must rupture at depth, or the fault would end there. King (1986) reasoned that a nonconservative barrier should be offset by only small slips at the rupture tips. He suggested that these small slips might not be large enough to penetrate the near-surface zone of stress relaxation and rupture the ground surface. This suggestion is consistent with any observed lack of surface rupture at ramps, warps, and unfaulted bedrock ridges. However, eventually these areas must rupture because strata cannot stretch indefinitely at low confining pressures as the structural relief increases at the fault.
2. Bruhn and Parry (this volume) suggested that stress corrosion, transient slip-induced changes in permeability and porosity, and fluid-rock reactions might enhance failure of asperities. Similarly, these processes also might affect the ability of dilational jogs to stop ruptures. As continuing slip on a lithologically and geometrically heterogeneous normal fault produces new asperities and jogs, these processes might shorten their effective lifetimes and reduce their persistence.

3. If the intermediate principal stress (S_2) is close in magnitude to the maximum (S_1) or minimum principal stress (S_3) on part of the fault, then slip nearby could perturb stresses so that S_2 interchanges with another principal stress. If S_2 is close to S_1 in a north-striking normal fault zone (fig. 4A), the perturbation could interchange normal slip on north-striking fractures with strike slip on northeast- or northwest-striking fractures. If S_2 is close to S_3 instead (fig. 4B), then perturbation could interchange normal slip on north-striking and east-striking fractures. The slip on east-, northeast-, and northwest-striking fractures could form the interlocking fracture network of a process zone, or might decouple adjacent parts of the main fault zone from each other. Either outcome would form a new segment boundary. Thus, a rupture tip entering a recently perturbed part of the stress field could encounter a new nonpersistent boundary. After perturbation ceased, slip would repeat itself, with constant sense on faults of constant strike. The repeated slip would fracture through the unrenewed process zone and end the nonpersistent boundary.

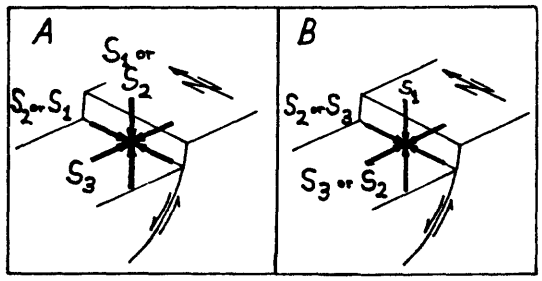

FIGURE 4.--Stress perturbation can interchange reactivation of differently oriented, preexisting fractures in a normal-fault zone. A, S_1 and S_2 are close in magnitude and interchange. Vertical S_1 favors normal reactivation of north-striking fractures, whereas vertical S_2 favors strike-slip reactivation of northeast- and northwest-striking fractures. B, S_2 and S_3 are close in magnitude and interchange. North-trending S_2 favors normal reactivation of north-striking fractures, whereas north-trending S_3 favors normal reactivation of east-striking fractures.

Criteria for Recognizing Persistent Boundaries

Wheeler and Krystinik (in press) identified four persistent segment boundaries on the Wasatch fault zone at large salients, which comprise bedrock ridges, and faulted and unfaulted footwall projections into the hanging wall (table 1). The salients have hundreds to thousands of meters of structural relief. From the estimated slip per rupture and age of the fault zone, Wheeler and Krystinik (in press) concluded that the salients acquired their structural relief by accumulating slip deficits at the ends of large rupture zones through much or all of the fault zone's history. Thus, salients and bedrock ridges with large structural relief identify persistent geometric segmentation of the Wasatch fault zone.

The geometry of the fault zone evolved by slip in thousands of individual rupture zones. Geometric segmentation of the fault zone does not imply seismic segmentation of the individual rupture zones. However, if scarps of the last rupture zones end at a salient or bedrock ridge suspected of being a persistent geometric boundary, then the geometric boundary is also a seismic boundary. This is the case at the four salients of the Wasatch fault zone (Machette and others, in press). Persistent boundaries in other fault zones

are also characterized by young scarp-ends that coincide with salients, transverse bedrock ridges, or similar changes in fault geometry that involve large changes in structural relief (table 1). Accordingly, these characteristics appear to identify persistent boundaries that will likely control the next few large ruptures near these boundaries.

CONCLUSIONS

A minimum criterion for identifying a segment boundary on a normal fault is that two individual large rupture zones on the same side of the proposed boundary have ends there. Study of multiple-event scarps or of the structures produced by large cumulative slip deficits can indicate that many ruptures have ended at the proposed boundary. If so, then fewer individual rupture ends are needed to meet the minimum criterion.

Interpretation of bends and dilational jogs as segment boundaries is simplified if the slip vector lies in the plane in which the bend or jog is viewed. Thus, using map views to identify bends and jogs is appropriate for strike-slip faults but misleading for normal faults.

Hazard evaluation needs to consider the persistence of segment boundaries as a guide to whether a boundary will likely control the next large ruptures. The boundaries that are most likely to do this are those that have persistently controlled large ruptures during the evolution of the fault zone, and at which the last one or more large ruptures have ended.

Many of the arguments and observations of this report can be recast to apply to reverse faults.

ACKNOWLEDGMENTS

The manuscript and I have benefited from discussions, preprints, unpublished data, and patient corrections from R.L. Bruhn, R.C. Bucknam, A.J. Crone, G.C.P. King, M.N. Machette, S.P. Nishenko, J.M. Pechmann, S.F. Personius, and R.H. Sibson.

REFERENCES CITED

Barrientos, S.E., Stein, R.S., and Ward, S.N., 1987, Comparison of the 1959 Hebgen Lake, Montana and the 1983 Borah Peak, Idaho, earthquakes from geodetic observations: Bulletin of the Seismological Society of America, v. 77, p. 784-808.

Boatwright, John, 1985, Characteristics of the aftershock sequence of the Borah Peak, Idaho, earthquake determined from digital recordings of the events: Bulletin of the Seismological Society of America, v. 75, p. 1265-1284.

Bonilla, M.G., Mark, R.K., and Lienkaemper, J.J., 1984, Statistical relations among earthquake magnitude, surface rupture length, and surface fault displacement: Bulletin of the Seismological Society of America, v. 74, p. 2379-2411.

Bruhn, R.L., Gibler, P.R., Houghton, W., and Parry, W.T. (in press) Structure of the Salt Lake segment, Wasatch normal fault zone--Implications for rupture propagation during normal faulting, in Hays, W.W., and Gori, P.L., eds., Evaluation of regional and urban earthquake hazards and risk in Utah: U.S. Geological Survey Professional Paper.

Crone, A.J., and Machette, M.N., 1984, Surface faulting accompanying the Borah Peak earthquake, central Idaho: Geology, v. 12, p. 664-667.

Crone, A.J., Machette, M.N., Bonilla, M.G., Lienkaemper, J.J., Pierce, K.L., Scott, W.E., and Bucknam, R.C., 1987, Surface faulting accompanying the Borah Peak earthquake and segmentation of the Lost River fault, central Idaho: Bulletin of the Seismological Society of America, v. 77, p. 739-770, 3 folded plates.

Das, Shamita, and Scholz, C.H., 1983, Why large earthquakes do not nucleate at shallow depths: Nature, v. 305, p. 621-623.

Dewey, J.W., 1987, Instrumental seismicity of central Idaho: Bulletin of the Seismological Society of America, v. 77, p. 819-836.

Doser, D.I., 1986, Earthquake processes in the Rainbow Mountain-Fairview Peak-Dixie Valley, Nevada, region 1954-1959: Journal of Geophysical Research, v. 91, no. B12, p. 12,572-12,586.

Doser, D.I., and Smith, R.B., 1985, Source parameters of the 28 October 1983 Borah Peak, Idaho, earthquake from body wave analysis: Bulletin of the Seismological Society of America, v. 75, p. 1041-1051.

Jackson, J.A., Gagnepain, J., Houseman, G., King, G.C.P., Papadimitriou, P., Soufleris, C., and Virieux, J., 1982, Seismicity, normal faulting, and the geomorphological development of the Gulf of Corinth (Greece)--The Corinth earthquakes of February and March 1981: Earth and Planetary Science Letters, v. 57, p. 377-397.

King, Geoffrey, 1983, The accomodation of large strains in the upper lithosphere of the Earth and other solids by self-similar fault systems--The geometrical origin of b-value: Pageoph, v. 121, p. 761-815.

King, G.C.P., 1986, Speculations on the geometry of the initiation and termination processes of earthquake rupture and its relation to morphology and geological structure: Pageoph, v. 124, p. 567-585.

King, Geoffrey, and Nabelek, John, 1985, Role of fault bends in the initiation and termination of earthquake rupture: Science, v. 228, p. 984-987.

Machette, M.N., 1986, History of Quaternary offset and paleoseismicity along the La Jencia fault, central Rio Grande rift, New Mexico: Bulletin of the Seismological Society of America, v. 76, p. 259-272.

Machette, M.N., Personius, S.F., and Nelson, A.R., 1986, Late Quaternary segmentation and slip-rate history of the Wasatch fault zone, Utah [abs.]: Transactions of the American Geophysical Union, v. 67, no. 44, p. 1107.

_____(in press) Quaternary geology along the Wasatch fault zone--Segmentation, recent investigations, and preliminary conclusions, in Hays, W.W., and Gori, P.L., eds., Evaluation of regional and urban earthquake hazards and risk in Utah: U.S. Geological Survey Open-File Report.

Myers, W.B., and Hamilton, Warren, 1964, Deformation accompanying the Hebgen Lake earthquake of August 17, 1959--The Hebgen Lake, Montana, earthquake of August 17, 1959: U.S. Geological Survey Professional Paper 435-I, p. 55-98, 2 folded plates.

Nur, Amos, and Booker, J.R., 1972, Aftershocks caused by pore fluid flow?: Science, v. 175, p. 885-887.

Richins, W.D., Pechmann, J.C., Smith, R.B., Langer, C.J., Goter, S.K., Zollweg, J.E., and King, J.J., 1987, The 1983 Borah Peak, Idaho, earthquake and its aftershocks: Bulletin of the Seismological Society of America, v. 77, p. 694-723.

Schwartz, D.P. and Coppersmith, K.J., 1984, Fault behavior and characteristic earthquakes--Examples from the Wasatch and San Andreas fault zones: Journal of Geophysical Research, v. 89, no. B7, p. 5681-5698.

Sibson, R.H., 1985, Stopping of earthquake ruptures at dilational fault jogs: Nature, v. 316, p. 248-251.

Slemmons, D.B., 1957, Geological effects of the Dixie Valley-Fairview Peak, Nevada, earthquakes of December 16, 1954: Bulletin of the Seismological Society of America, v. 47, p. 353-375, 1 folded plate.

Slemmons, D.B., Steinbrugge, K.V., Tocher, Don, Oakeshott, G.B., and Gianella, V.P., 1959, Wonder, Nevada, earthquake of 1903: Bulletin of the Seismological Society of America, v. 49, p. 251-265, 2 folded plates.

Snay, R.A., Cline, M.W., and Timmerman, E.L., 1985, Dislocation models for the 1954 earthquake sequence in Nevada, in Stein, R.S., and Bucknam, R.C., eds., Workshop XXVIII On the Borah Peak, Idaho, earthquake, 3-6 October, 1984, Proceedings, v. A: U.S. Geological Survey Open-File Report 85-290, p. 531-555.

Swan, F.H., III, Schwartz, D.P., and Cluff, L.S., 1980, Recurrence of moderate to large magnitude earthquakes produced by surface faulting on the Wasatch fault zone, Utah: Bulletin of the Seismological Society of America, v. 70, p. 1431-1462.

Tocher, Don, 1956, Movement on the Rainbow Mountain fault: Bulletin of the Seismological Society of America, v. 46, p. 10-14, 3 folded unnumbered plates.

Vita-Finzi, C., and King, G.C.P., 1985, The seismicity, geomorphology, and structural evolution of the Corinth area of Greece: Philosophical Transactions of the Royal Society of London, Series A, v. 314, p. 379-407.

Wallace, R.E., 1984, Fault scarps formed during the earthquakes of October 2, 1915, in Pleasant Valley, Nevada, and some tectonic implications: U.S. Geological Survey Professional Paper 1274-A, p. A1-A33, 1 folded plate.

_____1987, Grouping and migration of surface faulting and variations in slip rates on faults in the Great Basin province: Bulletin of the Seismological Society of America, v. 77, p. 868-876.

Wheeler, R.L., and Krystinik, K.B. (in press) Persistent and nonpersistent segmentation of the Wasatch fault zone, Utah--Statistical analysis for evaluation of seismic hazard, in Hays, W.W., and Gori, P.L., eds., Evaluation of regional and urban earthquake hazards and risk in Utah: U.S. Geological Survey Professional Paper.

Zoback, M.L., 1983, Structure and Cenozoic tectonism along the Wasatch fault zone, Utah, in Miller, D.M., Todd, V.R., and Howard, K.A., eds., Tectonics and stratigraphy of the eastern Great Basin: Geological Society of America Memoir 157, p. 3-27.

REPEATING EARTHQUAKES AND THE GEOMETRY OF FAULTS

William L. Ellsworth
U.S. Geological Survey
345 Middlefield Road
Menlo Park, California 94025

ABSTRACT

Geologic evidence of fault segmentation and the characteristic size of the coseismic slip on a given segment are combined with the seismological evidence for repeating earthquakes, the magnitude-independence of stress drop, and the Gutenberg-Richter frequency-magnitude relation to outline a conceptual model for seismicity. The persistence of individual segments through repeated slip episodes, as can be deduced from the geologic record, suggests that the geometry of the segments themselves plays a critical role in the rupture process. It is proposed that the observed self-similar distribution of segments forms the set of potential slip surfaces for the next rupture. If we further assume that individual fault segments fail along their entire length once dynamic rupture initiates, a scaling law for fault segments is derived. For faults with b-values of 1, it states that for each segment of a given size an equal area of the fault is segmented into an infinite number of smaller fault segments according to a power-law distribution.

INTRODUCTION

Multiple lines of geological and seismological evidence developed in recent years support the hypothesis that the amount of coseismic slip on a fault segment is a characteristic property of that segment (Schwartz and Coppersmith, 1984), with eventful slip at a fixed point on the segment varying by a factor of 2 from repeat to repeat (Sieh, 1986). It has also been recognized that the magnitude of the earthquake resulting from slip on the segment may also vary, particularly when adjacent fault segments either rupture or fail to rupture in the same event. Examples of this behavior range from variations in rupture length for great earthquakes in the Nankai Trough in southwestern Japan (Mogi, 1981) to seismically measureable differences in moment and source areas between successive repeats of events with common centroids on the San Andreas (Ellsworth and Dietz, 1987). While these observations collectively imply that the characteristic earthquake hypothesis, as originally posed by Schwartz and Coppersmith (1984) (equivalently, the uniform-earthquake model of Sieh, 1981), is not univesally valid, the central kernel of truth remains that segments rupture with a characteristic displacement.

In this paper the implications of this observation and the universal observation that faults are segmented structures are used to develop a conceptual model for seismicity.

Geometry of Faults

As any student of fault structure quickly learns that, faults are complex geometric structures which bear only a vague relationship to the "fault plane" that has been

employed with great success to study their kinematic properties. At any scale of mapping, segmentation of the fault into multiple dislocation surfaces is apparent, and this segmentation extends to smaller scale lengths in a scale-independent manner (Tchalenko, 1970). Thus, the geometric structure of faults appears to be without characteristic dimension, aside from that imposed by the finite length and width of the total fault zone, and it may be said that faults exhibit a fractal geometry (Okubo and Aki, 1987). From a purely mathematical standpoint, this implies that a power law describes the population density of segments of different size within any fault zone.

Another key, if almost trivial, feature of fault segments is their longevity. They must endure as slowly evolving features of the fault system. Otherwise, a fault would resemble a uniform gouge zone, with the most recent rupture appearing as an ephemeral marker. Instead, we know that pull-apart basins and pressure ridges characteristically form at jogs and steps in strike-slip faults, for example. They clearly represent the product of geometrically-stable, long-term movement of the fault in an amount that greatly exceeds the slip in any single event.

Given the presistence of individual segments through many earthquake cycles and the suggestion that event slip on a single segment falls in a narrow range, it is both reasonable and consistent to propose that individual segments fail in their entirety during the dynamic rupture of an earthquake. The amount of slip (u) is governed by the length ($2r$) of the segment itself, and the stress drop ($\Delta\sigma = u/r$) falls in a narrow range, as has been long-established from seismic observations (for example, Kanamori and Anderson, 1974). Should adjacent sements also fail in the same event, the magnitude of the earthquake will grow because of a greater extent of rupture and possibly because of dynamic effects which perturbs the slip on any given segment toward the upper end of its range.

Repeating Earthquakes

Geologic evidence of the behavior of individual segments is complimented by seismological evidence on multiple recurrences of the "same" earthquake. From observations of two to five repetitions of the same seismic source for earthquakes of about M 2 (Frechet, 1985), M 4 – 5 (Ellsworth and Dietz, 1987) and $M6$ (Bakun amd McEvilly, 1984), it is clear that many if not all positions on the San Andreas fault in central California are characterized by rupture in events of nearly fixed magnitude. Specifically, a region on the fault which fails in an event of M 4.0 fails only in events of this size, unless it is dynamically coupled to failure of a larger region, resulting in a substantially larger earthquake. Because the details of the stress-boundary conditions for any given point on the fault must vary from cycle to cycle, it seems implausible that the state of stress governs the size of the next event. Rather, it must be the enduring geometric features of the fault which control the nearly constant event magnitude which is observed.

At present, the seismological evidence is inconsistent with either the time-predictable, slip-predictable or uniform earthquake models, even after allowance is made for the observed variations in seismic moment. While the structure of the recurrence intervals currently lacks an obvious explanation, they scatter through the same time range about their mean value as has been found in geologic studies on recurrence at a single point on the fault (standard deviation of approxiately $\frac{1}{3}$ the mean). The mean interevent time

scales approximately as $M_o^{1/3}$, which is consistent with the constant-stress-drop hypothesis, and with a variability compatible with the observed range of $\Delta\tau$.

The short of the seismological evidence is that it too is compatible with the hypothesis that individual segments fail as a unit and produce earthquakes of nearly constant size. This suggestion is, of course, not new, and has been used as evidence for "stuck patches" or "asperities" on the fault plane. The critical difference here is the suggestion that the realization of these irregularities on the fault plane is the geometric nature of fault segmentation itself. In an attempt to tie these ideas together, we next examine their implications for earthquake statistics.

Scaling Law for Fault Segments

The Gutenberg-Richter relation between the frequency of earthquake occurrence (N) and their magnitude (M), $logN = a - bM$ can be transformed into a power law using the relation between magnitude (M) and seismic moment (M_o), $logM_o = C\,M + d$

$$N(M_o) = \alpha M_o^{-\beta}$$

where $\beta = b/c$.

Following Molnar (1979), the density function is $-dN/dM_o \equiv \alpha\beta\, n(M_o) = M_o^{-\beta-1}$. This formula describes how many times sources producing earthquakes of size M_o occur in the sample, but not how many sources exist.

Consider now a single fault composed of non-overlapping segments, each of which may produce only events with a fixed moment. If we also assume that the long-term slip rate is the same everywhere along the fault and that the stress drop, $\Delta\sigma$, is independent of M_o, it follows that the average time between repeated failure on a specific segment (T) is proportional to $M_o^{1/3}$. Measured over a time interval, t, the number of times each segment will fail is t/T, or inversely proportional to $M_o^{1/3}$. We may then write the density function $n(M_o)$ as

$$n(M_o) = \rho(M_o)\, M_o^{-1/3}\, k,$$

where $\rho(M_o)$ is the fault segment density distribution. It follows that $\rho(M_o)$ is given by the power law

$$\rho(M_o) = \alpha\beta\, M_o^{-\beta-2/3}.$$

Because smaller segments must produce many more events per unit time for this slip rate to keep pace with larger segments, the total number of such segments will be far fewer than that implied by the Gutenberg-Richter relation. Using typical values for $b = 1$ and $c = 1.5$ ($\beta = 2/3$), it is easy to show that the total number of segments grows by a factor of 10 for a two-unit change in M(10^3 change in M_o), while the number of events grows by 100-fold. A specific prediction of the model is the frequency-magnitude distribution of repeating earthquake sources and their interevent time distribution.

It is also of interest to examine the area of the fault plane occupied by segments of different sizes. Under the assumption of constant stress drop, the area of a single seg-

ment scales as $M_o^{2/3}$. The total area represented by all sources up through size M_o' is then

$$A = \int_0^{M_o} (M_o / M_o')^{2/3} \rho(M_o)\, dM_o$$

where the area of M_o' is taken as unity. Evaluating the integral with $\int_0^{M_o'} \rho(M_o)\, dM_o \equiv 1$, we find that $A = (\beta - 1/3)(1 - \beta)$. When $\beta = 2/3, A = 2$. This means that the total area covered by fault segments of size smaller than the segment producing an event with moment M_o' is equal to the area of that segment. A systematic study of the distribution of segments should provide a direct comparison with this prediction. However, it should be noted that the fractional area of the fault capable of seismic slip may be less than unity if it creeps or deforms ductally.

Concluding Remarks

At this stage, the model for seismicity outlined above is crude, untested, and subject to invalidation on both geoological and seismologial grounds. My main purpose is to suggest areas where future work may shed new light on the earthquake process. Among these are: (1) better definition of the observed relationship between segmentation and rupture termination, (2) elucidation of the systematics of repeating earthquakes over a wide magnitude range, particularly along a single fault segment, (3) development of dynamic models of faulting which incorporate fault geometry in as realistic a manner as possible, and (4) exploration of the physical basis of the emperical statistical laws of seismicity as governed by observable parameters of faults and the earthquakes they produce.

REFERENCES CITED

Bakun, W.H., and McEvilley, T.V., 1984, Recurrence models and Parkfield, California earthquakes: Journal of Geophysical Research, v. 89, p. 3051-3058.

Ellsworth, W.L., and Dietz, L.D., in press, Preliminary results on the temporal stability of coda waves in central California from high- precision measurements of characteristic earthquakes: In Proceedings of workshop on intermediate-term earthquake precursors: U.S. Geological Survey Open-File Report, 22 p.

Frechet, Julien, 1985, Seismogenese et doublets seismiques: These d'Etat, Universite Scientifique et Medicale de Grenoble, France, 207 p.

Kanamori, Hiroo., and Anderson, D.L., 1975, Theoretical basis of some emperical relations in seismology: Bulletin of the Seismological Society of America, v. 65, p. 1073-1095.

Mogi, K., 1981 Seismicity in western Japan and long-term earthquake forecasting, in, Simpson, D.W., and Richards, P.G., eds., Earthquake prediction An International review: Maurice Ewing Series 4, American Geophysical Union, p. 181-207.

Molnar, P., 1979, Earthquake recurrence intervals and plate tectonics: Bulletin of the Seismological Society of America, v. 69, p. 115- 133.

Okubo, P., and Aki, K., 1987, Fractural geometry in the San Andreas fault system: Journal of Geophysical Research, v. 92, p. 345-355.

Schwartz, D.P., and Coppersmith, K.J., 1984, Fault behavior and characteristic earthquakes–Examples from the Wasatch and San Andreas fault zones: Journal of Geophysical Research, v. 89, p. 5681-5698.

Sieh, K.E., 1981, A review of geologic evidence for recurrence times of large earthquakes: in D.W. Simpson and Richards, P.G., eds., Earthquake prediction–An International Review: Maurice Ewing Series 4, American Geophysical Union, p. 181-207.

_____1986, Slip rate across the San Andreas fault and prehistoric earthquakes at Indio, California [abs.]: EOS, Transactions, American Geophysical Union, v. 67, p. 1200.

Tchalenko, J. S., 1970, Similarities between shear zones of different magnitudes: Geological Society of America Bulletin, v. 81, p. 1625-1640.

CHARACTERIZATION OF INTRAPLATE SEISMIC SOURCE ZONES

by

Arch C. Johnston
Center for Earthquake Research
Memphis State University
Memphis, Tennessee 38152

ABSTRACT

The link between intraplate seismic source zones and paleoseismicity is one forged by necessity: most intraplate zones have such long recurrence intervals between significant earthquakes that paleoseismic investigations offer the best—or perhaps only—hope of quantifying the associated seismic hazard. A classification scheme is proposed with the objective of clarifying the definition and use of seismic source zones in intraplate and particular stable continental environments. Frequently in hazard analyses, seismic source zones are delineated on the basis of fragmentary evidence, far removed from the ideal of an identified seismogenic fault. This paper examines the criteria used in estimating seismic hazard in intraplate regions and discusses several promising research areas, especially paleoseismology, which can improve this admittedly imperfect process.

INTRODUCTION AND BACKGROUND

Paleoseismic studies have been applied most successfully along plate boundary seismic zones or in regions of geologically young (Mesozoic to Cenozoic) tectonic activity where active fault traces can be identified and analyzed. Much of the continental land mass of the world, however, is old and relatively stable. In these regions large earthquakes, though they exist, are rare, and surface expression of the faulting is rarer still. Recurrence intervals between significant events are roughly an order of magnitude greater than for plate boundaries, raising the fear that the historical seismicity record may at best be a poor indicator of future activity and at worst a misleading one. Paleoseismic methods—specifically the dating of liquefaction features preserved in unconsolidated sediments—only recently have been brought to bear on the recurrence estimation problem by Russ (1982) in New Madrid, and Obermeier and others (1985) and Talwani and Cox (1985) in the Charleston, S.C., vicinity.

The concept of a "seismic source zone" is in itself an admission of lack of knowledge. Abundant seismological evidence indicates that shallow earthquakes (and probably all earthquakes) are satisfactorily modeled as shear failures on planar or at least tabular features we call faults. Seismic source zones, then, represent a geographic region which is judged to contain at least one and perhaps a collection of seismogenic faults. Seismic parameters—principally the frequency-magnitude relation and maximum magnitude earthquakes—are assumed to be homogeneous throughout the zone. Along plate boundaries and large regions of the Western United States, seismic source zones can be restricted rather confidently to mapped fault zones, although the likelihood of surprise remains (for example, the Coalinga earthquake for which the causative fault was concealed by an anticline ridge structure of Pliocene and younger age (Clark and others, 1983)).

In the central and Eastern United States (CEUS) seismic source zones are discouragingly large, reflecting a high degree of uncertainty in their definition. Moreover, in an exercise in which 13 'experts' were requested by Lawrence Livermore

National Laboratory (LLNL) to independently zone the CEUS, the divergence of the maps was quite startling, as was the range of criteria that the experts applied in delineating the source zones (Bernreuter and others, 1984; fig. 3 in Anderson, 1986). Most weight was given to historical seismicity patterns, with tectonic structure and orientation to the regional stress regime also ranking in importance, but the emphasis and interpretation of each expert varied greatly.

One can conclude from the LLNL project, as well as similar ones conducted for the U.S. Geological Survey (Algermissen and others 1982) and the Electric Power Research Institute (EPRI, 1985), that the definition and delineation of intraplate seismic source zones in the absence of surface-fault rupture is a subjective, nearly intuitive, exercise. Given the present state of understanding of the earthquake process, it cannot be quantified. The purpose of this paper is to provide a more systematic, though still qualitative, framework for seismic source zonation through classification of generalized characteristics.

INTRAPLATE SEISMIC SOURCE ZONES

The proposed classification of intraplate seismic source zones (ISSZ) allows these regions to be usefully characterized for seismic-hazard analysis while incorporating current uncertainty as to just what constitutes an ISSZ. As used here, the term "intraplate" is best defined as what it is not; it excludes all features on which plate contact seismicity occurs or zones directly associated with plate margins in which it is clear that relative platemotions are accomodated, even though slip vectors may not be oriented subparallel to the relative plate motion vector. Examples of "interplate" seismic source zones include actual plate boundaries, subsidiary faults in the San Andreas system (for example, the Hayward, the Calaveras, the San Jacinto faults), and outer-rise or overriding-wedge earthquakes in subduction zones. ISSZs, then, would include all other regions in which earthquakes occur. The distinction between interplate and intraplate is most difficult in regions such as south- central Asia or the western North America Cordillera where plate motion is distributed over a broad zone. In this discussion, I will include these regions in the intraplate category. The intraplate designation can then be further subdivided according to whether a region is subject to significant Mesozoic/Cenozoic tectonic activity. If this is absent, I term the region "stable continental interior" (SCI). It is in these SCI regions that active surface faulting is rare, and consequently, precision and confidence in delineating ISSZs is lacking. In addition, oceanic intraplate seismicity is significant in some regions but will not be considered here.

ISSZ Classification

I propose a classification (table 1) for continental intraplate seismic source zones (ISSZs) in which all intraplate regions are assigned to one of six categories, depending on known (or unknown) tectonic, geologic, and seismological characteristics.

TABLE 1–Continental intraplate seismic source zones

CATEGORY	NAME	DESCRIPTION
1.	ASEISMIC	An ISSZ in which no significant seismic activity is known. Moreover, the region is understood well enough geologically and geophysically to exclude with high confidence the possibility future significant earthquakes.
2.	SEISMOGENIC	A specific geologic entity (usually a fault) which can be defined geologically or geophysically and, on which, earthquakes are known to have occurred, or there is evidence of prehistoric earthquakes.
3.	SEISMOTECTONIC	A clearly defined tectonic feature such as a fault zone, rift, suture, intrusion, etc. with which seismicity is spatially associated, but a clear association with a specific fault or faults is lacking.
4.	SEISMIC	A region where seismicity is "enhanced over background" and spatial clustering is evident, but data are insufficient to associate the activity with seismogenic or seismotectonic crustal structures.
5.	TECTONIC	Geologic or geophysical data resolve a crustal feature that elsewhere is known to be associated with earthquakes, but in this case no instrumental, historical, or paleoseismic data exist that suggest the feature has experienced significant seismicity.
6.	BACKGROUND	A region with no known significant seismicity or geological/tectonic feature capable of significant earthquakes, but the data are too poor to exclude with confidence their existence.

Categories 1 through 6 imply a steplike transition from abundant data that clearly define an ISSZ to a virtual lack of data for background zones. In actuality the transitions are, of course, gradational. Moreover, as new data are acquired and knowledge improves, geographic regions can be reclassified into new, better constrained ISSZs. One of the primary objectives of seismic hazard research is to move category 2–6 zones—where most continental intraplate ISSZs now would be classified—into category 1 or 2.

Examples

Several examples, drawn primarily from North America, are presented here to illustrate the proposed classification.

Aseismic ISSZ. In general, Precambrian continental shield interiors, for example, the Canadian, Brazilian and Siberian shields, but in areas removed from large-scale tectonic features such as suture zones or continental margins.

Seismogenic ISSZ. Identified active faults as in the Western United States intermountain belt or the Australian Yilgarn block (fig. 1). The Meers fault in southwest Oklahoma is a rare example of a seismogenic ISSZ in a SCI.

Seismotectonic ISSZ. The New Madrid seismic zone (fig. 2) is an archetypical example.

Seismic ISSZ. Charleston, S.C.; Anna, Ohio; the southern Appalachians of eastern Tennessee (fig. 3).

Tectonic ISSZ. The Grenville front (suture), and the Central North American rift system and the Cameroun line (rift) of west Africa are major tectonic structures that are nearly aseismic.

Background ISSZ. Most of the United States Atlantic seaboard; most of the Antarctic continent.

The fundamental problem of most intraplate seismic source zonation in SCI regions is that seismogenic faults cannot be identified. Surface rupture is usually absent even for large SCI earthquakes. Geophysical techniques have been unsuccessful in identifying individual active faults at depth. Until this situation improves, seismic zonation in stable continental interiors will suffer from high uncertainty in delineating ISSZs.

DISCUSSION AND CONCLUSIONS

A recent and ongoing study (Coppersmith and others, 1987) that assesses the occurrence of SCI seismicity on a worldwide basis provides a comprehensive look at these poorly understood events. To counter the probability that the observational record is neither sufficiently long nor complete, data from significant ($M \geq 5.0$) earthquakes in SCI regions throughout the world are combined to form a global data base. Stable continental interiors are defined as regions geologically and tectonically analogous to North America east of the Rocky Mountain Cordillera. Analogue SCI regions therefore are of continental character and contain no crust with Mesozoic/Cenozoic deformation or significant Neogene rifting or igneous activity. Worldwide, fewer than 20 earthquakes of magnitude $M \geq 7.0$ have occurred in SCI regions, and the level of seismicity varies widely on a continent-size scale. Most large events have been preceded by known historical or instrumental seismicity, and have occurred in Paleozoic-age rather than Precambrian-age crust. A compressive horizontal deviatoric-stress regime dominates, producing largely thrust and strike-slip earthquakes. The total data set of over 500 $M \geq 5.0$ earthquakes are most frequently associated with continental rifts of Mesozoic or younger age, continental margins, or suture zones. Earthquakes of magnitude 5-7 occur in a variety of tectonic environments, but those that exceed magnitude 7 are restricted nearly exclusively to zones of Mesozoic rifting (imbedded or continental margin).

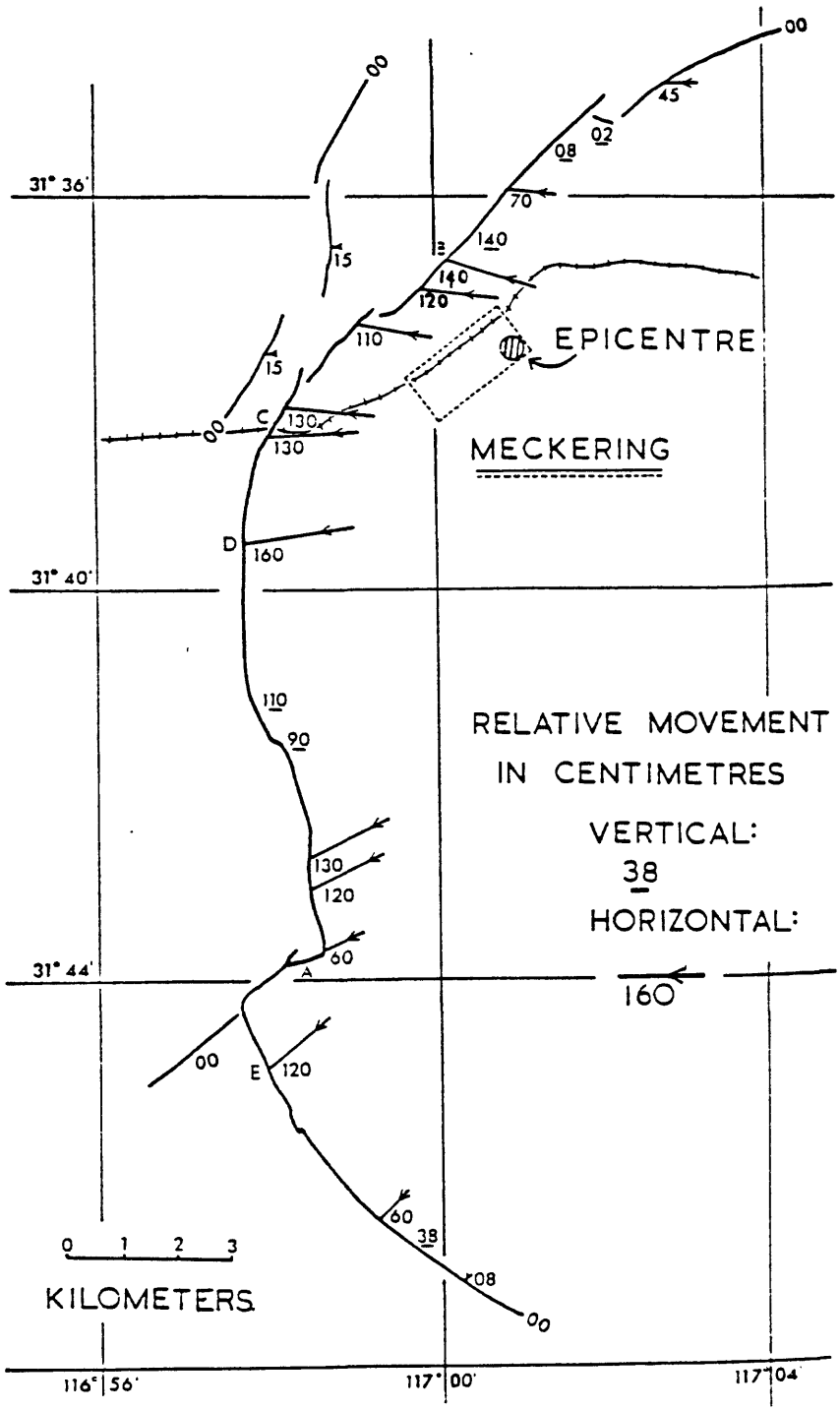

FIGURE 1.—Fault scarp of the 1968 M_s 6.8 Meckering earthquake in the Archean Yilgarn block of Western Australia (from Everingham and others, 1969). This is one of the rare examples of a SEISMOGENIC ISSZ (table 1) in a stable continental environment. Five of eight documented cases of surface rupture in SCI regions are from Australia.

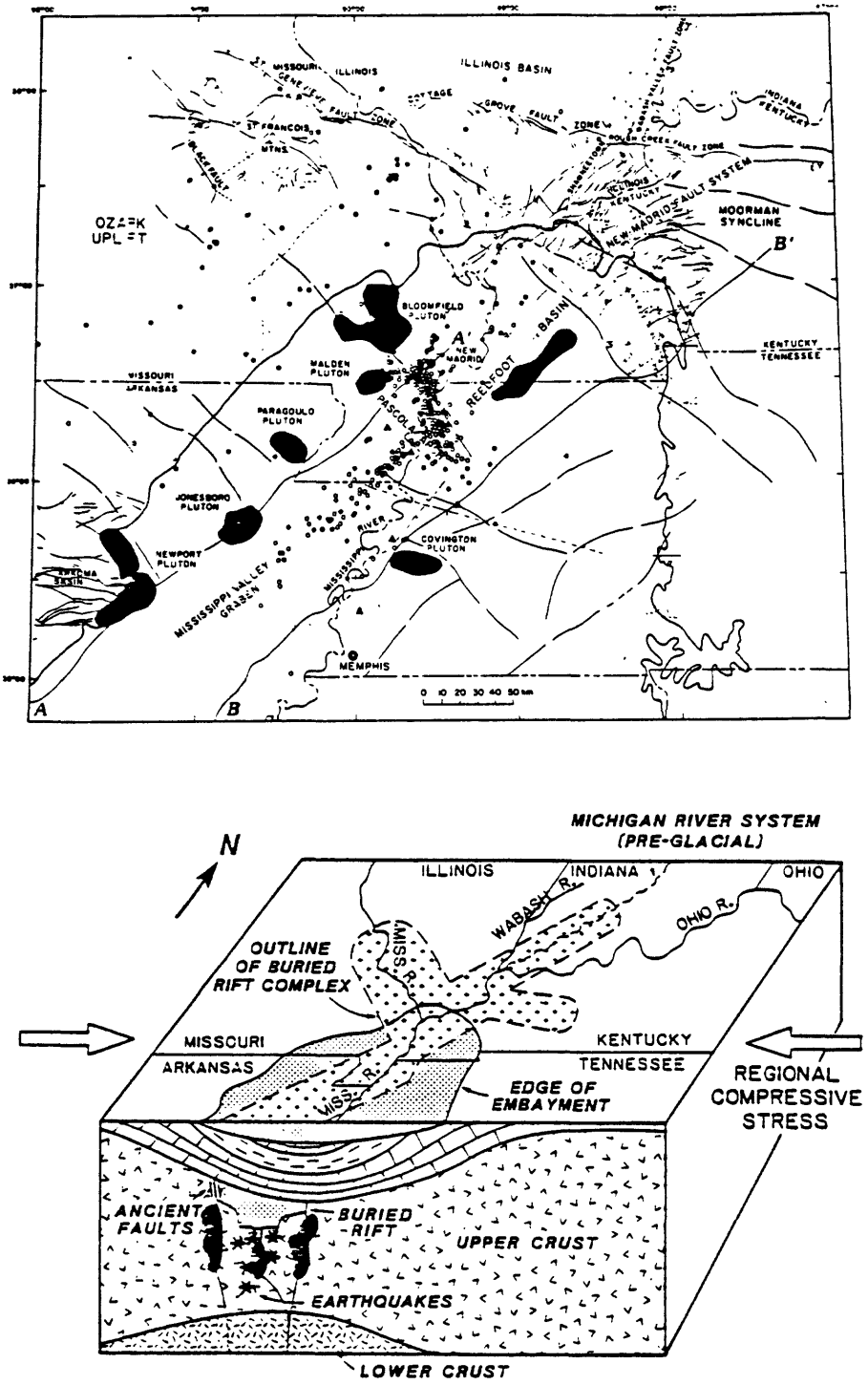

FIGURE 2.—Two perspectives of the New Madrid rift complex which illustrate how the tectonic structure localizes the seismicity. New Madrid is an excellent example of a SEISMOTECTONIC ISSZ (table 1). Top figure from Hildenbrand and others, 1982; bottom figure from Braile and others, 1984.

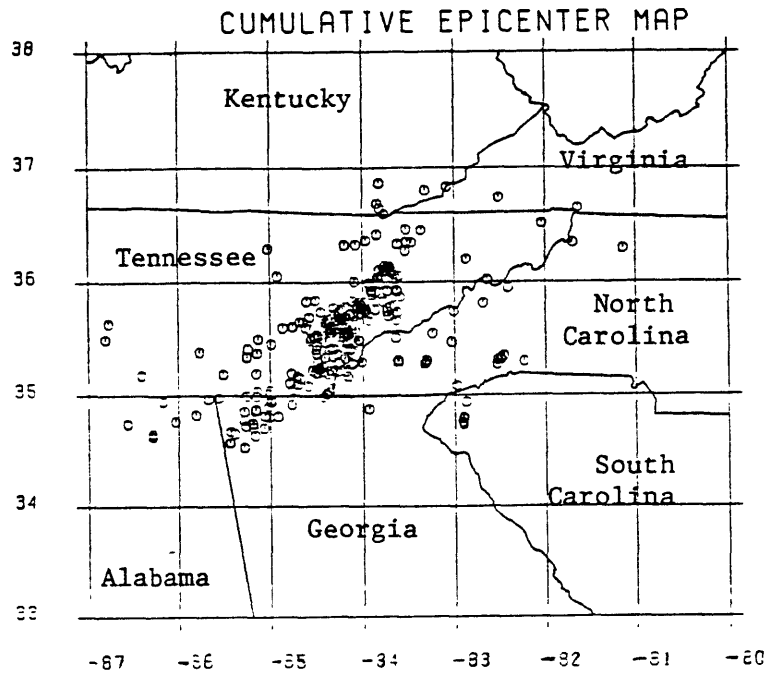

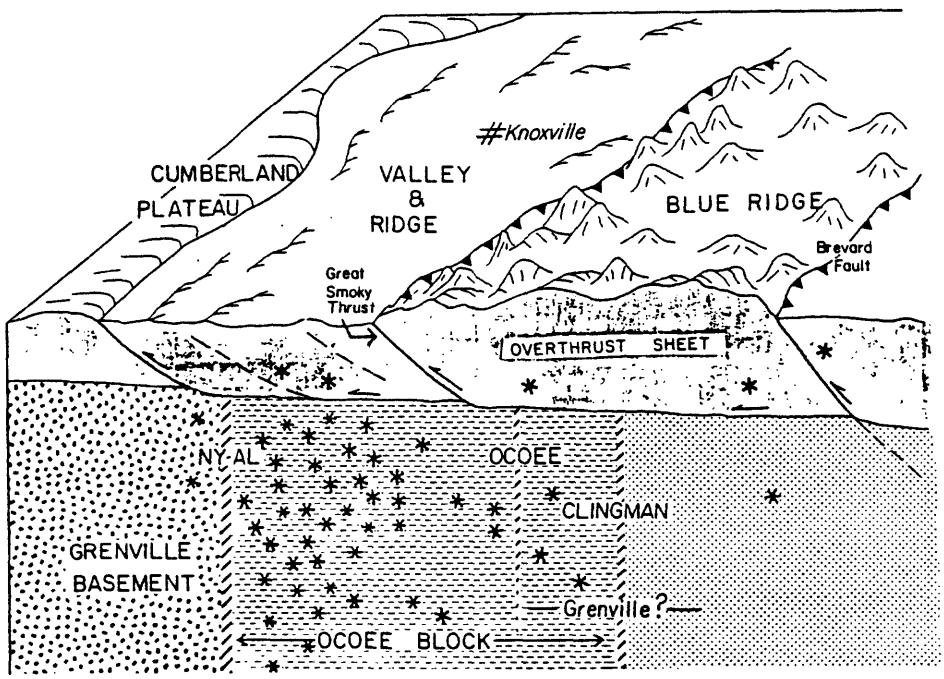

FIGURE 3.—(Top) Seismicity of the southern Appalachians for 1981-1986 (from Nava, 1986). (Bottom) Schematic representation of tectonic setting for the seismicity (from Johnston and others, 1985). Although major tectonic structures such as the Appalachian overthrust sheet and the New York-Alabama lineament are present, the seismicity does not correlate with them; hence it is a good example of a SEISMIC ISSZ (table 1).

For only ~2 percent of the SCI data set (eight occurrences) could surface-fault rupture be confidently documented. No SCI earthquake of magnitude 7 or greater has occurred worldwide in over 46 years since the M_L 7.2 Meeberrie, Australia earthquake of 1941.

Given the information compiled by Coppersmith and others (1987), how should one proceed with seismic zonation in SCI regions? I would argue that a strong constraint has been placed on source zone delineation by constraining the regions in which large ($M \geq 7.0$) SCI earthquakes can occur to a few types of tectonic environments. An ISSZ must have the same maximum earthquake assigned to the entire zone; thus boundaries should be based on mapped or geophysically-inferred structural boundaries, principally of Mesozoic-age rifts.

This problem has been addressed by Johnston and Nava (1985) in their analysis of recurrence probabilities of large New Madrid earthquakes. They conclude that although the crustal elastic-strain storage volume for the 1811-12 earthquake sequence must far exceed the Reelfoot rift boundaries of Hildenbrand and others (1982), major New Madrid earthquakes will be restricted to the principal fault segments within the rift flanks. The only other environments conducive to $M \geq 7.0$ earthquakes in North America are the Mesozoic/Cenozoic St. Lawrence rift and the Mesozoic Atlantic continental margin. Additional factors that localize earthquake occurrence within these environments (for example, impact structures, oceanic fracture-zone extensions) remain poorly understood.

The above arguments imply that there exists not only a difference in degree but also in kind between SCI earthquakes of magnitude $M \gtrsim 7.0$ and $M \lesssim 7.0$. (I am purposely avoiding defining M in specific terms such as M_s, M_L or moment magnitude in order to side-step the myriad scaling controveries surrounding intraplate earthquakes.) This section provides useful guidance in localizing the major, $M \geq 7.0$ earthquakes to a few locales, but what of the significant hazard contributed by events below this level? Sadly, the same familar uncertainties persist. One is forced to allow magnitude 5-6 events to occur almost anywhere—witness the 1982 $M5.6$ New Brunswick earthquake, the 1980 $M5.2$ Sharpsburg, Kentucky earthquake, or the 1986 $M5.0$ earthquake northeast of Cleveland, Ohio. Background seismicity serves as an unreliable, even misleading, guide to these events.

Other problems must be confronted when trying to use background historical or instrumental seismicity as a guide to seismic source zonation. The 1886 Charleston, S.C. (M_s 7.5, m_b 6.8) earthquake remains an enigma; it is close to but removed from the continental margin, no significant seismogenic tectonic structure has been confidently identified to place it on, paleoseismic evidence indicates repeated occurrences of major events, yet the background seismicity remains minor. In contrast, the southern Appalachian seismic zone (south of latitude 37.0° N.) is currently the most active region in the southeast (Johnston and others, 1985; Bollinger and others, in press), yet the largest known earthquake it has produced is the 1973 $M4.6$ Maryville, Tennessee earthquake (Bollinger and others, 1976). Both Charleston and the southern Appalachians would be classified as Seismic ISSZs (see table 1), but based on present understanding they would each be assigned significantly different maximum earthquakes. Could the southern Appalachian zone produce a Charleston-size event? Current 'wisdom' would say no, but the assessment remains intuitive.

Paleoseismological studies can aid in the dilemma of characterizing seismic source zones of SCI regions. First, they can demonstrate, as in the case of Charleston and New

Madrid, that major earthquakes can and have repetitively occurred on the same tectonic structures, possibly the same fault segments. Thus, they have validated the concept of "recurrence interval" as applied to SCI earthquakes. However, one caution is that paleoseismic evidence is selectively preserved in coastal plain or embayment sediments conducive to liquefaction and may be completely absent in other settings such as the overthrust Appalachians. Secondly, paleoseismology has the potential of providing perhaps the only nonstatistical estimates of the length and variability of recurrence intervals of major SCI earthquakes. As Johnston and Nava (1985) concluded for the New Madrid seismic zone: "The critical data required to constrain these estimates [conditional probabilities of recurrence] would be event chronologies based on paleoseismic evidence....Datable sand blows, slumps, or other liquefaction features produced by pre-1811 seismic episodes and preserved in these sediments offer the best hope of obtaining more tightly constrained forecasts of the future seismic behavior of the New Madrid zone". Given the great advances in paleoseismological methods as documented in this workshop, this observation is even more timely today. In the apt words of Hanks (1987), as paleoseismology matures as a science it carries the potential to free seismic hazard analysis "...from the prison of the historical record of earthquakes."

ACKNOWLEDGMENTS

Research support by the Electric Power Research Institute (Project 2556-12) and the Nuclear Regulatory Commission (contracts NRC-04-86-120 and NRC-04-85-107) is gratefully acknowledged.

REFERENCES CITED

Algermissen, S.T., Perkins, D.M., Thenhaus, P.C., Hanson, S.L., and Bender, B.L., 1982, Probabilistic estimates of maximum acceleration and velocity in rock in the contiguous United States: U.S. Geological Survey Open-File Report 82-1033, 99 pp.

Anderson, J.G., 1986, Seismic strain rates in the central and eastern United States: Seismological Society of America Bulletin, v. 76, p. 273-290.

Bernreuter, D.L., Savy, J.B., Mensing, R.W., 1987, Seismic hazard characterization of the eastern United States—Comparative valuation of the LLNL and EPRI studies: NUREG/CR-4885, U.S. Nuclear Regulatory Commission, Washington, D.C., 259 pp.

Bollinger, G.A., Langer, C.J., and Harding, S.T., 1976, The eastern Tennessee earthquake of sequence of October through December, 1973: Seismological Society of America Bulletin, v. 66, p. 525-547.

Bollinger, G.A., Johnston, A.C., Talwani, P., Long, L.T., Shedlock, K.M., Sibol, M.S., and Chapman, M.C., in press, Seismicity of the Southeastern United States, *in* Engdahl, E.R., ed., Seismicity Map of North America, Geological Society of America, Decade of North American Geology.

Braile, L.W., Hinze, W.J., Sexton, J.L., Keller, G.R., and Lidiak, E.G., 1984, Tectonic development of the New Madrid seismic zone, *in* Gori, P.L. and Hays, W.W., eds., Proceedings of the Symposium on "The New Madrid Seismic Zone": U.S. Geological Survey Open-File Report 84-770, p. 204-233.

Clark, M.M., Harms, K.K., Lienkaemper, J.J., Perkins, J.A., Rymer, M.J., and Sharp, R.V., 1983, The May 2, 1983 earthquake at Coalinga, California–The search for surface faulting, *in* The Coalinga Earthquake Sequence commencing May 2, 1983: U.S. Geological Survey Open-File Report 83-511, p. 8-11.

Coppersmith, K.J., Johnston, A.C., Metzger, A.G., and Arabasz, W.J., 1987, Methods for assessing maximum earthquakes in the central and eastern United States: Working Report, Electric Power Research Institute Research Project 2556-12, Electric Power Research Institute, Palo Alto, Calif., 107 pp.

Electric Power Research Institute, 1985, Seismic hazard methodology for nuclear facilities in the eastern United States: Volumes 1,2,3, draft reports, Electric Power Research Institute, Palo Alto, Calif., Research Project Number P101-29, v. 1-3.

Everingham, I.B., Gregson, P.J., and Doyle, H.A., 1969, Thrust fault scarp in the Western Australian shield: Nature, v. 223, p. 701-703.

Hanks, T.C., 1987, Seismology in the United States, 1983-1986, *in* U.S. National Report to International Union of Geodesy and Geophysics 1983-1986: Reviews of Geophysics, v. 25, p. 1131-1133.

Hildenbrand, T.G., Kane, M.F., and Hendricks, J.D., 1982, Magnetic basement in the upper Mississippi embayment region—A preliminary report, *in* McKeown, F.A. and Pakiser, L.C., eds., Investigations of the New Madrid, Missouri, Earthquake Region: U.S. Geological Survey Professional Paper 1236, p. 39-53.

Johnston, A.C., Reinbold, D.J., and Brewer, S.I., 1985, Seismotectonics of the southern Appalachians: Seismological Society of America Bulletin, v. 75, p. 291-312.

Johnston, A.C., and Nava, S.J., 1985, Recurrence rates and probability estimates for the New Madrid seismic zone: Journal of Geophysical Research, v. 90, p. 6737-6753.

Nava, S., 1986, TEIC Quarterly Seismological Bulletin: Tennessee Earthquake Information Center, Memphis State University, v. VII, no. 1, 64 pp.

Obermeier, S.F., Gohn, G.S., Weems, R.E., Gelinas, R.L., and Rubin, M., 1985, Geologic evidence for recurrent moderate to large earthquakes near Charleston, South Carolina: Science, v. 227, p. 408-411.

Russ, D.P., 1982, Style and significance of surface deformation in the vicinity of New Madrid, Missouri, *in* McKeown, F.A. and Pakiser, L.C., eds., Investigations of the New Madrid, Missouri, Earthquake Region: U.S. Geological Survey Professional Paper 1236, p. 93-114.

Talwani, P., and Cox, J., 1985, Paleoseismic evidence for recurrence of earthquakes near Charleston, South Carolina: Science, v. 228, p. 379-381.

SUMMARY OF DISCUSSION SESSION: THE BEHAVIOR OF SEISMOGENIC FAULTS

by

Anthony J. Crone
U.S. Geological Survey
Denver, Colorado 80225

Session Chairman: Anthony J. Crone, U.S. Geological Survey
Panel Members: Thomas C. Hanks, U.S. Geological Survey
Leonardo Seeber, Lamont-Doherty Geological Observatory
Kerry E. Sieh, California Institute of Technology
D. Burton Slemmons, University of Nevada, Reno

Fault segmentation is an significant new concept that has evolved out of the paleoseismologic research to characterize the behavior of seismogenic faults. Paleoseismologic data from several sites along a fault can help determine the extent of prehistoric ruptures which can then be used as guides to define segments. In some cases, we can use the geometry of a fault to define segments, but without additional data, we can only speculate on the stability of the segments during major earthquakes.

However, some ambiguity exists about how the terms "segments" and "segmentation" are used and defined. In some cases, the segments of a fault are identified by the physical characteristics of a fault zone (for example, fault geometry, changes in strike), and, in other cases, they are defined by seismicity or the extent of ground ruptures during historical earthquakes. At this stage of our research, perhaps the best basis for defining a segment is the behavior of a fault during a major historical earthquake. An obvious difficulty with this approach is that during great earthquakes like the 1857 Fort Tejon earthquake, more than one part of the fault may rupture.

Another problem with a rigorous definition is that the size and scale of segments varies depending on the techniques used to define them. A seismologist can resolve smaller-scale seismogenic features than those studied by geologists. Thus several seismologically defined segments may have to rupture simultaneously to produce a geologically recognizable feature. To confidently define all of the segments of a fault, we need a comprehensive case history of its past behavior. Then, the case history can be used to develop a probability models of the changes of future events rupturing one, two, or several segments. Ideally, the history should utilize both seismologic data which can provide good information on fault geometry and complexities at depth, and geologic data which can provide information on the fault's long-term behavior.

Until we have a better grasp on fault segmentation, perhaps a rigorous definition is unnecessary; perhaps segments should be described according to how they are defined, that is, historical segments, geometric segments, or seismologic segments.

Recent studies suggest the dilational jogs between en echelon segments can stop propagating ruptures, and thus can be guides to identifying possible segment boundaries. However, the effectiveness of dilational jogs at halting ruptures is a function of the dimensions of the jog, and the amount of strain that has accumulated on segments adjacent to the jog. For example, the

teleseismic data from the 1968 Dasht-y-Bayez, Iran earthquake indicates a very slow rupture velocity and suggests that the rupture associated with the main shock may have started and stopped several times. The 80-km-long part of the fault that broke has two prominent dilational jogs with en echelon offsets of 0.5-0.75 km. Apparently, in this case, sufficient strain had accumulated on several adjacent segments such that, when the main rupture encountered the jogs, the slowed but was not completely stopped. In other examples, dilational jogs appear to halt ruptures for periods of time ranging from days to many years. Thus the effectiveness of dilational jogs at halting ruptures encompasses a wide range of time-dependent behavior.

The structural and geometric features that apparently segment faults seem to respond differently to propagating ruptures under different conditions. To understand this variability, we must first use numerous case histories to document the ways these features respond to ruptures. Initially, we should focus on examples in which several historic earthquakes have repeatedly ruptured the same part of a fault. With these examples, we can directly compare similarities and differences between successive events which may offer clues about the nature of features that segment faults.

The model of characteristic earthquakes is based on the belief that similar amounts of seismic energy are released during successive failures of a particular fault or fault segment, thus producing similar magnitude earthquakes. However, we know of historic examples in which a single fault segment has ruptured during one earthquake, and several segments failed during another earthquake on the same part of the fault. Perhaps a better concept is one of a characteristic segment which would imply only that a specific segment behaves as a discrete unit, and would have no connotation about the size of the associated earthquake. Examples of historic earthquakes and (or) faults that might fit this idea of characteristic segments include the Parkfield and Carrizo Plain segments of the San Andreas fault, historic earthquakes in the Nankai trough of Japan, the parts of the Anatolian fault in Turkey that ruptured in the late 1930's and early 1940's, the 1983 Borah Peak, Idaho earthquake, the 1940 and 1979 Imperial Valley, California earthquakes, and possibly the Xianshuihe fault in southwestern China.

page 417 follows

ASPECTS OF SEISMIC-HAZARD ANALYSIS

GEOLOGICAL DATA AND SEISMIC-HAZARD ANALYSIS: PAST AND FUTURE

Steven G. Wesnousky

Center for Earthquake Research and Information
Memphis State University
Memphis, Tennessee 38152

ABSTRACT

Seismic-hazard analyses during the last [15-20] yrs have increasingly relied on geological data bearing on the seismic history of active faults. The reasons for this trend are the recognition that historical records of seismicity are generally too short to accurately reflect long-term rates of seismicity in many regions, and that available data show earthquakes which occur in regions of shallow seismicity generally have their origins on faults which show geological evidence of prehistoric earthquakes. Towards augmenting a limited historical data set, efforts to both recognize and develop geological methods to infer the past rate of seismicity on active faults have increased. Progress has been greatest in paleoseismic and fault slip-rate studies. Paleoseismic studies yield estimates of the dates of prehistoric earthquakes and fault slip-rate studies furnish information relating to the long-term rate of strain accumulation along faults. However, paleoseismic and fault slip-rate studies generally do not yield direct information regarding the sizes of earthquakes that have occurred in the past and which can be expected in the future. An estimate of the size of expected future earthquakes is fundamental to seismic hazard analysis and, as well, is necessary if earthquake repeat times are to be inferred from fault slip-rate data. In certain instances, estimates of expected earthquake size along a fault may be inferred from geologic or geomorphologic evidence of the amount of coseismic offset in past events, but such inferences are tenuous unless observations are available for many points along a fault. Observed relationships between seismic moment M_o and fault rupture length hold promise for quantitatively estimating the size of earthquakes expected to rupture mapped faults, but estimates of the length of a fault that will rupture are now largely subjective. It is the thesis of this discussion that the greatest promise toward significantly increasing the value of data provided by paleoseismic and fault slip rate studies to seismic-hazard analysis lies in a concerted effort to understand the physical factors that control the length of earthquake ruptures. Such efforts should include a systematic study of the structural and physical factors that have influenced the extent of historical earthquake ruptures and geological studies to determine the timing and offset history at many points along strike of active fault zones.

INTRODUCTION

The input of geological data to seismic-hazard analyses has increased markedly during the last 15-20 years. Several factors have led to this increase. The primary factor is that it is now generally recognized that earthquakes occurring in regions of shallow seismicity and active faulting generally have their origins on faults that show geologically recognizable evidence of prior (Allen, 1975; Sieh, 1978a) and, in certain instances,

similar-sized (Schwartz and Coppersmith, 1984) earthquake displacements in recent geologic time. The large uncertainty attached to seismic-hazard analyses based on the extrapolation of historical records to the future, particularly in regions where the historical record is short with respect to the average return time of earthquakes, has also provided an impetus to integrate geological data into seismic hazard analyses (Anderson, 1979; Wesnousky and others, 1984). The increased effort to incorporate geological data into seismic hazard analyses has led to advances in our ability to recognize and interpret the signature of prehistoric earthquakes as recorded in late Quaternary stratigraphy. In this paper, I will not be concerned with the details of how geological studies of active fault structures may be used to provide quantitative estimates of seismic hazard, since that has been discussed at length in earlier papers (Anderson, 1979; Wesnousky, 1986). Rather, I will briefly comment on what active fault studies currently provide for seismic-hazard analysis and what avenues of approach may likely provide the greatest increase in value of geologic data to seismic-hazard analysis in the near future. And finally, my comments will be concerned only with regions of shallow seismicity and active faulting like those in California and the Western United States.

DISCUSSION

Geological Methods

Fundamental to the increased role of active fault studies in seismic-hazard analysis is the recognition that faults which are seismically active commonly break Quaternary deposits and produce a characteristic and recognizable set of landforms. Hence, faults that break Quaternary deposits and exhibit such landforms are now commonly accepted as sources of seismic hazard, and geological and geomorphological studies are often the primary basis for locating potential seismic sources. In addition to locating seismic sources, geological studies of active faults frequently provide information regarding the long-term level of seismicity on faults.

The most well-known advances in assessing the long-term seismicity on faults have been made in the area of paleoseismology; the documentation of the dates of prehistoric earthquakes based on structural and stratigraphic analysis of sediments that have been repeatedly disturbed by earthquakes and, generally, exposed by the excavation of trenches across fault traces or liquefaction features (Sieh, 1978b; Wallace, 1981, Obermeier and others, 1985; Talwani and Cox, 1985). To my knowledge, the first such successful analysis was presented by Clark and others. (1972) for their study of the 1968 Borrego Mountain earthquake fault trace. They ascertained that the same fault ruptured in similar- sized events on the average of each 150-200 years during the last few thousand years. The importance of this study is magnified when it is realized that the historical record in Borrego Mountain region extends back in time 100 years at best (Toppozada and others, 1981). Now it is not uncommon to establish specific dates of earthquake ruptures that have occurred on faults during the last several thousand years (Sieh, 1978, 1984 [San Andreas fault]; Swan and others, 1980 [Wasatch Fault zone]; Tanna Fault Trenching Research Group. 1983 [Tanna Fault]; Obermeier and others, 1985 [Charleston area]; Rockwell and others, 1985 [Elsinore Fault]). Withstanding any uncertainties, these efforts have led to a far greater understanding of seismic hazard in the respective regions than could be gained solely from historical data.

Significant progress has also been made in geological methods to assess the long-term slip rate of active faults. Slip-rate estimates, the consequence of recognizing geo-

logical and geomorphological features of known age that are offset a given distance by a fault, have now been estimated from offset features that include, among others, Holocene stream channels (Sieh and Jahns, 1984), fluvial deposits (Adams, 1980), glacial moraines (Plafker and others, 1978), soils (Machette, 1978), and volcanic rocks (Dokka, 1983). Summaries of slip-rate determinations and the data on which they are based have most recently been summarized by the Research Group for Active Faults of Japan (1980), Sieh (1981), and Clark and others, (1984). The parameter of seismic moment M_o, a measure of earthquake size like magnitude, but which may be directly related to physical parameters that describe the earthquake source, such as fault length and coseismic slip, has further enabled quantitative estimates of long-term seismicity rates from geologic estimates of fault-slip rate, in terms of the *seismic- moment rate* (Wesnousky, 1986).

Contributions and Limitations of Geological Data to Seismic Hazard Analysis

Estimation of Earthquake Location

Within the context of seismic-hazard analysis, it appears that that geological studies currently play a most complete role in the identification of seismic sources. The geologic signature of active faults can be relatively easily documented by trained geologists. Moreover, the common coincidence between recent earthquake ruptures and preexisting and mappable Quaternary faults leads to confidence that maps of Quaternary faults and related fold structures provide a good indicator to the locations of future earthquakes. Such information forms the foundation on which seismic-hazard analyses are built.

Estimation of Earthquake Repeat Time

Paleoseismological or trenching studies provide the most direct measure of the past occurrence rate of moderate to large earthquakes on faults. However, the success of such studies is dependent on a unique set of geological conditions leading to preservation of a detailed stratigraphic record at sites along a fault. It is by no means certain that such sites exist along all active faults. Rapid urbanization is also eliminating many sites which would be conducive to paleoseismological analysis. Withstanding these problems, the potential of paleoseismological studies is yet largely untapped along most fault zones and future studies will certainly contribute more information to seismic-hazard analyses.

Fault slip-rates also give a measure of the long-term rate of activity of a fault and seem a more common result of active fault studies than stratigraphic constraints on the time that past earthquakes occurred. The fault slip-rate $\dot{u}$ is equal to U/T, where U is the geologically documented offset across the fault of a rock unit of age T. With knowledge of the fault length L and width W, the *seismic moment rate* $\dot{M}_o$ of the fault may also be estimated to equal $\mu LW\dot{u}$ (Brune, 1968), where μ is crustal rigidity. The average repeat time T between earthquakes on a fault is commonly interpreted from measures of $\dot{u}$ or $\dot{M}_o$ based on the equation

$$T = U^{exp}/\dot{u}^{g} \tag{1a}$$

or

$$T = M_o^{exp}/\dot{M}_o^{g}, \tag{1b}$$

where U^{exp} and M_o^{exp} are the values of coseismic offset and seismic moment expected to occur on the fault of interest, respectively (Wallace, 1970, Wesnousky and others, 1983). Thus, further assumptions regarding the size of earthquake expected to rupture the fault are necessary to convert measures of $\dot{u}$ or $\dot{M}_o$ to estimates of earthquake repeat time (RT).

Estimation of Earthquake Size

It is perhaps in the estimation of earthquake size that geological studies of active faults currently play their weakest role in seismic hazard analysis. Estimates of earthquake size are necessary to calculate the area which will be subjected to strong ground motions due to rupture of a fault. Further, estimates of earthquake return time from fault slip-rate data are critically dependent on estimates of the expected earthquake size (equation 1). Stratigraphy exposed along a trench wall or geomorphological features offset by a fault can sometimes provide information regarding the amount of offset that occurred coseismically at that site (Sieh and Jahns, 1984). However, such measures are generally limited to a small portion or site along a fault's entire length. An estimate of the offset along the entire length of a fault is desirable to correctly assess the size of past earthquakes. Recent earthquake ruptures show that variability of coseismic slip along faults can be very large. As a result, large uncertainty must be attached to estimates of earthquake size from point measurements of coseismic offset along a fault. Furthermore, many fault slip-rate studies report an estimate of fault slip-rate but are apparently unable to provide data regarding the coseismic offset of past earthquakes. Historical earthquakes may also provide direct evidence of the capability of the faults on which they occurred. However, it is my experience that, more commonly, empirical relations between earthquake magnitude M or moment M_o and rupture length l derived from recent earthquakes (fig. 1) must be relied upon to estimate the expected size of earthquakes on mapped faults, with the inference that the size of an earthquake will be proportional to the mapped fault or fault segment length.

The estimation of earthquake size from mapped fault length is simple in concept but difficult in practice. The difficulty stems from observations that earthquakes do not necessarily rupture the entire extent of the faults on which they occur. The great 1857 and 1906 California earthquakes are a well-known example of this behavior, each only rupturing 350-400 km of the total 1,000 km length of the San Andreas fault. Arising from this observation is the critical problem of identifying the segments of faults which will be the most likely source of future earthquakes. When coupled with the scatter observed in the empirical relationships between earthquake size and fault rupture length used to infer the expected size of future earthquakes (fig. 1), the uncertainty regarding estimates of the segments of faults expected to rupture during future earthquakes can translate into uncertainties in estimates of earthquake size and repeat time which are unacceptably large and not practically useful. The uncertainties are conveniently illustrated by a brief examination of the Elsinore Fault zone in southern California (fig. 2).

The Whittier-Elsinore Fault strikes southward from Los Angeles a distance of about 250 km. Displacement across the fault is primarily right-lateral. It may be inferred from the relations in fig. 2 that rupture along the entire 250 km length of the Elsinore fault would produce average displacements of 2.5-7.0 m (Wesnousky, 1986). A recent interpretation of offset geomorphic features along the southern Elsinore indicates the repeated occurrence of several earthquakes during the Holocene with coseismic offsets averaging about 1.4 m (Pinault and Rockwell, 1984), less than would be expected from a complete

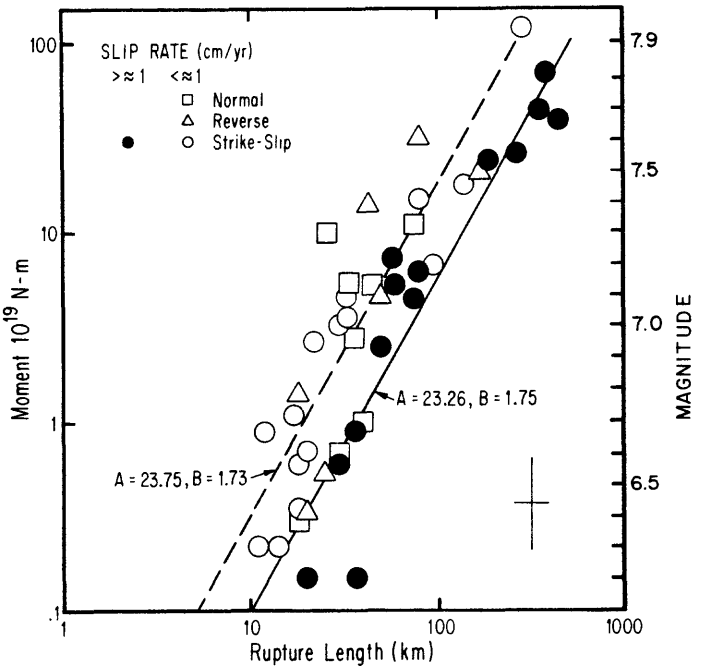

Figure 1. Seismic Moment M_o versus fault rupture length L for a set of historical earthquakes compiled by Wesnousky (1986). Solid symbols indicate earthquakes on major plate boundary faults generally characterized by a slip-rate of about 1 cm/yr or greater. Earthquakes on faults with lesser slip rates are shown by open symbols. Solid and dashed lines of form $logM_o = A + B \times logL$ are fit through the solid and open symbols, respectively. The vertical and horizontal bars of the cross in lower right corner of plot correspond to a factor of 3 in M_o and 50 percent in L, respectively. Estimates of earthquake size and repeat time in figure 3 are determined with the relationship shown by the solid line.

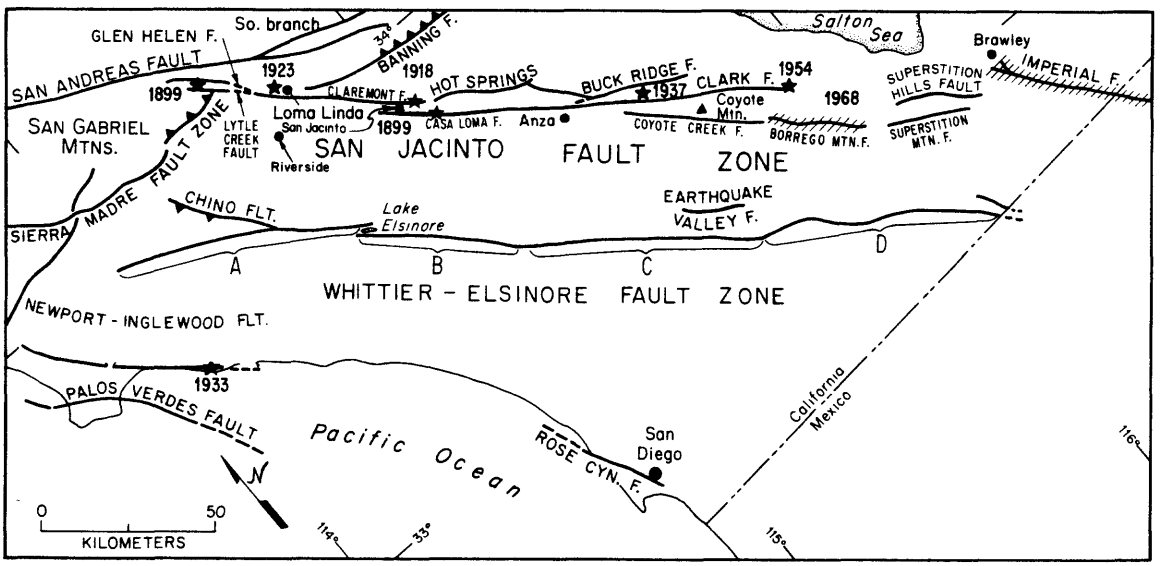

Figure 2. Location of Whittier-Elsinore fault zone in southern California. Labeled brackets show segments of fault which are divided on the basis of major steps or bends in the fault trace. Stars with dates are location of major historic earthquakes.

rupture of the fault zone. Historical data indicate that the Elsinore has not broken in its entirety during the last 150 years (Toppozada and others, 1980). Isoseismal data is, however, compatible with the occurrence of a moderate M=6.0 earthquake along the northern end of the fault zone in 1910 (Toppozada and Parke, 1982). It is entirely possible then, if not likely, that the Elsinore fault zone does not typically rupture in entirety during single earthquakes but, rather, breaks in sequences of lesser size events which are limited to specific segments of the fault zone. The possibility could be addressed by implementation of a suite of paleoseismic studies along strike of the Elsinore. Such a data set is not currently available nor is it certain that a sufficient number of sites suitable for paleoseismological analysis exist to provide such a data set. Estimates of earthquake size and repeat time must currently be based on data describing fault slip-rate and estimates of the length or segment of fault expected to rupture during the earthquake. The sensitivity of seismic hazard analysis to estimates of expected fault rupture length are, in part, schematically illustrated in fig. 3.

Figure 3 is a schematic map of the Whittier-Elsinore fault. The total 250 km length of the fault is divided into a various number of segments in figures 3a, b, and c, respectively. Available fault slip-rate studies (Wesnousky, 1986) are used to assume that the slip-rate along the entire fault zone is 4 mm/yr. In each case, individual segments of the fault are assumed to rupture in separate earthquakes. The size of earthquake expected on each segment is computed with the empirical relationship between fault length and seismic moment in fig. 1. The repeat time of the expected earthquake on each segment is estimated with equation 1b. Equations from Joyner and Fumal (1985) relating earthquake size–source to site distance–and strong ground motion are then used to estimate the distance from the fault to which peak strong ground accelerations equal to or greater than 0.2 gravity can be expected. Figure 3 illustrates that different assumptions regarding the length of fault expected to rupture during earthquakes yields strongly contrasting estimates of the size and repeat time of earthquake strong ground motions along a fault zone, even when disregarding the uncertainties inherent to fault slip-rate estimates and the uncertainty represented by the scatter in relationships between earthquake size and repeat time (fig. 1). Whereas the uncertainties associated with slip-rate estimates and empirical relations between earthquake size and seismic moment can be addressed in some quantitative fashion, estimates of the expected length of rupture are now primarily subjective. Thus, significant improvement to geological estimates of seismic hazard could be be realized if criteria were documented on which we could make statistically quantifiable estimates of the extent to which a fault will rupture in the future.

CONCLUSIONS

Geological studies of active faults now contribute, to varying degrees, to the asssessment of the expected location, size, and frequency of earthquakes in regions of active tectonics. The common coincidence between recent earthquake ruptures and preexisting and mappable Quaternary faults leads to confidence that maps of Quaternary faults and related fold structures are a good indicator to the locations of future earthquakes. Paleoseismology provides a tool to assess the past occurrence rate of earthquakes on active faults and, hence, a basis to estimate future behavior. Fault slip-rate studies, when combined with estimates of expected earthquake size, provide data bearing on the average expected repeat time of earthquakes on a fault. In certain instances, estimates of expected earthquake size for a fault can be gained by observations of geomorphic evidence of past coseismic offsets along the length of fault. It is more common, however,

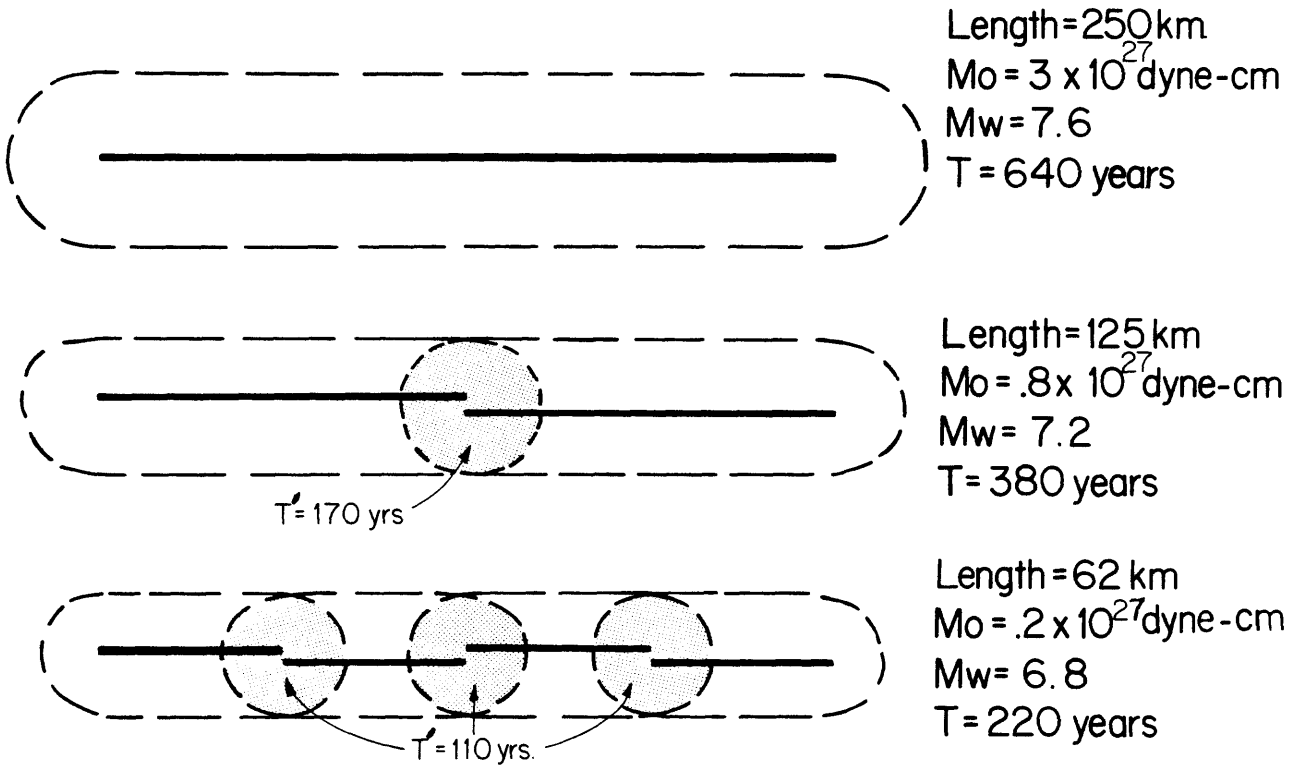

Figure 3. Schematic illustration showing how assumptions of fault segmentation strongly influence geological estimates of seismic hazard along a fault zone. Map view of 250-km fault trace shows fault divided into 250 km, 125 km, and 62 km segments in a, b, and c, respectively. The seismic moment M_o and moment-magnitude Mw expected for earthquakes rupturing individual segments are determined from empirical relationship in figure 1. The return time T of earthquakes on each segment is computed with equation 1b assuming $\mu = 3 \times 10^{11}\ dyne/cm^2$, fault width $W = 15$ km, and the fault slip rate is 4 mm/yr. The regions expected to experience 0.2-g peak ground accelerations or greater due to earthquakes on each segment are encompassed by dashed lines and computed with the equations of Joyner and Fumal (1985). The return time of 0.2-g ground shaking will be equal to the repeat time T of earthquakes computed for each fault segment in the unshaded regions encompassed by dashed lines. Regions near segment boundaries will be subjected to ground shaking from earthquakes on more than one segment (shaded regions) and, hence, the return time of strong ground motions T' will be less than the repeat time of earthquakes on individual segments. Estimates of the expected return time of ground shaking along a fault zone are thus strongly dependent on the assumed location and length of individual fault segments.

that estimates of earthquake size are made with empirical relationships between earthquake size (magnitude or moment) and fault length. Such estimates thus require some knowledge of the length of fault which will rupture. Since faults do not as a general rule rupture their entire length during an earthquake, estimating the extent to which a fault will rupture during future earthquakes is now largely subjective. In turn, estimates of earthquake repeat time from fault slip-rate data and earthquake size are often associated with unacceptable uncertainties. In this regard, the growing body of observations which suggest that points of structural complexity along faults strongly influence the initiation and extent of earthquake ruptures (Allen, 1968; Segall and Pollard, 1980; Lindh and Boore, 1981; Sibson, 1985; King and Nabelek, 1985) is an exciting and crucial development for seismic-hazard analysis. If systematic relationships can be established between the endpoints of earthquake ruptures and structural complexities along fault strike, much of the subjectivity involved in estimating the rupture length, expected size, and repeat time of earthquakes on mapped faults may be removed. Establishment of any such systematics will require a thorough examination of past earthquake ruptures coupled with extensive paleoseismologic efforts at many sites along particular fault zones. To summarize, it is my opinion that the greatest promise toward significantly increasing the value of data provided by paleoseismic and slip-rate studies to seismic hazard analysis lies in a concerted effort to quantify the extent to which structural and physical discontinuities along fault strike play a role in the rupture propagation process, and to determine whether or not the effects of these features are sufficiently systematic and large that they may ultimately be used with confidence as a predictive tool for assessing the likely length of earthquake ruptures.

ACKNOWLEDGEMENTS

This research was supported in part by NSF Grant No. EAR-8618314.

REFERENCES CITED

Adams, R., 1980, Paleoseismicity of the Alpine fault seismic gap, New Zealand: Geology, v. 8, p. 257-262.

Allen, C. R., 1968, The tectonic environments of seismically active and inactive areas along the San Andreas fault system, in Proceedings Conference on Geologic Problems of San Andreas fault system, edited by Dickenson, W. R., and L. Grantz, A., Stanford University Press, Stanford, California, p. 70-80.

Allen, C. R., 1975, Geological criteria for evaluating seismicity, Seismological Society America Bulletin, v. 86, p. 1041-1057.

Anderson, J. G., 1979, Estimating the seismicity from geological structure for seismic-risk studies: Seismological Society America Bulletin, v. 69, p. 135-158.

Brune, J. N., 1968, Seismic moment, seismicity, and rate of slip along major fault zones: Journal Geophysical Research, v. 73, p. 777-784.

Clark, M. M., Grantz, A., and Rubin, M., 1972, Holocene activity of the Coyote Creek fault: U. S. Geological Survey Professional Paper 787, p. 102-148.

Clark, M. M., Harms, K. K., Lienkaemper, J. J., Harwood, D. S., Lajoie, R., Matti, J. C., Perkins, J. A., Rymer, M. J., Sarna-Wojcicki, A. M., Sharp, R. V., Sims, J. D.,

Tinsley, J. C., and Ziony, J. I., 1984, U. S. Geological Survey Open File Report, 84-106, 12 p.

Dokka, R. K., 1983, Displacements on late Cenozoic strike-slip faults of the central Mojave Desert, California: Geology, v. 11, p. 305-308.

Joyner, W. B., and T. E. Fumal, 1985, Predictive mapping of earthquake ground motion, evaluating earthquake hazards in the Los Angeles region - An earth science perspective: U. S. Geological Survey Professional Paper, 1360, p. 203-220.

King, G., and Nabelek, J., 1985, Role of fault bends in the initiation and termination of earthquake rupture: Science, v. 228, p. 984-987.

Lindh, A. G., and Boore, D. M., 1981, Control of rupture by fault geometry during the 1966 Parkfield earthquake: Seismological Society of America Bulletin, v. 71, p. 95-116.

Machette, M. N., 1978, Dating quaternary faults in the southwestern United States by using buried calcic paleosols: U. S. Geological Survey Journal of Research, v. 6, p. 369-381.

Obermeier, S. F., Gohn, G. S., Weems, R. E., Gelinas, R. L., Rubin, M., 1985, Geologic evidence for recurrent moderate to large earthquakes near Charleston, South Carolina: Science, v. 227, p. 408-411.

Pinault, C. T., and Rockwell, T. K., 1984, Rates and sense of Holocene faulting on the southern Elsinore fault: Further constraints on the distribution of dextral shear between the Pacific and North American plates: Geological Society of America Abstracts with Programs, v. 16, p. 624.

Plafker, G., Hudson, T., Bruns, T., and Rubin, M., 1978, Late Quaternary offsets along the Fairweather fault and crustal plate interactions in southern Alaska: Canadian Journal of Earth Sciences, v. 15, p. 805-816.

Research Group for Active Faults of Japan–1980, Active fauts in and around Japan: The distribution and the degree of activity, Journal of National Disaster Science, v. 2, p. 61-99.

Rockwell, T. K., Lamar, D. L., McElwain, R. S., and Millman, D. E., 1985, Late Holocene recurrent faulting on the Glenn Ivy North strand of the Elsinore fault, southern California: Geological Society of America, Abstracts with Programs, v. 17, p. 404.

Schwartz, D. P. and Coppersmith, K. J., 1984, Fault behavior and characteristic earthquakes: examples from the Wasatch and San Andreas fault zones, Journal Geophysical Research: v. 89, p. 5681-5681.

Segall, P. and Pollard, D. D., 1980, Mechanics of discontinuous faults, Journal Geophysical Research: v. 85, p. 4337-4350.

Sibson, R. H., 1985, Stopping of earthquake ruptures at dilational fault jogs: Nature, v. 316, p. 248-251.

Sieh, K. E., 1978a, Slip along the San Andreas fault associated with the great 1857 earthquake: Seismological Society America Bulletin: v. 68, p. 1421-1448.

Sieh, K. E., 1978b, Prehistoric large earthquakes produced by slip on the San Andreas fault at Pallet Creek, California: Journal Geophysical Research: v. 83, p. 3907-3939.

Sieh, K. E., A review of geological evidence for recurrence times of large earthquakes, 1981, *in* D. W. Simpson and P. G. Richards, eds., Earthquake Prediction, American Geophsical Union Maurice Ewing Series 4, p.181-207.

Sieh, K. E., 1984, Lateral offsets and revised dates of large prehistoric earthquakes at Pallet Creek, southern California: Journal Geophysical Research: v. 89, p. 7641-7670.

Sieh, K. E., and Jahns, R. H., 1984, Holocene activity of the San Andreas at Wallace Creek, California: Geological Society of America Bulletin, v. 95, p. 883-896.

Swan, F. H., III, Schwartz, D. P. and Cluff, L. S. 1980, Recurrence of moderate to large earthquakes produced by surface faulting on the Wasatch fault zone, Utah: Seismological Society America Bulletin, v. 70, p. 1431-1462.

Talwani, P., and Cox, J., 1985, Paleoseismic evidence for recurrence of earthquakes near Charleston, South Carolina: Science, v. 229, p. 379-381.

Tanna Fault Trenching Research Group, 1983, Trenching study for Tanna fault, Izu, at Mhyoga, Shizuoka Prefecture, Japan: Bulletin of the Earthquake Research Institute, v. 58, p. 797-830.

Toppozada, T. R., and Parke, D. L., 1982, Areas damaged by California earthquakes, 1900-1949: California Division of Mines and Geology Open-File Report 82-17 SAC, 65 pp.

Toppozada, T. R., Real, C. R., and Parke, D. L., 1980, Preparation of isoseismal maps and summaries of reported effects for pre-1900 California earthquakes: Calilfornia Division of Mines and Geology Open-File Report 81-11 SAC, 182 pp.

Wesnousky, S. G., Scholz, C. H., Shimazaki, K., and Matsuda, T., Integration of geological and seismological data for the analysis of seismic hazard: A case study of Japan: Seismological Society American Bulletin, v. 74, p. 687-708.

Wallace, R. W., 1970, Earthquake recurrence intervals on the San Andreas fault: Geological Society of America Bulletin, v. 81, p. 2875-2890.

Wesnousky, S. G., 1986, Earthquakes, Quaternary faults, and seismic hazard in California: Journal Geophysical Research, v. 91, p. 12587-12631.

CONTAGIOUS FAULT RUPTURE, PROBABILISTIC HAZARD, AND CONTAGION OBSERVABILITY

by

David M. Perkins
U.S. Geological Survey, MS 966
Denver Federal Center, Box 25046
Denver, CO 80225

ABSTRACT

Earthquake ruptures are termed contagious if the occurrence of the rupture of one fault or fault segment increases the likelihood of the occurrence of a rupture on an adjacent fault or fault segment. Model systems of contagious fault segments may perform either as two-stage processes or as Poisson processes, depending on two parameters—the average contagion time and the standard deviation of the interoccurence time of ruptures on individual segments. Simulation studies of systems of idealized, identical faults have yielded a rule of thumb for those parameter values for which two-stage behavior is likely.

To determine whether parameter values would be observable with geologic-dating techniques, this rule of thumb is applied to a model Wasatch-fault system, in which the recurrence time for the individual faults is comparable to the average recurrence time observed on individual segments of the Wasatch Front fault. To assert the existence of contagion times sufficiently small to guarantee two-stage behavior, it would be necessary to observe that adjacent-segment ruptures have occurred 80 years apart, or less. To determine that the standard deviation of individual segment recurrence times was sufficiently small that contagions would be possible would require determining rupture times to an accuracy of 250 years or less. These accuracies seem to be beyond present standards of dating.

However, contagion could still be recognized if dating showed that all segments ruptured within several hundred years, with between-bunch quiescent times a factor of two or more longer. Even the information that there had been no large earthquakes on the Wasatch fault zone in the past 1,000 years would be very unlikely unless a strong contagion governed recurrences.

INTRODUCTION

Recently, the concepts of characteristic earthquakes and the near periodicity of their recurrence have led to probabilistic forecasts of such events (for example, Rikitake, 1974; Rikitake, 1975; Lindh, 1983; Sykes and Nishenko, 1984; Nishenko, 1985; Bakun and Lindh, 1985). These forecasts have been largely based on historical information of one or more cycles of recurrence. Geological-dating techniques would be needed to establish recurrence rates for those characteristic earthquakes whose average recurrence time, $\overline{T}$, is longer than the historical record. Wherever this data can be determined,

the impact on probabilistic estimates of recurrence in some future time window can be expected to be significant.

The more obvious impacts, and the ones most likely to be encountered in future work include the following:

1. The probability of the recurrence of a characteristic earthquake on a given fault segment during a forecast time window depends strongly on where the beginning of that time window is in the seismic cycle. This time-dependent probability may range from a small fraction to a large multiple of the constant probability obtained under the usual assumption of a Poisson process.
2. The recurrence rate given by the geologic data may be very different from that assumed by extrapolation of a Richter-Law fit to recurrences for lower-magnitude data (for example, Schwartz and Coppersmith, 1984).

These first of these characteristics is obvious to practitioners, but is a function of the mathematics and is not of much professional concern to geologists. The second impact depends directly on the precision with which geologists can recognize, date, and estimate the magnitude for past earthquake ruptures, but is not very interesting to illustrate. Accordingly, instead of these topics, this paper will address a topic in earthquake recurrence which has great impact on hazard estimates, but whose observability depends directly on the precision with which geologists can date ruptures.

Consider a system of multiple faults in which the occurrence of one rupture may increase the likelihood of the occurrence of a rupture on an adjacent fault. (Alternatively, consider several segments of a single fault, where rupture on one increases the likelihood of the rupture on an adjacent segment.) The time from the first event to the second is relatively short compared to the average recurrence time for a characteristic event on one fault. Because the tendency to rupture passes on from one fault to another, the process is termed a contagion, and the average time it takes to pass is termed the contagion time, t_c. Under certain conditions, the system can behave as a two-stage process: one stage having a high recurrence rate during the contagion process and a second stage having a long, quiescent inter-contagion time. The consequence for hazard estimates, even for relatively long time windows, can be dramatically different from that in which a Poisson process is assumed.

In the Poisson case, the average recurrence between the characteristic events on n segments of identical recurrence time, $\overline{T}$, would be $\overline{T}/n$, a relatively short time, making these events relatively likely within a time window for which mitigation of their effects would be required. In the two-stage case, the next characteristic event could occur only after a long period of time, if the beginning of the mitigation time window were early in the intercontagion time. A probability statement about this occurrence of the characteristic event during the quiescent time could yield a probability sufficiently low that mitigation of the characteristic earthquakes might not be considered very important.

THE MODEL AND TERMINOLOGY

Consider first the time-line of an individual fault or segment (fig. 1). Because the characteristic earthquakes are not completely periodic, there is some variation in the

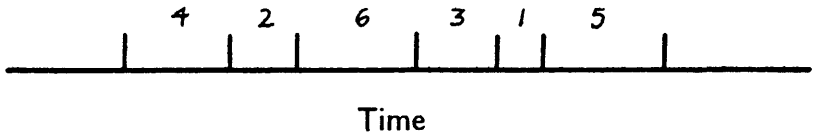

FIGURE 1.—Schematic representation of recurrence of characteristic earthquake events. Time is represented along horizontal line; uprights represent times of rupture events. Interoccurrence times are numbered in increasing order of length.

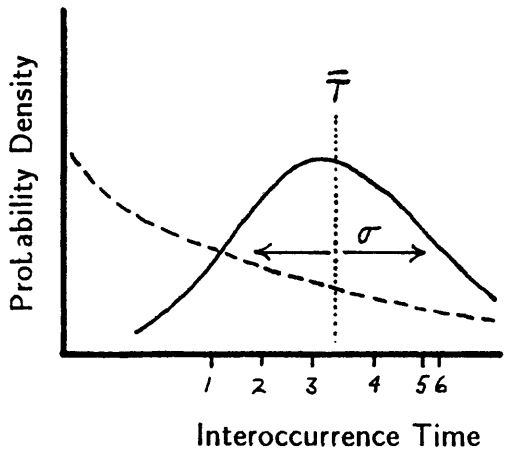

FIGURE 2.—Smoothed probability density function for the interoccurrence times of figure 1 (solid line) and a Poisson process having same average interoccurrence time (dashed line). The average value of the interoccurrence time is designated $\overline{T}$, and the standard deviation of the interoccurrence time by σ.

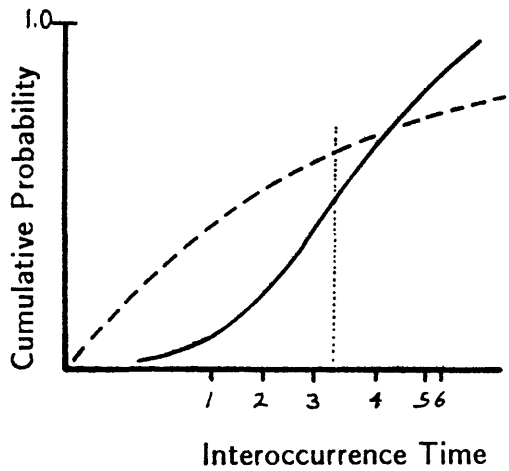

FIGURE 3.—Cumulative distribution function for the interoccurrence time of figure 1 (solid line) and for a Poisson process (dashed line).

interoccurrence time. Figure 2 shows a probability density function for the interoccurence time. Figure 3 shows the same information recast as a cumulative distribution function (CDF). It is contrasted with the CDF of a Poisson process, for which the interoccurrence times have an exponential distribution. There is a wider range of possible interoccurrence times in the exponential distribution, and the shorter the interoccurrence time, the more likely it is to occur.

Suppose there is another identical but independent fault, and we merge their two time lines. The average interoccurrence time for events on the merged time line would be half as large as before, and the standard deviation, coming from the variability of two processes, would be increased. In particular, there would be a greater likelihood of short recurrence times.

This procedure of merging independent time lines can be continued, and the resulting interoccurrence-time distribution comes more and more to resemble an exponential distribution. The smaller the σ of the individual time line, the more the merged time line resists looking random. However, for many faults, σ is not very small. Fault recurrences have been inferred to have a ratio of σ to $\overline{T}$ of about 0.20 to 0.33 (for example, Hagiwara, 1974, and Nishenko and Buland, 1987). I have performed simulation studies using such values and have found that as few as five time lines from independent faults having the same average recurrence produce merged time lines which statistically look very similar to samples of a Poisson process.

Consider now the time lines of two faults in which the occurrence of a rupture on one somehow produces an increased likelihood of an occurrence of a rupture on the other. The merged time line (fig. 4) shows the earthquakes to occur in pairs. The probability density function for the merged process (fig. 5) shows one peak for the interoccurrence time between the two events in the pair and one peak for the interpair interoccurrence time. If we continue the process of merging more contaged time lines, the pairs become bunches, the durations of the bunches increase, and the interbunch times decrease (fig. 6). The probability density function shows a large peak for the interoccurrence times within the contagion (fig. 7). This peak gets larger as n gets larger, because most of the interoccurrence times are between successive earthquakes in the same bunch. The smaller peak to the right represents the time between the last event in one bunch and the first event of the next bunch. This peak becomes relatively smaller and tends to shift more and more to the left, as the bunch time gets longer.

Clearly, the statistical distribution of interoccurrence times tends to look like a Poisson process as far as statistical parameters (mean and standard deviation) are concerned, but as long as we can count on a long inter-bunch time after a certain number of bunched events, there is information in the system which permits a useful probability statement to be made, both about the events in the bunch window and about the inter-bunch time. However, if the contagion time is relatively long, the inter-bunch time may approach the intra-bunch average time, and the process not only looks statistically Poissonian but also yields no interbunch time distinct from another contagion time. The process becomes no more predictable than an ordinary Poisson process.

The parameters σ, t_c, and n all play a role in whether the process looks two-stage or Poissonian. Although we can speculate about the relationship required between these parameters for a two-stage process to be possible (see appendix), modelling is required

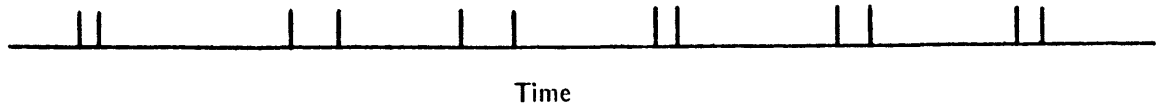

FIGURE 4.—Merged time lines for two faults, in which occurrence of an event on one time line potentiates the occurrence of an event on the other.

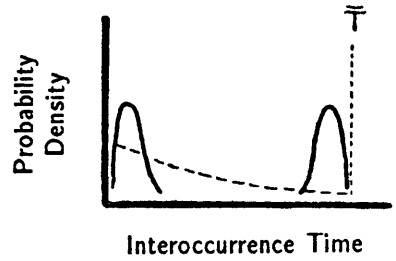

FIGURE 5.—Probability density function for the time line of figure 4.

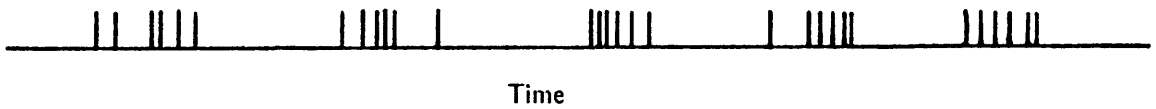

FIGURE 6.—Merged time lines for system of several contagious faults.

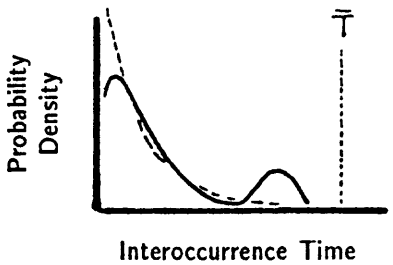

FIGURE 7.—Probability density function for the time line of figure 6.

to actually determine this relationship. In this paper, a brief parameter exploration study is presented. From this study, a preliminary parameter relationship is derived. Then a sample application is addressed for determining what standard of accuracy would be required for geological dating, in order that either the parameter values or the bunching behavior might be observable in the geologic record.

SOME SIMULATION RESULTS

Figure 8 shows a portion of a simulated eight-fault system. Although individual time lines do not show any unusual behavior, bunching caused by contagion is readily observed in the merged time line. Thus, dating the recurrences on a single rupture would not reveal the contagious behavior. One would have to date ruptures on adjacent faults and show that the differences in rupture dates were small compared to the random variability in occurrence for two independent faults of the same recurrence rate.

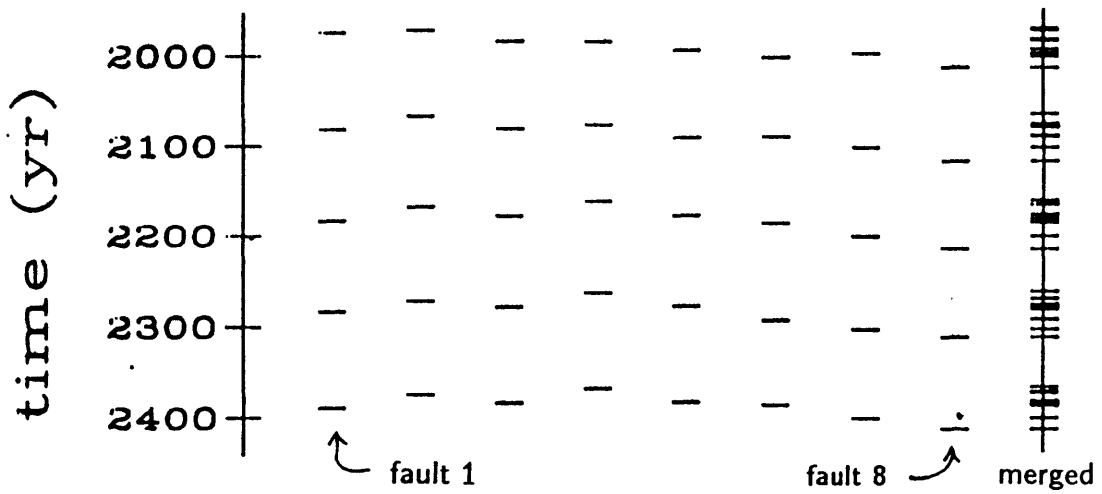

FIGURE 8.—Individual time lines and merged time line for system of eight contagious faults. Events on a single fault are shown as a stroke in the column representing that fault.

How small a time difference would dating have to discriminate? In figure 9, four illustrations show sets of CDF's for systems of 5 and 8 faults, for values of $\sigma' = \sigma/\overline{T}$ of 0.25 and 0.07. Contagion times, $t'_c = t_c/\overline{T}$, vary between 2 and 27 percent of the average recurrence time. Strong contagious behavior is shown when the CDF rises quickly to a value of $(1-1/n)$ and then levels off for a substantial fraction of time during the recurrence cycle. Poissonian behavior is shown by a continuing curving arc which becomes asymptotic to the value of 1.0. Intermediate behavior is shown by a CDF which rises with a first-stage rate clearly more rapid than the Poissonian rate to a value again near $(1 - 1/n)$, but which, instead of leveling off, merely lapses into a second-stage rate clearly slower than the Poissonian rate.

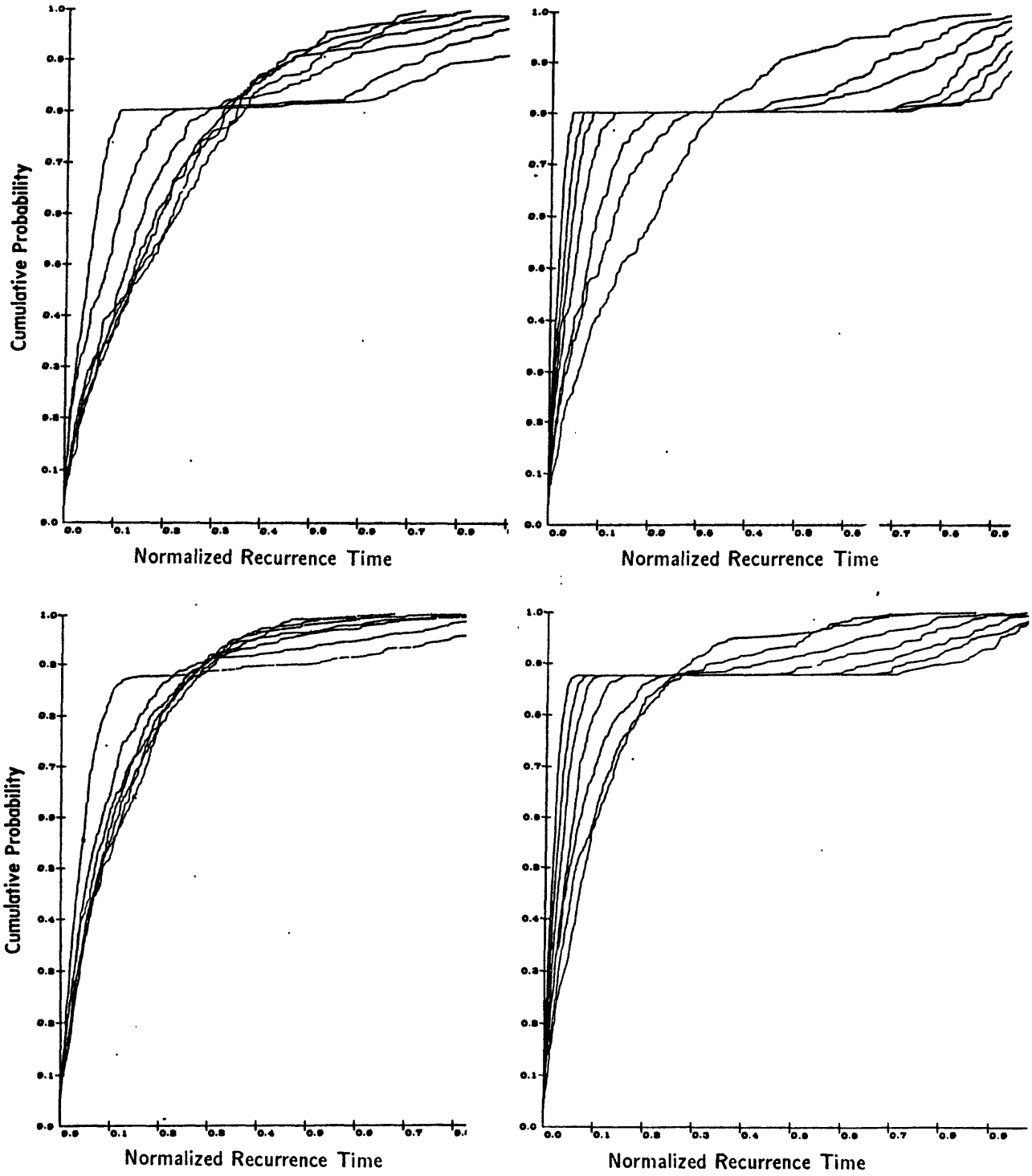

FIGURE 9.—Cumulative distribution functions for systems showing two-stage or Poissonian behavior, depending on value of t_c. Upper row, $n = 5$; lower row, $n = 8$. Left column, $\sigma' = 0.25$; right column, $\sigma' = 0.07$. Curves for the smallest values of contagion time rise earliest. Successive curves from left to right are for values of t_c' of 2, 3, 4, 6, 10, 15, and 27 percent, respectively.

In table 1 are gathered the values of σ', n, and t'_c which show clear to marginal two-stage behavior. The value of t'_c which produces marginally two-stage behavior is used to form the product of the variables. The product column shows that two-stage behavior for these simulations occurs when the product of the normalized values of the parameters is less than about 0.05. We can use this product as a rule of thumb to investigate whether the requisite values of the parameters can be observed by means of geologic dating procedures.

TABLE 1—Normalized Parameter Values for Two-Stage Processes, with Product for Marginal Processes

σ'	n	t'_c	$\sigma' \cdot n \cdot t'_c$
.25	5	.02, .03, .04	.05
	8	.02, .03	.06
.07	5	.02, .03, .04, .06, .10, .15	.052
	8	.02, .03, .04, .06, .10	.056
.10	8	.02, .03, .04, .06, .10	.08

Suppose we take $\overline{T}$ = 2000 yrs as an idealized model of the central five segments of the Wasatch Front zone. In order for the normalized product, $\sigma' \cdot n \cdot t'_c$, to be equal to 0.05, the product, $\sigma' \cdot t'_c$, must equal 0.01. If we take a value of σ' to be equal to 0.25, then t'_c must be equal to 0.04 or less, corresponding to unnormalized values of $2000 \cdot 0.25 = 500$ yrs for σ and $2000 \cdot 0.04 = 80$ yrs for t_c. A somewhat smaller value of σ' of 0.20 requires a t'_c of 0.05 or less, or 400 years and 100 yrs for σ and t_c, respectively.

To be able to directly observe parameter values this small requires dating large-earthquake occurrences on adjacent segments to within 50 yrs for t_c and requires measuring occurrence times on individual segments of the Wasatch fault to better than 250 yrs for σ. These accuracies are probably not currently achievable (M. N. Machette, U.S. Geological Survey, oral commun., 1987).

Does this mean that contagions for the Wasatch are not observable by current geological means? Not necessarily. If dating techniques permit us to establish that all of a group of segments consistently break over some time interval, say a 500- to 1000-yr time window, and that none of them break for the following time interval of 1500 to 1000 years, we might reasonably suspect two-stage process rather than a Poisson process. Even if one were only able to determine that none of the five segments had broken in the last 1000 years, this would indicate a low likelihood (probability of less than 3 percent) of Poisson behavior characterizing faulting for those segments.

DISCUSSION

In the simulations reported here, fairly stringent conditions are required in an ideal model to guarantee two-stage behavior under contagion. Is this model too ideal to be relevant? There are two reasons to think not, one based on how the model simulates the real world and one based upon the fact that contagions appear to be observable in the real world.

The contagion simulation represented here is governed by the use of an average contagion time t_c. Such an average time would be expected if this time represented the time it takes for a barrier between segments or faults to relax and transfer an additional stress load from one segment which has already ruptured to one which has not. The model uses this contagion time rather than using the unknown physics which underlies the contagion.

Whether such a contagion can occur or not depends not only on this stress load transfer but also on the physical state of the segment to which the load is being transfered. Back-contagion is physically unrealistic, because the segment which has just transferred a load is presumably not in a condition to do much with a load received back. Such back-contagion has been prevented in the model by nonphysical means—in part by a "toggle" which is set when the first fault passes the contagion to the second, and unset when the second fault tries to contage back. Back-contagion is also prevented in part by the role of σ. This variable not only models another recurrence characteristic observable in the real world but also, for reasonable values of σ and t_c, serves in the model to keep contagion bunches separate. The physics of the real world should operate this way as well.

The most artificial aspect of the model is the assumption that the average interoccurrence time for each segment is the same for all segments. This is a convenience rather than a restraint. Certainly if adjacent faults had very disparate recurrence times, a neighbor fault would rarely be physically ready to be contaged. Contagion would be rare. However such behavior would be difficult to model without some fairly explicit knowledge of the physics of the fault-rupture preparation process. On the other hand, if adjacent faults had roughly comparable recurrence times, neighbor segments would usually be in such a condition as to accept contagion. To assume that the recurrence times are identical in the model means nothing more than that the latter case is being assumed.

Nevertheless, these reassurances would not have much force if contagions were not actually observed in the world. In the literature, space-time diagrams may show show short time intervals between ruptures on adjacent segments and much longer recurrence times on individual segments (for example, Kelleher, 1970; Davies and others, 1981). Contagion seems to be involved in the last century of seismic activity in western Nevada on faults which have not previously ruptured for a period of time much longer than the interoccurrence times for recent events (Wallace and Whitney, 1984). Mogi (1974) shows periods of active seismicity followed by periods of inactivity for many of the world's chief seismic belts.

Indeed, contagion seems rather to be expected than to be surprising. The important thing is to be able to capitalize on knowledge about contagion in hazards analysis.

In the sample application presented here, it is possible that geological dating can be directed so as allow us to make a crucial choice in mitigation of hazard along the Wasatch Front, that is, whether to protect against large-magnitude characteristic events on the Wasatch fault itself, or to protect against the more likely, moderate-magnitude events historically observed west of the front.

REFERENCES CITED

Bakun, W. H., and Lindh, A. G., 1985, The Parkfield, California earthquake prediction experiment: Earthquake Prediction Research, v. 3, no. 3–4, p. 285–304.

Davies, J., Sykes, L., House, L., and Jacob, K., 1981, Shumagin seismic gap, Alaskan Peninsula—history of great earthquakes, tectonic setting, and evidence for high seismic potential: Journal of Geophysical Research, v. 86, no. B5, p. 3821–3855.

Hagiwara, Y., 1974, Probability of earthquake occurrence as obtained from a Weibull distribution analysis of crustal strain, in Rikitake, T., ed, Focal Processes and the Prediction of Earthquakes: Tectonophysics, v. 23, no. 3, p. 313–318.

Kelleher, J. A., 1970, Space-time seismicity of the Alaska-Aleutian seismic zone: Journal of Geophysical Research, Res., v. 75, no. 29, p. 5745–5756.

Lindh, A. G., 1983, Preliminary assessment of long-term probabilities for large earthquakes along selected fault segments of the San Andreas fault system in California: U. S. Geological Survey Open-File Report 83–63, 14 p.

Mogi, Kiyoo, 1974, Active periods in the world's chief seismic belts: Tectonophysics, v. 22, p. 265–282.

Nishenko, S. P., 1985, Seismic potential for large and great interplate earthquakes along the Chilean and southern Peruvian margins of South America—A quantitative reappraisal: Journal of Geophysical Research, v. 90, no. B5, p. 3589–3615.

Nishenko, S. P. and Buland, R., 1987, A generic recurrence interval distribution for earthquake forecasting: Bulletin of the Seismological Society of America, v. 77, no. 4, p. 1382–1399.

Rikitake, T., 1974, Probability of earthquake occurrence as estimated from crustal strain, in Rikitake, T., ed., Focal processes and the prediction of earthquakes: Tectonophysics, v. 23, no. 3, p. 299–312.

_____ 1975, Statistics of ultimate strain of the earth's crust and probability of earthquake occurrence: Tectonophysics, v. 26, no. 1, p. 1–21.

Schwartz, D. P., and Coppersmith, K. J., 1984, Fault behavior and characteristic earthquakes—Examples from the Wasatch and San Andreas fault zones, Journal of Geophysical Research, v. 89, no. B7, p. 5681–5698.

Sykes, L. R., and Nishenko, S. P., 1984, Probabilities of occurrence of large plate-rupturing earthquakes for the San Andreas, San Jacinto, and Imperial faults, California, 1983–2003: Journal of Geophysical Research, v. 89, no. B7, p. 5905–5927.

Wallace, R. E., and Whitney, R. A., 1984, Late Quaternary history of the Stillwater seismic gap, Nevada: Bulletin of the Seismological Society of America, v. 74, no. 1, p. 301–314.

APPENDIX

Getting a Feel for the Variables

To convince ourselves that the simulation results are sensible and to guide ourselves in searching for a rule of thumb governing relative parameter values which will permit contagion, it helps to get a heuristic feel for the role of the variables in the model. Below we consider the individual effects of σ and t_c, together with n.

First, suppose that σ is a "reasonable" value—that is, a modest, but not tiny fraction of $\overline{T}$ and somewhat larger than t_c. What happens as t_c gets smaller? Rupture times between adjacent segments get closer and closer together. The bunch time becomes strongly dependent on t_c: if the middle segment of a line of n segments breaks first, all segments will have broken within $((n-1)/2) \cdot t_c$, if n is odd, or $(n/2) \cdot t_c$, if n is even. If the end segment breaks first, all segments will have ruptured within time $(n-1) \cdot t_c$. Thus, on the average, the bunch time will be about $(3/4)(n-1) \cdot t_c$.

The remaining time until the first event of the next bunch, the inter-bunch time, is $\overline{T}-(3/4)(n-1)t_c$. Suppose we want the interbunch time to be three times the size of the bunch time. A little algebraic manipulation shows that this occurs when $t_c = \overline{T}/[3(n-1)]$. For values of $n = 3$, 5, and 8, corresponding values of t_c' would be 0.17, 0.08, and 0.05. The latter two values are about the size of the values in table 1 for $\sigma = 0.25$. Thus it appears that when σ is "loose," that is, reasonably large, but not so large as to prevent two-stage behavior, t_c seems to control the contagion fairly directly.

On the other hand, let us consider the case now when t_c is a "reasonable" number. As σ gets smaller, the recurrences on an individual fault time line get more and more regular. Once two segments get synchronized, they will tend to drift away from synchronization only very slowly. A modest contagion should arrest this drift. What is the role of the parameter n, in this case? Suppose all the fault segments are initially synchronized. The next rupture times of all the segments will be distributed according to the distribution function for interoccurence times. On the average they will span the $1/(2n)$-th to $(1-[1/(2n)])$-th fractiles of the cumulative distribution function (CDF). In interoccurrence time, the span will be from $t_1 = F^{-1}(1/2n)$ to $t_2 = F^{-1}(1-(1/2n))$, where $F^{-1}(x)$ means that value of time for which the CDF equals x.

Suppose the distribution function for interoccurrence times is roughly normal. Then the span in time is $2\sigma \cdot \Phi^{-1}(1-(1/2n))$ or simply $k\sigma$, where Φ^{-1} denotes the inverse of the central normal probability integral. For values of $n = 3$, 5, and 8, $k = 1.94$, 2.56, and 2.78. Suppose we want the interbunch time to be three times the size of this span. This occurs when $\sigma = 1/(4k)$. For values of $n = 3$, 5, and 8, corresponding values of σ would be 0.12, 0.10, and 0.09. The latter two values are about the size of those assumed in the lower part of table 1.

When σ is thus small enough to be controlling the bunching time, how "loose" can we expect t_c to be? The argument above suggests that one contagion can contain the σ-controlled bunch, so that $t_c = k\sigma$ or $t_c = 1/4$. This number is clearly too large compared to the values of t_c found in table 1. The reason is that the argument assumes that the contagion takes place exactly by time t_c. However, t_c is in the model a mean value; hence 50 percent of the time the contagion will take place after a longer period of time. In the model, t_c was chosen to have a normal distribution, with a standard deviation

equal to one-half the input value of t_c. To be more certain that the σ-controlled bunch is contained by the next contagion, one would expect a controlling time of t_c plus one or two standard deviations, that is, $1.5 \cdot t_c$ or $2 \cdot t_c$. For the latter case, $t_c = 1/8 = 0.12$, a value comparable to those shown in the lower half of table 1.

Thus, it appears that these heuristics roughly describe the results shown in table 1. Furthermore, it appears that when σ is loose, we need tighter, controlling values of t_c. Similarly, when t_c is loose, we need tighter, controlling values of σ. Thus, one would expect that their joint effect would tend to be compensating. This justifies the use of their product in searching for a rule of thumb for the modelled contagions.

PALEOSEISMOLOGY AND EARTHQUAKE-HAZARDS FORECASTING– A CONSUMER'S PERSPECTIVE

by

Stuart P. Nishenko
National Earthquake Information Center
U.S. Geological Survey
Denver, CO 80225

ABSTRACT

Probabilistic descriptions of earthquake recurrence along simple plate boundaries have become recognized as a valid means of expressing earthquake forecasts. Paleoseismology occupies a key position in hazard forecasting in that it can greatly extend the known earthquake history for many fault segments (hence, providing improved recurrence-time estimates), and can provide recurrence information for faults with no known historic earthquakes. To maximize the information content of paleoseismic data and to correctly interpret recurrence intervals based on these data, it is necessary to document the types and sizes of uncertainties present in the data.

INTRODUCTION

The use of probabilistic, time-dependent descriptions of earthquake recurrence along simple plate boundaries has grown during the last decade. These descriptions reflect the increase in the number of historic and geologic investigations of earthquake occurrence and the documentation of a nearly periodic distribution of characteristic earthquake recurrence-times along many individual fault segments. This observed behavior has already been exploited in the successful forecast of the 1985 M_S 7.8 Valparaiso, Chile, earthquake (Nishenko, 1985), and is presently being used as the basis for the Parkfield, Calif., earthquake-prediction experiment (Bakun and Lindh, 1985).

One of the basic problems that interferes with the application of a probabilistic approach to a specific fault segment is the relatively small number of data from which the recurrence interval and hence the forecast probability can be estimated. In general, distinguishing the most appropriate distribution function to generate probability estimates from a number of possible statistical functions requires more data than are available for individual fault segments. Previous attempts at applying probabilistic methods to forecasting earthquake hazards have used either *ad hoc* choices of probability distributions (for example, the normal or Gaussian distribution: Lindh, 1983; Sykes and Nishenko, 1984) or analogies to industrial failure-time statistics (for example, Weibull distributions: Hagiwara, 1974; Rikitake, 1976; Nishenko, 1985). While both approaches represent reasonable first attempts, the resolution possible with small data sets necessarily limited the reliability of the resulting answers.

THE LOGNORMAL DISTRIBUTION

Nishenko and Buland (1987) investigated the utility of a simple function, T/T_{ave}, to help define the overall distribution properties of characteristic earthquake recurrence

along simple plate boundaries. A characteristic earthquake is an event which repeatedly ruptures the same fault segment and whose source dimensions define that fault segment (see Schwartz and Coppersmith, 1984). For a series of characteristic earthquakes occurring along a specific fault or plate-boundary segment, T_{ave} is defined as the average recurrence interval for that segment, and T is the individual recurrence interval. Previous investigation of events in Chile (Nishenko, 1985) and California (Sykes and Nishenko, 1984) have indicated, for a limited number of examples, that the standard deviation of T/T_{ave} (or the coefficient of variation, $\sigma/mean$) appears to be roughly constant. This suggests that T/T_{ave} data from additional fault segments may also have the same statistical properties. If this is a general property of characteristic earthquake-recurrence intervals, then it allows the simultaneous analysis of all available recurrence data to determine the most appropriate distribution function. Recurrence data spanning two orders of magnitude in time and six orders of magnitude in seismic moment from both convergent and transform plate boundaries were used in the analysis. The primary assumption underlying the compilation of this diverse suite of recurrence intervals is that these data are all samples from a common population (that is, a single common process). This greatly increased data set allows for a more significant test to distinguish between various distribution functions. In particular, a larger data set allows a more thorough sampling of the tail areas of the distribution which have a large influence on estimating the statistical parameters of the function; hence the resulting forecast probabilities. For our purpose, the tails are the portions of the distribution that are far from the mean and therefore have small relative probabilities.

Two important results from the T/T_{ave} analysis are first, the identification of the *lognormal* distribution as the best-fitting distribution for earthquake-recurrence intervals along simple plate boundaries and the observation that the coefficient of variation, $\sigma/mean$, was approximately constant over the entire range of historical recurrence times analyzed ($\sigma/mean = 0.215$). That is,

$$f(T/T_{ave}) = \frac{T_{ave}}{T\sigma_D\sqrt{2\pi}} e^{-(\ln(T/T_{ave})-\mu_D)^2/2\sigma_D^2} \quad (1)$$

or that $\ln(T/T_{ave})$ is normally distributed with a mean of $\mu_D = -0.0099$ and a standard deviation of $\sigma_D = 0.215$. The second result of this analysis is the recognition of two sources of variability that affect the quality of recurrence-interval measurements. The first source of uncertainty, σ_i, involves estimating the length of a particular recurrence interval T_i. σ_i measures the reliability of each datum. Note that for historical events, $\sigma_i = 0$. The second source of uncertainty is the natural variability among recurrence intervals (the σ_D term in eq. 1). It measures how close an individual recurrence observation is likely to come to the average repeat time. As these two sources of variability are independent, the total variability of $\ln(T_i)$ is just,

$$\mathrm{var}[\ln(T_i)] = \sigma_i^2/T_i^2 + \sigma_D^2, \quad (2)$$

where σ_i is the uncertainty in estimating the length of a recurrence interval T_i. In other words, $\sigma_i = \sqrt{\sigma_1^2 + \sigma_2^2}$, where σ_1 and σ_2 are the uncertainties in the dates of the two

prior events that constitute the recurrence interval T_i. Both of these results provide valuable *a priori* information which helps improve the reliability and precision of the resulting earthquake-hazards forecasts.

Additionally, we also have a basis for comparing historical/geologic and laboratory observations of earthquake and failure behavior, as the T/T_{ave} results are scale-independent. Physically, the lognormal distribution is an appropriate description of failure processes in materials which have the property of strengthening as their lifetime increases (Gertsbakh and Kordonskiy, 1969). This type of behavior is similar to observations where fault strength increases with the logarithm of the time of fault contact (J. Dieterich, oral commun., 1987). Additionally, the use of the lognormal distribution can be motivated by a comparison with failure-time analysis in the materials science literature (Heller, 1972; Little and Ekval, 1981). Lognormal distributions are commonly used to describe the distribution of crack sizes, growth rates, and lives or failure times, and can be derived from a simple physical model of crack growth (Kao, 1965). Hence, our analysis indicates that the lognormal model may be not only the best-fitting model to the recurrence-time data but also the most appropriate.

Once we decide on the type of distribution function that best describes the recurrence information, we can ask the question: given the date of the last characteristic earthquake and the average recurrence time, what is the probability of another event occurring within some future time interval, provided the event has not happened yet? The answer to this question is termed the *conditional probability* and in many instances represents the final and most visible result for much of the work which is discussed in this volume. Examples of probability estimates for specific faults for future time intervals are shown in table 1. More detailed explanations and examples can be found in Nishenko (1985) and Nishenko and Buland (1987).

UNCERTAINTIES IN RECURRENCE-TIME ESTIMATES

While estimating the probability of recurrence for a particular fault segment is a step in the right direction, we also need to know the accuracy of that estimate. The usefulness or information content of the conditional probability statement can be evaluated by examining the range of probabilities within some predetermined confidence limits (for example, $\pm 1\sigma$, $\pm 2\sigma$, ± 90 percent). This conveys information about the precision of the forecast, and the range of numbers within the confidence limits represent the cumulative effect of all the uncertainties involved (see table 1 for examples). Two primary sources of uncertainty when dealing with historical data are determining the average recurrence time, T_{ave}, based on only a few observations, and describing the intrinsic variability of the recurrence process (σ_D). Both of these problems are addressed with the generic lognormal recurrence model (Nishenko and Buland, 1987). For geologically derived data, the above uncertainties are compounded by additional uncertainties associated with dating prior events. Dating uncertainties have two independent parts: (1) analytical uncertainty associated with a particular dating procedure and (2) field-sampling errors (that is, bad dates from picking a wrong or contaminated sample and the lack of enough samples to confidently date a particular stratigraphic horizon). For sites where the date of the last earthquake is only known through paleoseismic investigations, these errors and

Table 1. Lognormal recurrence time and conditional probability estimates

Region	Date of last event	Average repeat time (years)	Date of next event[1]	Conditional probability[2]		
Forecasts				**1987-1992**	**1987-1997**	**1987-2007**
Parkfield, Calif.[3]	1966	22	1987±8	70%(52-84%)	94%(85-98%)	100%(99-100%)
Pallett Creek, Calif.[3]...	1857	194	2052±84	2%(0-10%)	4%(0-19%)	10%(1-38%)
Indio, Calif.[4]	1680±20	220	1930±124	11%(5-22%)	22%(9-40%)	40%(18-64%)
Middleton Is., Alaska[3]..	1964	1021	3105±501	0%	0%	0%
East Oaxaca, Mexico[3]..	1965	37	2002±19	5%(0-53%)	21%(1-85%)	70%(19-99%)
Retroforecasts[5]				**1964-1969**	**1964-1974**	**1964-1984**
Middleton Is., Alaska[6]..	660	950	(1964)	3%(1-5%)	5%(2-10%)	10%(5-19%)
				1886-1891	**1886-1996**	**1886-1906**
Charleston, S.C.[7]	800	1086±131	(1886)	2%(0-6%)	3%(1-11%)	7%(1-21%)

Notes:

1. ± values are the 90% confidence limits on the date of the next event. For retroforecasts, dates in parentheses are actual dates of the next event.
2. Percentages in parentheses reflect the 90% confidence interval for the date of the next event.
3. Nishenko and Buland (1987).
4. Sieh (1986).
5. Retroforecasts are probability estimates computed just prior to the date of earthquake. Time intervals for retroforecasts indicated in bold print.
6. Based on pre-1964 marine terraces on Middleton Is. (Plafker, 1986).
7. Based on observed 800 A.D.-1886 recurrence interval (Weems et al., 1986).

uncertainties contribute to uncertainties in determining T_{ave}, hence the expected date of the next event.

All of the above uncertainties can be incorporated into earthquake-hazards estimates if, and only if, the values are known. In other words, it is becoming more and more important that researchers publish not only their dates but also the types and sizes of uncertainties associated with their data. For example, are the reported uncertainties $\pm 1\sigma$ or $\pm 2\sigma$? Are uncertainties analytic or associated with averaging a number of dates from a particular sample site?

PALEOSEISMOLOGY AND HAZARDS FORECASTING

Some of the implications of the above discussion that have a direct impact on earthquake hazards and paleoseismology are:

1. Uncertainties associated with dating prior events can be so large as to make the resulting forecast useless (that is, have an unacceptably large range of probability values within some confidence limit). Clearly, reducing the analytic errors and developing better dating techniques, as are discussed in the first section of this volume, can improve our estimates. Additionally, increasing the number of samples for analysis and using more more than one dating technique can also reduce our uncertainty.
2. Based on historical data for plate-boundary shocks, the property of a constant coefficient of variation indicates that earthquakes with short recurrence times ($\leq$ 30 yrs) can be "predicted" (that is, the recurrence time can be estimated to within a few years), while events with longer recurrence times (that is, $\geq$ 50 yrs) can only be "forecast" (that is, the recurrence time can only be estimated to within a decade or two). Hence, we are starting to see the types of results we can expect with standard types of data for various size earthquakes. In the forecast case, more precise statements which can narrow down the expected time of occurrence to within a few years, must await intermediate- or short-term precursory information. Since many of the earthquakes of interest to paleoseismologists have long recurrence times (that is, hundreds to thousands of years), the best we can hope to do with this type of recurrence information is to provide long-term earthquake forecasts.
3. For those earthquakes with very long recurrence times (that is, $\geq$ a few hundred years), conditional probabilities for any socially useful timeframe (typically one to two decades) will always be small numbers ($\leq$10 percent), since the time interval of interest is a small fraction of the recurrence interval. Hence, these events will always be viewed as relatively improbable and have a low social impact on a yearly basis. For example, using the marine terraces at Middleton Island, Alaska, that were formed prior to the great 1964 earthquake, the conditional probabilities in 1964 just before the earthquake for a repeat during the next 10 and 20 yrs (1964-1974 and 1964-1984) were at the 5- to 10-percent level. Similarly, using the observed 800-yr recurrence interval at Charleston, S. C., just before the 1886 earthquake the conditional probabilities for the next 10 and 20 yrs (1886-1896 and 1886-1906) were at the 3- to 7-percent level (table 1).

DISCUSSION

Seismologic and geologic research has finally reached the point where we can make time-dependent probabilistic earthquake-hazards statements for specific fault segments. This type of information, which is analogous to a weather forecast, can be readily communicated to governmental officials and the planning community, and provides a scientific rational for the development of hazard-mitigation programs for specific areas during specific time intervals. At present, the number of areas where these techniques have been applied is limited by the availability of recurrence data. The lognormal distribution appears to be the appropriate description for plate-boundary events. The generic properties of the lognormal distribution allow its use over a wide range of magnitudes and recurrence times. Additionally, by accounting for the uncertainties in both geologic and historic data, we can combine both types of recurrence estimates directly when producing earthquake forecasts.

Are the same ideas and distribution functions tranferable to *intraplate* earthquakes? At present, the evidence appears equivocal. Observations by Wallace (1984) and Schwartz and Coppersmith (1984) suggest bimodal recurrence behavior within the Great Basin, where periods of increased activity and perhaps repeated rupture on faults within a single subprovince are separated by long intervals of inactivity. Perkins (this volume) presents a discussion of this type of bimodal behavior.

Clearly, the trend for future progress in earthquake hazards-assessment is to make use of paleoseismic data, both to extend the record of past earthquake activity on historically active faults and to provide critical information for faults with no known historic activity. Additional geologic information from intraplate faults can help determine the applicability of the lognormal or perhaps another distribution function to describe intraplate earthquake hazards. Additional paleoseismic information from simple plate boundaries will also help refine our present understanding of how earthquake-recurrence intervals are distributed in time.

In general, due to the long recurrence times associated with many large and great earthquakes, the best we can do with these data is to provide the community with earthquake forecasts. Granted, earthquake forecasts are not as exciting as earthquake predictions. Nevertheless, accurate hazards forecasts require a thorough understanding, as well as proper treatment and presentation, of the uncertainties involved.

ACKNOWLEDGMENTS

Conversations with R. Madole, A. Nelson, D. Perkins, and R. Wheeler are gratefully acknowledged, as are the critical reviews by D. Perkins and R. Wheeler. This review was funded by Agency for International Development Agreement BOF-000-P-IC-4051-00.

REFERENCES

Bakun, W. H. and Lindh, A. G., 1985, The Parkfield, California earthquake prediction experiment: Science, v. 229, p. 619–624.

Gertsbakh, I. B. and Kordonskiy, Kh. B., 1969, Models of Failure: New York, Springer-Verlag, 171 p.

Hagiwara, Y., 1974, Probability of earthquake occurrence as obtained from a Weibull distribution analysis of crustal strain: Tectonophysics, v. 23, p. 313–318.

Heller, R. A., 1972, Probabilistic Aspects of Fatigue: ASTM Spec. Tech. Pub. 511, Philadelphia, PA, American Society for Testing and Materials, 203 p.

Kao, J. H. K., 1965, Statistical models in mechanical reliability: Proceedings 11th National Symposium Reliability and Control, p. 240–247.

Lindh, A. G., 1983, Preliminary assessment of long-term probabilities for large earthquakes along selected fault segments of the San Andreas fault system in California: U.S. Geological Survey Open File Report 83-63, p. 1–15.

Little, R. E. and Ekvall, J. C., eds., 1981, Statistical analysis of Fatigue Data: ASTM Spec. Tech. Pub. 744, Philadelphia, PA, American Society for Testing and Materials, 143 p.

Nishenko, S. P., 1985, Seismic potential for large and great interplate earthquakes along the Chilean and southern Peruvian margins of South America– A quantitative reappraisal: Journal Geophysical Research, v. 90, p. 3589–3615.

Nishenko, S. P. and Buland, R., 1987, A generic recurrence interval distribution for earthquake forecasting: Bulletin Seismological Society America, v. 77, p. 1382–1399.

Plafker, G., 1986, Geologic studies related to earthquake potential and recurrence in the "Yakataga seismic gap", in C. F. Shearer, ed., Minutes of the National Earthquake Prediction Council: U.S. Geological Survey Open File Report 86-92, p. 135–143.

Rikitake, T., 1976, Recurrence of great earthquakes at subduction zones: Tectonophysics, v. 35, p. 335–362.

Schwartz, D. P. and Coppersmith, K. J., 1984, Fault behavior and characteristic earthquakes– Examples from the Wasatch and San Andreas fault zones: Journal Geophysical Research, v. 89, p. 5681–5698.

Sieh, K., 1986, Slip rate across the San Andreas fault and prehistoric earthquakes at Indio, California [abs.]: EOS [Transactions American Geophysical Union], v. 67, p. 1200.

Sykes, L. R. and Nishenko, S. P. 1984, Probabilities of occurrence of large plate rupturing earthquakes for the San Andreas, San Jacinto and Imperial faults, California, 1983–2003: Journal Geophysical Research, v. 89, p. 5905–5927.

Wallace, R. E., 1984, Patterns and timing of late Quaternary faulting in the Great Basin province and relation to some regional tectonic features: Journal Geophysical Research, v. 89, p. 5763–5770.

Weems, R. E., Obermeier, S. F., Pavich, M. J., Gohn, G. S., Rubin, M., Phipps R. L., and Jacobson, R. B., 1986, Evidence for three moderate to large prehistoric Holocene earthquakes near Charleston, S.C.; in Proceedings Third U.S. National Conference Earthquake Engineering, v. 1, edited by Earthquake Engineering Research Institute, El Cerrito, CA, p. 3–13.

SUMMARY OF DISCUSSION SESSION: ASPECTS OF SEISMIC-HAZARD ANALYSIS

by

Anthony J. Crone
U.S. Geological Survey
Denver, Colorado 80225

Session Chairman: David P. Schwartz, U.S. Geological Survey
Panel Members: Stuart P. Nishenko, U.S. Geological Survey
David M. Perkins, U.S. Geological Survey
Robert E. Wallace, U.S. Geological Survey
Steven G. Wesnousky, Memphis State University

Transmitting hazard information to the appropriate public officials clearly and accurately is an very important part of hazard analyses. Considering the uncertainties in the geologic data on faults and the inherent uncertainty in probability estimates, it seems improbable that we will be able to confidently forecast the occurrence of large earthquake within time windows of less than 200 years. From a societal perspective, a 200-year span is very long, and therefore, the threat of a damaging earthquake may seem relatively remote and thus, may not warrant immediate attention. Even in a high-probability situation (for example, a very high probability of a large earthquake occurring within a 100-year time span), the chances of the event occurring in any single year are very small and probably would not stimulate adequate planning. Perhaps hazard information is better expressed to the public in the form of the chances of such an event happening is five times greater now than it was 100 years ago. Because we are dealing with events that have long recurrence times from a societal perspective, the absolute probabilities of such an event occurring within a one- or five-year interval will always be small. However, the small absolute probabilities may not accurately portray the actual threat to society in terms of injuries and damage.

In large part, seismic-hazard analyses are based on modeling the future behavior of a fault by combining probability functions with geologic data describing the fault's past behavior. The resulting hazard estimate partially depends on the kind of probability function used in the model. Sometimes models can yield unrealistic results. One advantage of a lognormal probability model over other models is that it gradually increases the hazard by an incremental factor with passing time. Thus it allows for a future forecasted earthquake to have a recurrence time longer than the average recurrence interval before it predicts 100 percent probability for the upcoming event.

Probability estimates define the general long-term earthquake hazard, but true short-term predictions will have to be based on physical clues that indicate a significant increase in the hazard. As we increase our understanding of the faulting process and learn more about premonitory signals, we will improve our ability to assess the short-term hazards. Paleoseismology will provide the much of the foundation for long-term forecasts, but, most likely, seismology and geodesy combined will provide the basis for short-term predictions.

We must fully utilize current and future technologies to identify and monitor the physical clues of increasing hazard. For example, an ideal way to

monitor geodetic changes would be to use global positioning satellites and lasers. Imagine a network of several hundred stations across California whose locations and elevations could be measured simultaneously and very accurately every day by satellite. With these data, we might be able to track the movements of microplates and actually observe progressive deformation and strain accumulation. These are lofty but not unattainable goals that we should envision as part of the future of earthquake prediction.

Despite efforts identify and map all potentially seismogenic faults near populated areas, an alarming number of recent damaging earthquakes on previously unmapped faults shows that our inventory is incomplete. Although we may not now (or ever) have an absolutely complete inventory of all seismogenic faults, most geoscientists feel that we have identified virtually all of the major faults or fault systems that might generate severe earthquakes. Considering our limited resources and personnel, we are faced with the choice of either concentrating on our mapping efforts to inventory all potentially seismogenic faults, or focusing on studies to decipher the paleoseismic histories of known faults. We must realize that damaging, moderate-magnitude events will occur in the future on ummapped faults in seismically active areas like California. Generally, seismic-hazard models accommodate these "random" events, so they are not completely ignored. But considering our available resources, seismic-hazard analyses can benefit the most from well-documented paleoseismic histories of the major faults and fault systems. These faults and fault systems pose the greatest and most obvious threat to life and property. Unfortunately, in some urban areas, documenting the histories of known faults is difficult or impossible because development has destroyed critical evidence.

Two of the most important kinds of paleoseismic data that affect seismic-hazard assessments are information on the earthquake recurrence interval and the time of the last event. For hazard models, it is critical to separate the faults with long recurrence intervals (for example, 25,000 yr) from those with short intervals (for example, 1,000 yr). In the above example, even if both faults have Holocene movement, the fault with a short recurrence interval poses a greater hazard. For hazard modeling, it is also very useful to know if the recurrence interval is regular and strongly periodic, or if the timing between successive events fluctuates a great deal.

The time of the last event combined with recurrence information can have a big impact on the estimated hazard. For example, a fault with a 1000±50-yr recurrence interval on which the last event 950 yr ago poses a greater hazard than the identical fault on which the last event was 100 yr ago. Thus, paleoseismologic data on recurrence intervals and the timing of the last event will permit improved hazard assessments.

Hazard assessments for critical facilities are faced with the difficult problem of determining the maximum-magnitude earthquake that can be generated by a specific fault. The paleoseismologic data that contributes to maximum-magnitude estimates is very important because of safety and financial considerations. Hopefully, paleoseismology can contribute to more reliable maximum-magnitude estimates through a better understanding of the mechanics of faults in different tectonic environments, and by providing a better data base to compare earthquake magnitude with various fault parameters.

Hazard assessments in the central and eastern United States are plagued by special problems. With a few notable exceptions (for example, the Meers fault, Oklahoma), surface faulting is rare. Therefore, identifying a hazardous fault and estimating recurrence times rely heavily on the patterns and characteristics of the modern seismicity. However, we know that hazardous

faults can be aseismic for long periods of time, and, in some cases, the recurrence estimates based on seismicity can be misleading. Dealing with these difficult problems is a major challenge for future research.

THE FUTURE OF PALEOSEISMOLOGY:

VIEWPOINTS OF PRACTITIONERS AND PROGRAM MANAGERS

RESEARCH IN THE GEOSCIENCES SUPPORTED BY THE NUCLEAR REGULATORY COMMISSION

Richard B. McMullen
U.S. Nuclear Regulatory Commission

ABSTRACT

The Nuclear Regulatory Commission (NRC) research budget for geosciences is about 4.5 million dollars per year. Approximately 2.5 million dollars of this supports the seismic networks deployed throughout the central and Eastern United States. The NRC and the U.S. Geological Survey signed an Interagency Agreement in November 1986, for the establishment of the eastern part of a national seismographic network. This will be accomplished over a period of 6 years with completion planned for Fiscal Year 1992. The new network will consist of about 55 three-component, broad-band, digital seismic stations east of the Rocky Mountains.

The remaining 2 million dollars of the current budget will fund contracts and grants for research carried out by academic institutions, consultants, other Federal agencies, State geological surveys, and national laboratories.

A major goal of NRC-funded geological, seismological, and geophysical research has been to define earthquake-source structures or source zones. In addition to maintaining seismic-monitoring capability, the current emphasis is on neotectonics, and identifying and defining seismogenic structures at hypo-central depths. Programs currently underway include research related to: (1) neotectonics of northeastern United States; (2) seismically induced soil-deformation features in Charleston, S.C., region and paleoliquefaction features on the Atlantic Coastal Plain; (3) geology and geophysics of the southeastern Piedmont, central Virginia, and Giles County, VA; (4) paleo-seismology of faults in the Wichita Frontal Fault System of southern Oklahoma; (5) ground-motion studies in California and in the New Madrid seismic zone; (6) paleoseismology in the Pacific Northwest; and (7) the state of stress in eastern and central United States.

The NRC is not a research organization as such; therefore, for a proposal to be funded, a direct relationship between the research and NRC regulatory responsibilities must be shown.

SUMMARY OF DISCUSSION SESSION: THE FUTURE OF PALEOSEISMOLOGY-- VIEWPOINTS OF PRACTITIONERS AND PROGRAM MANAGERS

by

Anthony J. Crone
U.S. Geological Survey
Denver, Colorado 80225

Session Chairman: Anthony J. Crone, U.S. Geological Survey
Panel Members: Clarence R. Allen, California Institute of Technology
William L. Ellsworth, U.S. Geological Survey
John A. Maccini, National Science Foundation
Richard D. McMullen, U.S. Nuclear Regulatory Commission
David P. Russ, U.S. Geological Survey
Robert E. Wallace, U.S. Geological Survey

In the past decade, paleoseismic studies have evolved from simply identifying and mapping "young" fault scarps to helping resolve complicated and sophisticated problems like earthquake recurrence intervals, maximum magnitudes, and fault segmentation. Geologists recognize the problems and uncertainties associated with paleoseismic data, but we can minimize these deficiencies with improved technology and additional research. Paleoseismology will continue to contribute to our understanding the behavior of seismogenic faults and to mitigating earthquake hazards in the future. However, the extent of these future contributions depends, in part, on the support that is available for paleoseismology. Thus, geoscientists need to be aware of the perception and philosophy of funding agencies toward paleoseismology.

As one of the major agencies of scientific research in the United States, the National Science Foundation (NSF) must constantly balance its support of "big" science against "small" science, that is, major, costly programs such as the Continental Lithosphere program, COCORP, and the Global Positioning Satellite program, versus comparatively small, inexpensive grants to individual scientists. The value and contributions of the major programs are obvious, and well publicized, but sometimes they overshadow the contributions of individual researchers. Unfortunately, these major programs have largely consumed the recent increases in the NSF budget. However, the NSF clearly recognizes the importance of individual scientists and continues to fund about 50 grants each year to individuals for research in fundamental earthquake studies.

The philosophy of the Nuclear Regulatory Commission (NRC) toward paleoseismic research has changed since the NRC first began funding earthquake-related studies in the late 1960s and 1970s. Initially, the NRC supported studies to map known faults and to determine if those faults were active according to NRC criteria. Next, the NRC funded research that concentrated on geophysical studies to characterize seismogenic structures. Most recently, the NRC has supported paleoseismic studies that document the long-term history of severe shaking in selected regions. Current research topics of interest to the NRC include (1) neotectonics and possible paleoliquefaction features in New England, (2) evidence of strong shaking in the Atlantic Coastal Plain, (3) structural geology and neotectonics of the

Central Virginia seismic zone, (4) neotectonics of the Wichita Frontal fault system in Oklahoma, and (5) evidence of major earthquakes in the Pacific Northwest.

The NRC is not a typical research-funding agency, therefore, proposals funded by the NRC must have a direct application to the nuclear licensing process. Severe recent budget cuts have reduced the NRC's funding for the geosciences, and much of the currently available support is dedicated to maintaining seismic networks. As a result, NRC support for paleoseismic studies is limited.

The U.S. Geological Survey's (USGS) studies in paleoseismology are supported by the National Earthquake Hazards Reduction Program (NEHRP), thus support for the agency's earthquake studies is funded directly from Congress. Annual Congressional reviews repeatedly emphasize the need for NEHRP to maintain a scientific and geographic balance. The program contains five elements: (1) current tectonic and earthquake potential studies, (2) earthquake prediction research, (3) regional earthquake hazards assessments, (4) data information and services, and (5) engineering seismology. Most paleoseismic research is funded by elements 1 and 3.

USGS-funded research under the NEHRP is divided in an "internal program" that supports studies by USGS personnel, and an "external" program that supports research by non-USGS scientists. At present, the "internal" program supports 37 projects that are generally related to paleoseismology.

During the past few years, administration of the "external program has changed and the procedure for awarding grants has been revised. The annual requests for proposals lists specific priorities for the program. These priorities are established by the managers for each of the program elements who balance the goals of the NEHRP with the input they receive from practitioners and scientists. The newly installed review and evaluation procedure for proposals to the "external" program is similar to that used by the NSF. After proposals are independently reviewed, a peer panel ranks the proposals according to their quality and their potential contributions to the program. Management then tries to fund as many of the proposals as possible within the existing fiscal constraints.

Paleoseismology has grown so rapidly and can expand in so many directions that there is neither sufficient talent nor adequate funds to pursue all of the possible tasks. Scientists involved in paleoseismic studies must develop a unified sense of direction to maximize their efficiency.

Paleoseismic studies initially focus on two key questions: when did an earthquake occur and how often do they recur. Both of these questions involve a time element and show the strong dependence of paleoseismology on geochronologic techniques. Novel and developing techniques may have great potential for widespread applications to paleoseismology, but typically, geologists are very hesitant to use their limited funds for dating on new techniques that may or may not yield useful results. Funding agencies must recognize this need and either provide support committed specifically to develop a technique, or fund field studies whose objectives include testing a particular technique.

Many geochronologic techniques are not developed by the field scientists who use them, so commonly proposals submitted to funding agencies to develop a technique do not include provisions for field testing. Funding agencies are commonly faced with the dilemma of funding either a laboratory-oriented or a field-oriented proposal. Ideally, the developers and users should plan to cooperatively test techniques, evaluate the sources of error, and thereby improve the technique's resolution while minimizing development costs.

Laboratories developing and refining new dating techniques require more stable and longer-term funding commitments than those allowed by the current system. Operating and maintaining a laboratory is an expensive endeavor, and without steady funding, scientists waste a great deal of energy supporting the daily operations of their laboratories. Stable, long-term funding would increase the scientist's productivity and maximize the opportunities to improve dating techniques.

There is a strong appeal and widespread support to the idea of applying many different numerical dating techniques to a specific paleoseismic problem at a selected site. This approach will allow geoscientists to compare the results from various numeric dating methods, especially some of the new, important techniques. With the age control from multiple numeric dating techniques, geologists can also calibrate other relative dating methods that do not directly yield numerical ages.

The sites where multiple dating techniques are initially tested should meet at least two important criteria. First, the basic geologic framework and chronologies should be well established using conventional, accepted methods. This approach provides a scientifically valid means of testing the specific dating methods although it is not as spectacular or exciting as developing a chronology in a new area. Without good geologic control to verify the results, the value and credibility of a program to test dating techniques would be severely reduced. Secondly, from both a technological and paleoseismic viewpoint, the site should contain deposits that span much of the late Cenozoic. This criteria would permit a variety of different techniques to be tested, and would also provide the kind of age control needed to compare short-term versus long-term fault histories.

In addition to the element of time, paleoseismologic studies must also wrestle with the difficulties of identifying prehistoric earthquakes in the geologic record and estimating the magnitude of those events. Detailed studies of recent large-magnitude (~7) historic events indicate that our overall interpretations of prehistoric earthquakes based on colluvial stratigraphy are generally valid. This observation emphasizes the importance of studying historic ruptures and stresses the need to continue such studies in the future.

Magnitude 6 or 6.5 events can cause substantial damage, and, in the past, hazard assessments have treated these events as part of the background seismicity in which such events could occur essentially anywhere. With detailed geologic mapping, and a refined understanding of structural patterns and regional seismicity, we may be able improve our ability to characterize tectonic regions and thus more accurately define seismotectonic provinces. As a result, we may be able to associate potentially damaging moderate-magnitude earthquakes with specific structures or structural provinces, and not be forced to treat all of these earthquakes as completely random events.

Another possible way of deal with the hazards from these moderate-magnitude earthquakes is to identify the causative faults from the geologic record. This requires that we determine our ability to resolve moderate-magnitude events in the geologic record. Can we confidently identify an eroded 20-cm-high scarp from stratigraphic relations? First we must establish our resolution limits by systematically studying the nature and extent of deformation associated with historic, moderate-magnitude events in different tectonic settings. For example, in the Basin and Range province, we suspect that the threshold magnitude for significant near-surface deformation is about M 6.5, but we have yet to collect the the data needed to support this suspicion.

Another difficult problem in paleoseismology is the conversion of slip measurements for prehistoric events to meaningful estimates of earthquake magnitude. Paleoseismic studies generally measure slip at a single point, but we know from historic ruptures that the amount of slip measured at the surface varies tremendously within short distances along strike. Should we regard these measurements of paleoseismic slip as estimates of the average slip or the maximum slip? The most reliable magnitude estimates are probably derived from slip measurements at several points along the fault, but obtaining these data through trenching and other detailed, site-specific studies is costly and time consuming. Scarp profiling is an efficient way to obtain numerous, reasonably accurate measurements of slip for faults whose movements are dominantly vertical. Obviously, the quality of the slip measurements depends on the careful selection of profile sites in the field, but overall, profiling is an underutilized method that can provide useful data on displacement for some faults.

Magnitude estimates of prehistoric events are derived from regression relations of surface displacement versus magnitude or rupture length versus magnitude for historic earthquakes. Engineers and planners rely heavily on these magnitude estimates for structural designs, but few realize the wide range in values and the variation in quality of the data set for historic events. A worthwhile endeavor in paleoseismology would be to reexamine and re-map important historic events to improve the data base for these widely used regressions relations.

Paleoseismology has grown rapidly and now plays an important role in our national earthquake program, but, without continued public support, it may not reach its full potential, or worse, it may fade into obscurity. Today, the program is healthy and active, but the geoscientists involved in paleoseismology cannot dwell solely on their science. To a degree, we must mount a public relations campaign to assure that paleoseismology can effectively compete with other physical sciences for the limited fiscal resources. Part of our efforts must focus on educating legislators, governors, and the public at large about the societal benefits of paleoseismic studies. We must aggressively advocate continued support for natural hazards studies in the ever-changing Federal and State programs for science. Dealing with the ever-changing political climate and research priorities requires organization, determination, commitment, and hard work, the same qualities we need to do competent science, but applied in a different way.

Scientific programs, funding initiatives, and research objectives change and evolve quickly. Currently, the NEHRP is being reevaluated and possibly, it's emphasis may shift from research to applications. However, today geoscientists are less naive than we were a decade ago, and more aware of the complexities of earthquake process. Now, we are much better prepared to tackle some of fundamental questions about earthquake mechanics. Geoscientists must be the strongest and most visible advocates of paleoseismology. We must constantly maintain a pool of fresh research ideas so we can utilize scientific unexpected opportunities. We must remember that proposals that seem too controversial or ambitious today, may be high research priorities in the near future. To maintain the vigorous growth of paleoseismology, we need explore new opportunities for research using new technologies, increase our visibility and activity in professional organizations, and encourage more formal academic training in paleoseismology and neotectonics. All of these activities will help maintain the momentum that we have developed during the past decade.